

NASA/CP-1999-208982/PART1



The Second Joint NASA/FAA/DoD Conference on Aging Aircraft

*Charles E. Harris, Editor
Langley Research Center, Hampton, Virginia*

Proceedings of a conference sponsored by the
National Aeronautics and Space Administration,
Federal Aviation Administration, U.S. Air Force
Materiel Command, U.S. Naval Air Warfare
Center, and U.S. Army Research Laboratory, and
held in Williamsburg, Virginia
August 31 - September 3, 1998

National Aeronautics and
Space Administration

Langley Research Center
Hampton, Virginia 23681-2199

January 1999

Available from:

NASA Center for AeroSpace Information (CASI)
7121 Standard Drive
Hanover, MD 21076-1320
(301) 621-0390

National Technical Information Service (NTIS)
5285 Port Royal Road
Springfield, VA 22161-2171
(703) 605-6000

Preface

The purpose of the conference was to bring together world leaders in aviation safety research, aircraft design and manufacturing, fleet operation and aviation maintenance to disseminate information on current practices and advanced technologies that will assure the continued airworthiness of the aging aircraft in the military and commercial fleets. The conference included reviews of current industry practices, assessments of future technology requirements, and status of aviation safety research. The conference provided an opportunity for interactions among the key personnel in the research and technology development community, the original equipment manufacturers, commercial airline operators, military fleet operators, aviation maintenance, and aircraft certification and regulatory authorities. Conference participation was unrestricted, with 623 participants from the international aviation community.

Conference Organizing Committee:

Charles E. Harris, General Chairman, NASA Langley Research Center
James C. Newman, Jr., NASA Langley Research Center
William P. Winfree, NASA Langley Research Center
William R. Elliott, WR-ALC/TIED, Robins Air Force Base
John W. Lincoln, ASC/EN, Wright Patterson Air Force Base
Joseph P. Gallagher, WL/CCI, Wright Patterson Air Force Base
Chris C. Seher, FAA, William J. Hughes Technical Center
Alfred L. Broz, FAA, Chief Scientist/Technical Advisor for Nondestructive Evaluation
Robert G. Eastin, FAA, Chief Scientist/Technical Advisor for Fracture
Mechanics/Metallurgy
Aubrey E. Carter, Technical Operations Center, Delta Air Lines, Inc.
Ulf G. Goranson, Boeing Commercial Airplane Group, The Boeing Company
Amos W. Hoggard, Jr., Douglas Products Division, The Boeing Company
Paul C. Hoffman, NAWCAD, Patuxent River
Feldon D. Bartlett, Jr., Vehicle Structures Directorate, Army Research Laboratory
Sonya Herrin, Conference Administrative Manager, Science and Technology Corporation

Sponsoring Organizations:

National Aeronautics and Space Administration, Langley Research Center
Federal Aviation Administration, William J. Hughes Technical Center
United States Air Force, Air Materiel Command
United States Naval Air Warfare Center, Aircraft Division
United States Army Research Laboratory



- TABLE OF CONTENTS -

PART 1

APPROACHES TO FLEET MANAGEMENT

Coast Guard Efforts to Deal with Aging Aircraft	1
Doug C. Connor, K. W. Devoe, J. E. Mihelic, M. E. Butt, M. S. Carmel, J. T. Baker, and P. J. Dwyer, U.S. Coast Guard Aircraft Repair and Supply Center, Elizabeth City, NC	
Risk Management of a Helicopter Fleet Containing Flight Safety Parts of Unknown Fatigue Strength	11
Robert W. Arden, Westar Corporation, St. Louis, MO	
Tracking Aircraft Structural Repairs from a Fleet Risk Management and Economic Standpoint	21
Robert D. Giese, Grant D. Herring, and James F. Bockman, Ogden Air Logistics Center, Hill Air Force Base, UT	
Influence of Undetected Hidden Corrosion on Structural Airworthiness of Aging Jet Transports	29
Aydin Akdeniz and Girindra K. Das, Boeing Commercial Airplane Group, Seattle, WA	
Achieving Total System Aging Aircraft Solutions	39
Steven M. Enloe, Boeing Information, Space and Defense Systems, Wichita, KS	
Eurofighter 2000 Structural Health and Usage Monitoring: An Integrated Approach	46
Stephen R. Hunt and Iain G. Hebden, British Aerospace Military Aircraft and Aerostructures, Preston, Lancashire, United Kingdom	
FSIP: The C/KC-135 Functional Systems Integrity Program	56
James Pappas, Jr., OC-ALC/LCRA, Tinker AFB, OK; Ralph R. Ward, Jr., Boeing Information Space and Defense Systems, Oklahoma City, OK	
An Application of Fracture Mechanics Principles in Determining a Service Life Enhancement Interval for The US Navy's C-2 Outer Wing	63
Alex R. Hocson and Tommy N. White, Naval Aviation Depot North Island, San Diego, CA	
Determining and Attaining Realistic Inspection Thresholds to Meet Durability and Damage Tolerance Requirements	70
Len Reid, Jude Restis, and Tom Swift, Fatigue Technology, Inc., Seattle, WA	
Support of Composite Structures on Naval Aircraft	79
Paul Mehrkam, Naval Air Systems Command, Patuxent River, MD	
Aging of Aircraft Transparencies	91
Michael P. Bouchard, Daniel R. Bowman, and Thomas J. Whitney, University of Dayton Research Institute, Dayton, OH	

Effects of Corrosion Inhibiting Lubricants on Avionics Reliability	101
William H. Abbott, Battelle Columbus, Columbus, OH	
Effective Method of Working Out an Optimum Inspection Schedule	116
Veniamin L. Raikher, Central Aerohydrodynamics Institute, Zhukovsky, Moscow region, Russia	
An Engineering Approach for the Assessment of Widespread Fatigue Damage in Aircraft Structures	124
Marc Balzano, Jean-Yves Beaufils, and Alain Santgerma, Aerospatiale Aéronautique, Toulouse, France	
Transport Risk Assessment Containing Widespread Fatigue Damage: TRACWFD Analyses of Longitudinal and Circumferential Splice Joints to Determine the Onset of Widespread Fatigue Damage and Its Probability of Occurrence	132
Robert E. Kurth, Battelle Memorial Institute, Columbus, OH; Catherine A. Bigelow, FAA William J. Hughes Technical Center, Atlantic City International Airport, NJ	
Operation and Maintenance of the Space Shuttle Orbiter	145
Frank V. Daniels, Boeing North American Reusable Space Systems, Downey, CA	
Composite Repair of Aging Metallic Structure P-Version 3D Finite Element Approach	153
Arnold Nathan, Israel Aircraft Industries, Ben Gurion International Airport, Israel	
Ensuring Damage Tolerance of Aging Aircraft Structures	163
Grigory I. Nesterenko, Central Aerohydrodynamics Institute, Zhukovsky, Moscow region, Russia	
TECHNOLOGIES FOR INSPECTION, MAINTENANCE, AND REPAIR	
Repair Development for Fatigue Cracks in the F-5E Vertical Stabilizer	173
Jennifer S. Elmore and Edwin L. Rosenzweig, Naval Air Warfare Center, Patuxent River, MD; Penelope Ulander and Douglas Perl, Naval Aviation Depot, North Island, San Diego, CA	
Air Force Cost of Corrosion Maintenance Study	183
Richard Kinzie, AFRL/MLS-OL, Robins AFB, GA; Garth Cooke, NCI Information Systems, Inc., Fairborn, OH	
Development of Novel Inspection Systems—Anticipating Operator Requirements	193
Christopher D. Smith, FAA William J. Hughes Technical Center, Atlantic City International Airport, NJ	
Expansion of the WR-ALC Fatigue-Arrest Composite Repair Capability	201
Steven F. Adams, WR-ALC/TIEDD, Robins AFB, GA	

Laser-Based Ultrasonics for Crack Detection	224
Pavel Fomitchov, Alexei Kromine, Sridhar Krishnaswamy, and Jan D. Achenbach, Northwestern University, Evanston, IL	
Reliability Study of Magneto-Optic Imaging (MOI) Inspection of C-5 Aircraft Fuselage	230
Jay L. Fisher, Gary L. Burkhardt, Jeffrey S. Stolte, Janet P. Buckingham, Peter C. Mckeighan, and Jack Fitzgerald, Southwest Research Institute, San Antonio, TX; George Burkhardt, SA-ALC/TIESM, Kelly Air Force Base, TX	
Quantitative Investigation of Surface and Subsurface Cracks Near Rivets in Riveted Joints Using Acoustic, Electron and Optical Microscopy	240
Zayna M. Connor, M. E. Fine, and J. D. Achenbach, Northwestern University, Evanston, IL	
Non-Contact Ultrasonic NDE Systems for Aging Aircraft	244
Robert E. Green, Jr. and B. Boto Djordjevic, Center for Nondestructive Evaluation, The Johns Hopkins University, Baltimore, MD	
Evaluation of the Self-Nulling Rotating Eddy Current Probe System	252
Donald Hagemaiier and Kent Rengel, Boeing, Long Beach, CA; Buzz Wincheski and Min Namkung, NASA Langley Research Center, Hampton, VA	
Thermal Wave NDI of Disbonds and Corrosion in Aircraft	265
Xiaoyan Han, L. D. Favro, and R. L. Thomas, Wayne State University, Detroit, MI	
Aging of Airframe Materials: Probability of Occurrence Versus Probability of Detection	275
D. Gary Harlow and Robert P. Wei, Lehigh University, Bethlehem, PA	
Crack Detection and Monitoring of Aging Airframes	284
Neal Phelps, U.S. Air Force, Ogden Air Logistics Center, Hill Air Force Base, UT; Scott May, U.S. Air Force; Eric Haugse, Tamara Leeks and Pat Johnson, Boeing Phantom Works; Steve Ziola and John Dorighi, Digital Wave Corporation	
Multi-Element Ultrasonic Linear Arrays for Rapid Lap-Joint Inspection	294
Robert A. Smith and Stephen J. Willsher, Defence Evaluation and Research Agency, Farnborough, United Kingdom	
Use of Acoustic Emission Monitoring to Detect, Locate and Measure Multiple Site Damage (MSD) Fatigue Crack Growth Underneath Rivet Heads	303
Stuart L. McBride, AEMS Acoustic Emission Monitoring Service, Inc., Kingston, Ontario, Canada; Jason P. Scott, Carleton University, Ottawa, Ontario, Canada; Graeme F. Eastaugh, National Research Council Canada, Ottawa, Ontario, Canada	
Bonded Repair Techniques Using Sol-Gel Surface Preparations	313
Kay Y. Blohowiak, Kenneth A. Krienke, and Joseph H. Osborne, Boeing Phantom Works, Seattle, WA; James J. Mazza, AFRL/MLSA, Wright-Patterson AFB, OH; Georgette B. Gaskin and Jonahira R. Arnold, Naval Aviation Systems Team, Patuxent River, MD; William S. DePiero and Joseph Brescia, US Army TACOM-ARDEC, Picatinny Arsenal, NJ	

A New Non-Contacting NDT System for Detection of Disbonds in Composite and Metal Structures	321
John M. Webster and T. Thevar, Holographics, Inc., Long Island City, NY; J. Mew, University of Portsmouth, Milton Campus, United Kingdom	
A Smart Patch Approach for Bonded Composite Repair/Reinforcement of Primary Airframe Structures	328
Alan A. Baker, Stephen C. Galea, and Ian G. Powlesland, Defence Science and Technology Organisation DSTO - Aeronautical and Maritime Research Laboratory, Fishermens Bend, Victoria, Australia	
Evaluation of Commercial Thermography Systems for Quantitative Composite Inspection Applications	339
Mike T. Valley, Dennis R. Roach, and Larry R. Dorrell, Sandia National Laboratories, Albuquerque, NM; Dennis M. Ashbaugh, SAIC, Albuquerque, NM; Roy T. Mullis, WR/ALC, Robins Air Force Base, GA	
Hidden Corrosion Detection Technology Assessment	349
Wally C. Hoppe, University of Dayton Research Institute, Dayton, OH	
Pre-Corroded Fastener Hole Multiple Site Damage Testing	359
Joe Luzar, Boeing Information, Space & Missile Systems, Wichita, KS; Patrick S. Johnson, Boeing Phantom Works, Seattle, WA	
Advanced Corrosion Resistant Coatings for Outer Mold Line Applications	369
Joseph H. Osborne and Kay Y. Blohowiak, Boeing Phantom Works, Seattle, WA; S. Ray Taylor and Chad Hunter, University of Virginia, Charlottesville, VA; Gordon Bierwagon and Brendon Carlson, North Dakota State University, Fargo, ND; Joshua Du and Matthew Damron, Chemat Technology, Inc., Northridge, CA; Michael S. Donley, Air Force Research Laboratory, Wright-Patterson AFB, OH	
Effect of Aircraft Washing on the Life of Corrosion Prevention Compounds	378
Krishnakumar Shankar, Australian Defence Force Academy, Canberra, Australia; Natasha Tindall, Royal Australian Navy, Naval Air Station, Nowra, Australia; Bruce Hinton and Maria Salagaras, Defence Science and Technology Organisation, Aeronautical and Maritime Research Laboratory, Melbourne, Australia	

PART 2

STRUCTURAL ANALYSIS METHODS

On the Assessment of the Criticality of Crack Scenarios with Respect to Widespread Fatigue Damage	387
Peter Horst, Technical University of Braunschweig, Braunschweig, Germany	

The Growth of Multi-Site Fatigue Damage in Fuselage Lap Joints	397
Robert S. Piascik, NASA Langley Research Center, Hampton, VA; Scott A. Willard, Lockheed Engineering and Sciences Company, Hampton, VA	
Residual Strength Pressure Tests and Nonlinear Analyses of Stringer- and Frame- Stiffened Aluminum Fuselage Panels with Longitudinal Cracks	408
Richard D. Young, Marshall Rouse, Damodar R. Ambur, and James H. Starnes, Jr., NASA Langley Research Center, Hampton, VA	
Residual Strength Analysis of Skin Splices with Multiple Site Damage	427
J. E. Ingram, Y. S. Kwon, K. J. Duffié, and W. D. Irby, Lockheed Martin Aeronautical Systems Company, Marietta, GA	
Fatigue Crack Growth Predictions in Riveted Joints	437
Scott A. Fawaz, Air Force Research Laboratory, Wright-Patterson AFB, OH; J. Schijve, Delft University of Technology, Delft, The Netherlands	
Nonplanar Fatigue Crack Growth in 7075-T73 Aluminum	452
Scott C. Forth and Leroy H. Favrow, United Technologies Research Center, East Hartford, CT; William D. Keat, Union College, Schenectady, NY	
Quantifying Spectrum Loading Effects on Fatigue Crack Growth	462
H. Lewis Zion, Georgia Tech Research Institute, Smyrna, GA; W. Steven Johnson, Georgia Institute of Technology, Atlanta, GA; Dale L. Ball, Lockheed Martin Tactical Aircraft Systems, Fort Worth, TX; Richard A. Everett, Jr., U.S. Army Vehicle Structures Directorate, Hampton, VA	
Analytical Framework for Assessment of Corrosion and Fatigue in Fuselage Lap Joint	472
Dale Cope, Patrick Johnson, Angela Trego, and J. Doug West, Boeing Information, Space, and Defense Systems, Wichita, KS	
Mathematical Model to Predict Fatigue Crack Initiation in Corroded Lap Joints	482
Gerhardus H. Koch, CC Technologies Laboratories, Inc., Dublin, OH; Le Yu and Noriko Katsube, The Ohio State University, Columbus, OH; Clare A. Paul, AFRL/VASE, Wright Patterson AFB, OH	
Analytical and Test Evaluations on the Linkup of Multiple Cracking in Stiffened Fuselage Panels	493
David Y. Jeong, U.S. Department of Transportation, Cambridge, MA; John G. Bakuckas, Jr., Federal Aviation Administration, William J. Hughes Technical Center, Atlantic City International Airport, NJ; Gopal Samavedam, Foster-Miller, Inc., Waltham, MA	
Benefits of Improved Fuselage Skin Sheet Alloy 2524-T3 in Multi-Site Damage Scenarios	503
Gary H. Bray, Robert J. Bucci, Michael Kulak, and Charles J. Warren, Aluminum Company of American, Alcoa Center, PA; Alten F. Grandt, Jr., Patrick J. Golden, and Darren G. Sexton, Purdue University, W. Lafayette, IN	

Fracture Analysis of the FAA/NASA Wide Stiffened Panels	513
B. R. Seshadri, J. C. Newman, Jr., D. S. Dawicke, and R. D. Young, NASA Langley Research Center, Hampton, VA	
Improved Engineering Methods for Determining The Critical Strengths of Aluminum Panels with Multiple Site Damage in Aging Aircraft	525
Bert Smith, Adil Mouak, Perry Saville, Roy Myose, and Walter Horn, Wichita State University, Wichita, KS	
Corrosion Pitting Cracks in Fuselage Joints	535
Nicholas C. Bellinger, Jerzy P. Komorowski, and Ron W. Gould, Institute for Aerospace Research, Ottawa, Ontario, Canada	
Towards a Predictive Design Methodology for Composite Laminate Patches Based on Physical Modeling of Failure Processes	545
Peter W. R. Beaumont, Cambridge University Engineering Department, Cambridge, United Kingdom; James M. Greer, Jr., United States Air Force Academy, USAF Academy, CO	
A CTOD Approach to Assess Stable Tearing Under Complex Loading Conditions	555
Claudio Dalle Donne, German Aerospace Center DLR, Cologne, Germany	
Residual Strength Predictions with Crack Bulging	565
David S. Dawicke, NASA Langley Research Center, Hampton, VA; A. S. Gullerud and R. H. Dodds, Jr., University of Illinois, Urbana, IL; R. W. Hampton, NASA Ames Research Center, Moffett Field, CA	
A Mixed-Mode I/II Fracture Criterion and Its Application in Crack Growth Predictions	575
Michael A. Sutton, Xiaomin Deng, and Fashang Ma, University of South Carolina, Columbia, SC; James C. Newman, Jr., NASA Langley Research Center, Hampton, VA	
Yield-Strip Models for Residual Strength of MSD Damaged Curved and Flat Panels	584
Karl-Fredrik Nilsson, Aeronautical Research Institute of Sweden, Bromma, Sweden	
Boundary Correction Factors for Elliptical Surface Cracks Emanating From Countersunk Rivet Holes	598
Anisur Rahman, Drexel University, Philadelphia, PA; John G. Bakuckas, Jr., Catherine A. Bigelow, and Paul W. Tan, FAA William J. Hughes Technical Center, Atlantic City International Airport, NJ	
Stable Tearing and Buckling Responses of Unstiffened Aluminum Shells with Long Cracks	610
James H. Starnes, Jr. and Cheryl A. Rose, NASA Langley Research Center, Hampton, VA	
Fracture Mechanics of Thin, Cracked Plates Under Tension, Bending and Out-Of-Plane Shear Loading	627
Alan T. Zehnder, C.-Y. Hui, Yogesh Potdar, Cornell University, Ithaca, NY; Alberto Zucchini, ENEA, Bologna, Italy	

Residual Strength Prediction of Fuselage Structures with Multiple Site Damage 635
 Chuin-Shan Chen, Paul A. Wawrzynek, and Anthony R. Ingraffea, The Cornell
 University Fracture Group, Ithaca, NY

POSTERS

**Fatigue Crack Growth Simulation for Complex Three-Dimensional
 Geometry and Loading** 657
 Thomas J. Curtin, Robert A. Adey, John M. W. Baynham, Phillip Marais,
 Computational Mechanics, Inc., Billerica, MA

**A Comparison of Numerical Methods of Fracture Analysis and Study with
 Helicopter Structure** 667
 George V. Bauer, Sikorsky Aircraft Corporation, Stratford, CT

Importance of Chemically Short-Crack-Growth on Fatigue Life 679
 Evan J. Dolley and Robert P. Wei, Lehigh University, Bethlehem, PA

Composite Coating of Jet Engine Air Intake as a Protection Against Acoustic Fatigue 688
 Jiří Fidranský and Jiří Fiala, Aero Vodochody a.s., Odolena Voda, Czech Republic

CF-18 Inner Wing Front Spar Cracking 697
 Yvan Francoeur and Daniel Adam, Bombardier Services Inc., Defence,
 Mirabel, Quebec, Canada

**Reduction in Fatigue Damage Incurred During Ground Operations
 on Rough Runways** 707
 Tony Gerardi, APR Consultants, Inc., Medway, OH; Doug Tritsch, University of
 Dayton Research Institute, Dayton, OH; Robert Knarr, Consultant, Beaver creek, OH

Optical Fiber-Based Corrosion Sensors for Aging Aircraft 716
 Jennifer L. Elster, Jonathan Greene, Mark E. Jones, Tim A. Bailey, and Shannon M. Lenahan,
 F&S, Inc., Blacksburg, VA; Ignacio Perez, Naval Air Warfare Center, Patuxent River, MD

Composite Patch Repair Applications to T-38 Lower Wing Skin 722
 James Helbling and Maro Heimerdinger, Northrop Grumman Corporation, El Segundo, CA;
 Mohan Ratwani, R-Tec, Rolling Hills Estates, CA

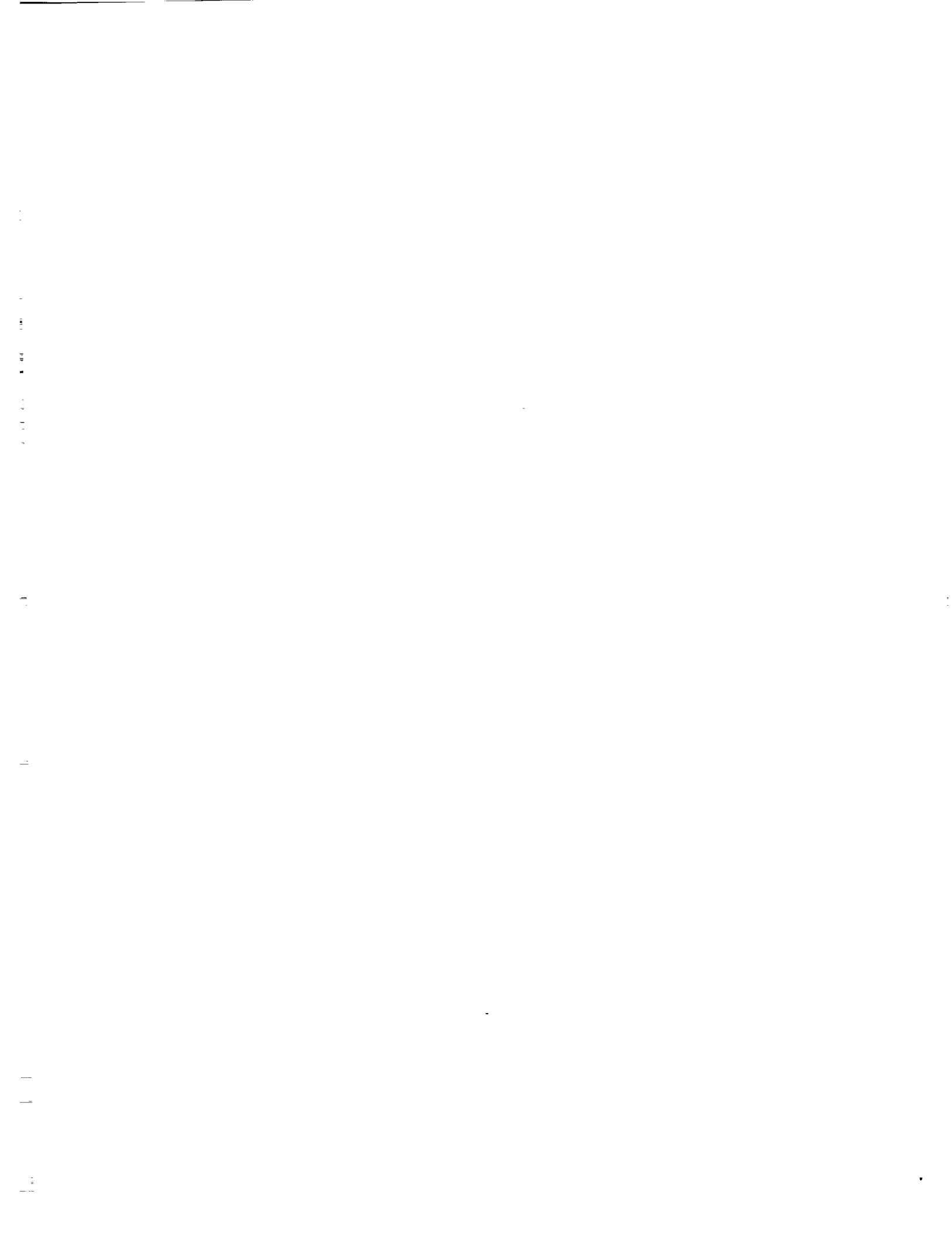
Lamb Wave Tomography for Corrosion Mapping 732
 Mark K. Hinders and James C. P. McKeon, The College of William & Mary, Williamsburg, VA

Experimental Results from the FAA/NASA Wide Panel Fracture Tests 741
 William M. Johnston, Analytical Services and Materials, Inc., Hampton, VA;
 Jeffrey D. Helm, University of South Carolina, Columbia, SC

**Novel NDE/I Probe for the Detection of Corrosion in Aircraft Metallic Structures
 Based on Electrochemical Impedance** 755
 Jinseong Kim, Anuncia Gonzalez and Dalibor Hodko, Lynntech, Inc., College Station, TX

Implementation of Filmless Radiography for Aerospace Applications	764
Timothy Kinsella, Liberty Technologies, Inc., Conshohocken, PA; Diana Carlin, Air Force Research Laboratory, Wright-Patterson AFB, OH	
3D Visualization of X-Ray Backscatter Images	774
W. Niemann, Joseph Kosanetzky, and K.-H. Fischer, YXLON International X-Ray GmbH, Hamburg, Germany; E. Siegel and S. Zahorodney, YXLON Inc., Alpharetta, GA	
Multiple Initial Coldworking with the Split Mandrel System	782
Anthony Leon, West Coast Industries, Seattle, WA	
NASGRO 3.0 - A Software for Analyzing Aging Aircraft	792
Sambi R. Mettu, V. Shivakumar, J. M. Beek, F. Yeh, and L. C. Williams, Lockheed Martin Space Mission Systems & Services, Houston, TX; R. G. Forman and J. J. McMahon, NASA Johnson Space Center, Houston, TX; J. C. Newman, Jr., NASA Langley Research Center, Hampton, VA	
Automatic Analysis of Data Derived from Scanning Acoustic/Laser Doppler Velocimeter	802
Jackie Mew and Robert G. Topp, University of Portsmouth, Hampshire, United Kingdom; John M. Webster and Thangeval Thevar, Holographics, Inc., Long Island City, NY	
Experimental Flight Test Vibration Measurements and Nondestructive Inspection on a USCG HC-130H Aircraft	811
David G. Moore and Craig R. Jones, FAA Airworthiness Assurance NDI Validation Center, Sandia National Laboratories, Albuquerque, NM; Joseph E. Mihelic and James D. Barnes, U.S. Coast Guard Aircraft Repair and Supply Center, Elizabeth City, NC	
Active Vertical Tail Buffeting Alleviation on an F/A-18 Model in a Wind Tunnel	821
Robert W. Moses, NASA Langley Research Center, Hampton, VA	
Corrosion-Fatigue Crack Initiation in 7000-Series Aluminum Alloys	831
Peter S. Pao, C. R. Jerry Feng, and Steven J. Gill, Naval Research Laboratory, Washington, DC	
Determination of the Corrosive Conditions Present within Aircraft Lap-Splice Joints	841
Karen S. Lewis and Robert G. Kelly, University of Virginia, Charlottesville, VA; Robert S. Piascik, NASA Langley Research Center, Hampton, VA	
Design of Visually Inspectable Fuselage Skin Repairs	853
P. C. Chen and David B. Roderick, Interpacific Technology, Inc., Alameda, CA	
Program for Probabilistic Stress Spectra Generation (Prospectra)	863
Mary W. Schleider and Robert A. Babb, Mercer Engineering Research Center, Warner Robins, GA	
Acoustic Detection of In Situ Corrosion in Aging Aircraft	872
Jeffrey N. Schoess, Honeywell Technology Center, Minneapolis, MN	

Modelling of Weak Bonds in Adhesively Fastened Joints	875
Krishnakumar Shankar and Dong Fei, University of New South Wales, Canberra, Australia	
Methods for Relating Fracture Surface Topography to Load Spectra	885
Donald A. Shockey and Takao Kobayashi, SRI International, Menlo Park, CA	
Aircraft Corrosion Inspection and Evaluation Technique Using Scanning Ultrasonic Methods	903
T. P. Sivam, Raytheon E-Systems - Waco, Waco, TX; Carl M. Ochoa, Vista Engineering Services, Inc., College Station, TX	
Aircraft Structural Integrity Monitoring System Development - Review of the Air Force/Navy Smart Metallic Structures Program	922
Craig B. Van Way and Jay N. Kudva, Northrop Grumman Corporation, El Segundo, CA; Mark N. West, Mission Research Corporation, Fountain Valley, CA; Steve M. Ziola, Digital Wave Corporation, Englewood, CO; V. Scott May and Michael N. Zeigler, AFRL/VASA, Wright-Patterson Air Force Base, Dayton, OH; James M. Alper, Naval Air Warfare Center, Patuxent River, MD	
APPENDIX A (AUTHOR INDEX)	933
APPENDIX B (LIST OF PARTICIPANTS)	937



APPROACHES TO FLEET MANAGEMENT

COAST GUARD EFFORTS TO DEAL WITH AGING AIRCRAFT
The Second Joint NASA/FAA/DoD Conference on Aging Aircraft

D. C. Connor, K. W. Devoe, J. E. Mihelic, M. E. Butt, M. S. Carmel, J. T. Baker, and P. J. Dwyer
U. S. Coast Guard Aircraft Repair and Supply Center
Elizabeth City, NC 27909, USA

ABSTRACT

The Coast Guard operates approximately 200 aircraft which include HC-130 transports, HU-25 Falcon Jets, HH-65 Dolphin and HH-60 Jayhawk helicopters all of which operate low level over salt water and in the case of the helicopters, hover in salt spray and deploy for extended periods on ships. Over time, we have developed both a maintenance philosophy and an engineering program to deal with these harsh conditions. In addition, the current and future projected budget climates will necessitate that we continue to operate our current fleet of aircraft well into the next century. This combination of operating in a severely corrosive environment and budgeting in an austere fiscal climate has induced us to develop an aggressive Aging Aircraft program. This paper will discuss our corrosion control program, two prototype sensor projects to monitor corrosion and structural loads on operational aircraft, plans to upgrade avionics equipment, our mature reliability centered maintenance program and service life extension plans which have been formulated for all of our aircraft. These individual projects make up our Aging Aircraft program. We are convinced that they will enable us to meet the immediate challenges and will position us for those that lie ahead.

INTRODUCTION

The Coast Guard is a small service with a relatively small fleet of aircraft and an even smaller budget to support those aircraft. As such, we depend heavily upon the Department of Defense (DoD), the original equipment manufacturers (OEMs) and commercial operators of our aircraft for the extensive engineering support necessary to maintain our fleet. This is especially true in the area of Aging Aircraft. In partnership with the DoD and OEMs, we have developed plans that will enable us to support our existing fleet of aircraft to the year 2010 and beyond. This plan addresses both the structural and economic service lives of our aircraft and it will enable us to efficiently use scarce Coast Guard recapitalization funds over the next several years when both ships and aircraft simultaneously reach the end of their planned service lives. This "near term aviation support strategy" calls for relatively minor structural enhancements, avionics upgrades, electrical rewiring and supplemental inspections for substantially less money than new aircraft procurements. Parts of this plan were initiated in 1994, and it is only in the last two years that it has been formalized into a comprehensive budget proposal. The implementation of this strategy strongly depends on our ability to identify, treat and prevent the long-term effects of corrosion on our aircraft.

CORROSION CONTROL

Corrosion prevention and control is absolutely essential to extending the life of our current fleet. Our operating environment is arguably the most severe of any aircraft operator, and efforts to ameliorate the affects of that environment must be a high priority. A recent study determined that corrosion costs the Coast Guard between 18 and 20 million dollars annually. This represents roughly 10% of the total annual operating and maintenance budget for Coast Guard aviation. This paper will discuss four key elements of

our corrosion control program: Programmed Depot Maintenance (PDM), Wash Water Quality Program, Corrosion Mapping during PDM and investigation of new sensors to monitor corrosion on aircraft.

PROGRAMMED DEPOT MAINTENANCE

The cornerstone of our corrosion control program is our periodic aircraft overhaul program, which we call Programmed Depot Maintenance (PDM). All of our aircraft are brought through PDM on a regular cycle to eliminate the effects of corrosion. PDM entails the complete disassembly of each aircraft, the stripping of paint to the maximum extent possible and the removal of all corrosion. During this process, we often must replace structural members that have experienced material loss due to corrosion. Our helicopters are generally brought into PDM every three to four years, while our C-130s are on a four-year schedule and the Falcon Jets are brought in every five years. Most of our recent efforts in this area have been geared towards developing environmentally friendly industrial capabilities, especially non-hazardous paint removal systems, coatings and corrosion prevention compounds. This is our greatest challenge in the near term to maintain our edge in the fight against corrosion.

WATER QUALITY PROGRAM

We have also partnered with our field units to maintain a strong corrosion control program. After every low over-water flight, and at least once a day when our aircraft fly, we wash them thoroughly to prevent the buildup of seawater and its associated products on them. Several years ago we realized that at some units, we were washing aircraft and engines with water that was not much better than the salt water we were flying over. We then tested the wash water at all units, assisted them with the development of corrective actions and implemented water quality standards to enhance the effectiveness of the aircraft wash procedures. After extensive research and discussions with OEMs, the Navy and the Air Force Corrosion Program Office, we implemented the following water quality standards: Dissolved Solids of less than 500 parts per million (ppm), Chlorides less than 50 ppm and pH (acidity) between 6 and 8. In order for units to maintain these levels, we mandated recurrent testing of aircraft and engine wash water at least annually or whenever an event occurred which might affect the values such as a new water source or suspected contamination. This program has been in effect now for three years.

CORROSION MAPPING

Another aspect of our corrosion program is our corrosion mapping during PDM. We have developed detailed grids covering all structural areas of each aircraft type. As an individual aircraft is inspected and treated, the technicians record the area where the corrosion is found, the type and severity of corrosion, and how many labor hours were required to treat it. These grids are then entered into a database that holds the aircraft identification and the history of where it has been stationed. With this information (four plus years worth of data), we have been able to identify the most corrosion prone areas of our aircraft and determine which field units have more corrosion problems. We use this information to develop material improvements and also send it to field units to assist with their corrosion prevention efforts.

CORROSION MONITORS

In an effort to obtain higher fidelity data, we have installed prototype corrosion monitors on four of our HH-65A helicopters. These monitors, developed by Dr. Vinod Agarwala at the Naval Air Warfare Center Aircraft Division in Patuxent River, MD, use bimetallic thin film sensors installed at inaccessible locations around the aircraft. The sensors capture the galvanic current generated when an electrolyte closes the circuit between the two dissimilar metals (two metals at opposite ends of the galvanic series). In addition to

the sensors, corrosion monitoring units (CMUs) consist of high impedance circuitry used for measuring the current and a data logger/memory unit for retention of both instantaneous and cumulative current. The CMU collects data from six sensors with data capture once every 30 minutes. The CMU also captures temperature and relative humidity to provide more clues as to why corrosion varies between aircraft. The ultimate goal of this project is to develop a condition-based PDM induction schedule, so we can reduce the corrosion variability of incoming aircraft and improve the business processes of depot maintenance. [1]

AVIONICS ISSUES

When discussing the topic of aging aircraft, the issues involving avionics often take a back seat. This can be a critical mistake. Today's aircraft are equipped with sophisticated and fully integrated avionics suites, crucial to the performance of assigned missions. In order to provide the operators with reliable and fully mission capable aircraft, maintenance program managers must address the reliability and maintainability of the avionics in their aging aircraft. A structurally sound, flyable airframe is of limited use if it cannot navigate to its destination, communicate with others, or provide for flight plan management and execution. With the plan to support our current aircraft until the year 2010, we have projects underway and on the horizon to modernize the avionics suites in our aging aircraft fleet. The processes to attack these initiatives for upgrading avionics were guided by several factors, common to all aircraft programs.

OBSOLESCENCE

This factor comes into play in two ways: (1) component maintainability and supportability, and (2) changes in the operational environment in which the aircraft is required to fly. Maintainability and supportability are factors due to the diminishing supply of repair parts or support equipment. The availability of piece parts for older avionics can become a major cost driver as manufacturers cease production in lieu of supporting newer avionics product lines or because of decreased demand for the parts as the number of installed components dwindles. This results in higher repair costs and longer lead times on repairs at a time when the Mean Time Between Failure (MTBF) is decreasing. Additionally, the actual black box may be serviceable but the equipment to support the component may not be. Operating environment changes play a significant role in the obsolescence of avionics. With the increased dependence on the Global Positioning System and the discontinued use of Loran-C and Omega, major changes to the integrated flight management systems installed in our aircraft needed to take place in order to safely navigate. New regulations and future initiatives from the FAA have also impacted avionics obsolescence. Requirements for Traffic Alert and Collision Avoidance Systems (TCAS) and Flight 2000, implementation of Local Area and Wide Area Augmentation Systems, and the decommissioning of ground-based navigation stations (NDB, VOR and TACAN) will require suitably equipped aircraft for aircrews to operate in controlled airspace. Most currently installed avionics will not meet the new standards. [2]

TECHNOLOGY LAG

The advancement of technology is growing at an exponential rate. A look at the home computer market illustrates this point. The consumer who purchased the top-of-the-line computer six months ago, is now lagging far behind the newest product lines. The latest software is developed to operate efficiently with the latest hardware, which makes machines purchased a year ago practically obsolete. When you combine this growth with the years required to design, engineer, and integrate modern avionics, it is easy to see that these 'new' systems are not far from being unsupportable the day they go into the aircraft. The perfect example is the new flight management system currently being installed in our HC-130 fleet. This system operates on a computer that has a 386 MHz processor, a component no longer used in industry. We are only half-

way through the implementation phase of this major avionics upgrade project. In an attempt to combat this problem, the contract for upgrading the HH-65A avionics suite contained two clauses. First, the vendor was required to define a maintenance support plan to ensure the equipment operates for 15 years after introduction. Secondly, the vendor was authorized to use the latest technology in manufacturing the production boxes as long as the form, fit, and functionality was not compromised, and with no additional costs incurred by the Coast Guard. This clause was primarily aimed at the 486 MHz processor to be used in the new flight management computer.

COMMONALITY

This factor has a variety of applications and can have a significant impact on avionics upgrade projects. For the HH-65A, the avionics upgrade will span four years. This will create a host of problems: training issues, standardization, maintenance and supply. For all practicable purposes, operational units will be required to fly and maintain two different models of aircraft. To lessen the impact, every effort was made during software development to keep the functionality between the two flight management systems the same. Only where significant improvements or safety of flight came into play were deviations made.

The Coast Guard currently has two major avionics upgrade projects in full swing. These projects will update the avionics suites for the HH-65A and the HC-130. In addition, plans are being formulated for HH-60J and HU-25 avionics upgrades. The above factors were a prime consideration in the design and integration of these new systems.

RELIABILITY CENTERED MAINTENANCE PROGRAM

The term Reliability Centered Maintenance (RCM) refers to a program of disciplined logic applied to realize the inherent reliability capabilities of equipment being maintained. It is a systematic approach to identifying preventive maintenance tasks for an equipment end item in accordance with a specified set of procedures and for evaluating and revising the established intervals between the performance of preventive maintenance tasks. Establishment of the proper intervals enables the equipment being maintained to meet its inherent reliability capabilities. Fundamental to RCM is the concept that reliability is designed into a component and cannot be improved with preventive maintenance; scheduled maintenance can only ensure that the designed reliability is achieved. The Coast Guard's RCM program monitors the performance of aircraft components by utilizing historical maintenance data and statistical methods. The historical maintenance data is supplied by our Aviation Computerized Management System (ACMS). ACMS is both a configuration management system and a maintenance procedure tracking system. This system identifies components installed on an aircraft by serial number, provides the complete history of every part and also catalogs all maintenance accomplished on each aircraft. This robust system has been in operation since 1985 and provides the data necessary to monitor the reliability of all Coast Guard aircraft. [3]

The RCM program continuously monitors the performance of the aircraft components and brings the problem areas to the attention of maintenance managers. As the fleet ages, this function becomes increasingly important in identifying and prioritizing equipment replacement and upgrades. Trend analysis, based on removal rate due to trouble in aircraft systems or components, serves to identify problem areas and initiate corrective action. Additionally, age exploration procedures are used to ensure the maintenance program remains efficient throughout the life of the equipment.

The RCM trending model is a time series model, which utilizes occurrence frequencies and relates these quantities to sequential time periods. This establishes the reliability trend of specific aircraft items. All the

data necessary for reliability trend analysis is extracted from the ACMS database. Unscheduled component removals and a computed trended value are compared against a standard of acceptable performance. The maximum allowable deviation from the acceptable performance of the system or component is termed the "Alert Value." This value is a multiple of the standard error of estimate computed using the trended values of the past twelve months. Maintenance managers set the constant by which the standard error of estimate is multiplied to yield the alert value. The computations required for the trending model are based on the Least Squares Regression method. If the alert value is exceeded by a component for two consecutive months then further analysis is undertaken.

Age exploration procedures supply the information needed to determine the applicability and evaluate the effectiveness of maintenance tasks. The information derived from age exploration is directed towards the optimization of existing maintenance intervals and procedures. This is obtained by studying the reliability of aircraft systems or components through utilization of the reliability function and the conditional probability of failure. The reliability function determines what percent of the population of the component survives to a specific age. The conditional probability of failure gives the probability of failure of the component during an age interval, provided the component survives to enter that interval. With this information it can then be determined if maintenance actions on a component are applicable and effective, as well as the scheduling interval of an action, age for specific failure modes, consequences of each failure, projection of sparing levels, and projected cost of ownership. Whenever applicable, the Weibull method of data evaluation is used due to its ability to be utilized as a forecasting method. [4]

Over the seven years of the program, scheduled maintenance accomplished on Coast Guard aircraft has been reduced by 80,000 maintenance man-hours annually across our 200 aircraft fleet. Most of these man-hours were redirected into fleet corrosion control. Additionally, numerous component overhaul intervals have been extended resulting in millions of dollars saved. The Coast Guard's RCM program, with its numerous success stories, has developed into an important tool in monitoring the status of our aging aircraft fleet. Trend analysis and age exploration techniques have allowed us to identify and project problem areas within the fleet prior to these problems becoming noticeable to the operational user. Additionally, the age exploration enables early identification of systems or components approaching wear out so that replacements or upgrades can be incorporated. We will next discuss the specific service life plans for each of our four aircraft types.

HC-130 LONG RANGE SEARCH AIRCRAFT

The Coast Guard currently operates thirty HC-130 Hercules aircraft at five Air Stations. The fleet is composed of "H" model aircraft broken down into three series (1500, 1600, and 1700 series). The 1500 and 1600 series aircraft are the oldest in the fleet having entered service in the 1970s while the 1700 series aircraft were obtained in the middle to late 1980s.

In 1997, CAE Aviation Ltd., now SPAR Aviation, was contracted to conduct an aircraft structural life extension engineering study to evaluate the current status of the Coast Guard's HC-130 fleet. The CAE report found that overall, the fleet is being maintained to a degree that it can continue to operate for the next 5 years before replacement of the 1500 and 1600 series aircraft would need to commence. However, by concentrating maintenance efforts in the area of improved "housekeeping," minor structural preventative maintenance programs, consolidating certain scheduled inspections and improving our existing corrosion control efforts, the existing fleet could continue in service until at least 2012. This additional maintenance would be accomplished annually at the unit level so as not to impact operational readiness or increase depot costs. In order to meet fatigue considerations for an extended service life, the report recommended a

fuselage structural refurbishment program to replace, modify or reinforce certain structural members and fittings. The structural refurbishment would be more like a heavy overhaul than a major Service Life Extension Program (SLEP), and would be accomplished as each aircraft cycled through its next PDM. Fortunately, the entire fleet is equipped with "H"-model outer wings, which incorporate 7075-T73 alloy vice T6 aluminum wing planks, so no major wing replacements are necessary. The report determined that with the incorporation of these relatively minor changes, we could continue to operate our existing aircraft well into the next century. [5]

Another aspect of our service life consideration is the application of a maintenance and inspection program tailored to the specific usage of the aircraft. We have worked with Lockheed to develop an Aircraft Structural Integrity Program (ASIP) for our HC-130 fleet. ASIP involves an analysis of operational usage, environmental data for each operational unit, mission profiles gathered from pilot interviews, flight records, aircraft ground and air loads data from USAF load surveys and a damage tolerance assessment. This information allows us to define critical airframe areas and actions required to assure the continued structural integrity of the aircraft. Once this is accomplished, base severity factors are developed and used to define equivalent flight hours for inspection purposes. The most severe operating unit (Barbers Point, HI) was selected as the baseline unit for purposes of comparison and severity factors were assigned to other units for specific aircraft structural members. See Table 1. These factors are updated periodically to ensure accuracy. [6]

TABLE 1. 1985 LOWER WING SURFACE SEVERITY FACTORS

Location	Elizabeth City	Clearwater	Kodiak	Sacramento	Barbers Point
Factor	0.44	0.63	0.50	0.33	1.00

As an example of how the severity factors are applied, an aircraft from Clearwater having flown 1000 actual flight hours would only have 630 equivalent baseline hours on the lower wing surface for inspection purposes. The use of these equivalent flight hours to monitor the condition of structures, the implementation of the CAE study recommendations and the ongoing avionics upgrades will give us a low-cost option for continuing our C-130 fleet in service for many years to come.

HU-25 MEDIUM RANGE SEARCH AIRCRAFT

The Coast Guard maintains a fleet of 41 HU-25 "Guardian" aircraft which are military derivatives of the Dassault Falcon Jet 20. This twin engine, medium range search and rescue platform has unique features that separate it from its civilian counterpart. These features include a side camera window, two large search windows, bottom drop hatch, Forward Looking Infrared Radar (FLIR), Side Looking Airborne Radar (SLAR), air-to-air combat radar, numerous radios, and an auxiliary fuel tank. Original delivery of these aircraft began in 1981, and the average age of aircraft in the fleet is 15 years of operational service.

The FAA originally certified the commercial Dassault Falcon 20 with an unlimited service life based on its fail-safe design and completion of fatigue tests to 100,000 cycles. However, in order to enhance the confidence of operators, the current Falcon 20 maintenance program calls for an *initial* service life of 20,000 flights or 30,000 flight hours. Upon completion of a Major Corrosion Inspection (MCI) and a Supplemental Structural Inspection Program (SSIP), the Falcon 20's initial service life is extended to 40,000 flights or 60,000 flight hours. The MCI consists of a detailed inspection of the aircraft structure and a curative and preventative corrosion treatment. The SSIP includes a damage tolerance assessment of main structural components supplemented by analysis of the results of partial testing and aging studies.

The commercial MCI and SSIP, however, do not apply directly to the Coast Guard's HU-25s because of the numerous modifications to our aircraft and our unique mission profiles.

We are currently in the process of developing an OEM originated or certified MCI and SSIP so that we can fly these aircraft with confidence well into the 21st century. Originally we planned to develop an SSIP through extensive aircraft instrumentation and loads monitoring of multiple aircraft. To help eliminate this requirement, we conducted in-flight mission studies and manually recorded data on over 730 flights to give Dassault a better understanding of how the HU-25 aircraft are flown. In addition, Dassault engineers visited the PDM line in late 1997 to review the comprehensive maintenance that we perform. Finally, we are investigating the possibility of developing the MCI separately from the SSIP, and implementing the MCI during PDM. Since corrosion plays a more significant role than fatigue in determining our maintenance strategy, it is believed that the MCI will be a lead indicator on the overall condition of the HU-25 fleet. This program, when implemented and combined with the research we have conducted with Sandia National Labs, should enable us to operate these aircraft well into the next century.

SANDIA NATIONAL LABORATORY AGREEMENT

In 1994, a Work for Others agreement was established between the Coast Guard and Sandia National Laboratories, the FAA's Airworthiness Assurance NDI Validation Center (AANC). The mutually agreed upon Scope of Work specified that Sandia would study and recommend nondestructive inspection techniques that could help the Coast Guard better inspect their assets to extend the service life of their fleet of HU-25 'Guardian' aircraft. Upon termination of this agreement in 1996, a new agreement was established which had a broader scope of work to include providing inspection of any Coast Guard aircraft on an as-needed basis as determined by the Coast Guard.

Upon entering this agreement, the Coast Guard transferred HU-25 tail number 2117 to Sandia's facility in Albuquerque, NM. Included with the transfer were a complete set of aviation maintenance procedure cards, aircraft publications and eventually a set of OEM wing drawings. During the first proposal period, work was directed at exploring the possibility of developing NDI procedures that could enhance or replace visual inspections in areas that were known or suspected of being problem areas in terms of corrosion or fatigue on the HU-25. This phase focused on activities that could provide a short-term payoff and immediate application. We expect to utilize this program more extensively as we implement the structural integrity and inspection programs for all of our aircraft in order to extend their service lives.

HH-65A SHORT RANGE RESCUE HELICOPTER

The Coast Guard accepted the first of 96 HH-65A "Dolphin" helicopters in late 1984 with deliveries continuing over the following 5-year period. The average fleet age is now over ten years and most aircraft have accumulated over 5,000 hours. In order to meet operational requirements under demanding and often hazardous mission profiles, we are focusing our aging aircraft efforts on the following areas: Structural Repair Capabilities, Kapton wire replacement (Rewire) program, fatigue crack prevention and engine improvements – both control systems and power enhancements.

STRUCTURAL REPAIR FIXTURE

In 1994, the Coast Guard acquired a structural repair fixture that allows us to correct any structural problems on the aircraft. The fixture is approved by the OEM, and all repairs are conducted with technical support from a Eurocopter representative. To date, 11 aircraft have been recovered from significant

crashes with this fixture. The capabilities provided by this fixture, along with the OEM commitment to continuously support the Dolphin with structural parts, will allow us to continue to maintain the main structure of the HH-65A indefinitely.

KAPTON WIRE REPLACEMENT

When the HH-65A was delivered to the Coast Guard, Kapton wiring was chosen due primarily to its low weight and the criticality of weight considerations on this aircraft. After several years of service however, Kapton wire coating becomes brittle, and the wire bundles are subject to flashover fires wherein all wires in a bundle are burned through as the result of a single short. In the early 1990s, the HH-65A community was experiencing regular equipment failures due to Kapton wire problems. On five occasions, all AC power was lost with a corresponding loss of primary flight instruments, due to Kapton flashover fires. In 1996, we commenced a four year comprehensive program to replace the Kapton wiring in all HH-65As.

FATIGUE CRACK PREVENTION

Several areas have been identified as subject to life/cycle cracking problems on the HH-65A. These include the upper 25-degree frame (pilot/copilot door), the 4630 bulkhead ("Texas" patch) area and the transmission deck crossbeam. The 25-degree frame and the 4630 bulkhead have received doubler-type repairs that are re-inspected during subsequent PDMs. The transmission deck crossbeam crack, if not caught in a timely manner, can cause cracking of the transmission deck itself. The Coast Guard is currently engaged in a 4-year, \$500K crossbeam replacement project.

ENGINE IMPROVEMENTS

The HH-65A's current electronic/mechanical/pneumatic engine control system was developed solely for the Coast Guard, and has been a safety concern since the early operational years. This system does not lend itself readily to in-flight problem diagnosis, and has been a troubleshooting nightmare for maintenance personnel. Full Authority Digital Engine Control (FADEC) is the new industry standard for engine control that will provide safety, training and reliability and maintainability benefits. In addition, the incorporation of FADEC will pave the way for power growth on this engine, to accommodate the aircraft/mission gross weight increases that have steadily accrued since the aircraft first entered service. The growth will be accomplished primarily through fine-tuning of the compressor section, and hot-section hardware upgrades. These projects, along with the avionics upgrade mentioned above, are projected to enable us to safely and effectively operate the HH-65A until the year 2015.

THE HH-60J MEDIUM RANGE RESCUE HELICOPTER

The HH-60J helicopter faces significant challenges as it ages, particularly given our goal to continue flying the aircraft until 2025. Two major challenges lie in the areas of structural integrity and dynamic component service life. We are addressing these challenges through partnership with the United States Navy, while tailoring individual programs to our specific needs. Two initiatives are currently underway. First, Coast Guard HH-60J helicopters will be outfitted with several portions of the Navy's H-60 SLEP. Secondly, a Coast Guard HH-60J helicopter is presently conducting in service testing of a Helicopter Integrated Diagnostics System (HIDS) designed by B. F. Goodrich.

HH-60J SERVICE LIFE EXTENSION PROGRAM

The Coast Guard is making plans to complete a SLEP on its 42 HH-60J helicopters to ensure the aircraft's structural integrity until 2025. The aircraft's production specification originally called for an airframe service life of 10,000 flight hours, and the oldest HH-60J will likely hit that mark no later than 2007. The SLEP's structural improvements are designed to address both fatigue modeling concerns generated by operation past 10,000 flight hours and numerous areas already shown to be fatigue sensitive based on current fleet experience. Specifically, the Coast Guard's version of SLEP is focused on preventing main transmission support beam cracks, improving the structural integrity around the cabin vibration absorbers, and reducing the likelihood of other upper fuselage cracks.

The Coast Guard's SLEP will consist of three major elements: An upper fuselage deck plug, upgraded cabin and nose vibration absorbers, and an upgraded tail gearbox support fitting. The upper fuselage deck plug will incorporate significantly redesigned main transmission support beams. The beam designs have been modified to increase resistance to cracks that historically occur in three different modes: Across the beam caps, longitudinally along the beam flange tabs, or across the station 343 web tie-in. An upgraded cabin vibration absorber will be installed together with the upper fuselage deck plug. The new absorber will incorporate bow-tie springs to enhance absorption efficiency and service life. The absorber assembly will be smaller and easier to remove so that recurrent maintenance may be performed on a workbench. We plan to begin our HH-60J SLEP in fiscal year 2004, and the SLEP elements will be installed during extended PDM cycles. The goal is to finish this effort by the end of fiscal year 2008.

HELICOPTER INTEGRATED DIAGNOSTICS SYSTEM

We are currently working with B. F. Goodrich and the Navy at Patuxent River to conduct an in-service evaluation of HIDS on one HH-60J helicopter. The primary goal of this two-year evaluation is to validate the system's advertised capabilities. These capabilities include: Reduced replacement costs for dynamic components, identification of current mission spectrums that cause significant fatigue damage, identification of life-limited components that require earlier removal due to current mission spectrums, and reduced maintenance check flight time required to comply with dynamic component track and balance limits. The HIDS is currently composed of the following elements: A structural monitoring module, an engine performance monitoring module, and integration with the Coast Guard's Aviation Computerized Maintenance System via a Unix-based ground station. Future plans include installation of an in-flight rotor track and balance monitoring system (ROTABS).

The structural monitoring module provides flight spectrum monitoring during each sortie, collecting data from more than 100 analog and digital channels, many via the aircraft's 1553 databus. With these data points, the HIDS identifies the flight regimes flown, their sequential order, and their individual duration. This information is downloaded into a UNIX-based ground station that is capable of cycle counting using Sikorsky Aircraft's accepted penalties for the flight regimes actually flown. The ground station is capable of tracking the configuration of an HH-60J's fatigue-sensitive components and comparing for each component the flight time flown against the fatigue damage incurred as expressed in flight hours. The Engine Performance Monitoring module uses several monitored channels to report on and record engine performance, as indicated by either the health integrity (HIT) check, or the maximum power check. The ROTABS will incorporate an optical tracker to baseline main rotor track in a hover as required by Sikorsky Aircraft. It will then use accelerometers and magnetic pick-ups to determine the vibration levels in key dynamic components such as the tail rotor, oil cooler drive shaft, main rotor, engine output shafts, and the vibration absorbers. The HIDS ground station will provide recommended adjustments to maintain

required vibration levels after each sortie, as desired. This module is still under development, and is due to fly on an H-60 helicopter late this year.

Planning for SLEP and evaluation of HIDS continue in a sustained effort to reduce the life cycle cost of the HH-60J. Emphasis on efforts such as these will only grow as the costs to replace the HH-60J with another medium range rescue platform continue to outpace inflation. The Coast Guard's partnerships with the Navy on these two efforts will ensure thorough operational testing of the proposed concepts prior to fleet wide adoption in Coast Guard aircraft.

CONCLUSION

These individual projects have provided the backbone to a robust Aging Aircraft program for the Coast Guard that will enable us to extend the lives of our current fleet of aircraft well into the next century. Our small size and overall lack of bureaucracy have made it possible for us to implement these individual projects in a systematic fashion over the past several years. As we have done so, we have established the momentum and the support within our system to build it into a comprehensive program. We believe that this program will enable us to continue to fly our current fleet of aircraft to at least the year 2010 and if necessary, it provides the foundation to extend them beyond that.

ACKNOWLEDGEMENTS

The authors would like to thank the numerous personnel at Coast Guard Headquarters and at the Aircraft Repair and Supply Center who developed these projects and put in the considerable staff work over the last several years to make this Aging Aircraft program a success.

REFERENCES

1. Agarwala, V. S. and Lerner, K. "Corrosion Monitoring System Installation and Operation Manual," Naval Air Warfare Center, Aircraft Division, Patuxent River, MD 20670, 1996.
2. Information on FAA initiatives and future plans can be found on their web site: www.faa.gov.
3. CGTO PG-85-00-30 "Coast Guard Reliability Centered Maintenance Process Guide," Revision 1, May 1997.
4. "Benefits of the Reliability Centered Maintenance Program for Coast Guard Aircraft Maintenance," Ogden Government Services Group, Task Number NON695012, October 1995.
5. CAE Aviation Ltd., "Final Report - HC-130H Aircraft Structural Life Extension Engineering Study" Report No. 20-351-USCG-001, January 1997.
6. "U.S. Coast Guard C-130 Aircraft Structural Integrity Program Master Plan," Lockheed-Georgia Company, August 1993.

RISK MANAGEMENT OF A HELICOPTER FLEET CONTAINING FLIGHT SAFETY PARTS OF UNKNOWN FATIGUE STRENGTH

Robert W. Arden
Westar Corporation
St. Louis, MO, 63044-2732, USA
(314) 298-8748 Ext. 303
Fax: (314) 298-0189
arden@westar.com

ABSTRACT

This paper describes the development and implementation of a risk management plan for critical helicopter components. It presents a brief overview of the fatigue methodology used in the original airworthiness qualification of the systems along with the analytical and test procedures required by the alternate vendor qualification program. The basis for the various methods used to derive the appropriate levels of risk is provided. Application of this risk management process to a specific aircraft system shows the calculation of component and system level risks. A comparison between the risk assessment based strength/life and the component test results ultimately achieved is presented. The overall approach is shown to be an effective tool in the assessment and management of fleet risk.

1. INTRODUCTION

For many years, the U.S. Army Aviation and Missile Command (AMCOM) has maintained an aggressive program for competitive procurement of fatigue critical rotor, flight control, drive system, and airframe components known as flight safety parts (FSP). The goal of this alternate vendor program is to establish manufacturing sources in addition to the original equipment manufacturer (OEM) for each critical FSP, and to allow competitive forces to reduce the unit cost while retaining the necessary quality standards.

1.1 ORIGINAL COMPONENT QUALIFICATION

Although damage tolerance techniques have been widely used throughout the fixed wing industry, they have been less successful in rotary wing applications, particularly on older systems. For this reason, virtually all of the U.S. Army's fatigue critical FSPs were qualified by OEMs using the safe life methodology shown in Figure 1. A brief overview of the essential elements of this approach for a typical system is presented below.

1.1.1 Usage Spectrum

The usage spectrum for these components was originally derived from user defined missions and tactics, based on the projected capability of the aircraft system and the threat environment. A rotary wing usage spectrum typically contains substantially more flight conditions than a fixed wing spectrum since helicopters can experience fatigue damage in virtually any flight condition including level flight. The spectrum is typically updated five to seven years after the system is fielded in

significant numbers to account for the inevitable expansion in usage. The update is based on pilot questionnaires and interviews with unit operations officers to accurately reflect current usage. U.S. Army helicopters currently do not have on-board flight recorders to monitor actual usage.

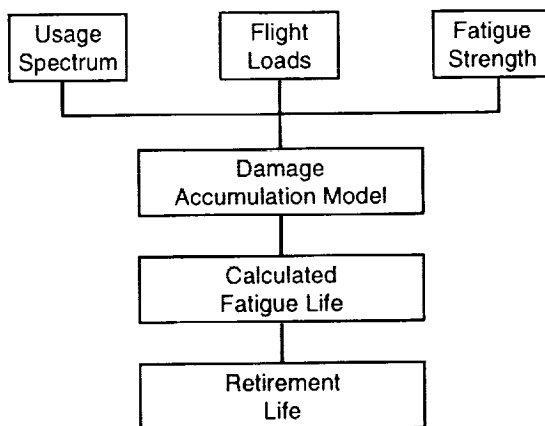


Figure 1. Safe life fatigue methodology.

1.1.2 Flight Loads

Component flight loads are obtained during a flight loads survey in which a test aircraft performs all flight conditions in the usage spectrum. The survey typically consists of approximately 1500 individual flight test points to account for all combinations of aircraft configuration, weight, center of gravity, and altitude. The test aircraft typically contains several hundred instrumentation parameters including strain gages on all FSPs. Component load time histories for each flight condition are electronically stored, and many are cycle counted prior to fatigue analysis. Helicopter fatigue loads have much higher frequencies than fixed wing aircraft being typically equal to the revolutions per minute (RPM) of the main or tail rotor or some multiple thereof. Flight loads may be replaced or revised by subsequent load surveys conducted when significant changes occur to the aircraft.

1.1.3 Fatigue Strength

Component fatigue strength is defined by an S-N curve as shown in Figure 2. Six full-scale specimens

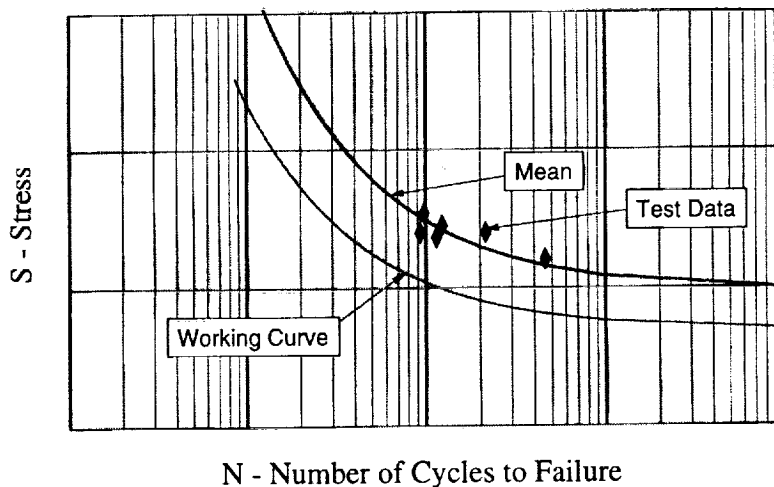


Figure 2. Typical S-N curve.

of each FSP are fatigue tested to failure at constant amplitude stress (or load) and the results are plotted as a function of the number of cycles to failure. A mean curve whose shape is based on extensive coupon testing is passed through these data points. At the runout point (approximately 10^8 cycles), a working curve is established by statistically evaluating the data scatter about the mean, and reducing the mean curve by three standard deviations (three sigma) or an equivalent fixed percentage. The working curve is used for all fatigue life calculations.

1.1.4 Component Fatigue Life

For each component, fatigue damage fractions are obtained for each flight condition by using the actual number of load cycles per fixed time period from the usage spectrum and the allowable number of load cycles from the component S-N curve at the flight load for the specific condition. The damage is summed using a linear cumulative damage hypothesis and the fixed time period divided by the total damage is the calculated fatigue life. The final retirement life is obtained from the calculated fatigue life and may be reduced to meet a specific maintenance interval or to provide additional conservatism.

1.1.5 Overall System Safety

At the component level, safe life fatigue methodology assures that each component has a very high probability of reaching its retirement life without failure. At the aircraft system level, the cumulative effect of individual component reliabilities is such that less than one failure will occur in the design life of the system.

1.2 FSP ALTERNATE VENDOR PROGRAM

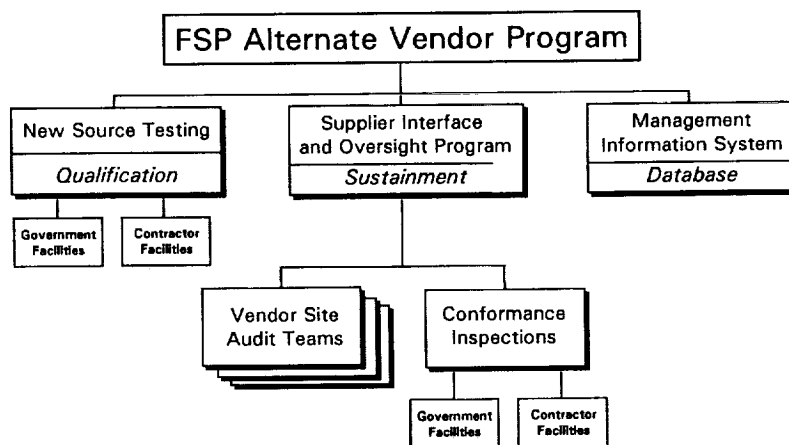


Figure 3. Alternate Vendor Program organizational structure.

The main elements of the alternate vendor program are depicted in Figure 3. Alternate vendors of FSPs manufacture components in accordance with a Technical Data Package (TDP). In addition to the normal manufacturing instructions, the TDP contains the requirement to freeze all production processes and defines the component critical characteristics that are attributes requiring special inspection and handling throughout the life cycle of the component. The first production lot from each vendor enters the New Source Testing phase of the program where two full-scale specimens are fatigue tested to failure. The test fixture, loads, phasing, and instrumentation are identical to the original qualification of the OEM component. The mean strength level demonstrated in the fatigue test is compared to that of the OEM and a post-test metallurgical investigation is conducted to ensure

that all dimensions, materials, manufacturing processes, and failure modes are also identical to the OEM. If all results are positive, the vendor is qualified as a tested source, and is eligible to compete for future production contracts for the specific component.

Long term sustainment of component quality is the function of the Supplier Interface and Oversight Program (SIOP). The SIOP consists of vendor audits and conformance inspections that work together to evaluate the production process and the final product. Vendor audits are conducted periodically at the production facility. These audits include review of the management structure, production processes, control of critical characteristics, inspection equipment and techniques, quality procedures, and control of sub-vendor processes. Conformance inspections are performed at an independent laboratory where a sample of each production lot is completely examined (including destructively) to determine conformance to the TDP and the frozen planning.

The list of qualified sources for each component is maintained in the FSP alternate vendor Management Information System (MIS), which is available to all qualified users through the Internet. The MIS also contains procurement history, maintenance publications, TDPs, new source test plans, and reports and is continuously updated to include the results of the latest vendor audits and conformance inspections.

2. RISK MANAGEMENT PLAN

As discussed above, an essential feature of the alternate vendor program is laboratory testing to ensure component structural integrity. The testing process, however, was overwhelmed by the enormous demand created by Operation Desert Storm. This allowed a significant number of untested FSP to enter the inventory and be installed on U.S. Army aircraft. Since immediate removal from service of all affected FSPs would result in the grounding of a significant percentage of the U.S. Army's rotary wing fleet, it was necessary to develop and implement a plan to manage the risk of continuing to fly with unqualified components. The goal of the plan was to eliminate the source of the risk within a one year time period.

2.1 TESTING PROGRAM

The first step in the risk management plan was to expedite the new source testing. All untested components in service were reviewed and a testing priority was established. The priority system criteria included the total number of components in service, normal retirement life, manufacturing complexity, and criticality of failure modes. When the priority list of components requiring testing was assembled, it was apparent the effort required was beyond the capacity of the Government's test facility and would also exceed the one-year completion goal. The testing program was dramatically increased as AMCOM contracted with nine separate test sources; including commercial test facilities, prime helicopter manufacturers, and Government test laboratories. Although the testing program ultimately required more than one year to complete, these facilities collectively tested more than 200 vendor/part number combinations consisting of more than 800 individual full-scale specimens.

2.2 COMPONENT LEVEL RISK

Given the estimated schedule to complete the required testing and knowing that wholesale component removal was impractical, it became necessary to conduct an assessment of the risk levels associated with allowing untested components with possible configuration, material, and/or process non-conformances to remain in service. To this end, several different methods were used to evaluate risk based on the components' service history, normal retirement life, and manufacturing complexity. The

initial time period for these risk assessments was one year in accordance with the overall risk management plan. Although the procedures were essentially identical across the affected aircraft systems, UH-60 Black Hawk helicopter data are used in the following discussion for purposes of numerical demonstration.

2.2.1 Weibayes Analysis

Untested components having significant service history were analyzed using Weibayes analysis, which facilitates the construction of a Weibull distribution when no failures have occurred.¹ A Weibull distribution provides a means for estimating the probability of future component failures.

Since there were no failures in service, the Weibayes method required that the Weibull slope parameter, Beta, be estimated. The determination of Beta was a two step process with the initial consideration being the failure distribution of fully conforming components. The generally accepted assumption is that fatigue life distributions are either normal or lognormal. Although full-scale test data sufficient to favor either distribution typically does not exist, the normal distribution is more critical in the region of interest (low failure probability) and is generally selected for conservatism. The second step in the Beta determination process was an evaluation of the possible impact of non-conformances on the failure distribution. Experience gained during the FSP testing program indicated the failure distribution of non-conforming components has essentially the same shape as conforming components, although the demonstrated mean strength is normally much lower. Data scatter about the mean may actually be less, as the non-conformance tends to concentrate the failure mode. Based on these considerations, Beta was assigned a value of 3.44, which is representative of a normal distribution.

For each vendor/part number combination, the characteristic life, Eta, was obtained from the assumed value of Beta and the flight times of the untested components. A Weibull distribution was developed from Beta and Eta, and each component was aged by adding the estimated flight hours for the one-year time period of the risk assessment. The number of expected failures (EF) was calculated from the Weibull cumulative failure distribution, the age of the components (in flight hours) and the number of components at each age. If the total EF for all components from a specific vendor/part number combination exceeded a desired value, the safe life was reduced, which eliminated the components with the highest flight time that contributed the most to the overall EF.

The Weibayes approach produces very conservative safe lives because it assumes the first failure is

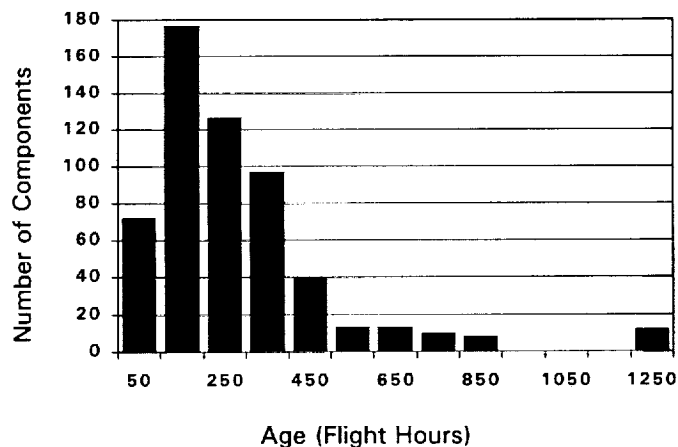


Figure 4. Typical age distribution.

eminent. The effect of this assumption can be seen by the relatively low life of approximately 300 hours that results from applying Weibayes methods to the typical age distribution shown in Figure 4.

2.2.2 Fatigue Strength Reduction

The evaluation of untested components with limited service history was based on the observation, discussed above, that component non-conformances reduce the overall fatigue strength while retaining the failure distribution shape. Accordingly, this analysis used a reduction in component fatigue strength to simulate the effect of potential non-conformances. Two methods of strength reduction were used depending primarily on the normal retirement life of the component. The most conservative approach, used on components with high or unlimited retirement lives, was based on a search of the existing test database to obtain the largest strength reduction that resulted from a non-conformance. Worst case strength reductions were obtained separately for aluminum and steel components. These maximum reductions were applied to the component mean strength that was further reduced by the reduction for data scatter. For the UH-60 aircraft system, this method produces working curves with total reductions from the mean of 52.4 percent for aluminum and 53.1 percent for steel.

A somewhat less conservative approach was used on components with lower retirement lives. The TDPs for these components were reviewed and all manufacturing processes were evaluated for complexity, impact on fatigue strength, and type of material. Each process was given a numerical score that was arbitrary in absolute terms, but had the correct magnitude relative to the other processes. The scores for all processes on each component were totaled, and the total scores for all components of the same material were reviewed. The range of total scores had three natural groupings, which is not unexpected given the technology and material choices available at the time the aircraft system was originally qualified. These three score subsets were taken to represent low, medium, and high risk. Component strength reductions were correlated to these risk levels by letting the maximum strength reduction described above represent a three sigma value associated with high risk. Medium and low risk became the two sigma and one sigma strength reductions respectively as shown in Table 1.

TABLE 1. STRENGTH REDUCTION AS A FUNCTION OF RISK LEVEL

Risk Level	Material	Component Strength Reduction			
		Relative Magnitude	Reduction from Mean (%)	Reduction for Data Scatter (%)	Total Reduction from Mean (%)
Low	Aluminum	1 σ	7	39	43.3
	Steel		11	30	37.7
Medium	Aluminum	2 σ	14	39	47.5
	Steel		22	30	45.4
High	Aluminum	3 σ (Maximum)	22	39	52.4
	Steel		33	30	53.1

The conservatism in the above strength reduction methods is substantial. A small reduction in fatigue strength produces a very large reduction in fatigue life. Table 2 shows the effect of fatigue strength reduction on a typical high life UH-60 component.

TABLE 2. IMPACT OF STRENGTH REDUCTION ON FATIGUE LIFE

Reduction from Mean (%)	Fatigue Life (Hours)
30 (Working Curve)	99,358 (Retirement Life)
35	57,025
40	10,989
45	1,167
50	563

One additional safety consideration was imposed on the strength reduction methods. If the reduction in fatigue strength resulted in level flight fatigue damage, the component was considered to have unacceptable risk, and steps were taken to immediately remove it from service.

2.2.3 Life Adjustment by Reliability Analysis

Although fatigue strength reductions can adequately account for component non-conformances, the resulting fatigue lives may be too low to be of practical value. This difficulty was addressed by using reliability-based methods that evolved from a Government/industry study conducted under the auspices of the Fatigue and Damage Tolerance Subcommittee of the American Helicopter Society (AHS).² The study was undertaken in response to a new U.S. Army requirement related to the design of future helicopter systems.³ The new requirement was for all fatigue critical components to have an individual component reliability level of .9, which the Army believed was synonymous with an overall system reliability of less than one fatigue failure in the life of the system. The principal purpose of the AHS study was to develop (and standardize if possible) the analytical tools required to evaluate component reliability.

As part of this AHS effort, the OEM for the UH-60 developed the methodology necessary for determining the structural reliability of helicopter dynamic components.⁴ The methodology was based on statistical distributions of component fatigue strength, flight loads, and the usage spectrum. These variables were combined using a Monte Carlo analysis to produce a probabilistic distribution of fatigue life. For a specific life, the component reliability equals the probability that the life is greater than the selected value. Data in the form of reliability versus fatigue life were plotted for several components in the UH-60 rotor and control systems. An additional benefit of this methodology development was the verification that the deterministic safe life methods then in use by the OEM produced fatigue lives with a reliability of approximately .9 as required for new systems.

In the current analysis, the individual component reliability plots were normalized and combined, and a conservative envelope was developed. The purpose of this single representation was to avoid conducting extensive Monte Carlo evaluations of all FSP in all UH-60 systems. This reliability versus fatigue life relationship was used to enhance the fatigue life of components at the expense of reliability. The component being evaluated begins with a relatively high fatigue life and the high reliability discussed above. To account for potential non-conformances, the fatigue life is reduced using one of the strength reduction techniques. The assumption inherent in this approach is that the reliability is unchanged by this reduction in life. The fatigue life is then increased and the reliability decreased, in accordance with the relationship previously described, to minimize the impact on

readiness while maintaining system safety. The EF for the component is obtained using the final reliability, enhanced fatigue life, number of components of the specific vendor and part number combination in service, and the estimated flight hours that will occur in the one year time period of the risk assessment as follows:

$$EF = \frac{(1 - \text{Reliability})}{\text{Fatigue Life}} \times \text{Number of components} \times \text{Flight hours} \quad (1)$$

The ten Black Hawk components with the highest contribution to the total system EF are presented in Table 3.

TABLE 3. UH-60 COMPONENT RISK

Component	Vendor	Number in Service	EF (1 Year)
M/R Shaft Extender	A	98	.001
M/R Shaft Extender	B	100	.001
T/R Hub Plate	C	93	.016
Fwd Bellcrank	D	312	.001
Swashplate Link	E	855	.002
Control Pushrod (-053)	F	434	.003
Control Pushrod (-054)	F	185	.001
Control Pushrod (-055)	F	341	.002
Control Pushrod (-056)	F	368	.003
M/R Cuff	B	68	.010

2.3 SYSTEM LEVEL RISK

The methods described above provide a convenient means for determining the individual contribution of each component to the overall system risk. Initially, an attempt was made to create a single most critical aircraft to represent the risk for the entire system. When the statistics for the distribution of new components throughout the fleet were evaluated, however, the probability of all untested components being installed on the same aircraft was extremely small. A more likely scenario from a probability standpoint was that a few potentially non-conforming components would be installed on many aircraft. It was decided that the sum of the EF from all aircraft in the system was a better indicator of system level risk. This total was then compared with the normal system EF for a one-year time period as shown in Table 4. The system life-time EF is based on 477,612 total components from 1500 aircraft with 180 critical components per aircraft, a usage rate of 250 hours per year, and a 40 year life.

TABLE 4. UH-60 SYSTEM RISK

Time Period	Reliability	EF
System Life-time	.96	.478
1 Year with Conforming Parts	.96	.012
1 Year with Untested Parts	Varies from .94 - .96	.058

3. RISK ASSESSMENT VALIDATION

Test results were ultimately obtained on 223 vendor/part number combinations (all aircraft systems) for which risk assessments were written based on the methods described above. A comparison of the risk assessment defined fatigue life with the actual test demonstrated life is summarized in Table 5. As shown by these data, 220 of the 223 total risk assessments provided a conservative estimate of the component safe life for a success rate of 98.7 percent.

TABLE 5. FATIGUE LIFE COMPARISON

Number of Components	Component Fatigue Life
218	Risk Assessment < Actual
2	Risk Assessment = Actual
3	Risk Assessment > Actual

Data for the three components having unconservative results were thoroughly reviewed to determine the cause. The first component exhibited low fatigue strength as a result of a dimensional error. The manufacturer had misinterpreted a drawing requirement, and produced components with less than minimum wall thickness in a critical section. Review of the TDP indicated the drawing was vague and subject to misinterpretation. Investigation of the second low strength component revealed another drawing interpretation error. A final dimension was to be obtained after the application of shot peening, which is a critical characteristic of the component. The manufacturer incorrectly produced this dimension by machining after shot peening which effectively removed the compressive stress layer and violated the requirements for critical characteristics and frozen planning. The final low strength component is a simple example of poor shop practice. The low strength was caused by grinding burns that should have been found during final inspection prior to shipment.

Investigation of these low strength components provided valuable lessons learned for the alternate vendor program. Improvements were made in the review of TDPs to ensure that all manufacturing instructions are clear and not subject to misinterpretation. Vendor audit teams were directed to reemphasize the importance of FSP critical characteristics and the need to maintain the frozen planning. Product assurance representatives were notified whenever it appeared that vendor manufacturing practices were deviating from alternate vendor program requirements.

CONCLUSIONS

The methodology described above is a useful and convenient tool for the risk management of critical helicopter components. The most significant limitation on the use of this risk management approach is the variability in the suppliers' capability to produce high quality components. Continued oversight and vendor education is necessary to ensure compliance with frozen planning requirements for FSPs and adherence to generally accepted manufacturing practices. Procurement documents such as TDPs must be clear and unambiguous, particularly the drawings and process specifications.

REFERENCES

¹ Abernethy, R. B., Breneman, J. E., Medlin, C. H., and Reinman, G. L., "Weibull Analysis Handbook", Air Force Wright Aeronautical Laboratories Technical Report AFWAL-TR-83-2079, Nov 1983.

² Everett, R. A., Bartlett, F. D., and Elber, W., "Probabilistic Fatigue Methodology for Six Nines Reliability", NASA Technical Memorandum 102757, AVSCOM Technical Report 90-B-009, Dec 1990.

³ Arden, R. W., and Immen, F. H., "U.S. Army Requirements for Fatigue Integrity", In proceedings of the American Helicopter Society National Technical Specialists' Meeting on Advanced Rotorcraft Structures, Oct 1988.

⁴ Thompson, A. E., and Adams, D. O., "A Computational Method for the Determination of Structural Reliability of Helicopter Dynamic Components", In proceedings of the 46th Annual Forum of the American Helicopter Society, Washington, DC, May 1990.

Tracking Aircraft Structural Repairs from a Fleet Risk Management and Economic Standpoint

Robert D. Giese Grant D Herring James F. Bockman
Ogden Air Logistics Center
Hill Air Force Base, UT 84056
(801)777-5292
giesero@hillwpos.hill.af.mil
<http://www.fleetlife.hill.af.mil/>

Abstract

The F-4 Structures Group at Hill AFB, UT has developed an Aircraft Structural Integrity Program (ASIP) management and engineering support software system. This software, called FLEETLIFE, includes analytical, fatigue tracking, individual aircraft tracking, configuration management, repair tracking, and other modules. These modules are designed to support the ASIP engineer and fleet manager in assuring the structural integrity of a fleet of aircraft. This paper will detail the risk management and economic aspects of the repair tracking module. In the repair tracking module all data concerning the details of structural repairs are cataloged. These details include the deficiency necessitating the repair, the action taken, and all archiving data. Several enhancements are in work for the software. One of these enhancements is the incorporation of cost and economic information into the repair tracking module. This paper will describe the effort, the approach and working solution for this effort. It will detail the incorporation of economic data into the repair tracking module and database. Repair cost data fields have been added to the database structure. The query engine has been defined to include search and accumulation of cost data. The cost data can be searched by repair discrepancy type. In this fashion, for example, the repair costs for corrosion initiated repairs can be retrieved. The report feature has also been modified to provide repair and modification costs trends. The module has been modified to track engineering hours, repair installation hours and repair material costs. The report feature can total these costs, determine average repair costs and can total repair costs per tail number. This data, while certainly not complete will be necessary inputs for a fleet economic life model. The paper will detail the approach used to track the types of discrepancies and how these discrepancies were detected. The types of discrepancies are, for example, corrosion, corrosion fatigue, fatigue, overstress, impact damage, and others. Examples of how discrepancies were detected are, routine inspections, special inspections, heavy maintenance, other maintenance, and others. Data concerning the types and magnitudes of discrepancies are accumulated. In this fashion trends can be detected and fleet risk lowered. Also, data concerning how defects are found and therefor the most effective inspection methods will be accumulated. The paper also describes in detail the database structure, look of the user interface windows, and report features.

1. INTRODUCTION

Managing the structural integrity of any fleet of aircraft is a task of balancing risk against economics. The goal, generally speaking, is to spend the minimum amount of money to reduce the risk to an acceptable level. This balancing act is primarily the result of the two different disciplines associated with this task: Engineering and Management. Structural Integrity Engineers strive to eliminate all risk of potential in-flight catastrophic loss or emergency events at any cost. Fleet Managers strive to spend the minimum amount of money to meet operational requirements at the minimum risk level. Accomplishing this minimization of risk with the



Figure 1. Balancing risk vs. cost

minimization of cost makes the structural integrity management task a very complex balancing act. An overemphasis on either side brings the optimal solution out of balance. To complicate the problem even further, information transfer and understanding between the two above mentioned disciplines is frequently limited. Engineers responsible for managing fleet risk usually don't have extensive economic or business training. Conversely, Fleet Managers often lack in-depth engineering backgrounds.

Given the complexity of balancing Risk vs. Cost in managing a fleet's structural integrity, it remains that effective decisions can only be taken from an enlightened point of view. In most cases, management functions easily quantify and measure the costs of aircraft maintenance and repairs. The Risk Avoidance Value associated with these maintenance and repair actions, on the other hand, are usually left undefined, unquantified, and unmeasured. Risk must be defined to allow comparing the money expended against the change in risk. This implies that not only must risk be defined but it must be quantifiable and measurable. Once risk is quantified and measured, those items representing the greatest risk can be identified and a plan can be devised to eliminate or reduce the risk of each of the items to an acceptable level. The plan, in turn, determines the minimum amount of cost needed to affect the largest risk reduction. This sequence of events constitutes a well informed process to balancing the Risk vs. Cost requirement. Subsequently, this process is continued until the overall fleet risk is reduced to or below the pre-defined acceptable level. As the balancing process is continued through the life of the fleet, a constant vigilance must be maintained for items emerging as new risk factors. Further, given the lead times for planning, acquisition, and implementation of corrective actions, the process must maintain its predictive nature.

There is a significant information management challenge in developing a process to balance low catastrophic loss risks and low maintenance and repair costs. In both cases enough information must be collected to provide a statistical base from which probability and economic models can be constructed. This is no easy task given the divergent nature of aircraft within a fleet. When a fleet is new, every aircraft is the same (in a general sense) as the

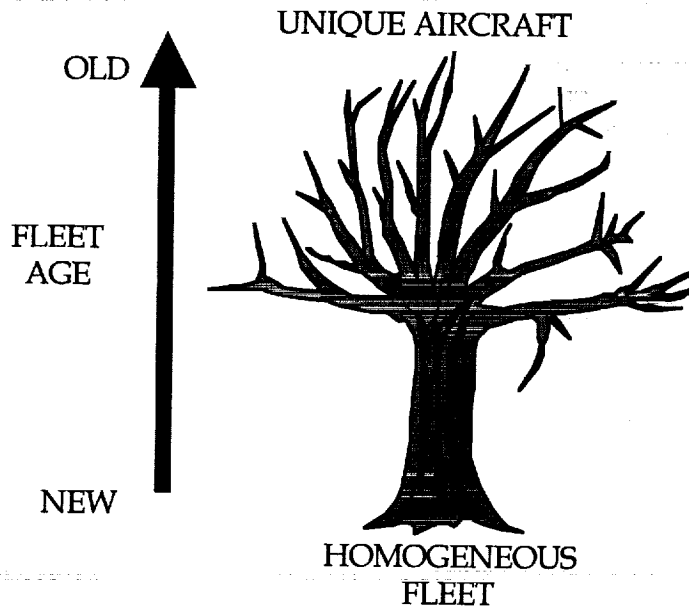


Figure 2. Effect of Fleet Aging on Fleet Data Content

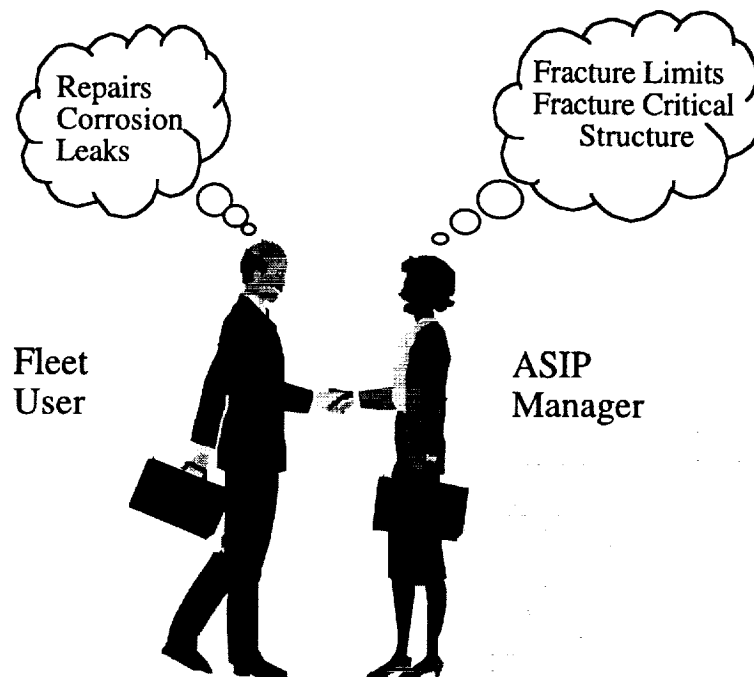
aircraft next to it. As the fleet ages, each aircraft becomes increasingly unique. Differences in many things contribute to this. How each aircraft is used, how it is maintained, and where it is stationed are some of the factors. It is therefore necessary to track risk and cost information for each individual aircraft. Information visibility is also required from the overall aged fleet as well as an individual aircraft perspective. The fleet perspective gives insight into potential trends that would necessitate proactive actions to be taken against individual aircraft.

To keep cost and risk in balance from an Aircraft Structural Integrity Program (ASIP) viewpoint, it is first necessary to define how cost and risk interact. The first risk/cost interaction is in minimizing the cost necessary to bring the risk of a catastrophic loss down to an acceptable level. The second interaction is in maximizing the risk reduction related to structural maintenance costs. Both of these items involve minimizing costs and risks. Both involve establishing "acceptable" limits.

For minimizing the cost required to bring the risk of a catastrophic loss down to an acceptable level, one approach taken in the past is rooted in probability analysis. There is some probability that an aircraft will experience a catastrophic structural failure on the next flight. The initial task is to establishing an arbitrary maximum limit to that probability. By defining the limit, say for example 1×10^{-7} , you are establishing the "acceptable risk criterion." There are several approaches for calculating the risk of a catastrophic fracture based on this initial limit value. One excellent approach is the PROFS software developed by Wright Labs. To accomplish the analysis using this tool, various input information is required. This includes several sets of data which must be collected. Examples of this collected data include inspection intervals, probability of detection functions, and crack size distributions. By accomplishing a sensitivity analysis on the input data, the most critical parameters can be determined. (It is interesting to note that several of these inputs are cost sensitive. Inspection intervals are directly impacted by cost. Better inspection methods used to improve the probability of detection are usually more expensive.) By working backwards using the acceptable risk criterion as a limit, only those things required to bring the risk to the acceptable level are accomplished. Using a sensitivity analysis, the lowest cost inspection necessary to meet the acceptable risk criterion can be determined. This approach is highly sensitive to the quality of the input data. Here again the information challenge presents itself. The amount of generated analytical data can rapidly become very large when doing sensitivity studies involving numerous locations on every aircraft in a large fleet. The management and presentation of this data is a very important part of the puzzle.

As noted earlier, the second part of the ASIP puzzle is to maximize the risk reduction related to structural maintenance action costs. This is a very complex problem to address. Maintenance actions run the gamut from annoying frequently occurring problems to major battle or crash damage induced rebuilds. In every case cost and risk must be balanced. When does it become cheaper to modify every aircraft rather than accomplishing a repetitive annoying small maintenance action? When should an aircraft be salvaged rather rebuilt following a mishap? Both of these decisions are fundamentally economic based but involve a hint of future operational risks. Both of these decision require cost and risk data from the alternatives. Costs associated with repetitive repairs must be known. Effects of major rebuilds on the risk of preventing future catastrophic failure must be determined. Once again, the management and presentation of this large body of information is critical.

In understanding risk and cost management of aircraft fleets, one must also consider the user's perspective. The users of a fleet often pose the question "How long will my fleet of aircraft last?" This question is usually posed to the structural integrity managers. An answer is provided. However, the viewpoint of what was asked and the viewpoint of the answer may be different. The users are concerned with the immediate and future maintenance costs, and assume the basic structure is sound. The structural integrity community is concerned with the future integrity of the structure and assume that routine maintenance will be accomplished. Both sides of this issue are equally important. Both sides of the question and answer need to be addressed.



How long will my fleet last?

Figure 3. Same Question - - Different View

To bridge this gap between user and ASIP manager, there needs to be a visible platform for information sharing and exchange. This platform should allow for information on routine maintenance, repairs, inspections, and predictive analysis to be visible to both parties. One method for establishing this desired understanding is to establish a common information database. Such a database is under development. FLEETLIFE is a joint USAF/USN effort to bridge the gap between the user perspective and the support management perspective. FLEETLIFE is presented here as a model of how repair and cost data can be fused into a single, useable information exchange platform. The first role of FLEETLIFE is to accumulate repair information. This may include both user initiated and ASIP manager initiated repairs. Figure 4 shows a screen shot of the repair data window. For any type of repair, basic accounting data must be documented for future reference. In FLEETLIFE, the controlling parameter is the Reference Number. This number could be the number of the engineering request paperwork or any user determined job number. For non-user generated repairs, engineering information is included with the repair. The engineer accomplishing the repair action and the number of hours he took to develop the repair are recorded. The structural component to which the repair is applied is recorded and can be used as a query variable. For example, in this fashion all repairs applied to the left main spar could be returned in a query. Another important sort variable is the deficiency type. Examples of deficiency type include corrosion, fatigue, and heat damage. If the ASIP manager or user were trying to see if corrosion on the left main spar was becoming a problem, the database could be searched for those two variables. The top portion lists all aircraft that a repair has been applied to. In this fashion reoccurring or nuisance type of maintenance actions become apparent to both the user and the ASIP manager. Standard repairs accomplished by the user can often affect decisions made at the support level. Therefore, it would be important to insure that all repairs made in the field are visible to the ASIP manager. Such a task could be provided by a data link between the FLEETLIFE software and the maintenance information system used in the field.

Aircraft Affected			Analysis	Deficiency	Repair
TAIL_NO	MODEL	CONFIGURATION			
162723	AV-8B	Day Attack			
Add Open Delete					
Ref No	Fleet	Engineer			
LES-70-CPA-1998	AV-8	W. Gay			
Deficiency Type	Eff. Date	Engr. Hours			
Heat Damage	04-28-1998	180			
Date Created	Main Structure				
04-28-1998	Wing				Fracture Critical

Figure 4. Repair Tracking - - Main Window

Information stored in a repair record would also need to contain Analysis, Deficiency, and Repair descriptions. This information would be crucial for understanding the impact of the repair on the overall aircraft. In FLEETLIFE, the tabs across the top of the window will control the information displayed in the upper portion of the window. The analysis tab will hold links to the analysis data associated with each repair record. Selecting the analysis tab will display a list of analytical file links. The details of the damage necessitating the repair will be contained in the deficiency tab. Selecting the deficiency tab will display a text box to record a written description. The caption box below it will contain an electronic image of the damage. The pictures can be transferred electronically from the aircraft station to the support engineer. The repair window will contain disposition instructions for repair of the deficiency. The top part of the window will contain the written instructions for the disposition. The bottom portion will contain a small repair drawing. It will also contain a link to other drawing packages, such as AutoCAD. As shown in Figure 5, cost information for each repair will be accumulated by tail number. All repair records associated with a particular tail number will be listed in this window. The total cost for all repairs will be shown in the cost total box.

The fracture critical box shown in Figure 4 will designate the selected repair record as an ASIP generated item. In this fashion repair costs will be definable as a mandated repair necessary to protect the fleet from catastrophic failure and a standard repair necessary to maintain the fleet. (This is beneficial from a cost/risk standpoint in that if the structural integrity engineer has visibility to the number of standard repairs being installed on aircraft in the fleet, he can assist in an economic analysis to decide whether to continue repair installation or modify the fleet.) In this fashion, both the user and the ASIP manager can gain greater understanding of the others' risk/cost requirements and perspective. The key to solving this problem is information.

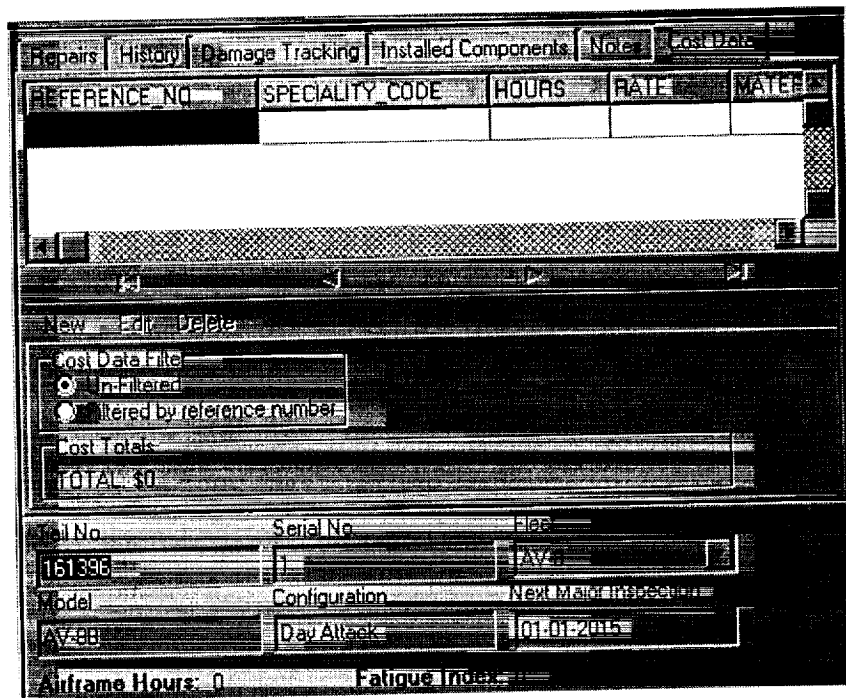


Figure 5. Aircraft Tracking - - Cost Tab

In the past, one major aspect that has been lacking in risk/cost analysis has been the visibility of engineering support. Currently in the Air Force, engineering hours are not recorded against a repair. This makes calculating the efficiency of design activities impossible. Conversely, structural integrity engineers do not have visibility to the number of standard repairs being installed nor the cost of standard maintenance actions. Structural integrity engineers need to know the cost impact of directed maintenance actions. That information may significantly influence the decisions that affect the fleet's risk/cost balance.

Information transfer in any risk/cost tracking of structural repairs is of critical importance. Since the volume of information that must be gathered, managed, and processed and

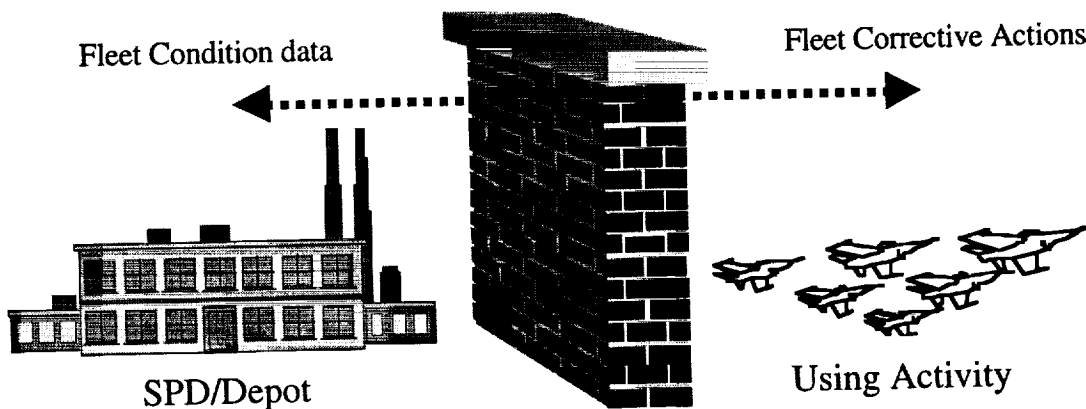


Figure 6. Information transfer is critical

presented is enormous, effective use of electronic hardware and software is extremely important. An effective ASIP program management tool should be divided into three major inter-related database management systems. These systems are the Force Management database, the Maintenance database, and the Cost/Economic Model database. These systems must be seamlessly integrated.

The Force Management database would contain the tools to predict and prevent major structural failures. It would contain historical and predictive aspects. In this system, the ASIP Brochure and Force Structure Maintenance Plan and associated data would be contained. The foundation of the database system would contain all original analysis and testing accomplished by the Original Equipment Manufacturer (OEM) and any additional analysis and testing accomplished by the using activity after delivery. Geographical location information of each aircraft would be archived on a regular basis to assist in developing an environmental spectra. Aircraft flight usage data and spectra would be stored; along with all critical aircraft structural details and associated analysis and testing results. The results of all types inspections would be cataloged and stored in this section. Finally, all future ASIP related plans, proposed modifications, proposed inspections and maintenance actions would be documented and stored for future reference.

The Maintenance database would need to contain all routine structural and system maintenance data. All standard structural repairs and inspections would be stored in relation to the aircraft's tail number. Major mechanical systems data would also include failure rate data on major mechanical system sub-components. In the future the system should allow maintenance personnel on the aircraft repair dock to electronically initiate and transmit a maintenance record for engineering support.

The Cost/Economic model database would be used to archive all man-hour and material cost data related to aircraft maintenance actions. It would also contain business models to assist in fleet modernization and modification planning. The cost data would be tagged by specific structural details and by aircraft tail number. This would allow visibility to "bad actors", both from a fleet wide and single aircraft problematic component view points.

The FLEETLIFE software referenced earlier is being developed to provide for efficient information transfer. Table 1 depicts the current, planned and development tasks being incorporated to provide decision makers with accurate information. Though formidable in nature, managing information flow between user and support organizations is the fulcrum to the risk/cost balance. (If you are interested in what we are doing with FLEETLIFE software and would like to participate please contact one of the authors.)

TABLE 1. FLEETLIFE development matrix

TASK	Current FLEETLIFE Task	Planned FLEETLIFE Task	Development Task
Force Management Database	X		
Historical			
Aircraft fleet/base/wing/squadron geographical	X		
Environmental data			
Individual airplane flight loads and usage data	X		
Current fatigue damage calculation by location and Tail number		X	
Full scale, coupon, environmental test results and teardown results both OEM and user generated for Baseline and modified configurations		X	
ACI and other directed inspection results by location and tail number		X	
Historical and in-service analysis by location and tail number	X		
In-service problems and observations by location and tail number	X		

Force Management Database	X		
Future Actions			
ASIP Brochure and supporting data		X	
SLEP modifications and scenarios		X	
Planned usage changes and effect on structural integrity	X		
Aircraft Maintenance Database			
Individual Airplane Maintenance history		X	
MRRB brochure and supporting data		X	
Routine -3 maintenance actions by location and tail number		X	
Results of routine -36 inspection results by location and tail number		X	
Catalog of corrosion inspection and maintenance actions by location and tail number		X	
Failure rate data for components in the primary mechanical systems		X	
Electronic entry and transmission of AFMC-202 and-107 forms			X
Cost/Economic Model Database		X	X
Maintenance action generated man-hour data by location and tail number			X
Engineering support man-hour data by disposition, location, and tail number.		X	
Material cost data by location		X	
Specific location cost data		X	
ASIP driven maintenance cost data		X	
High cost components and failure rates for primary mechanical systems			X
Corrosion related action cost by location and tail number			X
Business/Economic Models			X

In summary, as aircraft structural integrity management moves toward a more cost based business approach, the collection of accurate and detailed cost and risk data will become vital. Structural integrity engineers must have visibility to repair cost information. Fleet managers must have visibility to engineering and ASIP concerns. In many respects, the answer lies in efficient information management and exchange. Balancing future risks with current costs is a delicate art. The future success will require the use of effective and encompassing tools. Many of them already exist, some still need to be developed. Simple effective data input methods must be utilized. Current databases have holes and bad data. No system can give good results with bad inputs. Economic data must be fully integrated into maintenance and ASIP data bases. Without attacking the difficult tasks today the benefits can not be reaped in the future.

INFLUENCE OF UNDETECTED HIDDEN CORROSION ON STRUCTURAL AIRWORTHINESS OF AGING JET TRANSPORTS

Aydin Akdeniz and Girindra K. Das
Boeing Commercial Airplane Group
Seattle, WA 98124, U.S.A.
206-544-8541
Fax 206-544-8502
aydin.akdeniz@boeing.com

ABSTRACT

In this paper the implications of combined hidden corrosion and fatigue on structural integrity of aging jet transports are presented. The primary concern, the corrosion between the fay surface of the Principal Structural elements (PSE), is discussed. Examples of hidden corrosion that were found in older airplanes in the Boeing fleet are shown. Current maintenance programs for structural integrity of aging commercial fleet are discussed. Commercially available detection methods for hidden corrosion are described. Finally, recommendations to address hidden corrosion in older airplanes are proposed by supplementing existing visual inspections with subsurface nondestructive evaluation (NDE).

1. INTRODUCTION

Economic and market conditions have resulted in the use of commercial jet transport airplanes well beyond their original economic Design Service Objective (DSO). Increase in the active service life of commercial fleet is due to low fuel cost and increasing costs for fleet replacement. Supplemental inspections based on the damage tolerance philosophy provide continuing airworthiness until economics of repair and modifications dictate retirement of an aircraft from service. Safety will not be compromised if the mandated safety inspections and the scheduled maintenance are carried out. Air transport industry consensus is that older jet transport airplanes will continue to be in service despite anticipated substantial increases in the required maintenance.

Against this background, many aging jet transport airplane operators around the world are conducting economic impact studies to determine the feasibility of extending the use of the older airplanes in their fleet. Based on economical reasons, established operators may replace their airplanes well beyond their DSO with new ones. At the same time these older airplanes are sold to operators with little or no knowledge and experience with the aging airplane maintenance programs. Economic pressures coupled with lack of structural maintenance experience may reduce the additional attention needed to maintain continued airworthiness of these airplanes. As the air traffic continues to grow on every continent of the world, the likelihood for continued use of these older airplanes will only increase (Figure 1).

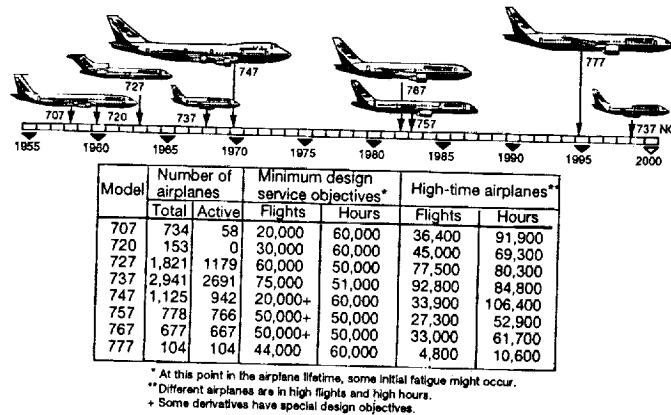


Figure 1. Basic commercial jet fleet summary (January 1998)

Standard Boeing practices to support continuing airplane structural integrity include inspection and overhaul recommendations contained in maintenance documentation and service bulletins. As airplanes exceed their DSO, the incidence of fatigue increases and corrosion may become more widespread. Since fatigue depends on flight cycles and corrosion depends on time, they may occur independently and their combined presence is hard to predict. Current industry practice is to keep corrosion under control by means of Corrosion Prevention and Control Program (CPCP) and develop maintenance for fatigue based on the assumption that the corrosion is under control.

Corrosion is controlled in the Boeing fleet by a CPCP that focuses on visual inspection of surface corrosion of safety critical areas, called PSEs. Once corrosion is controlled by CPCP, the FAA-mandated Supplemental Structural Inspection Program (SSIP) developed for fatigue can be effectively applied for structural integrity. This has worked very well for surface corrosion. However, undetected hidden subsurface corrosion in PSEs may influence the effectiveness of SSIP inspections for fatigue damage. (Ref. 1)

The objective of this paper is to raise the awareness of potential airworthiness concerns of older airplanes in the worldwide fleet with undetected hidden corrosion and present a proposed solution based on subsurface NDE inspections and extensive maintenance training. Timely preventive maintenance based on subsurface NDE inspection of PSEs to detect hidden corrosion should permit continued safe operation of aging jet transports until economics dictate their retirement from service.

1.1 MAINTAINING STRUCTURAL SAFETY FOR THE AGING COMMERCIAL FLEET

Criteria and procedures employed in the commercial aircraft design for the past three decades have resulted in long-life damage-tolerant structures with a credible safety record (Figure 2)(Ref. 2). This achievement is the result of diligent attention to detail design, manufacturing, maintenance, and inspection procedures.

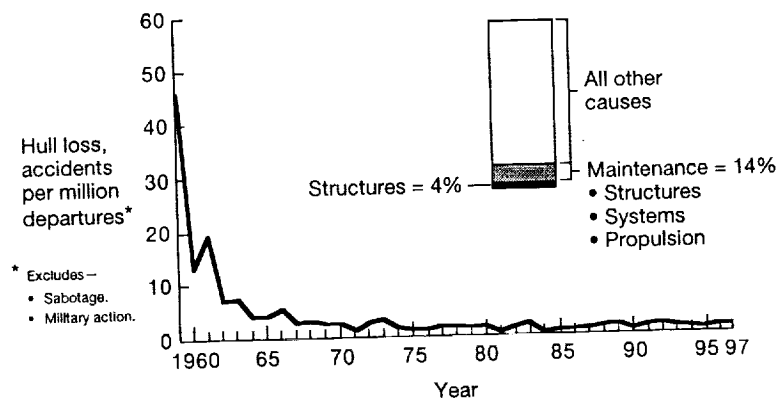


Figure 2. Safety record—worldwide commercial jet fleet (year-end 1997)

The design concepts, supported by testing, have worked well due to the system that is being used to ensure that the commercial fleets are kept flying safely throughout their operational life. The major participants of this system are the airworthiness authorities who establish rules and regulations, approve the designs, and oversee airline maintenance performance; the manufacturers who design, build, and support airplanes in service; and the airlines who operate, inspect, and maintain the fleet. Airplane safety depends on the diligent performance and participation by all the participants in the system.

Commercial jet airplane structures in the 1950s and 1960s were designed by using the fail-safe design concept, which ensures the ability of a critical component to maintain design capability and functionality with complete failure of a single element or an obvious partial failure of a single element. Experience has shown that the fail-safe design philosophy has generally been effective in allowing sufficient opportunities for timely detection of structural damage. However, failure modes were not always predicted with sufficient accuracy to ensure that structural failures would be obvious and within safety limits. Structural failures could progress in unanticipated ways, and a number of old airplanes were found with quite unexpected

defects. By the early 1970s it was clear that the airline operators were expected to find cracks that were difficult to detect, and inspection planning was recognized as a safety issue. This prompted the industry and airworthiness authorities to focus more on the adequacy of inspection programs for timely detection of structural discrepancy before they become critical. Combined industry and airworthiness authority activities in the late 1970s resulted in changes to the regulatory requirements to reflect state-of-the-art developments in fracture mechanics and embrace damage tolerance as a design philosophy. In addition to residual strength evaluations, damage growth and inspection requirements with consideration for damage at multiple sites were incorporated in 1978 in FAR/AC 25.571, Amendment 45 for new airplanes, and in CAA Notice 89 and AC 91-56 for development of SSIP for airplanes certified prior to 1978.

1.2 MAINTAINING AIRPLANES CERTIFIED DAMAGE TOLERANT USING MSG-3 PROCESS

For airplane models certified after 1978, maintenance for damage tolerance was developed using the Maintenance Steering Group-3 (MSG-3) process. The MSG-3 guidelines document, written by the Air Transport Association (ATA), provides procedures for developing initial maintenance programs for three principal sources of aircraft structural damage: fatigue, corrosion, and accidental damage (Figure 3).

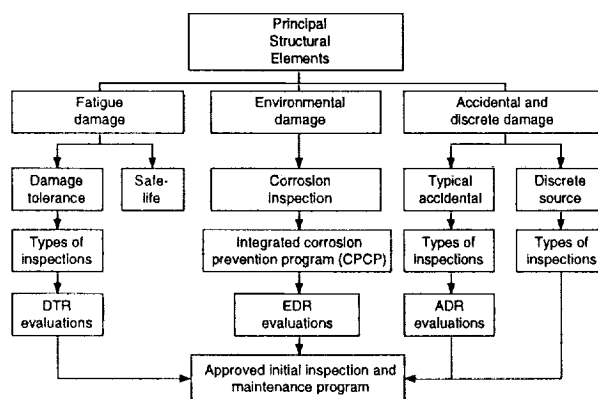


Figure 3. MSG-3 process for developing maintenance for principal damage sources

The guidelines provide for rating systems to be developed by the manufacturer as a means of determining inspection requirements. The rating systems are based on past practice and manufacturer/operator experience with similar structure. The rating systems used by Boeing are Accidental Damage Rating (ADR), Environmental Deterioration Rating (EDR) for corrosion, and Damage Tolerance Rating (DTR) for fatigue damage detection assessment.

The initial structural maintenance plan for a new model is directed toward detecting corrosion and accidental damage. Based on manufacturer and operator experience statistics, ADR and EDR for each PSE are established and initial inspections are developed. Simultaneously, feasibility study for fatigue damage detection is made to determine if a practical program can be constructed using the DTR system.

As the fleet matures, the risk of fatigue increases and the initial inspection program is reassessed using the DTR system. If the initial program is inadequate for finding fatigue cracks in significant structures, additional or supplemental inspections are required and provided by SSIP.

1.3 MAINTAINING THE AGING FLEET AGAINST COMBINED CORROSION AND FATIGUE

Corrosion in aircraft structures can occur under both static conditions and during missions, and it is a time-dependent phenomenon. Corrosion starts when applied protection systems become degraded and damaged. Degradation occurs due to exposure to ultraviolet rays, ozone, and moisture-induced leaching of inhibitors from primers and sealant. Accidental damage is a random event and is usually addressed by operator and manufacturer experience statistics. Fatigue, on the other hand, requires repeated loads and therefore depends on flight or missions. With time when airplanes accumulate more and more flights, both corrosion and

fatigue may occur simultaneously. Combined action of corrosion and fatigue tends to concentrate on joints due to high stresses caused by stress concentration and load transfer, crevices for moisture entrapment, fay surface contacts that wear out the protection system. Testing and fleet history have shown that the effect of corrosion on fatigue is significant and consistent (Ref. 3). Currently no simplified practical method to correlate the amount of corrosion to time is available. On the other hand, the science of fracture mechanics is well developed to predict fatigue crack growth and residual strength to a sufficient degree of accuracy.

Combination of severe corrosion and fatigue damage can significantly affect damage tolerance capability by reducing residual strength, increasing multiple site damage, accelerating crack growth rates, and larger initial damage size. Distribution of corrosion is unpredictable in the fleet and significantly reduces the safe damage detection period for fatigue damage.

An example illustrating the potential effect of fatigue damage occurring in the presence of severe corrosion is shown in Figure 4.

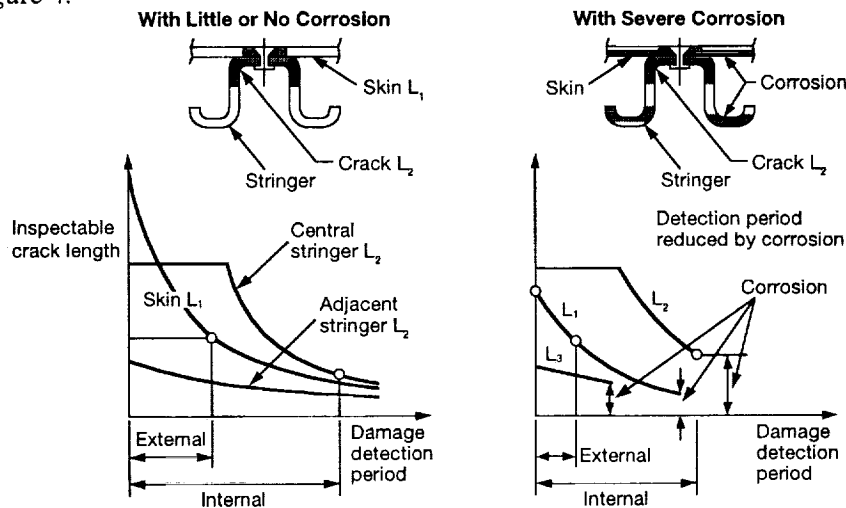


Figure 4. Reduction of damage detection period due to severe corrosion

Airplane structural integrity can be significantly affected by the reduced number of opportunities to detect damage, before it exceeds safe allowable limits.

Figure 5 shows typical fleet damage rate assumed for aging fleet assessments in the early 1980s when Supplemental Structural Inspection Documents (SSID) for fatigue cracking were developed. The fleet damage rate for corrosion was assumed to be fairly constant. However, surveys and events in the late 1980s have indicated an increasing number of corrosion problems in aging airplanes.

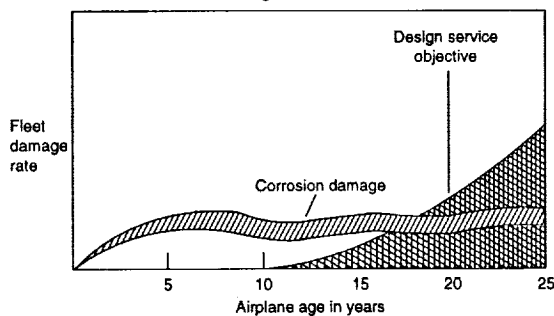


Figure 5. Assumed fleet damage rate

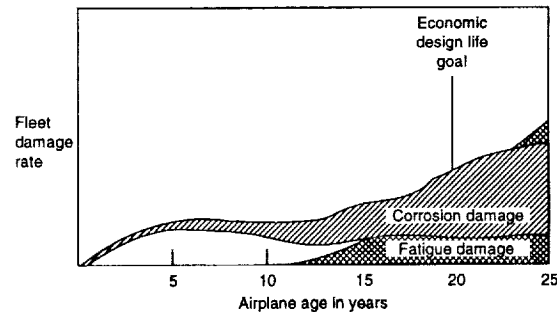


Figure 6. Observed fleet damage rate

Figure 6 shows the observed fleet damage rate during the same period as Figure 5, and 6 indicates a significant increase in the fleet damage rate due to corrosion. Some operators had taken effective action to prevent or control corrosion, but some did allow corrosion to progress to levels that required major repairs or re-

placement of parts. It became obvious that without changes in this trend, potential combinations of severe corrosion and fatigue cracking would require frequent inspection of all primary structure on all aging airplanes, to ensure continuing airworthiness. To avoid such impractical restrictions on an aging fleet, the industry approach was to prevent or control corrosion independent of fatigue, prior to any potential interaction with fatigue damage. The result was the CPCP (Ref. 4 and 5).

1.4 CORROSION PREVENTION AND CONTROL PROGRAM

The main objective of the CPCP is to establish minimum procedures for preventing or controlling corrosion that may jeopardize the continuing airworthiness of the aging fleet. The program is developed for each model by industry working groups called Structures Task Groups. A baseline program was developed for each jet transport model under FAA jurisdiction. The programs included a definition of levels of corrosion (Figure 7), inspection tasks, and implementation requirements, repeat inspections for each task, and reporting requirements for findings. Each operator must have an effective CPCP that controls corrosion to level 1 or better (Figure 7).

Corrosion Severity Relative to SRM Allowable Blend-out Limit	Corrosion Level for Given Extent and Number of Inspection Intervals to Reach Given Severity				
	LOCAL		WIDESPREAD		
	Single Interval	Multiple Interval	Single Interval	Multiple Interval	
Well Below	LEVEL 1	LEVEL 1	LEVEL 1	LEVEL 1	
Approaching	LEVEL 1	LEVEL 1	LEVEL 2	LEVEL 1	
At Limit	LEVEL 1	LEVEL 1	LEVEL 2	LEVEL 1	
Above Limit	(1)	LEVEL 2	LEVEL 1*	LEVEL 2	LEVEL 1*
	(2)	LEVEL 3	LEVEL 1**	LEVEL 3	LEVEL 1**

- (1) Corrosion is not an Urgent Airworthiness Concern.
- (2) Corrosion is an Airworthiness Concern.
- * Operator experience over several years has demonstrated only light corrosion between successive inspections, but latest inspection and cumulative blend-out now exceed allowable limit.
- ** Highly unlikely event following multiple applications of preventive measures and corrosion-inhibiting compounds.

Figure 7. Effects of corrosion extent and severity on corrosion level

In principle, the CPCP was developed based on general visual inspections without disassembly of permanently attached structure unless evidence of corrosion exists. CPCP has been effective for surface corrosion, where visual inspections are adequate.

1.5 THE BOEING APPROACH TO MAINTAINING FATIGUE AND CORROSION

In line with the above industry aging airplane philosophy, the Boeing approach to maintaining fatigue and corrosion has the following elements:

- Keep corrosion within level 1 or better by means of effective CPCP.
- Develop SSIP/SSID assuming effective CPCP keeping corrosion blend-out limits within damage tolerance assessments. This is done by normalizing damage tolerance methodology to a corrosion level of 1 or better.
- Consider effect of adverse environment in crack growth analysis methodology. Although full-scale presence of corrosion cannot be analyzed at present, the effect of corrosive environment on crack growth has been taken into consideration. Thus total absence of corrosion is not needed for damage tolerance analysis.

This approach has been working well for CPCP type surface corrosion.

1.5.1 CPCP and Hidden Corrosion

Despite having specific inspection requirements through some service bulletins and FAA Airworthiness Directives (AD), recent reports and inquiries from operators indicate that CPCP and other programs do not

have the full capability to detect hidden corrosion prior to becoming well beyond manufacturer's allowable limits. Furthermore, this is an issue for all PSEs, not just for structures defined by service bulletins and ADs.

1.5.2 Examples of Hidden Corrosion

Figure 8 shows a fuselage longitudinal lap splice in which severe corrosion underneath was not visible from outside.

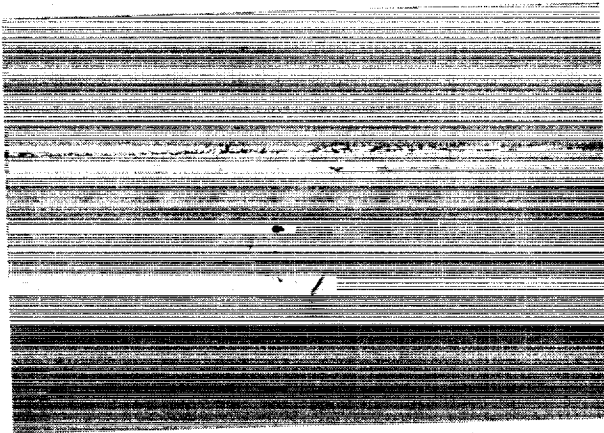


Figure 8. Hidden corrosion at advanced stage in a longitudinal lap splice

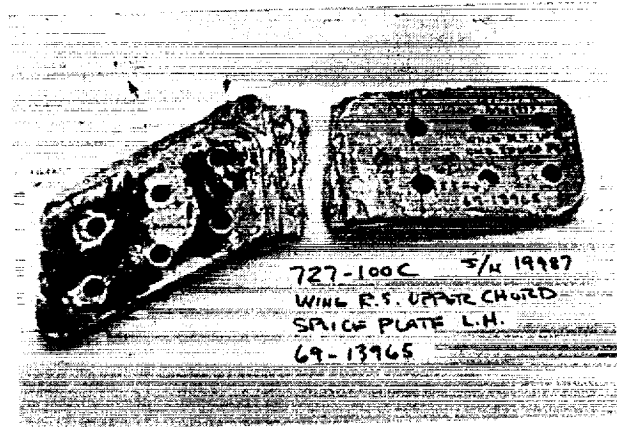


Figure 9. Corrosion in rear spar upper chord splice plate at side of body

Figure 9 shows a splice plate that splices the horizontal leg of the wing rear spar upper chord at the side of the body joint. Although the part was severely corroded, the only reason the corrosion was found was due to a fatigue crack in the spar chord that was found outboard of this joint, and the airline had elected to replace a portion of the chord from the side-of-body outboard.

Figure 10a shows hidden corrosion between the wing front spar lower chord and web in dry bay area. Previous visual inspection for this item was carried out multiple times without finding any corrosion. Corrosion became apparent during a visual (CPCP) inspection only after the web was totally corroded and was beyond fay surface of the chord and web. CPCP will not find similar occurrences in other areas until corrosion is well beyond allowable limits and level 2.

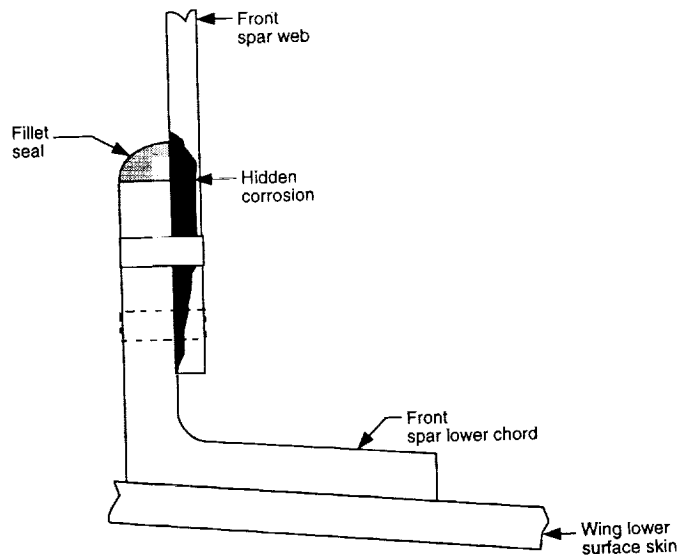


Figure 10a. Hidden corrosion in 747 wing front spar web

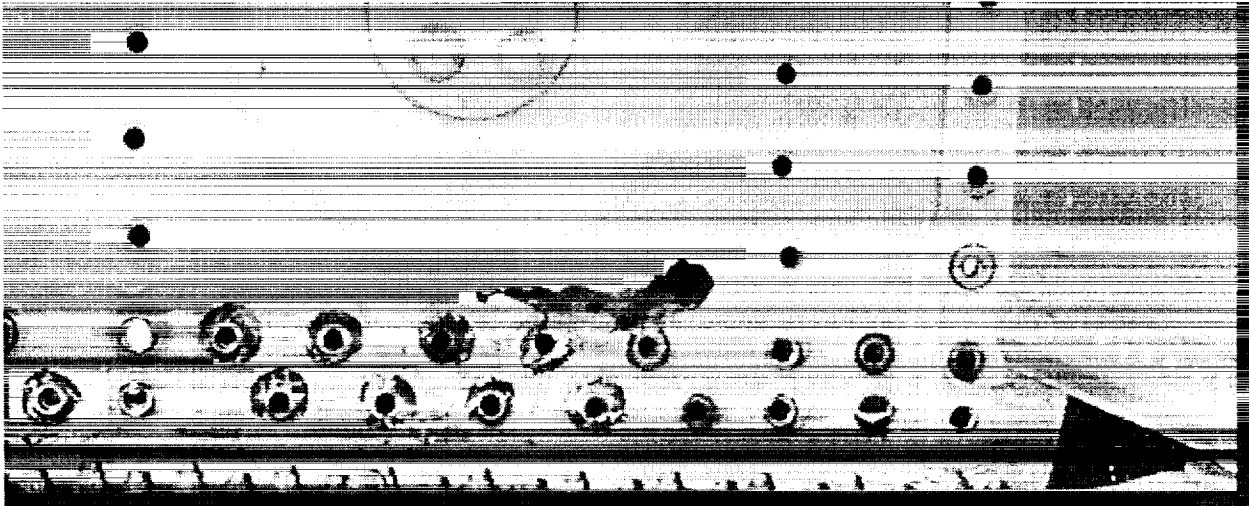


Figure 10b. From inside the tank

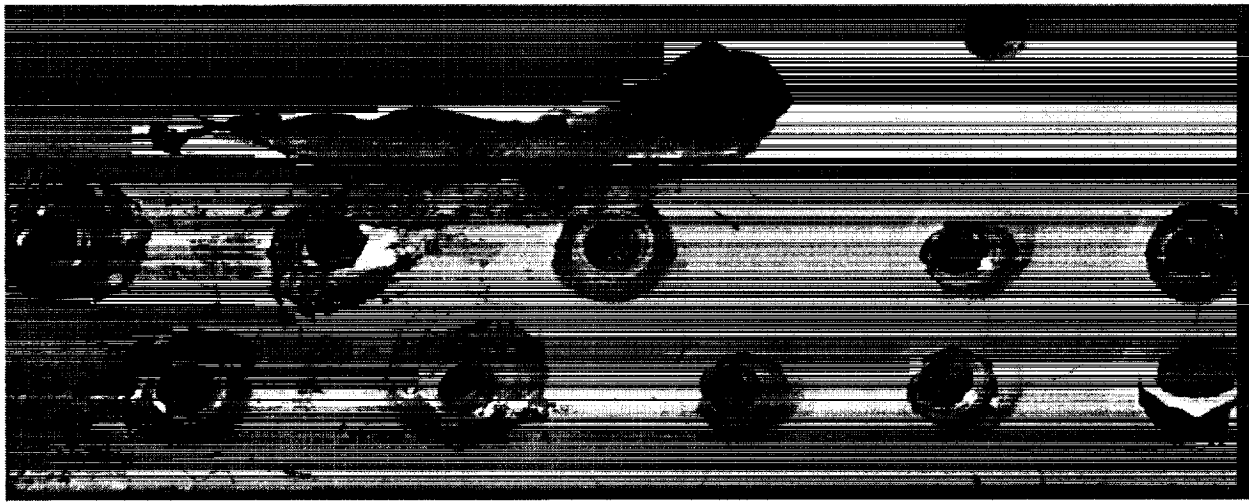


Figure 10c. From inside the tank

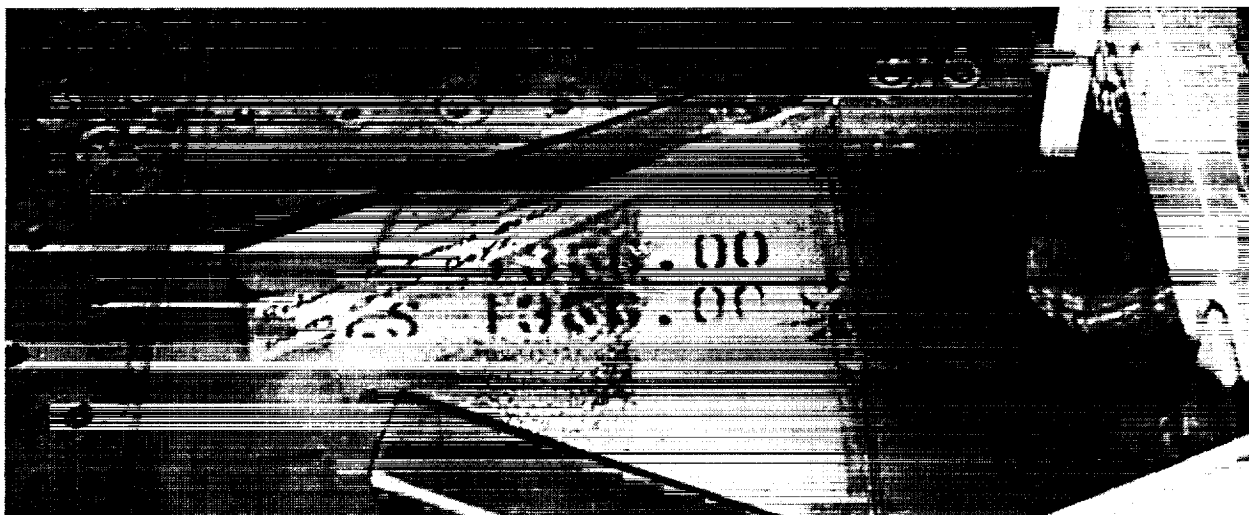


Figure 10d. From outside the tank

Figure 11 shows details of hidden corrosion between the belly skin and stringer reported by an experienced major operator. In this instance also the corrosion found was beyond level 2. By conducting NDE inspections, the operator discovered similar discrepancies at multiple locations. Once again CPCP visual inspections did not adequately detect hidden corrosion prior to becoming level 2.

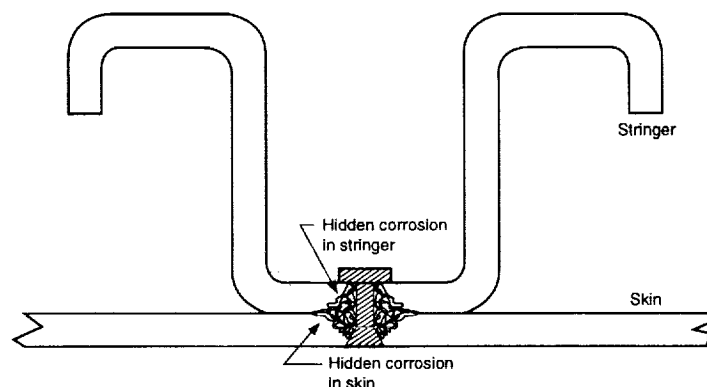


Figure 11 Hidden corrosion in bilge area skin and stringer

1.5.3 Impact of Hidden Corrosion

Surface corrosion can easily be detected by visual or other surface inspections. CPCP provides for such inspections and therefore, corrosion can be detected in a timely manner and repaired before it becomes a safety concern. Thus, once corrosion is under control, inspections for fatigue can be developed using fracture mechanics methods, which assume no significant interaction of corrosion on fatigue. Therefore, resulting SSIP is effective in detecting fatigue cracking in a timely manner before it becomes a safety concern. Hidden corrosion, on the other hand, will not be detected by mandated CPCP and may not be detected until it reaches or exceeds critical levels at multiple locations. Therefore, SSIP for fatigue inspections may be unconservative. Cracking patterns for structure with potential for hidden corrosion must be adjusted accordingly. Thus, for the example in Figure 11, the detection period could be based on the assumption of failed stringer flange at the skin surface rather than crack growth from the edge of a fastener hole. These cracking pattern assumptions for damage tolerance detection assessments will be a function of visual versus NDE methods employed in the SSIP.

1.5.4 Hidden Corrosion Detection

Recent visits to experienced aging airplane operators show that detecting hidden corrosion in aircraft structure is a challenging task. Of particular concern is the corrosion that is not visible or does not have tell-tale signs. Use of NDE is essential in ensuring airworthiness of aircraft that are used well beyond their DSO. However, utilization of NDE to ensure safety by means of hidden corrosion detection in a large commercial fleet can only be relied upon once it has proven to be effective by virtue of its track record. The other problem with NDE is that although its reliability for fatigue is well established, that for corrosion is not yet well defined.

Early detection of hidden corrosion, prior to exceeding allowable limits, is the key to maintaining aircraft safety. Hidden corrosion usually can be detected by subsurface inspections only. Therefore, it may be essential that subsurface nondestructive inspection methods be used to effectively detect hidden corrosion prior to becoming well beyond allowable limits.

1.5.5 NDE Methods for Hidden Corrosion (Ref. 6,7, and 8)

Traditional methods for subsurface inspection include low frequency eddy current (LFEC), ultrasonic, and radiographic methods (X-ray). LFEC is capable of detecting material loss (thickness loss) in the first and

second layers, ultrasonic is capable of accurate measurement of material loss in the first layer, and X-ray is used for detection throughout the full thickness of the structure. Thermal techniques are also used to detect 10% or more material loss for large areas.

Among emerging techniques, two are promising for rapid, wide area inspection. The first method is an optical double-pass retro-reflection surface inspection technique (D-sight). Although a surface technique, it is very sensitive to surface bulging (pillowing) effects caused by the confinement of the subsurface corrosion products and has potential for lap splice subsurface corrosion detection. The second method is thermal wave imaging, which is capable of imaging wide areas of subsurface corrosion in lap splices, tear straps, and other areas of the aircraft fuselage.

1.5.6 Detection of Hidden Corrosion in the Commercial Fleet

In the commercial fleet two NDE methods are commonly used: LFEC and Ultrasonic.

-LFEC inspection can be basically classified into two groups:

- Single-frequency LFEC inspection where only first-layer hidden corrosion may be detected. Using this method, reliable detection can be obtained for corrosion of 10% or more of the thickness, and it can be used for thicknesses up to 0.125 inch.
- Dual-frequency LFEC inspection, in which second-layer corrosion can be reliably detected for corrosion of 10% or more of the thickness can be used for thicknesses of up to 0.125 inch. The dual frequency allows the inspection technique to separate the signals from the gap between the two parts and thereby this technique allows inspectors to detect corrosion in the second layer.

Note that no effective practical method exists for third-layer corrosion for a commercial fleet.

-Ultrasonic Inspection

- Ultrasonic inspection can be used to detect first-layer crack only and works better with thicker plates. Essentially, they act as thickness gages and determine the thickness loss due to corrosion. They can detect corrosion of over 10% of the thickness, although more reliable resources can be obtained in the range of 10% to 30% (or higher).

-Thermography:

- Another promising method is thermography, which is currently used to detect ice in honeycomb structure. But the equipment needed to detect corrosion seems to be expensive at this time.

1.6 CONCLUSIONS AND RECOMMENDATIONS

Hidden corrosion affects damage tolerance of PSEs and, if detection is not timely the continuing airworthiness of the aircraft will be impacted. Very old airplanes operated by less experienced operators are most vulnerable.

To avert this situation, current CPCP may have to be expanded to include subsurface NDE in addition to existing visual inspections. Alternately, a new program primarily with subsurface NDE may have to be created to supplement the CPCP. Simultaneously, SSIP may have to be modified to include cracking scenarios to account for hidden corrosion. Industry training coupled with improved inspection techniques for early detection of hidden corrosion should be an integral part of this program.

REFERENCES

1. U. G. Goranson, "Damage Tolerance - Facts and Fiction", 17th Symposium of International Committee on Aeronautical Fatigue, Stockholm, Sweden, June 1993.
2. R. T. Watanabe and T. D. Scheumann, "Structural Integrity Criteria for Commercial Transport Aircraft", Effects of Product Quality and Design Criteria on Structural Integrity, ASTM STP 1337, St. Louis, Missouri, May 1997.
3. R. J. W. Wanhill, J. J. De Luccia and M. T. Russo, "The Fatigue in Aircraft Corrosion Testing (FACT) Programme", AGARD Report No. 713, February 1989.
4. A. Akdeniz, "Airplane Structural Maintenance and Corrosion Prevention", *Aircraft Engineering and Aerospace Technology*, Volume 68, No. 3, 1996, West Yorkshire, England.
5. A. Akdeniz, "Corrosion Prevention and Control Programs", *Airliner Magazine*, March 1996, Boeing Commercial Airplane Group, Seattle, Washington.
6. J. P. Komorowski, K. Shankar, R. W. Gould, and O. L. Hageniers, "Double pass retroreflection for corrosion detection in aircraft structures", 79th AGARD, Seville, Spain, October 1994, Paper 7.
7. D. A. Bruce, "Non-Destructive Detection of Corrosion for Life Management", 79th AGARD, Seville, Spain, October 1994, Paper 9.
8. J. H. Heida and W. G. J. 't Hart, "Eddy Current Detection of Pitting Corrosion around Fastener Holes", 79th AGARD, Seville, Spain, October 1994, Paper 11.

ACHIEVING TOTAL SYSTEM AGING AIRCRAFT SOLUTIONS

Steven M. (Mike) Enloe
Boeing Information, Space & Defense Systems
P.O. Box 7730, MC K84-47
Wichita, KS, USA 67277-7730

Abstract

The initial focus of aging aircraft efforts, and the development of resolution plans, has primarily been applied to the corrosion and structural areas. These solutions have typically been developed and applied in a singular manner, constrained by limited or incremental funding availability. In addition, the focus has primarily been on the necessity of resolving single critical issues, without assessment of the overall system effects. As corrosion and structural issues are resolved, weapons systems operators continue to experience degradation of availability and readiness due to systems, equipment, and support limitations of aging aircraft. These include: 1) equipment item obsolescence, 2) mission requirements changes, 3) diminishing manufacturing sources, 4) age degradation of the systems/equipment, 5) reduced manpower levels (both skills and numbers of personnel) and, 6) funding constraints. In addition, recent changes and DoD initiatives relative to Acquisition Reform and Flexible Sustainment are causing increased scrutiny of the nature and effectiveness of support systems management and application. The DoD continues evolving towards improved support practices, and modernization requirements (such as Global Air Traffic Management (GATM) and Future Air Navigation Systems (FANS)) constantly emerge. As a result, the need for new methods of analysis and forecasting is becoming critical. In order to rapidly assess and quickly respond to these concerns, a comprehensive approach to identifying aging aircraft issues, providing resolution, and assessing total system implementation effectiveness is required.

Application of the systems engineering process to aging aircraft issues provides for: 1) identification of all issues pertinent to the equipment and its support system, 2) development of assessment criteria to allow ranking of the issues in order of magnitude, 3) assessment of the impacts on availability as well as operating & support (O&S) costs, 4) development of alternatives, 5) preparation of a roadmap for the resolution of issues, 6) assessment of newly emerging issues against the roadmap, and, 7) continued evaluation to maintain the health of both the equipment and the support system. The systems engineering approach, applied to the weapon system (including the support infrastructure), provides a method of determining and obtaining total system objectives. Assessments will provide measures of the cost savings necessary to fund zero net dollar improvements in the current cycle of shrinking defense budgets. Return on investment can be maximized while reducing the overall time required to realize O&S savings. Impacts to the existing support infrastructure can be minimized while optimizing capabilities to support constantly evolving mission requirements.

Introduction

Aging aircraft system costs continue to increase while the ability to obtain funding has become a competitive environment. Fleets have been operated beyond their anticipated chronological service lives, usually in conjunction with mission profile changes that have significant impact on the structural and/or systems life of the aircraft. In the meanwhile, operational requirements have continued to increase due to

shrinking force sizes and multiple force commitments. Add to this the tendency to focus aging aircraft solutions on (generally) structural issues, overshadowing subtler (but just as significant) systems issues.

Weapon system management of emergent issues has traditionally been handled on a “case by case” basis with the emphasis on maintaining system performance, not overall system economics. The development of resolutions should be managed and measured at the overall level and needs to involve business cases. Latest DoD initiatives are based on achieving “Best Value” for overall life cycle support. In order to do this, weapons systems managers need new metrics and new processes.

Commercial aircraft operators make rapid, cost-based decisions because they track and assess impacts and changes based on cost of ownership (e.g. “dollar cost-per-seat-mile”). They collect data in sufficient detail, and in a consistent manner, to support standardized analysis. This allows evaluating each issue against the overall cost of ownership of their respective system. While commercial processes are generally applicable to aging aircraft, the specific metrics need to be developed based on sensitivity to systems unique perspectives such as the chronological age of the systems being measured exceeding the forecast service life period.

Utilizing the systems engineering process, the weapon system manager can identify sustainment requirements, allocate these requirements into plans, analyze and validate the achievement of goals, and update requirements as necessary. Using analytical tools to develop true cost per unit of operation (e.g. flight hours, sortie, out-of-service hour, etc.), the system manager can also track actual costs of ownership. This helps to determine the most profitable planning of expenditures to support known or forecast operational service requirements of the weapon system. In addition, it provides a means of weighing the out-year cost effects of occasional short-term needs to delay or bypass correcting a systems problem.

A systems manager cannot expend all of their available funding on the latest trendy technology or topic at the expense of the safety or operational degradations, which are existent or emerging. By managing cost for profitability, they can effect out-year cost avoidances that will provide for future modernization activities. These are necessary to retain a viable warfighting capability well into the year 2020 and beyond.

Requirements for Increased Systems Cost Effectiveness

In order to effect increased cost effectiveness, first establish metrics for success. For aged or aging weapons systems, success exists when the following occur:

The cost of continuing the current support approach is a constant, stable value that will incur no growth due to obsolescence, loss of industry base, planned improvements or restorations, etc.

The cost of planned improvements or restorations “pay for themselves” in actual out-year savings, and within the period of their respective obsolescence.

Economic analysis indicates that the Net Present Value of changes is less than or equal to their obligated funding.

Current in-progress activities are consistently being accomplished at or under their cost and schedule targets.

Weapons systems maintenance and support is a decreasing, not increasing cost.

It becomes immediately obvious that systems managers must look at cost in a new and more comprehensive manner. The trap inherent in increased workloads and operational tempos is the lack of time to evaluate everything at a detailed level. True, an economic analysis will not and should not be used to support urgent mission requirements. But the fact remains that the primary purpose of system managers is to provide for the real needs of the crews to fly, the maintainers to have tools and spares, and the planners to have equipment available to support missions. Doing so involves maximum utility in forecasting future needs, and the costs associated with achieving these goals.

If an organization has a computer with a higher end spreadsheet and calculation application (such as Microsoft® Excel, etc.), they most likely have more than one person with the mathematical background to build models. The key point is that sophisticated models are generally a product of the functions they utilize and not the data they require. As long as a comprehensive set of data is available, and the data is accountable, simpler functions can be utilized in a repetitive manner to accomplish the same results as complex functions.

What is a systems engineering approach? Nothing more than identifying requirements for the system (top-level model), allocating those requirements (building cost factors and groundrules), validation of success (verifying cost effectiveness of decisions), and documenting results (maintaining the model(s)). Most importantly, it is the assessment of each item against the total system, both current and planned, from a cost perspective, to ensure that the most cost-effective solution for total system support is being used. It allows the “what if” assessment for alternatives while providing the means to assess the most cost effective timeline for accomplishment – or delaying the efforts - based on the planned approach for overall system management.

Approaches for Documenting Assessments and Impacts

Understand the system/equipment, as well as all related costs. In order to determine the impacts of change, one must first document a baseline of what is actually being expended today. All future decisions will be based on the effect against this baseline, so be diligent in data gathering. Define the operational and support commitments of the existing weapon system. These elements include such things as:

systems supported, # locations, foreign or CONUS, deployment cycles, utilization, supply support, repair support

Don't be hasty to neglect such items as direct personnel costs, facility and support costs, surcharges, etc. One method of identifying “buried” costs is as follows: observe “routine” activities and whenever one observes an activity, or the consumption of an item, or the use of equipment or facilities, attempt to find out where the costs are tracked and how they relate to the system. Every single item that occurs has some cost associated with it. And while these costs may not be reflected in system specific appropriations, there is a benefit from the ability to forward cost benefits upward to the appropriate staffs.

Look for subtle drivers. These are the typical cause of most faulty analyses for profitability. Subtle drivers are those items that at first (or even third) glance do not obviously contribute to the specific issue under evaluation. As a result, overlooking them is easy, yet they may cause one to miss true requirements by large amounts.

Example

A command is replacing a wing skin at a cost \$20,000 per aircraft for 500 aircraft. (\$10 M). This drives a need to replace all the fasteners with the next oversize at an additional (hidden) cost of \$30,000 per aircraft (\$15 M). It is decided to be conservative and obligate 125% of this amount to cover contingencies (\$31.25 M). After obtaining headquarters approval based on the estimates developed, and funding is allocated.

The subtle drivers are: 1) some of the fasteners are already oversized, and will drive rework of stringers on 20% of the aircraft for the replacement of these fasteners during reskin at a cost of \$40,000 per aircraft (\$4 M) PLUS 10% of the stringers (6 per a/c average) will crack out and need replacement, but the replacement is 30 month lead time and a \$10,000 item (\$6 M). This drives a cum program cost (excluding contingencies) of \$35 M – leaving a potential \$3.75 M shortfall in the program. In addition, there are issues of out-of-service costs, depot facility delays due to schedule impacts, and increased utilization of other aircraft resulting from the out-of-service effects. Now a decision is required, do they delay this program or will some other maintenance or modernization issue be reduced or delayed in order to meet this requirement.

Define groundrules and restrictions. These include not only the known quantitative items (reliability, cost, etc.), but also the unknown, therefore qualitative, items (utilization forecasts, inflation, forecast scrap factors, etc.). These groundrules are the basis of decision making as to whether or not a global strategy change is necessary to effect profitability. In addition, the documentation of groundrules and assumptions provides the continuity to future managers so that they understand all the reasons behind decisions.

Use available tools to gather data. Regulatory Changes. New and pending regulatory changes can provide good insight into future operational, support and modernization requirements. It takes a good amount of research to identify and validate these forecasts, but the results can provide sufficient lead-time to develop weapon system management strategies that can utilize currently obligated funding in a streamlined manner.

Aircraft Sustainment Master Plans (ASMP): ASMPs are an effective tool for compiling and prioritizing weapon system issues, concerns, strategies and assessments. Use of ASMPs provides the means to document results of analyses and future utilization predictions in a single document. This facilitates the development of “roadmaps” for systems management, as well as building a repository of data to support rapid turnaround of command requests and emergent funding opportunities. The ASMP serves as the “business plan” for the system management.

Aircraft Structural Integrity Program (ASIP). ASIP is used to monitor, predict and forecast structural integrity of an aircraft, including degradation effects of cracks and other structural failures. The inherent drawback of ASIP is that it is based on pristine (undamaged) structural materials. The effects of corrosion on structural integrity are being developed through testing and conceptual model analysis. As these tools become perfected, the ability to forecast impacts will be enhanced and streamlined.

Functional Systems Integrity Program (FSIP). Aircraft were designed, and initially qualified, for a service life based essentially on structural integrity. As time has elapsed, these service life predictions have been modified due to testing, rework and analytical study. One effect is that the systems installed on the aircraft have been used for a far greater period than designed, even as the technology involved in the systems has become obsolete or extinct. An FSIP program performs failure analysis on a system – identical to the initial Failure Modes and Effects Analysis (FMEA) performed by the OEM. The emphasis of FSIP is to determine how age, modification and other factors effect the system, as well as recommending how to manage and/or improve the system. FSIP is typically applied from a safety

perspective, e.g. how does a failure affect mission or personnel, but could also be applied from an operational or support perspective. FSIP is a handy tool for systematically assessing the effects of age on systems and equipment.

Corrosion Prevention/Control Plans (CPCP). CPCPs are used to develop corrosion prevention strategies, identify corrosion prone areas of the aircraft, and forecast future corrosion repair requirement potential. Some elements of a CPCP include corrosion zone mapping of potential problem areas, corrosion predictive modeling

Cost Of Ownership (COO) Modeling. COO provides the tools for accumulating the knowledge, and assessing the overall impacts of changes. They allow evaluating potential changes for impact to funding, or estimate impacts of reallocating current work. COO modeling is the means by which value determinations are made as a result of gathering data.

Define future changes to the baseline, both known and anticipated. The past can be an indicator of the future, either for better or worse. In documenting future changes, focus on those items that cannot be managed or affected today. These include such things as obsolescence, operational utilization, modernization, etc. By documenting these factors using realistic values, the baseline includes a planned growth factor for use in comparing growth issues. If one cannot obtain a planning factor, develop one, but ensure that it is documented clearly in the groundrules for future reference.

Programs such as ASIP and FSIP provide data that is extremely helpful in looking forward. These programs can provide concise and accurate information on obsolescence, emergent utilization or safety issues, and projected maintenance increases. The more data that can be obtained, the more proactive the modeling.

Know what it's going to cost to get there. Develop and use a mathematical cost model to provide numerical as well as graphical interpretations of the data. As mentioned earlier, this can be as complex as can be afforded, or as simple as desired. The goal is to display the global system cost issues, so that all changes can be assessed based on their impact to the baseline. As a point of reference, the easier it is to use the model, the more likely it will be used. And the more it is used, the more it will come to be depended on as another tool for the decision making process.

Insert disruptions that will have predictable results to validate the model. Pay special attention to the selection of sensitivity analysis criteria – analysis of the wrong metrics will provide skewed results.

Use the model to assess hardware/software changes, determine impacts of future trends, evaluate options related to modernization and maintenance, and analyze operational or support system changes and their effects. Relate costs back to the baseline to evaluate if there is economical payback of the proposed change. In the event that safety or operational changes are going to negatively impact funding profiles, determine the most economical method of re-allocating current or planned projects to get back into a profitable position.

Don't forget to plan for updating the model as projects are activated, cancelled or modified. The more the model is utilized, the faster it will be to use because it contains the most current data. But if allowed to become too outdated, it will become too time consuming to update on demand and therefore not of value for decision making.

Make sure to include the support system. Another critical, but often overlooked area of cost is the support system for the equipment. There is general recognition of spares and technical manuals as support costs. But investigating further reveals the costs of repairing the spares, costs to update the

manuals, costs of developing and fielding the new support equipment required due to the forecast obsolescence or other replacement requirements for system equipment, etc. More difficult than the current costs are the projections of support system impacts resulting from future requirements or changes in strategy. It has been widely documented that Operating and Support (O&S) costs are the real drivers in system Life Cycle Cost (LCC). One cannot model future profitability without including the support system in the analysis.

Picking the “best value”. How does one assess which item is the best candidate to delay? How does one decide if they can delay this item? How did one reach the conclusion that this was the right item to work first? Lacking the mandatory nature of safety items, many candidates for modernization or maintenance improvement should be evaluated based on qualitative measures. Lacking good cost of ownership models, these evaluations become victims of subjective measures.

No one wishes to hit the brick wall of aircraft retirement due to landing gear or cockpit modernization problems because all of the available funding is being consumed in an incremental manner for corroded lap joints? And are they being cleaned because it is needed, or just because it has always been done that way?

These decisions will most likely be self-generating if a model adequately addresses the key elements:

1. What are the operational and support (maintenance) objectives of the system/equipment – now & future?
2. What are the impacts on the “as-designed” equipment and support system?
3. What alternatives are there?
 - Use the planned approach now
 - Delay
 - Do Nothing
 - Do something else
4. What effect does each alternative have on total system cost of ownership? Rank the alternatives based on the weighting criteria most appropriate to the analysis.

Breakthrough Opportunities

With recent DoD changes that place more emphasis on profitability, there are areas where breakthroughs can and should occur. These breakthroughs will either simplify decision-making, or increase the options available to the systems manager for creating the most profitable approach possible. These include such items as the following:

- True cost of ownership and operational documentation.
- Detailed work-level cost collection for modernization and maintenance.
- Forecasting models and analysis approaches that are utilized consistently by DoD agencies.
- Legislative/regulatory issues (color of money).
- Long-term (>5 years) funding obligation capabilities.
- Standard systems engineering approach model for use by all DoD agencies.
- Standardized metrics.
- New data sources and collection techniques.
- New processes and/or streamlining of existing processes.

CONCLUSIONS

There are significant benefits, both short-term and long-term, to be derived from total systems assessment. Most notable is the decreased probability of funding obligations which later prove incapable of sustaining mission and support metrics. Proper evaluation of age issues includes analysis of weapons system utilization and performance, detailed assessment of all cost elements affected, and determination of support system impacts. These analyses can provide the methods for determining how to prioritize limited available funds for the best return on investment. As the O&S costs are brought more under control for fiscal efficiency, the out-year savings can be re-applied to meet increased system improvements and/or modernization objectives. All of this can be accomplished with a “net zero dollar” impact to current obligation and funding plans under the cognizance of using and managing commands.

DoD has committed to long-term sustainment of aging aircraft. By developing enhanced technologies, methods, materials and systems, managers will have greater opportunities to ensure that weapon systems will continue to fulfill current and future missions. It is dependent upon industry to develop a standard support metric and leverage commercial expertise. DoD has a corresponding role by increasing “best value” management, providing data to industry, and streamlining existing processes to increase efficiencies. Industry and DoD need to work to jointly evolve support processes as well as developing new data sources and collection techniques.

EUROFIGHTER 2000 STRUCTURAL HEALTH AND USAGE MONITORING: AN INTEGRATED APPROACH

Stephen R. Hunt and Iain G. Hebden

British Aerospace Military Aircraft and Aerostructures,
Warton Aerodrome, Preston, Lancashire,
PR4 1AX, United Kingdom
iain.hebden@bae.co.uk

ABSTRACT

This paper outlines the Structural Health Monitoring system being developed for Eurofighter 2000. The system is designed as an integral part of the avionics system, both on and off-aircraft, enabling the customer to perform fleet-wide monitoring of fatigue life and significant structural loading events.

1. INTRODUCTION

Eurofighter 2000 (EF2000) is a four-nation collaboration between Germany, Italy, Spain and the United Kingdom. The Structural Health Monitoring (SHM) system being developed for EF2000 is resident on each aircraft and will enable the operators to monitor accurately fatigue consumption and significant structural events, thereby safeguarding the structural integrity of the aircraft. The information obtained can be used to plan maintenance actions effectively, and to manage the fleet fatigue life pro-actively by the rotation of aircraft.

British Aerospace have system design responsibility for the EF2000 SHM system. The SHM is integrated with both the on-aircraft avionics systems and the ground support system. The on-aircraft software is part of the Integrated Monitoring, test and Recording Sub-system (IMRS). The IMRS is also responsible for crash data recording, video voice recording, management of equipment maintenance messages and provides the engine health monitoring interface with the ground.

The SHM ground analysis is performed by the Ground Support System (GSS), which is responsible for both mission and engineering support activities for EF2000. An overview of the SHM system is shown in Figure 1.

Different customer requirements for the SHM system has lead to the development of a flexible system which can be configured, without recourse to software change, as either a parametric based or strain gauge based fatigue monitoring system.

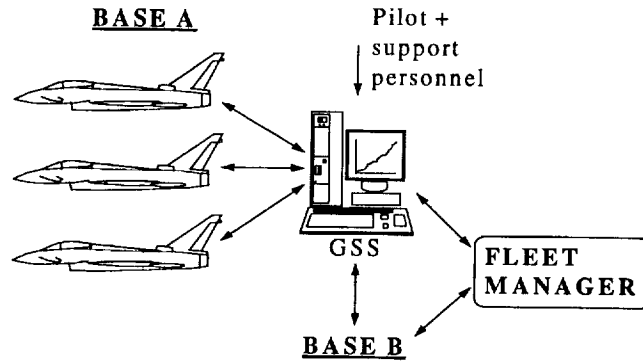


Figure 1. Overview of aircraft and ground SHM systems

2. ON-AIRCRAFT SYSTEM

The SHM algorithms form part of the IMRS software fitted to each EF2000 and as such have access to the majority of the data within the avionics systems e.g. flight control system. The IMRS software is written such that on entry into service a growth potential of 100% is present (both processing and memory).

The SHM system performs real-time fatigue calculations and determines the life consumed by the airframe. Significant structural events and flight performance parameters are also monitored. A facility exists to record parameter and strain gauge time histories, if requested by the operator, for ad hoc studies (Figure 2).

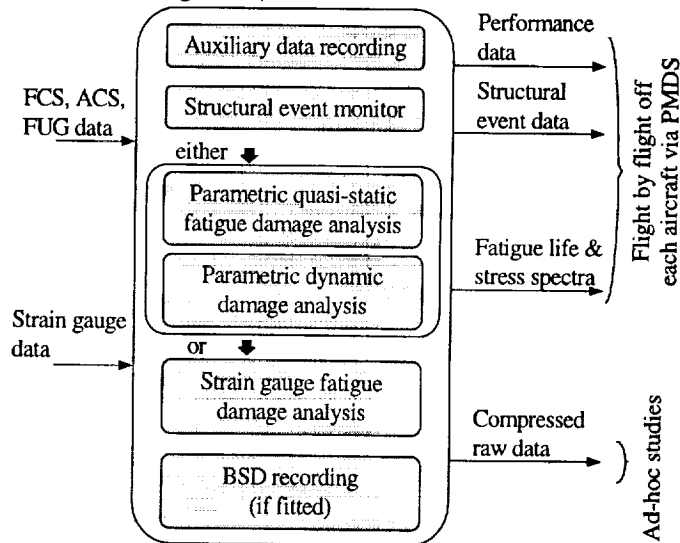


Figure 2. Schematic diagram of aircraft SHM system

The SHM data are available from the aircraft via two sources: Maintenance Data Panel (MDP). The MDP is an on-aircraft equipment which displays information to the support personnel allowing them to query on-aircraft systems data. The SHM data available on the MDP are details of the total life consumed by each SHM monitored location and information on SHM event messages which have occurred on the previous sortie.

Portable Maintenance Data Store (PMDS). The PMDS is a solid state memory device approximately the same size as an cigarette packet ($\approx 100*60*25$ mm). The PMDS is used to transfer SHM, engine and maintenance data to and from the aircraft. The PMDS can store data for up to five individual flights.

In addition to the above equipment the aircraft has an optional recording device, the Bulk Storage Device (BSD), which can be used to record a set of parameters requested by the support personnel.

2.1 Fatigue Calculation

Two SHM versions are being developed. These reflect the customer requirements for either a parametric based or strain gauge based fatigue monitoring system. Both versions will be validated by comparison with flight test data correlated to fatigue test results.

The SHM calculates fatigue life consumed at specified locations on the airframe. A single software is fitted to the aircraft which provides the operator with the facility to define, via data uploaded by the support personnel, whether each location is to be either parameter or strain gauge based.

For parametric based locations, real-time data are captured from the Flight Control System (FCS), Armament Control System (ACS) and the Fuel Gauging System (FUG). The FCS provides aircraft altitude, velocities and accelerations, the ACS provides information on the aircraft weapons configuration and the FUG provides fuel mass information. These data are fed into the SHM which calculates the stress at each location by comparison with approximately 17500 "templates" held in internal memory. Each template, derived from finite element analysis and results of ground based airframe fatigue tests, corresponds to a particular aircraft configuration and set of flight parameters. The process iterates, generating a history of stress. The stress history is subjected to a real-time range-mean-pairs cycle counting analysis to calculate stress spectra and fatigue damage (Figure 3).

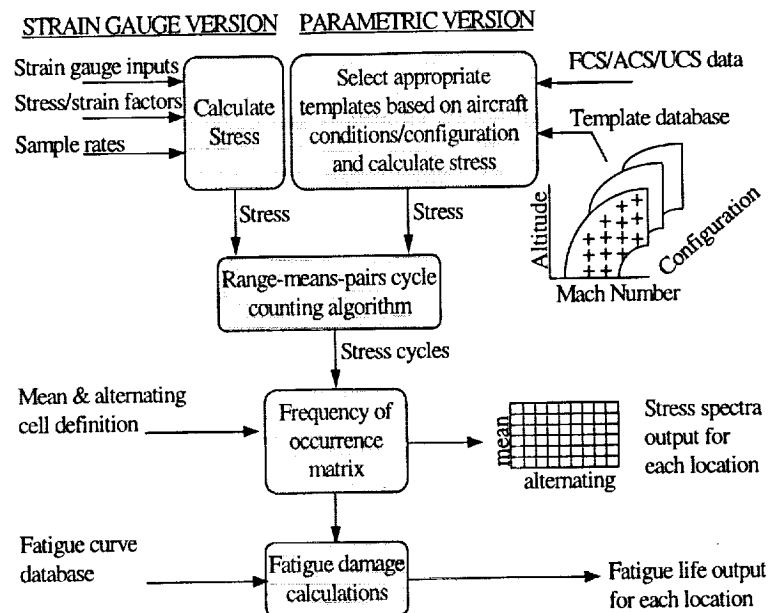


Figure 3. Overview of fatigue calculations

For strain gauge based locations, the stress is calculated directly from strain gauge measurement at an iteration rate defined by the user. A real-time range-mean-pairs cycle counting analysis, identical to the parametric locations, is performed to calculate stress spectra and fatigue damage.

The health of the data input to the SHM algorithms from external sources i.e. flight control system and strain gauges, are monitored. These, together with data indicating the health of the SHM data, are also available for off-aircraft analysis.

Typical SHM locations are given in Figure 4.

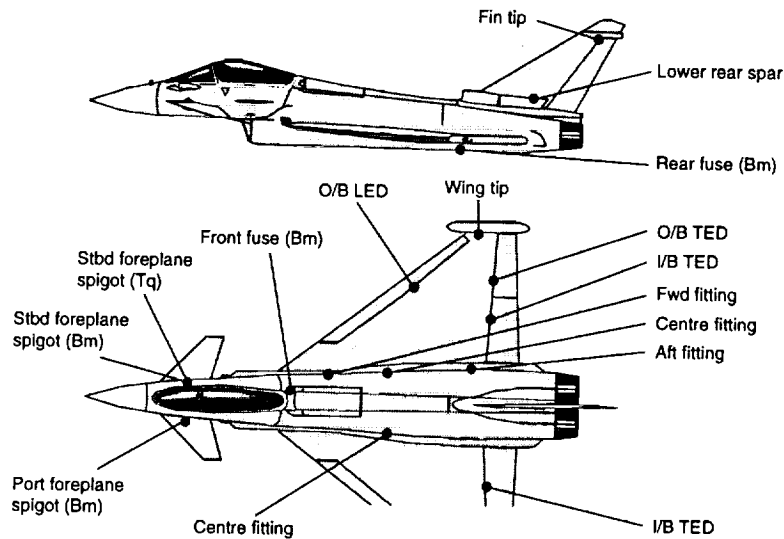


Figure 4. Position of SHM locations

2.2 Dynamic Damage Calculations

For the strain gauge system the sample rates are user definable, allowing the operator to select a sample rate sufficient to capture dynamic loading on the airframe.

For the parametric system a more complicated method has been designed, see Figure 5. The data provided to SHM from the FCS etc. is insufficient in both rate and content to measure directly dynamic loading on the airframe. The method employed by the SHM to calculate dynamic damage is as follows.

The SHM measures and records the length of time spent within multi-dimensional regions (e.g. incidence vs. dynamic pressure vs. airbrake angle) within which the aircraft is subject to dynamic loading and hence dynamic damage. A corresponding multi-dimensional envelope containing damage rates for each region subject to dynamic damage is held within the software.

Multiplying each cell in the duration matrix by the corresponding damage rate and summing all the resultant damages gives a total dynamic damage for that flight.

The shape and cell size of the duration matrix and corresponding damage rate matrix are identical and are both user-definable.

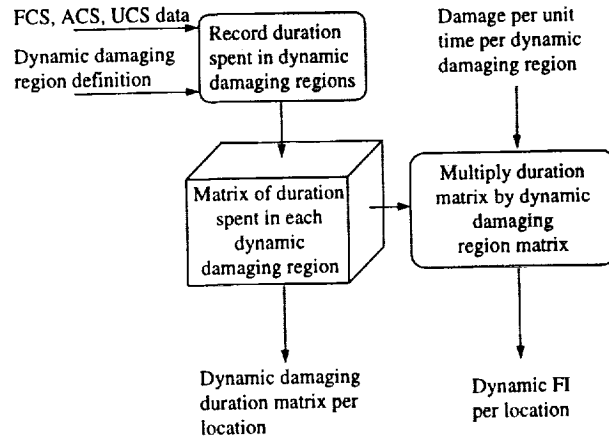


Figure 5. Parametric dynamic damage calculations

2.3 Event Monitoring

The SHM monitors in real-time the allowable parameter envelopes for structurally significant events and displays to the support personnel, via the MDP, any excursions outside these boundaries. Additional data are available on the PMDS for down-load to the GSS where further investigations using crash recorder data and bulk storage device data, if available, can be undertaken.

The definition and validation of the relevant parameter envelopes and the event corner points will be performed during aircraft development.

Up to seven envelope types can be monitored, each envelope being dependent on up to six configurations (e.g. clean, tanks). Up to five sub-factor envelopes and corner points for these envelopes/configurations can be defined to the aircraft software. An illustration of the functionality is shown in Figure 6.

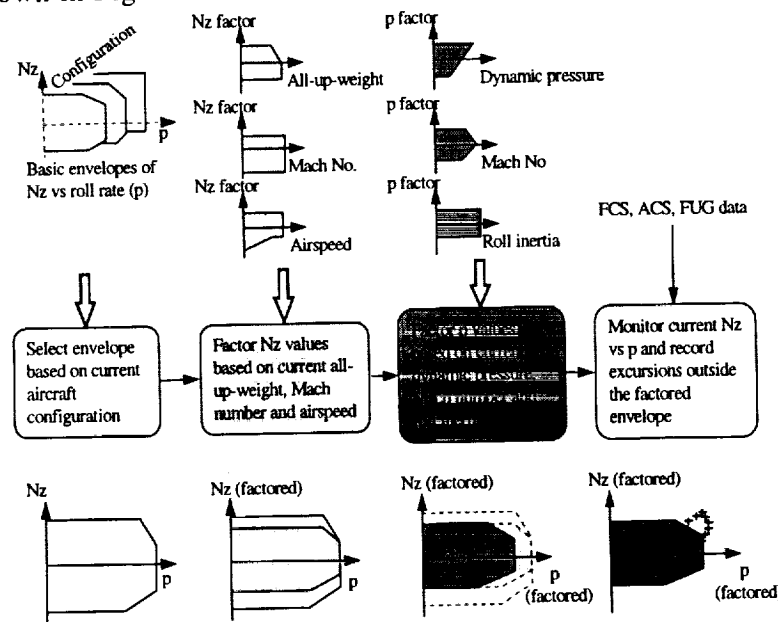


Figure 6. Example of structural event monitoring

2.4 Auxiliary Data

The SHM calculates auxiliary data. This consists of data traditionally collated in the flying log, and additional design/performance parameter summaries (Figure 7).

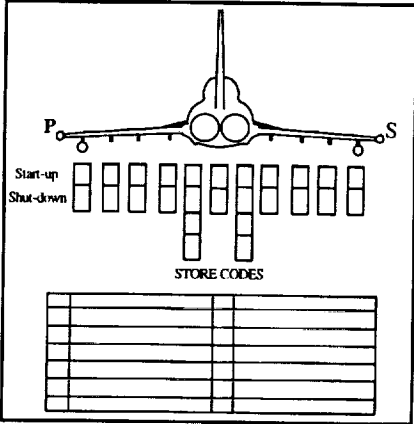
In order to reduce the work load of the support personnel the following data are made available by the on-aircraft SHM system for each flight: flight date, take-off time, flight duration, stores configuration, mass of stores/fuel at each take-off and landing, number and type of landings (roller, touch and go, arrested etc.).

In addition, the following performance parameter summaries are available from each flight: number of airbrake operations, undercarriage cycles and refuelling probe deploys/refuels. Tabulation of "fatigue meter style" recordings of Nz in various aircraft mass and "points in the sky" bands are recorded together with Nz vs. roll rate tables. Maximum and minimum values of airspeed, altitude, Nz, and roll rate within one minute bands are also available.

Tail No.	Flight No.	Unit Code	Station/Unit/Sqn

Flight Details					
Date (Day/Month/Year)					
Take-off Time					
B/F Total Aircraft Hours					
Duration					
Total Aircraft Hours					
% Supersonic	Sortie Code				
Number of Crew	Airbrake Ops				

Mass in kg					
Basic Aircraft Weight					
AAR No.	Fuel Recvd.				
Fuel at Take-off					
Fuel at Landing					
Ballast Mass					
Ammo Mass	Take-off	Landing			



RECORD OF LANDINGS			G COUNTS			ROLL RATE COUNTS			SERIAL NUMBERS		
Roller Landings This Flight			Level	Subsonic	Supersonic	Level	Subsonic	Supersonic	Port Wing		
Total Roller Landings			1			1			Starboard Wing		
Touch & Go Landings This Flight			2			2			Fin / Rudder		
Total Touch & Go Landings			3			3			Port Foreplane		
Full Stop Landings This Flight			4			4			Starboard Foreplane		
Total Full Stop Landings			5			5			Port Flaps		
Arrested Landings This Flight			6			6			Starboard Flaps		
Total Arrested Landings			7			7			Airbrake		
Total Number U/C Cycles			8			8			Undercarriage		
			9			9					
			10			10					
			11			11					
			12			12					

Captain's Name: _____	(Service No) _____	Tradesman's Name _____
-----------------------	--------------------	------------------------

Figure 7. Example of auxiliary data output

2.5 Bulk Storage Device

A BSD can be fitted to each EF2000 for special studies purposes. The system is designed to compress and record data for a ninety minute flight, depending upon number of parameters and their sample rates and resolutions, and upon flight activity. The definition of which data time histories are recorded, and the rates and resolutions of those data, is controlled via the ground support system.

Any data entering the IMRS can be accessed, including the twenty analogue channels. Internal SHM data can also be accessed e.g. stress at each location. This gives the operator the ability to perform ad hoc studies e.g. operational load monitoring exercises, on any aircraft at any time, without the expense of special recording equipment.

3. GROUND SUPPORT SYSTEM

The GSS provides the mission and engineering data processing for the aircraft and the management of the interface between EF2000 systems and the respective in-service ground based systems to support the aircraft operational staff at squadron level. In addition the GSS also supports engineering staff in the maintenance of the aircraft. The design of the SHM ground based analysis is integrated into the engineering support facility (Figure 8).

The quantity and complexity of the SHM data retrieved on a flight by flight basis from the aircraft is prohibitive to the support personnel. A full understanding of all the data would require specialist knowledge and training. As the support personnel are not expected to have detailed specialist knowledge, the SHM ground based analysis is designed to be used by an operator with a minimum of training.

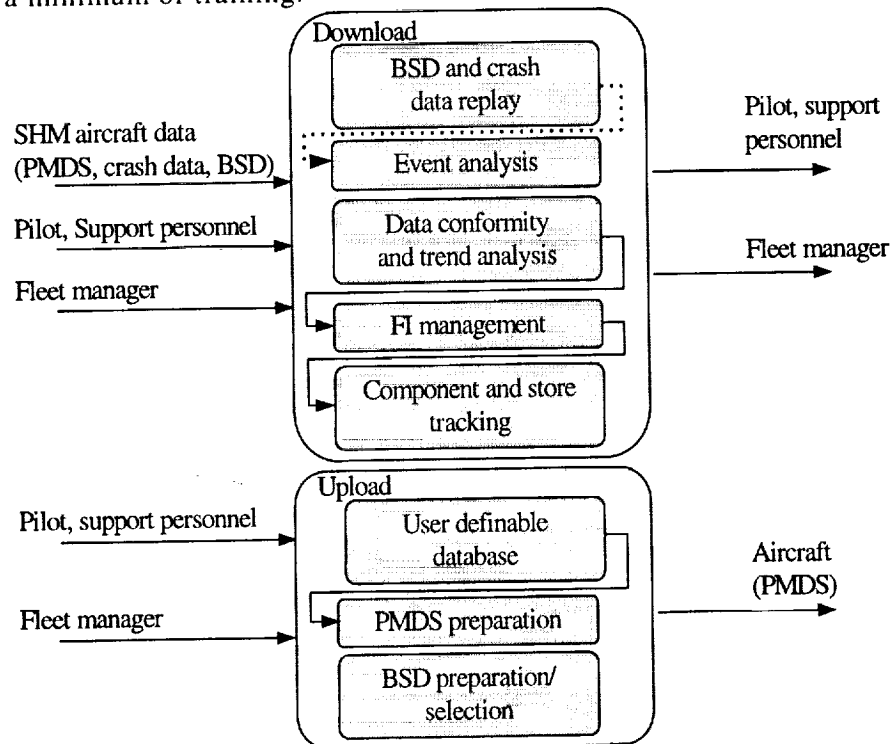


Figure 8. Schematic diagram of ground SHM system

Note: The volume of SHM data retrieved per flight from each EF2000 is approximately 350 times the volume of fatigue data currently retrieved and stored for a Tornado aircraft.

3.1 SHM Ground Analysis

The PMDS can store up to five flights' worth of data. On receipt of a PMDS the GSS demultiplexes the SHM data into individual flight files and scales the data into engineering units. The GSS checks for completeness and data integrity. Identification of a failure, either in the data or in the transfer of data from the PMDS to the GSS will result in the GSS operator inserting a new PMDS into the aircraft and down-loading data stored in non-volatile memory on-board the aircraft. Post-flight the pilot is required to enter a profile code describing the sortie flown. This profile code is used in the verification of SHM data retrieved from the aircraft and will assist in fleet planning activities.

The SHM analysis assesses the validity of retrieved SHM data by comparison of individual aircraft results with that aircraft's history of fatigue data collected and by comparison with fleet trends. The GSS analyses the SHM health messages to determine the quality of the data. The system automatically calculates the values for any "unmonitored" flying using formally agreed rules.

The SHM validated flight records are stored in a database within the GSS. This database also stores both the aircraft component and role equipment serial numbers. This validated information can be transmitted to national information centres for fleet planning.

The database of SHM results held by the GSS at a base can be queried by authorised support personnel in order to manage their aircraft. A variety of standard query formats and chart types are provided, together with the facility to answer ad-hoc queries. Typical examples of data formats are given in Figures 9 to 10.

Fleet utilisation by sortie profile code for year 2006

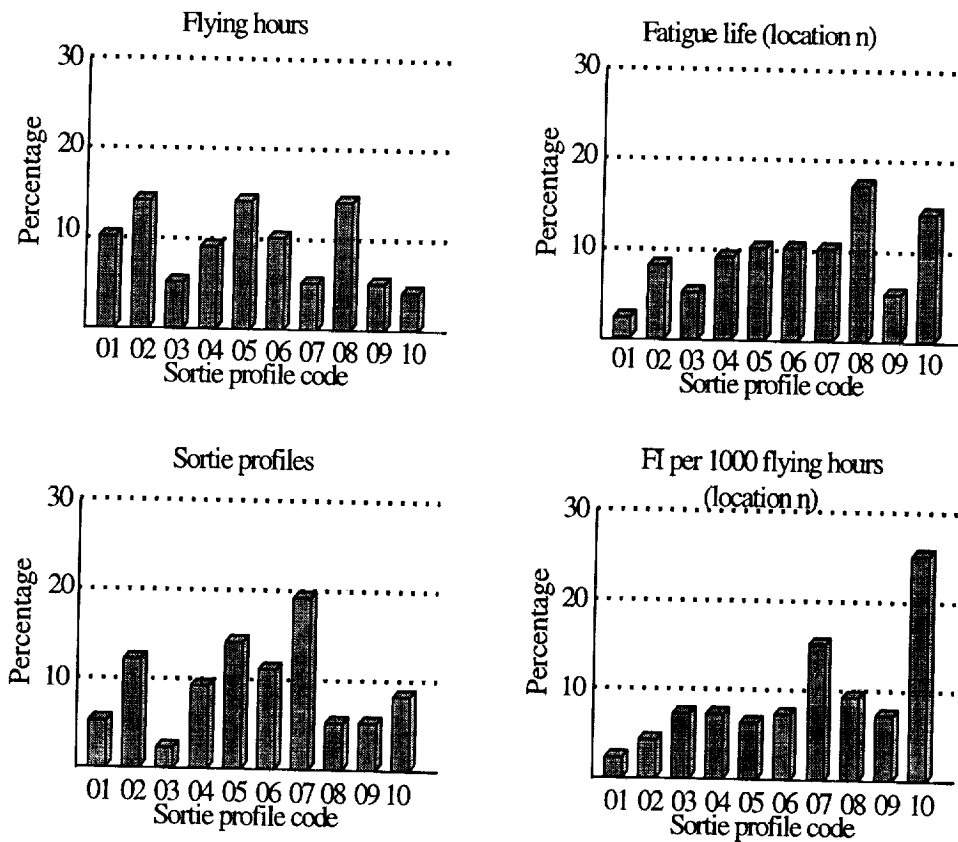


Figure 9. Typical ground analysis queries

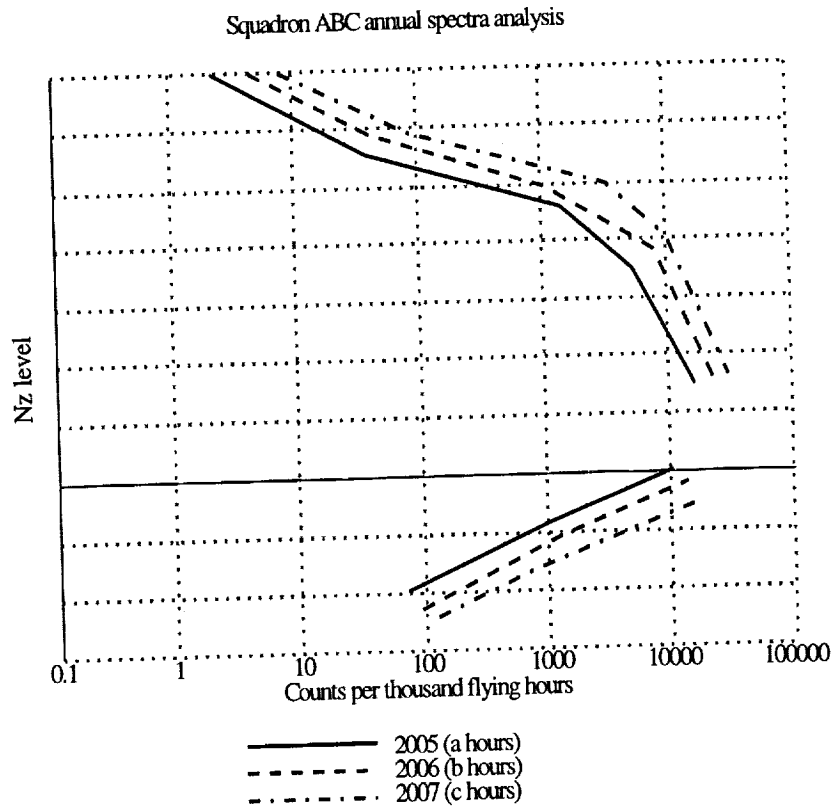


Figure 10. Typical ground analysis query

SHM data retrieved from the aircraft is electronically tied to the aircraft component and stores by the GSS. This allows the operator to query a component or store and retrieve the history of that component.

The system also allows the user to access the crash recorder data and BSD, if available, to display the significance of any event messages produced by the aircraft system.

3.2 SHM Up-load Data

The system controls the SHM definable data to be up-loaded onto the aircraft. This SHM data defines to the aircraft software the number and type (parametric or strain gauge) of fatigue locations to be monitored. The relevant structure and values of the stress templates for the parametric locations and the stress equations and sample rates for the strain gauge locations are also definable.

The SHM up-load data also defines to the aircraft software the number of parameter event envelopes to be monitored. The relevant parameters to be monitored and the event envelope corner points are also definable.

The ground system controls the preparation of the up-load file defining the data to be recorded on the bulk storage device. All data entering the IMRS system can be selected for recording (not just SHM specific) and their required recording rates and resolutions defined.

4. SYSTEM SUMMARY

The EF2000 SHM provides a complete structural health and usage monitoring facility incorporating:

1. Maximum automation on- and off-aircraft
2. Integration of the systems on- and off-aircraft for minimum maintenance
3. Minimum specialist training required for operators on the Base
4. 100% growth potential for on-aircraft system (processing and memory) at initial entry to service
5. Fatigue life consumption, stress spectra and parameter exceedance reporting available on a flight-by-flight basis for each aircraft.
6. Up to five flights of individual SHM data available for down-load to the GSS
7. Flexibility to alter the SHM locations (up to twenty) to either parameter based or strain gauge based calculations or a combination of both, without recourse to software change
8. Ad hoc facility for recording user selected flight parameter time histories
9. Tracking of aircraft components and stores

CONCLUSIONS

The EF2000 SHM is the latest in a line of monitoring systems (1) and supplies information never previously available on a fleet-wide basis. The system is designed to maximise the long-term benefits to the aircraft operator, and marks the initial phase of a BAe initiative aimed at exploring "smart" structural health monitoring systems for military combat aircraft.

ABBREVIATIONS

ACS	Armaments Control System
BSD	Bulk Storage Device
EF2000	Eurofighter 2000
FCS	Flight Control System
FUG	Fuel Gauging System
GSS	Ground Support System
IMRS	Integrated Monitoring, test and Recording Sub-system
MDP	Maintenance Data Panel
Nz	Normal Acceleration
p	Roll Rate
PMDS	Portable Maintenance Data Store
SHM	Structural Health Monitoring

LIST OF REFERENCES

- (1) Gill, L. and Wright, B.D., "Demonstration of the potential of Operational Loads Measurement", I. Mech. E. Aerospace Industries Division Seminar, Operational Loads Measurement", University Of Bristol, 1993

FSIP:

The C/KC-135 Functional Systems Integrity Program

Captain Jim Pappas
Structural and Mechanical Systems Engineer
C/KC-135 Systems Program Office
OC-ALC/LCRA Tinker AFB OK
Telephone: 405-736-3832
Fax: 405-736-5604
James.Pappas@tinker.af.mil

Mr. Ralph Ward
Principal Engineer C/KC-135 FSIP Program
Boeing Information Space & Defense Systems
Oklahoma City, OK
Telephone: 405-739-1488
Fax: 405-739-1416
Ralph.Ward@OKC.Boeing.com

Abstract

After several C/KC-135 mishaps in the early 1990's that resulted from system failures or malfunctions, the -135 System Program Director (SPD) recognized that a logical, organized, and disciplined approach to ensure or monitor the safety and durability of aircraft functional systems did not exist. This was true even though system failures or anomalies have caused most mishaps within the last five years involving USAF large body transport type aircraft. At this same time, HQ AMC/CC tasked the SPD's managing the aircraft within their command to develop a Functional Systems Integrity Program (FSIP) to ensure the safety and durability of aircraft systems much like the Aircraft Structural Integrity Program ensures the safety of aircraft structures. Since a generic FSIP process did not exist, the -135 SPD volunteered to develop a FSIP process which would be adaptable to all aircraft based on recent experience with analysis and problem resolution of -135 fuel systems. The requirement for a generic FSIP process was subsequently canceled. However, the -135 Board of Directors decided that any -135 sustainment program must include a thorough and pro-active evaluation of system integrity especially in the light of the aging problems, changing aircraft roles and missions, subtle system degradations that may have been induced during years of system sustainment, etc. Accordingly, the SPD tasked Coral Reach, the C/KC-135 Aging Aircraft Integrated Production Team (IPT), to develop and execute a FSIP process. Coral Reach then expanded their Integrated Product Team (IPT) with the -135 OEM to accomplish this effort. This paper presents the -135 FSIP process, and the activity and progress made to date.

Overview/Purpose:

The Functional Systems Integrity Program was developed in response to two high profile aircraft accidents in late 1993. The cause of each accident was traced to a fuel system related problem. The second accident, which claimed six lives, was the explosion and fire of a KC-135 Stratotanker due to a faulty fuel pump. After this accident the Commander of Headquarters Air Mobility Command (AMC), General Ronald Fogleman directed the AMC aircraft community to 'find the next fuel pump' before another accident occurred. As a result of such high level involvement, the Secretary of the Air Force for Acquisition (SAF AQ) made functional systems integrity a Program Objective Memorandum (POM) Initiative.

In September 1995 the C/KC-135 System Program Office began the initial groundwork to develop a health assessment model for the functional systems of the C/KC-135. Following the logic of existing integrity programs such as the Airframe Structural Integrity Program (ASIP) the Functional Systems Integrity Program (FSIP) was developed to provide a systematic approach of evaluating aircraft systems. Boeing, the OEM of the -135 was placed on contract to develop the FSIP model with initial delivery in December 1996 for validation and verification.

The purpose of FSIP is to PROACTIVELY ensure safety of flight for both the aircrew and aircraft, and ensure the durability of aircraft functional systems. FSIP focuses on the aging aspects of functional systems as airframes are continually flown well past their original intended design life. FSIP is intended to supplement existing integrity programs such as ASIP, ENSIP, and RCM, with a long-term goal of becoming as effective as ASIP.

Organization:

The FSIP team is organized under the Coral Reach Program, the aging aircraft program for the C/KC-135 SPO and is staffed by both government and contractor personnel forming an Integrated Product Team. Joint USAF and Boeing IPT co-chairs located at Boeing's Oklahoma City office and at Tinker AFB provide leadership for FSIP. Boeing maintains a staff of dedicated FSIP engineers at their Wichita offices and the KC-135 SPO provides a lead FSIP engineer. HQ AMC personnel at a Tinker AFB Operating Location (OL) provide direct representation for the using commands of the aircraft offering valuable expertise and work as a liaison to field level experts as needed. Other Air Logistics Centers provide support as required depending on the subsystem involved.

Objectives:

The "bottom line" objectives of FSIP are very straightforward:

1. Identify systems, subsystems, and/or functions that have a reduced safety margin due to aircraft age or changing roles and missions. In today's Air Force, current weapon

systems are repeatedly asked to fly beyond original service lives and to take on additional missions, most of which were never considered in the original design.

2. Identify single and multiple potential failures within functional subsystems and components that could jeopardize the safety of the flight crew (including maintenance personnel) and/or the aircraft.
3. Provide a *systematic* approach to review all systems, subsystems, and their functions. Without systematic guidelines to follow, considerable time is added to the execution of any task or procedure.
4. Risk management, reduce the at risk nature of operating an aging fleet of aircraft.

Other program specific objectives are also in place and are not germane to this paper.

The FSIP Process:

The FSIP process is a systematic approach to investigate each aircraft system for safety and durability problems/concerns. Each system was rank-ordered based on the GO-50 Health Of Weapon System Report plus a study conducted by the Flight Safety Foundation and published in Flight Safety Digest in December 1994¹. The GO-50 report gives an indication of overall systems health and performance by showing reliability data for each system by work unit code (WUC) and the Flight Safety Foundation report investigated the cause of most major jet transport accidents from 1958 to 1993. The study showed the number of accidents caused by each major system on an aircraft. Using this data the FSIP team rank ordered each C/KC-135 system in order of importance to determine which systems to investigate first.² The prioritization was completed in April 1996 and reaffirmed in May 1997.

At the initiation of an FSIP project, a detailed description of the system is developed. A system compliance check is then performed to ensure that every component listed by WUC for the system is an actual part of the system and that no component is left out of the system description (in case it is listed by another WUC.) A spreadsheet is then developed that contains all pertinent data for the system: components, part numbers, stock numbers, WUC's, engineering authority, and maintenance data such as Mean Time Between Failures (MTBF). The spreadsheet is used for tracking purposes to record all actions taken on a particular component.

After the system description is complete, the FSIP team takes a "big picture" approach to evaluate the system. The system is analyzed using Reliability Centered Maintenance (RCM) type criteria, which explores the consequences of each potential failure. The critical failures for the system are developed using Failure Effects and Modes Analysis (FEMA) and Failure Effects and Modes Criticality Analysis (FEMCA)

¹ See Appendix A

² Ibid.

data if available, and user inputs from both maintenance and flight crew personnel. For example a critical failure for the landing gear system is obviously the gear failing to extend and lock, however depending upon the timing of the failure, gear failing to retract may have a safety impact by distracting the flight crew. The failures are then tested against a set of questions to determine the criticality of each failure. The questions are as follows: Is there a direct impact on safety? Is there a loss of a redundant system and no notice of the loss to the crew? Could the timing of the failure have a direct impact on safety? Will the failure cause a secondary failure that has a direct impact on safety? These criteria are used to help eliminate components from consideration to ensure that only safety critical items are reviewed. At the initiation of the FSIP program, emphasis was placed on safety items first and review of durability items will commence after all systems have been reviewed for safety of flight concerns.

When the critical failures have been determined and prioritized, the system is evaluated to determine which components can cause the failures to occur, either directly or indirectly. These components are then flagged for closer scrutiny during the FSIP process. At any time components can be added or removed from the priority list based on any information obtained which would change the criticality of the component.

The FSIP process consists of five steps denoted as Task A through Task E.

Task A is a health assessment of the system. A system health baseline is established and system performance and usage is evaluated. All available safety data is accumulated and assessed for any obvious trends/problems. System requirements are evaluated against system performance, using both original requirements and any post production requirements. All available maintenance data is reviewed to determine if any trends or other health indicators exist.

Task B is a more detailed investigation covering many of the areas of Task A. Maintenance and safety records receive a detailed review to further explore any trends/indications of problems. The system is investigated to determine if any documented or undocumented changes have occurred since the original design and if these changes are adequate. User feedback data from overhaul facilities is solicited and evaluated. Detailed component studies such as condition inspections are done if deemed necessary.

Products from Task A and B are categorized as either "Significant Findings" or "Issues." Significant Findings are discoveries that may have an immediate direct safety impact. Issues are items that do not have an immediate safety impact but may become significant over time.

Any Issue or Significant Finding that warrants further action is tracked as a Task C effort. In Task C, candidate solutions are developed and evaluated. Possible solutions may involve simple changes to technical data or wholesale redesign of a system. If any new procurement is required, standard Air Force acquisition practices are followed.

Solutions are implemented through a Task D effort. Task D activities include production implementation, technical data changes, spares procurement, training, and any other documentation required. Health monitoring strategy for the solution is also developed at this time.

Task E efforts involve the long term health monitoring of each system and any solutions implemented in Task D. Any data requirements are evaluated and data collection devices are developed.

The Gaseous Oxygen System (GOx) was chosen to verify and validate (V&V) the FSIP model since it is non complex with very few moving parts. During the V&V process several changes were made to the FSIP model to streamline the process and guarantee the focus remains safety related, such as the inclusion of RCM logic when evaluating each system. Continuous improvement is an underlying goal of FSIP and the program is organized in an IPT structure to easily implement any changes that are required.

Findings to Date:

The evaluation of the GOx system is complete and work is currently in progress on the Landing Gear and Brake system and a few significant findings were discovered. During the GOx review the FSIP team discovered that the GOx system on the KC-135 does not have any type of pressure relief for the twelve storage tanks located in the aft fuselage. A problem may arise during any type of overheat condition such as a fire. The tanks could overpressure and rupture, which could injure personnel or increase the intensity of a fire. In the landing gear system the team discovered that the Landing Gear Emergency Extension (LGEE) system is not inspected for component wear. The LGEE is the backup system to extend the landing gear if the primary system fails and it was being treated as a fly-to-fail item. Through investigation of the braking system, the FSIP team discovered if the antiskid system is lost to one entire truck, the brakes on that truck may lock, potentially blowing all tires on that side of the aircraft. The pilot's ability to maintain directional control of the aircraft is diminished, potentially allowing the aircraft to depart the paved surface of the runway, an extremely unsafe situation.

Program Challenges:

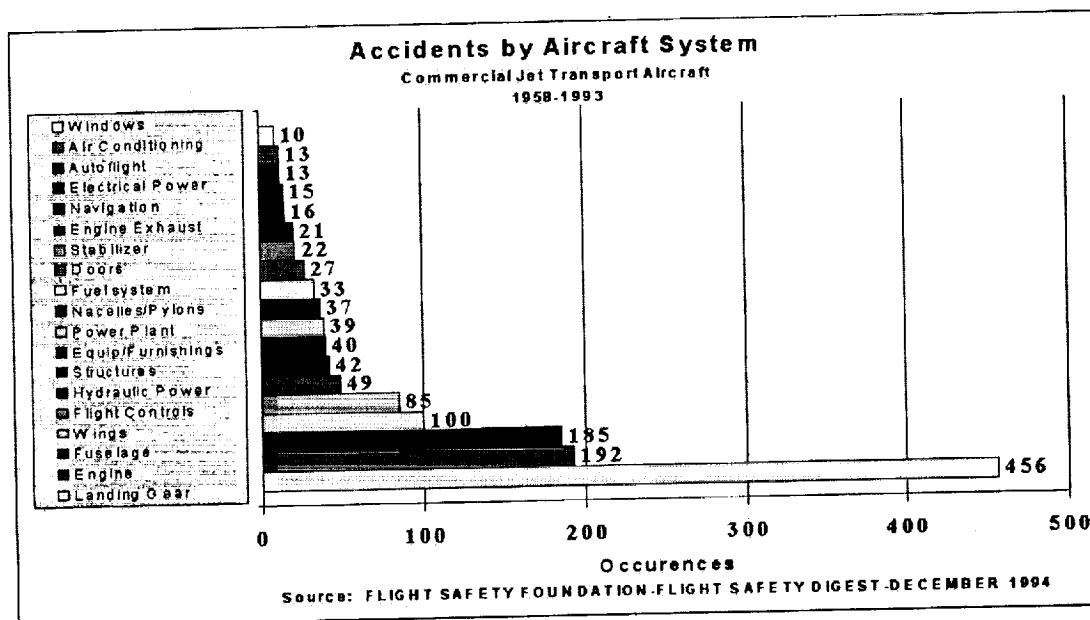
One of the toughest challenges for FSIP to overcome is the determination of what actually constitutes a serious safety problem. In the ASIP world, crack growth is very well understood and mathematical models exist that calculate how many cycles it will take for a crack to grow to the critical crack length for a given material. For FSIP, no such model exists, and modeling mechanical systems is still not yet robust enough to consider every possible failure mode of a system. Unless a "smoking gun" is found, the only tool available to make such determinations is often sound engineering judgement and practical experience. Once an item is called a significant finding, convincing the rest of the aircraft community of the importance of the finding is usually the most difficult part of FSIP.

Several programmatic challenges have also greeted the FSIP process and many more continue to surface as the program is executed. When conceived, no aging systems program was in place either in the Air Force or industry. All aging aircraft related activity revolved around fatigue and corrosion of the airframe so there was not a large database to draw upon as the FSIP model was developed. Until TWA Flight 800, all major aging related aircraft mishaps that received widespread attention involved structural failure of the airframe, and as with any mishap, the level of concern decreases after the investigation is complete. Accuracy of the available data can hamper investigation by increasing the time needed to review the data set. Access to vendor information is often limited due to proprietary rights and an atmosphere that FSIP investigators are "out to get" them. Many of these roadblocks will be easily overcome with more general acceptance of FSIP in both government and industry circles.

Summary:

The C/KC-135 Functional System Integrity Program was developed in response to ever increasing occurrences of safety and durability problems due to flying aircraft well beyond their original service lives. The effects of aging on aircraft functional systems is not well documented or understood in government or industry organizations which deal with flying operations on a day to day basis. The FSIP process provides a systematic approach to investigate aircraft functional systems and provides a health assessment to the operations and support communities while providing a means for long term monitoring of these systems.

APPENDIX A



Priority	Project	WUC
V&V	Oxygen System	47
1	Landing Gear	13
2	Fuel System	46
3	Flight Control	14
4	Hydraulic & Pneumatic Power Supply	45
5	Instruments	51
6	Airframe: Non ASIP	11
7	Autopilot	52
8	Turbojet/Turbofan Power Plant	27
9	Cockpit & Fuselage Compartment	12
10	Engine: Non ENSIP	23
11	Electrical Components	42
12	Air Conditioning, Pressurization, & Surface Ice Control	41
13	Radar Navigation	72
14	Aux. Power Plant	24
15	Interphone	64

Table 1 C/KC-135 System Prioritization List

AN APPLICATION OF FRACTURE MECHANICS PRINCIPLES IN DETERMINING A SERVICE LIFE ENHANCEMENT INTERVAL FOR THE US NAVY'S C-2 OUTER WING

Alex R. Hocson and Tommy N. White
Office of Research and Engineering
Naval Aviation Depot North Island
San Diego, California, 92135, USA
(619) 545-3922
(619) 545-4765
white_t@a1.nadepni.navy.mil

ABSTRACT

The Navy's C-2 aircraft have suffered unaccounted fatigue damage from a phenomenon not considered a likely source during the original design and determination of their service life. This phenomenon, the addition of spectral loading caused by thermal expansion of the outer wing panels (OWP's) in a stowed condition when exposed to turbine engine exhaust, produced compressive field stresses in the wing's lower skin. These compressive stress magnitudes were as much as 30 to 40 percent of the lower skin field stresses experienced from maximum service loads. As such, this unaccounted condition has diminished the projected useable life of the affected structure. Structural enhancements to extend the wing's fatigue life are being developed and tested to establish an extended service life. This effort requires a corrected useable life for the original design so as to establish a suitable life interval for enhancement incorporation. Since fleet requirements preclude the time necessary to accomplish an additional fatigue test incorporating the thermal loading, a tear down examination of several relatively high service time outer wing panels was elected as a representative and conservative sample of fleet assets. The tear down revealed small embedded cracks, less in size than what is normally accepted as an initial flaw size for damage tolerance philosophy. Because safe life predictions incorporating thermal expansion effects were considerably less than the tear down specimen lives, a life to a removable flaw size, was desired for establishing an enhancement life. To accomplish this, a modified damage tolerance approach was adopted. To obtain the required life, crack growth data from thermally adjusted spectrum tested coupons was used. The life for a flaw equivalent to the tear down findings to grow to a removable, thus repairable flaw size, was determined and combined with the thermally adjusted life of the full scale fatigue test (FSFT) article. This combined life was then factored with the appropriate scatter factors, as dictated by Navy safe life policy, to obtain a life interval needed to define the enhancement schedule.

INTRODUCTION

According to safe life philosophy as practiced by the US Navy, aircraft and their component service lives are primarily determined from FSFT's. The method is to obtain crack initiation lives by adjusting test lives to remove any crack growth contribution beyond a predetermined crack size. Where upon, an appropriate life reduction factor is applied to correct for statistical scatter in order to define the service lives. As such, in this time of austere resources, alternate approaches are sought to maintain reliable service of the fleet. A natural extension of this accepted method is applied here.

1. BACKGROUND

1.1 CONFIGURATION

The current version of the C-2A (Greyhound) aircraft outer wing panel (OWP) has a structural configuration identical to the current E-2C (Hawkeye) OWP, see figures 1 and 2. Both aircraft OWP attachment structures are also identical and are made up of mating lug and clevis assemblies for the forward, main, and aft beam, upper and lower caps. The aft beam attachments act as a hinge arrangement for stowage when the main and forward beams attachment pins are extracted hydraulically. As well, both aircraft stow the OWP in the same fashion. This is by rotating and folding the OWP leading edge down and lower side aft about the hinge design of the rear beam attachment via hydraulic actuation. A lock mechanism in the panel contacts a mating device on the outboard vertical fins to lock the OWP in it's stowed position. Since the turboprop propulsion system mounts in an under wing nacelle located just inboard of the OWP fold joint, the stowed position of these OWP's places the lower cover into the turbine engine exhaust stream, as shown in figure 3.

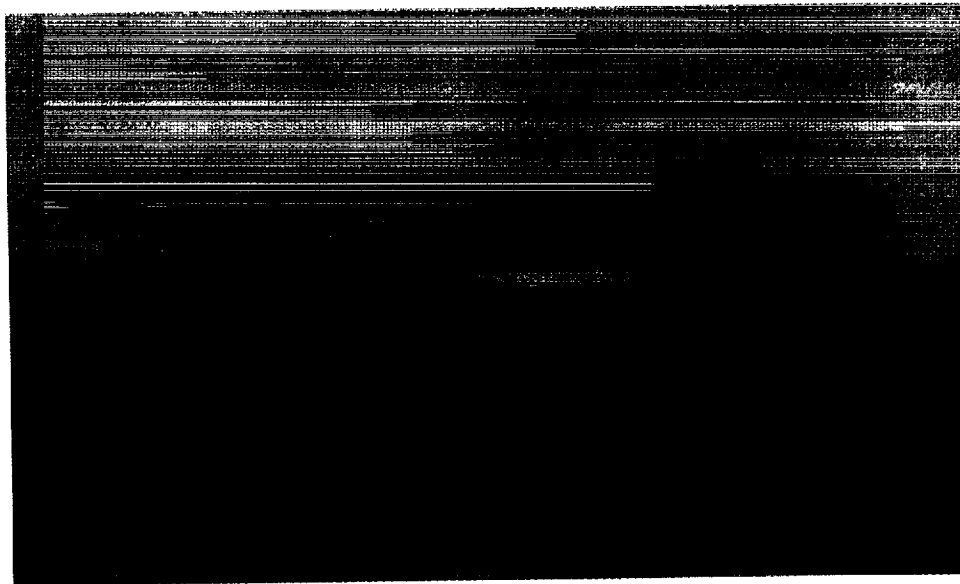


Figure 1. C-2A(Reprocured) Configuration (Wings Extended)

1.2 SERVICE LIFE

The original design specifications for both the E-2C and C-2A(R) aircraft specified a 10,000 flight hour service life for the aircraft including its major structural components.¹ Analytical assessment of the E-2C FSFT revealed that the OWP configuration required enhancement to reach a test goal needed to demonstrate a 10,000 flight hour service life.^{2,3} Early fleet incorporation of this enhancement revealed cracks in OWP's at lives far short of design life. Subsequent destructive examination of two of these E-2C OWP's with crack sizes which exceeded repair and enhancement limits substantiated that the OWP lower cover fatigue life was below design life.^{4,5} Later C-2A OWP tear downs have produced similar findings.⁶

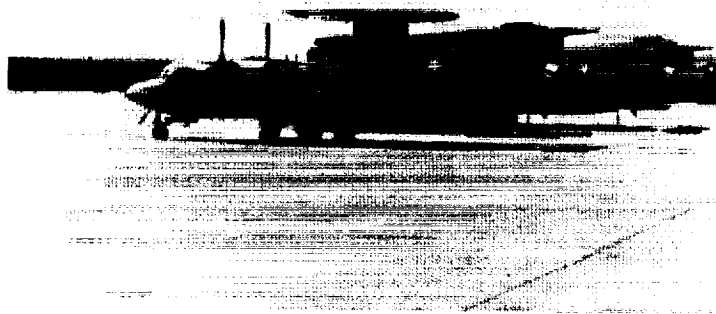


Figure 2. E-2C Configuration (Wings Folded)

1.3 INVESTIGATION

The results of continued contractor investigations into the reason for this lower than expected life, proposed that thermal expansion of the OWP lower cover produced additional damaging stress excursions in the spectrum. This thermal exposure to the OWP lower cover occurs from the impingement of turbine engine exhaust on the lower cover with the OWP in a stowed position. Subsequent OWP lower cover thermal and strain surveys taken during engine exhaust impingement for both E-2C and C-2A have shown that peak temperatures in the range of 280 degrees Fahrenheit.⁷ Thermal analysis of temperature profiles predict compressive stresses at a maximum magnitude of 16 Kips per square inch (Ksi), about 40 percent of the maximum tensile operating stress magnitude, were observed.⁷ However, follow on metallurgical analysis of coupon specimens taken from tear down and surveyed OWP assets showed inconclusive evidence of over aging or material property alteration due to the thermal exposures.⁶ This increase in the stress excursion adds to fastener hole notch stresses thus their fatigue damage accumulation rates.⁸



Figure 3. Exhaust Residue on stowed E-2C Outer Wing

1.4 LIFE EXTENSION

Improvements to the E-2C's OWP's limited service life had been provided in the way of structural fatigue enhancements.⁹ However due to the advent of new requirements, introduced by Health of Naval Aviation (HONA), E-2 and C-2 service was extended to the year 2015. An OWP service life extension, requiring additional enhancements, is in development to reach these new goals. These enhancements, in the form of hole cold working and interference fit fasteners, extend the fatigue life of the affected structures by providing a means to reduce the fastener hole notch stress, cyclic damage. The enhancement is applied by first removing any detectable crack damage through machining. Next hole cold working is accomplished, then an additional ream is applied to remove undetectable damage beyond the crack removal. Finally interference fit fasteners are installed to provide maximum fatigue life enhancement. The key to extracting the maximum benefit from these enhancements is the timing of their incorporation. If applied early when the accumulated fatigue damage is too little, then the total life improvement benefit is limited primarily to the enhancement life. If the enhancement is applied late when accumulated damage is too great, then the condition is non-repairable and the enhancement provides little benefit. This is primarily due to reduced ligaments from damage removal using extended hole sizes. Suitably, the enhancements incorporation should be timed to allow the most removal of prior accumulated damage while restoring the structure to a new fatigue life based on the enhancement life. This provides an optimally extended, total life which includes the enhanced life plus all previously accumulated life.

2. ANALYSIS

2.1 FLEET SAMPLING

As referenced in the background of this paper, destructive examination of select C-2 OWP's removed from service revealed early evidence of accumulated fatigue damage.⁶ The most significant damage detected was noted in fastener holes along the main beam lower cap, aft horizontal flange where the higher compressive stresses from thermal expansion were predicted, see figure 4.¹⁰ These predictions were based on earlier thermal measurements made on E-2C aircraft as well as later C-2A thermal measurements.⁷

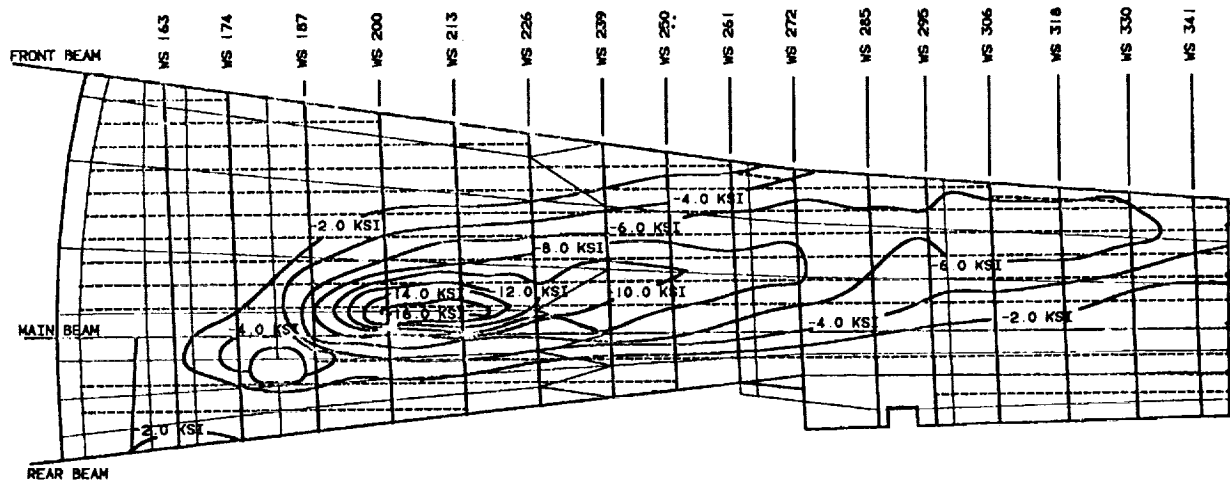


Figure 4. Typical Thermal Expansion Stress Contours for E-2 & C-2 Outer Wing Lower Covers

2.2 LIFE DETERMINATION

Maximization of the OWP service life to accommodate the HONA goals requires some innovation. First, a repairable crack size is determined for the structure being assessed. In the case of the C-2A OWP the maximum allowable crack is that which is removable by machining the fastener hole to a one sixteenth inch larger in diameter. This provides for a 0.032 inch allowable crack size. Next, crack growth lives are determined by applying the defect sizes discovered from C-2A(R) tear down (0.007 inch) as initial crack sizes with a 0.032 inch crack size as a final crack size to coupon developed crack growth curves which produced an additional 1900 unfactored flight hours, figure 5.¹¹ The crack growth life obtained here is reduced for statistical scatter by applying a reduction factor of two then combined with the thermally adjusted analytical FSFT life which is factored by four to define a new service life.

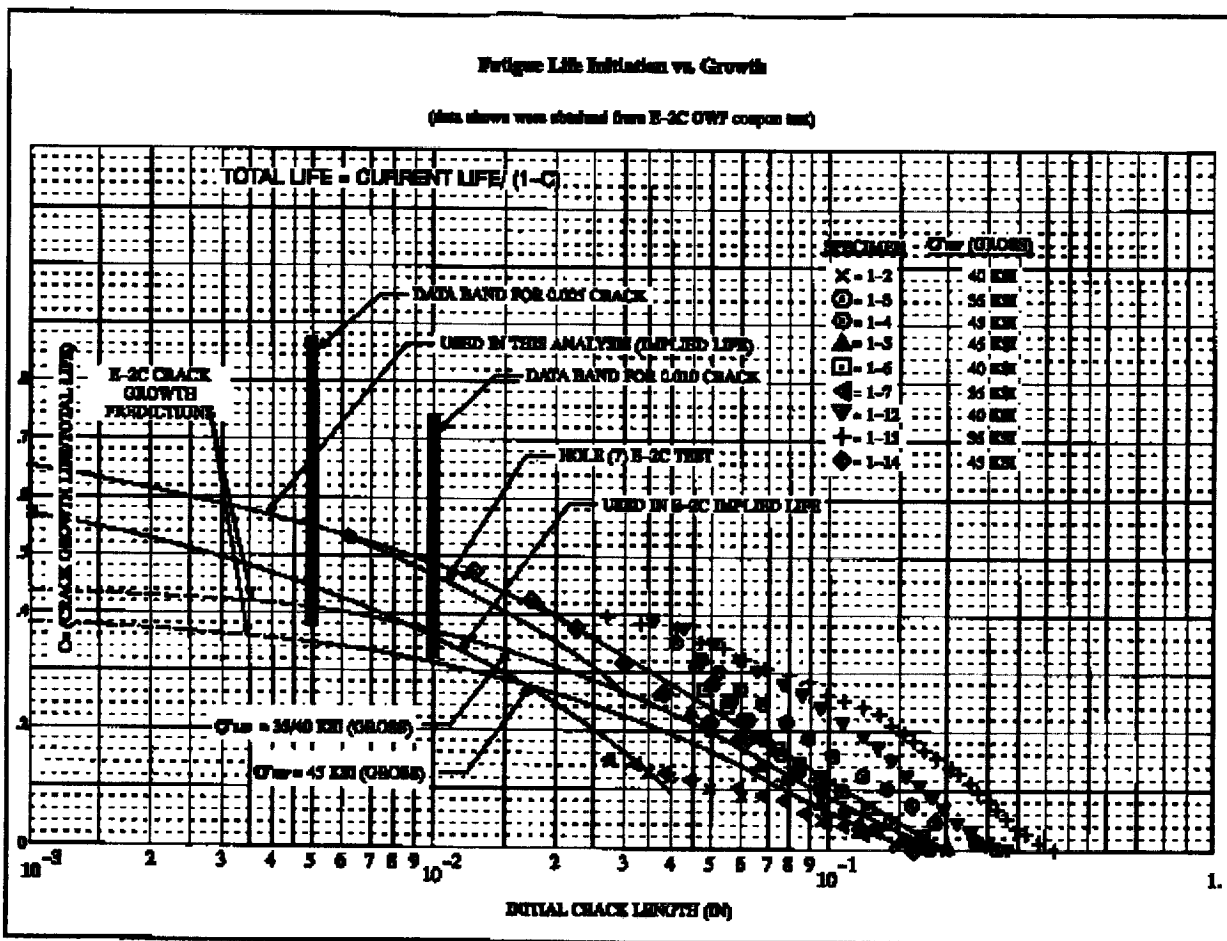


Figure 5. E-2C Outer Wing Fatigue Coupon Crack Growth Data

2.3 ANALYTICAL NOTES

Extrapolation of the crack growth curves is required for the small initial crack sizes. Although small cracks do not grow as do larger cracks like those studied in the referenced coupon test, this approach is considered conservative since the small cracks are seen to grow at decreased rates over that of those larger coupon cracks. This is evident by the fact that the stress intensity for small elliptically shaped cracks is inversely dependent on both the value of the elliptical integral of the second kind and the shape factor for part through elliptically shaped cracks.¹² Both values are found to be greater than 1.0, which have the effect of reducing the stress intensity and in turn providing a lower da/dN for crack growth rates. Also, it can be seen that there are values for shape factors for these part through cracks which approximate through cracks. Since the initial cracks were many smaller cracks which have linked up, they produced cracks which were very shallow compared to their total length on the surface of the fastener hole, i.e. depth to length (a/c) \sim 0.25 or less, so their shape factors are very close to 1.0 thus causing their growth rates to behave much more like through cracks.

2.4 FLEET RESTRICTIONS

This extended life for OWP's is applied with a flight restriction on future service to provide an added conservatism. A vertical acceleration limit of 3.3 times the acceleration of gravity (g 's) for C-2A (R) aircraft was reduced to 2 g 's.

CONCLUSIONS

The new service life, up to the enhancement interval, can be and is determined by combining the appropriately factored individual crack growth and initiation portions. This extension of service life is applied along with the added conservatism of limiting vertical accelerations during flight. Although simply an extended application of practices currently being used, this approach can add a much needed service life extension however small to systems suffering urgent requirements and tight schedules required to prolong their service life.

ACKNOWLEDGMENTS

Credit is extended to James Candela of the Naval Air Systems Command for suggesting this approach, and Randy Lefler also of the Naval Air Systems Command for the executing of the approach. Special thanks is extended to Leigh-Ann Waughtel of Naval Aviation Depot North Island for the appropriate and timely dissemination of the newly established service life to our fleet. A special credit is extended to the co-author Alex Hocson for managing, executing, and reporting the findings of the several C-2 tear downs and examinations conducted to assess the health of our fleet. Also, much thanks to my associate, Tracie Okada, of the Naval Aviation Depot North Island, San Diego, California for her unfailing efforts to provide quality support for those last minute issues.

REFERENCES

1. "C-2A(Reprocured) Design Specification," Naval Air Specification SD-551-1-3, 17 August 1981 and "E-2C Design Specification," Naval Air Specification SD-527-2-6, 12 January 1978.
2. "Summary - Structural Fatigue Life E-2C Airplane," Grumman Report No. 3821.2A, 19 August 1985.
3. "E-2C Airframe Change No. 353," Naval Air Technical Directive.
4. "E-2C, Aircraft No. A-33 Outer Wing Panel Tear Down Inspection Report," Grumman Report No. AV123-U-RP-280, 28 February 1989.
5. "E-2C, Aircraft No. A-26 Outer Wing Panel Tear Down Inspection Report," Grumman Report No. AV123-U-RP-281, 7 April 1989.
6. "C-2A(R) Outer Wing Panel (OWP) Tear Down Inspection Report for S/N A1-G77-008 (Port), BUNO 162147, S/N A1-G77-015 (Stbd), BUNO 162154, and Heat damage Evaluation of Ten Selected C-2A (SLEP) and E-2B OWP's," Naval Aviation Depot Aeronautical Engineering Report No. 001-96, 8 February 1996.
7. "C-2A(R) Outer Wing Panel Thermal Heating Differences Due to High Speed Ground Idle and Low Speed Ground Idle with the Wing Folded," Grumman Report No. 3807.21G Appendix A, 29 Jan. 1993.
8. "C-2A(R) Outer Wing Panel Thermal Analysis Fatigue Life Curves," Grumman Report No. 3807.21G Appendix C, 13 January 1995.
9. "E-2C Airframe Change No. 378," Naval Air Technical Directive, Preliminary.
10. "C-2A(R) Outer Wing Panel Fatigue Analysis Including Thermal Effects," Grumman Report No. 3807.21G, Appendix D, 15 April 1995.
11. "C-2A(R) Outer Wing Panel (OWP) Fatigue Analysis of Selected Tear Down Holes"- Northrop Grumman Corporation, Appendix A of Report No. 3807.21G APP.D Rev. B, 31 May 1996.
12. "Stress Intensity Factors for a Wide Range of Semi-Elliptical Surface Cracks in Finite Thickness Plates," *Engineering Fracture Mechanics*, Volume 11, 1979, p 817-829.

DETERMINING AND ATTAINING REALISTIC INSPECTION THRESHOLDS TO MEET DURABILITY AND DAMAGE TOLERANCE REQUIREMENTS

Len Reid Coauthor, Jude Restis Coauthor
Fatigue Technology Inc.
Seattle, Washington 98188, USA
Telephone: 206-246-2010
Fax Number: 206-244-9886
E-mail: Engineering@fatiguetechnology.com

Tom Swift Coauthor
Fatigue Technology Inc. Consultant

ABSTRACT

A recent revision to the regulations governing fatigue and damage tolerance for commercial aircraft (FAR 25.571 amdt. 96) requires inspection thresholds for certain types of structure based on crack growth from likely initial defects. The industry challenge is how to economically achieve these requirements in new design.

For certain situations, the USAF currently allows the damage tolerance analysis to take credit for fatigue enhancement fastening systems and cold expanded holes by assuming a smaller initial flaw size. Testing and in-service experience has shown this method to be conservative. More quantitative means of accounting for the benefits of these fatigue-enhancing processes is needed. A method of determining a "modified" stress intensity factor for fastener holes that have been processed to be fatigue resistant, using split sleeve cold expansion, was developed by Boeing Wichita. This paper compares the smaller initial flaw size concept and the Boeing method for predicting crack growth life with hole cold expansion to determine inspection thresholds.

1. BACKGROUND AND INTRODUCTION

FAR 25.571 states that for fail-safe structures with large damage crack arrest capability, the inspection thresholds can be established using either fatigue analysis or crack growth methods assuming initial manufacturing flaws. For single load path structures or multiple load path structures which behave like single load path structures, when the proper cracking scenario is considered, the inspection threshold must be based on crack growth assuming initial manufacturing flaws.

All of the current aging fleet of commercial transport aircraft was certified to be fail-safe based on the single principal structural element failure concept at limit load. However, there are a number of locations on these aircraft that behave like single load path structures when the proper fatigue-cracking scenario is considered. Under the new requirements the thresholds for these areas will have to be based on crack propagation analysis assuming appropriate initial manufacturing damage. In the past, particularly on military aircraft, appropriate initial manufacturing damage has been simulated by assuming that a 0.050-inch radius corner crack exists at a fastener hole in the most critical location in each principal structural element. This initial crack has become known as the "rogue flaw." In addition, 0.005-inch cracks have been assumed to exist at each fastener hole, representative of equivalent initial quality, for continuing damage calculations. The rogue flaw and continuing damage flaw sizes have been assumed in the absence of specific data for the particular fastening system used. When fatigue enhancement fastening systems have been used, the Air Force has allowed smaller initial crack sizes to represent the rogue flaw. For example, on the KC-10 program in areas where Gemcor rivets or fasteners in interference fit holes were

used, the Air Force allowed 0.030-inch radius cracks to be used to represent the rogue flaw. In the case of cold expanded holes the rogue flaw has been simulated by 0.005-inch corner cracks. These reduced crack sizes have been used merely as an analytical expedient to simulate the rogue flaw due to the complexity of calculating crack tip stress intensity factors in the residual stress field surrounding the fasteners.

Several attempts have been made in the past to calculate stress intensity factors in the complex residual stress field created by cold expansion [1-4]. However, to simplify the analysis most manufacturers, on both military and commercial programs, have used the 0.005-inch crack. Testing and in-service experience has shown this method to give very conservative predictions of fatigue life improvement.

Fatigue Technology Inc. (FTI) has been investigating an engineering approach to account for the effects of hole cold expansion (Cx), which is more satisfactory than using the arbitrary 0.005-inch crack to determine inspection thresholds. Boeing Wichita has developed an engineering approach to account for the effects of hole cold expansion in relatively simple analytical methods, which will account for both the degree of cold work and fastener edge distance effects. This paper will discuss the development of this approach.

2. CRACK RETARDATION THROUGH HOLE COLD EXPANSION

Generation of permanent compressive stresses around holes has long been recognized as a means to extend fatigue life, by retarding crack growth [5]. Split sleeve cold expansion generates a large controllable residual compressive stress zone around and through the total depth of the hole [6]. These compressive stresses reduce the effective crack opening displacement. The primary effect is to retard the crack growth rates by reducing the stress intensity factor range (ΔK) and the stress ratio (R). Additionally, the presence of residual stresses may change the critical crack length for unstable fracture, because it reduces the static stress intensity factor. The resultant reduction in crack growth rate and the increased critical crack length significantly improves the damage tolerance of the structure.

These life improvement benefits have been utilized to reduce/eliminate frequent inspections. However, the life improvement factor applied is often very conservative and considered inadequate because it is generally determined by a small number of test specimens. An alternate analytical method to the commonly used smaller initial flaw size (typically 0.005 inch) is needed, which would compensate for actual structural geometry and variations in the amount of cold expansion (applied expansion).

3. EXISTING METHODOLOGY FOR IMPLEMENTATION OF SPLIT SLEEVE COLD EXPANSION IN DAMAGE TOLERANT DESIGN

Although damage tolerance specifications have long been in place for both commercial and military aircraft, there are no consistent rules as to how to incorporate the beneficial effects of hole split-sleeve cold expansion in damage tolerance design. To date, the best available guidelines are found in the USAF specifications, such as MIL-A-83444 (Section 3.1.1.1, paragraph c). These guidelines essentially state that cold expansion can be used to comply with flaw growth requirements for fastener holes provided the benefits from this process are demonstrated by laboratory testing of joints with precracked holes. The specimens must be representative of the actual structure.

Because cold expansion residual stresses and their effect on fatigue life are difficult to predict analytically, the USAF damage tolerance specifications allow the design of a cold expanded (Cx) hole to be based on analysis for the same size non-cold expanded (NCx) hole with a reduced initial assumed flaw size and considered as a filled hole, under non-clamped up joint conditions. The assumed initial flaw

cannot be smaller than a 0.005-inch radius corner flaw on one side of the hole. In contrast, the typical assumed initial flaw geometry for a non-cold expanded hole is a 0.050-inch radius corner flaw.

The assumed initial flaw size for a cold expanded hole is dictated by considerations such as material characteristics, hole geometry, fastener type and fitup (if applicable), loads, and cold expansion parameters. A commonly used technique for determining the assumed initial flaw size for a cold expanded hole is illustrated in Figure 1 for a 2024-T3 aluminum test coupon with a 5/16 inch nominal diameter hole (FTI internal test data). Other design considerations such as structural weight growth potential can be factored in by increasing the initial flaw size beyond the value calculated by this method.

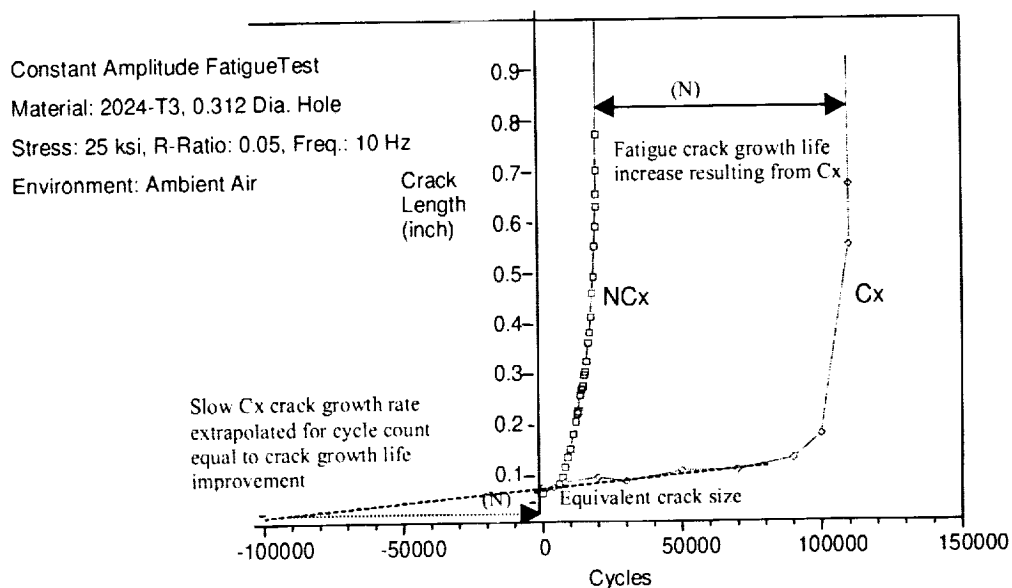


Figure 1. Calculation of Equivalent Cx Initial Flaw Size (Example)

Once an initial flaw size has been defined, a flaw growth analysis can be used to build a crack growth curve for the cold expanded hole condition, and establish the proper inspection intervals. The general practice is to then validate the analysis by fatigue testing of representative sub-elements or full-scale components using the standard initial flaw size (e.g., 0.050-inch corner crack) on the cold expanded holes. Figure 2 shows how this approach compares with actual test data taken from [7] for a standard 0.050-inch through-the-thickness crack in specimens with non-cold expanded (NCx) and cold expanded (Cx) holes. The typically high degree of conservatism resulting from the use of a reduced initial flaw size approach is apparent in these results.

By using this reduced initial assumed flaw size approach, the structural designer does not need to have a precise knowledge of the magnitude and extent of the residual stresses surrounding the cold expanded hole. Furthermore, this technique facilitates damage tolerance analysis tasks by enabling the use of stress intensity factor and crack growth formulations normally used for non-cold expanded holes. The drawback of this approach is that the size of the assumed initial flaw is arbitrary, and therefore that size must be carefully selected.

Despite the high degree of conservatism inherent to the assumed initial flaw size range permitted by USAF specifications, MIL-A-87221 (Appendix Section 3.12.1, para. G) cautions that "to maximize safety of flight and to minimize the impact of potential manufacturing errors, it should be a goal to achieve compliance with the damage tolerance requirements of this specification without considering the

beneficial effects of specific joint design and assembly procedures such as interference fasteners, cold expanded holes, or joint clamp up.”

This recommendation stems from a concern that poor airframe manufacturing and assembly practices involving cold expansion could result in ineffective processing. However, with proper training and certification of shop floor personnel involved in cold expansion processing, strict adherence to cold expansion specifications, and the use of certifiable tools and equipment (all of which FTI strongly advocates), the risks associated with use of this process are negligible, and compliance with the aforementioned goal in MIL-A-87221 should no longer be necessary.

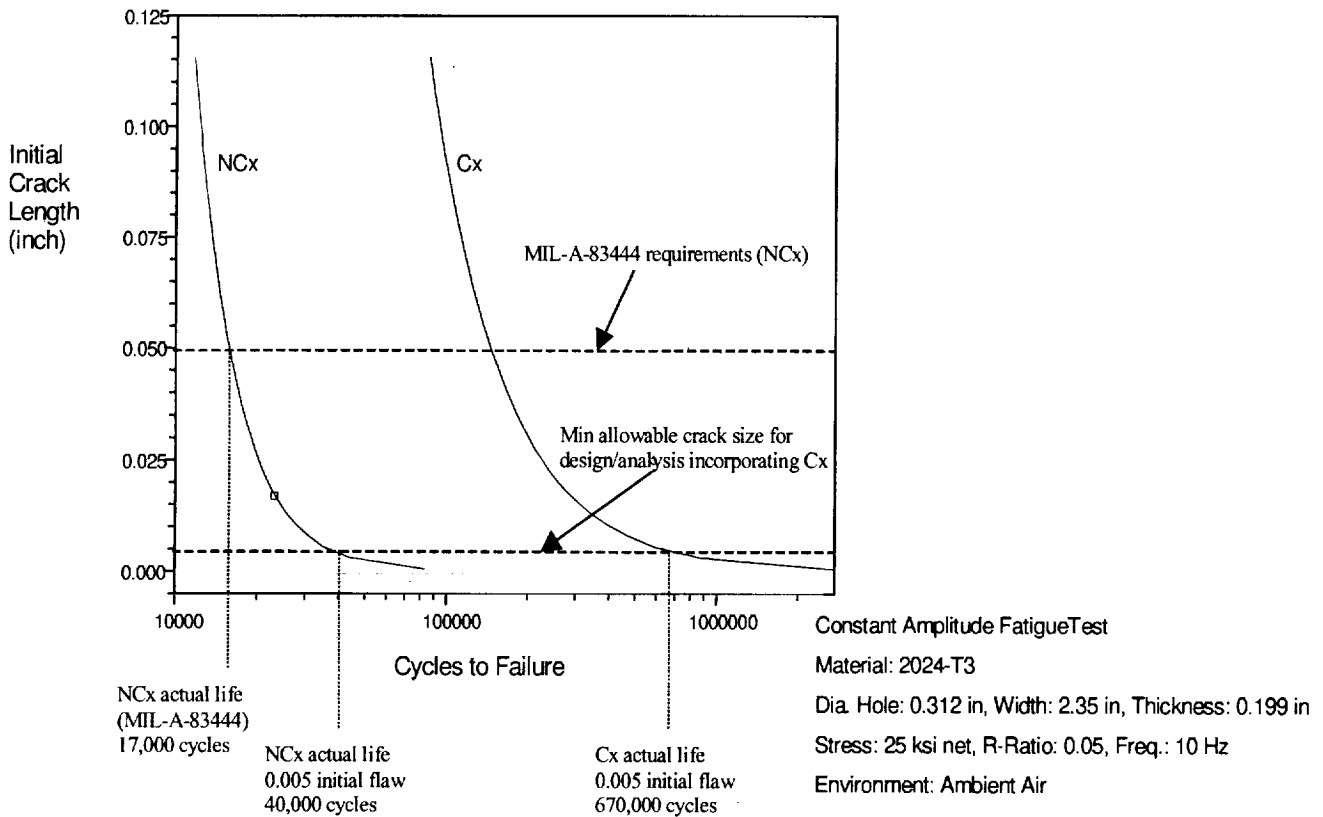


Figure 2. Reduced Initial Flaw Assumption vs. Test for Precracked Cold Expanded Holes

4. PROPOSED NEW METHODOLOGY

The revised requirements of FAR 25-571 to establish inspection thresholds for certain types of structures based on crack growth from initial flaws/defects, will encourage manufacturers/repair facilities to incorporate fatigue enhancing methods in the design of critical locations. Methods such as hole cold expansion will be beneficial in attaining realistic inspection thresholds or indeed could eliminate inspection requirements.

A convenient analytical method to account for the beneficial effects of hole cold expansion is required by industry. One such method was developed by Boeing Wichita for the USAF B52G/H Strut Front Spar Life Improvement Program [8]. The approach assumes a modifier to the stress intensity factor for the cold

expanded hole. This modifier assumes the ratio of β for the cold expanded hole to the non-cold expanded hole varies exponentially from zero at the edge of the hole to 1.0 at the free edge of the component. (Refer to Figure 3.)

The stress intensity factor $K = \sigma[\pi a]^{1/2}\beta$ in general. Equation (1)

Where

σ = applied gross stress

a = crack size

β = effects of geometry

The modifier takes the form $\beta_{Cx}/\beta_{NCx} = 1 - [(1 - a^m/b^m)e^{-a/b}]$
Equation (2)

Where

β_{Cx} = effect of geometry and residual stress field for the cold expanded hole

β_{NCx} = effect of geometry for non-cold expanded hole

a = crack size

b = distance of hole boundary to free edge

m = exponent F (% cold expansion)

F = empirical factor obtained from crack growth tests

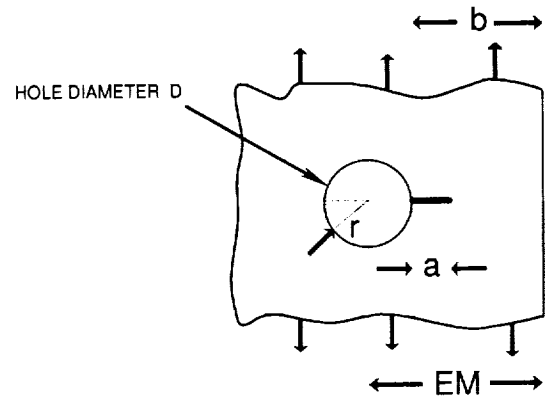


Figure 3. Single Crack at Hole Propagating Toward a Free Boundary

The empirical value F is obtained from crack growth tests and then multiplied by the percentage of cold expansion to form the empirical exponent m . For example, in the Boeing study the value of F was determined to be 0.1167. For 2% cold expansion the value of m would be $2(0.1167) = 0.2334$.

The exponent m in equation (2), obtained from crack growth test results, controls the ratio of crack tip stress intensity factors for the cold expanded hole relative to the non cold expanded hole β_{Cx}/β_{NCx} . An example of how this ratio varies with the ratio of crack size to ligament size a/b is illustrated by Figure 4.

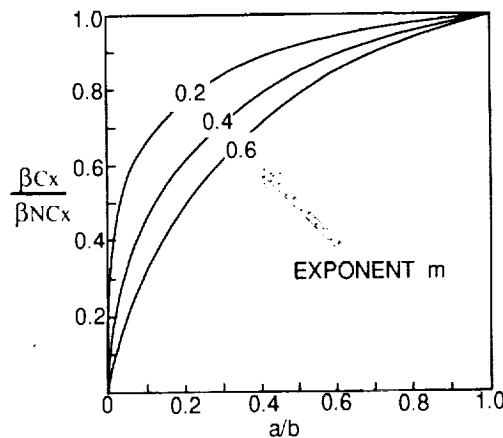


Figure 4. Example of the Influence of m in Equation (2)

An example problem will be considered for illustration purposes.

Example problem (Reference Figure 5.)

Assumptions:

Hole diameter $D = 5/16 = 0.3125$ inches

Edge Margin $EM = 2d = 0.625$ inches

$b = 0.625 - 0.15625 = 0.46875$

Percent cold expansion 2%, 3% and 4%

$m = (0.1167)^2, (0.1167)^3$ and $(0.1167)^4$

(From Boeing Tests)

$b^m = 0.83791$ for 2%

0.76700 for 3%

0.70209 for 4%

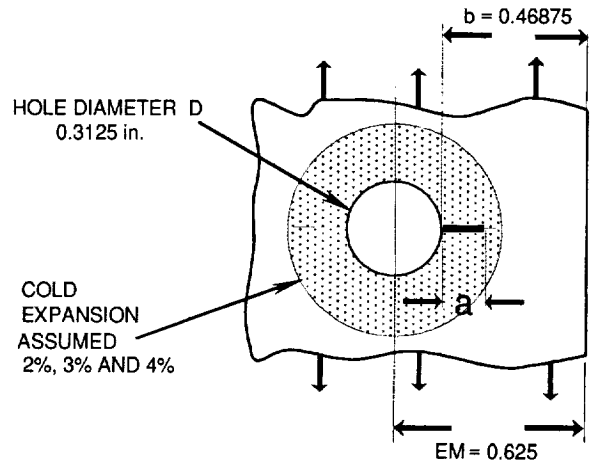


Figure 5. Example Problem

$$\beta_{Cx}/\beta_{NCx} = 1 - [(1 - a^{0.2334}/0.83791)e^{-a/0.46875}] \text{ for 2\% cold expansion}$$

$$\beta_{Cx}/\beta_{NCx} = 1 - [(1 - a^{0.3501}/0.76700)e^{-a/0.46875}] \text{ for 3\% cold expansion}$$

$$\beta_{Cx}/\beta_{NCx} = 1 - [(1 - a^{0.4668}/0.70209)e^{-a/0.46875}] \text{ for 4\% cold expansion}$$

These values are calculated in Table 1.

In order to further illustrate this method β_{NCx} will be determined for a through crack using the Bowie solution for the effect of the hole and the Feddersen solution for the free boundary effect.

For the non cold expanded hole:

$$\beta_{NCx} = \beta_b \beta_f$$

β_b is shown in Figure 6

$$\beta_f = [\text{Sec } \pi(a+r)/2EM]^{1/2}$$

β non-cold expanded hole:

$$\beta_{NCx} = \beta_b [\text{Sec } \pi(a+r)/2EM]^{1/2}$$

$$2EM = 1.25$$

(Calculated in Table 2.)

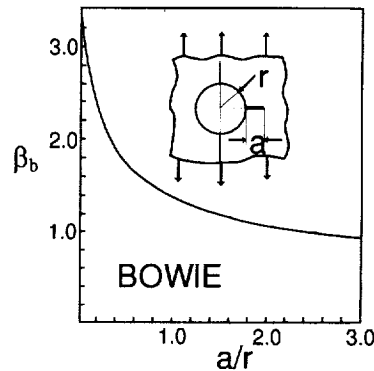


Figure 6. Bowie Solution for Single Crack

Values of β_{Cx} for the three percentages of cold expansion are calculated in Table 3 and shown on Figure 7 for illustration purposes.

TABLE 1. VALUES OF β_{Cx}/β_{NCx}

a	a/b	β_{Cx}/β_{NCx} 2% Cold Expansion	β_{Cx}/β_{NCx} 3% Cold Expansion	β_{Cx}/β_{NCx} 4% Cold Expansion
0.00	0.0	0.0	0.0	0.0
0.01	0.0213	0.41989	0.27564	0.18357
0.02	0.0427	0.50069	0.35936	0.26155
0.03	0.0640	0.55581	0.42030	0.32197
0.04	0.0853	0.59876	0.46970	0.37286
0.05	0.1067	0.63429	0.51175	0.41737
0.10	0.2133	0.75543	0.66250	0.58490
0.15	0.3200	0.83043	0.76113	0.70046
0.20	0.4267	0.88233	0.83171	0.78588
0.25	0.5333	0.91995	0.88411	0.85082
0.30	0.6400	0.94784	0.92373	0.90084
0.35	0.7467	0.96876	0.95392	0.93958
0.40	0.8533	0.98452	0.97699	0.96960
0.45	0.9600	0.99637	0.99457	0.99278
0.46875	1.0000	1.00000	1.00000	1.00000

TABLE 2. NON-COLD EXPANDED HOLE β_{NCx}

a	a/r	β_b	(a+r)	(a+r)/2EM	β_f	β_{NCx}
0.0	0.0	3.39	0.15625	0.125	1.0404	3.527
0.01	0.064	2.86	0.16625	0.133	1.0460	2.992
0.02	0.128	2.56	0.17625	0.141	1.0521	2.693
0.03	0.192	2.30	0.18625	0.149	1.0586	2.435
0.04	0.256	2.12	0.19625	0.157	1.0655	2.259
0.05	0.320	1.98	0.20625	0.165	1.0730	2.125
0.10	0.640	1.60	0.25625	0.205	1.1183	1.789
0.15	0.960	1.39	0.30625	0.245	1.1800	1.640
0.20	1.280	1.25	0.35625	0.285	1.2646	1.581
0.25	1.600	1.15	0.40625	0.325	1.3834	1.591
0.30	1.920	1.08	0.45625	0.365	1.5589	1.684
0.35	2.240	1.02	0.50625	0.405	1.8442	1.881
0.40	2.560	0.98	0.55625	0.445	2.4117	2.363
0.45	2.880	0.94	0.60625	0.485	4.6074	4.331
0.46875	3.000	0.94	0.62500	0.500	∞	

TABLE 3. β COLD EXPANDED HOLE

a	2% Cold Expansion			3% Cold Expansion			4% Cold Expansion		
	β_{Cx}/β_{NCx}	β_{NCx}	β_{Cx}	β_{Cx}/β_{NCx}	β_{NCx}	β_{Cx}	β_{Cx}/β_{NCx}	β_{NCx}	β_{Cx}
0.00	0.0	3.527	0.0	0.0	3.527	0.0	0.0	3.527	0.0
0.01	0.41989	2.992	1.2563	0.27564	2.992	0.8247	0.18357	2.992	0.5492
0.02	0.50069	2.693	1.3484	0.35936	2.693	0.9678	0.26155	2.693	0.7044
0.03	0.55581	2.435	1.3534	0.42030	2.435	1.0234	0.32197	2.435	0.7840
0.04	0.59876	2.259	1.3526	0.46970	2.259	1.0611	0.37286	2.259	0.8423
0.05	0.63429	2.125	1.3479	0.51175	2.125	1.0875	0.41737	2.125	0.8869
0.10	0.75543	1.789	1.3515	0.66250	1.789	1.1852	0.58490	1.789	1.0464
0.15	0.83043	1.640	1.3619	0.76113	1.640	1.2483	0.70046	1.640	1.1488
0.20	0.88233	1.581	1.3950	0.83171	1.581	1.3149	0.78588	1.581	1.2425
0.25	0.91995	1.591	1.4636	0.88411	1.591	1.4066	0.85082	1.591	1.3537
0.30	0.94784	1.684	1.5962	0.92373	1.684	1.5556	0.90084	1.684	1.5170
0.35	0.96876	1.881	1.8222	0.95392	1.881	1.7943	0.93958	1.881	1.7673
0.40	0.98452	2.363	2.3264	0.97699	2.363	2.3086	0.96960	2.363	2.2912
0.45	0.99637	4.331	4.3153	0.99457	4.331	4.3075	0.99278	4.331	4.2997

The crack tip stress intensity factor K to be used for crack growth analysis would then be:

$$K = \sigma[\pi a]^{1/2} \beta_{Cx}$$

Where β_{Cx} would be given by Figure 7

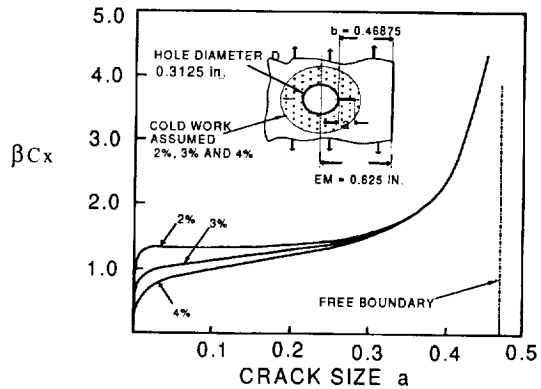


Figure 7. Effect of % Cold Expansion on β_{Cx}

Crack growth analysis was performed to illustrate the effect of different percentages of cold expansion compared to the non-cold expanded hole.

Assumptions:

Initial crack size 0.05 inch

Fracture Research crack growth program

2024-T3511 extrusion

Constant amplitude gross stress 20 KSI, $R = 0$

Paris crack growth equation $da/dN = 3.599E-10(\Delta K)^{3.7}$

For comparison a crack growth analysis was performed starting with a 0.005-inch crack generally approved by the authorities to represent the effects of cold expansion. The results are shown on Figure 8.

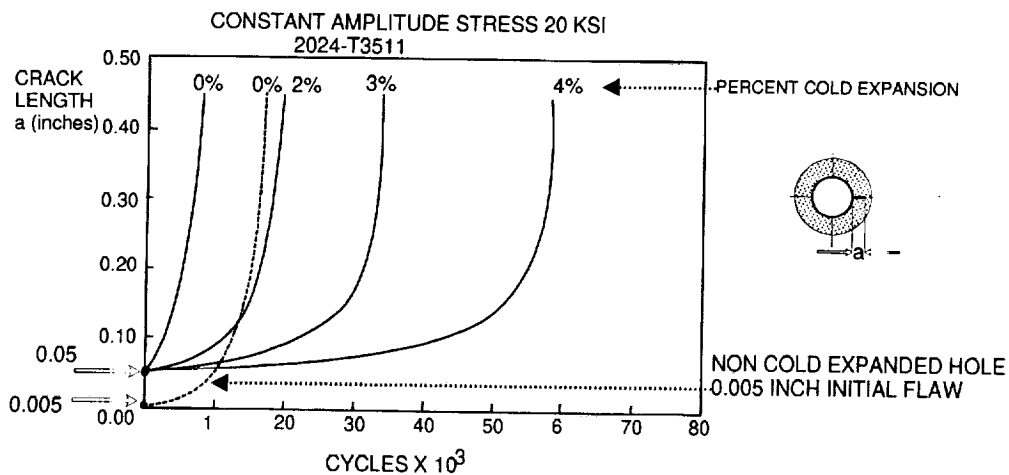


Figure 8. Effect of Cold Expansion on Crack Growth

SUMMARY

The investigation above was performed to assess the merits of the Boeing Wichita method of accounting for the effects of cold expansion on the crack tip stress intensity factor. The intention was to develop a more viable approach than the previous approach where certifying authorities have allowed a smaller initial crack size to represent the rogue flaw when the fastener hole was cold expanded. The Boeing approach is empirical in that it depends on the development of an exponent m from crack growth test results. The results shown here merely use the same exponent m developed by Boeing. Boeing tests have shown this analysis method to be conservative; however, it does provide a better estimate of potential crack growth after cold expansion than the 0.005-inch initial flaw analysis. It accounts for hole geometry, edge margin and percentage applied expansion. Fatigue Technology Inc. will be conducting a follow-on test program to independently determine the modifying exponent and to validate this approach for more general usage.

The modified stress intensity factor solution for fatigue critical holes incorporating cold expansion produces a better and less conservative analytical solution for use in determining realistic inspection thresholds required by the new FAR 25-571 regulation.

REFERENCES

- [1] Rich, D.L. and Impellizzeri, L.F., "Fatigue Analysis of Cold-Worked and Interference Fit Fastener Holes," ASTM STP 637, 1977.
- [2] Clark, G., "Modeling Residual Stresses and Fatigue Crack Growth at Cold Expanded Fastener Holes," Fatigue Fracture of Engineering Materials Structures, Vol. 14, No. 5.
- [3] Grandt, Jr., A.F., "Stress Intensity Factors for Some Through-Cracked Fastener Holes," International Journal of Fracture, Vol. 11, No. 2, April 1975.
- [4] Armen, H.; Levy, A.; Eidenoff, H.L.; "Elastic-Plastic Behavior of Coldworked Holes," Proc. 24th AIAA/ASME/ASCE/AHS Structures, Structural Dynamics, and Materials Conference, May 1983 (AIAA Paper 83-0865-CF, pp. 1-11).
- [5] Petrak, G.J. and Stewart, R.P., "Retardation of Cracks Emanating from Fastener Holes," Engineering Fracture Mechanics, Vol. 6, Pergamon Press, 1974, pp. 275-282.
- [6] Reid, L.F.; Easterbrook, E.T.; Rufin, A.C.; "Production and Repair of Fastened Joints Incorporating Cold Expansion," SAE Aerofast '92 Conference Paper #922400, October 1992.
- [7] Ozelton, M. W. and Coyle, T. G., "Investigation of Fatigue Life Improvement by Cold Working of Holes in Aircraft Materials," Final Report for Contract N00019-82-C-0364, Northrop Corp., 1983.
- [8] Boeing Report, No. D500-12540-1, Contract No. F34601-88-C-0392, "Cold Expanded Hole Testing Summary," (ETA) 88-B52B1-4, dated September 26, 1990.

SUPPORT OF COMPOSITE STRUCTURES ON NAVAL AIRCRAFT

Paul A. Mehrkam
Naval Air Systems Command, Patuxent River, MD

ABSTRACT

Since the first composite structures on navy aircraft were introduced in the early 1970's, the Navy has developed extensive composite repair experience for maintaining the fleet which includes current, emerging, and aging aircraft. To be presented will be composite repair experiences and developments for F-14, F-5, F/A-18A/B/C/D, AV-8B, CH-46, F/A-18E/F, and V-22. This will include solutions to specific repair problems such as ambient storable repair materials, reduced temperature vacuum bag cure of repair materials, support equipment for composite repair, and rapid composite repair procedures. This repair experience and technology was developed through teaming between Naval Air Systems Command (NAVAIR), Naval Air Warfare Center Aircraft Divisions (NAWCAD), Naval Aviation Depots (NADEP), Air Force agencies, international organizations, and aircraft manufacturers.

1. INTRODUCTION

In order to sustain mission readiness, the Navy has a requirement to repair and maintain aircraft at carrier and field locations. Repairs must be performed in both peace time and battle conditions. At these locations, freezer storage is limited or non-existent. Only vacuum bag pressure and heat blankets are available to cure the repair materials. Support equipment must be portable and compatible with a variety of aircraft. The repairs in the battlefield must be performed rapidly using existing repair materials and restore structural integrity for a minimum of 100 hours of operation.

Current Navy aircraft contain both monolithic and honeycomb composite structures. Honeycomb structures require a much lower cure temperature, 200-250°F (93-121°C), to prevent damage due to entrapped moisture. At high cure temperatures, 300°F (149°C), the entrapped moisture changes to steam and creates enough pressure within the honeycomb cells to disbond the face sheets.

Emerging aircraft such as the F/A-18 E/F Super Hornet, V-22 Osprey, and the Navy versions of the Joint Strike Fighter (JSF) will contain 19-40% by weight of composite structures. These new structural materials come with a new set of requirements that may include operational temperatures ranging from -67 to 550°F (-55 to 288°C), high cycle fatigue, thermal cycling, thermoset and thermoplastic materials, and post buckle composite structures. The Navy is involved in many development programs to meet these new requirements.

2. DISCUSSION

2.1 In-Service Experience Of Aging Composite Aircraft Structures The Navy's composite repair experience began with small amounts of composite structures introduced on the F-14, F-5, and CH-46 in the early 1970's. The F/A-18 and AV-8B were later introduced in the early 1980's which contained more structural composite weight. Many of the early field level composite repair techniques were limited to minor non-structural damages. As repair technology improved, the repair capability was expanded in many areas.

2.1.1 F-14 Fixed Winged Interceptor The F-14 contains boron/epoxy monolithic and composite honeycomb skins. Some honeycomb structures have bonded thin aluminum face sheets. Composite usage on the F-14 is roughly 4% of the total airframe weight.

Structural F-14 repairs on boron/epoxy components require the use of Cytec FM400 film adhesive which cures at 350°F. This high temperature cure posed potential damage problems for the honeycomb horizontal stabilizer. Cold-wall autoclave procedures were developed to minimize damage during the repair. The autoclave would provide the pressure while a heat blanket would only heat the repair area [1].

Another problem of using the Cytec FM400 film adhesive was that it required freezer storage at a time when none existed in the fleet. A small amount of freezer storage is now available on most carriers today. However, the minimum buy for this adhesive is a production size 40 inch (101 cm) wide roll which does not fit properly inside some freezers. Also, there is a lack of information for fleet personnel in handling, shipping, storage, sealing, and shelf life monitoring of this material.

The matrix of the F-14 boron/epoxy composite was very brittle and prone to delamination damage. Bonded patch repairs were developed to repair these delaminations [1].

To perform composite repairs, a hot bonder controller and composite machine tool set was developed specifically for the F-14. The hot bonder consists of a hefty hand truck unit to be wheeled around.

The 2024 honeycomb core used on the F-14 horizontal stabilizer and inlet walls is untreated which means that no corrosion protection is used. This has resulted in extensive corrosion and exfoliation of the core. The inlet wall has the most trouble. The skins are aluminum and through holes are present that lead to moisture intrusion. Currently repair involves removal of the corroded core and replacement with the same type of core [2].

2.1.2 F-5 Aggressor Squadron Aircraft The F-5 contains bonded aluminum skins over aluminum honeycomb and bonded leading edges with Cytec FM73. The potential for corrosion of the core exists as in the F-14. Surface preparation for bonded repairs of the honeycomb involves a scuff sand, solvent wipe, and the optional use of primer [3]. This type of surface procedure is known to degrade very quickly. However, this land based F-5 does not experience the salt water corrosive environment of carrier aircraft.

2.1.3 CH-46 Cargo/Transport Rotary Wing The CH-46 has longest in-service performance of 10,000 hours for epoxy/fiberglass composite rotor blades. The blades have experienced wear damage and delamination from flying debris. Composite stub wings used on some aircraft are susceptible to impact damage. Bonded repairs are often performed on these components.

2.1.4 F/A-18A/B/C/D Multirole Aircraft The F/A-18A/B/C/D contains 10% carbon/epoxy (Hexcel 3501-6) in monolithic and honeycomb structures. The maintenance history primarily focuses on the bonded repair of thin composite skins over aluminum honeycomb core, and composite access panels and doors. The majority of these structures are located in impact damage prone areas which are low on the aircraft, around the aircraft perimeter, and in maintenance areas. Removable access doors are also susceptible to fastener hole wear and edge damage. Thick monolithic structures, such as the wing skin, proved to be very durable and rarely experienced damage [1].

During the early introduction days of the F/A-18, film adhesive Cytec FM300 and core splice foaming adhesive Cytec FM404 were used primarily for the repair of honeycomb structures on the flaps, rudder, gear doors, and horizontal stabilizer. These materials required autoclave pressure and 350°F (177°C) cure which posed potential damage during the repair [4]. Like the F-14, cold-wall autoclave procedures with reduced pressure were developed. Later on, a stage embossing technique was developed for the Cytec FM300 to minimize porosity formation during a vacuum bag cure. Small kits of the embossed FM300 adhesive were made available by NADEP North Island to be supplied to the fleet. Out of the autoclave processing techniques were developed for the Cytec FM404 foaming adhesive. Reduce cure temperature cures at 300°F (149°C) were utilized for both adhesives to reduce the potential of over pressurization damage. However, studies have shown that cure temperatures above 275°F (135°C) can still lead to skin core disbond. At cure temperatures of 300-350°F (149-177°C), heat blankets have large temperature gradients across the repair with cold spots that can under cure the adhesive and hot spots that can either disbond the face sheet or heat damage the composite [4, 5].

Low temperature curing two part paste adhesives, Hysol EA9321 and wet lay-up resin EA956, were used more extensively latter on in the fleet. However, these materials still require refrigerated storage.

Unfortunately, the freezer storage capability in the fleet did not improve when the F/A-18 was first fielded. Much of the film adhesives degraded during shipment. Two part

adhesives which require refrigerated storage were stored at ambient conditions for long periods. To this day, a significant amount of repair material is disposed as hazardous waste because of degradation under these conditions.

Many bonded patches consisted of thin precured composite sheet stock cut to shape and bonded in layers. Bolted and bonded titanium patches have also been used. The chromic acid surface treatment for titanium is too hazardous and cannot be performed at the field level. Wet lay-up patches made with Hysol EA956 are cured with a release film on the structure to be removed and secondarily bonded with adhesive. Thick wet lay-up patches cannot be used, because porosity prevents non-destructive verification of the bondline.

There is a high potential for water intrusion into F/A-18 honeycomb structures with thin composite skins and fastener hole attachment points. Once the water passes the intrusion point it can travel to multiple locations within the honeycomb structure by saturating the adhesive bondline between the skin and core and the adhesive node bonds between the core ribbons. The moisture can weaken the core nodes and skin to core bonds. This type of degradation can cause damage to the part during bonded repairs.

To perform composite repairs, a hot bonder controller and composite machine tool set was developed specifically for the F/A-18. The first prototype of the hot bonded was two large cases, each weighing over 100 lbs. The second iteration was three cases, each weighing 65-93 lbs.

2.1.5 AV-8B VSTOL Aircraft The AV-8B contains 24% airframe weight in composite monolithic structures. Four composite types are utilized: graphite/epoxy, graphite/bismaleimide, glass/epoxy, and glass/bismaleimide.

A variety of operational and design problems had to be overcome after the AV-8B was first introduced. Flight procedures for vertical landing and take off were modified to minimize heat damage on strake fairings and trailing flaps. Bolted titanium doublers were added to the heat damaged areas. Although there always was a potential of debris damage during take off and landing, very few incidents have been reported. The acoustical fatigue present during the flight operation of this aircraft lead to excessive hole wear damage on composite panels. New fastener designs were implemented to prevent this type of damage.

The AV-8B contains many durable thick composite structures which were rarely damaged during service. However, delaminations occurred in some of the earlier components by the use of non-conformable metal skins. A combination of resin injection and bolted metal plate repairs were applied to the delaminated regions. Also, manufacturing measures were taken to prevent this type of factory induced damage.

The thick monolithic structures on the AV-8B allowed the extensive use of bolted metallic patches [1]. A composite machining and drill kit was developed to specifically support the AV-8B.

Very few bonded repairs are performed on thinner structures using ambient curable two part adhesives. Like the F/A-18, the AV-8B experienced similar problems of material degradation during storage for these materials.

2.1.6 Early Evolution Of Composite Repair Common trends have been developed that affect field repairs at carrier and field locations for all of the aircraft discussed. Cure of repair materials required high temperatures and autoclave pressure. Freezer storage requirements of the repair materials were not being met and lead to significant amounts of material disposed as hazardous waste. Aircraft specific support equipment cause logistical burden for fleet units with multiple types of aircraft. Field repairable applications were limited since repair materials formed significant amounts of porosity that prevented non-destructive verification of the patch and adhesive bondline.

The Navy requirements for composite repair are a small market niche for many manufactures. Some of the needs are very expensive to produce and availability is extremely limited. Throughout the years, the Navy has successfully developed many new materials and common support equipment. However, vendors change their free enterprise marketing strategies and stop producing products for the Navy to pursue a more profitable market share.

2.2 Navy Repair Developments In the early 1980's, the Navy began development programs for repair materials, structural design concepts, and support equipment. The inclusion of a repair programs were mandatory for emerging aircraft such as the V-22 and F/A-18E/F. All of these development programs required the coordination of the Naval Air System Command, Naval Aviation Depots, Naval Air Warfare Center Aircraft Divisions, Air Force, Army, and commercial industry.

2.2.1 Development Of Repair Materials Several requirements were established in the evaluation and development of repair materials. Low temperature cures, 200-250°F (93-121°C) were required for repair of moisturized in-service composite structures. Repair materials need to be cure under vacuum pressure without creating significant amounts of porosity. The materials need to have high mechanical properties and to be easily non-destructively verified for patch quality and bondline integrity. Repair materials also need to be ambient storable to reduce logistic constraints associated with freezer storage. Battle field repairs need to be performed quickly utilizing the current repair materials and support equipment.

Previously, navy ambient storage conditions were originally defined by the Navy as 12 months at 70-80°F (21-27°C) or 6 months at 100°F (38°C). Various candidate repair materials were initially developed and tested under these ambient conditions. However, navy storage conditions were redefined in the early 1990's as 2 weeks shipping/transit storage at 140°F (60°C) followed by 12 months storage at 100°F (38°C). Although many materials may meet the storability requirements of 6 months at 100°F (38°C), they may not withstand the increased exposure temperature of 140°F (60°C) in combination with the extended shelf life time of 12 months at 100°F (38°C).

2.2.1.1 Magnolia Plastics Magnobond 6363 Adhesive As part of the Navy developmental efforts during the 1980's, a two part ambient storable adhesive was developed [6]. The initial formulated adhesive had a very low viscosity and foamed under vacuum bag pressure. A second generation was developed to prevent the viscosity from going below 100 poise during cure to prevent void formation under vacuum [7]. The second generation was then supplied commercially by Hysol and qualified to MIL-A-85705A during the early 1990's [8]. Characterization studies were performed for use on the V-22 repair development programs [9, 10, 11]. However, implementation of a new structural repair material requires lengthy qualification ranging from material characterization, design allowable development, coupon repair testing, to full scale subcomponent testing. New aircraft programs, such as the V-22, that would incorporate this adhesive would not be fielded until after the year 2000. The product was discontinued by the vendor since the Navy market niche was too small and too far into the future [12].

In the early 1990's, formulation efforts were pursued on a separate program to develop a third generation adhesive with increase the hot wet operation performance up to 250°F (121°C) [13]. The amine-to-epoxy mix ratio and toughener concentration were modified to increase performance of this adhesive. A vendor, Magnolia Plastics, supplied candidate formulations for evaluation by the Navy [14]. The down selected candidate was made commercially available as Magnobond 6363 which is utilized on the V-22 and MH-53E repair programs.

Testing has shown that Magnobond 6363 bipacks and quart kits meet the Navy's shipping and ambient storage requirements for up to 6 months based on the physical and mechanical properties testing for cold temperature, room temperature and 180°F (82°C)/wet conditions [15, 16].

2.2.1.2 Dexter Hysol EA9390 Resin This is a two part epoxy system for wet lay-up fabrication of composite patches. This impregnation resin will be qualified for structural repairs on the F/A-18 E/F, V-22, and MH-53E aircraft. The resin is ideal for wet lay-up applications because it can be stored at ambient conditions, has low viscosity for impregnation, and has a long pot life. Studies have shown that the material can be stored at room temperature for up to 12 months at 38°C (100°F) [17]. Double vacuum processing of this material has resulted in laminate qualities comparable to autoclave processed materials.

Although the previous NAWCADPAX study showed that Hysol EA9390 to be ambient storable. The increase exposure temperature of 140°F (60°C) has a detrimental effect on the material properties. Testing has shown that special handling and storage conditions would have to be implemented for Hysol EA9390 bipacks since the Navy's shipping and ambient storage requirements cannot be met. The Hysol EA9390 bipacks will have to be shipped frozen and stored in freezers. According to a study by Boeing St. Louis, Hysol EA9390 quart kits can be shipped under navy ambient shipping conditions but must be stored in freezers.

2.2.1.3 Dexter Hysol EA9394 Adhesive This thixotropic two part paste adhesive system can be used for potting, filling, and liquid shim applications. Hysol EA9394 adhesive will be used for the F/A-18 E/F and V-22 aircraft because it can be cured at either room or at elevated temperatures.

Testing has shown that Hysol EA9394 bipacks and quart kits can withstand the Navy's shipping environment. However, the Hysol EA9394 bipacks must be stored in freezers once the destination point has reached. According to a study by Boeing St. Louis, Hysol EA9394 quart kits may meet navy ambient shipping and storage conditions. However, after the storage of 12 months at 100°F (38°C), hardening of the part A resin on the top surface can occur which should be removed prior to use.

2.2.1.4 Dexter Hysol EA9396 Resin This is a room temperature curable, two part epoxy system for wet lay-up fabrication of composite patches. The F/A-18A/B/C/D program and commercial industry is strongly considering replacing Hysol EA956 with EA9396 for wet lay-up applications. The main benefit of Hysol EA9396 is that it meets the ambient storability requirement for the Navy in the quart kit form, according to a study by NADEP North Island [18].

The resin has a short pot life which prevents the use of double vacuum processing and other debulking procedures to minimize porosity. Also, the material has low hot wet properties which prevent its use in many structural repair applications.

2.2.1.5 Cytec FM300-2 Film Adhesive This is a 250°F (121°C) curing film adhesive with metal-to-metal bond properties similar to Cytec FM300. A stage embossing procedure was developed so that NADEP North Island can supply this adhesive in kit form. Structural analysis methods were evaluated and revised to incorporate this material on the F/A-18A/B/C/D and F/A-18E/F programs. Although this change in material solves the high temperature curing problems, it does not resolve the freezer storage requirement.

2.2.1.6 Cytec FM410-1 Core Splice Foaming Adhesive This is a 250°F (121°C) curing core splice foaming adhesive. Core splice procedures have been modified to used for Cytec FM404 repair applications to account for the reduced expansion ratio and increased film thickness of FM410-1. Structural analysis methods were evaluated to incorporate this material on the F/A-18A/B/C/D and F/A-18E/F programs. Like the Cytec FM300-2, this change in material solves the high temperature curing problems and does not resolve the freezer storage requirement.

2.2.1.7 Repair Material Requirements The benefits in developing repair materials that are ambient storable were not fully realized. The newly developed materials cannot be readily implemented into existing aircraft. Structural repair manuals (SRM's) must be evaluated for aircraft specific processes and applications. Many other types of repair material needs that are aircraft specific need to be addressed.

The requirements of 2 weeks shipping/transit storage at 140°F (60°C) followed by 12 months storage at 100°F (38°C) degraded the structural repair materials. Freezer storage on the F/A-18A/B/C/D and F/A-18E/F programs is still required for the low temperature curing film and foam adhesives.

2.2.2 Navy Stock System Improvements For Repair Materials An evaluation has been performed on the Navy stock system for composite repair materials. The findings showed that the supply system was not responsive to current or projected needs for maintaining advance composite materials in the fleet environment. Current navy stocking procedures for composite materials results in large amounts, up to 88%, of unusable material that is discarded as hazardous waste. Two part materials are treated as sheet metal regardless of the vendor requirement for refrigerated or freezer storage. Perishable repair materials are shipped and stored without temperature controls, shelf life is not maintained, and field quality control tests do not exist for many materials.

Under these shipping/storage conditions, unusable material is supplied to the end user. Repair actions may be delayed until acceptable material is resupplied. The material may be unusable for various reasons such as expired shelf life, hardening of the paste or film adhesives, improper storage/shipping conditions, or a combination of these situations. Some repair activities may request large quantities of repair materials in order to get a few usable units. The resulting hazardous waste is expensive to process and is expected to be more costly as emerging aircraft contain increasing amounts of composite structure.

To improve fleet readiness and to reduce logistical costs, the Naval Air Systems Command (NAVAIR) has teamed with Naval Inventory Control Point (NAVICP), NADEP North Island, NADEP Cherry Point, and NADEP Jacksonville. The purpose of the team is to recommend solutions for improving the quality of repair materials being supplied to the fleet. The team's investigation focused on impact of material quality on fleet readiness, structural repair needs, shipping/storage temperature controls, distribution time frames, storage conditions, and shelf life. The general findings are that material temperature controls vary throughout the distribution system, multiple agencies involved in material management resulting in process variation and complexity, and lack of information and training in handling perishable materials.

Some of the recommendations will include 0°F (-18°C) shipping for all perishable repair materials, implement freezers at all stocking storage and transit points, set-up long term contract with vendors for direct delivery, increase prioritization for faster transportation times, improved training for stock personnel and end users, and common repair materials among the aircraft platforms. The results sought from these recommendations are improved safe affordable readiness by preserving the mechanical properties of the repair materials, maintain weapon system readiness by improving material

availability and logistic response time, and comply with mandates for reduced hazardous waste reduction.

2.2.3 Development Of Rapid Composite Repair Procedures Composite repairs performed on naval aircraft during peace time must be capable of fully restoring the structural strength for the life of the aircraft. Often these repairs are time consuming due to the long heat cycles for the repair materials. In a battle field situation, these repairs must be performed rapidly to return the aircraft to "mission capable" within a few hours. Some repairs may not be required to fully restore the structural strength and need only last for 100 operational hours. Many of the current qualified repair materials do not meet the needs of rapid field repairs because they require freezer temperature shipment/storage and high temperature cure cycles.

To expedite these repairs, the Navy has investigated rapid heating methods and rapid curing materials. Some of the heating methods investigated were ultraviolet, ultrasonic, and induction heating. These rapid heating methods would require specialized equipment, calibration, and training. The rapid cure adhesives and composites that were investigated would require a lengthy qualification process prior to use on naval aircraft. The new heating methods and rapid curing materials would be a significant logistical constraint since they can only be used for battlefield conditions. To maintain reduced logistics costs, rapid repair methods must be adaptable with current qualified repair materials and equipment.

Qualification of wet lay-up material, Hysol EA9390, for repairing composite structures in a remote field location is nearing completion on the F/A-18 E/F, V-22, and MH-53E aircraft. Current wet lay-up repair procedures require 6 to 8 hours. Three hours of this repair time is used for vacuum bag curing of the repair. Developmental efforts at the Naval Air Warfare Center, Aircraft Division, Patuxent River, Maryland led to the evaluation of shorten double vacuum processes and cure cycle dwell times [19]. Hysol EA9390 impregnated AS-4 plain weave fabric wet lay-up composite was tested to determine mechanical strength and thermal stability in a 180°F (82°C) wet environment for 100 hours of operation.

Magnolia Plastics Magnobond 6363 will be qualified for structural bonded repairs on the V-22 and MH-53E aircraft utilizing a cure cycle that takes over 3 hours to complete. An evaluation by Naval Air Warfare Center, Aircraft Division, Patuxent River, Maryland showed that cure cycles can be shorten by as much as 110 minutes and still meet thermal stability requirements for 100 hours with a hot wet operation temperature of 180°F (82°C) [15].

In a battle field situation, the shorten cure cycles for Hysol EA9390 and Magnolia Plastics Magnobond 6363 provide the ability to complete repair actions and return the aircraft to immediate mission readiness.

2.2.4 Development of Support Equipment For Composite Repair In order to reduce inventory, maintenance, and training costs, the Navy has invested and developed standard support equipment that can service a variety of aircraft. The equipment being used for composite repair is very critical with regards to quality control and providing reproducible results. Each aircraft has its own set of requirements and manufacturers will custom fabricate the additional support equipment at extra cost. Currently, the Navy uses tool kits to machine composites and temperature vacuum hot bonder controllers to cure materials. The V-22 program is developing a field portable double vacuum tool for processing Hysol EA9390 wet lay-up patches. Some of the candidate support equipment that the Navy plans to investigate are heating systems for curing on complex shaped structures, sensors for detecting moisture in composites, and rapid tooling equipment and materials for duplicating complex shaped parts.

2.2.4.1 Temperature Vacuum Hot Bonder Controllers The Navy has several types of hot bonder controllers in its inventory manufactured by BriskHeat, Grumman, McDonnell Douglas, and etc. During the early 1990's, the Navy developed and awarded a contractual specification for a generic temperature/vacuum hot bonder control set (P/N 1935AS100-1). This system has the combined repair material cure requirements of several air platforms. The generic temperature/vacuum hot bonder control set is larger and heavier (65 lbs. for the controller case) than commercially available hot bonders, because of the built-in rugged requirements. Navy rugged environmental test requirements include drop and shock resistance, electromagnetic interference (EMI), magnetic pulse, chemical-biological agent cleanability, and many more.

2.2.4.2 Composite Repair Tool Sets Composite machining is very specific to the types of structures being repaired. Likewise the tool sets sold by the aircraft manufacturers were very specific for the platform intended and could not be directly used on other platforms. The Navy developed a common support tool kit that combined all of the different air platform requirements.

2.2.4.3 Field Portable Double Vacuum Tool Aircraft programs such as the F/A-18 E/F, V-22, and MH-53 will be soon qualifying Hysol EA9390 wet lay-up repair patches made with the double vacuum process. The double vacuum debulk procedure requires the use of a rigid enclosure over a flexible vacuum bag. Vacuum is applied to the vacuum bag and rigid enclosure. Under these conditions, the laminate plies are exposed to a vacuum but no consolidation force is applied to the laminate. At a given point in the process, the vacuum in the rigid enclosure is vented which allows the bag to collapse onto the ply stack surface. Consolidation of the plies occurs under this vacuum pressure. Void free laminates with Hysol EA9390 resin result with good mechanical properties. Currently, V-22 is the only program developing the field portable double vacuum tool. The Navy needs to supply this tool as a common support equipment for used by other programs such as F/A-18E/F and MH-53E. Otherwise, field support personnel will have to construct the double vacuum tool in the field from wood.

3. SUMMARY

The Navy has been involved in many programs to develop state-of-the-art composite repair materials, processes, and support equipment. This type of development requires team work between Naval Air Systems Command (NAVAIR), Naval Air Warfare Center Aircraft Divisions (NAWCAD), Naval Aviation Depots (NADEP), Air Force and Army. The repair programs meet the requirements of emerging, current, and aging navy aircraft.

Most ambient storable materials do not meet the newly define navy storage conditions of 2 weeks shipping/transition storage at 140°F (60°C) followed by 12 months storage at 100°F (38°C). The increased exposure temperature of 140°F (60°C) had a detrimental effect on stored materials. To improve storage conditions and minimize hazardous waste, recommended changes are expected to be implemented in the Navy stock system. Shorten cure cycles for Hysol EA9390 and Magnolia Plastics Magnobond 6363 provide the ability to complete repair actions rapidly and return the aircraft to immediate mission readiness. Standard common support equipment to be used with all current and emerging aircraft have strong costs benefits for reduced inventories and training.

4. ACKNOWLEDGEMENTS

The author thanks the contributing efforts by Jim Fuss, Rob Hartel, and Ken Workman of NADEP Cherry Point; Doug Perl and John Hill of NADEP North Island; Don Knapp of NADEP Jacksonville; Rob Dompka, Denver Witworth, Mike Marvin, and Tom Reilly of Bell Helicopter Textron; Philip Persaud, Adam Sawicki, and Dave Stone of Boeing Philadelphia; Alex Rubin and Harlon Ashton; of Boeing St. Louis; Chris Jones and Ed Serinco of Northrop-Grumman; Brett Bonnet, Diane Kleinschmidt, Jim Thompson, Jennifer Elmore, Ed Rosenzweig, Tony Martinelli, Tom Mixon, Tracy Larson, Dennis Bellevou, and Chanda Sanders of the Naval Air Systems Command, Patuxent River, MD.

5. REFERENCE SECTION

1. T.M. Donnellan and E. Rosenzweig, "Supportability of Composite Components on Navy Systems," Naval Air Development Center, Warminster, PA, Report No. NADC 91083-60, Oct. 1991.
2. Don Knapp, Naval Aviation Depot, Jacksonville, FL.
3. Doug Perl, Naval Aviation Depot, North Island, San Diego, CA
4. D.R. Perl, "Evaluation of Damage To F/A-18 Advance Composite Honeycomb Sandwich Parts Caused By Elevated Temperature Cure Cycles," Proceedings of 39th International SAMPE Symposium and Exhibition, Society for the Advancement of Material and Process Engineering, Covina, CA, April 1994.

5. M.E. Marien, D.R. Perl, and K. Gaenzle, "Applications of Thermal Analysis In The Repair Of Advance Composite Structures," Proceedings of 39th International SAMPE Symposium and Exhibition, Society for the Advancement of Material and Process Engineering, Covina, CA, April 1994.
6. D.J. Crabtree, Adhesives for Field Repair of Graphite Epoxy Composite Structures, Naval Air Development Center, Warminster, PA, Report No. NADC 79286-60, Nov. 1981.
7. R.C. Cochran, T.M. Donnellan, J.G. Williams, and J.J. Katilaus, "Adhesive for Field Repair of Composites," Naval Air Development Center, Aircraft Division, Warminster, PA, Report No. NADC-88072-60, June 1988.
8. Military Specification Mil-A-85705A, "Adhesive, Aircraft, for Structural Repair," Feb. 27, 1987.
9. P.A. Mehrkam, M.F. DiBerardino and T.M. Donnellan, "Low Temperature Cure Adhesive for Honeycomb Repair Applications," Proceedings of 23rd International SAMPE Technical Conference, SAMPE, Covina, CA, October 1991
10. P.A. Mehrkam, M.F. DiBerardino, R.C. Cochran, and I.S. Lim, "Low Temperature Cure Adhesive for Honeycomb and Composite Repair Applications," Proceedings of 6th International Symposium on Structural Adhesives Bonding, American Defense Preparedness Association, May 4-7, 1992, pp 192-200
11. P.A. Mehrkam, R.C. Cochran, and R.E. Trabocco, "Cocure of Wet Lay-Up Patch and Toughen Adhesive for Composite Repair Applications," Proceedings of 25th International SAMPE Technical Conference, SAMPE, Covina, CA, October 1993.
12. Memo Form Dexter Hysol, M. Cichon, "EA 9346 And XEA 9391 Being Discontinued," February 28, 1994.
13. P.A. Mehrkam and T.M. Donnellan, "Development of 121°C Adhesive for Composite Repair Applications," Closed Proceedings of 22nd International SAMPE Technical Conference, SAMPE, Covina, CA, November 1990, pp 81-93.
14. P.A. Mehrkam and R.C. Cochran, "Development of Ambient Temperature Storable Repair Adhesive" Proceedings of 40th International SAMPE Symposium and Exhibition, SAMPE, Covina, CA, May 1995
15. P.A. Mehrkam and B. Bonnet, "Cure Cycle Optimization of Ambient Temperature Storable Adhesive," Closed Session Proceedings at the 28th International SAMPE Technical Conference, SAMPE, Covina, CA, November 4-7 1996.
16. P.A. Mehrkam, B. Bonnet, and D. Kleinschmidt, "Ambient Storability Evaluation Of Two-Part Epoxy Composite Repair Materials," Closed Proceedings of 42nd International SAMPE Symposium and Exhibition, Society for the Advancement of Material and Process Engineering, Covina, CA, May 1997.
17. M. DiBerardino, J. Dominguez and R.C. Cochran, "Bonded Field Repair Concepts Using Ambient Storable Materials," Closed Proceedings of 34th International SAMPE Symposium and Exhibition, Society for the Advancement of Material and Process Engineering, Covina, CA, 1989, pp 75-86.
18. M.E. Marien and D.R. Perl, "Ambient Temperature Storable Adhesives," Composite Repair Engineering Development Program, NADEP North Island, Document No. CRE003-92, October 23, 1992.
19. P.A. Mehrkam, D. Wong, D. Alley, and C. Fuller, "Development of Rapid Wet Lay-Up Repair Procedures," Closed Session Proceedings at the 41st International SAMPE Symposium and Exhibition, March 1996.

AGING OF AIRCRAFT TRANSPARENCIES

Michael P. Bouchard, Daniel R. Bowman, and Thomas J. Whitney
University of Dayton Research Institute
300 College Park Dr., Dayton, OH, 45469-0110, USA
Phone: (937) 229-3030
Fax: (937) 229-4251
E-Mail: bouchard@udri.udayton.edu

ABSTRACT

Aircraft transparencies (windshields, canopies, and windows) are structural components that must withstand flight and ground loads. This paper seeks to demonstrate that transparencies, like metal airframe components, are subject to aging with attendant reductions in structural capability, and therefore transparency aging must be adequately considered when addressing aircraft structural integrity. Typical transparency construction and aging mechanisms are described, and case histories demonstrating the impact of aging on structural life and safety are presented. Approaches for managing transparency aging, including design, removal for cause, inspection, and life extension, are described. The discussion is based on experience with military aircraft transparency system design, development, research, and problem solving.

1. INTRODUCTION

This introduction provides a general description of aircraft transparencies, followed by a discussion of transparency aging mechanisms and effects, and a summary of the objective and scope of the paper.

1.1. TRANSPARENCY DESCRIPTION

Aircraft transparencies, which are comprised of windshields, canopies, and windows (Figure 1), provide the aircrew with an optically clear view of the outside environment while protecting them from flight loads such as wind blast, temperature, pressure, and foreign object impact. Transparency structural integrity therefore is important to ensure aircrew safety as well as operational readiness. Transparencies are subject to aging, which can and does affect structural integrity.

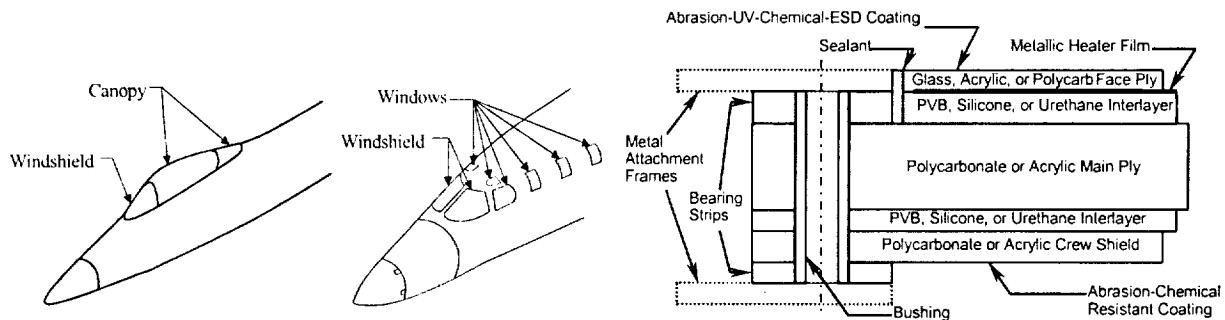


Figure 1. Aircraft Transparencies and Transparency Construction.

Aircraft transparencies may be single-layer (monolithic) or multi-layer (laminated) in construction, consisting as required of structural plies, adhesive interlayers, protective coatings, embedded metallic heater films, and edge attachment hardware such as bushings and bearing strips (see Figure 1). Transparencies typically are fabricated using structural polymers (acrylic and polycarbonate), adhesive polymers (urethane, silicone, PVB), and/or glass.

1.2. TRANSPARENCY AGING MECHANISMS

Transparencies, like metal airframe components, are subject to aging. Some of the aging mechanisms of transparencies are similar to, while some are different from those experienced by metal components. As with metals, transparencies are subject to fatigue when exposed to cyclical loads at high stress concentration locations such as bolt holes, which can result in reduced bird impact resistance (see Section 3.1). Classical galvanic corrosion can be an issue with respect to the metal bushings that contact metal frame members and conductive films or coatings (see Section 1.2.2). Degradation due to moisture, chemical attack, and ultraviolet light is an issue with respect to polymeric materials. The chemicals, particularly in conjunction with residual or installation stresses, can cause surface defects, such as crazing and haze, delamination, and more insidiously, bolt hole cracking. Abrasion due to dust, dirt, and other airborne particles leads to significant haze build-up and pitting, which can become craze initiation sites.

In addition to the above aging mechanisms, the polymer materials in aircraft transparencies also are subject to physical (thermal) aging.¹⁻⁶ Physical aging is a property of plastic materials that has been recognized for many years. Plastics age because they are in a non-equilibrium state that is constantly relaxing. The relaxation is in the form of molecular ordering which often causes the material to lose ductility, increase stiffness and density, and reduce craze resistance. For transparent plastics, optical properties also are affected, as degradation often manifests itself as increases in haze and loss of light transmission. The time required for a certain degree of relaxation (or aging) is a function of temperature; increasing the temperature can accelerate aging.

Acrylic and polycarbonate are the two primary polymers used for aircraft transparency structural plies. Aging issues associated with each material follow.

1.2.1. Acrylic Aging

Acrylic can be used in either the as-cast condition, or it can be stretched to improve various properties. While acrylic is relatively stable, it is subject to aging, and stretched acrylic has been shown to degrade on the order of 10% in terms of tensile strength in the first several years of service, and after 8 to 10 years the strength falls off rapidly.⁷ Acrylic, while very stiff and strong, is very brittle and is therefore limited in impact strength. Acrylic transparencies have had problems with distortion and cracking. The leading edge of stretched acrylic F-15 windshields often have distortion ridges. These ridges are caused by relaxation of the stretched acrylic during high temperature missions or by heating from the hot air duct (stretched acrylic relaxes to its unstretched shape and size at 220 to 230 degrees F). F-4 and F-15 acrylic canopies have had in-plane cracking problems at the edges caused by mismatches between the thermal coefficients of expansion of the edge attachment and the transparency. Changing from fiberglass/phenolic edge reinforcements to nylon/acrylic edge attachments has solved these problems.^{8,9} The AV-8B acrylic canopies have had bolt hole cracking problems caused by drilling of the edge reinforcement too close to the edge attachment/transparency interface¹⁰. Service lives for acrylic transparencies have been reported to range from 5 to 8 years.

1.2.2. Polycarbonate Aging

In contrast to acrylic, polycarbonate is a very ductile and tough material with very high impact strength. Consequently, polycarbonate is utilized in applications where birdstrike protection is critical. Polycarbonate

is not used in the unprotected condition, as it is susceptible to chemical attack and UV attack, although it does have higher temperature capability than acrylic (the use temperature approaches 300 degrees F). Typically, the polycarbonate is protected with a laminated acrylic or glass outer ply, or with a coating. Extensive evaluation by UDRI of the polycarbonate in F-111 windshields showed no degradation of the bulk polycarbonate for service lives up to 6.4 years.^{4,5} Evaluation of in-service aged F-16 canopies by Texstar, Inc., has shown no evidence of polycarbonate degradation. Texstar has in fact stripped and recoated monolithic F-16 canopies as much as three times with ages as high as ten years.^{11,12} In several cases, specifically for the F-111 and F-16, the laminated polycarbonate windshields have experienced problems with bolt hole cracking. For the F-111 this cracking caused a reduction in birdstrike capability (see Section 3.1 for a detailed discussion). For the F-16, birdstrike testing has shown that bolt hole cracking has no effect on birdstrike capability. The cause of the cracking has been traced by Sierracin/Sylmar Corp. to an airplane wash fluid in combination with steel fasteners, a solar coating, and a grounding bus-bar which induced a galvanic cell and a corrosive environment. A change in the bushing, the sealant, and the grounding bus-bar eliminated this problem.¹³ UDRI has conducted research to determine service lives of F-16 laminated transparencies. Average service lives for laminated polycarbonate F-16 canopies range from 36 to 54 months for transparencies manufactured between 1984 and 1988.¹⁴

1.3. EFFECTS OF TRANSPARENCY AGING

Transparency aging affects both structural and non-structural transparency performance. For example, aging can degrade pressure, thermal, and bird impact resistance (see Section 3 for examples), and also can degrade optical clarity due to haze, crazing, scratching, pitting, and yellowing. Transparencies typically are replaced due to degradation of optical functionality before structural integrity has been compromised due to aging. This is a fortunate, albeit somewhat unintentional circumstance, especially given the relatively fragile, "unhardened" nature of the polymeric materials (compared to metal components). This fortuitous circumstance can be masked for glass-faced transparencies since the glass provides outstanding abrasion and chemical resistance, and therefore may retain acceptable optics and remain in service for long periods of time. In addition, certain windows may be non-critical to mission performance, and therefore even optics can be compromised without removing the window, thereby allowing aging mechanisms to affect structural integrity.

Aging can significantly shorten the service life of aircraft transparencies. The Air Force has had a long-standing goal of a four year service life for its transparencies,¹⁵ but typically obtains 2-3 years of life from its high performance aircraft. Cracking of the glass face ply on B-1 windshields is limiting service life to about 24 months.¹⁶ Acrylic-faced F-16 canopies have fared better, with haze and crazing of the acrylic face ply limiting service life to 36-54 months or less. Repair procedures (e.g., for minor coating peeling, acrylic scratches, and delamination) and refurbishment programs (e.g., supplier programs to strip and re-coat F-16 canopies) do help extend the useful lives of transparencies. However, operational readiness, supply logistics, and cost of ownership all are affected by relatively short service lives of transparencies.

2. MANAGING STRUCTURAL INTEGRITY OF AIRCRAFT TRANSPARENCIES

Approaches for managing aging of transparencies are similar to those used with airframe components and systems, but vary somewhat in specific details. Descriptions of several approaches appropriate for managing structural integrity (in contrast to optics or other non-structural issues) follow.

2.1. DESIGN

Ideally, transparency systems should be designed from the beginning (or during a transparency system upgrade) to minimize degradation due to aging. Bolt holes tend to be particularly susceptible to degrada-

tion. Therefore one approach that has been utilized is to eliminate altogether the bolt holes through transparencies by trapping the transparency in a "C"-shaped frame with a generous overlap region and sealant. There are tradeoffs related to transparency replacement when using this approach. Depending on design, it may be very time consuming or virtually impossible to separate the transparency from its frame, so that the entire assembly becomes a costly disposable item. For designs with bolt holes, precision drilling, cold working, and the use of interference-fit bushings can significantly reduce crack susceptibility (see Section 2.4). Barrier coatings should be used to completely seal edges and bolt holes to prevent contact from aggressive chemicals, which can initiate cracks. The sealants and cleaners specified for use for transparency installation and maintenance must be compatible with constituent polymer materials in the transparency. All cleaners and wet sealants should be tested to ensure compatibility with each polymer material, and then maintenance directives written to specify only these cleaners/sealants to install and maintain the transparency. Dry rubber or foam sealants eliminate chemical incompatibility problems and provide for rapid change-out should the transparency need to be replaced (wet sealants must be scraped from the aircraft frames, a laborious process).

2.2. REMOVAL FOR CAUSE CRITERIA

A removal-for-cause criterion links replacement to unacceptable levels of structural degradation of the windshield. The degradation can be detected on a case-by-case basis via routine inspection of individual parts, or can be statistically based on the service life of the part. A general methodology for developing removal for cause criteria requires definition of critical failure modes; understanding the processes that result in the failure mode; testing to determine conditions favorable to the failure mode process; and correlating field removal data to the occurrence of conditions in the field. Once a positive correlation is established, removal criteria can be stated in terms of the occurrence of the condition. For instance, for an inspection-based criterion, windows exhibiting a certain number and/or length of structural ply cracking would be replaced. Or, for a service life based criteria, those parts exceeding a certain age would be removed since, according to correlation data, they would have an unacceptable probability (10%, for example) of failing. Section 3.2 illustrates the development of a service life based removal-for-cause criteria.

2.3. INSPECTION

Inspection can be a very useful tool to detect and monitor transparency aging for those cases in which the aging-induced damage can be visually detected. Visual inspection is used to detect flaws such as scratches, gouges, pits, and cracks in transparency structural plies. Flaws present in the main viewing area are straightforward to detect by looking through the transparency from various positions to observe light reflections off the flaws. Edge and bolt hole cracking are more difficult to detect due to edge attachment hardware which often blocks a direct view of this region. An optical prism, fabricated from acrylic, can be used to facilitate inspection in this region. As shown in Figure 2, images in the edge region can be viewed clearly with the prism. Glycerin provides an optical coupling medium (index of refraction similar to acrylic) between the transparency and prism, and keeps the prism from scratching the transparency. A flashlight also aids illumination of the edge region.

The Navy currently uses the prism technique to inspect its AV-8 transparencies for bolt hole cracking.¹⁷ Three AV-8B canopies failed in flight because of cracks emanating from bolt holes, prompting the inspection. The inspections are performed on all new transparencies and those considered for rework.

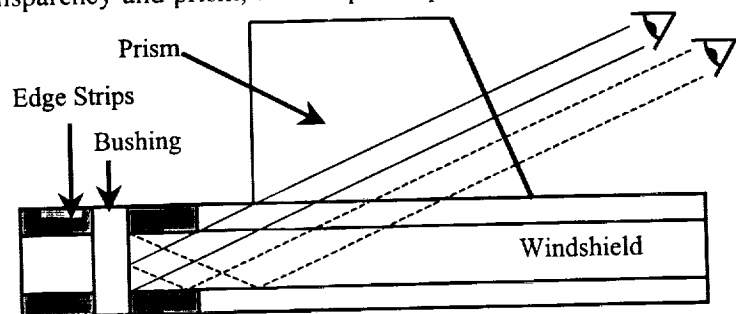


Figure 2. Use of Optical Prism for Edge Inspection.

2.4. LIFE EXTENSION

Bolt holes have proven to be one of the more vulnerable areas of a transparency for crack initiation and growth, with resulting degradation in structural integrity. Several life extension techniques have been investigated and have shown promise in reducing crack initiation and extending fatigue life. Initial research focused on hole preparation techniques, such as drilling and polishing.¹⁸ Step drilling resulted in a smooth hole surface finish which improved fatigue life compared to conventional techniques which resulted in rougher hole surfaces. Bolt hole cold working is a technique used in metallic structures to extend life, and was investigated for applicability to aircraft transparencies.^{18,19} Cracks initiate from excessive tensile stresses in the surface of the bolt holes. Cold working yields the material near the surface and induces a permanent compressive stress at the surface. This compressive stress must be overcome to produce a crack-inducing tensile stress. Various levels of cold working were produced in polycarbonate bolt holes by pushing an oversize mandrel through the hole. Fatigue testing was then conducted to determine the benefit of the cold working over the as-drilled holes. It was found that an interference of 10-14% (i.e., mandrel diameter 10-14% larger than hole drill diameter) resulted in an order of magnitude increase in fatigue life (Figure 3). Another technology investigated for life extension is the interference fit bushing. Basically these are oversize bushings that are forced into the bolt holes, thereby inducing a compressive stress state at the hole surface. As with cold working, this compressive stress must be overcome to produce a tensile crack-inducing stress. Fatigue testing showed that an interference of 6-9% (i.e., bushing diameter 6-9% larger than hole drill diameter) resulted in up two orders of magnitude increase in fatigue life (Figure 3). These technologies have been successfully demonstrated in the laboratory but require some further study prior to flight demonstration (long-term durability simulations, craze testing, temperature effects).

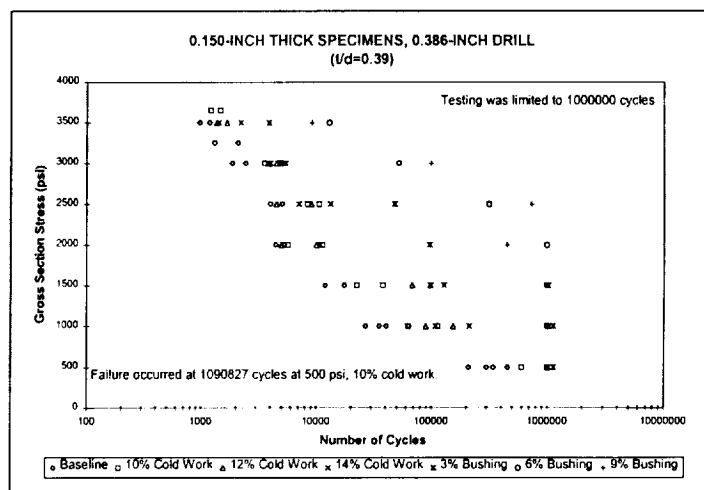


Figure 3. Improvement in Fatigue Life Due to Cold Working and Interference Fit Bushings.

3. CASE HISTORIES

The following case histories illustrate the effects of bolt hole cracking/fatigue and physical aging on transparency structural integrity, and the approaches taken to mitigate damage and extend life.

3.1. AGING OF F-111 ADBIRT WINDSHIELDS

The original F-111 windshield was glass having a four-pound bird impact resistance of 136 knots. This low level of protection coupled with the aircraft's low-altitude, high-speed penetration mission resulted in the loss of one aircraft per eight-month time period due to bird impact on the windshield. The F-111 ADBIRT (Advanced Development Bird Impact Resistant Transparency) was developed to provide four pound bird impact protection up to a minimum of 470 knots. The ADBIRT consists of two polycarbonate structural plies and a floating outer acrylic ply, bonded together either with silicone or urethane interlayers (vendor dependent). The entire F-111 fleet was retrofit with ADBIRT windshields, resulting in numerous aircraft saves from what would otherwise have been catastrophic birdstrikes.²⁰

Test programs to study the effects of simulated UV/humidity and flightline thermal environments indicated that there may be significant degradation in impact resistance of F-111 ADBIRT windshields. As a result, UDRI then conducted full-scale bird impact testing of 22 F-111 ADBIRT windshields to determine the effect, if any, of in-service aging on bird impact resistance capability.²¹ In-service aging was defined as the amount of time the transparency was on the aircraft. The structural integrity (birdstrike resistance) was found to be significantly reduced by the in-service aging, from over 470 knots when new to 360 knots after two years of service to an asymptotic minimum value of 325 knots after five years of service.

A test program was conducted to determine the cause of degradation.^{4,5} Aging mechanisms investigated included physical aging, moisture, chemical, and UV attack, and fatigue. Laboratory coupon tests of in-service aged and baseline new ADBIRT coupons were conducted to assess physical aging. Craze testing was performed to evaluate the sealants, cleaners, and other chemicals used to install or clean the transparency. Fractography was utilized to investigate bolt hole integrity. Finite element analysis (FEA) was conducted to determine stress levels in the edge attachment.

Physical aging was thoroughly assessed using a variety of tests, as shown in Table 1. The testing detected no performance degradation, and therefore no physical aging, of the bulk laminate and its constituent materials.

TABLE 1. TESTS TO ASSESS PHYSICAL AGING

Test	Purpose – Assess:
Optical haze and light transmission	Optics degradation due to bulk laminate aging
Torsional shear and flatwise tension	Interlayer strength, stiffness, and bond integrity
High rate MTS 3-point beam	Ply embrittlement (loss of impact strength)
Falling weight 3-point beam	Ply embrittlement (loss of impact strength)
Air cannon	Ply embrittlement (loss of impact strength)
Tensile testing	Polycarbonate toughness, strength, and elongation
Fracture toughness	Polycarbonate fracture toughness
Fatigue crack growth	Polycarbonate fatigue crack growth rate
Dynamic mechanical analysis (DMA)	Polycarbonate polymer structure changes
Differential scanning calorimetry (DSC)	Polycarbonate thermal history (annealing)
Gel permeation chromatography (GPC)	Polycarbonate molecular weight

Crazing is yielding in polymers characterized by a spongy void-filled fibrillar structure,²² typically formed by the combined action of aggressive chemicals and applied stress. Crazing negatively affects optics, causing an irritating glint, but also can degrade structural integrity by becoming crack initiation sites. Chemical craze testing of the “approved” sealants and cleaners for the F-111 windshield revealed that most caused crazing, and were not suitable for use with polycarbonate. In addition, machined surfaces, such as bolt holes and windshield edges, were more susceptible to crazing than the optical surfaces.

Edge sealants and reinforcements were removed and fractography used to evaluate the condition of the bolt holes in the structural polycarbonate plies. Many cracks were found in virtually all of the windshields, with the number of cracks increasing with transparency age, and with the majority of the cracks occurring on the inner ply. The cracks showed significant propagation due to fatigue. Tensile tests of coupons fabricated from transparency edges showed over a factor of three reduction in edge strength due to these bolt hole cracks.

FEA was conducted to compute the state of stress in the vicinity of the edge for various combined cabin pressure and temperature loads. The analysis showed that all but one load case resulted in higher stresses in the outer ply, not the inner ply where most of the cracks were observed. In general, the results indi-

cated that stresses in the inner ply were not high enough to initiate cracks independent of other contributing factors, but were of sufficient magnitude to propagate the cracks.

The results of this extensive investigation led to the following explanation for F-111 ADBIRT windshield degradation: crazing initiated in the polycarbonate structural ply bolt holes due to the combination of aggressive sealants and cleaners and service-induced stresses. The cyclic stresses were of sufficient magnitude to propagate these cracks due to fatigue. The resulting cracks were the direct cause of degradation of birdstrike resistance of F-111 ADBIRT windshields.

Specific action taken to remedy the problem included field inspections for bolt hole cracking, along with windshield replacement when cracks were found. The change from the T.O. wet sealant (which was shown to attack polycarbonate) to a non-aggressive dry sealant resulted in a reduction of observed cracks by 80%.²³

3.2. AGING OF KC-135 CELESTIAL NAVIGATION WINDOWS

There have been two catastrophic in-flight failures of KC-135 celestial windows resulting in rapid decompression of the aircraft and two fatalities. The location of the celestial windows is shown in Figure 4. The window is a 13 in by 15 in glass/PVB/glass laminate. The PVB was designed as a fail-safe ply to maintain pressure in the event the inner glass ply should fracture. The cause of glass ply failure was unknown, however the PVB was determined to have failed due to PVB degradation and subsequent fatigue cracking of the PVB at the edge of the window.²⁴

KC-135 celestial windows had been replaced only when optical requirements could not be met. There was no requirement for structural service life and replacement. As of 1991 the average age of the KC-135 fleet was over 27 years, while the average age of the overall cargo fleet was 23 years. The celestial window failures in conjunction with the high average fleet age and the widespread use of PVB interlayers throughout the fleet led to general concern over structural degradation of interlayers due to aging.

The near term solution to the celestial window failures was to first reinforce the window with an aluminum skin and later, pending availability, to replace the entire window with an aluminum plate. Although effective there was an obvious vision penalty. In 1991 the Air Force initiated an aging study of the celestial windows to develop a removal for cause criteria that would ensure replacement of degraded aged windows while permitting continued use of undegraded windows.²⁵

Nearly 50 celestial windows were obtained for testing. Service age was determined as the date of removal minus the date of installation. When date of installation was not available, date of manufacture was used. When date of removal was not available, date of shipment for test was used. Uncertainties due to use of these dates rather than actual installation/removal dates was estimated and included in the service life estimate. Service lives ranged from less than 30 months to over 180 months. Note that actual flight hours, which may have been a more realistic measure of age, and the effects of chemicals, humidity, and temperature could not be considered due to lack of data.

Pressure testing was conducted using a facility consisting of two test cells, one each matching the curvature of the left and right side windows. Other key components were a holding tank with an impact-

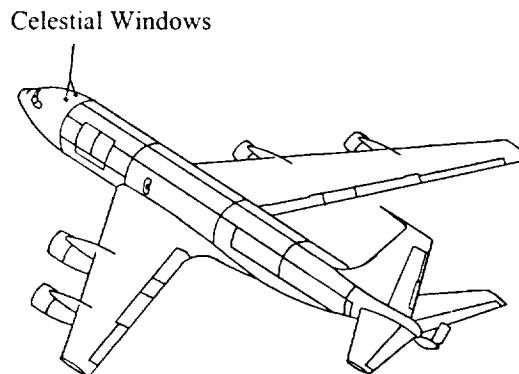


Figure 4. KC-135 Celestial Windows.

resistant polycarbonate lid to contain catastrophic failure; an air compressor; computer controlled pressure regulating hardware; data acquisition system to record pressure; and video camera to record each test. A proof test of up to 50 psi was conducted on each window to assess its ability to withstand high pressure.

Once a window passed proof testing, burst testing of the PVB was conducted. The inner glass ply was fractured using a hammer blow in a corner. The window was then pressurized until it could no longer hold pressure, terminating the test. A post-test visual failure analysis of each window was conducted.

Failures ranged from small PVB tears near the edge to "blowout" of the entire window. Burst strength as a function of service life is presented in Figure 5, along with a linear least square regression fit and 95% and 99% confidence intervals. The data indicates a gradual reduction of PVB strength over time. The 99% confidence line indicates the pressure below which one percent of windows from a random sampling at a given service age would likely burst. For a minimum burst pressure of 10 psi, the 99% confidence interval lower bound extrapolates to a service age of 313 months.

A risk assessment was conducted in accordance with MIL-STD-882C²⁶ to assist in defining a removal-for-cause criteria. Given its failure history, pressure burst of the PVB layer is considered a Category I, Catastrophic hazard, which is defined as death, system loss, or severe environmental damage. Hazard probabilities were assigned based on the proposition that more than two failures per year fleet-wide is "frequent." The associated failure risk is about 5/100 (95% confidence bound).

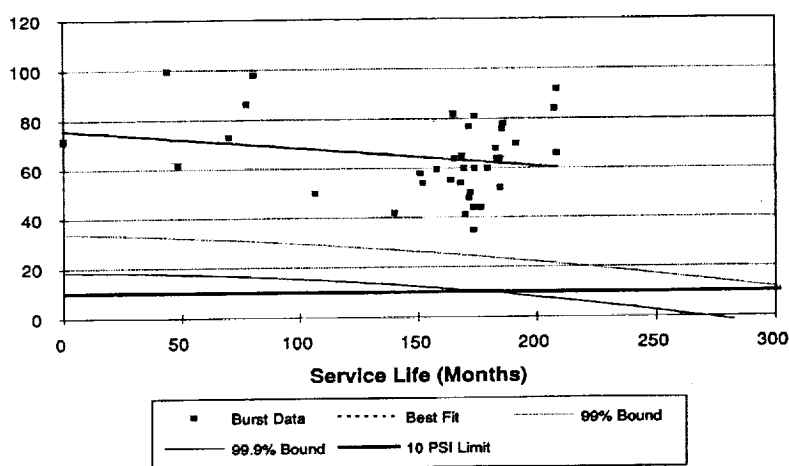


Figure 5. PVB Burst Pressure Versus Service Life.

Table 2 summarizes the hazard probabilities and service lives.

TABLE 2. HAZARD PROBABILITY LEVELS AND SERVICE LIVES

Probability	Level	Fleet Description	Number of Occurrences*	Number of Fleet Occurrences**	Service Age (months)
Frequent	A	Continuously Experienced	>5	More than 0.5 (>2 per year)	>424
Probable	B	Will Occur Frequently	0.5 – 5	0.08 – 0.5 (0.32-2 per yr.)	273-424
Occasional	C	Will Occur Several Times	0.1 – 0.5	0.025 – 0.08 (0.1-0.32 per yr.)	178-273
Remote	D	Unlikely, But Can Reasonably Be Expected to Occur	0.05 – 0.1	0.017 – 0.025 (0.068-0.1 per yr.)	126-178
Improbable	E	Unlikely to Occur, But Possible	<0.005	Less than 0.017 (<0.068 per year)	<126

* Per 100 windows in service. ** 1st Row: Per 100,000 flight hours
2nd Row: Assuming 275 Flight Hours/Year, 1460 windows in service

MIL-STD-882C requires that for Catastrophic hazards, Frequent, Probable, and Occasional probabilities must be prevented. The Occasional probability requirement (0.5 occurrences per 1000 service aged windows) would be satisfied by replacing windows when they reach a life of 126 months (10.5 years). This removal-for-cause criterion represents a substantial reduction (nearly factor of 5) in risk since over a hundred parts at the time of this work had service lives over 22 years, yet still provides a reasonable service life over which to spread replacement costs.

4. CONCLUSIONS

Aircraft transparencies have been demonstrated to be aging components, with potentially serious ramifications to structural life and safety if not adequately addressed. Aging mechanisms were discussed and approaches for managing transparency aging, including removal for cause, inspection, and life extension, were described. Case histories illustrating aging transparency problems and their solution were presented. It is recommended that aircraft transparencies be carefully considered and included in plans and programs for assessing and controlling the structural integrity of military and civilian aging aircraft.

5. ACKNOWLEDGEMENTS

Much of the work described herein was performed under various contracts for USAF AFRL/VACE, Wright-Patterson AFB, OH. The sponsorship and leadership of Mr. Ralph Speelman and Mr. Robert McCarty, and the enthusiastic contributions of the rest of the Air Force "Windshield Gang" over the last twenty years are gratefully acknowledged.

6. REFERENCES

1. Struik, L. C. E., *Physical Aging in Plastics and Other Glassy Materials*, in *Polymer Engineering and Science*, 1977, 17 (3), p. 165-173.
2. Brostow, W. and R. D. Corneliusen, *Failure of Plastics*, 1986, New York: Hanser Publishers.
3. Whitney, Thomas J. and Daniel R. Bowman, "Transparency Durability Test Criteria: Phase II Literature Survey," UDR-TR-93-16, February 1993, University of Dayton Research Institute.
4. Bowman, Daniel R. and Blaine S. West, "The Cause and Effect of Structural Degradation of In-Service Aged F-111 ADBIRT Windshield Transparencies," *Conference on Aerospace Transparent Materials and Enclosures*, WRDC-TR-89-4044, April 1989.
5. Bowman, Daniel R. and Blaine S. West, "An Investigation into the Structural Degradation of In-Service Aged F-111 ADBIRT Windshield Transparencies," UDR-TR-90-34, University of Dayton Research Institute, June 1990.
6. Hinds, B. G., "The Study of Polycarbonate Aging - A Review of Existing Data," ER90012, February 1990, Sierracin/Sylmar Corp.
7. Ursell, C. R., "Investigation of the Effect of Age on the Structural Integrity of F-5 Canopies," June 1981, Southwest Research Institute.
8. Mulville, D. R., I. Wolock, and R. J. Thomas, "Crack Formation in F-4 Aircraft Canopies," *Proceedings of the Conference on Transparent Aircraft Enclosures*, Las Vegas, AFML-TR-73-126, 1973.

9. Frank, Geoffrey J. and Gregory J. Stenger, "Crack Formation in F-15 Canopies," UDR-TR-90-110, October 1990, University of Dayton Research Institute.
10. Francis, Cheryl A., Naval Aviation Depot, Cherry Point, North Carolina, Private Communications, June-August 1993.
11. Teten, Lance, "Methods for the Determination of the Degradation of Polycarbonate," *Conference on Aerospace Transparent Materials and Enclosures*, WRDC-TR-89-4044, April 1989.
12. Teten, Lance R., Texstar, Inc., Private Communications, Various Dates.
13. Hinds, B. G. and J. A. Raffo, "In-Service Cracking of F-16 Windshield/Canopies," *Conference on Aerospace Transparent Materials and Enclosures*, WRDC-TR-89-4044, April 1989.
14. Whitney, Thomas J., Alan P. Berens, and Daniel R. Bowman, "Transparency Durability Test Criteria Interim Technical Operating Report (Phase III Field Service Data Analysis)," UDR-TR-96-23, February 1996, University of Dayton Research Institute.
15. Smith, Gen. R., Keynote Address at the *Conference on Aerospace Transparent Materials and Enclosures*, Monterey, CA, WRDC-TR-89-4044, April 1989.
16. Private Communications, Air Force Flightline Maintenance Personnel for B-1B Aircraft, Dyess AFB, TX and McConnell AFB, KS, September 1997.
17. Francis, Cheryl A., "T/AV-8B Local Engineering Specification," CP 70-30-AA-7840, Department of the Navy, Cherry Point, NC, June 1993.
18. Bowman, Daniel R., "An Experimental Evaluation of the Effect of Hole Fabrication/Treatment Techniques on Residual Strength and Fatigue Life of Polycarbonate Specimens with Holes," WL-TR-93-3086, Aeropropulsion and Power Directorate, Wright Laboratory, Wright-Patterson AFB, OH, August 1993.
19. Huelsman, Marc A. and Daniel R. Bowman, "The Effects of the Cold Working Process and Interference Fit Bushings on the Fatigue Life of Polycarbonate Specimens with Holes," WL-TR-97-3110, Flight Dynamics Directorate, Wright Laboratory, Wright-Patterson AFB, Ohio, April 1997.
20. West, Blaine S., "Development of Bird Impact Resistant Crew Enclosures for Aircraft," Proceedings of the *International Conference on Structural Impact and Crashworthiness*, Volume 2, Editor J. Morton, Imperial College, London, Elsevier Applied Science Publishers Ltd., 1984.
21. Bowman, Daniel R., G. J. Stenger, and B. S. West, "Full-Scale Birdstrike Testing of In-Service Aged F-111 ADBIRT Windshields," WRDC-TR-89-3075, Flight Dynamics Laboratory, Wright Research and Development Center, Wright-Patterson AFB, Ohio, August 1989.
22. ASTM F791-96, "Standard Test Method for Stress Crazing of Transparent Plastics," American Society of Testing and Materials, December 1996.
23. Kelley, Malcolm E., WL/FIVR, Wright-Patterson Air Force Base, Private Communication, Oct. 1993.
24. Griffen, Sandra J., "Analysis of KC-135 Navigator's Window In-Flight Mishap," Materials Engineering Report 88-417, December 5, 1988.
25. Whitney, Thomas J., D. R. Bowman, and R. A. Smith, "Pressure Burst Testing of KC-135 Celestial Navigation Windows," Proceeding of the *1993 Conference on Aerospace Transparent Materials and Enclosures*, San Diego, CA, WL-TR-94-4083, March, 1994.
26. Military Standard for System Safety Program Requirements, MIL-STD-882C, October 1991.

EFFECTS OF CORROSION INHIBITING LUBRICANTS ON AVIONICS RELIABILITY

W.H. Abbott
Battelle Columbus
Columbus, Ohio 43201

614-424-4198 (P)
614-424-4065 (F)
abbott@battelle.org

ABSTRACT

Studies were conducted on the effects of corrosion inhibiting lubricants on the electrical performance of gold plated connectors. The basis for the work was the premise that a significant number of typical No Defect (ND), Can Not Duplicate (CND), and Retest OK (RTOK) maintenance actions may be due to environmental corrosion of connector surfaces. This may include typical gold plated I/O connectors as well as ground connections.

The objectives of the work which was conducted in several phases were as follows. First, field and laboratory studies were conducted to evaluate the electrical performance and potential risk versus benefits associated with the use of Commercial Off The Shelf (COTS) materials conforming to MIL-L-87177A and MIL-C-81309E. Materials from 12 vendors were evaluated.

Second, it was planned that if satisfactory results were obtained in Phase I, a field study would be conducted in which selected lubricants would be applied to the I/O connectors on specific Line Replaceable Units (LRUs) of operational aircraft. This was, in fact, initiated with the F-16 aircraft as the test vehicle. To date, flights tests have involved nearly 150 aircraft spread over 10 bases in CONUS.

The Phase I studies produced several important conclusions. Among the lubricants which were evaluated there was a **wide range** of performance. One unique material was identified which actually appeared to **degrade** performance. A number of materials showed little benefit compared to the unlubricated state, and only several showed an excellent combination of corrosion inhibition in severe environments and good electrical performance under a wide range of environmental extremes. These results indicate that a few lubricants can be used in such applications with no identified engineering risk, but lubricants must be thoroughly qualified to a far greater extent than is required in existing specifications.

The Phase II studies have yielded positive results. Most important is the confirmation that such materials can be routinely applied in the field with no identified or perceived risk to the aircraft systems or with any objections from maintenance personnel. Beyond this, the results from several years worth of flight tests have produced variable results/benefits among different LRUs as might be expected. However, on specific LRUs there have been significant reductions in ND and NR values as well as Maintenance Man Hours/Flight Hour. Results comparing maintenance actions for aircraft with lubrication against comparable data for the entire fleet of aircraft within the same command have been favorable.

While these results have been positive, there is one overriding conclusion which must be stressed. Lubricants for such applications cannot be selected in an arbitrary manner. Thorough qualification data

must support these decisions. Such data do not appear to be available from historical qualification requirements.

1. INTRODUCTION

1.1 CORROSION

It is well established that gold plated connector products can degrade in natural, operating environments (1,2). The degradation which is the subject of this study may be termed corrosion, but it often takes the form of very thin films even below the limits of visual detection. Such reactions are somewhat insidious, since they cannot often be observed by maintenance personnel. However, in keeping with both contact theory and experiment such thin films are often sufficient to produce unpredictable effects, failure without warning, intermittent operation (3,4), etc: Such faults may just as suddenly "clear" to produce the familiar CND/ND/RTOK observations.

There is no suggestion that in gold plated product it is the precious metal which is corroding. Instead, the corrosion films are produced from both natural and induced defects in the precious metal coatings. These defects which include sub microscopic porosity as well as wear provide paths for the natural environment to access the underlying reactive base metals. The resultant corrosion products which are, of course, non conductive may be transported by several mechanisms out and onto the precious metal surfaces (5,6).

It is often believed that "corrosion" of this type may only occur in very severe environments such as coastal/marine environments. This is clearly not the case as has been demonstrated by the author in numerous field studies worldwide and which are discussed, in part, in this paper. The marine scenario would be an unfortunate impression, since it might lead to the conclusion that at inland location similar corrosion is not a factor in reliability. This is anything but the case, and as we will demonstrate, virtually all ambient environments are **sufficiently** severe that this type of corrosion can occur **if** the natural environment actually reaches the connector surfaces.

Closely associated with this common belief about the marine environments is the thought that corrosion may occur only in the presence of high levels of salt and/or humidity. Modern research has shown that this is anything but the situation. In fact, there exist in natural environments any number of critical air pollutants and at concentrations measured in sub-parts per billion (ppb) which can, together with even moderate humidity levels, drive these corrosion mechanisms. In view of these findings, it is not surprising that virtually all operational environments are **sufficiently** severe to drive corrosion on metal surfaces directly exposed to such environments. Recent work has shown that these conclusions extend even to the highly attenuated environments indoors and within vehicles/aircraft.

1.2 CORROSION INHIBITING LUBRICANTS -HISTORICAL

There are several approaches to the problem of connector corrosion. However, they all reduce to the concept of keeping the reactive environment away from reactive surfaces. One such approach is the use of organic lubricants which may also be referenced as corrosion inhibiting compounds (CPCs). This is actually a very old technology which has been widely discussed in technical conferences, but is one which is not widely practiced in the industrial world. The use of such materials is apparently permitted within the military as found, for example, in T.O. 1-1-689. However, we have found little indication of the use of these materials on electrical/electronics systems or even much knowledge about these materials within the military.

Discussions with both industrial and military personnel have yielded similar reasons for a reluctance to embrace lubrication technology. These can be described as either 1) common myths, or 2) inadequate technical information to support their use and to evaluate perceived risks. A summary of most of these factors is given in Table 1.

TABLE 1. LUBRICATION CONCERNS

-
- | | |
|---|--|
| ■ | Lubricant is an insulator |
| ■ | Effects of amount applied |
| ■ | Long-term aging effects/degradation |
| ■ | Effects of hardening at low temperatures |
| ■ | How long will it last |
| ■ | Effects of duct attraction and retention |
-

A large number of materials have been evaluated as classical contact lubricants (7). However, it is only in recent years that even these materials were evaluated in a comprehensive manner for use as corrosion inhibitors (8). This later work led to the important conclusion that few, if any, of the materials that were "known" to the contact/connector community would survive a comprehensive qualification program under a wide range of environmental extremes. Furthermore, few provided sufficient corrosion inhibition potential for consideration in this study.

1.3 FACTS LUBRICATION STUDY

In 1994, a program was initiated from the F.A.C.T.S. office at Wright Patterson Air Force Base to conduct an evaluation of several classes of materials for potential use as corrosion inhibiting lubricants and to eventually test the thesis set forth in the first part of this paper. The study had the constraint of being restricted to materials which were both COTS items and were covered by existing military specifications. This limited the study to most of the qualified sources under two specifications -- MIL-C-81309E and MIL-L-87177A.

It is interesting to note that both of these materials were generally unknown to the industrial, contact/connector community. In addition, at the time this study was initiated there was little, if any, hard data which could be found relating to qualifications for the intended applications.

2. RESEARCH PROGRAM

This work was done in two overlapping phases. The first was a laboratory evaluation and ground based field study. The second was a flight test program in which selected lubricants were applied on electrical connectors in the F-16 aircraft.

The first phase of this program has been completed. These results have been published (9) and for this reason this paper will not discuss the experimental details other than as an overview. The second phase is still in progress, but some important findings will be presented in this paper.

2.1 GROUND BASED STUDIES

2.1.1 Lubricants

At the time this program was initiated there appeared to be about 12-13 vendors of qualified lubricants. In reality, some of these materials were no longer routinely available but were supplied by some of the vendors.

As a result a total of 12 lubricants were evaluated in both field and laboratory studies. These consisted of 10 from the 81309E group and 1 from the 87177A group. The 12th material did not conform to either, but was a material which a vendor was promoting to the military for such use.

Most of these materials were available in the form of aerosol sprays. Those which were not applied by spraying using a small device as available from artists supply stores and with a CO₂ propellant. In fact, a requirement in this program was that all materials used should be free of ODC materials.

It should be noted that the identification of specific vendors has been avoided in this paper as a matter of Battelle policy. This information is available in reports made available to the funding organization.

2.1.2 Test Articles

The primary test vehicle used in this work was a gold plated, edge card connector. This item was used for a variety of reasons including experimental convenience. However, for purposes of this paper we may cite the most important reasons as 1) a high pin count allowing large numbers of electrical readings to be made for statistical purposes, 2) an "open" structure allowing free environment access to the contact interface, and 3) a relatively porous gold plating to provide for a worst case corrosion susceptibility.

It is recognized that this approach can be criticized as being unrealistic of many applications (open,unsealed, structure) and as a result overly severe. The counter to this was the program need to obtain degradation within a reasonable period of time. In addition it was argued that if corrosion inhibition could be demonstrated for this worst case situation the result could be viewed as very positive.

The second test article can be described as corrosion monitors. These were specially prepared metallic coupons which were deployed mainly at the field sites to document the corrosion conditions encountered during the field exposures.

Details of all of these items can be found in Reference 9.

2.1.3 Field Studies

Samples were deployed at 10 sites in CONUS. These ranged from severe coastal to less severe inland locations. Eight sites were at military bases and 2 sites were at the Battelle Corrosion Test Site at Daytona Beach Florida.

At these 10 sites, 8 points of sample placement were in the outdoor base environments (and DAB). Two were indoor but in uncontrolled environments.

At each location a relatively large test matrix was installed in a compact plastic test rack. Independent

connector samples were installed with each of the 12 lubricants plus an unlubricated reference and corrosion monitors.

These samples were exposed over a minimum period of 12 months. At 3 month intervals the samples were returned to Battelle for electrical measurements after which the same connector samples were returned to the field. Corrosion monitors were replaced at 3 month intervals.

The objective of the field studies was to support the laboratory work and to add to evaluation the complex synergistic effects including dust which can never be achieved in laboratory tests.

2.1.4 Laboratory Studies

Space is not available in this paper for a full discussion of the laboratory test phase of this work. Interested readers can find such information in Reference 9. It is important to note that the laboratory studies were designed to evaluate the performance of the same types of samples in a controlled manner and under a wide range of environmental conditions. The objectives in this work were to address the concerns listed in Table 1 and to provide a risk assessment for the use of any of these materials in subsequent flight tests.

2.1.5 Flight Tests

2.1.5.1 Lubrication

On the basis of positive findings from the Phase I studies a decision was made to proceed to flight testing in 1995. The F-16 aircraft was designated as the test vehicle due to its high reliance on electronic systems. This work which is still in progress has involved 12 bases (11 ANG, 1 AFR) and nearly 150 aircraft.

For this work 2 lubricants were selected for to be used. These were equally divided among bases as opposed to mixing lubricants within a given base. The lubricants selected were among the very few which survived comprehensive laboratory evaluations.

This work was originally designed as a limited, engineering study of lubricant effectiveness. The term limited means that a small number of LRUs were designated for treatment. These were mainly from the 74 (avionics) and 75 (weapons) systems on the aircraft. These were selected on the basis of high CND rates and/or high maintenance actions. While most bases in the program did comply with the Minimum Designated LRU requirement, the program met with sufficient enthusiasm that most bases have treated various LRUs in numbers far beyond this minimum.

This work was an engineering study in the sense that minimal instructions were given to the maintenance personnel who performed all of the connector lubrication. The general guideline was to apply ant cleaning and/or lubrication in accord with T.O. 1-1-689 in which the details surrounding the spray application (time/amount/etc:) were not specified. Actually, this somewhat informal approach was supported by the prior ground based studies as having no effect on results.

2.1.5.2 Data Analysis

The results from the flight tests are being evaluated in two ways. One is feedback from base personnel regarding both their opinions about the use of lubrication as well as their perceptions about effect. The

second and more quantitative analysis is from the Maintenance Data reported into the REMIS database by 5 digit Work Unit Code (WUC).

3. RESULTS

3.1 Connector Field Exposure

3.1.1 Unlubricated Connectors

Figure 1 shows the contact resistance data distributions for all data from all sites as a function of time and for connectors without lubrication. For the reader not familiar with this method of data presentation or the interpretation of such results the following brief analysis will be given.

A design goal or one which indicates no degradation would be a flat line graph extending to the extreme right end of the X axis and with low resistance values. Conversely, a high resistance "tail" is a measure of degradation by corrosion and high risk.

The data in Figure 1 clearly show that test samples of this type can degrade severely in practically any base environment. As significant is the fact that if such environments actually reach the contact surfaces, degradation can be rapid.

3.1.2 Lubrication Effects

Figures 2 and 3 take the data from one (and the most severe) site and show the effects of the various lubricants. Actually, these two graphs summarize many of the important conclusions from this work at all sites. The data have been compared to the unlubricated condition for this site.

The results clearly show a large variation among materials and should serve as a note of caution about the arbitrary use of lubricants in the absence of extensive qualification data. Specifically, these results show that at least two materials appeared to **degrade** performance (4,5, and 7) and another three showed marginal benefits at best (9,10, and 12).

At the same time, the very positive finding was that a few lubricants could provide an exceptionally high degree of protection and with no apparent adverse effects.

It must be emphasized that Figures 2 and 3 address only the corrosion issues. They do not address other potential risks such as thermal degradation of lubricants and low temperature performance all of which are important to aircraft operation. For an evaluation of these effects reliance was made of the laboratory test data as given in Reference 9. When this was done and combined with all of the corrosion test results, no more than 3 lubricants were considered to have no known engineering risk and suitable for flight tests. Those lubricants were the ones identified as Lubes 1 and 6 in Figures 2 and 3.

3.2 Flight Test Phase

This section of the paper will present several types of data. It will show both ground level monitoring results and then preliminary analyses of LRU performance data. The purpose of the ground level monitoring is to place in proper perspective the severity levels of the environments in which the aircraft were based and for which performance data will be summarized. We will also attempt to show how this

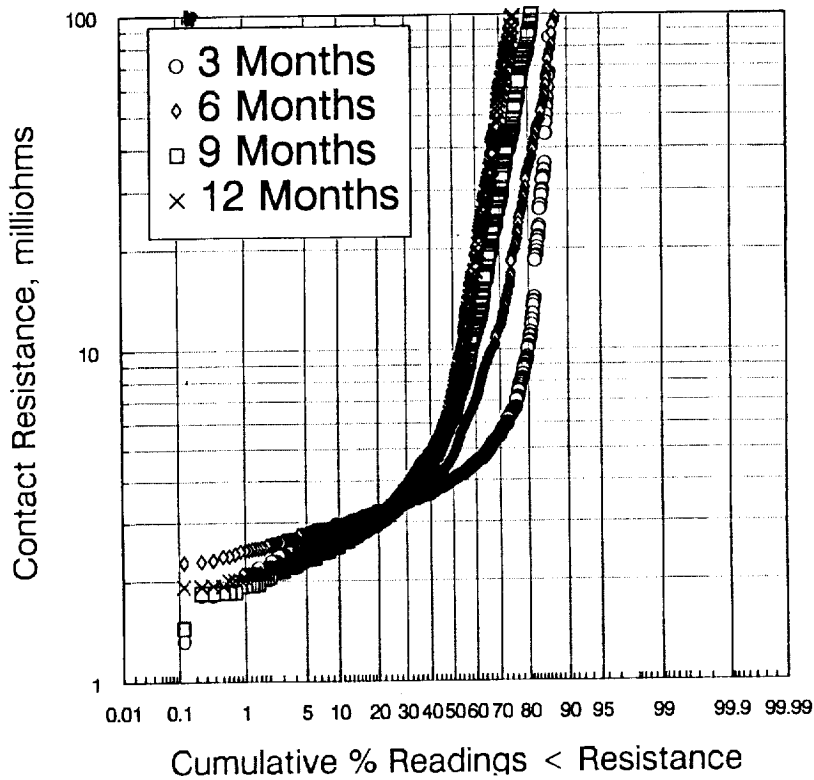


Figure 1. Contact resistance of mated, gold-plated connectors exposed at all field sites; 12/94 - 12/95, no lubrication.

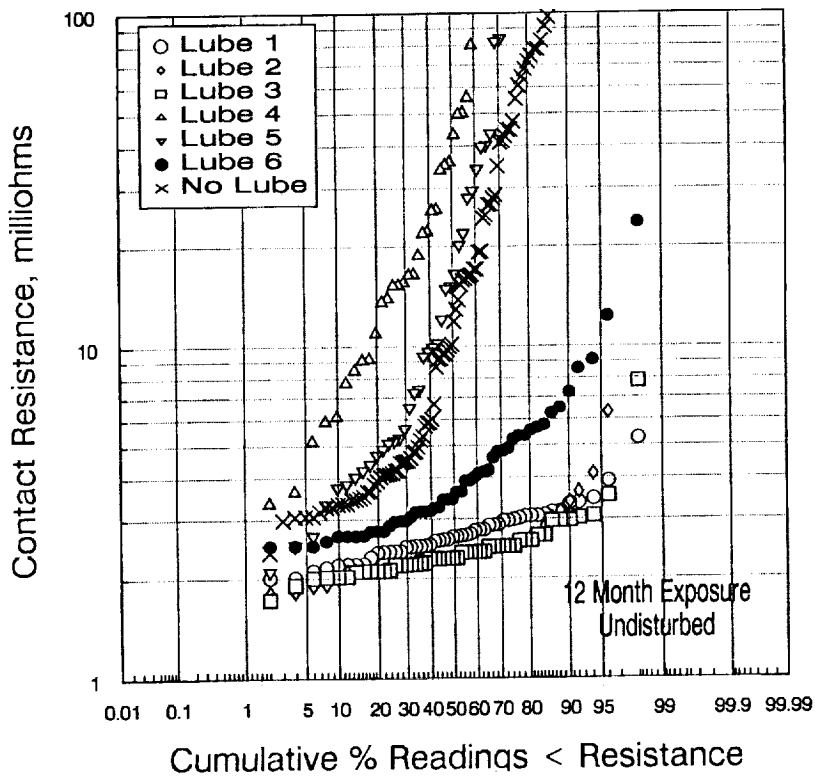


Figure 2. Contact resistance of aged mated gold-plated connectors at Daytona Beach (outdoors); 12/94 - 12/95.

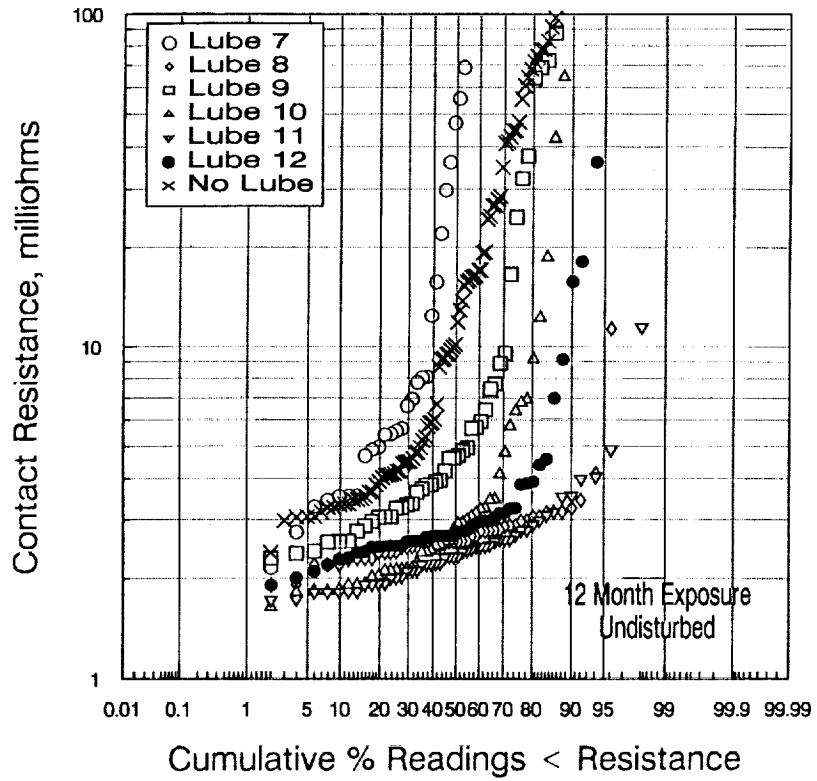


Figure 3. Contact resistance of mated, gold-plated connectors at Daytona Beach (outdoors); 12/19 - 12/95.

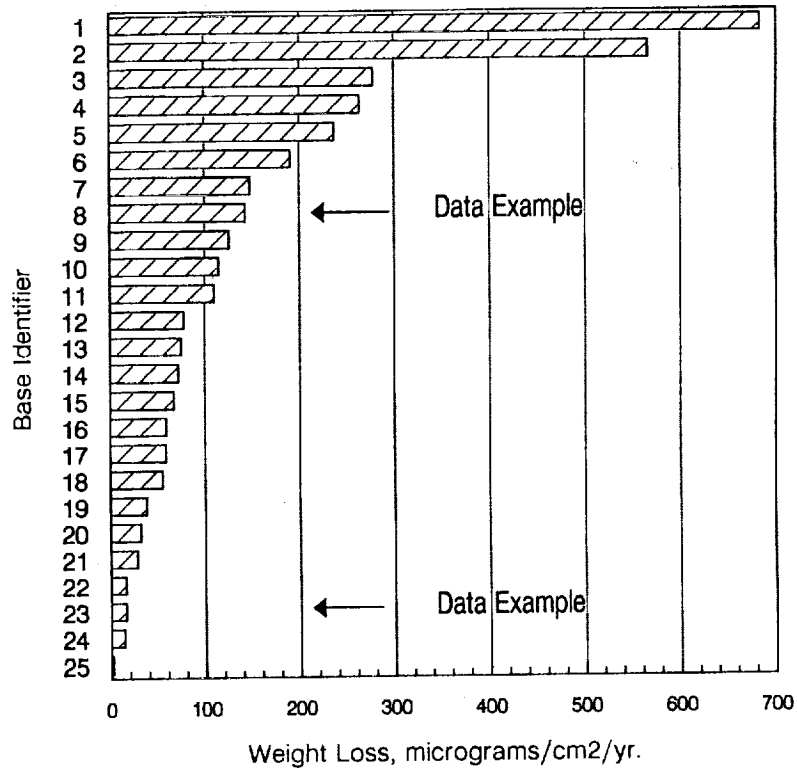


Figure 4. Weight loss on 6061 aluminum at outdoor field sites 270-365-day exposures normalized to 1 year.

subset of corrosion severity data for the F-16 fleet in CONUS compares to corrosion data at a wider range of sites being surveyed in other Air Force studies (10).

3.2.1 Base Level Corrosion Monitoring

Figure 4 shows the results from outdoor corrosion monitoring at 25 bases most of which are in CONUS. These particular data are for measurements made on 6061-T6 aluminum sensors, but we may note that additional data from other metallic sensors have given a similar rank ordering among sites. The bar heights, therefore, give measures of relative base severity.

As indicated earlier, the 12 bases with F-16 aircraft at which lubrication work is being done are a subset of the results in Figure 4. The actual range is Base 8 (highest) to Base 25 (lowest).

The corrosion measurements taken alone may mean little and serve only as a point of reference to describe the external base environment. The real questions for the purposes of this paper are 1) do even the test connectors corrode in these environments and, if so, how quickly, 2) is lubrication effective on these test items, and 3) is there any evidence of probable effects of lubrication on LRU performance?

To consider these questions, the results at 2 bases will be shown by way of examples. These are bases 8 and 23 as referenced in Figure 4.

Data are shown in Figure 5 for the test connectors exposed in the base environments and for three conditions -- no lube, and with Lubes 1 (an 81309E material) and Lube 6 (an 87177A material). The sample exposure was 1 year. It is clear that at Base 8 degradation on the No Lube connectors was severe (and rapid). At Base 23 with a relatively mild environment, there was measurable degradation sufficient to pose a risk to high reliability connector systems.

In both cases, either type of lubricant was totally effective for corrosion inhibition. It is also important to note that one characteristic of the Base 23 environment is a high level of dust/dirt as could be seen on the samples. In spite of this, there was no measurable effect on contact resistance. This latter result is consistent with the Phase I results concerning dust collection and retention by lubricants. To a large degree, such effects appear to be cosmetic rather than functional.

Finally, Figure 6 shows additional data on the rates of test connector degradation in the external environments of 3 bases in the flight test program. For purposes of illustration, the variable which is plotted is contact resistance taken from a fixed point on the distributions such as that shown in Figure 5. The only reason the values at the 70th percentile were selected was to keep the data on-scale, since values at a more meaningful level such as 95 or 99% were essentially at open circuit levels for the non lubed samples at Bases 9 and 17.

The significance of the data in Figures 5 and 6 is simply to emphasize what was stated earlier. This is that every effort should be made by whatever means to prevent ingress of ambient environments to connector interfaces. If this cannot be assured, and no supplemental protection such as lubrication is used, there is a reasonably high probability that corrosion will occur.

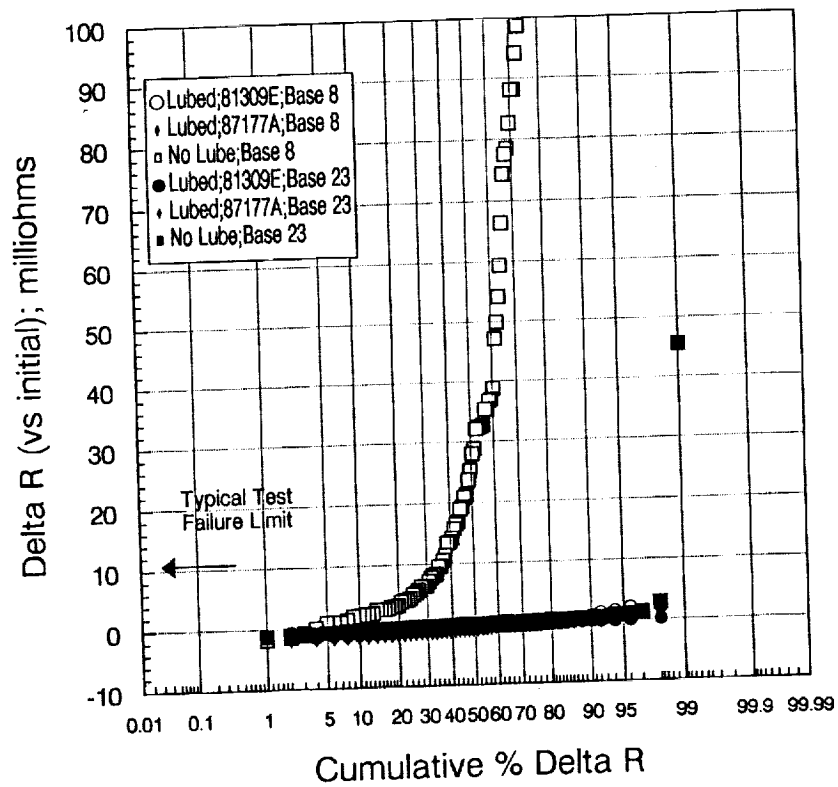


Figure 5. Contact resistance change of gold-plated connector test samples with and without lubricants; Base 8 and Base 23; exposed 1 year..

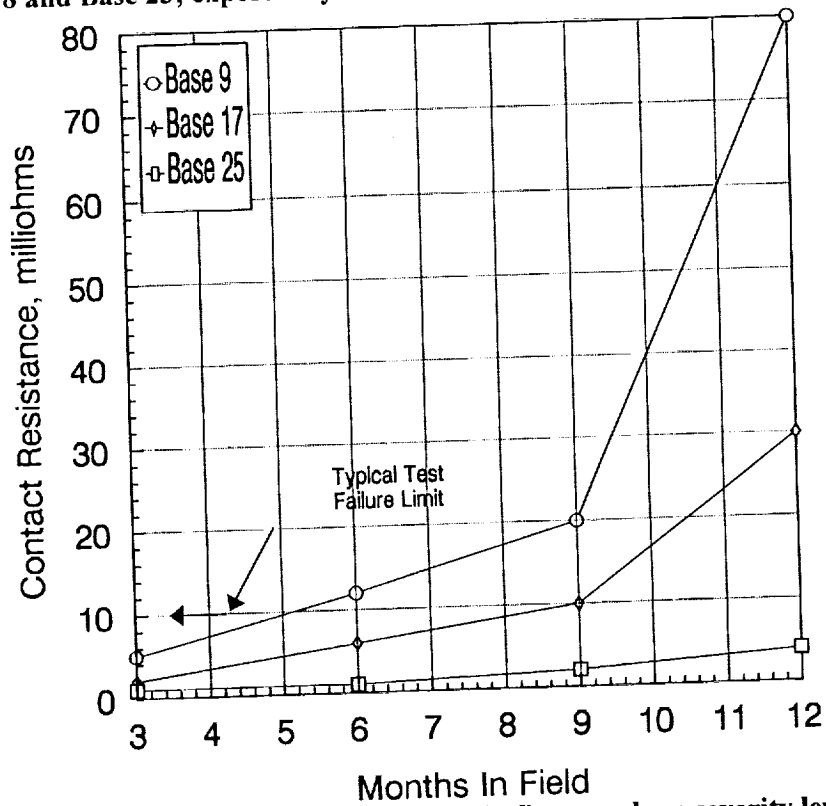


Figure 6. Typical connector degradation rates (electrical) versus base severity level; 70 percent percentile statistics.

3.2.2 LRU Performance

3.2.2.1 Base Feedback

To date, no negative feedback has been received from any participating base. No implementation problems have been reported. This includes subjective items such as touch, smell, etc:

3.2.2.2 LRU Data

It must first be noted that in work of this type it is nearly impossible to conclusively prove a cause and effect relationship. This is in sharp contrast to results such as those in Figure 5 where unique measurements can be made. Instead, the procedure has been to track data over time, compare results on the same basis against the rest of the F-16 fleet (presumably without lubrication), and attempt to develop a circumstantial argument for or against the benefit of lubrication treatment.

For purposes of this paper and as a summary, the data for Base 8 will be shown. Other reasons for discussing these particular results include a complementary analysis from this base to indicate substantial cost savings attributable to reduced LRU removals and the resulting reduced exchange costs. These results were claimed for only about 60% of the fleet completed.

At this base about 25 LRUs were reported to have been treated. These included 10 from weapons systems and 15 from avionics. Although data have been analyzed by 5 digit WUC, these data would be too voluminous to present here. Instead, the results for all treated items have been summed. For comparison data have been summed for the same items and time period for the entire ANG F-16 fleet.

Data are shown in Figures 7 and 8 for two measures of failures -- No Defect and Removals. Figure 9 shows On Equipment Labor trends against these particular items for the same period. While we must note that similar analyses by individual item/WUC will produce variable results as might be expected, the overall conclusions for this base remain favorable.

Final examples are shown in Figures 10-12 for one particular LRU, the 74AN0. The data from this particular base illustrates the need to follow results over a long period of time. The results suggest an increasing failure rate on this LRU for the subset of this aircraft population coming in phase to be treated. As the treatments were completed the data have become quite favorable particularly for removals, but the monitoring period since completion of the planned portion of the fleet has been short. As a result, we cannot determine what the long term effects will be or the effects as additional aircraft are completed.

4. CONCLUSIONS

The results obtained to this point in time must be viewed as favorable for the use of corrosion inhibiting lubricants as one means of reducing corrosion related failures in aircraft electrical systems. The treatments are attractive since the materials are inexpensive, implementation costs are low to negligible, and there is almost no effect on routine maintenance activities.

So far no adverse effects have been identified from the flight tests, and none are expected on the basis of laboratory studies. These conclusions, however, come with a repeated note of caution. This is that even though many of these materials may be qualified to existing specifications this does not mean that they

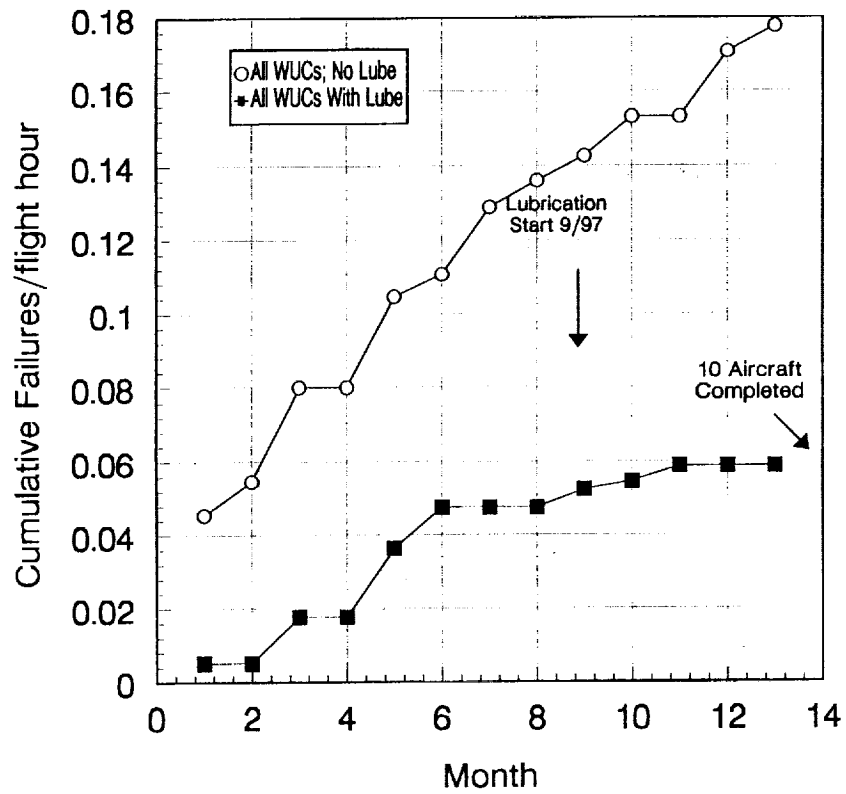


Figure 7. PPS (on) data for type-6 (no defect) failures for Base 8 with and without lube; Month 1 = January 1997.

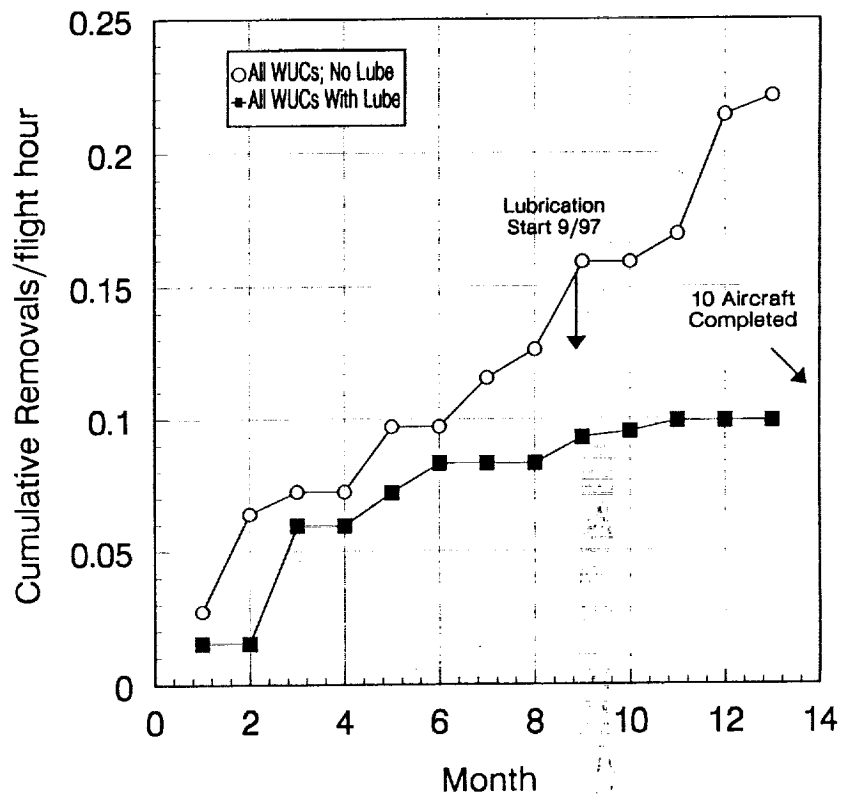


Figure 8. PPS (on) data for removals/flight hour; all WUCs for Base 8 with and without lube; Month 1 = January 1997.

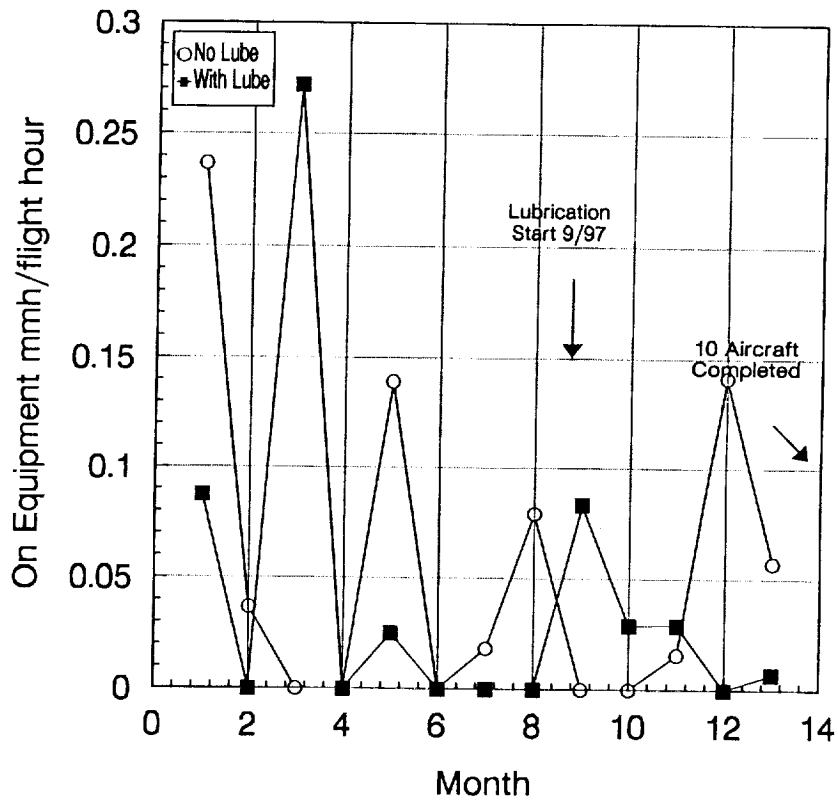


Figure 9. On equipment labor hours/flight hour; 74ANO for Base 8 with and without lube; Month 1 = January 1997.

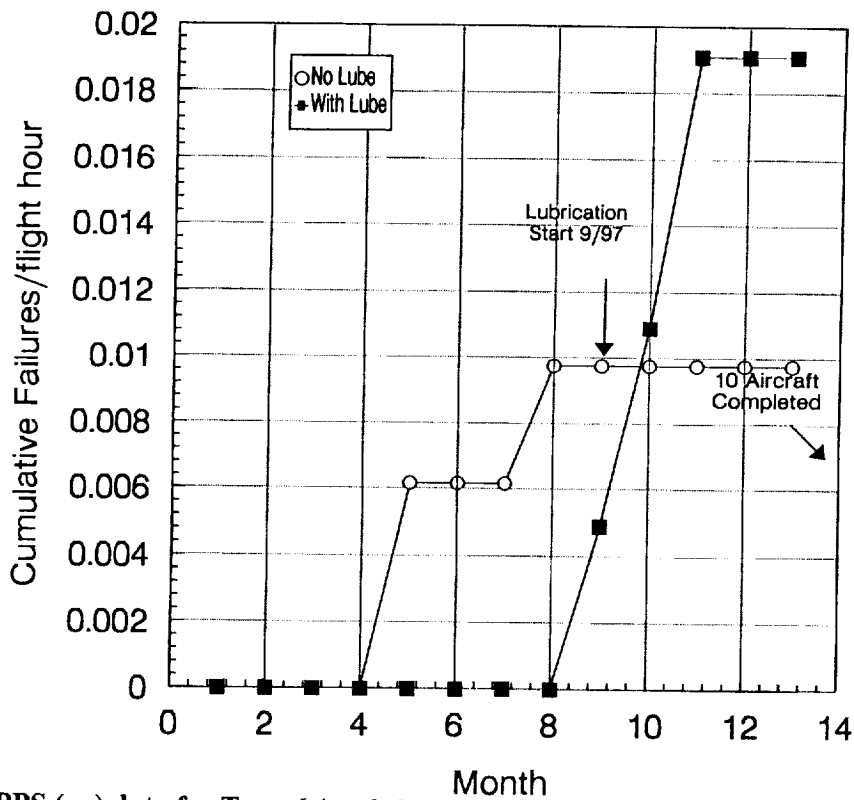


Figure 10. PPS (on) data for Type-6 (no defect) failures; 74ANO for Base 8 with and without lube; Month 1 = January 1997.

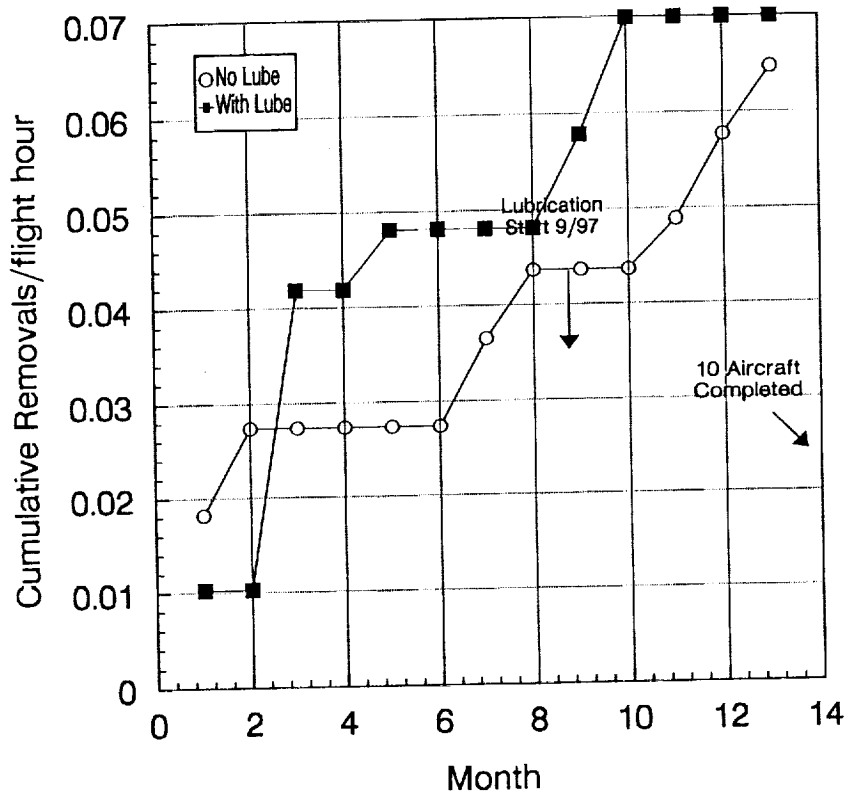


Figure 11. PPS (on) data for removals/flight hour; 74ANO for Base 8 with and without lube; Month 1 = January 1997.

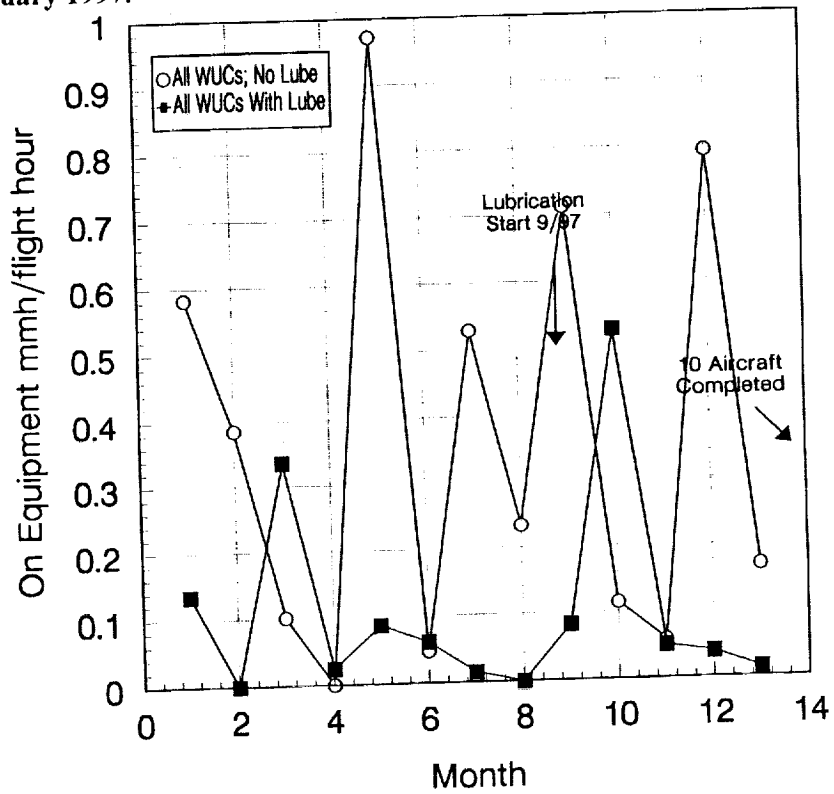


Figure 12. On equipment labor hours for all WUCs for Base 8 with and without lube; Month 1 = January 1997.

are equivalent in performance. In fact, some may pose an unacceptable risk but this conclusion has not been demonstrated on operating hardware.

In view of this situation, two recommendations should be made. One is that qualification requirements need to be upgraded considerably. The second is that corrosion inhibiting lubricants should not be used unless comprehensive test data are available to support vendor's claims.

References

1. Abbott, W.H. ; The Development and Performance Characteristics of Mixed Flowing Gas Test Environments; Proc. IEEE Holm Conf. On Electrical Contacts; 63-78, (1987)
2. Rice, D.W. ; Corrosion In The Electronics Industry; Corrosion/85, March 1985, Boston, paper No. 323
5. Abbott, W.H. ; The Corrosion Of Porous Gold Platings In Field And Laboratory Environments; 13th Int'l Conf On Electrical Contacts, Lausanne, 1986, pp343
3. Abbott, W.H. and Schreiber, K.L.; Dynamic Contact Resistance Of Gold, Tin, and Palladium Connector Interfaces During Low Amplitude Motion; Proc Holm Conf. On Electrical Contacts; 211-220, (1981)
4. Murrell, S.R. and McCarthy, S.L.; Intermittence Detection In Fretting Corrosion Studies Of Electrical Contacts; Proc IEEE Holm Conf. On Electrical Contacts; 1-6, (1997)
6. Abbott, W.H.; The Effects Of Test Environment On The Creep Of Surface Films Over Gold; 12th Int'l Conf On Electrical Contact Phenomena; Chicago, 1984, p. 47
7. Antler, M.A.; Corrosion Control and Lubrication Of Electronic Connector Contacts: Wax-Oil Barrier Coatings; Proc. IEEE Holm Conf On Electrical Contacts, 1995
8. Abbott, W.H. and Antler, M.A.; Connector Contacts: Corrosion Inhibiting Surface Treatments For Gold-Plated Finishes; Proc. IEEE Holm Conf On Electrical Contacts; 97-123; 1995
9. Abbott, W.H.; Field And Laboratory Studies Of Corrosion Inhibiting Lubricants For Gold-Plated Connectors; Proc. IEEE Holm Conf On Electrical Contacts; 414-428; 1996
10. Abbott, W.H.; unpublished data; work in progress

EFFECTIVE METHOD OF WORKING OUT AN OPTIMUM INSPECTION SCHEDULE

Veniamin L. Raikher
Central Aerohydrodynamics Institute (TsAGI)
Zhukovsky, Moscow region, 140160, Russia
Fax: (095) 556 4407

ABSTRACT

Two durations from total Fatigue Life Depleting Process are taken into account:

- the duration t up to reaching the critical damage size which characterizes the Limit State of the Structural Significant Item considered;
- the duration v of crack growth between Maximal Undetectable Size (MUS), which is such a crack that can be missed (with small allowable probability) during the inspection, and the critical size. MUS depends sufficiently on the used inspection means and methods.

Both durations are random values. Their joint probability characteristics are considered as a $t - v$ System. An effective approach is described which gives an opportunity in a simple and uniform manner to calculate all necessary probability values for any probability characteristics of $t - v$ System and for any inspection schedule. The method is based on the procedure of forming on a $t - v$ Plane of some zones which correspond to possible properties of different structure copies if the individual $t - v$ Point «hits» into the corresponding zone.

The main features of probability characteristics of the $t - v$ System are investigated using the results of different type cyclic tests conducted in TsAGI during the 1960 - 70s. About 300 copies of the same Al-alloy D16 sheet coupon having a central hole have been tested. The derived qualitative results may be considered apparently as typical features for many aircraft structures.

1. INTRODUCTION

Modern approach to ensure safe aircraft operation is based on application of Damage Tolerance concept. Fig. 1 illustrates the relation between four fundamental ideas:

- critical state (critical damage size l_{cr});
- total life from operation start till critical state;
- maximal undetectable damage size l_0 and
- detectable damage growth duration from the state of Maximal Undetectable damage Size (MUS) till critical state.

The critical state is assumed to be the state, corresponding to the residual strength required (as a rule, it is no less than 67% of the initial one). The decrease of the structural strength level at any time moment lower than this limit value should be practically impossible.

MUS is defined as the maximal crack length that can be undetected during the inspection but with tolerable small probability; this size substantially depends on the inspection tools and techniques.

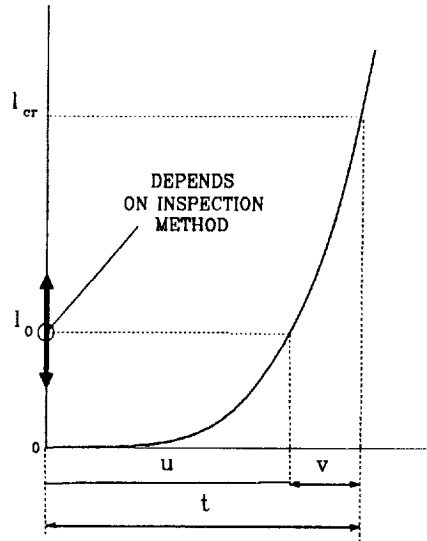


Figure 1. Notations.

The knowledge, first, of total life from operation start till critical state and, second, of detectable damage growth duration till critical state allows to define such inspection schedule (the inspection threshold and the inspection intervals), that could have ensured practical improbability of critical state achievement. The same requirement should be satisfied in case the inspections are not carried out at all by some reasons, while the structure is replaced or repaired at the moment when the first inspection is to be done, i.e. Safe Life concept is applied.

2.COMBINED DISTRIBUTION METHOD (CD - METHOD)

We must emphasize the approved account of very large scatter that is unfortunately accompanying this physical phenomenon. Both total life from operation start till critical state and damage growth duration from state of MUS till critical state are random values, corresponding to each separate copy of the same structure. Only the knowledge of their combined probabilistic properties considered as a system of two random values enables efficient but safe enough determination of inspection schedule required.

2.1.PLANE OF PROPERTIES

Let us consider the plane of random values t and v (see Fig.1) and according to refs.[1] and [2] define the properties of various copies of the same structure corresponding to the location of random $t - v$ Points inside different zones in the area of possible states.

If the operational time (without any inspections!) is T_{end} , all the copies having their $t - v$ Points inside the triangular of possible properties (Fig.2.1) must be failed because their total lives t are less than T_{end} .

If an inspection is conducted by the moment T_{insp} the damage of copies whose $t - v$ Points are inside the «Area of Detectability» (Fig.2.2) should be detected as the differences t minus v (i.e. u - values, see

Fig.1) are less than inspection time T_{insp} .

When a number of n successive inspections at the moments $T_1, T_2 \dots T_i, T_{i+1}, \dots T_n$ is conducted the general picture on the $t - v$ Plane is shown in Fig.2.3. The lowest row of zones (triangular marked with «0») indicates the «zones of unsafety» where the damage won't be detected by any inspection. The higher row of zones marked with «1» indicates the «zones of safety» where the damage will be detected by the previous (single!) inspection. The next rows indicate the «zones of high safety», because the damage may be detected by two or more previous inspections (marked in the Figure with «2»,...«k»,... etc); i.e. the loss of, for example, one inspection does not lead directly to loss of safety.

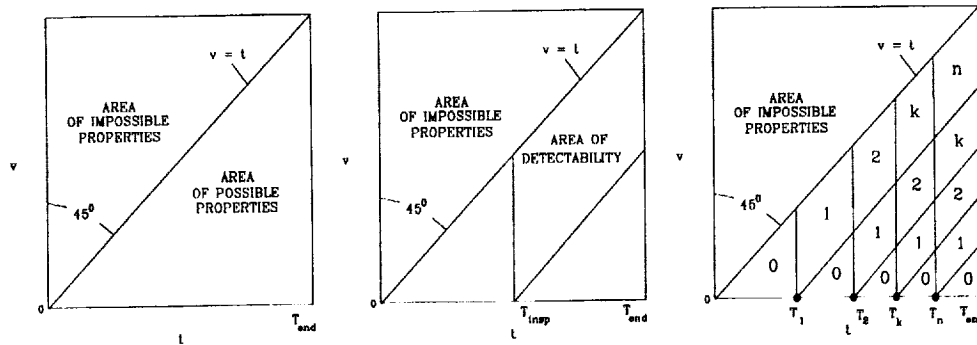


Figure 2. Plane of properties: 1 – without inspections in operation up to T_{end} ; 2 – one inspection in operation; 3 – many inspections in operation.

If combined distribution $f(t,v)$ of random values t and v is known, then the probability of points location inside any zone is calculated as $p = \int_{(zone)} f(t,v) dt dv$ and the necessary accumulated probability is

$$P = \sum p_i .$$

2.2.SOME IMPORTANT FATIGUE TEST RESULTS

In 1960 - 70s TsAGI performed extensive cyclic fatigue tests of different specimen types («smooth» and having stress concentrators, total of more than 2000 specimens) manufactured from various Al - alloys. Cylindrical specimens were tested by the bending during rotation, while the flat ones were affected by tension - compression. Test data and their analysis results are presented in ref. [3]. The main feature of this experiment was that fatigue was analyzed as two stage process; for some specimen types their number (4 - 5 and more for each loading mode) allows to get rather adequate statistical assessments of probabilistic properties.

Most comprehensive tests (about 300 similar specimens) were conducted under tension - compression of Al - alloy D16-T sheets 24 mm wide and 2.3 mm thick ($\sigma_b = 45 \text{ kg/mm}^2$, $\sigma_{0.2} = 28 \text{ kg/mm}^2$, $\delta = 12\%$) having central round hole 4 mm in diameter. The tests were conducted using 5 - 7 cycle amplitude values (from the following: $\sigma_a = 4; 5; 6; 7.6; 8; 9.2; 10; 12$ and 14 kg/mm^2) for each of different levels of the average cycle stress σ_m ($\sigma_m = 0; 3; 6; 10; 14$ and 20 kg/mm^2). During the tests each specimen was periodically (approximately after each 5 10% of the average life expected) inspected using penetrant

to detect fatigue crack. Each specimen properties were defined in terms (see Fig.1) of cycle number u till the crack length of $l_0 = 0.15 - 0.3$ mm, duration v of the following crack growth and total life t (till complete specimen failure! Therefore values v and t differ a little from the ones symbolized above). Unfortunately, crack growth process was not investigated in more detail at the time; experimental data of the kind including «continuous» fixing individual properties of life duration process started to appear much later (ref.[4]); but they contained the data only about the growth stage of the crack being initiated . In 1996 the results were published in ref. [5] of the unique experimental study of individual properties (for each of approximately 100 similar specimens) during the whole life duration. However the detailed statistical processing of these data (from the point of view of two stages) is impracticable due to the lack of initial experimental data (e.g. in the tabulated form) in the publication. As for TsAGI experiment, there are all initial data sufficient for additional more detailed statistical processing. The results of such processing are given in Figs.3 - 5.

As numerous investigations showed that the distributions of random lives u , v and t are approximately log-normal, the values to be analyzed are not lives themselves, but their decimal logarithms $\log u$, $\log v$ and $\log t$. In all the cases the mean value of any X is shown by the line above the letter (as \bar{X}), the sample estimate of root mean square deviation of X is symbolized by $S(X)$, and for the sample estimate of correlation factor between random values X and Y the symbol $r(X,Y)$ is assumed. The stress values are presented in kilograms per square millimeter.

The analysis gave the following important results:

1.The hyperbolic type relation (refs.[6,7]) for total fatigue life between the root mean square deviation (RMS) in life logarithm and its mean value is also verified by these experimental data. The similar relation is as well realized for each stage of life duration process. For all three durations the scatter increases much both for high and low lives (related to the scatter for the mean value of $10^4 - 10^5$ cycles). The general pictures of RMS for any life duration stages are approximately the same (Fig.3).

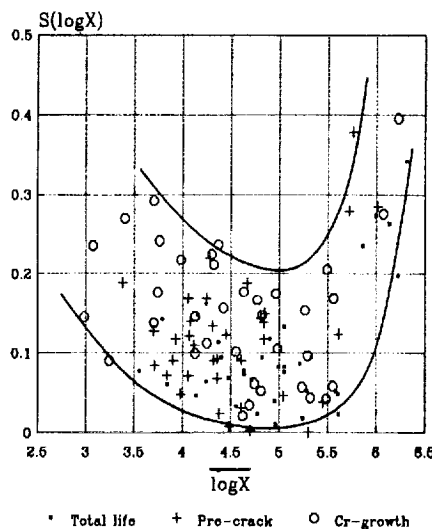


Figure 3. The influence of mean duration on scatter.

2.The mean relative crack growth duration v/t shows an obvious trend with maximal value of the cycle (Fig.4). This phenomenon may be explained as a result (only!) of decreasing the crack length by the failure (i.e. of shortening the duration of crack propagation stage) with increasing the maximal value of

the cycle. Therefore it may be supposed that the average relative crack growth duration \bar{v}/\bar{t} is independent of cycle characteristics and may be independent of loading structure in general.

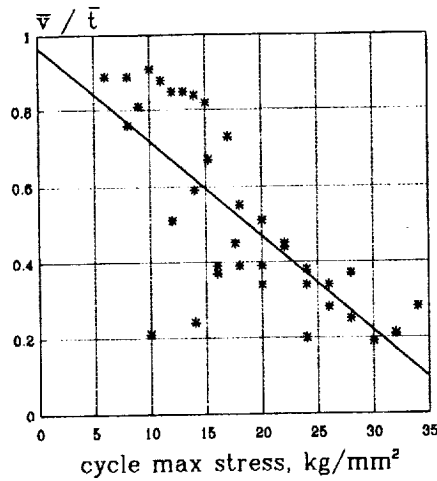


Fig.4. Relative crack-growth duration as a function of maximum value of the cycle.

3. The degree of correlation between the durations of two stages in the life duration process: u and v can be arbitrary; correlation factor has any values from the whole theoretically possible range $-1 < r < 1$ (Fig.5.1) and no relation with loading conditions or with relative duration of two stages is shown. However correlation factor between v and total life t (Fig.5.2) is positive in the great majority of cases and it is close to one for high \bar{v}/\bar{t} values, as it should surely have been.

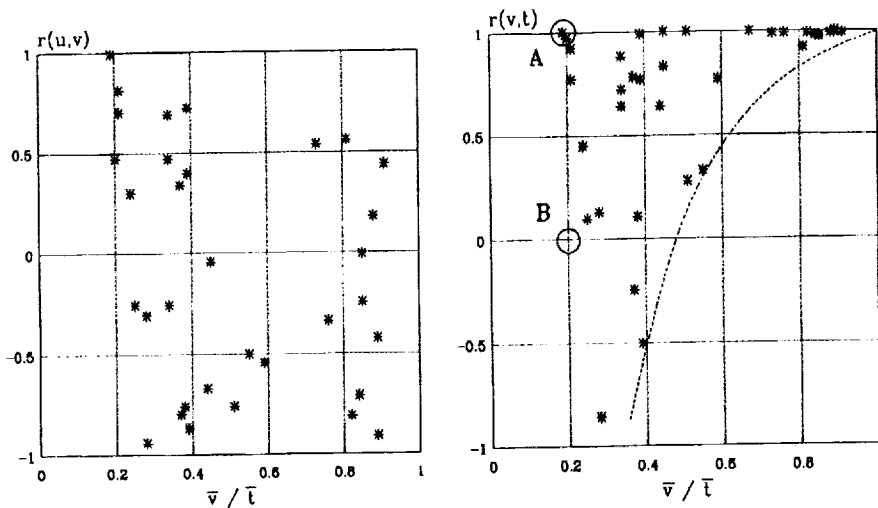


Figure 5. Correlation between crack-growth duration and: 1 – pre-crack duration; 2 – total life.

4. If the strong positive correlation exists between v and t the connection between $\log t$ and $\log v$ is linear, as a rule, witnessing that there is a proportion $v = kt$ in this case. It follows from this equation that $S(\log v) = S(\log t)$.

It seems possible to consider these quality laws obtained on «narrow» test conditions and test object being discussed here to be rather typical for such aircraft structures as plates, panels, etc.

2.3 EXAMPLES

Now let us consider two examples on the basis of the described approach that take into account the principal qualitative results of test data analysis.

2.3.1 STRONG POSITIVE CORRELATION BETWEEN t AND v

Let $r(t, v) = 1$ (point A in Fig.5.2) and $\bar{v}/\bar{t} = 0.2$, that reflects realistically enough the typical average relation between the crack growth duration for the crack detected in operation (as a rule, visually) and the total life. Let us determine the schedule of structure inspection in operation in accordance with the current Aircraft Regulations (ref.[8]) and Methods of Compliance (ref.[9]), that are:

- first inspection moment T_1 is mean life \bar{T} divided by reliability (scatter) factor $\eta = 3$;
- inspection interval ΔT is mean detectable crack growth duration $\Delta T = 0.2 \bar{T}$ divided by reliability factor $\eta = 2$;
- specified service life is assumed equal to mean life \bar{T} divided by reliability factor $\eta = 2$.

The resultant situation is illustrated in Fig.6 where the «zones of unsafety» are hatched. As $r(t, v) = 1$, all random points, representing the individual values t and v would lie on the straight line $v = kt$ starting from the coordinate zero and crossing point (\bar{t}, \bar{v}) .

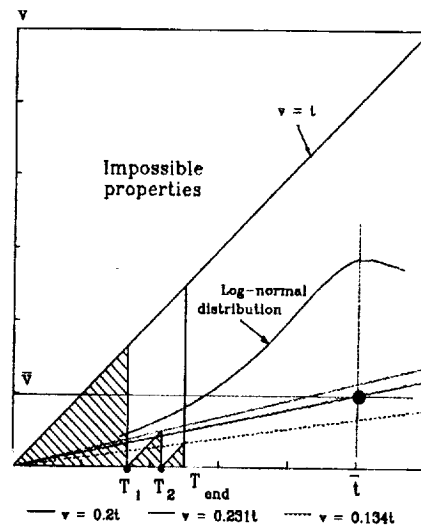


Figure 6. Example 1. Strong correlation between crack-growth duration and total life.

Random value t distribution is assumed log normal (according to the assumption, being the basis to determine Standard Reliability Factors) and having the standard value of root mean square deviation of $\log t$, equal to $S(\log t) = 0.15$. It should be reminded that as it has been noted above the same scatter is valid for $\log v$.

It is seen in Fig.6 that the straight line $v=0,2 t$, where all possible realizations of random values t and v are located, is crossing the zones of unsafety only up to the first inspection moment and between the first and the second inspections. The probability values of random point «location» on the straight line parts inside «triangulars of unsafety» are determined using simple analysis based on Gaussian distribution

tables. These values are equal to $p_1 = 0.00074$ and $p_2 = 0.00206$. Accumulated probability $P = 0.0028$ (of the order of 10^{-3}) outlined by the assumed basic data can be considered reasonable.

However this probability value will greatly depend on the relation v / t . When such inspection methods are used where MUS decreases and consequently the relation v / t will increase and exceed the value $v/t=0.23$, then «the straight line of possible properties» will never cross the triangular between the first and the second inspections. Accumulated probability P of «unsafe properties» will be completely defined by the moment of the first inspection and will have its minimum value $P = p_1$. (It may be generally noted that if the limit life T_{end} is not established one may choose such inspection schedule that the straight line will never cross the triangulars and the inspection intervals will be increased (!) one after another).

On the contrary, when v / t decreases, as it is seen in Fig.6, accumulated probability will start increasing. For $v / t < 0.134$ the straight line will already cross all three triangulars; for very low v / t the inspections being recommended in current Methods of Compliance will give small effect (Fig.7); the interval between them must be much shorter.

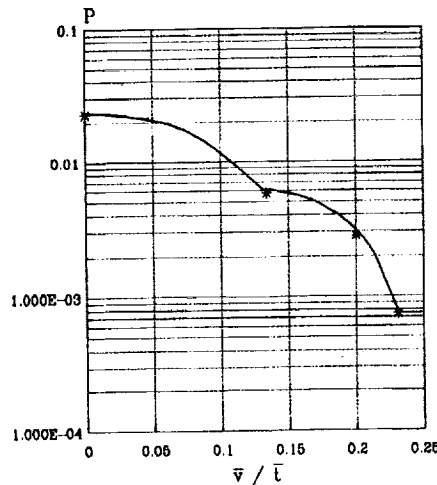


Figure 7. The influence of relative crack-growth duration on the probability that the crack will not be detected.

2.3.2. NO CORRELATION BETWEEN t AND v

Let $v/t = 0.2$ as earlier, but $r(t, v) = 0$ (point B in Fig.5.2). As t and v have log-normal distribution, the application of double logarithmic coordinates $\log t - \log v$ is more suitable. Inspection intervals are naturally like in the previous example, however, as it is seen in Fig.8, «triangulars of unsafety» have obvious deformation (they are also hatched). Random values $\log t$ and $\log v$ are independent and their combined distribution is illustrated by the system of scatter ellipses, where the values of probability of locating inside the appropriate ellipse are marked. Scatter characteristics of random values $\log t$ and $\log v$ are assumed standardized, i.e. $S(\log t) = 0.15$ and $S(\log v) = 0.10$ (their equality is not obligatory now). As it is well known for two dimensional Gaussian distribution there are no simple methods to analyze the probability of «locating» inside the zones of complicated form: the required assessments can be done by means of specific computer based statistical simulation (Monte Carlo method). However it is obvious from Fig.8 that for the conditions assumed this probability is very poor, as in the previous example; it

will increase substantially when the relation v/t decreases, i.e. when ellipse system displaces down the scale $\log v$.

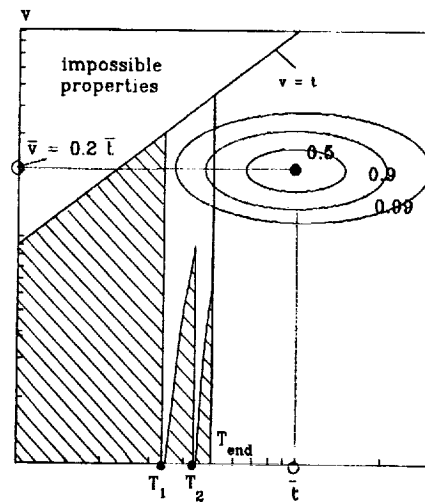


Figure 8. Example 2. No correlation between crack-growth duration and total life.

CONCLUSIONS

The principal role of combined distribution of crack growth duration and total life in inspection schedule planning is emphasized. Effective and very simple method of working out an optimum inspection schedule is proposed. On the basis of experimental data the importance of the crack growth duration relative contribution (related to total life) is discovered. When this contribution decreases:

- the indefiniteness in correlation factor between complete life and crack growth duration increases;
- with the inspection schedule selected the probability of reaching the critical state by the structure increases substantially.

REFERENCES

1. Zimont, Ye.L. (1977). TsAGI Scientific Notes, 8, 1 (in Russian).
2. Luchinskaya, Ye.L. and Raikher, V.L.(1997). TsAGI Scientific Notes, 28, 2 (in Russian).
3. Yekimenkov, L.N. (1974). Thesis, TsAGI, Zhukovsky, Russia, (in Russian).
4. Bogdanoff, J.L. and Kozin, F. (1985). Probabilistic Models of Cumulative Damage. John Wiley & Sons, Inc., New York – Chichester – Brisbane – Toronto - Singapore.
5. Liao Min, Xu Xiao fey and Yang Qing Xiong. (1996). In: Proceedings of ICAS 96 Conference, Sorrento, ICAS 96 6.6.4.
6. Raikher, V.L. and Selikhov, A.F. (1988). In: Mechanics Progress in Science and Technology, 4, Science, Moscow (in Russian).
7. Raikher, V.L. (1994). In: Proceedings of FAA/NASA International Symposium on Advanced Structural Integrity Methods for Airframe Durability and Damage Tolerance, Hampton, USA, NASA CP 3274, part 2, pp.621- 634.
8. Aircraft Regulations, part 25, AR 25.571. Airworthiness Standards. Airplanes of Transport Category. (1994). Interstate Aviation Committee, Moscow (in Russian).
9. Methods of Compliance (MOC) to AR 25.571. (1996). Aviation Register, Moscow (in Russian).

AN ENGINEERING APPROACH TO THE ASSESSMENT OF WIDESPREAD FATIGUE DAMAGE IN AIRCRAFT STRUCTURES

Marc Balzano, Jean-Yves Beaufiles, and Alain Santgerma
Aerospatiale Aeronautique
Dept A/BTE/CC/CM - Route de Bayonne, 316
Toulouse, 31060, France
Tel.: 33 5 61 93 82 05
Fax: 33 5 61 18 37 03
E-mail: alain.santgerma@avions.aerospatiale.fr

ABSTRACT

According to the recommendations of Advisory Circular AC91-56A, a full structural evaluation for Widespread Fatigue Damage (WFD) will be completed at Aerospatiale as part of the Airbus A300 extended service life activities. The approach followed in this evaluation is based on a specific calculation method, supported by experimental results provided by tear-down and analysis on a full-scale fatigue test and representative component tests. Research activities on the WFD phenomenon were done at Aerospatiale a few years ago in the framework of a thesis conducted concurrently with European research program on the same subject. Based on the Finite Element Method and Monte-Carlo simulations, an overall prediction method has been developed to automatically simulate multiple crack development in a structure in a realistic way. The two main particularities of this phenomenon, scatter at crack initiation and interaction effects, are taken into account. The same process allows different ranges of analysis to be completed, depending on the required objective. Calculation results have been successfully compared with tests performed on simple open hole and lap joint structures. This approach is now applied to the A300 aircraft structure.

1. INTRODUCTION

A full life extension program has been launched by Airbus Industrie to extend the high time A300 fleet operation beyond its initial Design Service Goal (DSG). A complete review and update of the maintenance program or modification will be needed to cover at least 25% additional service life objective. As part of the life extension program, the aircraft manufacturers committed themselves in the Airworthiness Assurance Working Group¹ (AAWG) to perform a full structural evaluation for Widespread Fatigue Damage (WFD). The Airbus Industrie partners – Daimler-Benz Aerospace Airbus, British Aerospace Airbus, Construcciones Aeronauticas S.A. and Aerospatiale – have thus initiated a specific WFD program.

The Advisory Circular AC91-56A² provides guidance for an acceptable means of accomplishing a structural evaluation for WFD. According to these recommendations, this activity will be conducted at Aerospatiale through a comprehensive approach: tear-down and analysis on extended full scale fatigue tests already performed on similar structures, calculations, additional partial and representative tests.

This paper presents the Aerospatiale assessment approach followed in this structural evaluation program, with particular emphasis on the developed analysis method.

2. AEROSPATIALE PHILOSOPHY FOR WFD ASSESSMENT

According to AC91-56A, the aim of this structural evaluation program is firstly to identify the primary structure susceptible to WFD, then to predict when this phenomenon is likely to occur and finally to establish, if necessary, the additional maintenance or modifications actions required to ensure the continued safe operation of the aircraft.

2.1 SUSCEPTIBLE STRUCTURES

The Industry Committee on WFD² listed generic locations potentially susceptible to WFD. A complete review of these areas has been carried out in order to identify the susceptible primary structures in the specific case of the A300.

2.2 WFD ASSESSMENT APPROACH

The figure 1 describes the comprehensive WFD assessment approach followed by Aerospatiale. It is mainly based on a specific calculation method to analyse the WFD behaviour on each susceptible area, supported by experimental results to provide input data and to validate this method. This approach has been chosen because, up to now, no experience of WFD has been found in-service. Some instances of non critical MSD /MED (Multiple Site Damage/Multiple Element Damage), in areas previously well identified by full-scale tests have been experienced.

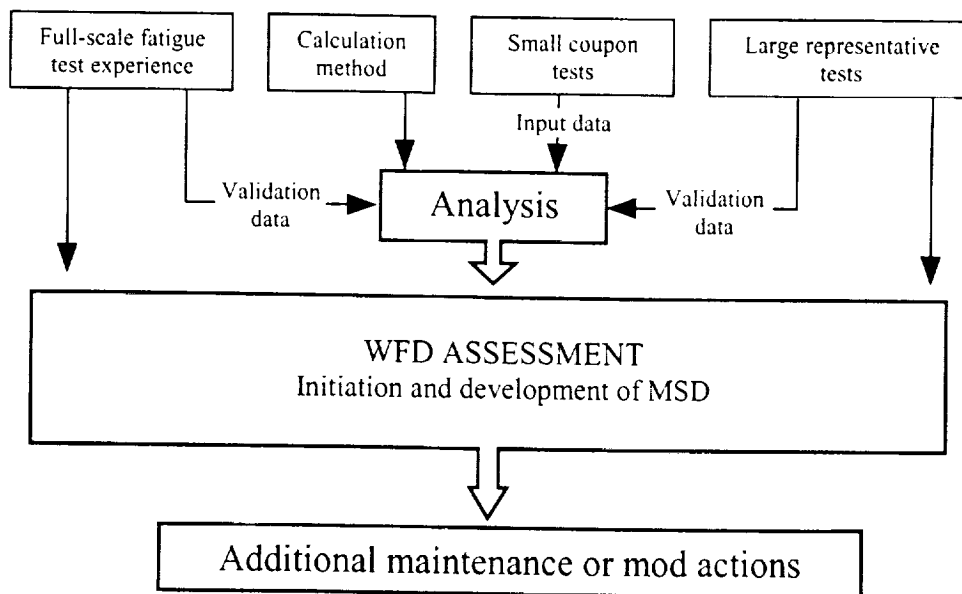


Figure 1. Aerospatiale approach to WFD assessment

Full-scale fatigue test experience. A300 full-scale fatigue test represented between 2 and 2.5 A300-B2 Design Service Goal. The areas in which MSD/MED occurred were identified by tear-down inspections and fractographic analysis.

Among the susceptible areas, some of them where no damage was found may be covered up to extended DSG without any further investigation if a sufficient number of cycles has been simulated (appropriate test-to-structure and scatter factor must be applied).

Additional tear-down of in-service aircraft and full-scale tests will be done to complement the analysis.

Calculation method. A specific calculation method has been developed at Aerospatiale in the framework of a thesis conducted concurrently with the Brite-Euram European research program Structural Maintenance of Ageing Aircraft (SMAAC), which is in its last stage. A complete and accurate analysis of the initiation and development of multiple cracks in a structure can be done, taking the scatter at crack initiation and the interaction effects into account. The major benefit is to investigate accurately the phenomenon without a large number of tests. A detailed description of this calculation method is presented in chapter 3.

Small coupon tests. The calculation method must be supplied with realistic data, including for instance scatter at crack initiation. This is why small coupon tests representative of the A300 structural areas will be performed.

Representative tests. An experimental program has been launched for this structural evaluation. Representative component test results will be used to assess the initiation and development of WFD, particularly where no reliable calculation method can be applied (thick structure assembly). Validation data for the calculation method will also be provided by some of these additional tests.

3. WFD SPECIFIC CALCULATION METHOD

Aerospatiale initiated research activities a few years ago to improve the understanding of WFD phenomenon³. The European Garteur and Brite-Euram research programs have also supported these activities, carried out as part of a thesis⁴. They have led to the development of an overall prediction method at Aerospatiale.

3.1 WFD PARTICULARITIES

The first step of these research activities was to investigate the basic behaviour of the WFD phenomenon. Two particularities have been identified that strongly distinguish it from the classical fatigue problem. Due to identical stress levels at critical sites, several cracks may initiate independently at different locations. But propagation of these cracks increases the local stresses at adjacent locations, speeding up initiation of new cracks. Furthermore, link-up of two or more cracks can lead to a major crack, which can behave dramatically. It is therefore essential to have an overall approach to this phenomenon. Accurate prediction of this complex behaviour needs not only determination of the precise original stress distribution but also exact stress evolution during the process.

Time to initiation of a crack is dependent on the local stress field and several random parameters like material quality, ... In the same stress conditions, crack initiation life can exhibit very large scatter. Thus, when several critical sites are equally loaded, a lot of initial crack scenarios are possible, each of them leading to very different crack evolutions and subsequently times to failure. This scatter must be taken into account. These particularities support our development of an overall methodology with a stochastic approach to crack initiation followed by a deterministic calculation of crack growth, link-up and fatigue failure. Determination of accurate stress fields will be achieved by means of the Finite Element Method.

3.2 DETAILED FEATURES

Limits of the study and assumptions. Fuselage skin joints are particularly susceptible to WFD and this method has mainly been developed to investigate this kind of structure. Some assumptions have been made:

- Plane thin sheet riveted or bolted joints are considered.
- Homogeneous and isotropic aluminium alloy is used.
- Uniaxial constant amplitude loading is applied (positive constant stress ratio R).
- Cracks are assumed to initiate at maximum hoop stress locations. They are immediately becoming one millimetre long through cracks, growing perpendicularly to the loading direction (Mode I). Short crack propagation is not taken into account and is assumed to be included in the initiation stage in conformity with material data.
- A small-scale yielding stress field is assumed, and therefore Linear Elastic Fracture Mechanics may be applied.
- Plane stress conditions.

Crack initiation criterion. S-N curves, or Wöhler curves, express initiation life versus applied stress for given loading, material and geometric conditions. These data, including scatter, are determined by representative small coupon fatigue tests for each structure analysed.

Increase in local stress at uncracked locations is taken into account by the Palmgreen-Miner⁴ linear damage accumulation rule.

Crack growth prediction. It has been demonstrated, throughout several test/calculation comparisons, that multiple fatigue crack growth does not reveal any particularity³. Accurate predictions may be achieved using Linear Elastic Fracture Mechanics assumptions, e.g. Stress Intensity Factors (SIF) and crack growth law (A Paris or Forman law). Nevertheless, an accurate method is needed to compute SIF, in order to take the interaction phenomenon into account (between cracks or between a crack and other “boundaries” i.e. holes, stiffeners...).

Crack link-up. An intuitive criterion was proposed by Swift to predict crack link-up⁶. It assumes that failure of the ligament occurs when plastic zones ahead of crack tips meet. Irwin, Dugdale or other approximations may calculate plastic zone sizes.

The Swift criterion is defined for two collinear cracks. We extended its application to the scenario of a crack reaching a hole.

Residual strength. Research activities on this topic are still in progress in the Brite-Euram project. A reliable method to predict residual strength of a structure in the presence of MSD is still under development, taking the discrete source problem into account.

3.3 OVERALL ASSESSMENT METHOD

Calculation of local stresses and SIF. The Finite Element Method is used to compute the local stresses at uncracked holes as well as Stress Intensity Factors at crack tips, as shown in figure 2. The structure is meshed with membrane elements (2D problem). SIF's are derived from the displacement field around the crack tip, where quarter-node isoparametric elements are situated in order to represent stress singularity⁶.

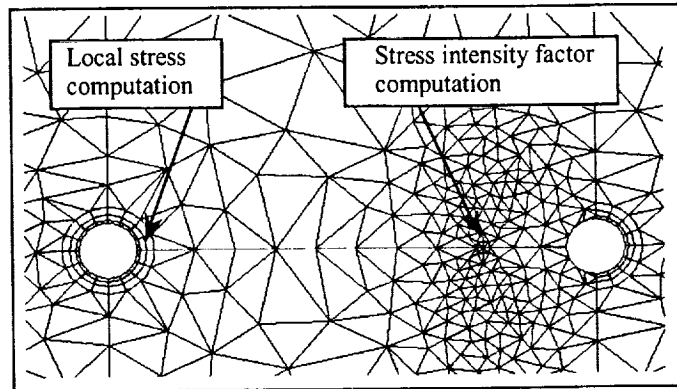


Figure 2 – Finite Element analysis

Overall tool. The Monte-Carlo method is very well suited to problems exhibiting complex random events and where a statistical solution is difficult to obtain. Simulating a lot of fictitious experiments thus approaches the solution of the physical problem. Regarding the WFD problem, several initial random scenarios are defined. The method consists in randomly setting a time to initiation at each critical location using the S-N curve and its scatter.

A numerical process named FENTOMAS allows an automatic simulation of initiation, crack growth, link-up and failure according to the criteria described above (figure 3). It is built around the Finite Element Method code SAMCEF®. A first crack, one millimetre long, is initiated at the “weakest” location. Propagation of this crack is simulated while damage accumulation, taking stress re-distribution into account, is performed at the other critical locations. When the “second weakest” location is reached, a second crack is automatically created. This process is then performed until failure of the structure, automatically determining a new initiation of crack and crack link-up. The tool has been developed with Unix shell and Fortran 77 languages.

In the Monte-Carlo simulation, this whole process is repeated several times. Between 100 and 150 scenarios must be performed to have a reliable approximation of the results, whatever the number of random parameters (critical sites). The process is described in figure 3. Detailed results are provided for each scenario and statistical post-processing of the results is accomplished, giving normal or lognormal distributions of the parameters to be discussed.

Deterministic simulation can be achieved with the same tool by defining the initial scenario with set values. These values can come from the mean S-N curve, or any kind of failure probability S-N curve.

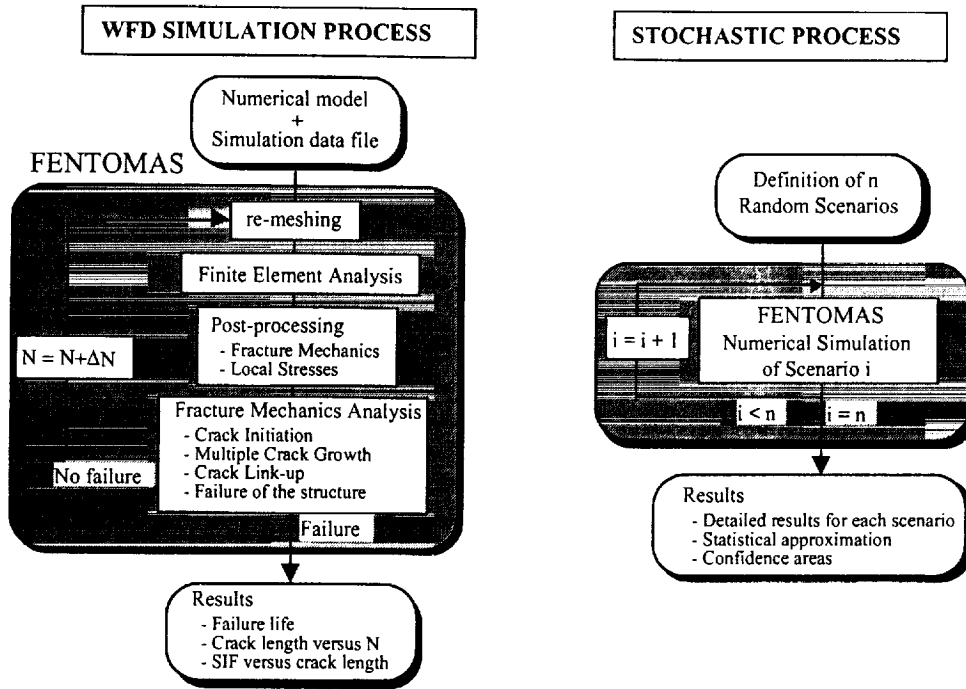


Figure 3 – Overall Assessment tool

3.4 APPLICATION

An application of the assessment tool on a simple structure is presented. Several comparisons with test results and other calculation methods were made, giving interesting results.

Test program. Fatigue tests were performed on six simple 14-open hole specimens made of 2024 T3 thin sheet (figure 4). A constant amplitude tension loading was applied ($R=0.1$ and $\sigma_{max}=100$ Mpa). Crack initiation and growth up to failure were followed by optical measurement.

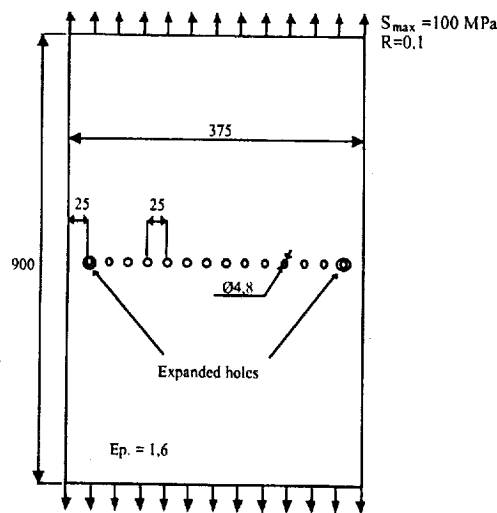


Figure 4. 14-open hole specimen

Analysis. Two kinds of analysis were made with a deterministic and a stochastic approach. 400 random scenarios have been simulated with the FENTOMAS process for the latter. Figure 5 shows an example of result for one simulated scenario. The geometric locations of the 14 holes are plotted along the X axis and the fatigue life plotted on Y. The number of cycles up to detectability of at least one crack is represented by the horizontal solid line.

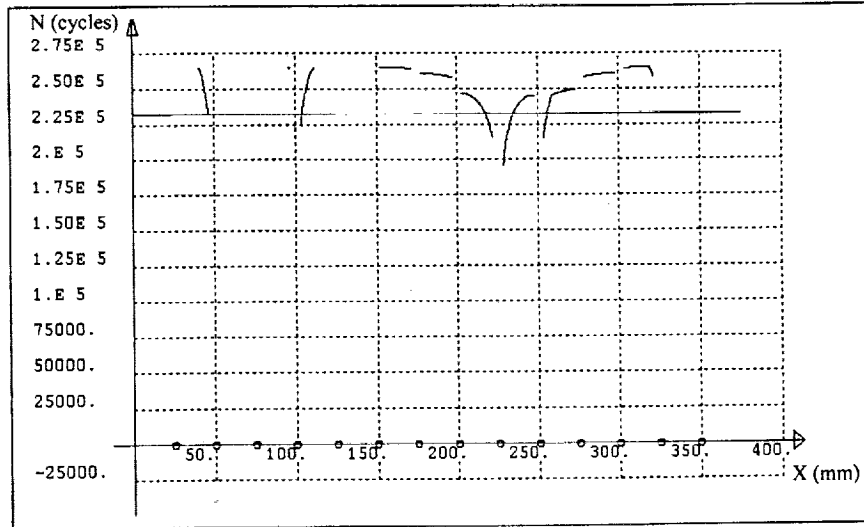


Figure 5. Example of stochastic simulation result

Statistical laws have been used to exploit the meaningful values from stochastic analysis. The comparison with test results shows that the behaviour is quite well represented, in terms of fatigue life to initiation, propagation phase and number of cycles to failure.

The probability of occurrence of a particular scenario may be determined from the stochastic analysis. The likelihood of at least 2 or 3 adjacent cracks being present in the structure are compared in figure 6 with those calculated using a theoretical solution (probability calculation derived from the basic crack initiation law by binomial law application). Significant differences between the 2 approaches are observed particularly for 3 adjacent cracks, because the stress evolutions at uncracked locations are taken into account in our approach.

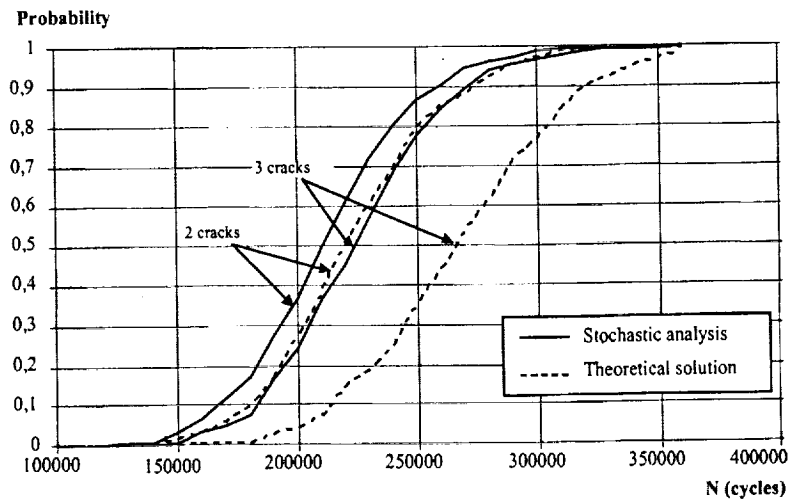


Figure 6. Probability of at least k adjacent cracks being present

3.5 FEATURES OF THE ASSESSMENT TOOL

Due to the FENTOMAS architecture, several different ranges of exploitation are possible with the same assessment tool. Depending on the required analysis, a stochastic or deterministic approach may be applied with either an overall simulation – including crack initiation, crack growth and failure – or a partial simulation, crack growth for example. This feature will be very useful in this WFD evaluation.

CONCLUSIONS

The Aerospatiale structural evaluation for WFD will be carried out according to AC91-56A recommendations. The philosophy is based on the use of a specific prediction method, supported by experimental results (full-scale fatigue tests, representative panels and small coupon tests).

An overall assessment method has been developed at Aerospatiale to predict the behaviour of multiple cracked structures. The originality of this method consists in coupling an advanced calculation method, the finite element method, and a stochastic approach, the Monte-Carlo simulation method. The simulation is carried out taking interactions and scatter at crack initiation into account. The tool developed allows different kind of analyses to be achieved : stochastic/deterministic approach, complete simulation or only crack growth simulation,... Initial comparisons on simple open hole and lap joint structures show a very good agreement between test and calculation results. Analysis is now in progress on A300 riveted joint structures.

Scatter at crack initiation constitutes one of the main particularities of the MSD phenomenon, which is difficult to take into account by fatigue tests only. The use of a calculation method together with fatigue tests seems to be the best way to perform a complete and accurate analysis of the MSD phenomenon.

REFERENCES

- (1) Industry Committee on Widespread Fatigue Damage. « Structural fatigue evaluation for aging airplanes. Final report of the AAWG, October 1993.
- (2) Advisory Circular n° 91-56A. "Continuing structural integrity program for large transport category airplanes". Draft 6/23/97.
- (3) Santgerma, A., "Développement d'une méthodologie de prévision du comportement des structures d'avions civils en présence de dommages multiples de fatigue", Thesis report, I.N.S.A. Toulouse, December 1997.
- (4) Miner, M.A., "Cumulative damage in fatigue", Trans. ASME, J. Appl. Mech., vol. 67, 1945, pp. A159-A164.
- (5) Swift, T., "Damage Tolerance Capability", Specialists Conference on Fatigue of Aircraft Materials, Delft University of Technology, 1992.
- (6) Barsoum, R.S., Int. J. Num. Meth. Eng., Vol. 10, 1976, pp. 25-37.

TRANSPORT RISK ASSESSMENT CONTAINING WIDESPREAD FATIGUE DAMAGE: TRACWFD ANALYSES OF LONGITUDINAL AND CIRCUMFERENTIAL SPLICE JOINTS TO DETERMINE THE ONSET OF WIDESPREAD FATIGUE DAMAGE AND ITS PROBABILITY OF OCCURRENCE

Robert E. Kurth
Battelle Memorial Institute

Catherine A. Bigelow
FAA William J. Hughes Technical Center

ABSTRACT

A probabilistic analysis tool has been developed over the last two years to assess the damage progression in aging aircraft and such damage's impact on the onset of widespread fatigue damage, the residual strength, and maintenance and inspections. The analysis tool combines the results of previous Federal Aviation Administration, US Air Force, and National Aeronautics and Space Administration developments into a fast, efficient mechanics model for the aging aircraft fleet. Studies have been concluded examining a narrow-body jet longitudinal lap splice, wing, and circumferential lap and butt splices. Several predictions of the time-dependent probability of the onset of widespread fatigue damage and the loss of residual strength have been made. More importantly, the minimum crack sizes that must be able to be detected to maintain a risk level have been predicted. Times between inspections, the impact of wall thinning due to corrosion, and initiation predictions can be studied with this tool. This paper will present an overall description of the model and some of the results generated to date.

INTRODUCTION

As aircraft age, damage accumulates throughout the structure. Many researchers at universities, private companies, and government facilities have worked diligently to develop models to assess this damage progression as well as reconcile the results of such modeling with experimental and flight results. In 1996 the Federal Aviation Administration (FAA) William J. Hughes Technical Center began the development of a model that would act as an integrator for the major deterministic models of aircraft damage in the context of risk. The onset of WFD, as well as the structure's residual strength, are not deterministic quantities, rather there is some probability that either the onset of WFD has occurred or the residual strength has fallen to unacceptable levels. Not only are these calculations a function of the underlying physical processes but they are also a function of the maintenance and inspection procedures performed on the aircraft.

Thus, a program was initiated in 1996 to develop a computer model that would encompass all of the physical processes important in aging aircraft. Even for those processes for which detailed deterministic models are either unavailable or not yet validated, "place-holders" are to be included in the model to provide for the future expansion into those areas of investigation. For example, corrosion related wall-thinning rates together with the associated reduction in strength are not well understood. However, the phenomena has been included in the analysis model in a first order manner. Because of the program's initial emphasis on WFD, and the calculation of the risk associated with such phenomena, this computer model has been named **TRACWFD** – Transport Aircraft Risk Assessment Containing Widespread Fatigue Damage. Phase I of this program has been completed, and a tool has been delivered to the FAA William J. Hughes Technical Center to evaluate the risk associated with aging in aircraft structures.

To assess the risk of failure of an aircraft structure, it requires detailed knowledge about the materials, loadings, applied stresses, damage mechanisms, and failure modes of the structure. In addition to detailed knowledge concerning the nominal behavior of each of these processes, it is also critical to define the uncertainty in their behavior. Only by adequately quantifying these uncertainties can one develop an estimate of the structural integrity and risk. However, this is not a simple task.

The ability to model an aircraft from a good as new condition to ultimate structural failure also requires that the processes associated with aging be addressed. Thus, corrosion, corrosion fatigue, material degradation due to fretting, fatigue crack initiation, and so forth must be included in the model. This cradle to grave analysis capability implies that the model must be able to decide which processes are important to address depending upon the service history of the aircraft. Thus, it is generally not important to include corrosion models in the risk analysis of an aircraft when first placed into service. Similarly, it is generally not important to model fatigue crack initiation processes in an older aircraft that has already been exposed to 75,000 pressurization cycles. This kind of logic has allowed analysts to limit the variables being considered and to perform deterministic structural analyses in a manageable fashion. The introduction of risk into the analysis makes these calculations much more difficult. This is because there is some probability, albeit small, that a rogue crack will develop in the structure or that the structure will suffer significant corrosion damage after only several hundred pressurization cycles. Thus, such a risk calculation requires that many complex structural calculations be performed simultaneously for much of the aircraft's service life. Unless handled properly, this risk assessment process can become very time consuming and cost prohibitive.

TRACWFD: OVERVIEW

The computer program TRACWFD is a powerful tool for assessing the effect of a variety of factors on the overall risk of commercial and military aircraft operation under the conditions of aging. A variety of conditions have been used in the engineering community to describe aging. Some of the damage mechanisms that can be addressed with TRACWFD are:

- ◆ Crack initiation
- ◆ Linear and nonlinear curved-panel stress analyses
- ◆ Fatigue crack growth
- ◆ Corrosion
- ◆ Corrosion fatigue
- ◆ Nondestructive inspections (NDI)
- ◆ Residual strength analyses
- ◆ Multisite damage (MSD)
- ◆ Multielement damage (MED)

The use of the computer program has been divided into two phases. The first phase of the analysis for a particular aircraft structure is deterministic, wherein the nominal behavior is calculated in terms of local damage conditions, stress concentrations, and crack driving forces. The second phase of the analysis involves the probabilistic modeling of the mechanics models, loads, and inspection procedures.

CRADLE TO GRAVE: SETTING UP AN AGING AIRCRAFT ANALYSIS

To use TRACWFD, the user must develop a detailed plan. To start off the analysis with a pristine aircraft and carry the calculation forward to the end of its life is the goal. However, reaching this goal in incremental steps is ultimately the most efficient.

The major steps in designing a cradle to grave analysis of an aging aircraft structure are:

- ◆ Define the aircraft geometry
- ◆ Define the initial damage condition
- ◆ Define the fatigue crack growth model
- ◆ Define whether corrosion will be considered
- ◆ Select the residual strength model
- ◆ Set inspection intervals at selected time intervals or based on specified risk conditions

Each of these steps is complex. It is not possible to define a widespread fatigue damage analysis of an aircraft without having a working knowledge of structural mechanics. However, TRACWFD does allow for an easy analysis of the risk factors associated with an aging aircraft once a consistent mechanics model has been developed.

To develop a consistent mechanics model for an aircraft structure, TRACWFD contains a detailed finite element model based on physical parameters. Thus, if a standard stringer, rib, frame, etc., is used, then by simply specifying the dimensions and spacings of the structural components a detailed stress analysis model can be developed. Figure 1 shows the result of such a model construction exercise.

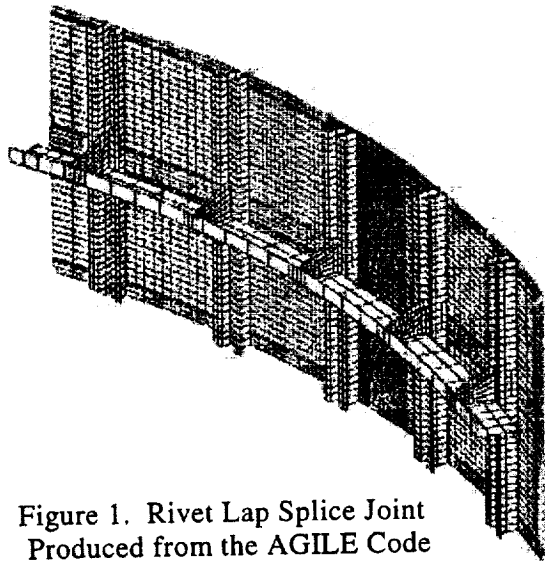


Figure 1. Rivet Lap Splice Joint
Produced from the AGILE Code

Once the global model has been developed, TRACWFD performs detailed stress analyses of the structure using the NASA Langley-developed code, STAGS (Structural Analysis of General Shells), for the global stress analysis and the FEAM (Finite Element Alternating Method) code, developed by the FAA William J. Hughes Technical Center for local stress and crack growth analysis. STAGS was developed specifically for curved-shell analysis, thus it provides very accurate solutions for fuselage analyses. The FEAM code allows cracks to be inserted anywhere in the local model. This is critical for subsequent probabilistic fatigue and fracture analyses.

The available probabilistic methodologies include Monte Carlo, discrete probability distribution methods¹ (DPD) developed for NASA Johnson Space Center², PROF developed for the USAF³, and Level II reliability methods developed for NASA Lewis Research Center.⁴ The primary probabilistic engine is the DPD method, however, each is used as appropriate for efficient calculations. For example, the residual strength calculation is performed exclusively with level II methods.

The results of the STAGS analyses are integrated into the TRACWFD analysis in several ways. First, stress concentrations can be used to identify initiation sites. The local crack driving force, usually defined by the mode I stress-intensity factor, K_I , is also developed from this analysis. The residual strength of the structure is subsequently calculated using the STAGS/FEAM analysis. Finally, a coupling of the probabilistic fatigue crack growth analysis and the residual strength analysis leads to a determination of the likelihood of the onset of WFD. To illustrate the capabilities of TRACWFD, some sample calculations are discussed in the following sections.

SAMPLE TRACWFD CALCULATION: FUSELAGE RIVETED LAP SPLICE

One of the standard analyses that are carried out for every program that addresses WFD is that of the rivet fuselage lap splice joint. This is the location of the only known component failure due to WFD.* Most studies compare the results of the analyses to the Foster-Miller data.⁵ However, in 1997 an extensive study by Piascik and Willard⁶ was published. This study provides much more detailed information on fatigue cracks in curved panel, riveted, lap splice joints. Therefore, we will use the results of this study to assess the accuracy of TRACWFD.

LAP SPLICE JOINT MODEL PHYSICAL DESCRIPTION

The lap splice joint chosen for study has the physical characteristics typical of a narrow-body commercial jet. The first step in the TRACWFD analysis is the construction of the stress analysis model for the area of interest on the aircraft. The construction of the stress analysis model was based on the STAGS⁷ and FEAM⁸ stress analysis codes. The stress analysis procedure uses a global-intermediate-local hierarchical procedure. In this procedure STAGS performs the global and intermediate analysis while FEAM performs the local stress analysis. This procedure was selected because of the probabilistic nature of the analysis. To perform a probabilistic analysis requires many solutions of cracks growing in a structure under a variety of conditions. Because the FEAM method only requires the inversion of the stiffness matrix one time, we are able to solve the global-intermediate stress problem once and store this solution. After this single solution, FEAM is able to analyze any combination of MSD cracks within the local model to predict the crack growth behavior.

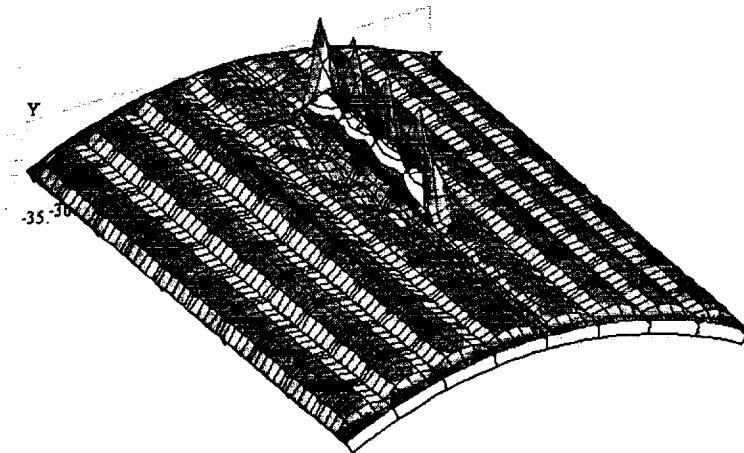


Figure 2. Global Solution of Riveted Lap Splice Joint by AGILE/STAGS

AGILE/STAGS solution procedure. The final result, the local solution, generated by FEAM is also controlled in a similar manner. Thus, after the initial inputs describing the physical characteristics of the aircraft component being analyzed, AGILE/STAGS/FEAM will automatically generate the necessary solutions without any further user interaction. The results of a local model solution are shown in Figure 4.

Figure 2 shows a global solution for the stress produced from the STAGS analysis. This solution procedure was enhanced for aircraft structures through the development of a module labeled AGILE. AGILE is an interface code that allows a user to simply specify frame spacing, rivet hole diameter, stringer type, stringer spacing, and so forth to automatically generate a finite element grid for STAGS and FEAM solution. Additionally, all file transfers, boundary conditions, and so forth are controlled by AGILE so the interface between STAGS and FEAM is invisible to the user. Thus, the intermediate solution, shown in Figure 3, is automatically generated during the

* While it is true that the Aloha accident was a tremendous tragedy, the aircraft did land after the large failure of skin and stringers, thus this would be classified as a component failure not an aircraft failure.

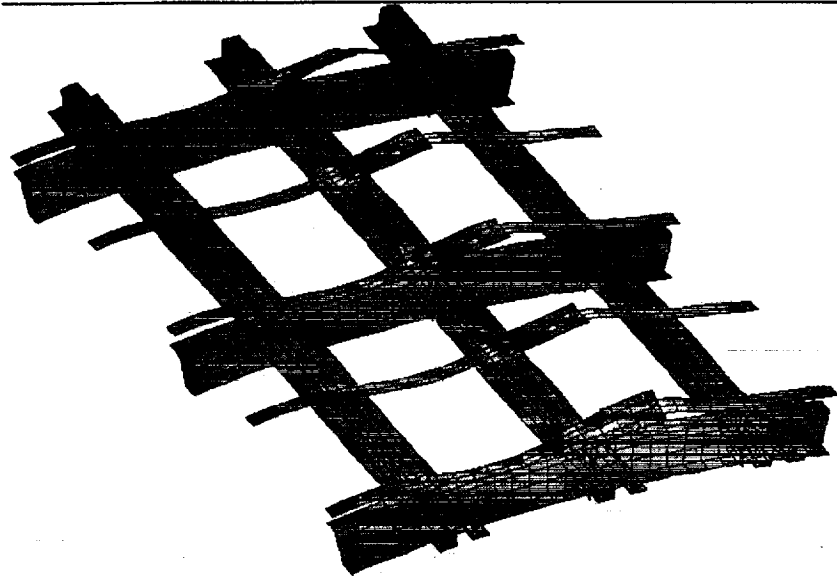


Figure 3. Intermediate Solution of Riveted Lap Splice Joint by AGILE/STAGS

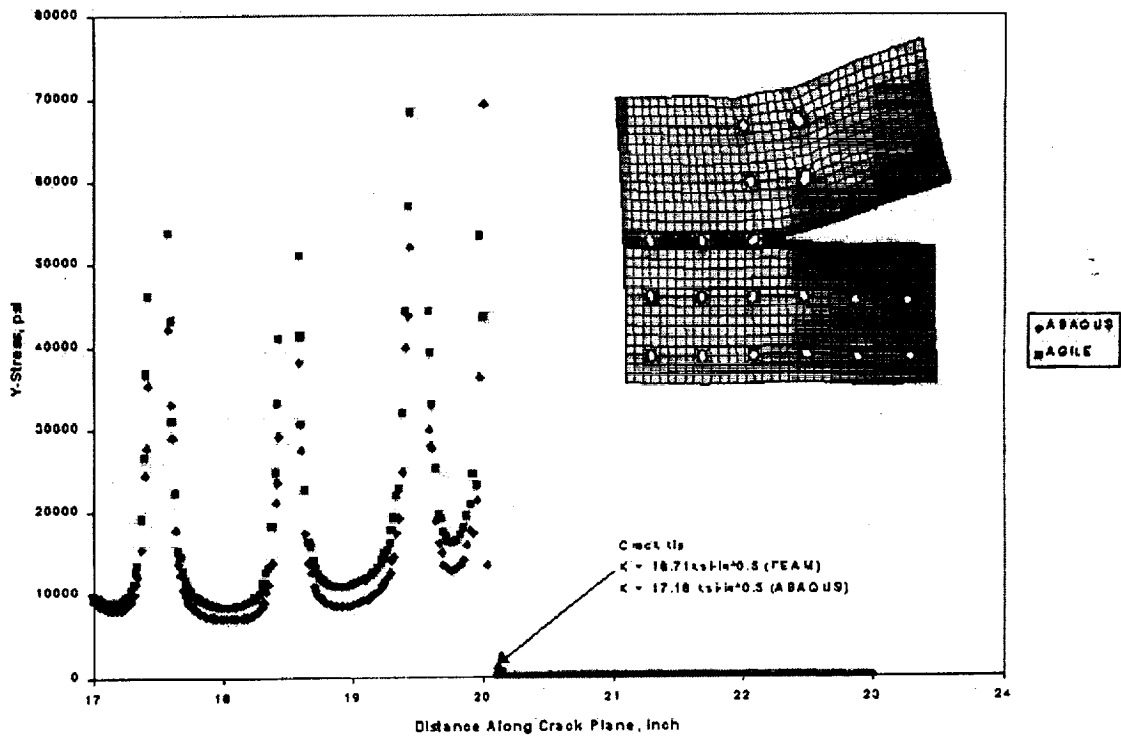


Figure 4. Local Solution of Riveted Lap Splice Joint by AGILE/STAGS and Comparison to ABAQUS

STAGS and FEAM are well-established programs. However, they are still, in a relative sense, new. Therefore, also shown in Figure 4 is a comparison of the STAGS/FEAM solution to an ABAQUS

solution. Extensive verification studies were conducted by comparing the results of this solution procedure to both ABAQUS and ANSYS results. The stress analysis procedure developed for this program agrees with other commercially available programs.

At this point we have developed several important inputs for the TRACWFD analysis. First, we have defined the stress concentration factors at each location. Second, we have calculated stress-intensity factor values for the crack growth procedures. The former results can be used in a crack initiation model if one desires to use a linear damage accumulation model for initiation. The stress-intensity factor solution is even more critical. As Figure 5 indicates, while there are many solutions for cracks in a variety of geometries, not all situations are covered by existing solutions. In Figure 5, the solution for the stress-intensity factor for two cracks at a rivet hole is shown. Both the FEAM and ABAQUS solutions are plotted. These are also compared to the TC05 and TC09 NASGRO solutions. The NASGRO solutions shown are for a single crack growing out of a rivet hole while the FEAM and ABAQUS solutions are for a crack growing out of both sides of the hole. Clearly, there are significant differences. Equally clear, if we are restricted to known solutions, then we have a significant chance of error.

The stress solutions generated by AGILE/STAGS/FEAM are automatically sent to the probabilistic analysis portion of TRACWFD. The global-intermediate solution results are stored in a system of files organized into a library structure. The FEAM solution kernel, denoted tkALT, is linked directly to the probabilistic analysis solution. MSD cracks can be inserted into the calculation at any point in time to assess the stress-intensity factor and the residual strength.

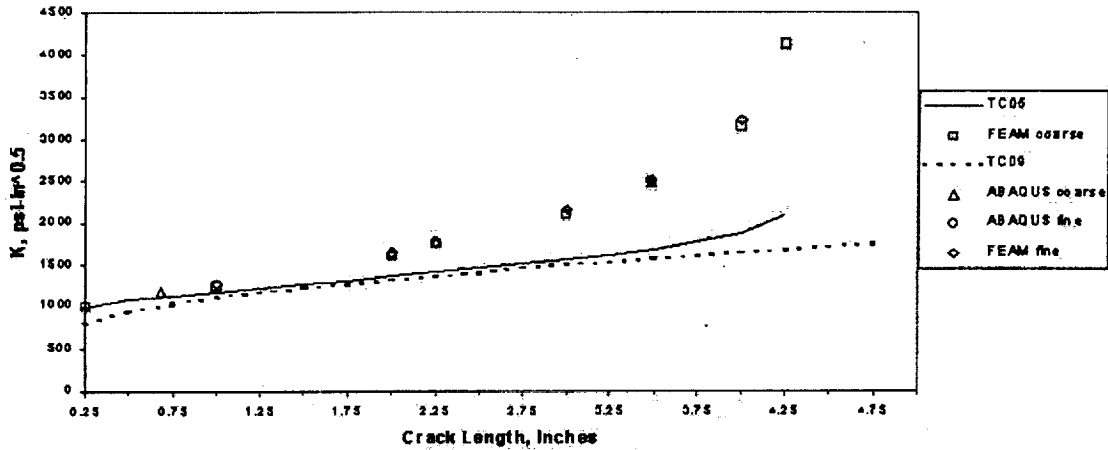


Figure 5. AGILE/FEAM Solutions for Two Rivet Hole Cracks Growing Out of Both Sides of the Rivet Hole

As Figure 4 indicated, and as many other analyses not reported here have demonstrated, the accuracy of AGILE/STAGS/FEAM has been verified. By verification we mean the code has been checked out thoroughly against existing theoretical solutions and standard accepted commercial solutions. What is now needed is a validation of the overall analysis procedure. To perform a validation, it is necessary to compare the code predictions to actual experimental results. This topic is described in the following section.

TRACWFD: VALIDATION FROM EXPERIMENTAL RESULTS

The previous analyses of riveted lap splice joints have almost exclusively relied upon data generated by Foster-Miller.⁵ While this was valuable data, recently more extensive data has been obtained in a study performed by Piascik and Williard.⁶ In this study, detailed crack growth, linkup, and fractography

data were obtained. Using TRACWFD we have predicted the results of this study to identify strengths and weaknesses of TRACWFD as well as validate TRACWFD. We first describe the results and data to be used in the comparisons.

CRACK GROWTH DATA

There were two sets of data given in reference 2. For each of two bays, labeled Bay 3 and Bay 4, crack growth data were measured. Not surprisingly, there was significant scatter in the data. Based on the current lap splice model developed for the AGILE/STAGS/FEAM analysis, it was found that Bay 3 more closely fit the geometry of our model.[†] Parameters for the fatigue crack growth law were derived based on this data, and an Equivalent Initial Flaw Size (EIFS) model was developed.

Figure 6 shows the results of the TRACWFD crack growth curve predictions for various rivet hole locations. While the NASA data does differentiate crack sizes among various rivet hole locations, we compare to an average crack size. As Figure 6 indicates, the parameters for the EIFS model are appropriate since the TRACWFD predictions are very close to the NASA data.

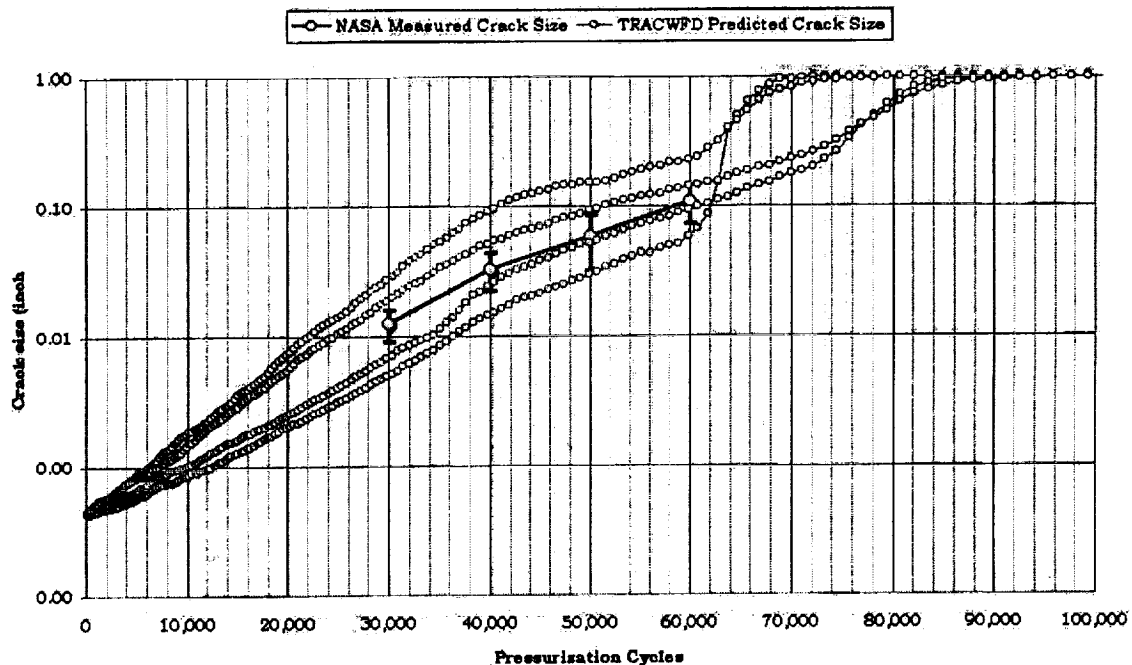


Figure 6. AGILE/FEAM Solutions for Two Rivet Hole Cracks Growing Out of Both Sides of the Rivet Hole

CRACK BEHAVIOR

The next analysis examines the time at which cracks begin to link up. Piascik found that the first linkup occurred at 58,200 pressurization cycles, and all cracks linked within an additional 500 pressurization cycles. This is shown, with the TRACWFD results, in Figure 7.

[†] An exact model for the geometry in the NASA study is being developed; however, for the time being we approximate the stress intensity solutions with existing analyses.

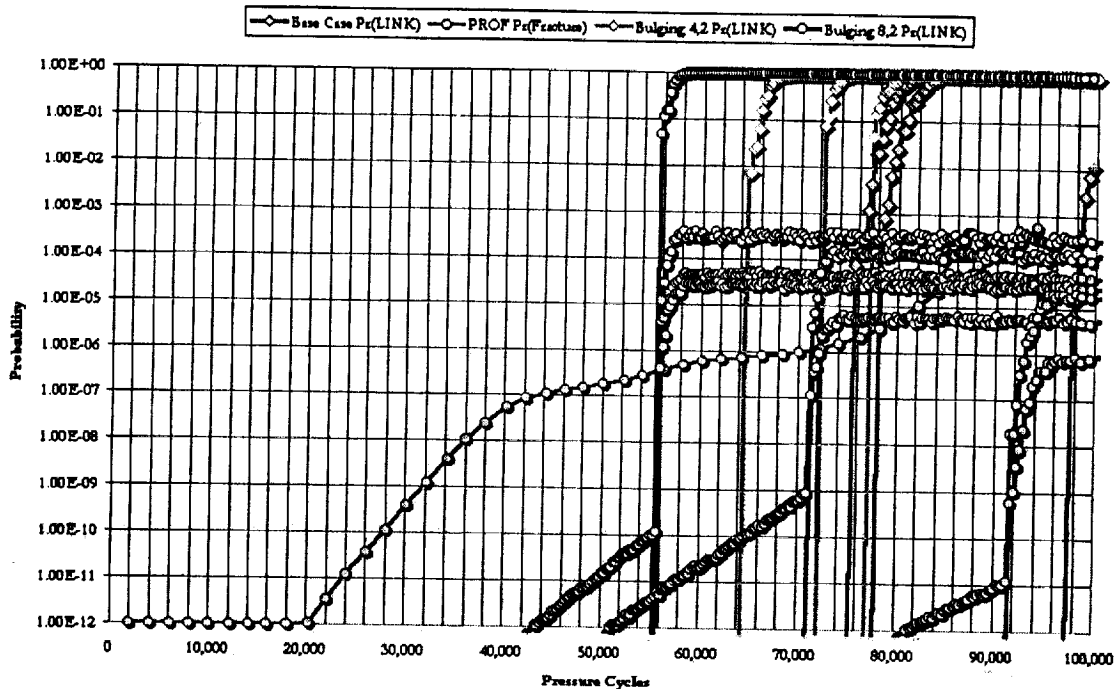


Figure 7. AGILE/FEAM Solutions for Two Rivet Hole Cracks Growing Out of Both Sides of the Rivet Hole

The initial TRACFWD analysis predicted crack linkup to occur at 67,000 cycles. The linkup of cracks was predicted based on plastic collapse of the remaining ligament using a model developed by Jeong⁹. In this model there is a factor for the effect of bulging. In the initial analysis the bulging factor was set to 1.0; i.e., there is no impact of bulging on the ligament collapse. By adjusting the bulging factor, as well as its uncertainty, we can calibrate TRACWFD to match the existing data. Through a sensitivity study it was found that the bulging factor described by a Weibull distribution with a mean value of 4.0 and a standard deviation of 2.0 adequately predicted the crack linkup as seen in the NASA data. Of course other explanations for the experimentally observed time of crack linkup are possible; however, the purpose here is to illustrate how TRACWFD can be used to investigate experimental results analytically. The full explanation of all of the NASA generated data requires substantially more analyses than can be contained in the limitations of this paper.

RESIDUAL STRENGTH AND THE ONSET OF WFD

Finally, we examine the change in the residual strength of the structure and how this impacts the onset of WFD. To do so requires a definition of the onset of WFD. There is currently on-going discussions about the final definition of the onset of WFD. However, to calculate such a probability some definition must be adopted. To this end we adopt the definition used by Dr. Jack Lincoln of the US Air Force.¹⁰ Swift originally proposed this definition.¹¹

Widespread Fatigue Damage. Characterized by the simultaneous presence of cracks at multiple structural details that are of sufficient size and density whereby the structure will no longer meet its damage tolerance requirements; for example, not maintaining required residual strength after partial structural failure.

Thus, while a structure may be able to continue in operation for its entire predicted service life with small cracks at many locations, it is certified to continue under much more severe structural damage conditions. Classically, in the lap splice of a commercial aircraft, this additional damage has been referred to as the two-bay crack. For each fatigue critical location, a similar type of damage is defined under which the aircraft must be able to sustain limit loads. These damage conditions are referred to as discrete source damage (DSD). However, when we begin to perform such calculations it must be emphasized that the probability of the DSD existing is assumed to be equal to 1.0. This is because the onset of WFD is defined to be the point in time when the partial structural failure is defined to be a two-bay crack.

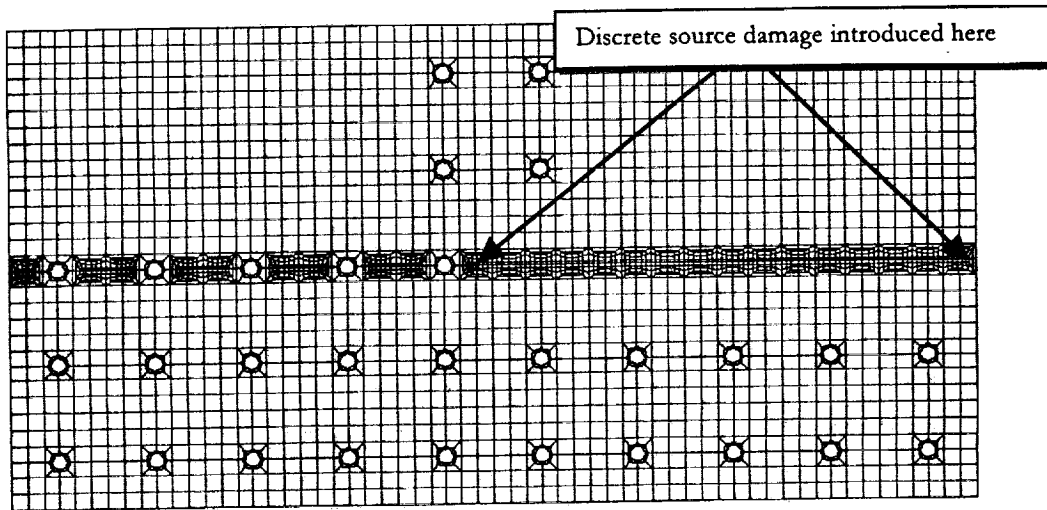


Figure 8. Local Model for DSD Analysis of Lap Splice Joint

TRACWFD can conduct an analysis for virtually any definition of the onset of WFD. Because of the modular design of the program, the current routine performing these calculations can be changed at any time as the definition changes. However, the definition shown above was used for the calculations presented in this paper.

For the narrow-body lap splice joint, the DSD is shown in Figure 8. In this figure we show ten rivet locations from the FEAM local model. Five of the rivet holes do not show up in this figure because the DSD, in the form of a large lead crack, is inserted at this point. This is the partial structural failure we investigate for the onset of WFD.

In the FEAM program there are two methods for calculating residual strength. The first is based on T^* (or, in the case of linear stress analysis, the equivalent J) and K_C . For this paper we only investigate the residual strength calculations based on K_C . The FEAM code predicts the residual strength of the structure and we use a Level II reliability analysis to estimate the probability that the residual strength is less than zero.

Plotted in Figure 9 are the results of the analysis when there is no DSD and the subsequent calculation of the onset of WFD. In this figure we are only plotting the results of the analysis for the three holes closest to the DSD. For the analysis in which there is no DSD, the onset of WFD does not occur until nearly 50,000 pressurization cycles with a probability of occurrence greater than one in 1012 pressurization cycles. In order for the probability of the onset of WFD to exceed one in 10,000 pressurization cycles, nearly 70,000 are needed. When the large lead crack DSD is introduced the situation changes dramatically. This is also illustrated in figure 9. Here we see that at 12,000 cycles there is some probability (albeit extremely remote) for the onset of WFD. By 18,000 cycles there is a 1 in 100 chance that the onset of WFD has occurred. The other side of the coin is that after crack linkup between two rivet holes there is still a 50% chance that the onset of WFD has not occurred.

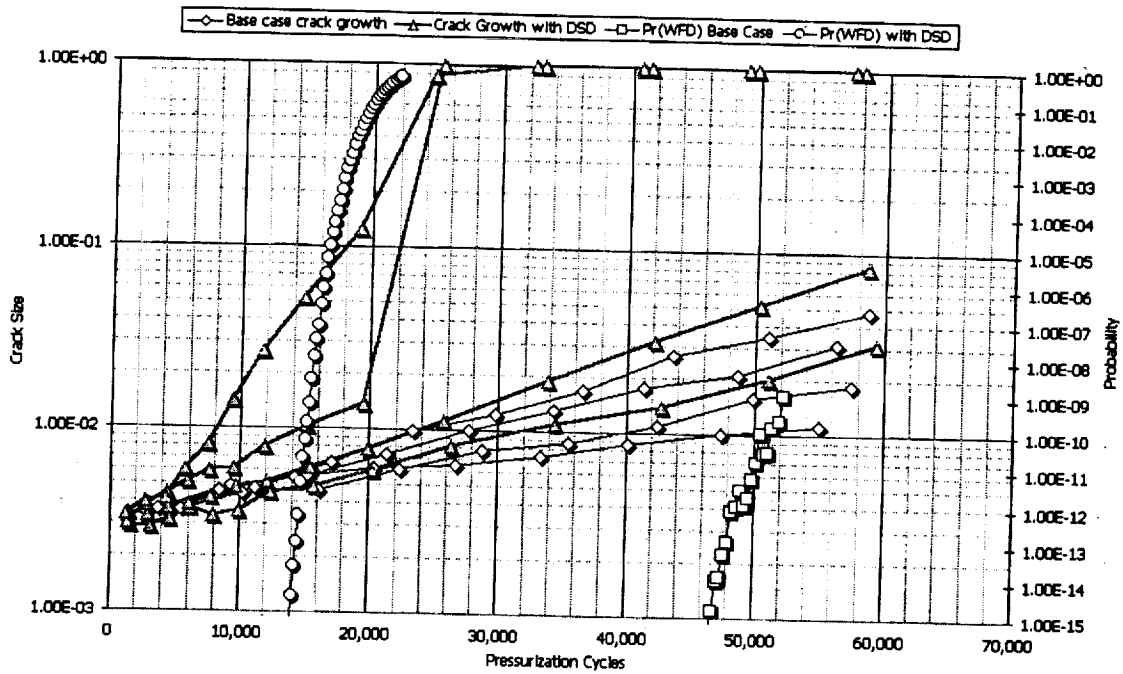


Figure 9. DSD Effects on the Probability of the Onset of WFD

TRACWFD AS AN ANALYSIS TOOL

While we have presented a fair amount of detail about the lap splice joint we now present some results of other analyses to simply demonstrate some of TRACWFD's capabilities. In these analyses we

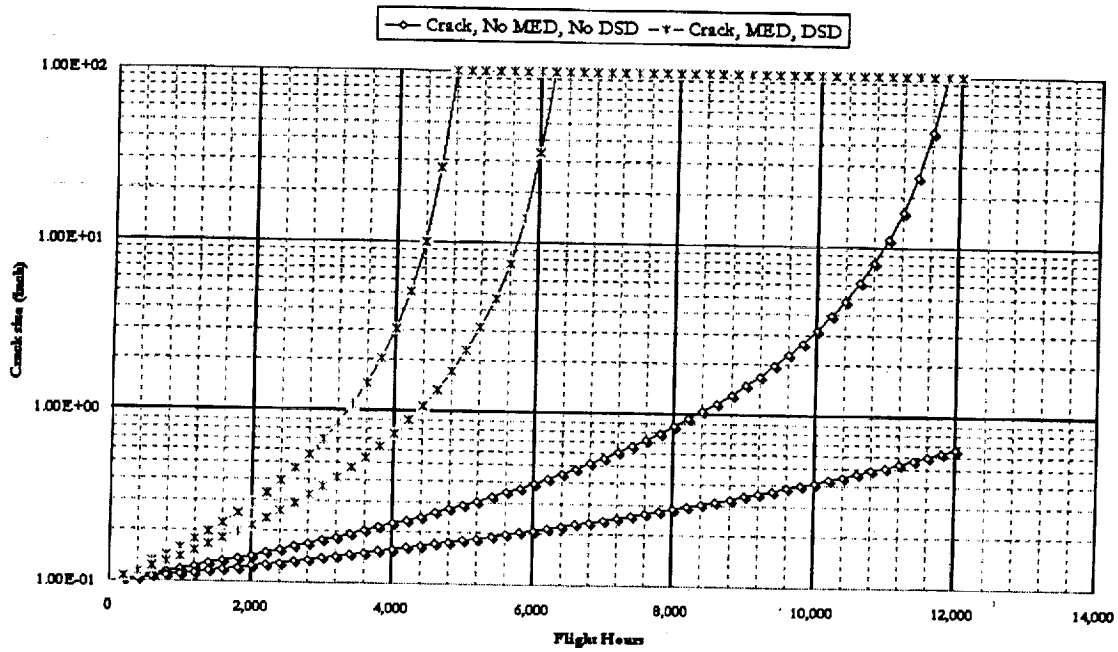


Figure 10. Lower Wing Skin Panel Crack Growth for Pristine Structure and MED with DSD Case

examine the lower wing skin panel of another narrow-body commercial jet. Figure 10 shows a comparison of the crack growth for two cases. First, the pristine structure is shown. Also plotted in the same figure is the crack growth for a broken stringer (MED) and a large lead crack (DSD). These are deterministic analyses in which all probabilistic analysis has been turned off. In addition, for the MED and DSD case, analyses from the original equipment manufacturer (OEM) were available. Using AGILE we obtained stress solutions that were within 10% of the manufacturer's analysis. Therefore, we have confidence that the analysis is reasonable.

Figure 11 shows the impact of performing risk constrained inspections. If we wish to limit the probability that K exceeds the critical value of the stress-intensity factor (K_C) to less than 1 in 1,000,000,

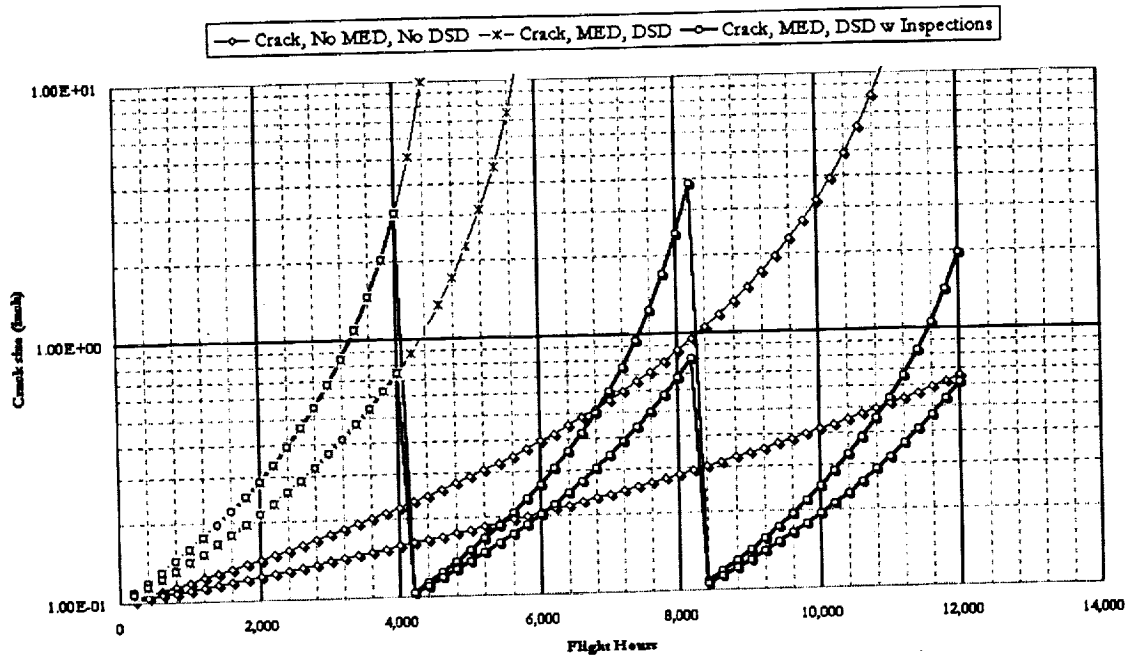


Figure 11. The Impact of Inspections on the Lower Wing Skin Panel Crack Growth for Pristine Structure and MED with DSD Case

then the inspection schedule must follow that shown in Figure 11. In this case there is an almost equal cycle[†] interval between inspections of approximately 4,000 cycles. At the large crack sizes predicted it is necessary to inspect with almost 100% efficiency to achieve this schedule. Finally, Figure 12 examines the effect of corrosion wall thinning on the predicted results. Not surprisingly, there is a significant impact. In the presence of corrosion the number of inspections almost triples. Additionally, equal cycle interval inspections are no longer adequate.

SUMMARY

The use of TRACWFD to analyze crack growth behavior in fuselage joints and wings has been illustrated. Many different analyses can be performed using TRACWFD. Initial crack size distribution effects, initiation models, corrosion impacts, the use of more advanced inspection methods, and repair techniques can all be studied with TRACWFD. Detailed estimates of the aircraft's residual strength and the point at which the onset of WFD occurs can both be calculated.

[†] This does not imply an equal time interval.

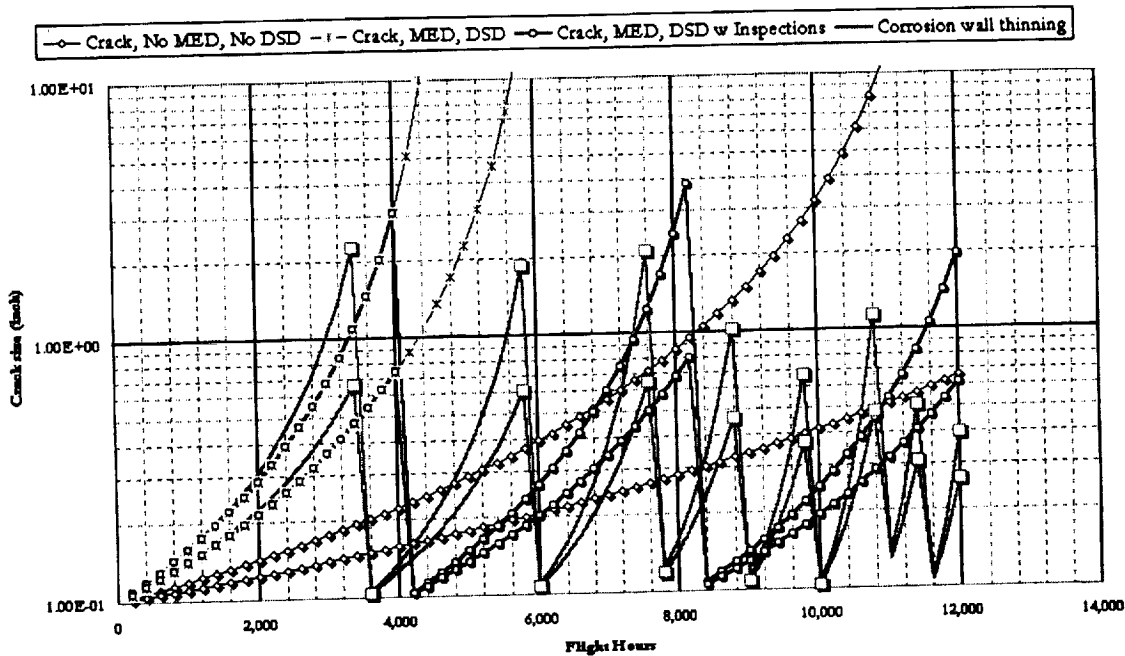


Figure 12. The Impact of Corrosion on the Lower Wing Skin Panel Crack Growth for Pristine Structure and MED with DSD Case

ACKNOWLEDGEMENTS

This work was supported by the FAA William J. Hughes Technical Center and the United States Air Force under the DEP contract. Knowledge Systems, Inc. under contract to Battelle Memorial Institute developed the AGILE/FEAM solution procedure.

REFERENCES

- ¹ Kurth, R. E., and Cox, D. C., *An Investigation of Discrete Probability Distributions for Probabilistic Fracture Mechanics Analysis*, Risk Analysis: An International Journal, 5, No. 3, 1985.
- ² Kurth, R. E. and Woods, K. S., *Probabilistic Damage Tolerant Analysis to Improve Aging Aircraft Maintenance and Inspection Schedules*, Invited paper, 1994 ASME International Mechanical Engineering Congress and Exposition, November 6-11, 1994, Chicago IL.
- ³ Berens, A. P. (1989), *Risk Analysis for Aging Aircraft Fleets; Task 1 Interim Report*, University of Dayton Research Institute Report UDR-TR-89-09.
- ⁴ Hopkins, D. A., Chamis, C.C., *Probabilistic Structural Analysis methods: SSME Propulsion Components*, Advanced Earth-to-Orbit Propulsion Technology, 1, NASA Conference Publication 2436, 1986.
- ⁵ Samavedam, G., Hoadley, D., *Fracture and Fatigue Strength Evaluation of Multiple Site Damaged Aircraft Fuselages - Curved Panel Testing and Analysis*, DOT/FAA/CT-94/10, January 1994.
- ⁶ Piascik, R. S. and Willard, S. A., *The Characteristics of Fatigue Damage in the Fuselage Riveted Lap Splice Joint*, NASA/TP-97-206257, November 1997.

⁷ Brogan, F. A., Rankin, C. C., and Cabiness, H. D., *STAGS User Manual Version 2.0*, Lockheed Palo Alto Research Laboratory, LMSC Report P032594, 1994.

⁸ Wang, L., Brust, F. W., and Atluri, S. N., Predictions of Stable Growth of a Lead Crack and Multiple Site Damage Using Elastic-Plastic Finite Element Method and Elastic-Plastic Finite Element Alternating Method, *Proceedings of the FAA-NASA Symposium on the Continued Airworthiness of Aircraft Structures*, DOT/FAA/AR-97/2, 1997.

⁹ Jeong, D. Y., *Analyses of Residual Strength and Multiple Crack Linkup Based on Plastic Collapse*, Volpe Center Report, 1994.

¹⁰ Lincoln, J. Communication via Capt. Scott Fawaz from *Definitions for AC No. 25.571-1A*.

¹¹ Swift, T., *Widespread Fatigue Damage Monitoring Issues and Concerns*, Proceedings of 5th International Conference on Aging Aircraft. 16-18 June 1993, Hamburg, Germany.

OPERATION AND MAINTENANCE OF THE SPACE SHUTTLE ORBITER

Frank V. Daniels
System Safety and Product Assurance Engineering
Boeing North American Reusable Space Systems
12214 Lakewood Blvd. M/C AB71
Downey, CA 90242
Phone: (562) 922-5126
Fax: (562) 922-3602
Email: frank.v.daniels@boeing.com

ABSTRACT

The Space Shuttle is the only manned reusable system in the world. Since its first flight in April of 1981, the Space Shuttle has flown 91 missions to deliver payloads, repair satellites, and carry crew and supplies to the Russian Mir space station. It is poised to begin the delivery of the first elements of the International Space Station later this year.

The Space Shuttle consists of a fully reusable orbiter, an expendable propellant tank, and two reusable solid rocket boosters. This paper focuses on the orbiter vehicle only. It briefly describes the criteria used in its design and the manufacturing and assembly process and discusses in detail the operations and maintenance that take place after each flight and during orbiter maintenance periods.

INTRODUCTION

When the Space Shuttle contract was awarded in 1972, the criteria were that the orbiter would be designed as a safe-life vehicle, fly 100 missions (with a scatter factor of 4) in 10 years, and operate from both the Eastern Test Range and the Western Test Range. (The Western Test Range was subsequently dropped as a launch site.) Now, 26 years after contract award and 17 years since its first flight, the orbiter continues to be a reliable means of manned space transportation. In order to maintain this reliability and safety, a routine maintenance and inspection plan was devised. Some structural inspections are required after each flight (defined as turnaround flow), more inspections are required after a few flights, and a majority of the inspections are required every 3 years. This plan has been in operation since the mid 80s and has resulted in well-maintained vehicles.

The turnaround inspections are performed at the Kennedy Space Center (KSC) in Florida, and the 3-year inspections are performed as part of orbiter major modifications (OMMs) at Palmdale, CA. Portions of the orbiter, including the orbital maneuvering system (OMS) pods and the forward reaction control system (FRCS) module, remain at KSC for the required inspections. The OMS pods and the FRCS module, which contain hypergolic propellants, are inspected at the Hypergolic Maintenance Facility at KSC. A Problem Report and Corrective Action (PRACA) system tracks all of the discrepancies found during these inspections at KSC. A detailed structural inspection report prepared after each OMM summarizes the findings and categorizes the types of discrepancies. These reports have been very helpful in establishing trends and revising the frequency and level of inspections. The PRACA system and the structural inspection reports provided the data used to develop this paper.

ORBITER DESIGN CRITERIA

The orbiter design criteria state that it will be a safe-life vehicle for 100 missions with a scatter factor of 4, for a total of 400 missions, and 10 years. A mission begins when the Space Shuttle lifts off from the launch pad and continues through ascent, orbit, reentry, descent, and landing. It may also include a ferry flight if the vehicle lands at a site other than KSC. A manned factor of safety of 1.4 is applied to design limit loads. Since the orbiter has a thermal protection system (TPS) bonded to the external surface, it must be shear resistant up to 115% of design limit loads during ascent and 100% of design limit loads on descent. This requirement was imposed because most of the TPS is a brittle silica glass tile that cannot tolerate excessive out-of-plane deflections. A sketch of a typical tile installation is shown in Figure 1. In order to satisfy life certification requirements, static stress, durability, and fracture analyses were performed.

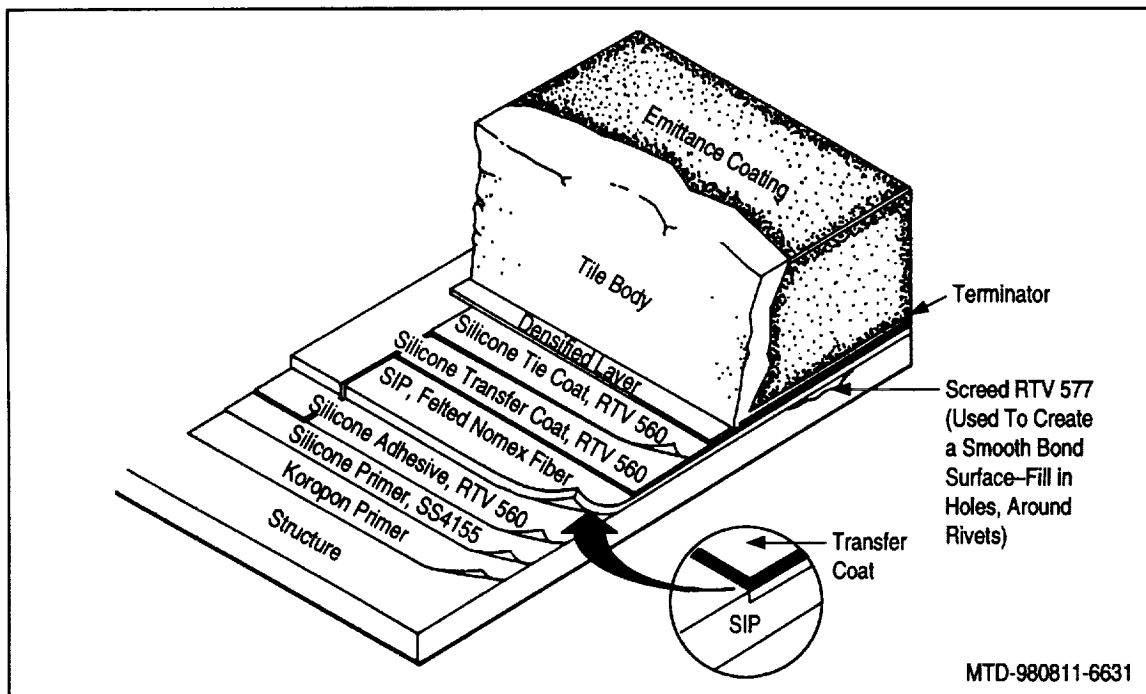


Figure 1. Typical tile installation

In order to satisfy the 10-year life requirement from a corrosion standpoint, a coating of Koropon was applied to the skins, frames, stringers, and other parts. This corrosion inhibitor is supplemented with a dry air purge whenever the vehicle is outside of its controlled environment in the Orbiter Processing Facility (OPF) at KSC. The only unpurged areas are the movable aerodynamic surfaces, the nose cap, and the wing leading edges.

ORBITER MANUFACTURE AND ASSEMBLY

The orbiter structure was produced by many subcontractors around the United States (see Figure 2). The majority of the structure is aluminum, but some titanium, Inconel, graphite/epoxy and beryllium were used in the construction. Each material was chosen for a specific purpose (e.g., temperature, strength, weight, or stiffness requirements).

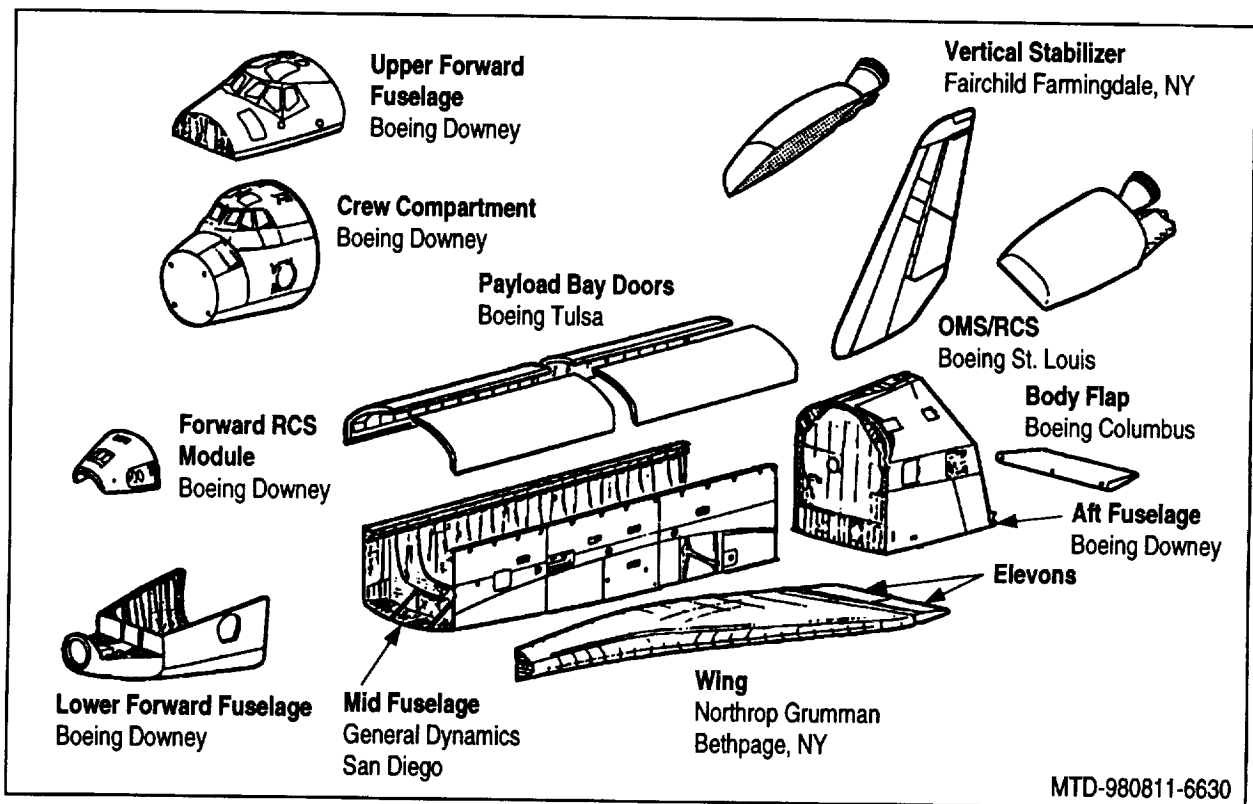


Figure 2. Orbiter structural elements and manufacturers

The outer shell of the orbiter contains no lap joints. All skin splices are butt joints at either frames/bulkheads in the longitudinal direction or at longerons in the circumferential direction. This type of splice was used to maintain a flat surface to minimize problems during the subsequent bonding of TPS to the outer shell. It eliminated steps and irregularities in the outer shell surface.

All of the components were shipped to the Boeing North American (BNA) facility in Palmdale for final assembly. The completed vehicles were then placed atop a NASA Boeing 747 and ferried to KSC, where they were rolled into the OPF for final vehicle processing before flight. Six orbiters were assembled in Palmdale. Enterprise (OV-101) was used for approach and landing tests only. Columbia (OV-102), Challenger (OV-099), Discovery (OV-103), Atlantis (OV-104), and Endeavour (OV-105) were delivered to KSC for orbital operations. Table 1 lists the orbiters and other pertinent information. Challenger was lost in an accident in January 1986.

TABLE 1. ORBITER VEHICLES

Orbiter Vehicles	Delivery Date	First Flight	No. of Flights	No. of OMMs
Enterprise (approach and landing tests)	5/76	2/77	8 captive 5 free flight	
Columbia	3/79	4/12/81	25	2
Challenger	7/82	4/4/83	10	0
Discovery	10/83	8/30/84	24	2
Atlantis	4/85	10/3/85	20	2
Endeavour	5/91	5/8/92	12	1

Note: Total orbital flights = 91 (as of Sept. 3, 1998)

ORBITER OPERATIONS

After the NASA Boeing 747 and orbiter arrive at KSC, they are placed under a mate/demate device, and the orbiter is lifted off of the aircraft. It is then rolled into the OPF, where the temperature and humidity are controlled constantly. Here final processing is completed. The vehicle is rolled out of the OPF and into the Vehicle Assembly Building (VAB), where it is mated with the external tank and two reusable solid rocket boosters (RSRBs) on a mobile launch platform. A dry air purge is initiated on the orbiter within 72 hours of its leaving the OPF. The "stack" is then rolled out from the VAB to the launch pad. The vent doors on the orbiter begin opening 28 seconds before liftoff to minimize the delta pressure across the outer shell. As the vehicle ascends, the internal pressure drop trails the external pressure drop, causing a slight burst pressure across the outer shell. After burning for approximately 2 minutes, the RSRBs are released, their parachutes deploy, and they drop into the Atlantic Ocean to be retrieved by two specially equipped ships. The RSRBs are towed back to Cape Canaveral, FL, for refurbishment. The three Space Shuttle main engines continue to burn for another 6 minutes and are shut down. If necessary, the OMS pod engines complete the final insertion into orbit.

At the end of the mission, the orbiter reenters the Earth's atmosphere. Its vent doors are closed prior to entry and are opened at approximately 70,000 feet. The vehicle lands on a special runway (3 miles long) at KSC or at an alternate site if weather conditions are poor in Florida. Figure 3 presents a typical mission profile.

As soon as the vehicle rolls to a stop, the ground purge is begun as quickly as possible. The vehicle is then rolled back into the OPF to begin turnaround processing.

ORBITER MAINTENANCE

The orbiter structural inspection requirements are contained in the Operation Maintenance Requirements and Specification Document (OMRSD). Structural inspections are performed in zones similar to those shown in Figure 4. There are three levels of inspection: surveillance, detail, and special detail. Surveillance inspections are performed over large areas with the unaided eye. Detail inspections, which concentrate on specific areas, are generally visual but allow the use of magnification glasses. Special detail inspections require the use of borescopes and/or some type of nondestructive inspection technique (e.g., radiography, ultrasonic, eddy current) and focus on specific areas of the vehicle. Some of these inspections are performed at KSC during turnaround operations when the OMRSD requirements call for inspections before the 3-year OMM at Palmdale.

Of the approximately 600 structural inspection requirements for the orbiter, about 120 are performed at KSC by United Space Alliance personnel, and the remaining 480 are performed at Palmdale by BNA personnel. Approximately 85% of the structural inspections are surveillance inspections, and the remaining 15% are either detail or special detail.

Unique inspection methods were developed to minimize the amount of disassembly required for access. In areas where bolts had to be removed, ultrasonic shear wave inspection methods were developed to eliminate the need to remove the bolts. This type of inspection was especially useful in the vertical tail and thrust structure areas. The vertical tail inspection required the removal of eight bolts in the aft attachment that were installed in close-tolerance holes. The bolt holes were visually inspected with a borescope and then inspected with an eddy current probe for possible cracks in the bore. This was a time-consuming task, and there was also a very good chance that the hole bores would be damaged during the extraction of the bolts. A novel inspection method that used the ultrasonic shear wave approach was developed to inspect these bolt holes without removing the bolts. A large, thick washer was notched to

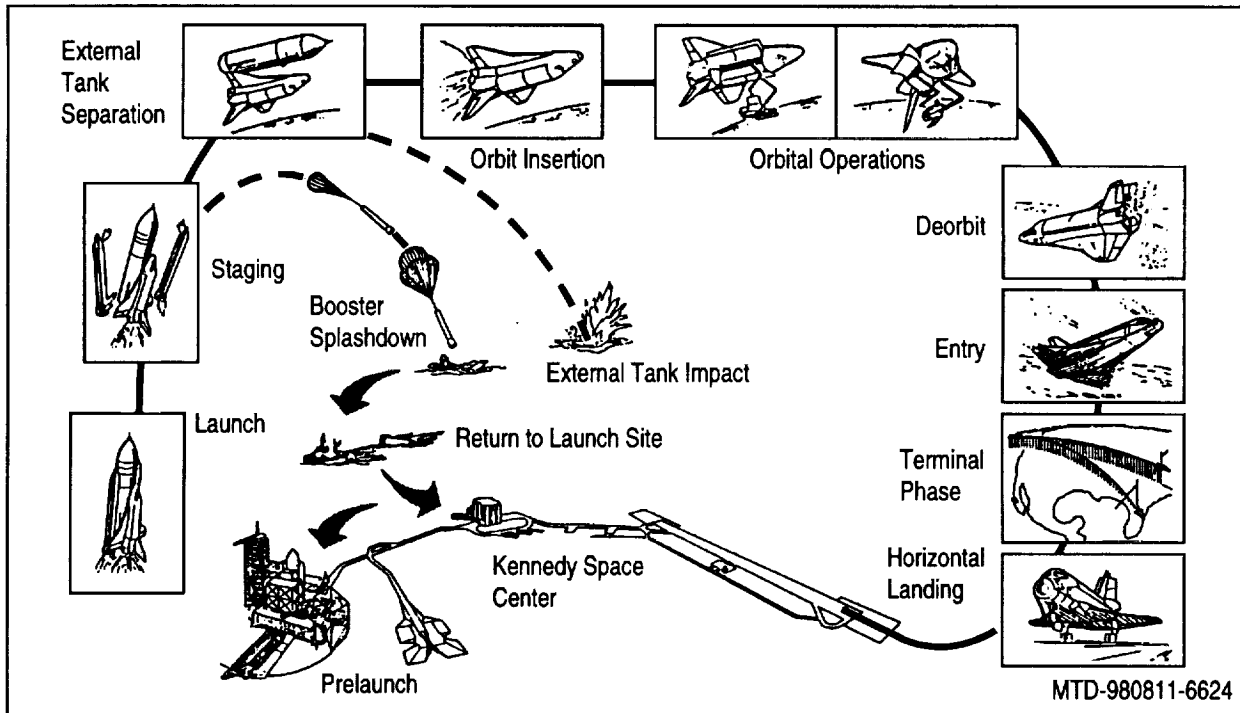


Figure 3. Typical mission profile

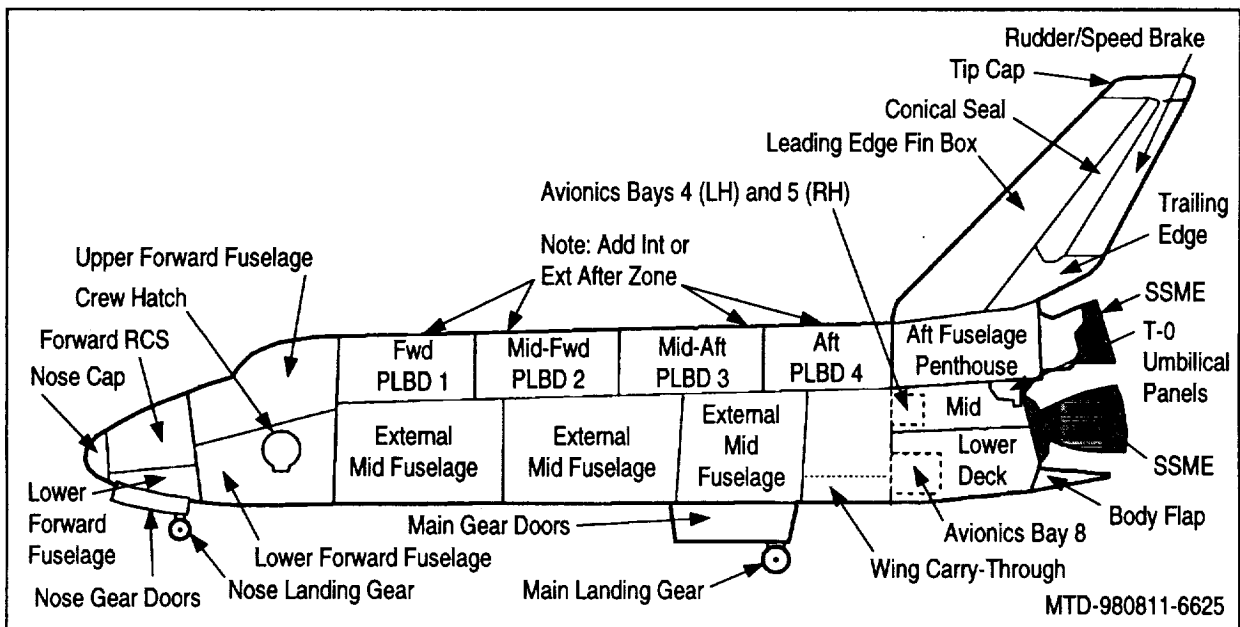


Figure 4. Orbiter major and submajor zones—left side

accept an ultrasonic shear wave transducer. This assembly was placed over the bolt head or nut and then rotated 360 degrees to inspect the titanium fittings for flaws greater than or equal to 0.10 inch long.

Radiography is used in areas that have limited accessibility, such as the area between the crew module and the forward fuselage, the wing tip, and portions of the vertical tail.

The forward fuselage/crew module area is closed out and has very few access panels. To maintain adequate temperature control of the crew module, thermal blankets cover the structure, further complicating the inspection effort. As an added inspection method, borescopes are used extensively in this area. The borescopes are fed in through avionics antenna openings and manipulated under the thermal blankets to inspect either the inner surface of the forward fuselage or the outer surface of the crew module. This results in a sampling of the structure.

Vertical tail forward attachment bolt preloads are measured with an ultrasonic bolt gage and recorded. The bolts are retorqued if the preload drops below the design requirement.

RESULTS OF THE STRUCTURAL INSPECTIONS

Figures 5 through 8 summarize the findings of the structural inspections. A review of these figures reveals that the number of nonconformances is rather small compared to the total number of inspections. Most of these findings are due to normal wear and tear. No serious degradation of the structure has been observed.

The corrosion shown in Figure 5 for Columbia is attributed to the use of dissimilar metals in the forward wing spar area. In that area, aluminum honeycomb face sheets are insulated from the high temperatures behind the wing leading edges with Inconel thermal blankets. Since this area is unpurged, moisture is trapped between the aluminum and Inconel while the orbiter is on the launch pad, and corrosion ensues. The entire front spar was stripped of its Koropon primer, the corrosion was neutralized, and two coats of Koropon and a thick coat of room temperature vulcanizing material were applied to separate these two metals. It should be noted that OV-102 is the only orbiter with an aluminum honeycomb front spar. Later orbiters have an aluminum corrugated front spar.

The gouges and nicks are mostly caused by routine maintenance operations.

CONCLUSIONS

The orbiters have flown a total of 91 flights (as of Sept. 3, 1998). Columbia has the most number of flights (25) and is the oldest of the vehicles (it was delivered to KSC in March 1979). The minimal findings during the structural inspections are testimony to the design, manufacture, assembly, and maintenance of each vehicle. If the care and maintenance of these vehicles continue, they will be able to fly well into the 21st Century and make the orbiter the DC-3 of manned space vehicles.

ACKNOWLEDGMENTS

The author would like to thank the following BNA personnel for compiling the data for this paper and assisting in its preparation: Gerry Mintz, Dan Montoya, Don Parker, Jeff Hausken, Ken Melick, Sandy Pilon, and Mike Tullius.

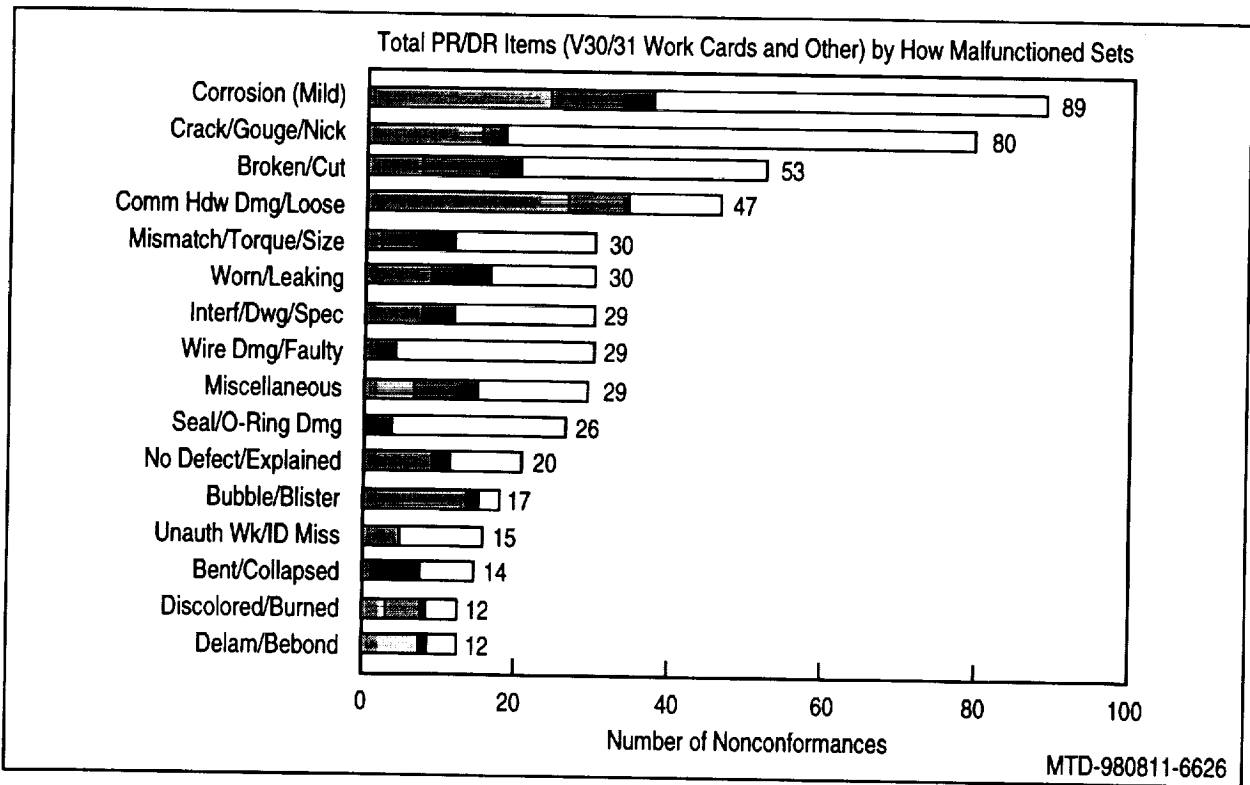


Figure 5. OV-102 Nonconformances

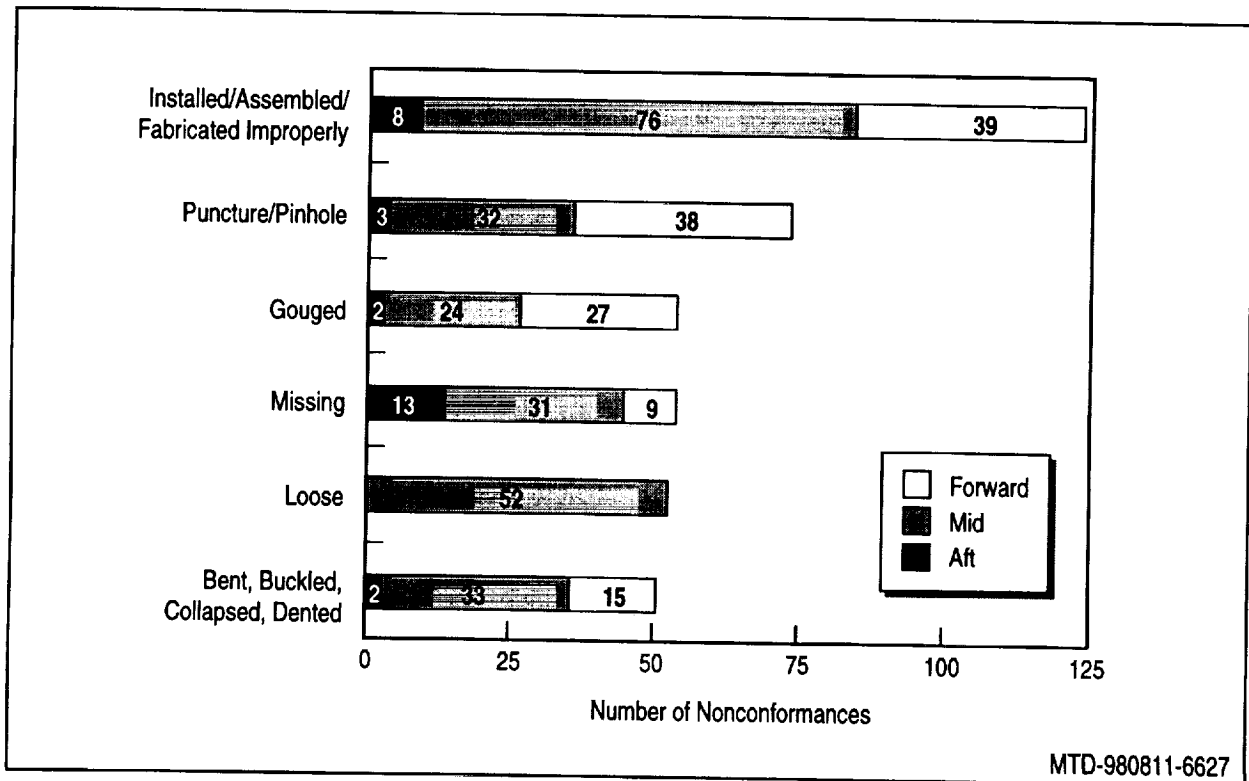


Figure 6. OV-103 OMDP nonconformance findings (50 or more)

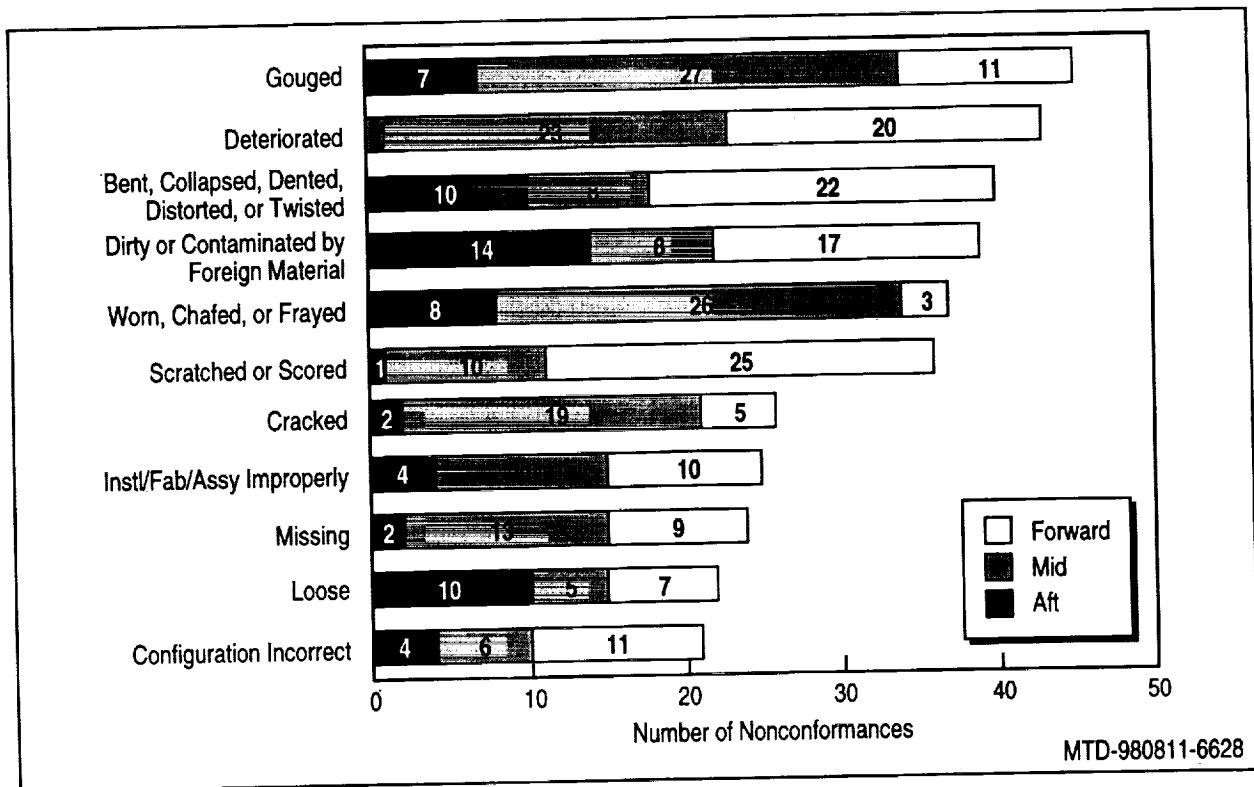


Figure 7. OV-104 OMDP nonconformance findings (21 or more)

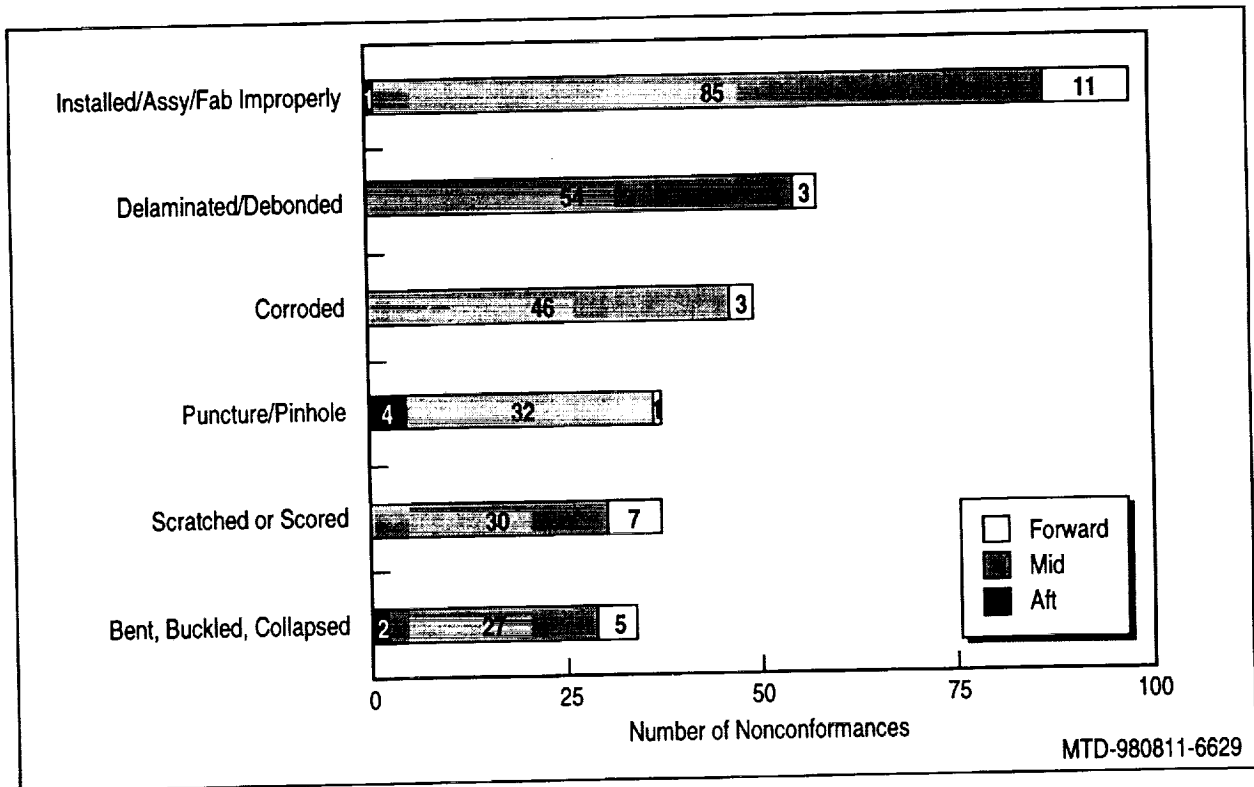


Figure 8. OV-105 OMDP nonconformance findings (34 or more)

COMPOSITE REPAIR OF AGING METALLIC STRUCTURE P-VERSION 3D FINITE ELEMENT APPROACH

Arnold Nathan
Israel Aircraft Industries
Department 4441 - Engineering Division
Ben Gurion International Airport, 70100 Israel
Telephone: 972-3-935-3868
Telefax: 972-3-935-5055
e-mail: natanfam@netmedia.net.il

ABSTRACT

A quick, easy and relatively accurate method to calculate the effect of composite material repairs bonded to metallic structure is addressed in this paper. P-version, three dimensional, parametric, finite element analysis is used to calculate load transfer to the repair as well as stress intensity factors for cracks in the parent metallic structure. Cracks by cutouts under composite patches are also analyzed. The parametric nature of the model allows simple changes in geometry or crack size.

1. INTRODUCTION

One of the approaches to help deal with the issue of aging aircraft is the use of bonded composite repairs. The bonded composite patch has numerous advantages over the metallic fastened repair including:

- lowering of stress concentrations by eliminating fastener holes
- sealed interface thus lessening corrosion and fretting under the repair
- only one side access is required
- no damage to structure or hidden components

The problem of calculating the load transfer to the patch as well as the stress intensity factor for crack growth under the patch are essential in quantifying the beneficial effects of the composite repair.

P-version, three-dimensional finite element analysis was used to solve this problem. A completely parametric model was built representing the parent material, adhesive and composite patch. Thus a change in geometry may be easily modeled by adjusting only one of the parametric dimensions, for example, patch thickness, plate width or crack size.

Certain aspects of the work will be presented in this paper:

- solutions for both a center crack and for a *crack by a cutout under a composite patch*
- different methods to use the finite elements to calculate K_I for a crack under the composite patch
- parametric modeling which helps isolate the dominant factors of composite patch design
- P-version finite element solutions for simple modeling of complex problems
- Residual stresses due to difference in thermal expansion coefficient between the patch and aluminum
- Typical Application: Composite patch over cutout in fighter aircraft front spar web

2. P-VERSION FINITE ELEMENT MODEL

The P-Version finite element program STRESS CHECK was used to model the composite repair over the metallic cracked structure. STRESS CHECK, a trademark of Engineering Software Research and Development Inc. of St. Louis, Missouri, is a user friendly, motif based finite element program which allows for control of discretization errors by increasing the polynomial degree of the elements (p-extension). Meshing in the presence of cracks is relatively effortless because refined meshes are not required around the crack tips.

Three dimensional modeling, including thermal loading was also included in the work effort described in this paper. STRESS CHECK allows virtually all inputs to be defined parametrically which allows easy changes in geometry or crack size without remodeling the problem. Parametric studies to isolate dominant parameters are simply performed.

Certain investigators have mentioned the potential difficulties in using 3d finite element solutions for studying composite material repairs. They fear the high computational costs and high aspect ratio elements due to the thin adhesive and patch layer (See Reference 1). Both of these obstacles are significantly less problematic with the "p-version" finite element models.

Three dimensional models of a repair over a center crack and a crack by a hole are presented as Figures 1a and 1b. Only one-eighth of the geometry is modeled due to symmetry in the length width and thickness directions. With these constraints applied, the repair is symmetric (a patch on each side of the thickness) and the crack by a hole is actually a crack at each side of the hole. The case of a non-symmetric patch was also studied, and will be presented in this paper.

Figure 1: STRESS CHECK three dimensional finite element model

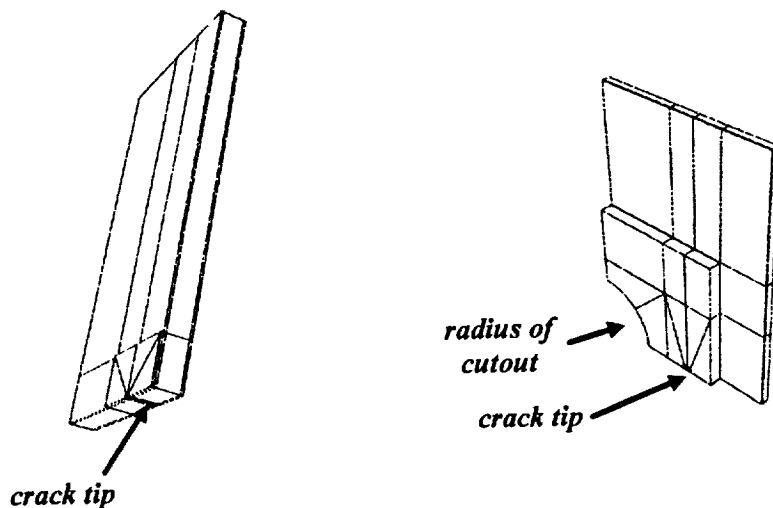


Figure 1a: Center Crack - 1/8th model

Figure 1b: Crack by Hole - 1/8th model

3. STRESS INTENSITY CALCULATION USING 3D FINITE ELEMENT ANALYSIS

The stress intensity factor, K_I , describes the stress field at the crack tip. It is well known that the stress intensity factor may be related to the strain energy of the structure and also may be related to the displacement distribution in front of the crack. Since the finite element solution can provide displacements and strain energy, the stress intensity solution may be calculated from the finite element model.

Calculation of Stress Intensity Factor - Strain Energy Method:

$$K_I = \sqrt{\frac{\Delta U \cdot E}{\Delta a \cdot \frac{1}{4} t}} \quad (\text{note the } 1/4 \text{ in the denominator is due to fact that } 1/8\text{th plate is modeled}) \quad (1)$$

with:

ΔU = change in strain energy

Δa = change in crack length

t = thickness of plate

Note that in the strain energy method, the stress intensity is related to the *change* in strain energy due to the change in crack size. Thus this method entails performing two finite elements runs, with a small difference in crack size, and calculating the “delta” strain energy for the two runs. STRESS CHECK allows multiple parametric runs, thus simplifying this task.

Calculation of Stress Intensity Factor - Displacement Extrapolation Method:

$$K_I = \frac{V \cdot E \cdot \sqrt{2\pi}}{4 \cdot \sqrt{r}} \quad \text{Where } V \text{ is displacements of a set of points behind crack tip at a distance } r \quad (2)$$

Multiple values of K are plotted vs distance r . The curve is then extrapolated back to $r=0$ to derive the stress intensity at the crack tip. See for example Figure 2.

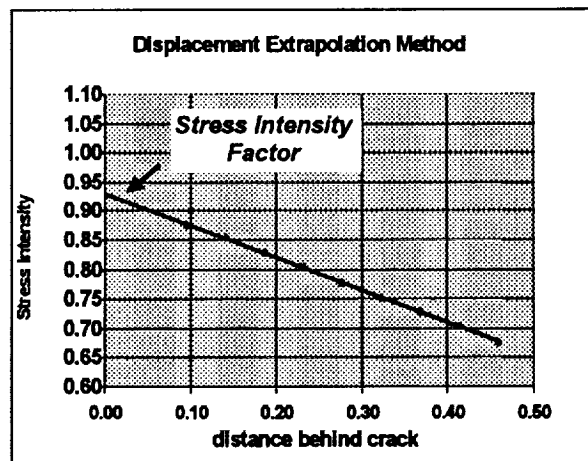


Figure 2: Displacement Extrapolation method to calculate K_I

These methods for calculating the stress intensity factor, have been well established and proven with 2 dimensional H-version finite elements models. In this study, the applicability of these approaches will be demonstrated using three-dimensional finite element solutions, and specifically higher order, large aspect ratio, P-version elements with less refined meshes.

3.1 VERIFYING THE METHODOLOGY

The 3D P-version accuracy and applicability of the strain energy method and the displacement extrapolation method were verified as follows:

- solve a simple crack configuration and compare to a known solution
- solve a more complex problem with both energy and displacement methods and compare the solutions to each other.

Both verifications were performed for the models and crack configurations in this paper. The stress intensity solutions resulted in reliable and accurate results.

For example, Table 1 below compares the results of a 3D P-Version center crack model (with no repair) to the known solution in the literature. The stress intensity results differed by less than 1%.

TABLE 1: CENTER CRACK - COMPARISON OF STANDARD SOLUTION TO F.E. ENERGY METHOD WITH 3D STRESSCHECK

R_1, R_2	U_{p-v} STRESSCHECK	ΔU_{p-v} STRESSCHECK	R_{ave}	$\beta_{(known)}$ "KNOWN SOLUTION"	K_{p-v} STRESSCHECK	$K_{-cr/\pi a \beta}$ "KNOWN SOLUTION"	%diff
1 0.9	8.002479×10^{-7} 7.926858×10^{-7}	7.562×10^{-9}	0.95	1.036	1.78	1.79	<1%
1 1.05	8.002479×10^{-7} 8.043766×10^{-7}	4.129×10^{-9}	1.025	1.042	1.86	1.87	<1%
0.8 0.9	7.860191×10^{-7} 7.926858×10^{-7}	6.667×10^{-9}	0.85	1.029	1.67	1.68	<1%

Note: Unit stress applied

Similarly, for a case of a composite patch over a cracked metallic material, the strain energy stress intensity results were compared to the displacement extrapolation calculation. The comparison illustrated below is typical for crack sizes and configurations of interest.

The displacement extrapolation stress intensity factor calculation for the case of a crack under a patch is presented as Figure 3, and results in a value of approximately 0.95. The strain energy calculation below results in practically the same number:

Calculation of Stress Intensity Factor - Strain Energy Method:

$$K_I = \sqrt{\frac{\Delta U \cdot E}{\Delta a \cdot \frac{1}{4} t}} = \sqrt{\frac{1.55 \times 10^{-7} \cdot 7.17 \times 10^4}{0.05 \cdot \frac{1}{4} \cdot 1}} \quad (3)$$

= 0.943 (virtually identical to the value calculated below with the displacement extrapolation method)

(note that E is given in N/mm² and that Δa is given in mm)

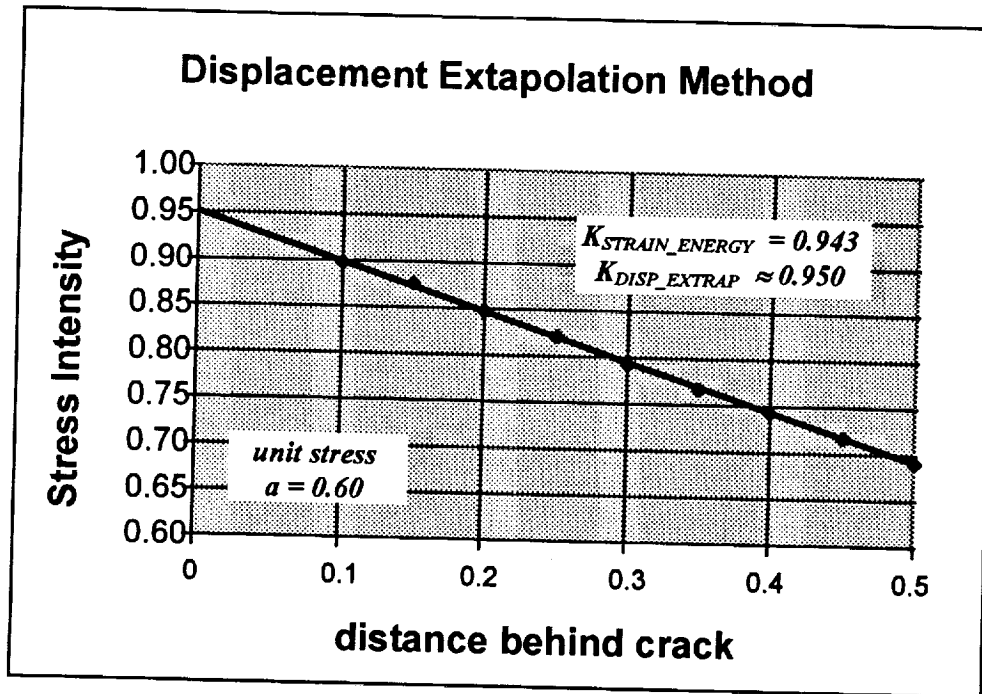


Figure 3: Comparison of stress intensity results using two different methods (3D P-version Finite Element Analysis)

4. PARAMETRIC STUDIES

One of the advantages of the STRESS CHECK model is the ease in changing geometric parameters while studying the composite repair problem. Varying different dimensions allows isolation of the dominant parameters which effect the specific problem type. As mentioned above, multiple geometric cases with varying parametric values may be calculated in one STRESS CHECK run.

Figure 4 illustrates an example of such a parametric study. The stress intensity is plotted vs. crack size for various ratios of plate stiffness to patch stiffness. As expected, the stress intensity in the cracked parent material decreases as the relative stiffness of the patch increases.

Another interesting observation is the nearly constant stress intensity, K_I , as a function of crack size, "a". This is consistent with results reported using the Rose model developed by Rose and his colleagues (See References 2,3, and 4). Also note that the graphs below in Figure 4 were derived for a defined patch width.

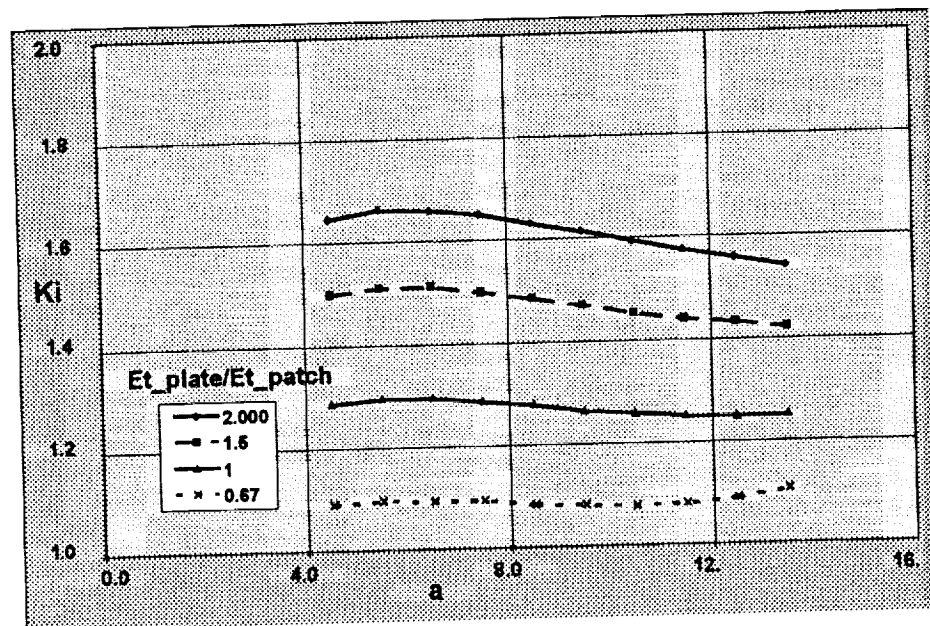


Figure 4: Parametric Study - Stress intensity as a function of plate/patch stiffness

Among the other significant conclusions which were derived from parametric studies were:

- small errors/inaccuracies in adhesive thickness did not significantly effect the stress intensity results
- small errors/inaccuracies in adhesive modulus did not significantly effect the stress intensity results
- a first attempt to derive a non-dimensional all inclusive stress intensity correction factor graph seemed promising. We were able to receive consistent curves for β vs "a" for constant values of λ ; with:

$$\beta = K_{I(WITH_PATCH)}/K_{I(NO_PATCH)}$$

a = crack size

$$\lambda = (2 \times "a" \times E \times thickness)_{PLATE}/(E \times thickness \times Width)_{PATCH}$$

Upon further study, it was found that these graphs are only consistent for certain specific conditions.

5. COMPOSITE PATCH OVER A CUT-OUT

One of the important crack configurations for composite repair, which is not often found in the analytical literature, is the case of a composite patch over a crack by a hole or cut-out. A 3D P-version finite element model was built for such a case (See again Figure 1b).

To verify that the model was reasonable and that the results were relatively accurate, the unrepaired model was compared to the known Bowie solution for a crack by a hole. In addition, the two analytical methods, strain energy and displacement extrapolation stress intensity results were compared to each other. Figure 5 presents a unrepaired "p-version" finite element *parametric* model of a crack by a hole. Again, the comparisons demonstrate that the model and methodology give reasonable results.

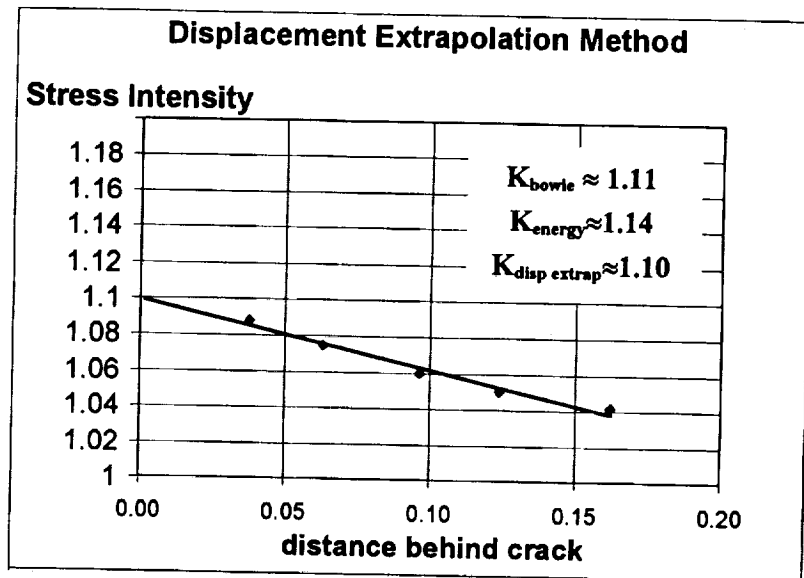


Figure 5: Crack by hole: Stress intensity comparison 3D p-version finite element solutions to known solution

An interesting conclusion regarding the composite patch by a cutout case is the necessity at times to reduce the thickness of the patch by the high K_T or to move the patch away from the hole. A stiff patch by the edge of a hole may draw too much load, thus causing failure in the adhesive or composite patch.

6. RESIDUAL STRESSES DUE TO THERMAL STRESSES

Temperature is usually applied when bonding the composite patch to the metallic material either for the bonding process of the adhesive in the case of a pre-cured patch, or for curing and bonding in the case of a co-cured type patch. Since the area is eventually cooled off, the differences in coefficient of thermal expansion will cause residual stresses around the crack in the parent material. In the usual case, the graphite or boron patch will contract less than the aluminum material to which it is bonded. Thus, as the parent material tends to contract, and the patch is restraining the contraction and thus residual tensile stresses occur around the crack. This case is illustrated in Figure 6 which presents the aluminum under

the patch after cooling. In this case the thermal expansion coefficient used for the aluminum was 2.36×10^{-5} in/in/°C while the composite material's coefficient was 3.9×10^{-7} in/in/°C. The resultant stresses illustrated are in the vertical Y direction and are thermal residual stresses due to a change in temperature of -60°C. As expected, the area under the patch (which surrounds the crack) has the highest tensile residual stress (darkest shade). At the edge of the patch, we find residual compressive stresses which are expected and necessary to equilibrate the body.

These damaging residual tensile stresses provide an incentive in certain cases to find an alternate repair solution. One possibility mentioned by investigators is the GLARE patch (See for example References 5 and 6). Due to the similarity in thermal expansion coefficient to the aluminum parent material, a GLARE patch does not result in such pronounced residual tensile stresses.

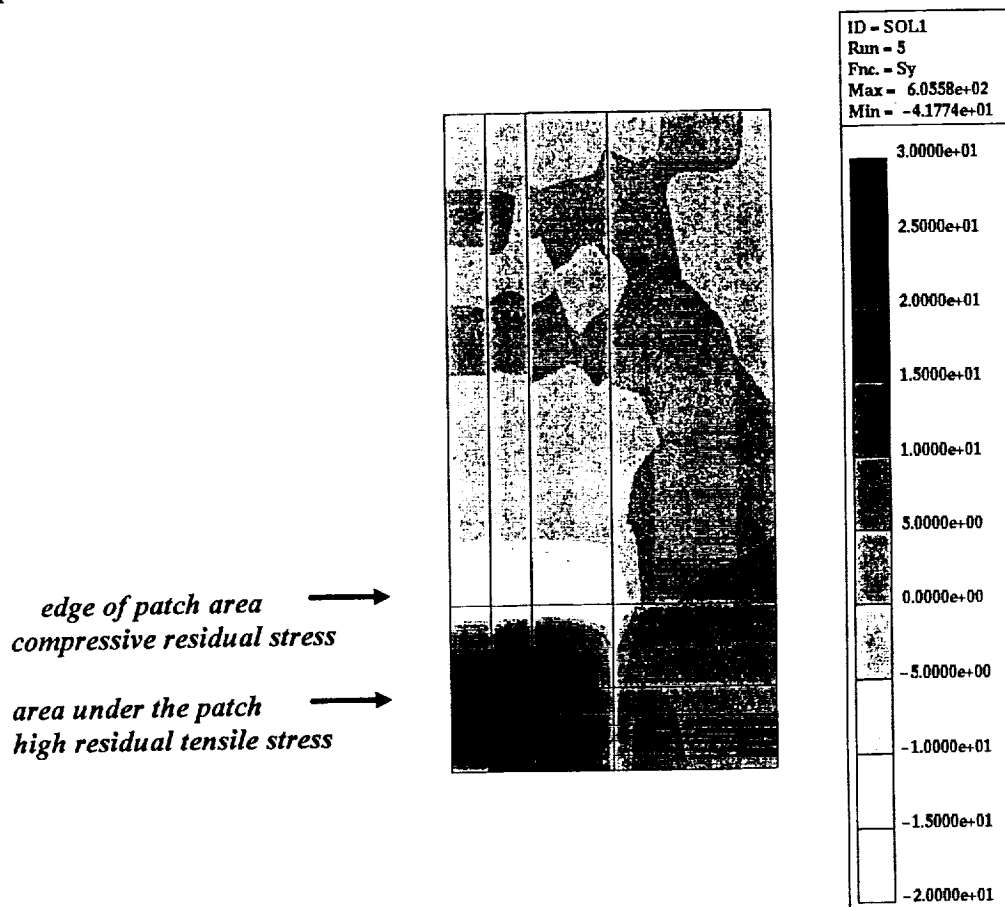


Figure 6: Residual stresses in aluminum parent material due to thermal loading

7. FIGHTER AIRCRAFT FRONT SPAR COMPOSITE PATCH

As part of a composite bonded repair development program, a graphite epoxy co-cured repair was designed for a critical cutout of a fighter aircraft front spar. In this specific case, a patch is only on one side of the structure. Thus the symmetry in the thickness dimension is not modeled. Certain challenges of this specific problem include:

- a lip on one face of the web and the asymmetric patch cause out-of-plane bending

- the high stresses in this spar and stress concentration of the cutout make it difficult to find a suitable material system
- high service temperature requirements also add difficulty to this specific repair
- the relatively thick web will require a thick repair

A spectrum fatigue test of this area is planned. EDM notches will be inserted in both the unrepaired and repaired specimens, precracking performed, and then the beneficial effect of the composite repair will be verified by damage tolerance spectrum testing. The analytical tools described in this paper have been used to predict the improvement in life due to the composite repair. The reduction in stress intensity due to the repair was calculated and is presented as Figure 7. An improvement of at least a factor of three is expected in crack growth life. Again note the nearly constant “ K_I ” which results for the case with the patch, which is consistent with the Rose model mentioned above. The testing should be performed in September 1998, and thus the validity of the models and methodology may be further verified.

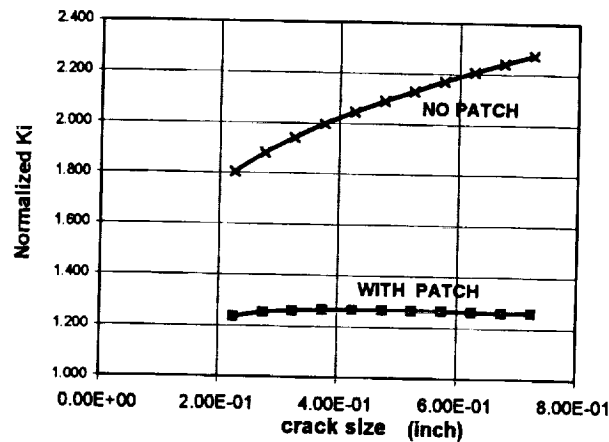


Figure 7: Stress intensity calculation with and without a patch by spar web cut-out

SUMMARY AND CONCLUSIONS

- Composite patches were modeled over metallic structure with a “center crack” configuration and also for a *repair of a crack by a cutout*. Load transfer to the repair and stress intensity factors for the cracks were calculated.
- Both the strain energy finite element method and the displacement extrapolation method were used to compute the stress intensity by the crack. The finite element results were compared to known solutions as well as the results of one method compared to the values of another solution. All of these comparisons resulted in consistent values, thus lending credibility to the methodology and models.
- The effect of thermal residual stresses were modeled.

- "P-version" three-dimensional parametric finite element analysis is an efficient tool to calculate load transfer and stress intensity factors for a composite patch over a metallic structure. The STRESS CHECK "p-version" finite element program allows coarse, easy modeling of the problem and relatively accurate results are attained. P-version finite elements do not have the computational costs or element aspect ratio limitations which prevented other investigators from using a three-dimensional finite element approach. Repairs over complex geometries or cutouts may be modeled with relative ease.
- Once the basic four repair configurations are modeled (center crack/crack by cutout each with a symmetric and asymmetric patch), numerous practical cases may be effortlessly solved, due to the parametric nature of the models.
- Parametric studies were performed to isolate dominant factors which effect the stress intensity calculation of the composite repair
- An interesting observation resulted for the case of a patch over a crack by a hole. There is a necessity to optimize the thickness and position of the patch with respect to the high stress concentration area . A balance must be found between sufficient load drawn from the cracked area and not too much load transferred to the patch which can cause premature failure in the repair or adhesive.
- A test of a graphite/epoxy co-cured patch over a crack by a cutout in a fighter aircraft spar web was modeled and is presently being tested. An improvement in life due to the composite patch of at least a factor of three is expected.

REFERENCES

- 1) Lena, M. R. , Klug, J. C., and Sun, C. T., "Composite Patches as Reinforcements and Crack Arrestors in Aircraft Structures", *Journal of Aircraft*, Vol. 35, No. 2, 1998.
- 2) Rose, L.R.F., "An Application of the Inclusion Analogy for Bonded Reinforcements", *Int. J. Solids and Structures*, Vol. 17, 1981.
- 3) Rose L.R.F., in Baker, Jones, eds. *Bonded Repair of Aircraft Structures*, Martinus Nijhoff Publishers, 1988.
- 4) Rose, L.R.F., "A Cracked Plate Repaired by Bonded Reinforcements", *Int. Journal of Fracture*, Vol. 18, No. 2, 1982.
- 5) Fredell, R., Guyt, C., Mazza, J., Knighton, S., Collas, E., "Repair of C-5 Fuselage Cracking With Bonded GLARE Patches", 41st International SAMPE Symposium, 1996.
- 6) Vlot., A., Soerjanto, I., Yeri, I., Schelling, J. A., " Residual Thermal Stresses Around Bonded Fibre Metal Laminate Repair Patches on an Aircraft Fuselage", 41st International SAMPE Symposium, 1996.

ENSURING DAMAGE TOLERANCE OF AGING AIRCRAFT STRUCTURES

Grigory I. Nesterenko
Central Aerohydrodynamic Institute (TsAGI)
Zhukovsky, Moscow region, 140160, Russia
Tel.: 7 095 5564002
Fax: 7 095 5564337

ABSTRACT

The principles of ensuring damage tolerance in Russian aging aircraft structures are outlined. The test scopes are presented for fatigue and damage tolerance tests of full-scale structures for various new and long-operated aircraft. The residual strength study results are generalized for full-scale wing and fuselage structures of various aircraft types affected by widespread fatigue damages (WFD). Test values of crack resistance for the specimens cut out of new materials are compared with those taken from long-operated aircraft wing and fuselage skins. Test data in fatigue and damage tolerance of new and long-operated structures are presented. The results are given of determining corrosion damage growth time by measurement of corrosion in high-time structures using probabilistic methods. The examples are presented of operating the aging aircraft structures with cracks.

1. INTRODUCTION

One of the most important problem in contemporary aviation is the problem of ensuring safe operation of aging aircraft. Many types of Russian aircraft have reached limits of their service lives and lifetimes assigned at their design. As it is impossible in the nearest future to replace old aircraft types by the new ones, then service lives and lifetimes of old aircraft should be prolonged over the design values.

Now aircraft companies, operators and research institutions in Russia ensure the increase in 1.5 - 2 times as compared to design values of service lives and lifetimes for Antonov, Ilyushin, Tupolev, Yakovlev aging aircraft. The problem of aging aircraft is being solved on the basis of analyzing the data on loading and technical state of operated aircraft, fatigue and damage tolerance tests of long-operated aircraft structures, calculations of fatigue, crack growth rate and residual strength of the structures. The system is applied to prolong service lives and lifetimes of separate aging aircraft copies.

To solve the aging aircraft problem the damage tolerance of the structure having widespread fatigue damages is investigated alongside with the degradation of crack and fatigue resistance characteristics in long-operated structures as well as defining corrosion damage growth duration based on the analysis of in-service data by methods of mathematical statistics. The experience^(1,2,3) of solving the above mentioned problems is outlined below.

2. TESTS OF FULL SCALE STRUCTURES

The Airworthiness Regulations⁽²⁾ for the USSR civil aircraft paid much attention to the laboratory test results for full-scale fatigue and damage tolerance tests. There are no types of Russian aircraft whose full-scale structure was not fatigue tested with large safety factor as related to design service life. Several copies of full-scale aircraft structures of each type were tested including those after operation (Table 1). The cycle number of the structures under fatigue tests was more than three times larger than the design service lives.

It was shown by calculations⁽¹⁾ that the cycle number of the structure during the tests is to be no less than three specified service lives in order to find out the possibility of occurrence of multi-site (widespread) fatigue damage in such structures during operation.

TABLE 1. FATIGUE AND DAMAGE TOLERANCE TEST VOLUMES FOR AIRCRAFT STRUCTURES

Aircraft	New structures			Structures after operation		
	Full-scale aircraft	Wing	Fuselage	Full-scale aircraft	Wing	Fuselage
An-10	3			2		2
An-12	2			4		
An-22	1					
An-24	1	1	3	3	2	
An-124	1					
Il-18	1	3	1	3		
Il-62	2	1			1	
Il-76	1	2	2			
Il-86	1	2	1			
Il-96	1		1			
Tu-104	1	5	1	2		2
Tu-114	1	1		1		
Tu-124	1				1	
Tu-134	1	2	2	1	1	
Tu-144	3					
Tu-154	4		1	1		
Tu-204	2					
Yak-40	1	1		1		
Yak-42	2		1			

On the basis of full-scale structure test result analysis some criteria were defined for residual strength of structures with widespread fatigue damages, and degradation of fatigue and damage tolerance characteristics was investigated.

3. RESIDUAL STRENGTH OF STRUCTURES WITH WFD

Widespread fatigue damage (WFD) initiates in primary structural sections including a lot of elements having almost identical values of fatigue life. Table 2 gives residual strength data for full-scale structures with WFD⁽³⁾. The apparent fracture stresses in the net section, $\sigma_{fr.net}^{app}$, were defined with due regard to reduction of the section area in primary elements due to the presence of holes and initial cracks. The structural cross section length where the net area and $\sigma_{fr.net}^{app}$ were calculated was stated as follows. The initial length was equal to the length of the zone with WFD. In the calculation this initial length was "extended to the left" by adding two lengths of the leftmost crack, and "to the right", by adding two lengths of the rightmost crack. While calculating critical fracture stresses $\sigma_{fr.net}^c$, additional attention was paid to section weakening due to crack length increase during stable crack growth stage. The values of these stresses were compared to the yield strength $\sigma_{0.2}$ values. Stress intensity factors K_{fract} at which the structure fails were calculated according to usual (approved) methods. These factors were compared to

TABLE 2. RESIDUAL STRENGTH OF FULL-SCALE AIRCRAFT STRUCTURES WITH WIDESPREAD FATIGUE DAMAGES

Damaged principal structural element	Material	$\frac{\sigma_{fr.net}^{app}}{\sigma_{0.2}}$	$\frac{\sigma_{fr.net}^c}{\sigma_{0.2}}$	$\frac{K_{fract}}{K_{app}}$	$\frac{K_{fract}}{K_{1c}}$
Skin and stringers near stringer splice in wing lower surface	D16ATNV D16T	0.8	1.0	0.5	-
Skin, stringers and spar of lower wing surface around stiffening lap edges	D16ATNV D16T	0.9	1.0	0.6	-
Skin and stringers of lower wing surface around stiffening lap edges	D16ATV D16T	0.9	1.0	0.5	-
Skin and stringers of monolithic stiffened panel of wing lower surface near fuel holes in stringer	D16T	0.7	0.83	1.0	-
Spars and shapes of upper wing surface	D16T	0.3	0.47	0.5	-
Splice shapes of upper wing surface	D16T	0.7	1.0	0.75	-
Stringer and lap for circumferential skin splice of pressurized fuselage	D16ATV D16T	0.75	0.88	1.0	-
Pressurized fuselage skin near three-row longitudinal riveted splice	D16ATV	0.57	1.0	0.5	-
Pressurized fuselage skin near two-row longitudinal riveted splice	D16ATV	0.63	1.05	0.9	-
Pressurized fuselage skin near two-row longitudinal riveted splice	D16ATV	0.48	0.85	0.7	-
Pressurized fuselage skin between two frames and between two stringers (19 through-the-thickness notches) (experiment)	D16ATV	0.9	0.9	1.0	-
Pressurized fuselage skin between two frames and between two stringers (19 through-the-thickness notches) (experiment)	D16ATV	0.85	0.85	1.0	-
Strip joining the cylindrical pressurized fuselage with spherical pressure bulkhead	D16ATV	0.16	0.17	0.45	-
Skin and stringer of lower wing surface around stiffening lap edges	V95AT1V V95T1	0.45	0.46	1.0	-
Lap joining the skins of lower wing surface	V95T1V	0.4	0.41	0.4	1.0
Wing pivot assembly	V93T1	0.4	0.40	-	1.0

fracture toughness for plane strain, K_{1c} , or to the apparent fracture toughness for plane stress state, K_{app} . The apparent fracture toughness K_{app} was determined by using sheets with free bulging near the crack.

Structural residual strength criteria are those fracture parameters whose relative values are 1.0. It follows from Table 2 that for structures made of brittle materials (like V95T1 and V93T1) residual strength criteria are linear fracture mechanics criteria $K_{fract}=K_{app}$ or $K_{fract}=K_{1c}$. For many structures made of plastic

materials (like D16T) having WFD with interacting cracks residual strength criterion is the stress $\sigma_{r,rem}^e$ equal to the yield strength $\sigma_{0.2}$ calculated with correction for stable crack growth. Some structures failed at $\sigma_{r,rem}^e < \sigma_{0.2}$; this can be explained by the effect of local bending stresses difficult to calculate. During residual strength test of two pressurized fuselages with skin notches simulating the through multiple-site cracks no notch growth was observed. It should be noted that during residual strength test of one pressurized fuselage with multiple-site circumferential skin cracks in the upper part a substantial stable crack growth was detected. Test results for this fuselage are not included into Table 2, as the structure did not completely fail. There are also such multiple-site fatigue crack patterns (in structures made of the plastic alloy D16T) for which the residual strength criterion may be formulated as $K_{fract} = K_{app}$.

4. ON CRACK AND FATIGUE RESISTANCE DEGRADATION

In the early 1980s special tests were conducted on wide specimens cut out of aircraft wing and fuselage skins operated for 25 years (from the late 1950s) and on newly fabricated materials of the same types manufactured in the early 1980s. Tested were clad sheets of naturally aged copper-based alloys (D16ATV and D16ATNV) as well as clad sheets of artificially aged zinc-based alloy (V95AT1V); extruded panels of naturally aged copper-based alloy (D16T) and extruded panels of artificially aged zinc-based alloy (V95T1). The specimens were tested with free bulging near cracks. The ultimate strength σ_b , yield strength $\sigma_{0.2}$, and elongation δ were determined using other specimens. The crack growth rate was found by testing the same wide specimens that were thereafter used for determining residual strength. Fatigue crack growth rate (d2a/dN) tests were conducted for stress increment $\Delta\sigma = 130$ MPa, cycle stress ratio $R=0.05$, and loading frequency $f=0.2$ Hz. Table 3 presents experimental study results on apparent fracture toughness K_{app} , while Table 4 shows the fatigue crack growth rate d2a/dN for the stress intensity factor range $\Delta K = 31-62$ MPa \sqrt{m} . The specimen numbers in Tables 3 and 4 are unified. The numbers with index "o" are for specimens of old aircraft skins, while the numbers with index "n" are for specimens of newly fabricated materials. Some general tendencies are observed with the materials of all aircraft types studied:

- residual strength of materials in airplanes operated for a long time (from the late 1950s) is lower than that of new materials of the same type made in the early 1980s;
- ultimate and yield strength of materials in high-time aircraft is higher than the characteristics of new materials of the same type;
- fatigue crack growth rate for the range $\Delta K = 31-62$ MPa \sqrt{m} in the materials of high-time aircraft is higher than that of new materials of the same type.

In 1998 an additional experiment was carried out to compare fatigue crack growth rate of narrow specimens (160-mm wide) made of D16ATV. The narrow specimens were cut out of wide specimens tested earlier. Test methods and results for wide specimens are described above. Narrow specimens were tested at the same stresses, cycle stress ratio and loading frequency as wide specimens. Results of this experiment may be seen in Fig. 1; these converge with results of testing wide specimens (Table 4).

It should be noted that in the experiments described it was difficult to separate the effects of the sheet manufacture process and the service duration on crack resistance. Alloys 1163T and V95pchT2 having less silicon and iron (and with improved process) are utilized instead of alloys D16T and V95T1 (respectively) in structures of Russian advanced aircraft.

TABLE 3. MATERIAL STRENGTH IN WING AND FUSELAGE SKINS

Aircraft type	Alloy	Semi-finished item	σ_b , MPa	$\sigma_{4.1}$, MPa	δ , %	Si, %	Fe, %	Specimen number	W, mm	t, mm	2a, mm	K_{app} , MPa \sqrt{m}
Wing												
1	D16ATV	sheet	424-443	312-319	21-22	0.28	0.38	1.1n	566	4.9	176	98
			472-483	355-367	18-20	0.27	0.4	1.2n	565	4.9	171	100
2	D16ATN V	sheet	462-490	386-405	8-12	0.28	0.28	1.1o	568	5	250	91
			476-501	395-425	11-13	0.24	0.3	1.2o	565	5	170	81
3	D16T	extruded panel	509-547	374-417	12-13	0.27	0.38	2.1n	754	3.8	255	102
			535	440	10			2.2n	754	3.8	243	103
4	V95ATI B	sheet	545	510	10-11			2.3n	754	3.8	245	103
			561-588	506-550	8-9	0.07	0.28	2.1o	710	3.8	225	83
5	V95TI	extruded panel	603-634	575-588	7-8	0.22	0.3	2.2o	747	3.9	220	82
			561-588	506-550	8-9	0.07	0.28	2.3o	713	4.8	223	91
			561-588	506-550	8-9	0.07	0.28	2.4o	692	3.7	152	69
			535	440	10			3.1n	500	6	150	103
			545	510	10-11			3.1o	494	3.2	150	96
			561-588	506-550	8-9	0.07	0.28	3.2o	494	3.2	175	87
			603-634	575-588	7-8	0.22	0.3	3.3o	494	3.2	150	91
			561-588	506-550	8-9	0.07	0.28	4.1n	500	4	160	62
			561-588	506-550	8-9	0.07	0.28	4.2n	500	4	163	60
			603-634	575-588	7-8	0.22	0.3	4.1o	580	4	160	53
			561-588	506-550	8-9	0.07	0.28	4.2o	580	4	142	56
			603-634	575-588	7-8	0.22	0.3	4.3o	580	4	140	56
			561-588	506-550	8-9	0.07	0.28	5.1n	500	6	160	86
			603-634	575-588	7-8	0.22	0.3	5.2n	500	6	160	87
			561-588	506-550	8-9	0.07	0.28	5.3n	500	6	160	89
			603-634	575-588	7-8	0.22	0.3	5.1o	500	6	160	63
			561-588	506-550	8-9	0.07	0.28	5.2o	500	6	160	63
			603-634	575-588	7-8	0.22	0.3	5.3o	500	6	160	54
			561-588	506-550	8-9	0.07	0.28	5.4o	500	6	160	49
			603-634	575-588	7-8	0.22	0.3					

TABLE 3(continued). MATERIAL STRENGTH IN WING AND FUSELAGE SKINS

Aircraft type	Alloy	Semi-finished item	σ_b , MPa	σ_{e2} , MPa	δ , %	Si, %	Fe, %	Specimen number	W, mm	t , mm	2a, mm	K_{app} , MPa \sqrt{m}
Fuselage												
6	D16ATV	sheet	430-440	320-328	17-19	0.21	0.32	6.1n 6.1o 6.2o	1200 1195 1185	1.3 1.1 1.2	599 597 598	84 83 87
7	D16ATV	sheet	460-471	356	13-15	0.35	0.27	7.1n 7.2n	1200 1200	1.5 1.5	600 600	96 100
			483-488	359-364	13-17	0.35	0.3	7.1o 7.2o	1180 1246	1.5 1.5	620 600	77 91

TABLE 4. FATIGUE CRACK GROWTH RATE IN WING AND FUSELAGE SKIN MATERIALS

Aircraft type	Alloy	Semifinished item	Specimen number	$(d2a/dN)_{aver.}$, mm/kilocycle at $\Delta K=31$ MPa \sqrt{m}	$(d2a/dN)_{aver.}$, mm/kilocycle at $\Delta K=62$ MPa \sqrt{m}
Wing					
1	D16ATV	sheet	1.1n, 1.2n 1.1o, 1.2o	8.5 36	131 970
2	D16ATNV	sheet	2.1n, 2.2n, 2.3n 2.1o, 2.2o, 2.3o, 2.4o	7.5 17	154 491
3	D16T	extruded panel	3.1n 3.1o, 3.2o, 3.3o	12	265
4	V95ATIV	sheet	4.1n, 4.2n 4.1o, 4.2o, 4.3o	20 58	1000 5527
5	V95TI	extruded panel	5.1n, 5.2n, 5.3n 5.1o, 5.2o, 5.3o, 5.4o	13 20	300 1200
Fuselage					
6	D16ATV	sheet	6.1o, 6.2o	5.7	712
7	D16ATV	sheet	7.1n, 7.2n 7.1o, 7.2o	3.8 8.5	208 895

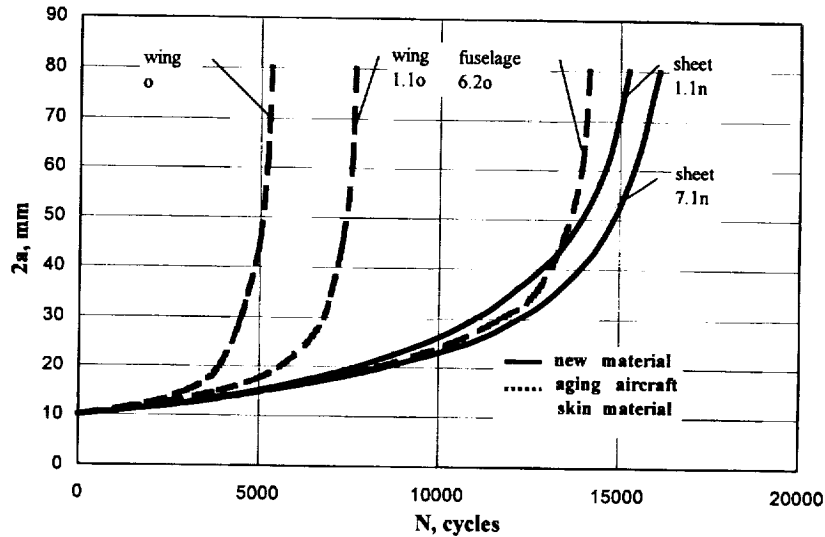


Figure 1. Crack growth duration in D16ATV specimens.

Full-scale structures with WFD were investigated in terms of fatigue crack growth during fatigue tests and in operation (Figs. 2 and 3). Relative service times \bar{T} are the ratio of the current service time to the service time at which the structure with WFD has been destroyed. Operational data are presented by the points showing crack size and lifetime of those aircraft where WFD was detected. On the basis of these data and by means of statistical analysis ⁽⁴⁾ some crack growth curves were generated corresponding to probability $p=0.5$; 0.05 and 0.001. Experimental data of Figs. 2 and 3 show that multiple-site fatigue cracks initiate much earlier and grow much faster in high-time aircraft structures than in new structure tests.

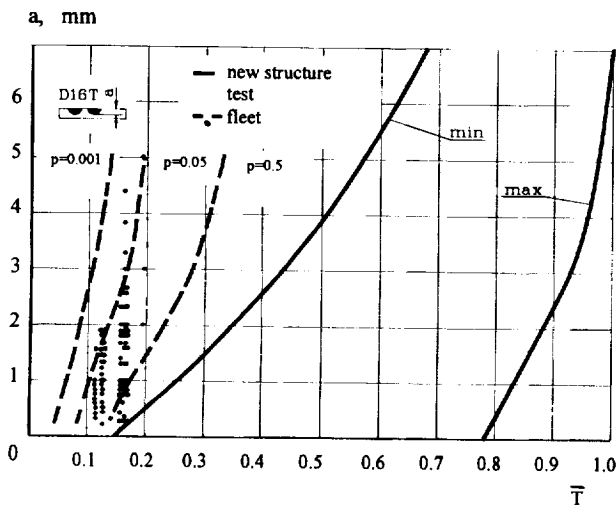


Figure 2. Relative MSD growth time: upper wing panel attachments.

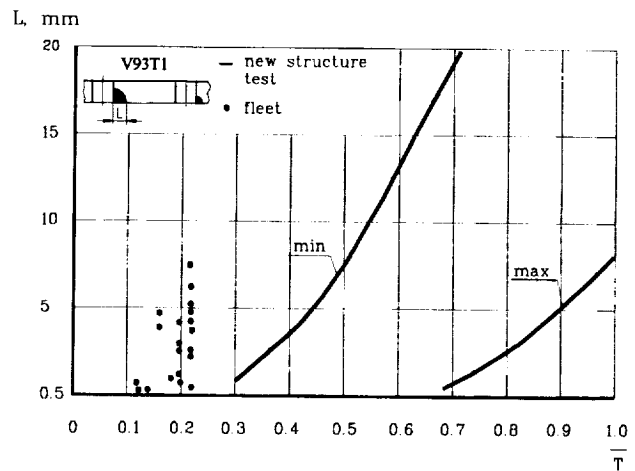


Figure 3. Relative MSD growth time: lower wing panel attachments.

New aircraft full-scale structures and those taken from the fleet were fatigue tested. Both new aircraft and those with different service times were fatigue tested in the laboratory using similar loading programs. The lives of new and operated aircraft structures of the same type were compared taking into account fatigue damage equivalents for tests and operation. Figure 4 presents experimental and analytical data on residual life of four aircraft wings of the same type but having different service times, while Fig. 5 shows experimental and analytical data on residual life of four pressurized fuselages of a different type with

various service times. Linear hypothesis of fatigue damage accumulation was used in residual life calculation. It follows from Figs. 4 and 5 that experimental residual life of aircraft structures being operated is much lower than the predicted one.

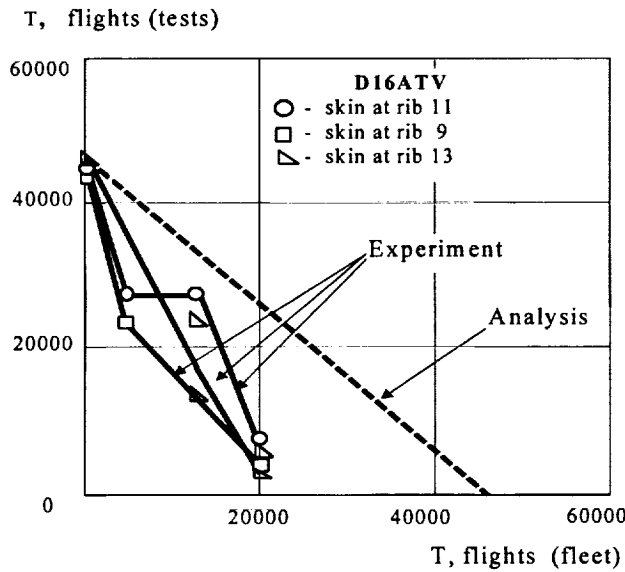


Figure 4. Residual life of turboprop aircraft wing.

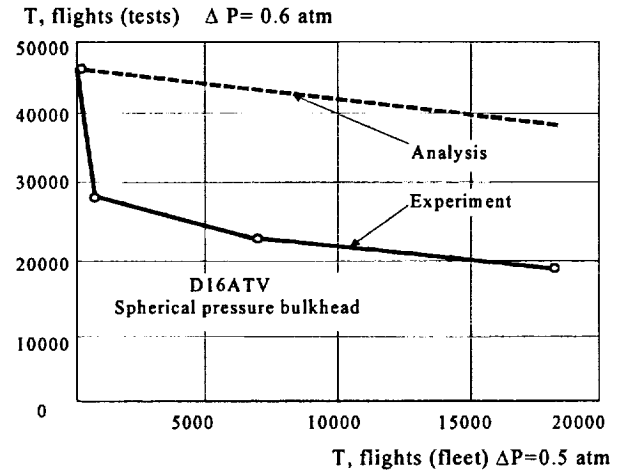


Figure 5. Residual life of turbojet aircraft fuselage.

5. CORROSION

The corrosion damage growth time is predicted analytically, based on operational sizes of detected corrosion damages and duration of aircraft service with detected damages. The same methods of mathematical statistics as for estimating fatigue crack growth⁽⁴⁾ are employed. Examples of estimating corrosion growth in wing and fuselage skins are presented in Figs. 6 and 7.

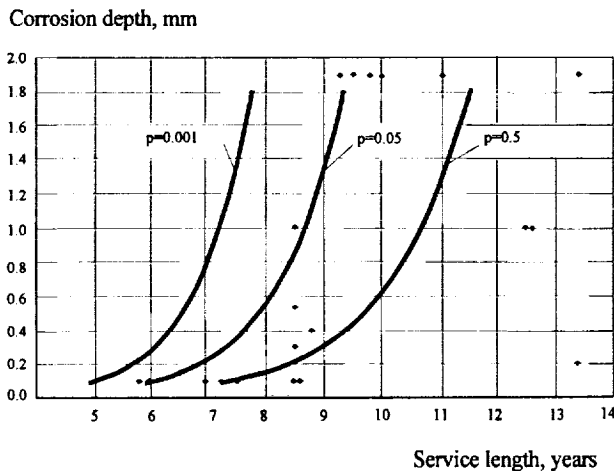


Figure 6. Corrosion growth in fuselage skin.

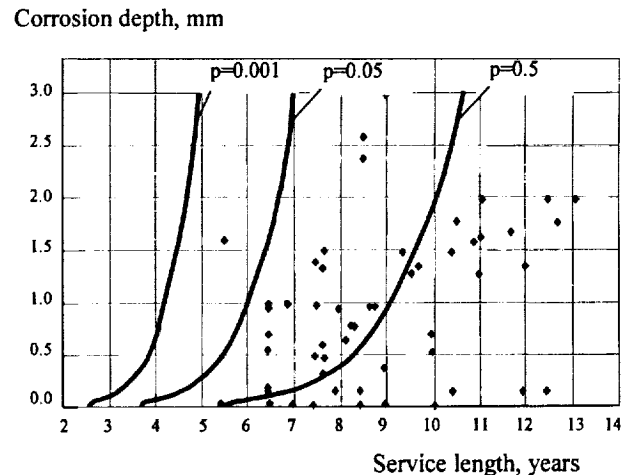


Figure 7. Corrosion growth in wing skin.

6. SAFE OPERATION OF AGING AIRCRAFT

Safe operation of aging aircraft structures is ensured according to damage tolerance concept. Damage tolerance characteristics of aging aircraft structures are refined by test results from long-operated aircraft (Table 1). The inspection initiation dates and intervals for aging aircraft structures are refined based on comparing the data from testing new and long-operated aircraft (Figs. 4 and 5), comparing the data from testing full-scale new structures with data on detected cracks in operated structures (Figs. 2 and 3). To calculate the damage tolerance of aging aircraft structures a data bank is generated on crack resistance of aging aircraft materials (Tables 3 and 4).

On the basis of such complicated test-analytical investigations dealing with service life prolongation are given for separate aging aircraft copies. In some cases these, documents permit operating the structures with cracks detected in them. Fig. 8 shows an example structure. Here, inspection intervals and tolerable crack lengths are defined in accordance with the damage tolerance concept.

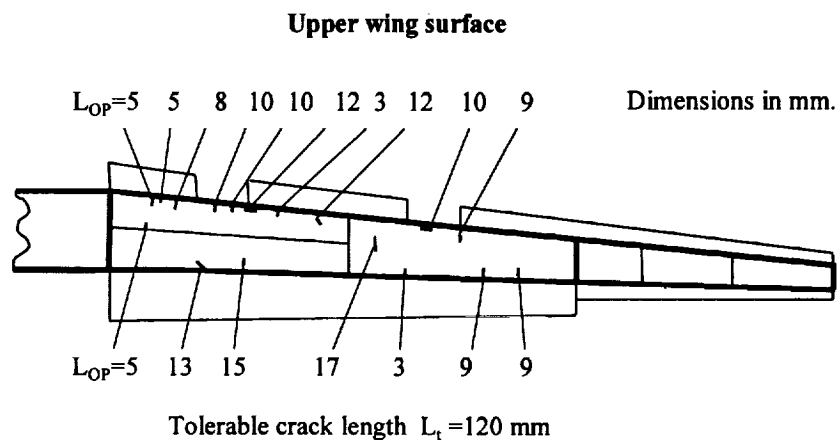


Figure 8. Operation of aircraft structures with crack

CONCLUSION

Residual strength criteria are studied for full-scale wing and fuselage structures having widespread fatigue damage. It is stated that fracture of several structures having such damage may be described by linear fracture mechanics criteria – material fracture toughness under plane strain or under plane stress. Many structures manufactured of plastic materials fail under stresses equal to the yield strength for a net section. These stresses should be calculated with consideration of stable crack growth.

The following experimental data were compared: crack resistance and fatigue strength of wing and fuselage skin materials of high-time aircraft and new materials; multiple-site fatigue crack growth duration in new structures during tests and in operation. Theoretical and experimental values of residual and fatigue lives of operated structures were compared. Crack resistance and fatigue strength of high-time aircraft turned out to be decreased in comparison with new structures.

For many types of aging aircraft, corrosion damage growth was estimated on the basis of fleet data. These data are used to specify structural inspection intervals for aging aircraft.

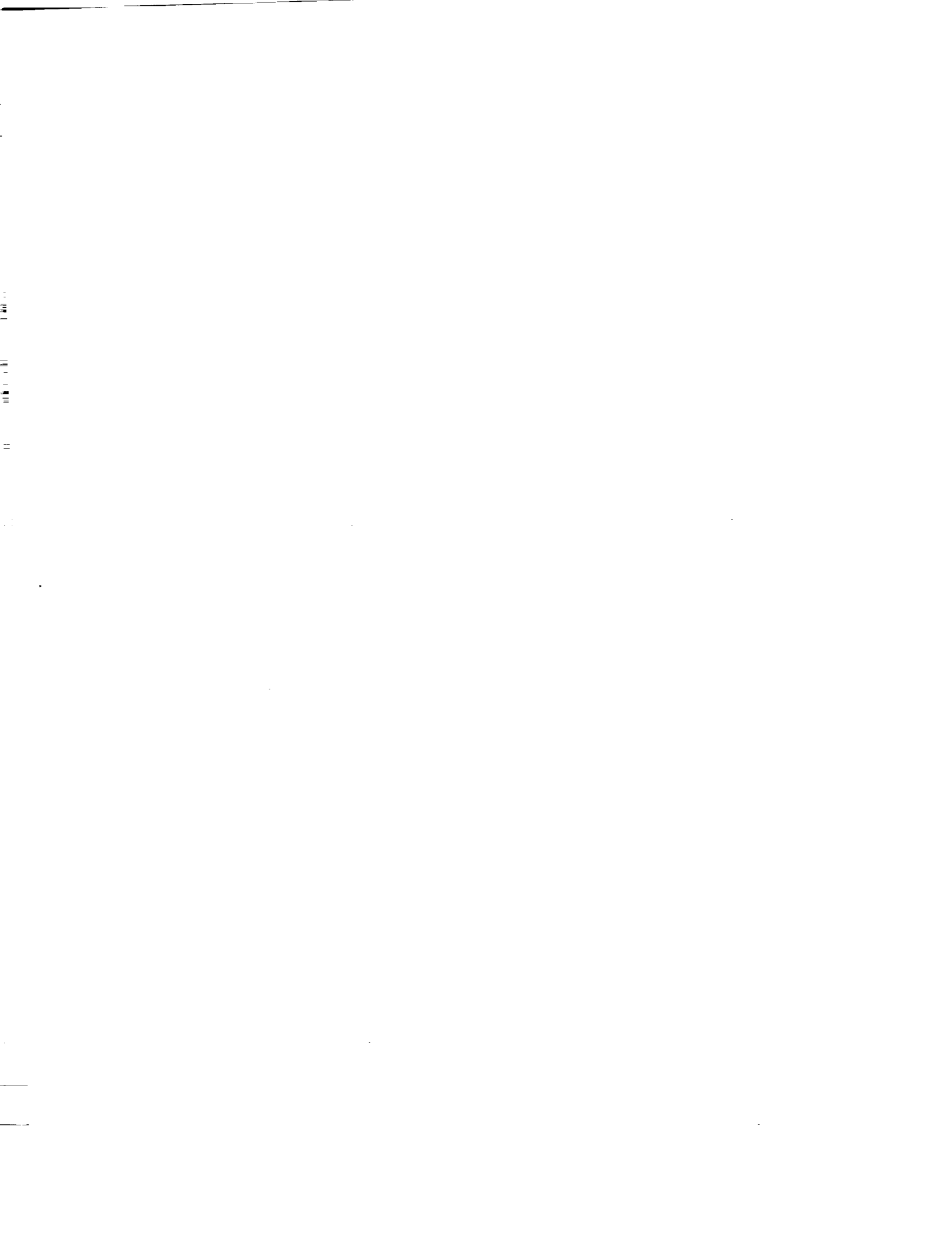
Safe operation of Russian aircraft is ensured by using results of comparing fatigue lives of new and operated full-scale structures; comparing crack resistance of wide specimens cut out of high-time aircraft

skins and new skin sheets; generalizing fleet experience (damage data collection and processing using mathematical statistics methods).

REFERENCE

1. Nesterenko, G.I. "Damage Tolerance of Aircraft Structures". Joint Higher School Scientific Proceedings: Strength, Reliability and Life of Aircraft Structures, issue 2, Kiev, 1976, p.60-70 (in Russian).
2. Raikher, V.L., Dubinsky, V.S., Nesterenko, G.I. and Stuchalkin, Yu.A. "The Features of Aircraft Structure Fatigue Resistance Certification and Airworthiness Maintenance in Contemporary Conditions". Test Facilities and Aircraft Certification International Symposium, Zhukovsky, Russia, Aug. 22-25, 1995, p.233-245.
3. Nesterenko, G.I. "Fatigue and Damage Tolerance of Aging Aircraft Structures". Proceedings of the 19th ICAS Symposium, Fatigue in New and Aging Aircraft, v.II, 1997, Edinburgh, Scotland, p.731-742.
4. Senik, V.Ya. "Analysis of In-Service Fatigue Crack Growth in Aircraft Structural Elements". Trudy TsAGI, issue 1671, Moscow, Russia, 1975, p.17-27 (in Russian).

**TECHNOLOGIES FOR
INSPECTION, MAINTENANCE, AND REPAIR**



REPAIR DEVELOPMENT FOR FATIGUE CRACKS IN THE F-5E VERTICAL STABILIZER

Jennifer S. Elmore and Edwin L. Rosenzweig

Structures Engineering

Naval Air Warfare Center

Patuxent River, Maryland 20670-1906

(301)342-9354

(301)342-9412

Elmore_Jennifer%Pax5A@mr.nawcad.navy.mil

Penelope Ulander, F-5 Team Lead

Douglas Perl, Materials Engineering

Naval Aviation Depot, North Island

San Diego, California 92135-7058

ABSTRACT

This paper describes the experience gained by the Navy in the development of composite patch repair techniques for the F-5E vertical stabilizer. The F-5E is used by the Navy as an aggressor aircraft in the Dissimilar Air Combat Training (DACT) program. In this role, the aircraft has sustained different and more severe fatigue loading than originally designed. Fatigue cracking was discovered at the termination of the integral blade stiffeners in the aft section of the vertical stabilizer. These fatigue cracks occur randomly at five different vertical stabilizer stations (VSS). Bulges due to plastic deformation were also found in the skins at some repair stations. Due to the long lead times and costs associated with the manufacturing of new stabilizers, the decision was made to engineer and apply a bonded composite repair concept. This paper outlines the approach followed in the planning, development, certification and application of repairs to arrest or retard crack growth thereby restoring original structural life and elaborates on critical stages in the process and important lessons learned. A grit blast/silane surface preparation technique developed by the U. S. Air Force was selected. A double vacuum debulk and staging process was developed for Textron 5521 Boron/epoxy to improve patch quality, inspectability and formability over the plastically deformed bulges in the skin. The overall engineering and certification methodology also required extensive design and analysis efforts to properly size, shape and locate the patch on the post-buckled structure. Also, limited coupon testing was performed to verify critical processes, certify personnel, and establish material design allowables. Subcomponent design and fatigue testing were required to replicate skin loads, demonstrate crack initiation, and validate the repair design and crack growth retardation predictions. Finally, NDI methods were developed to monitor crack growth rate and detect possible failures. Initially, the repaired stabilizers will be inspected using eddy current, the patch bondline by thermography. As confidence in the repair process grows, the inspection intervals will be lengthened to account for the beneficial effects of the repair on structural integrity and durability.

1.0 INTRODUCTION

The use of composites to repair metallic structure has been steadily rising as the average age of an aircraft increases. Airplanes designed in the 1960's and 1970's are now expected to be flying to 2005 and beyond. As spares are consumed, and the cost and lead time for new parts for these aircraft become prohibitive, repair to existing structure becomes an attractive alternative.

The F-5E is used by the U. S. Navy for aggressor training. Due to being flown at a spectrum the airplane was not originally designed for, fatigue cracking is occurring in the vertical tail. There are currently 15 airplanes out of a fleet of 33 aircraft that have exhibited cracking. Of these, 6 aircraft are grounded. Three alternatives were investigated, reskinning, repairing, or replacing the tails. The lead time for replacement tails or skins was estimated at 2 years from contract initiation, leaving repair as the most feasible course of action.

The vertical tail is exhibiting two types of damage, fatigue cracking and bulging of the metal skin. The bulging phenomenon is seen in areas with and without cracks, and is believed to be plastic deformation of the metal skin. Of the fifteen damaged aircraft, only ten have been deemed repairable. The VSS displaying the most damage is 61.5, with 12 cracks in nine tails. Using this information, the details necessary to implement a bonded repair were defined.

2.0 REPAIR CONCEPT

The F-5E vertical tail has exhibited fatigue cracks emanating from the compound fillet at the intersection for the integral skin stiffeners and the machined skin lands for the ribs. These cracks are all aft of the 50% spar and have been detected at six Vertical Stabilizer Stations (VSS). Repair alternatives were evaluated. A bolted metal repair had been installed by the Air Force, however, the repair did not prevent the crack from growing. It was decided to evaluate a bonded repair concept.

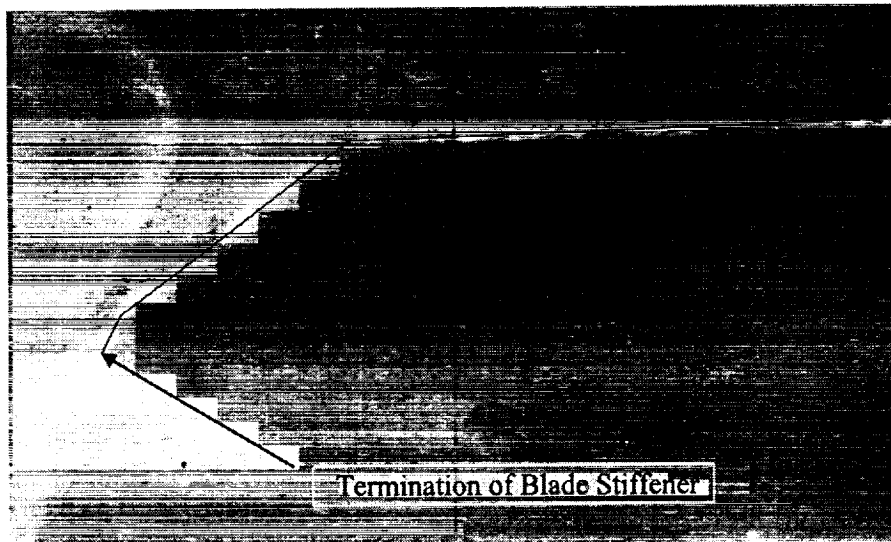


Figure 1: Termination of blade stiffener. Fatigue cracks are appearing at the termination of the integral blade stiffeners.

2.1 OBJECTIVES OF REPAIR

The intent of the repair is to retard the crack growth rate, or to be used as preventative maintenance and applied to uncracked stations to delay crack formation. Due to geometry restrictions, a repair could not be developed for VSS 25.5. Consequently these tails will be reskinned when the cracks at VSS 25.5 exceed 0.25". The repair is intended to be for fatigue enhancement only, and repaired stabilizers will be inspected at the same intervals established before repair.

2.2 REPAIR DESIGN

Northrop-Grumman was tasked to evaluate the stabilizer and provide the design for a bonded doubler. The following design assumptions were established: the patch is designed for the vertical tail station exhibiting the most severe cracking (VSS 61.5); the patch is designed to retard the crack growth rates of two 0.5" cracks impinging on each other; and the patch may be applied at any station, cracked, bulged, or undamaged.

With these baseline assumptions a repair patch was designed using autoclave cure Boron 5521 and FM 300-2 mechanical properties. The final repair patch design is a seven-ply symmetric layup [0/+45/-45/0/-45/+45/0] that has a standardized width of 5.3" for all VSS, the length varies by VSS. The patch edges have a taper ratio of 30:1 and is octagonal to relieve peel stresses at the corners. Since the vertical tail is considered a post-buckle structure, particular emphasis is placed on out-of plane material properties.

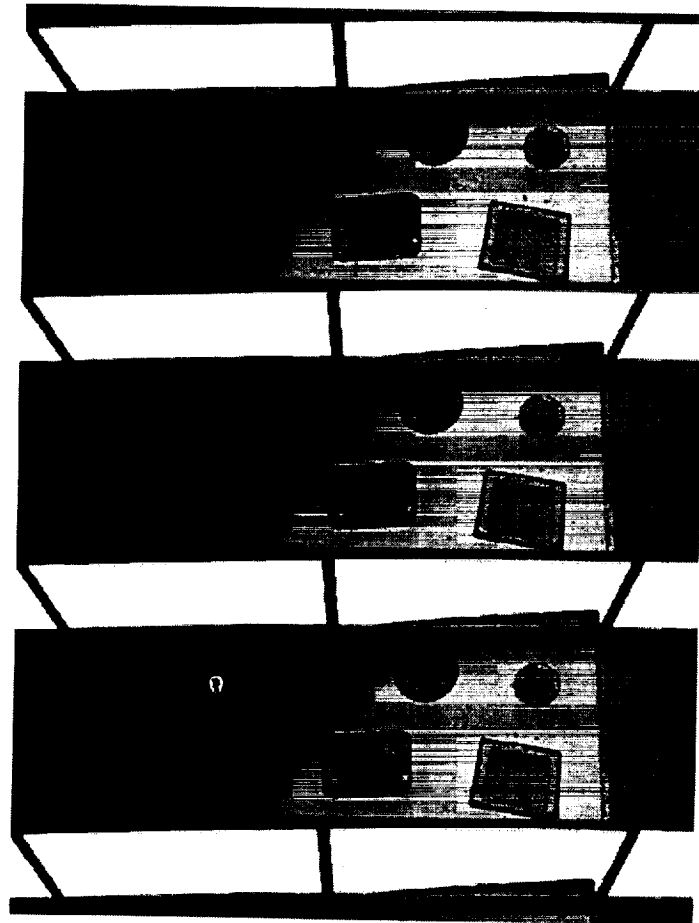


Figure 2: Repaired vertical stabilizer. The bonded boron repair doubler installed at VSS 34.5.

Detailed design and analysis is necessary to verify the repair configuration. For the F-5 vertical stabilizer repair analysis, three models were created. The initial model, developed by Northrop Grumman, was a linear analysis model of the stabilizer using plate elements in the skin and bar element in the stringers [8]. This model was used to determine the gross stresses and highest loaded bay. The second model, developed by NAWC Pax, was created to evaluate the buckling and post-buckling behavior of the repaired and unrepaired stabilizers [7]. This non-linear model was generated for the highest loaded stringer and adjacent bays using plate elements in the skin and stringer, and imposing thermal loading for the repaired configuration. Models indicated that the bays between the stringers would buckle at 60% of limit load, and redistributed load from the bays to the stringers would crack the skin at the stringer runouts. To analyze this case, a series of pre and post buckled load cases were imposed on the second model to determine edge displacements of the repair patch and input to a third 2D model of the bonded repair joint in cross-section. Two local cross-section models of the patch to skin joint were generated and analyzed at the location of the maximum lateral deflection in the center of the bay and adjacent to the stringer. Maximum lateral deflection was predicted to be 0.22 inches. Peak bondline shear strains, normal tension stresses, patch interlaminar shear stresses, and normal tension stresses were determined and compared against individual material allowables. A combined failure mode criteria was used to determine margins of safety. For combined failure modes, both the bondline and patch transverse shear and transverse normal tension stresses were input to a Tsai Wu type quadratic formula. Additional A4EI elastic/plastic bonded joint analyses were conducted for the joint adjacent to the stringer to model the effects of the bondline plastic behavior. The findings from the non-linear analyses were that interlaminar failure and failure at the edge of the patch adhesive adversely affected crack growth retardation due to the redistribution of the load adjacent to the stringer.

The F-5 repair analysis used a spectrum analysis from flight data from Nellis AFB. Damage tolerance analysis and crack growth analysis were conducted unrepaired and repaired to optimize patch design, determine inspection intervals, and predict life extension. Stress intensity factors (K_I) were calculated at different crack lengths and used to create a crack length stress intensity curve. This data is iterated through the spectrum loading and used to create Crack Length vs. Flight Hours curves for the repaired and unrepaired configurations of each VSS. This data was initially used to establish inspection criterion. Due to the weight addition and balance requirements, the stabilizer was also analyzed for flutter. Analysis indicated the increased stiffness and weight of the tail due to the repair patches were not a concern.

3.0 PROCESSING AND PROCEDURES DEVELOPMENT

Due to the urgency of repairing this aircraft, as many decisions as possible had to be made early in the program. Surface preparation, inspection, training, and lessons learned were incorporated directly from the experiences of the U. S. Air Force [1-3]. The Air Force has used this technology to repair C-141 fuel tanks, F-16 wings, and many other aircraft. However, for other parameters, such as boron processing and allowables generation, it was necessary to investigate and develop alternative solutions.

3.1 BORON/EPOXY PROCESSING

For the vertical tail, three damage situations were discovered. The vertical stabilizer stations could be cracked, bulged, or cracked and bulged. The bulges discovered extended approximately 0.04" out of plane. These bulges were attributed to localized plastic deformation of the aluminum skin. For these areas, a precured repair patch was not an option due to the stiffness of the repair patch, causing excessive void formation in the bondline. It was decided early in the program to only consider the Boron 5521 resin system. This was done due to the 250°F cure required for this system opposed to a 350°F cure

required for the Boron 5505 resin system. The lower cure temperature induces less residual stresses in the bondline. Two other processing options were investigated for the 5521 resin system.

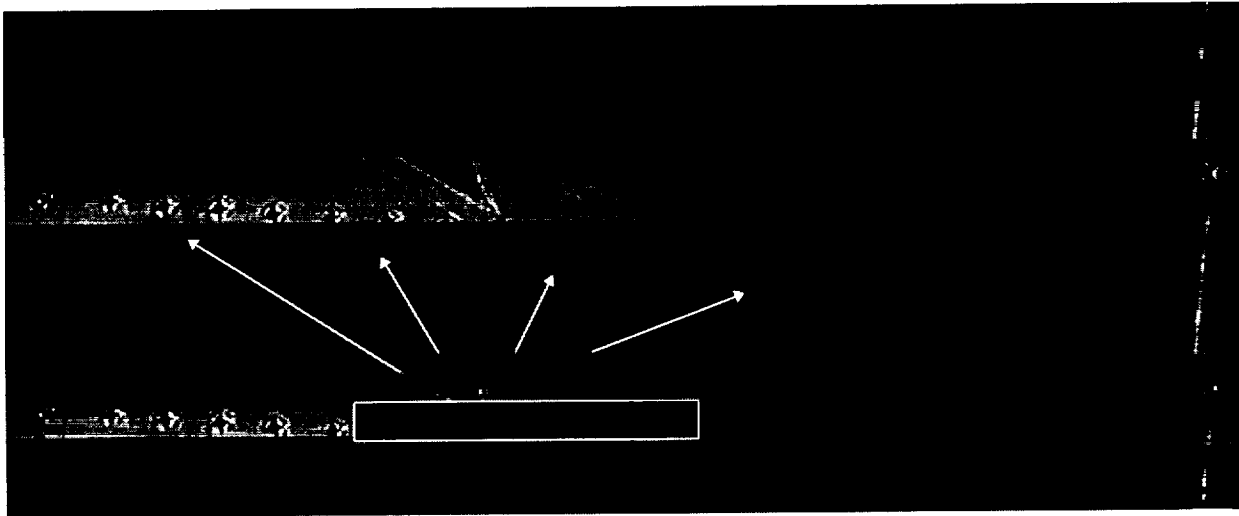


Figure 3: Bulged and cracked VSS skin. The cracks in the vertical tail initiate at the compound fillet at the intersection of the integral skin stiffeners and the machined skin lands for the ribs.

In order for the repair patch to form over the bulged area, formability of the laminate was required. The structural analysis indicated that a vacuum bagged repair patch would not have sufficient interlaminar properties. The first alternative investigated was a staged/compacted autoclave cure cycle that was formed from some information provided by the Canadians [4]. In this cycle the laminate is heated and compacted in the autoclave for a short period of time in order to reduce the porosity in the laminate. The patch is then removed from the autoclave, still formable, and vacuum bag cured to the stabilizer. The second alternative developed involved characterizing the resin with a variety of thermal analysis techniques and forming a double vacuum debulk (DVDB) cycle [5-6]. Double vacuum bag debulking is a processing technique used to manufacture composite laminates with reduced porosity levels without an autoclave. This technique uses two vacuum bags to remove the air from between the plies of a laminate, then the outer bag is collapsed and the laminate is compacted to prevent air from forming between the plies of the laminate. This technique has been used successfully with the Hysol EA 9390 resin system and AS4/3501-6 carbon pre-preg. To evaluate these processing techniques, interlaminar shear testing was performed per ASTM D2344. The results are shown in Table 1. Flange bending testing was performed to determine interlaminar tension values, shown in Table 2.

Test Condition	Autoclave Cured	DVDB	Staged and Compacted	Vacuum Bag Only
-65°F	14.5 ksi	14.3 ksi	13.7 ksi	11.9 ksi
75°F	13.7 ksi	12.8 ksi	12.2 ksi	10.4 ksi
180°F/wet*	5.4 ksi	6.0 ksi	4.4 ksi	4.4 ksi

* 48 hour water boil conditioning

Table 1: Interlaminar shear test data for Boron/Epoxy 5521.

Test Condition	Autoclave Cured	DVDB	Staged and Compacted
-65°F	5.4 ksi	4.1 ksi	4.7 ksi
75°F	5.7 ksi	3.3 ksi	3.7 ksi
180°F/wet**	2.0 ksi	1.0 ksi	0.95ksi

** 45 days @ 140°F/95%RH

Table 2: Interlaminar tension test data for Boron/Epoxy 5521.

Due to the significant reductions in interlaminar properties, the problems with forming the boron fibers over the vertical stabilizer stations with bulges, strict NDI requirements, it was decided to precure the repair doublers in the autoclave and secondarily bond them to the vertical tail. The repair patch is vacuum bagged onto the vertical tail at the VSS it will be bonded to later and release film is placed between the patch and vertical tail skin. The entire vertical tail assembly is rolled into the autoclave and the structure is heated to 175°F. A heat blanket placed over the repair patch is used for the final repair patch cure at 250°F. The location of the repair patch is carefully marked, particularly on the bulged stations. Exact placement of the repair patch is required to ensure proper fit-up and eliminate porosity in the bondline during the secondary bond cycle.

3.2 SURFACE PREPARATION

Two surface preparation techniques are generally used for this type of repair, a grit blast/silane surface treatment, and the Phosphoric Acid Containment System (PACS). Both of these techniques have documented procedures and have been proven to work through coupon testing and actual aircraft application [3]. Due to time considerations a decision was made in the beginning of the program to only develop the organic capability for the grit blast/silane surface preparation technique. This technique was the most attractive because the tail configuration only allows a one sided repair of a through crack. The PACS technique is generally simpler and less operator sensitive, however, the ability to seal a through crack to guarantee no acid entrance to the inside of the vertical tail could not be quickly answered. Consequently, the grit blast/silane procedure was preferred.

NADEP NI implemented the grit blast/silane surface preparation procedures provided by Wright Labs Materials Directorate. The depot used floating roller peel testing (ASTM 3167) and wedge crack testing (ASTM 3762) to evaluate their progress in adopting these procedures. The results of their test panels were compared to the test results provided by Wright Labs for similar testing configurations and conditions. The acceptance criterion for a successful wedge crack specimen was defined as less than 0.2" crack growth after 24 hours at 140°F/95% RH in 24 hours with a cohesive failure mode. Any specimens deviating from this criterion was designated a failure.

3.3 INSPECTION REQUIREMENTS

Due to the short lead time for implementing these repairs, inspection requirements were largely adopted from the quality specifications for the Air Force's C-141 Weepole Repair program [2]. It was decided that ultrasonics would be used to inspect the precured composite doublers, thermography to inspect the bondline for porosity and voids after patch installation, and eddy current would be used to detect the crack growth under the repair patch. A peel strip is used as a witness coupon to verify the quality of the surface preparation. The inspection criteria for the program are summarized as follows:

- a. Each precured repair doubler shall be inspected using through transmission ultrasonics. The through transmission decibel loss shall not exceed a 5 dB increase over an autoclave standard. Small areas, less than 1/16" diameter, can exhibit up to a 9 dB loss over an autoclave standard. A 5 MHz transducer shall be used for the inspection.
- b. For the adhesive bondline, thermography shall be used to detect voids or porosities. No voids larger than 1/8" diameter are acceptable in the edge and transition area. In the central area, up to 1% of the area may be disbonded with no one disbond exceeding 0.5 square inches. An example of unacceptable bondline porosity is shown in Figure 3.
- c. An aluminum peel strip shall be bonded concurrently with the repair patch. This peel strip will be tested after patch cure by pulling it off in the 90° direction. The peel strip shall fail at an excess of 24 piw and exhibit a cohesive failure mode. If the peel strip does not meet this criterion, the repair patch shall be removed, the surface prep repeated and the patch reapplied.
- d. Eddy current shall be used to inspect for further crack initiation or growth under the repair patch. The target crack growth monitoring resolution is 0.05".

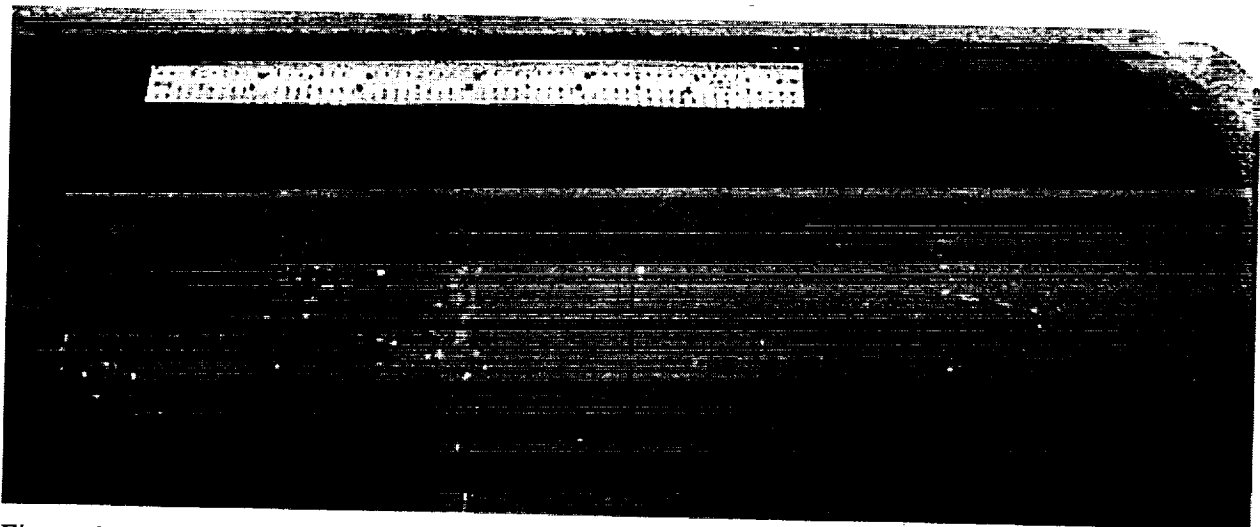


Figure 4: Unacceptable bondline porosity. The uneven bondline and voids in the center of the repair patch can be seen in this verifilm check of the vacuum bag bonding procedures.

After installation of the repair patch at the depot, the cracks under the repair patch will be initially inspected every 50 flight hours. Component test results indicate the cracks will not detectably grow and after some time in service, this inspection interval will be increased. There is no in service bondline inspection.

3.4 QUALIFICATION AND TRAINING

Artisan qualification and training is a major factor in the success or failure of composite repair to metallic structure. Because the surface preparation is so critical and the bond strength cannot be detected by any non destructive means, it is crucial an intensive training program is initiated. NADEP NI developed and implemented this program which includes one week of lecture followed by a written exam and hands on training. Each artisan is required to make two wedge crack panels on consecutive days that pass the less than 0.2" crack growth after 24 hours at 140°F/95%RH with a cohesive failure mode criterion.

4.0 SUBCOMPONENT TESTING

In order to validate the repair, a section of uncracked vertical stabilizer skin was removed from an unrepairable stabilizer. This stabilizer had over 3,000 flight hours and cracks were detected at VSS 61.5. The goal of this component testing was to verify the predicted repaired crack growth curves provided by Northrop-Grumman's [8] analysis.

4.1 Panel Configuration

The test section panel consisted of the area from VSS 34.5 to VSS 52.5 and cut from the 12% spar to the 46% spar. Both skins and the corresponding substructure was provided for the test component. Two through notches, 0.15" wide x 0.25" long, were milled into the skin at the termination of the lower, middle blade stiffeners at VSS 43.5. These locations were the most frequent occurrence of cracks at this vertical stabilizer station. The notches were milled to minimize residual stresses at the notch edges. The original substructure was bolted to the skin to provide stability. Fiberglass load introduction tabs were bonded to the ends of the test panel with Hysol EA 9309. Large metal plates were bolted to the fiberglass end tabs to introduce load through shear, not bearing. These load introduction plates were installed at approximately a 6° angle in order to introduce load perpendicular to the blade stiffeners.

4.2 Test Spectrum

Spectrum loading for the test specimens was done by reducing 1000 flight hours of data provided from the Nellis AFB spectrum. This spectrum was more severe than the original DACT flight spectrum. All values less than the predicted onset of buckling at 36% CLL, were clipped from the spectrum. Similarly, all low level tensile cycles were clipped from the spectrum. This provided a manageable test spectrum of 19,000 load pairs.

After the test panel assembly, the specimen was proof loaded in tension and compression. Proof loading was performed to establish the maximum tensile and compressive loads in the spectrum. The specimen was loaded in tension until an average of 1700 $\mu\epsilon$ was achieved across the test section. This load was set as 100% tensile limit load. Similarly, an average of 1400 $\mu\epsilon$ was generated across the test section, VSS 43.5, and the load set as compressive limit load. The entire test spectrum was then modified to reflect the new limit loads of 15,500 lbs in tension and 12,000 lbs in compression.

After proof loading and establishing the final spectrum loading, the test specimen was fatigued at R=0.1, maximum load 13,000 lbs, to grow cracks from the notches milled in the test specimen. After approximately 7,000 cycles at this load level, a crack was initiated out of one edge of each of the milled notches. After documenting the pre-repair crack length, the specimen was removed from the test frame for repair installation.

4.3 Patch Installation

The repair patch was installed in the high bay area of the NAWCAD structures test floor, with the large doors open, in February to reflect realistic conditions. Qualified NADEP North Island personnel performed the patch installation. After successfully performing the grit blast/silane surface preparation procedure, the patch was co-cured to the test panel. Co-curing is considered a higher risk than pre-curing and secondarily bonding the repair patch. The peel strip failed cohesively at acceptable load levels. Pre-test NDI indicated a dime size void in the bondline.

4.4 Test Results

During compression proof loading of the unrepaired and repaired test component, no buckling was observed. All back-to-back strain gauges placed in the center of the bays between blade stiffeners remained in compression. This leads to the conclusion that the assumptions made for the modeling were conservative. Unfortunately, during compression proof loading, a mechanical error caused the specimen to be overloaded and bent at VSS 25.5. The test component was repaired and fatigue testing proceeded in tension-tension only. The lack of compression loading affects the test of patch durability, but was deemed to not affect crack growth behavior.

The patch reduced the strains on the back side skin in the test section by over $625\mu\epsilon$, or 36% at tensile limit load. The unpatched strains on the top side of the skin in the test section averaged $1,300\mu\epsilon$. The strains on top of the repair patch in the same locations averaged $525\mu\epsilon$.

The test specimen was cycled for an equivalent of 4,500 flight hours or 88,000 cycles. Catastrophic failure occurred the repair at VSS 25.5. Ultrasonic inspection detected no growth in the dime size disbond found after cure, no edge delaminations, and no edge of patch disbonds. The bondline was intact, no additional defects were detected. Eddy current inspection detected no crack growth. To verify this, the test panel was disassembled, and the cracks were reinspected using dye penetrant. This confirmed no detectable crack growth for the 4,500 equivalent flight hour test spectrum. According to the crack growth curves provided by Northrop Grumman, for an initial crack length of 0.34" and an additional 4,500 flight hours at VSS 43.5, the crack should have gone catastrophic after 2,500 flight hours. Clearly the predicted crack growth curves are very conservative for this VSS.

5.0 CONCLUSIONS

Composite repair of metallic structure is a viable repair technique for aging aircraft. Selection of the proper repair materials, processing techniques, surface preparation techniques, and inspection techniques is essential to the success of this type of repair. The establishment of strict training requirements for Navy personnel, through classroom and hands on experience, is equally essential.

There is no cookbook approach to the design and analysis of bonded repairs. Each potential repair application must be evaluated for that specific structure. The stress analysis of the F-5 vertical tail indicated the need for a repair patch that would not only slow crack growth, but also accommodate the interlaminar shear and tensile loads in a post buckle structure.

Subcomponent fatigue test results indicate the repair patch reduces the strain in the test area, has good bondline durability, and prevents crack growth. These test results will be used to increase the inspection interval for crack growth under repaired vertical stabilizer stations after some in-service flight time.

ACKNOWLEDGEMENTS

The authors would like to express their gratitude to Jim Mazza, Jay Fiebig, and Harold Banks from the U.S. Air Force for their assistance in the surface preparation technology transfer, Randy Cramer for the thermal analysis work performed to develop the processing cycle, Lee Rosenstadt, Sgt. Mike Kirby, George Boerke and Mike Bosak for the panel fabrication and testing effort, and Paul Kulowitch for inspecting the sub-component during the fatigue test.

REFERENCES

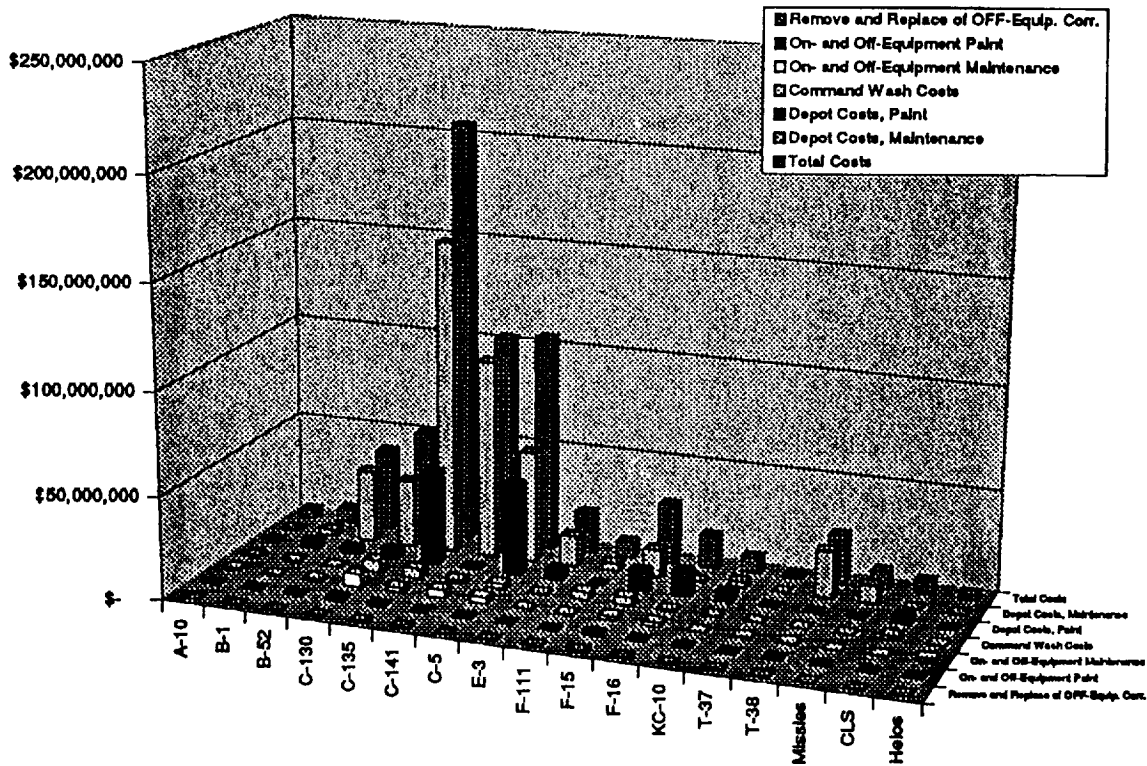
1. Sivam, T. P., Edwards, D., Mason, S., and Guy, P., "The Evolution of Composite Patch Repair Technology at CTAS in Meeting the Challenges of the C141-B Drop-In-Repair Program for WRALC," SAE Technical Paper Series, No. 961255, April, 1996.
2. "Quality Specification for Installation of Composite Repairs on C-141 Aircraft," Warner-Robbins AFB Specification No. 93-LJLE-021, Revision 6, August, 1994.
3. "Aluminum Surface Preparation for C-141 Repair," WL/MLSE Report No. ML 94-144.
4. Raizene, M. D., Heath, J. B. R. and Benak, T. J., "Processing Specification for CF-5 Upper Wing Skiing Boron5521/4 Fatigue Enhancement Doubler", LTR-ST-1884, National Research Council of Canada, June 1992, Revised 1 November 1992.
5. Mehrkam, P. A., Cochran, R. C., and DiBerardino, M. F., "Composite Repair Procedures for the Repair of Advanced Aircraft Structures," NAWC Warminster, Report No. 92091-60, September, 1992.
6. Bergerson, A., Marvin, M., Whitworth, D., Fuss, J., and Elmore, J., "Fabrication of a Void Free Laminate by Optimizing a Non-Autoclave Cure," SAMPE, April, 1997.
7. Rosenzweig, E., Elmore, J., Ulander, P., and Perl, D., "A Navy Approach to Bonded Repair of Metal Structures," First Joint NASA/FAA/DoD Conference on Aging Aircraft, Odgen, UT, July, 1997.
8. "Composite Patch Repair of F-5E/F Vertical Stabilizer Skin," Northrop Grumman Report No. 96-021, Contract No. F41608-94-D-0322, January, 1997.

Air Force Cost of Corrosion Maintenance Study

In 1990 the annual direct cost of corrosion maintenance was determined for USAF systems. This extensive database has been widely used and is the only one of its kind. A new study has now been completed using a 1997 base year. This new study not only provides updated cost figures but it also provides a snapshot in time for determining trends and changes in the costs of corrosion. These figures include all Air Force assets but exclude facilities, real property installed equipment, classified systems, and some indirect costs associated with corrosion.

Corrosion costs the Air Force in excess of \$795 million per year in direct maintenance expense. The results show that while the fleet size has decreased nearly 20% between the two studies, the costs of corrosion have gone from \$720 Million in 1990 to \$795 Million in 1997. Corrosion costs per aircraft have risen drastically for nearly all systems. This trend is especially important when it is realized that significant numbers of the retired assets were those requiring the most corrosion maintenance. In the 1990 study 53% of the corrosion costs involved the 5 aging weapon systems. Today 50% of those costs involve just 3 of the oldest systems (C-135, C-5, and C-141).

This Cost of Corrosion database gives costs by command, location, and weapon system as well as field level vs. depot level expenditures. The field vs. depot corrosion cost distribution has remained almost constant between the two studies. This information is summarized below:



Corrosion Costs (and cost elements) of Air Force Weapon Systems

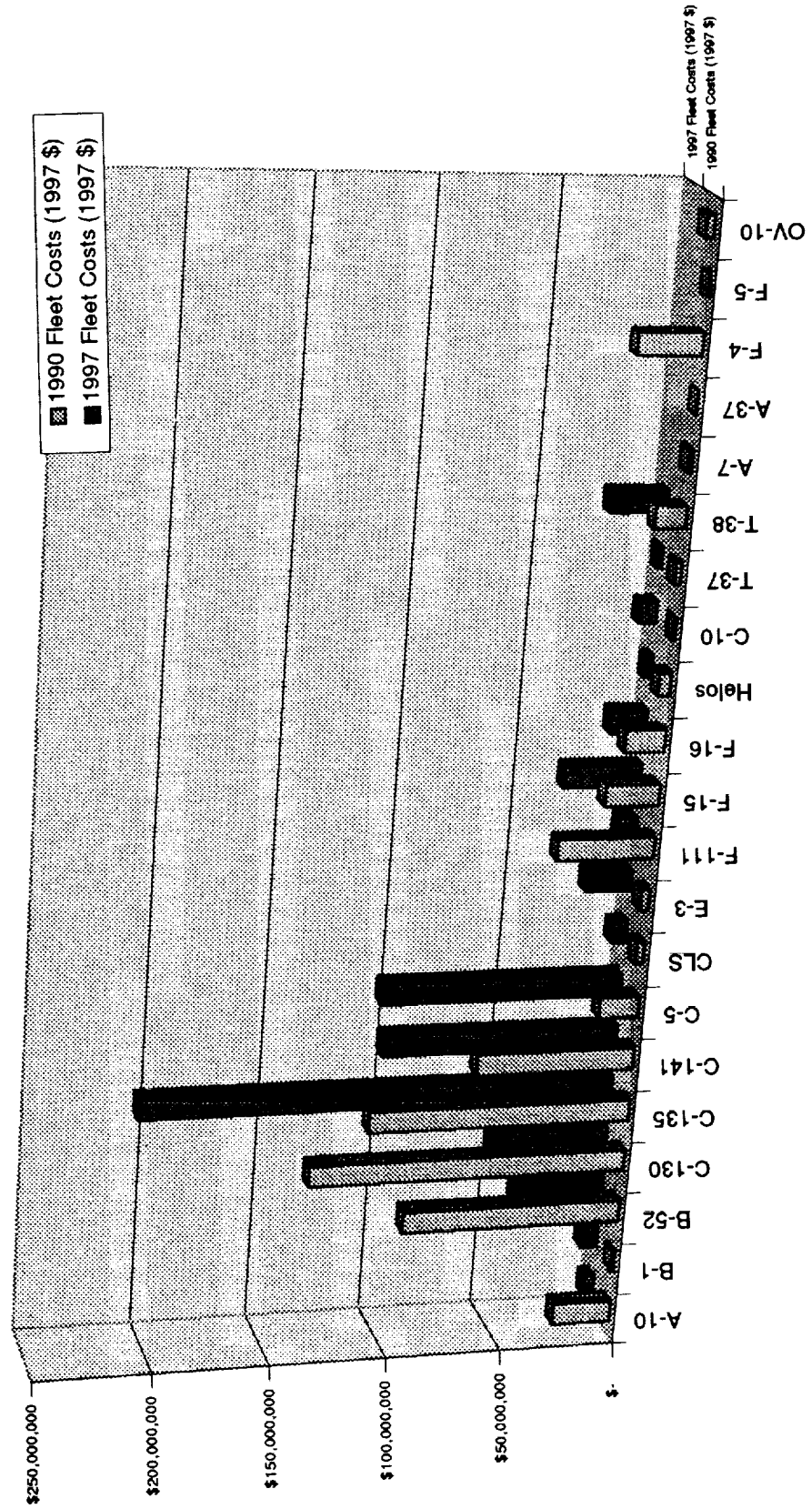
Corrosion Maintenance Definition

- **Direct corrosion maintenance includes:**
 - All Corrosion treatment
 - Application of sealants
 - All painting
 - All protective coating removal and re-application
 - Washing
 - Inspection for corrosion
 - Repair and replacement of corroded parts

Exclusions

- **Direct corrosion maintenance does not include:**
 - Cost of A/C downtime
 - Depreciation
 - Facilities
 - Training
 - Deferred maintenance

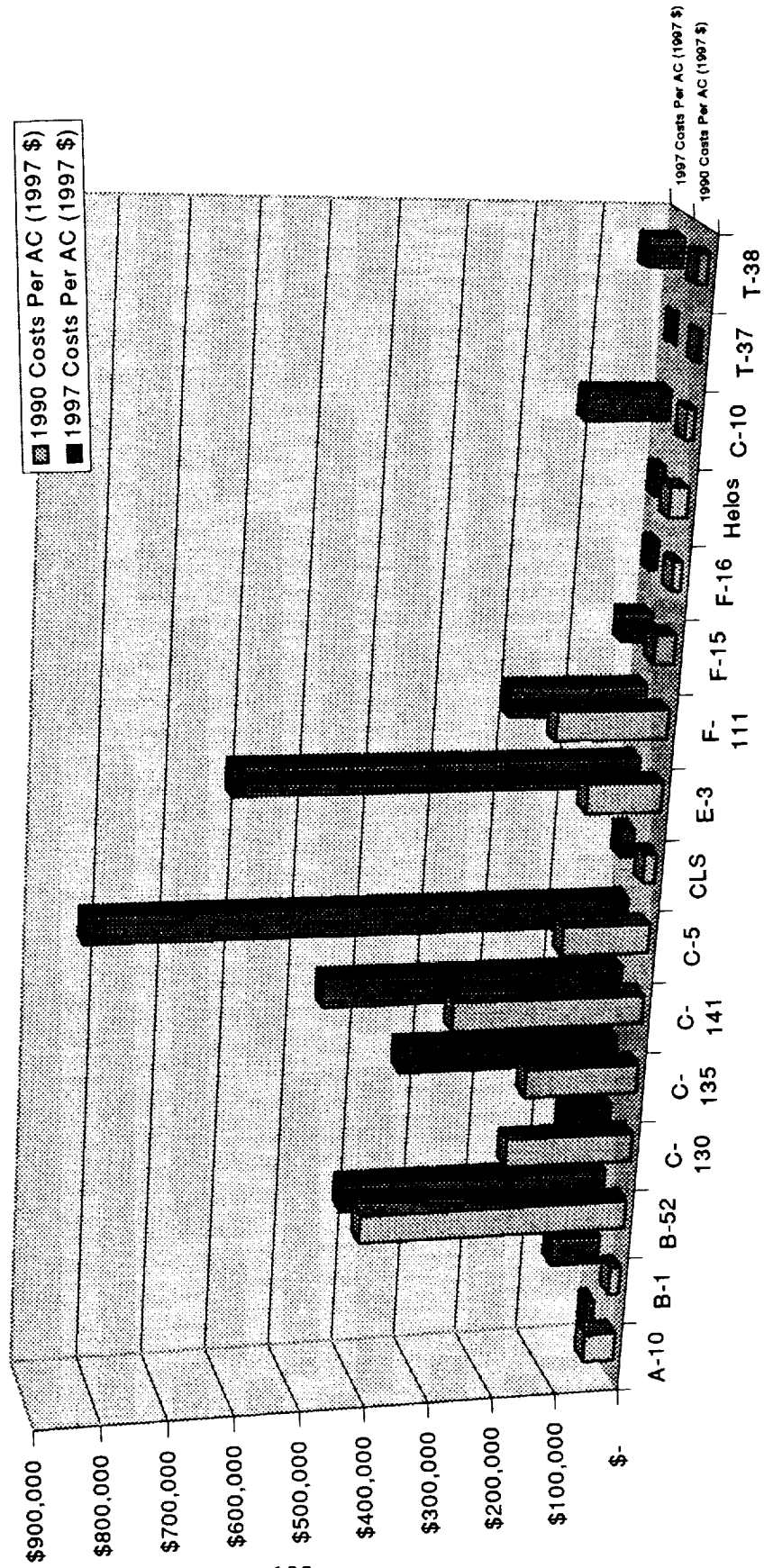
A/C Fleet Corrosion Maintenance Costs (1990 & 1997)



Fleet Corrosion Maintenance Cost Observations

- Three fleets (C-5, C-135, C-141) account for ~ 50% of all direct corrosion maintenance costs. (In 1990 study, five fleets)
- A-10 a success story; addressed serious corrosion problems plus basing less severe
- Significant B-52 decrease due to force reduction
- C-130 reduction deceiving due to wing mod completion
- C-141 increase due to Center Wing rework
- C-5 increase due to B model PDM start

Corrosion Maintenance Cost Per Aircraft (1990 & 1997)



Observations on Corrosion Maintenance Cost per A/C

- Force structure reduced by 28%, corrosion maintenance increased by 4% (1998 \$)
- F-16 decrease is illusory, reflects additions to force structure with constant depot costs
- B-1 and E-3 fleets started PDM, both have larger than average percentages of fleet going through PDM
- B-52 cost per A/C has remained constant despite retirement of G model
- F-111 PDM reduced dramatically due to projected phase out.
- T-38 Queen Bee flow remains unchanged despite reduction in force structure

Conclusions

- Direct corrosion maintenance costs remain a significant part of USAF maintenance expense
- Aging fleets consume most of the corrosion maintenance resources
- Force structure decreases have not resulted in commensurate reduction in corrosion maintenance workload

Corrosion Maintenance Philosophy

- Current Philosophy-Find and Fix
 - “If you find it, you must fix it”
 - All corrosion is equally “bad”
 - “Pay me now or pay me [more] later
 - Embedded in Engineering Practice, Technical Data, and Maintenance (Training, Processes, and Procedures)
- Proposed Philosophy-Anticipate & Manage
 - Identify, Assess, Act, and Document

Recommendations

- Re-examine corrosion maintenance philosophy and resultant practices with shift from “find and fix” to “anticipate and manage
- Develop tools and techniques that will facilitate tail number management and focused corrosion inspections

DEVELOPMENT OF NOVEL INSPECTION SYSTEMS—ANTICIPATING OPERATOR REQUIREMENTS

Christopher D. Smith

FAA William J. Hughes Technical Center, AAR-433
Atlantic City International Airport, NJ, 08405 USA
609 485-5221
609 485-4569
SmithC@admin.tc.faa.gov

ABSTRACT

The establishment of maintenance programs to support a fleet of transport aircraft is an extremely difficult task which often results in the application of inspection technologies and procedures that may seem primitive to the casual observer. A thorough review of the maintenance operation usually shows that the selection of inspection mode and technology is optimal or nearly optimal for the given organization at that time. This does not, however, mean that such operations will stay optimal or that technology solutions will stay adequate. The FAA's long-term investments in inspection research are selected based on anticipated changes in airline maintenance requirements. This paper will discuss four classes of inspection-related technologies being developed to address anticipated inspection needs. In particular it will discuss FAA- and government-sponsored initiatives in distributed damage assessment, large-area inspection, robotic inspection, and the application of emerging computational resources to aircraft inspection.

1. INTRODUCTION

Two years ago at an aging aircraft conference, Quincy Howard of Boeing Commercial Aircraft delivered a very well-received paper entitled "The Applicability of Wide-Area Inspection Techniques on Boeing Airplanes." The paper set out to answer the question "What existing inspection requirements for in-service airplanes could be performed with current and emerging wide area inspection systems?" The paper correctly concluded that there were few if any existing requirements which could be addressed by these systems.

The most fundamental problem with managing wide-area inspection system development, or any sophisticated inspection system development, is that directed inspection requirements arise abruptly and are often soon eliminated with a terminating action (structural repair or modification). Development of still immature technology for specific existing requirements is usually a futile exercise.

This does not, however, imply that system development for aviation applications is impossible or irrelevant. In fact, the aviation industry's extreme requirements for inspection system capability and reliability make it incumbent on the aviation industry (and government agencies) to be in the vanguard of inspection system research and development. To rise to this challenge the industry must *anticipate* requirements and advance technologies to a point where their near-term application is possible and practical. The FAA will not always be successful in picking technologies, but by using our collective

experience and common sense and employing sound judgment and trend analysis, we can maximize successful technology implementation.

1.1 A CLASSIFICATION OF RESEARCH AND DEVELOPMENT

Clearly a relatively safe and essential part of a research and development program is the adaptation and enhancement of relatively mature technologies currently popular in aircraft inspection. The FAA's development of pulsed eddy-current techniques and dual-probe ultrasonics are examples of this strategy. It is a safe bet that these inspection modalities will be around for the foreseeable future and that inspection requirements will arise requiring the application of these derivative technologies.

A slightly more risky approach is to develop advanced technologies which look and feel like current technologies but which have substantially greater capability, reliability, or applicability. Superconducting Quantum Interference Device (SQUID) eddy-current devices, laser ultrasonics, and self-focusing ultrasonics are examples of technologies in this category.

Technologies in both these categories could (if validated) be considered in the class "or equivalent" for many service bulletin applications. That is to say that they do not change the way we do business. Concepts such as calibration, signal-to-noise ratio, reproducibility, and thresholds need little or no modification for these techniques.

There are, however, other technologies which offer great technical promise but do not fit the current inspection paradigm. Some of these novel technologies will require new concepts for inspection specification, and some of these technologies will require (or promote) aircraft maintenance management changes. Inspection technologies producing image base results will require substantial effort on the part of inspection engineers to specify objective and reproducible flaw detect criteria. Information technology and robotic devices may allow operators to maintain their airplanes differently.

1.2 MANAGEMENT ISSUES FOR EFFECTIVE RESEARCH AND DEVELOPMENT

Though novel technologies are some of the most exciting technologies, they are also the most problematic to manage. Focusing on the technical possibilities may be personally satisfying for the technology enthusiast but will usually lead to impractical solutions to real problems or solutions to nonexistent problems. The management challenge is to identify application potential. Some of the things to consider in this regard are the following.

- An aging commercial fleet: Aircraft were designed to be inspected visually, and an imperfect design (all of which are) often results in specific directed inspections prior to retirement from service. The requirement for these directed inspections may be established at the aircraft's time of introduction to service but more likely are the result of service experience. As the aircraft ages, these inspections become increasingly more problematic: inaccessible areas, multiple failure modes, and unique structure all complicate the inspection. Many of these inspections will be even more difficult if the repeat interval forces operators to perform the inspections at other than a regularly scheduled heavy maintenance check.
- Widespread fatigue damage: Aircraft suffering from widespread fatigue damage (WFD) pose a substantial threat to safety, yet the identification of widespread fatigue damage is not at all straight forward. Damage at multiple sites in some local area may or may not be WFD. Though the precise risk of WFD to aircraft is the subject of continuing research, it is fairly clear that, for an equivalent level of risk, critical crack lengths are smaller for WFD than for discrete damage.

- Regulatory requirements: The Federal Regulations regarding the detectability and detection of damage on aircraft are rather precise and may not allow the timely application of an improved inspection. Inspection technology must be validated with respect to the prevailing damage tolerance philosophy for airframes and the safe-life philosophy for engine components.
- Organizational/operational constraints: Operators schedule inspection and maintenance to optimize safety, maximize utilization, and minimize *overall* maintenance/operational costs. Focusing on only the cost of the inspection misses the point.
- Technology plums: Every once in a while a technology comes along with features so appealing that we are compelled to make larger changes to accommodate that technology. It has been our experience that system developers have unrealistic expectations of this potential.

In the context of these issues, this paper will discuss FAA and other government initiatives in distributed damage assessment, large-area inspection, robotic inspection, and the application of emerging computational resources to aircraft inspection. This is not meant to be a complete survey of inspection R&D or even R&D in these areas. Instead it is meant to open a dialog on the potential aviation application of certain technologies on the cutting edge.

1.2.1 Rapid Imaging Inspection

Rapid imaging inspection may be the next substantial change in airplane inspection practice. Inexpensive computational power (for data processing and display) and increasingly long and complex inspection tasks may foster the near term implementation of such techniques.

As we approach the fundamental limit on the signal-to-noise ratio for a given technology, to improve inspection capability, we must either identify new technologies unconstrained by this limit or relax our requirements on the signal-to-noise ratio. By applying scanning technologies in conjunction with an existing technique, we can generate data which allows us to reliably detect flaws just above the noise floor. This is accomplished by supplementing signal-to-noise criteria with subjective and objective pattern recognition criteria.

While the ability to supplement signal-to-noise ratio with other criteria is a scanner's most appealing feature, it is also the source of one of the most major obstacles to implementation of the technology. Perhaps the greatest obstacle to implementation of these techniques is the adoption of criteria for establishing a precise and reproducible correspondence between the indication and a flaw. Exceedance of a threshold is a concept that can be extended to multivariate data, but not in a way which clearly correlates indication with flaw size. (This is somewhat akin to trying to establish a precise correspondence between penetrant indication size and actual flaw size.)

Examples of the FAA's interest in rapid imaging techniques include our activities in thermal wave imaging (figure 1) and magneto-optic imaging. Efforts previously supported by the FAA, some of which are now being supported by other government agencies, include shearography and D-sight. The DoD has several efforts in real time radiography which also fall into the category of rapid imaging technology.

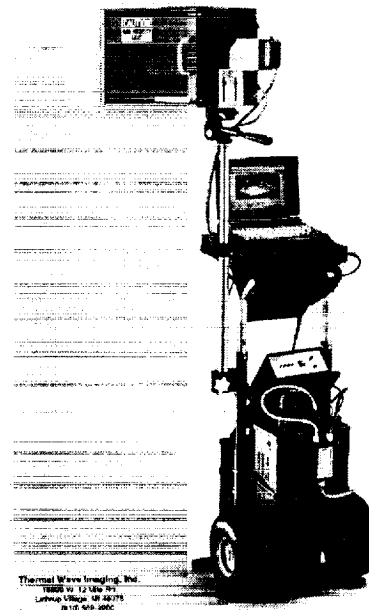


Figure 1. Modern Thermal Imaging System

Bridging the gap between rapid imaging and robots is a class of inspection devices called scanners. Many special purpose scanners are already used for in-service inspection (i.e., figure 2). These systems are still quite expensive, slow, and somewhat limited in their application potential. What they do offer is the sensitivity of point measurement systems with the imaging capability of the technologies mentioned above. Scanners will become even more popular as they become faster and more versatile.

Rapid imaging systems and scanners both have the additional virtue of enabling or enhancing surveillance inspection done in conjunction with a specified directed inspection. Examination of a lap joint for cracks with the Magneto-Optic Imaging (MOI), for example, could easily result in the incidental detection of pitting corrosion between rivets.

1.2.2 Robotics

Perhaps because they've captivated the imagination of the scientists and engineers, robots have been subject to an overzealous technology push and inflated claims of potential. More serious than this is the seeming ignorance of implementation considerations which will determine the success or failure of robots in aviation maintenance. Robots are not a universal replacement for people presently doing skilled or unskilled manual labor. Robots are useful in inspection situations where 1) the environment is too hostile for humans; 2) the accessibility is too restrictive for humans; 3) precise, repeatable probe alignment or positioning is required; or 4) the speed of the robot and length of the inspection make the robots application more cost effective.

Relative to the climatic conditions inside a volcano or on the surface of Mars, environmental conditions for aircraft are generally mild. In any case, it is not likely that an operator invests in a robot to spare personnel the risk and the inconvenience of aircraft inspection. One exception to this is the hazardous environment created by high energy radiation inspection. In fact the only fully programmable robots in common use for aircraft fuselage inspection are located at the McClellan AFB radiographic inspection facilities.

There are in fact inaccessible areas on aircraft (particularly engines) where robotic devices may be of value to a maintenance operation. Strangely, most robotic solutions to aircraft inspection requirements are more constrained than the existing human-based solution. Anyone who has observed a fuel tank inspection or seen the staging around an aircraft during a heavy maintenance check will attest to the difficulty of accessing the aircraft to perform the inspection.

Mel Siegel of Carnegie-Mellon University presented a paper at the 1997 Joint DoD/FAA/NASA Conference on Aging Aircraft which discusses at some length the history of and potential for robotic devices for aircraft application. That paper also presents a rationale for using robots for aircraft inspection which focuses on three concepts: thoroughness, correctness, and recordability. These concepts relate to the issue I identified as precise, repeatable probe alignment or positioning. Dr. Siegel's arguments are some of the most realistic I've heard, though I am still not convinced of his conclusions, including his prognosis for robots.

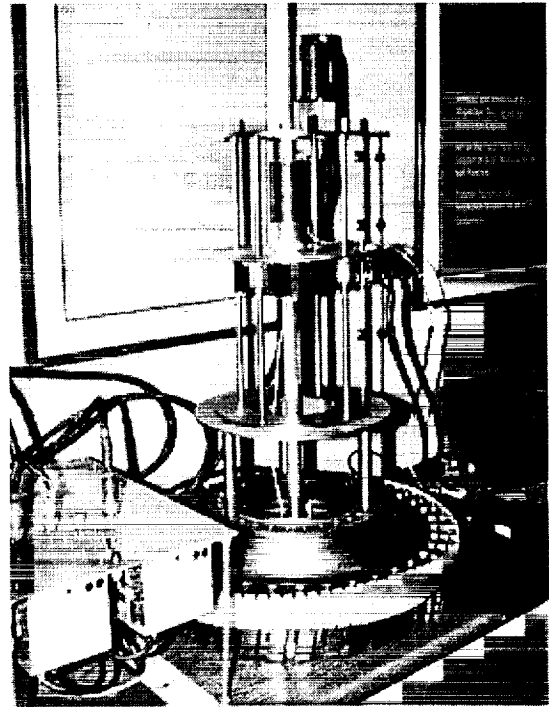


Figure 2. Engine Titanium Consortium Portable Scanner

It is interesting to consider that application of robotic devices to aircraft inspection may be delayed by technology advancements in other areas. In particular, rapid imaging technology may facilitate human-based inspection to a degree where robots are a clearly the inferior solution. In particular, rapid imaging technologies can alleviate the need for precise, repeatable probe alignment or positioning, while at the same time increasing the speed of the inspection.

A conservative and reasonable approach to robotic R&D is to identify near-, mid-, and long-term potential for robots and foster the long-term potential by following an evolutionary path which does not by-pass the near- and mid-term potential applications. Scanners should first evolve into smart scanners which can intelligently adapt scanning patterns in response to unexpected structural details (e.g., protruding rivets) and inspection results (e.g., intensification of scan at indications). Such scanners might be combined with emerging robot technology for aircraft painting and paint stripping to evolve into fixed-based robots and then finally may evolve into mobile robots.

For many years now, the FAA has chosen not to invest R&D funds in mobile robot development. From our recent assessment of the field, we have determined that this stance will probably not change in the near future. We feel that current efforts at NASA and in the DoD are more than a sufficient level of effort for this type of research. These efforts include:

- A 12 degree of freedom manipulator arm developed by NASA's Jet Propulsion Laboratory (JPL). This robot is being developed for space station borescope inspection, but the concept—a multisegment arm with universal joints—might be appropriate for aircraft inspection as well. The structure and control mechanism designs were established not for specific inspection requirements but rather for on demand inspection.
- A walking robot with suction cups developed by NASA's JPL. This robot was designed with Air Force support for a C-5 aircraft inspection. The robots are similar to—but smaller than—the FAA-sponsored Carnegie-Mellon Research Institute (CMRI) Automated NonDestructive Inspector (ANDI).
- A treaded robot. Both Boeing and NASA have sponsored the development of a treaded robot developed by Autocrawler, LLC. The robot is a fast moving platform that was designed to serve various needs in addition to inspection.
- A fixed-based robot. Several years ago Engineering Incorporated proposed a fixed based on tracks to inspect commercial aircraft. The concept is similar to that of a USAF-sponsored SAFARI robot. NASA and the USAF are now considering a similar proposal.

The FAA will, however, continue to fund research which is simpler automation (e.g., scanners). The FAA's present interests in this area include: an immersion quality on-aircraft ultrasonic inspection system (a.k.a. dripless bubbler) developed by the Center for Aviation Systems Reliability and a versatile portable scanner for on-wing inspection of engine disk bores and webs and bench top inspection of broach slots.

1.2.3 Distributed Damage Detection

Distributed damage detection is the detection of structural degradation by indirect means which indicate (but do not necessarily isolate or characterize) damage. An inspection device might, for instance, be sensitive to unusual structural deformation indicating altered load paths or elastic properties.

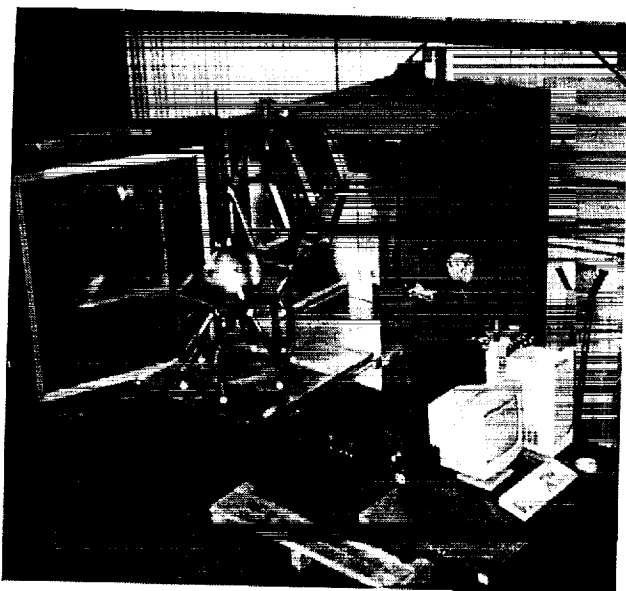


Figure 3. Halon Bottle AE Tester

Acoustic Emissions (AE) testing (figure 3) was perhaps the first technology to challenge our typical inspection paradigm. Though claims have been made regarding the ability of AE to locate and characterize cracks, their real virtue is probably their sensitivity to the *cumulative* presence of active cracks somewhere in a localized area of the structure. Eddy current is no more sensitive to isolated cracks than to a crack associated with widespread fatigue damage. AE (when it works) should be more sensitive to multiple cracks than individual cracks since crack growth is probabilistic in nature and does not necessarily produce the optimal signal for AE on each load cycle.

Other emerging techniques challenge our inspection paradigm in different ways. Residual stress measurements tell us something about the stress state of a component without telling us about the individual flaws which might exist in the component. Though our common sense and experience tells us that this information is useful, it is hard to see how it could fit into a damage tolerance philosophy of airworthiness which focuses on discrete flaws. Such techniques could be used to screen-out bad components, but cannot be used to verify the airworthiness of good components. The application of such technology to safe-life parts does not raise such concerns but most safety-critical, safe-life parts (e.g., engine disks) are lifed without consideration of the beneficial effects of residual stress.

One FAA-sponsored technology which may change inspection practice is nonrelative eddy current (for lack of a better name). Systems such as Jentek's Meandering Winding Magnetometer (MWM) probe may be able to identify conductivity changes in components which may in turn be indicative of a distressed state. Though such information would probably not alleviate the need for a more conventional inspection for discrete flaws, it could help inspectors determine whether a series of flaws is a series of isolated flaws or a condition indicative of widespread fatigue damage.

Because many of these techniques are not directly sensitive to discrete flaws, most present applications are noncritical. In fact, AE is used extensively in monitoring fatigue tests. MWM may find a similar application in monitoring coupon, component, and full-scale tests before it becomes a widely accepted in-service inspection tool.

1.3 APPLICATION OF EMERGING COMPUTATIONAL RESOURCES TO AIRCRAFT INSPECTION

Advanced computational tools are helping the aircraft inspection in at least three distinct ways:

- Advanced information systems: Information technology (IT) is allowing operators to collect, archive, and analyze data in ways which were impossible just a few years ago. The ability to access inspection data across time and fleets will allow an inspector to assess a condition more completely and with less effort than previously. If an inspector can quickly access the results of a previous inspection he might assess a condition as pre-existing and benign. If a maintenance manager can identify recurring flaw detections he can analyze the economic and safety impact and take additional remedial action.

- **Inspection System Enhancements:** This category includes any computational tool which improves the on-line performance of an inspection system. Data fusion, signal processing, and neural nets are some the tools presently being considered for this role. The emergence of imaging techniques will both enable and encourage the development of these computational add-ons.
- **Inspection Optimization Tools:** Inspection efficacy is the result of operator performance and inspection system design. Computational tools are now being used to maximize operator performance through computer-based training and optimize inspection design through physical modeling of the inspection system.

The FAA has sponsored efforts in all three areas. Efforts in the first area, advanced information systems, are not, however, sponsored by the FAA Inspection R&D Program. Inspection-related IT efforts include:

- Continued development of the Safety Performance Analysis System (SPAS) which incorporates risk analysis models and critical safety performance indicators.
- Development of an Aviation Safety Management System (ASMS) and analytical tool for identifying possible situations with adverse safety impact.
- Development of a monitoring process for aviation safety data quality improvement, Aviation Safety Attribute Mapping (ASAM).
- Development of a Maintenance Malfunction Information Report System, an Automated SDR system borrowed from the helicopter community.
- Development of a methodology for evaluating and assessing aircraft system maintenance.

FAA sponsored efforts to develop computational tools for inspection optimization include the following.

- Development of XRSIM, an x-ray simulator, for optimization of x-ray inspection parameters (figure 4). XRSIM has also demonstrated significant potential as a training tool.
- Development of a computational tool to facilitate dual probe ultrasonic inspection engineering. This is an extension of the dual-probe technology originally applied to the DC-9 T-Cap inspection.
- Finite element modeling of magneto-optic imaging to determine the ultimate potential of MOI inspection.
- Development of a comprehensive ultrasonic model for inspection. This effort grew out of Engine Titanium Consortium Phase I research on Titanium billet inspection. The objective Phase II work is to develop an ultrasonic model which incorporates sufficient system and material parameters and which has sufficient predictive capability to make the model a useful tool for inspection engineers.

Perhaps the greatest benefit of the application of advanced computational resources lies in the direct incorporation of computers in inspection equipment. Of course, the computer itself is worthless without validated algorithms incorporated in its software. The FAA has sponsored some dedicated tasks in the area of algorithm development, such as signal processing for eddy-current inspection, but most efforts have been incorporated in complete system development activities.

All FAA sponsored imaging technologies and many advanced point methods require advanced signal processing algorithms requiring enormous computational power. Self-focusing ultrasonics, for example, would be impossible without very substantial computational power.

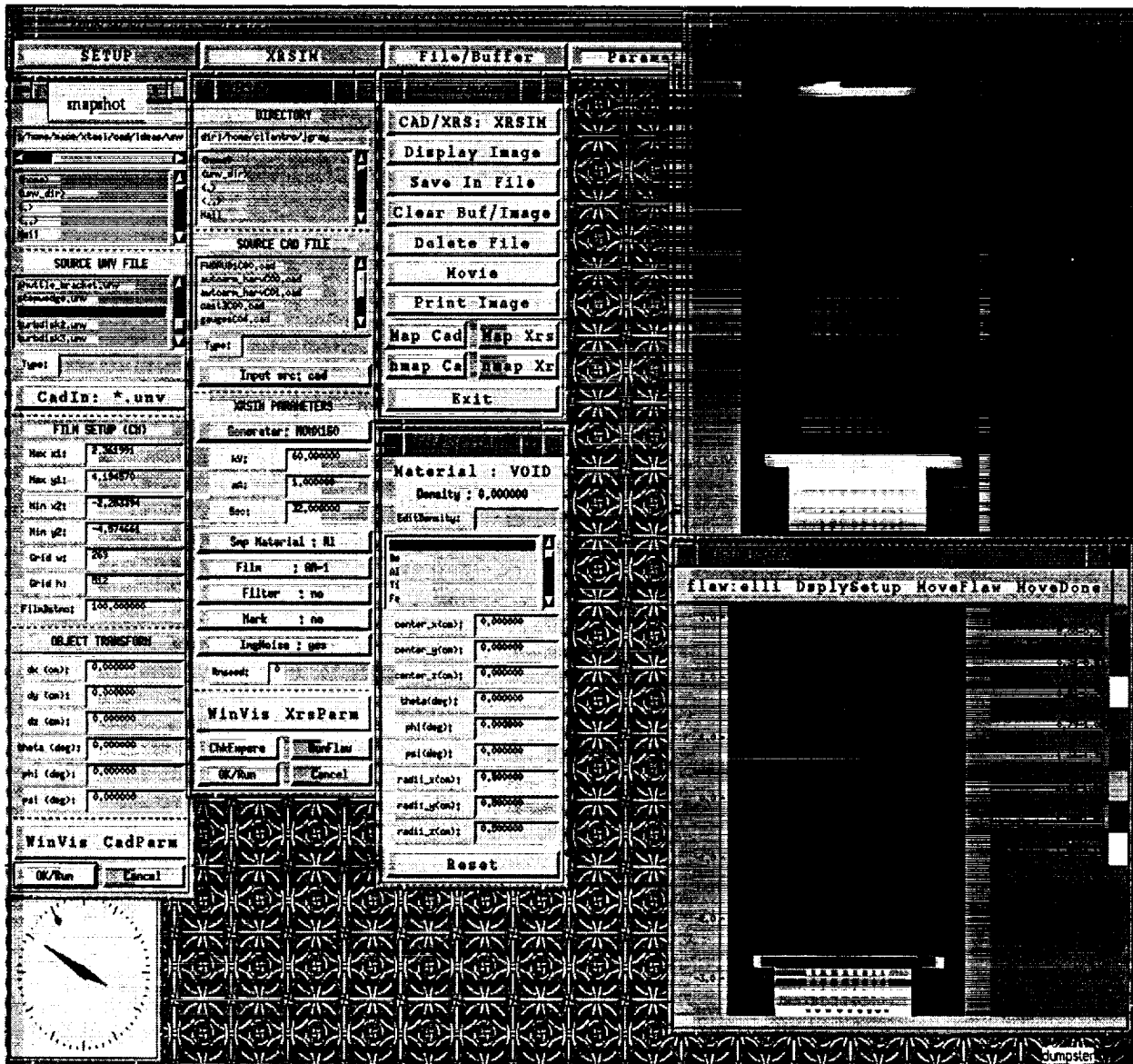


Figure 4. XRSIM x-ray simulator

Many of the enabling algorithms have already worked their way into prototype software, and some have even been incorporated in systems available commercially. CASR-NU's Additive-Subtractive Phase Modulated Shearography has been licensed by LTI for incorporation in their systems. CASR-NU also combined its dual-probe ultrasonic technology and dedicated ultrasonic algorithms with SAIC's proprietary hardware and software to enable an AD-compliant DC-9 T-Cap inspection system.

CONCLUSIONS

State of the art technology offers exciting promise but requires cautious well-focused development. The FAA's long-term investments in inspection research are selected based on anticipated changes in airline maintenance requirements. By frequent formal and informal contacts with the aircraft and engine manufacturers, aircraft operators, and system developers, the FAA intends to maximize its near- and mid-term return on investment.

EXPANSION OF THE WR-ALC FATIGUE-ARREST COMPOSITE REPAIR CAPABILITY

Steven F Adams
WR-ALC/TIEDD
420 2nd St Suite 100
Robins AFB GA 31098-1640

Warner Robins Air Logistics Center (WR-ALC) has been performing fatigue-arrest boron-epoxy repairs for over four years and has designed and installed almost 500 repairs of primary structure on various U.S. Air Force and Foreign Military Sales (FMS) aircraft. All of these repairs, however, have been designed to survive a similar environment of cyclic fatigue typical of primary wing or fuselage structure, and they have been almost exclusively boron-epoxy patches of similar stiffness ratio on aluminum alloy substrate. WR-ALC has a great deal of research data quantifying the design requirements and performance of this type of repair as well as the fleet-wide statistical base of the in-service C-141 repairs, but opportunities exist within the Air Force for fatigue arrest repairs for which the existing repair methodology or knowledge base may not be satisfactory. This paper will focus on three in-house engineering efforts that have been geared towards establishing the effectiveness of this type of bonded crack-arrest technology outside this existing repair envelope - areas where potential workload exists or where limitations of the existing repair methodology currently limit its applicability. These efforts are:

- A) Low-stiffness ratio repairs for thin structure or fatigue-critical areas,
- B) Non-aluminum substrate fatigue repair such as titanium, high-strength steel, etc., and
- C) High cycle fatigue applications, such as structure subjected to turbulent flow or acoustically-excited thin structure.

These efforts were intended to assess concept feasibility prior to a full-scale repair development and therefore are not exhaustive engineering studies, but rather cursory first looks attempting to identify a potential Achilles' heel prior to a full repair development effort being undertaken.

A. Low Stiffness Ratio Bonded Fatigue Repairs

1.0 ABSTRACT

Very low stiffness ratio repairs were designed and fatigue tested under constant amplitude loading. Fatigue arrest performance was predicted using finite element analysis (FEA) and closed form analytical methods. Very good agreement between predicted growth rates and testing was obtained.

2.0 WR-ALC BONDED CRACK ARREST HISTORY

All of the existing fatigue-arrest bonded composite repairs designed and installed by WR-ALC have repair to substrate stiffness ratios in the range of 1.1 to 1.5, with the target stress reduction under the repair being 50 to 55%. The overwhelming majority of these repairs are C-141 weep hole repairs, many of which have been in service for over four years. During that time, no bondline failures have occurred on any of the properly installed grit-blast/silane/primer repairs. C-141 weep hole repairs are still being designed and installed by WR-ALC as new cracks are detected during inspections. Very thorough finite element modeling to explicitly define adhesive shear and peel stresses and strains, patch stresses, load attraction and proximity stress effects has been performed on the existing repair configurations. Crack growth analysis using these FEA stress and strain results predict millions of flight hours for a typical existing crack to reach the unrepaired critical length, although none of the repairs are likely to see over 15,000 flight hours prior to aircraft retirement. This extremely conservative repair approach was adopted during the weep hole repair program for a number of reasons, the most compelling of which was the time constraint on the development and implementation of the repairs. In August of 1993, 45 C-141's were grounded and 116 more were prohibited from in-flight refueling until their weep hole cracks were repaired or removed. This action caused considerable scrutiny and subsequent wholesale shortening of the repair development and implementation timetable. With very little time available for design verification, the engineering decisions became very conservative. The patches were designed with stiffness ratios equivalent to conventional bolted repairs, and in fact even the crack growth predictions performed at the time by both Lockheed and WR-ALC/TIEDD assumed a repaired stress-intensity vs crack-length dependency similar to that of a bolted repair.¹ Configuration control essentially set these early designs in concrete, and so it remains to this day. Air Force repair guidelines are equally conservative, as they mandate that the adhesive remain within the elastic limit at Design Limit Load, even though excellent adhesive durability at strains well above yield has been repeatedly demonstrated.² In fact, current Air Force policy prohibits the use of a bonded repair on any crack which could become critical before the next two inspection intervals if it were left unrepaired.

2.1 Proximity Effects

As a result of the conservative design approach taken, the existing repairs are quite robust in durability and virtually impervious to fatigue damage, but the resulting large repair footprint and high stiffness ratio produce significant stress increases at the patch ends. In addition, repairs placed close enough together interact and intensify this stress increase. A pre-existing crack in one of these high stress areas would grow at a significantly accelerated rate, and extensive FEA was performed to quantify the magnitude and location of the high stress areas induced by weep hole repairs. Considerable effort was made to avoid placing an obvious initiation site in the high-stress window, and often the repairs had to be lengthened or even combined with other repairs to avoid such a condition due to the sheer number of fasteners and attaching structure. This has led to several repairs over 30 inches in length which produce stress kicks in excess of 60% being designed and put into service.

2.2 Thermal Stress

Thermal stresses in the aluminum substrate under the repair footprint increase with repair stiffness ratio as the boron stiffness becomes more and more dominant. In the case of the weep hole repairs, these thermal stresses are comparable in magnitude to the stress induced under the repair by limit flight load.

The aluminum substrate is subjected to considerable tensile stress just by exposure to cold, serving to increase the R-ratio of the fatigue loading, since flight loads add to the thermal loads in the aluminum. Since the limit stresses are very low compared to yield stress on the C-141 lower wing surface, the additional thermal stress was tolerable. In addition, the resulting crack growth rate increase caused by the higher effective R-ratio is completely overwhelmed by the ΔK reduction produced by the repair, so fatigue life remained far more than adequate.

The thermal loads do significantly affect bondline shear stresses, however, as shear stress in the adhesive at the patch ends is at a maximum at zero flight load when cold. Flight loads actually reduce the adhesive shear stress in this region as the boron, which is under compressive stress, is stretched back towards its stress-free length with loading. This is not the case at the crack site, however, as shear stress in the adhesive from flight loads add to thermally-induced shear, since both loads attempt to open the crack. Preliminary analysis predicted near plastic adhesive strains at the crack and caused great concern, but actual strain gauge data collected during repair cure cycles on C-141 lower wing skins revealed a lower expansion differential than predicted. This is due to the restraint effect of the unheated surrounding structure, which lowers the apparent coefficient of thermal expansion of the aluminum substrate by resisting expansion of the heated area. Our strain gauge data, however, which produced a measured effective CTE of over 7×10^{-6} in/in^oF, revealed significantly less restraint than is predicted by Rose's radial constraint model for the cure cycle³. In flight, the expansion restraint is removed as the entire aircraft is cooled at altitude, so in-service thermal stresses are still quite high, typically on the order of 10 ksi tension at -65^oF as shown in figure 1.

It has been postulated that adhesive creep at load may serve to remove a great deal of this thermal stress⁴, but one-sided fatigue coupons tested at WR-ALC showed little relaxation of curvature after significant load cycling. This cycling was accomplished typically 1 hz or less because the adhesive modulus stiffens appreciably and crack growth rate slows at higher rates, but perhaps this is still too fast to permit relaxation that could be seen in service.

RESIDUAL THERMAL STRESS C-141 WEEPHOLE REPAIR

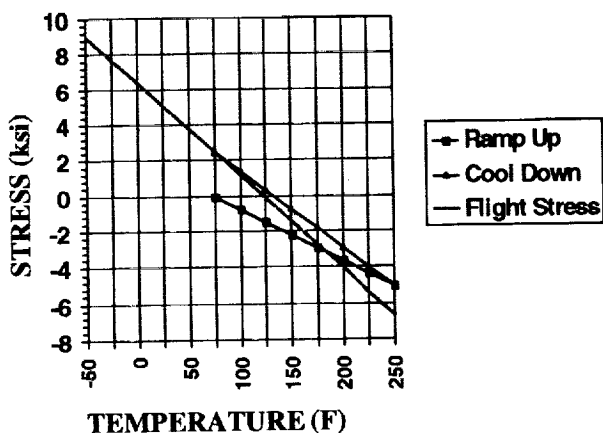


Figure 1.

3.0 THE PLAN

Given the apparent over-design from a crack growth standpoint, it was believed that in some cases, such as those situations where existing repair size was a problem or repairs near each other interacted, or existing structure created initiation sites which the existing repairs were too large to avoid, that significant improvement could be achieved through more closely matching the repair stiffness requirement to the life-extension goals from a crack propagation standpoint. Since this would constitute a deviation from the conservative design precedent established, a more thorough, ground-up understanding of how cracks grow under bonded repairs and how design parameters actually affect crack retardation was needed for accurate life predictions to be made.

4.0 CRACK PROPAGATION AND ARREST

For a typical structure which has service loads high enough for crack initiation, crack propagation as a function of time can be represented by a curve whose slope increases with the square root of crack length. The rate of crack growth is primarily a function of crack tip stress intensity or crack opening displacement and therefore crack length and applied stress. The static strength of a structure decreases with crack growth, and critical crack length is reached when the residual strength becomes insufficient to carry the highest service load, or locally, when crack tip stress intensity at limit load exceeds the fracture toughness of the material. A repair of a cracked structure must address these two problems: reduction of crack growth rate to an acceptable level, and the restoration of required static strength.

5.0 PREDICTING CRACK GROWTH RATE

Several closed-form solutions exist for calculating the repaired stress-intensity factor K_r for a semi-infinite cracked plate with a bonded repair, the most well-known being presented by Rose.⁵ This solution or some form of it is commonly used in modern patch design computer programs to determine the repaired stress intensity factor, and the concept is rather straightforward.

5.1 Repaired Stress and Joint Stiffness Analysis

Typically, the stress reduction is first calculated under the repair assuming there is no crack present. An adhesive shear transfer length is then calculated based on cracked substrate stiffness, repair stiffness, adhesive shear modulus and thickness. For a typical adhesive with a shear modulus of around 1×10^5 psi, this length is quite short and varies with substrate stiffness and bondline thickness. It is rather impervious to repair stiffness ratio, though the repaired stress intensity, which is a function of both the joint flexibility and the stress reduction under the repair, is directly affected by stiffness ratio. Through-thickness shear stiffness of the substrate and repair are generally ignored, but shear lag in the boron and the aluminum substrate, both of which are much stiffer in shear than the adhesive, can nonetheless accumulate for thick repairs and affect joint stiffness.⁶ Explicit 3-D FEA modeling should be performed to validate the closed form prediction, especially for thick or reinforced structure.

5.2 Determination of Repaired Stress Intensity

Once the repair stress reduction and adhesive properties are determined, the crack is then introduced into the analysis, and using the repaired substrate stress under the patch, an upper bound for the repaired stress intensity, K_∞ , is calculated. Since it is highly dependent on the adhesive transfer length as well as applied stress, the big drivers for K_∞ are adhesive stiffness (shear modulus and thickness), and substrate thickness, which affect shear transfer, and patch stiffness ratio, which affects the applied stress at the crack. K_∞ is derived through an energy balance, using the displacement of the crack face due to joint stiffness as crack face stresses are relaxed to zero. The assumption is made that the crack tip is far enough away that it provides no opening restraint, meaning that the stress intensity calculated represents K_∞ . This value is not valid for short cracks, however, where significant restraint is provided by the crack tip and the displacement energy from the crack face opening is small. In the limit, the displacement energy of the joint goes to zero as crack length goes to zero, and the stress intensity then approaches the classical $K_0 = \sigma \sqrt{\pi a}$. This represents the initial value and slope for K . An interpolated value for K_r , which satisfies these boundary conditions, as shown in figure 3, is typically created.

Interpolated Stress Intensity

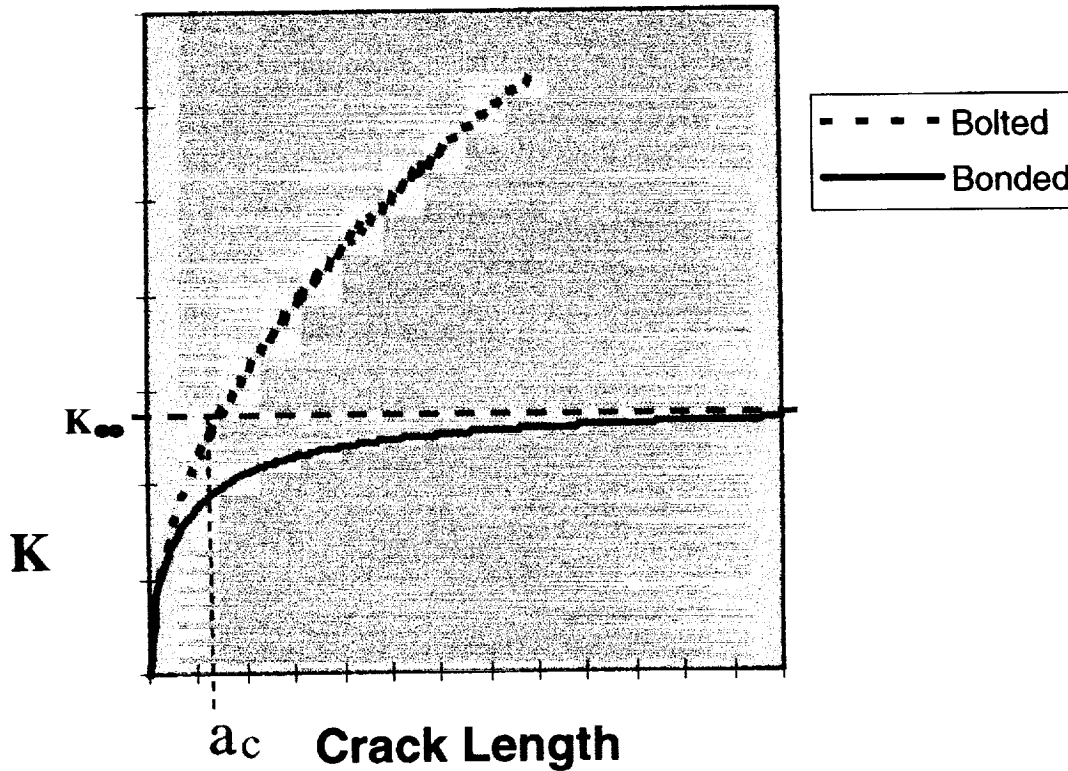


Figure 3.

The characteristic crack length for the bonded repair, a_c , which is essentially the crack length which would produce K_{∞} at the repaired stress level, can be derived from the repair properties alone and is independent of applied stress or actual crack length in theory. In actuality, if the adhesive goes plastic, then the shape of the shear distribution vs length in the vicinity of the crack changes, and an elastic-plastic adhesive shear model must be used to accurately predict K_r . Since a_c is typically very short, β -factors to account for finite width or other geometric effects approach their initial value. In the case of a center-cracked panel, $\beta \rightarrow 1$.

6.0 REPAIR DESIGN

With the tools currently available for predicting bonded repair crack growth rates and an understanding of how the repair parameters affect crack growth rates under the repair, it should be possible to accurately design a repair to meet a target fatigue life with reasonable accuracy. Towards that end, fatigue test coupons were designed and tested to compare actual with experimental crack growth rates. Five two inch wide by 0.050 inch

4.1 Bolted Repairs

Traditional bolted fatigue repairs impede crack growth by reducing the apparent far-field stress applied, and the crack growth rate is primarily a function of the repair to substrate stiffness ratio. In the somewhat linear range for $\log (da/dn)$ vs $\log (\Delta K)$ for most aluminums, crack growth rate is roughly proportional to the third power of ΔK , as shown in figure 2, meaning that a 50 percent reduction in ΔK would typically slow crack growth rate roughly one order of magnitude. Reducing stresses in the repair area by significantly more than 50 percent is difficult with a bolted repair, as stress concentrations at the fasteners become life-limiting. In general, the design of bolted repair is bound by the existing crack growth rate on one side and initiation and growth of new cracks at attachment points on the other side. A ten-fold increase in fatigue life over the remaining unrepaired life is often a very short life extension when compared to remaining service life. Additional life extension maneuvers such as stop-drilling and cold-working are often employed where possible for this reason.

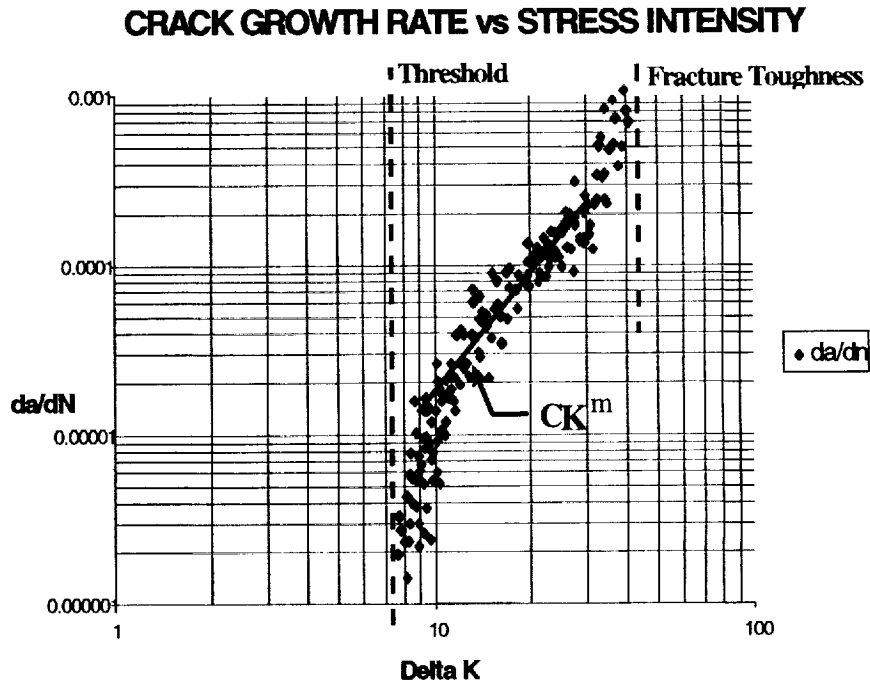


Figure 2.

4.2 Bonded Repairs

Bonded fatigue arrest repairs have long been considered superior to bolted repairs in theory, but environmental durability problems with on-site bonding procedures generally prohibited their use. This all changed with the introduction of grit-blast/silane/prime surface preparations to the aerospace industry. Since that time, they have been used quite extensively by the USAF, and their crack arrest performance, which typically produces several orders of magnitude life extension over the unrepaired remaining life, far exceeds any type of bolted repair capability. Crack tip stress intensities are reduced so much that in many cases the pre-existing plastic zone at the crack, produced by typical in-service loads, retards further crack growth for the remainder of the aircraft service life. The tremendous fatigue arrest improvement bonded repairs provide cannot be attributed to the elimination of attachment hole stresses or improved stress reduction in the substrate. The mechanism by which bonded repairs reduce crack tip stress intensity is much more effective than bolted repairs, especially for relatively long cracks, as the crack growth rate under a bonded repair does not significantly increase with crack length. Contrary to the predictions of early crack growth analysis techniques for bonded repairs, stress reduction under the repair, which is the mechanism for crack retardation in bolted repairs, is generally not the greatest contributor to life extension in bonded repairs. The crack opening restraint provided by bondline continuity, which physically requires strain compatibility between the repair and the substrate, overwhelms the stress reduction contribution to crack growth rate in all but the very shortest cracks. This restraint serves to redistribute the stress field in the substrate in the immediate vicinity of the crack through adhesive shear. More simply put, in order for the crack to open, the adhesive which attaches the repair to the cracked substrate must deform in shear. The reduction in ΔK is usually so great for bonded repairs that the $\log(da/dN)$ vs $\log(\Delta K)$ relationship, whose slope changes from a 3rd power relationship to essentially asymptotic near the fatigue threshold, produces much slower growth rates than a linear log-log dependency would suggest. For very short cracks, the crack opening displacement is small, so the adhesive shear deformation, and therefore the opening restraint, is small. Very little crack retardation over that provided by apparent far-field stress reduction is produced. For this reason, bonded repairs are about as effective as bolted repairs for very short cracks. As the crack lengthens, the crack opening displacement becomes larger, meaning that more adhesive shear stress is produced and more crack retardation occurs. Crack growth stabilizes when the crack length is long enough to allow complete load transfer through adhesive shear from the center of the crack. The change shear stress in the adhesive as one moves from the crack tip towards the crack center then increases to some maximum value and becomes constant to the center of the crack. Further crack growth does not produce further crack opening; the length of the constant adhesive shear stress zone along the crack merely lengthens. Stress intensity at the crack tip does not increase with crack length from this point on, producing constant crack growth, until the crack emerges from under the repair, where crack growth once again accelerates with length as the crack tip moves away from the adhesive restraint.

thick, one-ply, two-sided repair coupons, as shown in figure 4, were manufactured for fatigue testing. Two were cycled at 30 ksi, one at 25 ksi, one at 20 ksi, and one at 10 ksi.

Fatigue Test Coupon Configuration

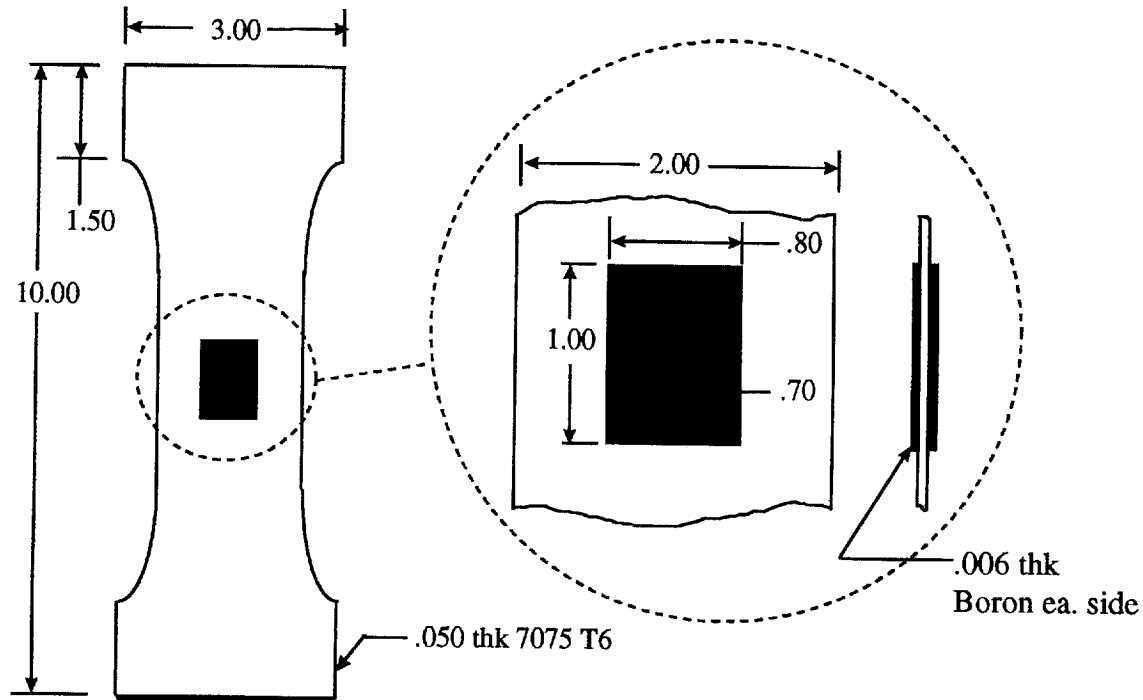


Figure 4.

6.1 Coupon Substrate Design

The substrate chosen was 0.050 inch thick 7075 T6. Explicit da/dn vs ΔK data was generated for this sheet of aluminum through constant amplitude loading of EDM-notched three inch wide fatigue specimens to provide a reliable baseline and to try to eliminate some of the inaccuracy associated generalized material data. Residual strength testing was then performed on these cracked coupons to determine fracture toughness. The residual strength curve for a three inch wide coupon is shown in figure 5. A hypothetical limit stress of 30 ksi was chosen, and the coupons were then pre-cracked to 0.7 inch from a center EDM notch, critical length at 30 ksi for our two inch coupon width.

Residual Strength Curve (7075 T6, 3inch width)

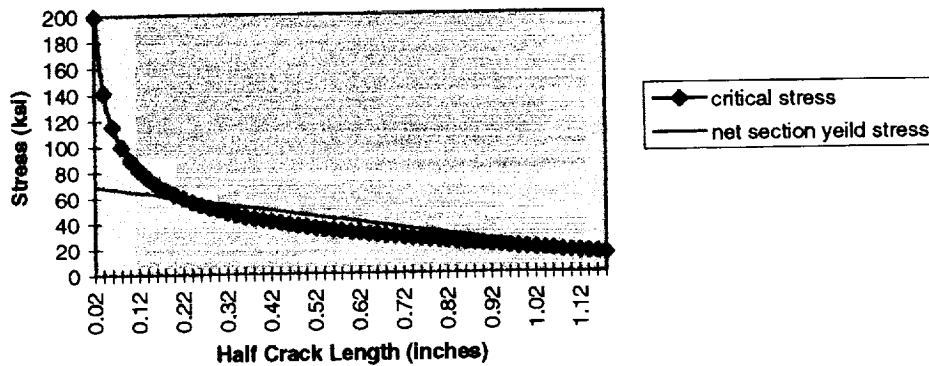


Figure 5.

6.2 Patch Design

The patch was designed for minimum strength of 45 ksi far-field stress, or 1.5 times limit load. This produced a patch thickness 0.010, or two plies. By contrast, a standard boron repair of typical stiffness ratio for this substrate would be five plies thick. One ply 0.80 inch wide by 1.00 inch long was placed on either side of the crack to eliminate bending stresses. At 45 ksi far-field, FEA predicted the boron tensile stress, which is maximum at the crack center, to be 208 ksi.

6.3 Residual Strength Testing

Repaired residual strength testing produced initial fiber breakage at 48.20 ksi minimum, with catastrophic failure at 53.80 ksi average for four coupons. The failure mode was not one discreet failure as expected, as boron fibers at the crack center began to fail about 5 ksi before maximum load was reached. This allowed the crack to progressively open, thereby dumping load back into the substrate. As the applied load increased, more and more fibers began to fail and fast fracture of the crack finally occurred after perhaps 25% of the fibers had failed. Thermographic inspection detected no adhesive failures in any of the failed specimens. Failure scatter for four coupons was within 4%.

6.4 Adhesive Stress Analysis

Nonlinear 3-D FEA was used to determine adhesive shear stresses and strains as well as stress reduction under the repair. For a two-sided repair, the shear transfer area is doubled and the effective thickness of the substrate is also cut in half, meaning that peak adhesive stresses and strains are dramatically reduced at the crack for a given load. In fact, plastic adhesive strain did not occur in the FEA model short of about 38 ksi external load, and reliable bondline durability in excess of 50 ksi, which exceeded the boron strength, was predicted from a shear strain standpoint. No shear failures occurred during repaired residual strength testing.

7.0 FATIGUE LIFE VERIFICATION

Since the coupons were all pre-cracked to 0.7 inch prior to repair and the patch width was 0.80, crack growth of only 0.050 inch was required to reach the patch edge. Pre-cracking the five fatigue specimens prior to repair had to be performed at very low stress levels to ensure the crack tip plastic zone would be small enough that it did not retard growth after the repair.⁷ This meant keeping K_{max} below $9 \text{ ksi}\sqrt{\text{in}}$ for the 30 ksi specimens and $6 \text{ ksi}\sqrt{\text{in}}$ for the 20 ksi specimens. Two coupons were cycled at 30 ksi, R-ratio $\cong 0$, until the crack could be detected. The crack growth rate was calculated and compared to the da/dn -vs- ΔK curve generated for this material at the predicted repaired ΔK value. This procedure was repeated for one coupon each at 25 ksi and 20 ksi. These results were plotted on a log (da/dN) vs log(ΔK) scale, shown in figure 6, along with the 7075 T6 fatigue test data previously collected. In addition, one repaired coupon was cyclically tested at 10 ksi, R-ratio $\cong 0$ for 250,000 cycles, with no growth detected. The repaired ΔK value at this applied stress level was calculated to be about $3 \text{ ksi}\sqrt{\text{in}}$, well below the apparent threshold for crack growth.

Correlation of Predicted Stress Intensity to Fatigue Test Data

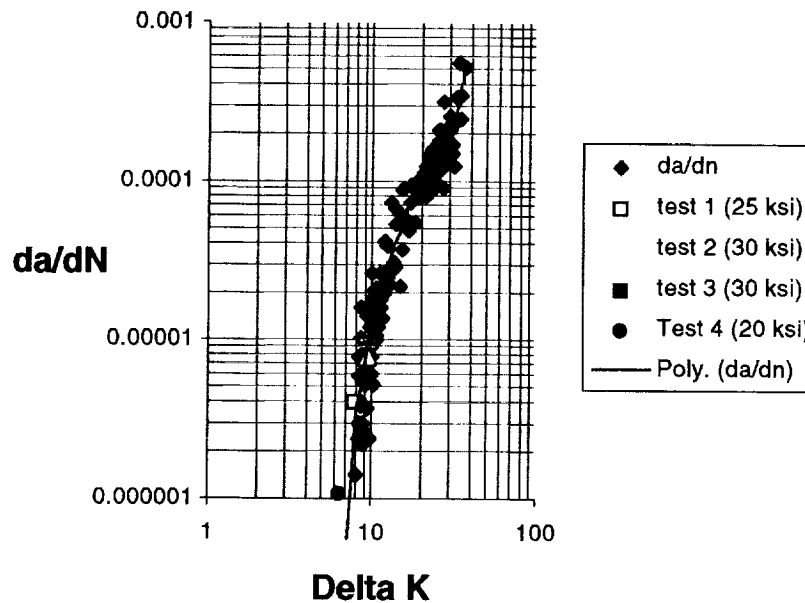


Figure 6.

8.0 RESULTS AND CONCLUSIONS

The predicted crack growth rates compared extremely well with the crack growth data generated for the bare coupon substrate material, meaning that the combination of FEA and closed form joint analysis produced accurate values for the repaired stress intensity. It is clear from these results that crack growth rates for bonded repairs can be effectively

tailored through patch design and accurate life predictions made using simple closed-form analysis techniques. While these results are based on constant amplitude loading of fatigue specimens, it should be rather straightforward to accurately predict damage accumulation from spectrum loading as well, since determining the stress intensity under the repair is the key in either case. Complex geometry and changing material thickness complicate matters as the repaired stress level and characteristic crack length are no longer constants, but FEA modeling can explicitly determine substrate stress levels under the patch, and summation of predicted crack growth rate in steps small enough to accurately map the predicted gradient should yield accurate results, since redistribution of the stress field, which is rather drastic in the vicinity of the crack for bolted repairs, is prevented by the bondline. For external reference stress approaches, the difficult task of accurately calculating beta factors as a function of position and crack length, which tends to make traditional life predictions for such structure a black art⁸, becomes relatively unimportant for a bonded repair since, in general $\beta \rightarrow 1$ for cracks as short as typical effective bonded crack lengths. This simplification becomes less accurate as the characteristic crack length increases. For thick structure and an energy compliance method which accounts for shear deformation of the substrate and repair should probably be used. Lowering stiffness ratio to meet some life extension goal with minimal proximity stress effects produces higher adhesive shear stresses at the crack, however, because the stress level under the patch which must be sheared into and out of the repair at the crack is proportional to stiffness ratio. This is not a problem at the patch ends, as tapering lowers the shear stresses through compliance. This is not possible at the crack, however, where adhesive stresses are highest. If limit stress must be carried without exceeding the elastic adhesive shear limit at the crack, the stiffness of the repair may be driven by this requirement, especially for thicker repairs or highly-loaded structure, and very little reduction in stiffness ratio may be acceptable. Adhesive durability testing has repeatedly demonstrated this elastic requirement to be extremely conservative, as significant plastic deformation can occur without cumulative damage. If the joint is simply designed to withstand ultimate strength without failure and the adhesive is permitted to yield at limit stress, even the stiffness ratio of one-sided, relatively thick structure repairs can be safely reduced. The use of a lower stiffness adhesive or thicker bond line can be used to reduce the adhesive stress at the crack to counteract the effects of stiffness ratio reduction, but a flexible joint increases the repaired characteristic crack length, and faster crack propagation ensues. On the other hand, for thin or lightly loaded structure, a stiffer adhesive could be used even with a minimum strength patch without exceeding adhesive properties. The ability to reliably design composite repairs for a given fatigue life extension goal will hopefully find useful application soon in those areas where repair size, external stress increases, or residual thermal stresses are considered problematic and must be kept to a minimum.

B. Non-Aluminum Substrate Bonded Fatigue Arrest Repairs

1.0 ABSTRACT

Boron-Epoxy repairs were installed on 0.100 inch thick 8Mn titanium fatigue test coupons using the grit-blast/silane/prime surface preparation technique. Excellent bondline durability was demonstrated at extremely high strain values. All coupons failed in the grips and no bondline degradation or crack extension was detected.

2.0 BACKGROUND

The purpose of this test program was to attempt to expand the application of bonded composite fatigue enhancement repairs to non-aluminum structures and systems. An extensive knowledge base has been accumulated for the application of such repairs on aluminum through design and testing work performed for the C-141 weep-hole program in the areas of bondline durability and crack retardation performance, but the applicability to other substrate materials is questionable due to differences in strength, fracture toughness, working stress, modulus, and surface preparation. It was decided for the purpose of this test to use an annealed titanium substrate material, since its combination of high strength and relatively low modulus, coupled with a very high fracture toughness, demands a patch and bondline performance which lies well outside the envelope of conventional aluminum repairs. In addition, an existing annealed titanium fatigue failure problem currently exists in a U.S. Air Force weapons system. Very high fracture toughness and low yield strength tend to make for relatively long critical crack lengths, and bonded repairs are much more effective at reducing the stress intensity for longer cracks. While limit stress for aluminum in a fatigue sensitive application rarely exceeds 30 KSI, 60 KSI is not uncommon for an equivalent titanium structure, and in fact very near yield stress may be seen in a typical fighter fatigue spectrum.

3.0 FATIGUE COUPON DESIGN

The testing procedure involves designing and installing a boron-epoxy repair for a test coupon which has been pre-cracked to three inches. The design parameters were that the structure should carry 120 ksi without static failure, and it should withstand fatigue loading at 60 ksi, R-ratio zero, without adhesive failure. The coupons were made of 0.100" thick, 10 inch wide and 24 inch long annealed TI-8MN as shown in figure 7.

3.1 Test Assumptions

The coupon and crack geometry was driven by several factors, most notable of which was the extremely high fracture toughness of alpha-beta annealed titanium.. It was decided that far-field stress would be around 60 ksi, thereby producing twice the stress level and 1.5 times the strain seen in a typical aluminum repair. This limited the coupon width to not more than 10 inches, since the grips in our fatigue tester were only capable of producing 60,000 pounds tension. It was also decided to cyclically test the first repaired specimens at or near critical load for the cracked section, meaning that the residual life of the panel prior to repair at this load level would be essentially zero.

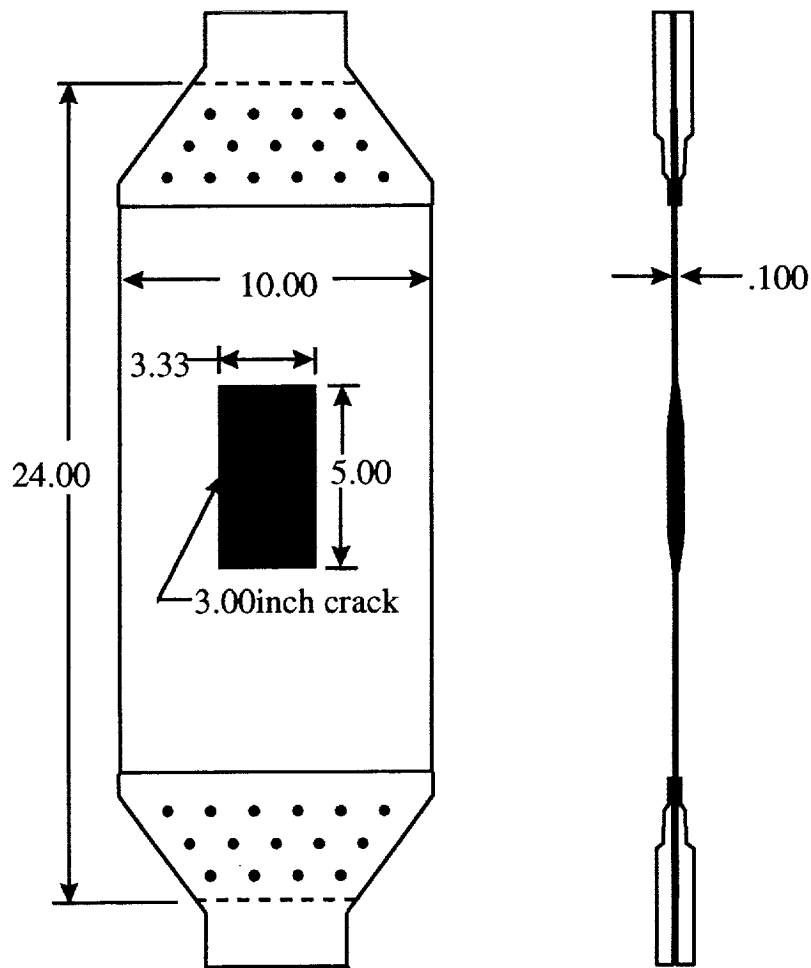


Figure 7.

3.2 Substrate Design

In order to obtain an actual fracture toughness value for our specific mill run of 0.100 thick TI-8MN sheet, four 10 inch wide coupons were pre-cracked from a center notch to a crack length of 3" and then pulled to failure on a tension tester. Existing fracture toughness data interpolated between 0.250 and 0.050 thickness (longitudinal, rolled sheet data) predicted a fracture toughness, K_{Ic} between 140 and 160 $KSI\sqrt{IN}$, but our 4 pre-cracked coupons failed at an average of 72,690 psi far field stress (± 2200 psi), giving a fracture toughness of 167 $KSI\sqrt{IN}$. It should be noted that due to the extremely high fracture toughness in relation to yield strength that slow stable tearing occurred prior to fast fracture and had to be corrected for. In order to actually obtain fast fracture instead of net section yielding at 60 ksi, panel width had to be a minimum of nine inches. It is recommended that the critical stress should not exceed 80% of yield stress for a given crack geometry for accurate residual strength testing, meaning that a 10 inch wide

specimen was required. This same fracture testing difficulty arises in 2024 T3 as well and is due to the extremely high fracture toughness in relation to material yield point⁹. In order to obtain a low enough residual strength to place critical panel load near 60 ksi for a 10 inch wide coupon, a crack-length on the order of 3 inches was required. The residual strength curve for a 10 inch wide coupon is given in figure 8.

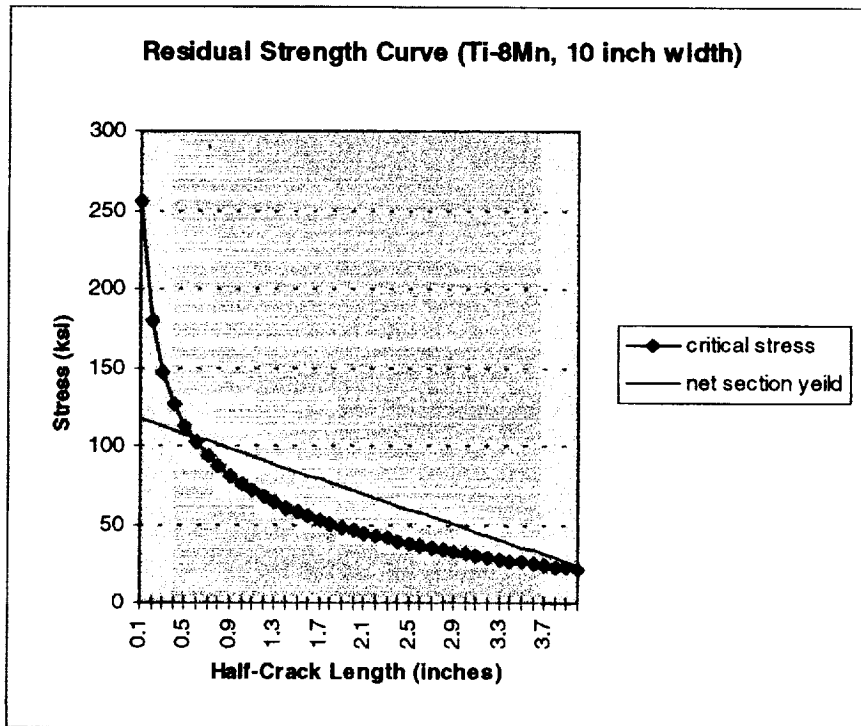


Figure 8.

It was observed from previous FEA modeling that convergence on infinite plate load attraction gradients began to occur at about 3:1 patch to coupon width ratios, so the width constraint limited our boron patch width to around 3.33 inches. In order to allow reduced strain under the patch without causing an artificial stress spike from the stiff coupon grips, coupon length was set at 24 inches. This provided enough distance from the patch end to the grip (which essentially produces a constant displacement across the coupon width) for shear lag to redistribute strains around the stiffened patch area, producing a stress field similar to an infinite-length panel.

3.3 Patch Design

In order to produce a patch capable of transferring loads up to yield stress of 130 ksi from a 0.100 inch thick substrate, 14 plies were required. This was achieved by bonding 7 plies of unidirectional boron to each side of the coupon, producing about a 50% reduction in stress intensity under the patch in an infinite panel. In order to eliminate bending displacements, a two sided symmetrical Boron patch was used. This tensile strength-driven design produced a stiffness ratio of 1.2 to 1. The higher this stiffness ratio, the more severe the proximity effects for a given geometry. The tradeoff is that a higher

stiffness ratio patch reduces the severity of the adhesive stress kick at the crack face. The magnitude of this adhesive stress is a function of the substrate stiffness (i.e., the modulus and thickness) as well as the magnitude of the stress under the patch. The adhesive plastic zone at the crack face is a critical design factor, since adhesive failure there removes the crack-closure restraint and can increase crack-growth rate by an order of magnitude or more depending on crack length, even if the remainder of the repair is intact. Proximity stresses and adhesive shear limitations in the crack region serve to bound the acceptable stiffness ratio of a given repair.

A taper ratio which varied linearly from 100:1 at the patch end to 25:1 at three plies and then remained constant was used in order to provide bondline damage tolerance should peel failures start to occur in the first ply or in the corners. Standard Baker criterion transfer length was used, producing a 5.0 inch long patch. A patch width of 3.33 inches was used to maintain a 3:1 width ratio. This left less than 0.20 inch from the crack tip to the patch edge on each side, meaning if the repair life was crack-growth limited, the adhesive durability would not be explicitly determined, and the test would need modification. This represents a worst-case loading spectrum for both the patch and bondline, however, as essentially the entire patch footprint is severed. For this reason it was felt that bondline durability would be the weak link for this repair and not crack growth.

4.0 CRACK GROWTH PREDICTION

In order to accurately predict crack growth under the repair, it would be necessary to determine the stress reduction under the repair for the coupon geometry using FEA and then determine the repaired stress intensity. This prediction would then be validated by measuring repaired fatigue growth and comparing it to the unrepaired growth rate at the same ΔK . A 3-D FEA model was made of the repair configuration in order to more accurately determine the stress reduction under the repair for crack growth analysis. In addition, analysis of the adhesive shear stresses and strains, especially in the vicinity of the crack, was obtained. This required the use of a nonlinear adhesive stress-strain curve as adhesive deformations were well into the plastic range at the crack. Ignoring the crack-opening constraint of the bonded repair and taking into account only the stress-reduction at the crack predicted due to patch stiffness (similar to a bolted doubler fatigue analysis), a crack-growth life of less than 8,000 cycles to reach critical crack length for 32 ksi (the predicted stress level under the bonded repair at 60 ksi applied) is predicted. This very short life is a result of the very high delta K values associated with a 3 inch crack. This type of analysis is obviously very conservative, however, if the repair is fully bonded in the area of the crack, since crack opening is restricted by the bonded repair, and therefore the dependency on crack length to tip stress is removed¹⁰. The Rose model, which takes into account this crack-opening restraint, predicts around 80,000 cycles just for the crack to grow 0.166 inch to the repair edge and become externally detectable, but assumes that no delamination around the crack occurs. Since FEA of the repaired panel predicted plastic adhesive deformation in the crack region at 60 ksi., it was felt that adhesive shear failure in the vicinity of the crack would eliminate the crack-closure retardation mechanism, and growth rates approaching the bolted repair rate would soon occur.

5.0 STATIC AND DURABILITY TESTING

Prior to manufacture and testing of the pre-cracked panels, bondline durability testing and static strength testing for the grit-blast/silane/prime surface prep was performed. Two three inch wide coupons and two coupons two inches wide, each manufactured from 0.100 thick Ti-8Mn sheet were completely severed and then patched together using full width, five inch long, seven-ply boron patches bonded to each side. The two inch wide coupons were then loaded to static failure. As expected, no bondline failures occurred and all coupons failed by fiber fracture after significant yielding had occurred in the titanium substrate. Average failure load was 28,200 pounds for the two coupons; minimum was 27,020 pounds. This corresponds to 201 ksi in the boron and 141 ksi in the titanium. The four remaining three inch specimens were then cyclicly loaded from zero to 60 ksi at 2 hz. Thermography inspection was performed every 10,000 cycles. None of these specimens exhibited any bondline degradation, and all failed from fatigue outside the repair between 200,000 and 300,000 cycles.

6.0 Results

Based on the successful bondline durability testing, the pre-cracked fatigue specimens were manufactured and tested at 1 hz at 0 to 60 ksi. The first two coupons failed in the grip area with a total accumulation of about 40,000 cycles each. Through thermographic inspection of the repair every 10,000 cycles, no degradation of the bondline was observed. A redesign of the grips resulted in the remaining two coupons surviving about 80,000 and 120,000 cycles respectively before fatigue failure occurred, once again in the grip area. No bondline failure was detected. No measurable crack growth occurred on any of the specimens, even though the repaired stress intensity was about $16 \text{ ksi} \sqrt{\text{in}}$, which should have produced around 1×10^{-6} inches per cycle crack extension based on material fatigue testing, give or take about half an order of magnitude. This lack of crack extension can only be attributed to retardation from the pre-cracking of the specimens prior to repair. A closer look at coupon manufacturing revealed that retardation was in fact the culprit. Although the peak stress applied was only 15 ksi during pre-cracking, this corresponded to a stress intensity of over $34 \text{ ksi} \sqrt{\text{in}}$ at the final crack length of 3.00 inches, which is more than double the repaired stress intensity at 60 ksi. While correlation between measured and predicted crack growth rates for the repair could not be obtained due to retardation, excellent bondline durability for a grit-blast/silane/prime surface preparation on a titanium substrate was demonstrated.

C. Durability Testing of the Grit-Blast/Silane/Prime Surface Preparation in a High-cycle Fatigue Environment

1.0 ABSTRACT

Three aluminum panels with boron-composite reinforcements bonded to them were subjected to high vibration forces on a one-axis electromagnetic vibration shaker table. No deterioration of the adhesive bond or the patches occurred, and eventually fatigue failures of the aluminum substrate limited the test duration on the first two coupons. The stress concentrations around the hard mount points which caused the fatigue cracks on the first two coupons were eliminated on the third coupon, and it was tested for 100 hours and over 32 million cycles, with no bondline failures or patch degradation.

2.0 BACKGROUND

A number of high-cycle fatigue applications for fatigue enhancement bonded composite repairs are being pursued by private contractors for application on various U.S. Air Force or DoD weapon systems. In some cases, no durability testing was performed prior to implementation of those repairs and some of these efforts are now plagued with bondline durability problems. WR-ALC decided to determine the robustness of the existing grit-blast/silane/prime bonded composite repair process in such a high-cycle fatigue environment. This was done in a preemptive maneuver in order to answer the question of survivability of our process under vibration before it was asked or required for a repair effort.

3.0 TEST SET-UP AND PROCEDURES

Three boron composite patches were bonded to 12 x 16 x 0.190 inch thick 6061 T3 aluminum panels, using the standard grit-blast/silane/prime surface preparation common to all WR-ALC-installed weep-hole repairs. The boron patches were centered on the aluminum panel and were 4.5 inches wide by 10 inches long and consisted of 16 plies of pre-cured unidirectional boron epoxy bonded with one layer of AF163 adhesive. This produced a repair-to-substrate stiffness ratio of 1.25:1. The three coupons were labeled S/N 001, 002 and 003 for tracking purposes. The test was performed on a horizontal axis shaker table, and each panel was to be excited at or around the first modal resonance until some failure was detected through periodic thermographic bondline inspection. All three coupons were inspected for disbonds prior to testing.

The panels were mounted to the horizontally flat shaker table and feedback and control was accomplished through the mounting of two accelerometers: a drive accelerometer on the shaker table and a monitoring accelerometer on the panel at a point of maximum displacement during excitation. From the G-forces and frequency data provided by this

accelerometer, displacements, and therefore strains and stresses, could be computed. To select a test frequency, a low G-level sinusoidal sweep from 5 to 2000 Hz was performed to locate the natural frequencies for a given mounting configuration. The lowest natural frequency was used initially on each panel, as this produces maximum deflection and therefore maximum stress and strain. The shaker controller was programmed to sweep from just below to just above the natural frequency in order to detect resonant shift caused by compliance increase induced by bondline failure or material fatigue failure. Sweep time was arbitrarily set at one minute.

4.0 TEST RESULTS

The test results on each panel will be discussed separately in the sequence they were performed.

4.1 Panel S/N 002:

This panel was initially mounted to the shaker table with eight bolts and spacers, with four bolts on either end of the panel aligned in a line perpendicular to the long axis of the coupon as shown in figure 9.

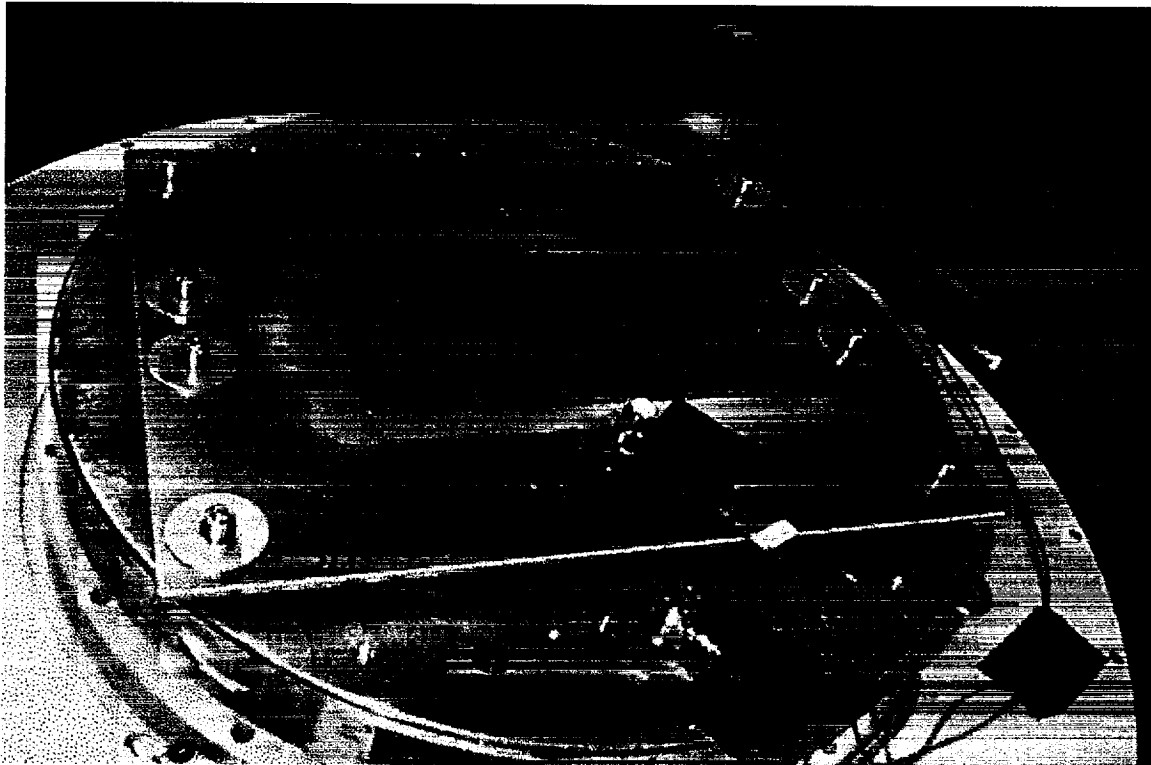


Figure 9.

This was done in order to ensure first-mode freedom, though the bolts themselves clearly produced a partial rotational constraint due to their bending stiffness. It was hoped that this would not be significant, and to prevent fatigue failure of the bolts they were replaced every eight hours. The first resonant frequency occurred at 214 Hz, so the one minute sweep was set from 205 to 220 Hz and testing initiated. With a 2.5 G drive table forcing function, the monitoring accelerometer read 330 Gs. This equates to a peak-to-peak deflection of 0.150 inch, and given the coupon geometry, a peak alternating stress in the aluminum substrate under the patch of about 10 ksi. After 12 hours of run time at this setting, or 9.25 million cycles, the first mode natural frequency began to shift downward. Since no visual problems with the mounting points could be seen, it was assumed that bondline failure was reducing the flexural stiffness of the panel. No failure could be detected through thermographic inspection, however, so testing resumed. The natural frequency continued to drift downward, and the drive table frequency was adjusted as required during the test to bracket the resonance with the programmed sweep. After 17 total hours, or 12.8 million cycles, the natural frequency had fallen to 180 Hz and was dropping rapidly. Thermographic inspection turned up no bondline failure, so the plate was removed and inspected. Cracks were found at all of the mounting point holes, two of which had propagated over two inches. Four new mounting holes were drilled two inches inboard of the initial mount points at each corner, and testing resumed at an equivalent 330 G level, though the natural frequency was now 300 Hz due to the shortening of the span between mounting points.

After about 2 hours, or 2 million cycles, the natural frequency again began to shift downward. Since no disbond could be detected, mounting hole cracking was suspected. It was theorized that the high rotational deflection caused by first-mode displacement was causing the cracking of the mounting holes. The drive table was then run at 1414-1430 Hz for 8 hours, or 41 million cycles, at a monitoring accelerometer reading of 300 Gs. Cracking around all of the mounting points was again detected, but no bondline failure was produced. The drive table frequency was then reduced to 250 Hz and tested for five hours, or 4.5 million cycles before the existing cracks approached link-up. After some 60 million cycles at over 300 Gs, no bondline failure could be detected. As a last-ditch effort to fail the bondline, the mounting configuration was changed to a center constraint, leaving the ends of the test coupon free to deflect as shown in figure 10.

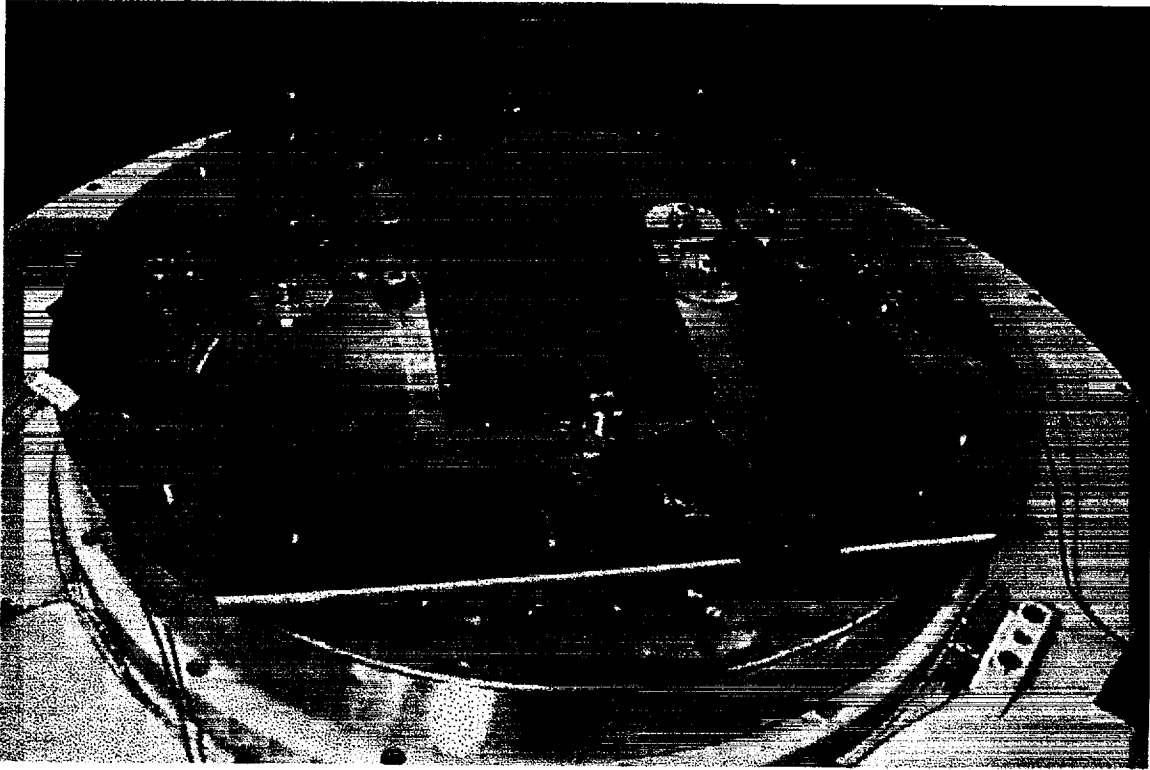


Figure 10.

The panel was then shaken at 125 Hz at over 400 Gs, or a deflection of 0.420 inches. This produced a stress in the base aluminum under the patch of over 20 ksi. Ten hours of run time in this configuration, or 4.5 million cycles, produced panel failure in the form of a fatigue crack that ran completely under the patch from each mounting point. Thermographic inspection revealed no bondline failure more than 0.25 inch from the crack path. Total accumulated run time was 43 hours.

4.2 Panel S/N 001:

This panel configuration was identical to the first test article and was mounted to the shaker table in the same configuration as the last run of panel S/N 002. The panel was shaken at 125 Hz and 300 Gs for 1.5 hours, or 600,000 cycles, before a crack from one of the mounting holes propagated under the patch and caused the test to be halted. Rapid crack initiation indicated a substantial initial flaw or stress concentration at the mounting hole.

4.3 Panel S/N 003:

The final panel was physically identical to the previous two panels, but in an effort to eliminate the mounting point failures which affected the first two panels, a holding fixture was constructed to eliminate the bending loads at the mount point. The ends of this panel were free to rotate along the short panel axis but were constrained from translation. The configuration is shown in figure 11.

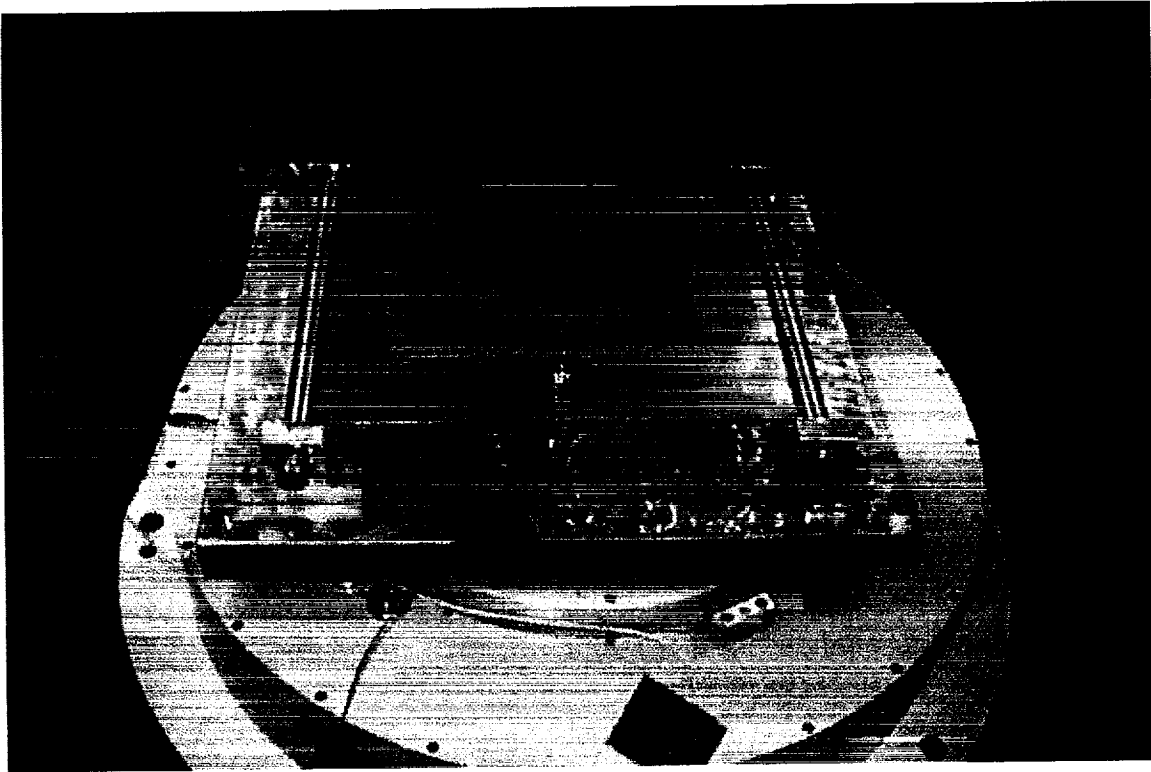


Figure 11.

This configuration was driven at its first resonant frequency of 90 Hz at 56 Gs, or 0.125 inch peak-to-peak deflection. This deflection produced an alternating stress in the aluminum under the patch of about 6 ksi. This load level and configuration was run for 100 hours, or 32 million cycles without bondline or patch degradation. No base material failures were induced on this test. Testing was suspended at 100 hours.

5.0 SUMMARY

All three composite patches survived extremely rigorous vibration testing without failure. The testing indicates that the existing repair methodology is extremely durable under vibratory excitation, and the fatigue endurance of the aluminum substrate should be the life-limiting factor in a typical repair in such an environment.

References:

1. D.R. Lee and D.C. Register, *Damage Tolerance Analysis of C-141 Weep Hole Cracks with Boron Composite Repairs*, WR-ALC/TIEDD Report DTA94-C141-009 (1994).
2. R.W. Hertzberg and J.A. Manson, *Fatigue of Engineering Plastics*, Academic Press, (1980).
3. L.R.F. Rose, *Theoretical Analysis of Crack Patching*, in: *Bonded Repair of Aircraft Structures*, A.A. Baker and R. Jones (Editors), 90-92 (1988).
4. J.G. Williams, *Stress Analysis of Polymers*, Longmans, London, 225-243 (1973).
5. L.R.F. Rose, *Theoretical Analysis of Crack Patching*, in: *Bonded Repair of Aircraft Structures*, A.A. Baker and R. Jones (Editors), 77-106 (1988).
6. A.A. Baker, *Crack Patching: Experimental Studies, Practical Applications* in: *Bonded Repair of Aircraft Structures*, A.A. Baker and R. Jones (Editors), 138-142 (1988).
7. P.C. Paris, *The Growth of Fatigue Cracks Due to Variations in Load*, Ph.D. Thesis, Lehigh University (1962).
8. D.J. Cartwright, *Methods of determining Stress intensity Factors*, RAE TR73031 (1973).
9. C.E. Feddersen et al, *An Experimental and Theoretical Investigation of Plane Stress Fracture of 2024 T351 Aluminum Alloy*, Battelle Mem. Inst. Rep. (1970).
10. L.R.F. Rose, *Theoretical Analysis of Crack Patching*, in: *Bonded Repair of Aircraft Structures*, A.A. Baker and R. Jones (Editors), 77-79 (1988).

LASER-BASED ULTRASONICS FOR CRACK DETECTION

Pavel Fomitchov, Alexei Kromine, Sridhar Krishnaswamy and Jan D. Achenbach
Center for Quality Engineering and Failure Prevention
Northwestern University
Evanston, IL 60208, USA
Telephone - 847-491-5527
Fax - 847-491-5227
e-mail - achenbach@nwu.edu

ABSTRACT

Laser-based ultrasonic (LBU) techniques provide a number of advantages over conventional ultrasonic methods such as higher spatial resolution, non-contact generation and detection of ultrasonic waves, and ability to operate on curved and rough surfaces. In this paper we present a new laser based technique -- the Scanning Laser Source (SLS) technique -- for the detection of small surface-breaking cracks on rough and curved surfaces. This technique allows detection of flaws by monitoring the variations of ultrasonic amplitude and frequency (flaw signature) as the laser ultrasonic source is scanned across the object and passes over any defects. Typical flaw signatures for different kinds of surface breaking defects are obtained. The results of application of the SLS technique to detection of cracks in attachment slots of a turbine disk are presented.

1. INTRODUCTION

Laser generation of ultrasound and the detection of the ultrasonic waves using laser interferometry are areas of active research¹. In earlier papers, the present authors have described fiberized tunable laser ultrasonic sources^{2,3}, and fiber optic heterodyne and Sagnac interferometers for detection of ultrasound^{4,5}.

Conventional ultrasonic flaw detection methodologies require the generation of an ultrasonic wave packet that travels through a structure, and the subsequent detection of reflections of this wave packet from any existing flaws within the structure. Laser-based ultrasonics has thus far followed the same methodology expect that the generation and detection of the ultrasonic wave packets were done using lasers. The limitations on the size of flaws that can be detected using this approach are set by the ultrasonic reflectivity of the flaws for the particular wavelength used, and by the sensitivity of the particular ultrasonic detector used. In view of their expected small reflectivity, the reflected wave packets from very small flaws are often too weak to be detected with existing laser detectors, which typically have significantly lower sensitivity than conventional piezo-electric transducers (PZT).

Scanning Laser Source (SLS) Approach

We now propose an alternate approach for ultrasonic detection of surface-breaking small cracks using laser-based techniques. In this approach, the ultrasound generation source, which is a point or line-focused high-power laser beam, is swept across the test specimen surface and passes over any existing surface-breaking flaws (Figure 1).

The generated surface ultrasonic wave packet is detected at a fixed location on the test specimen. It is found that the amplitude and frequency of the measured ultrasonic signal have specific variations

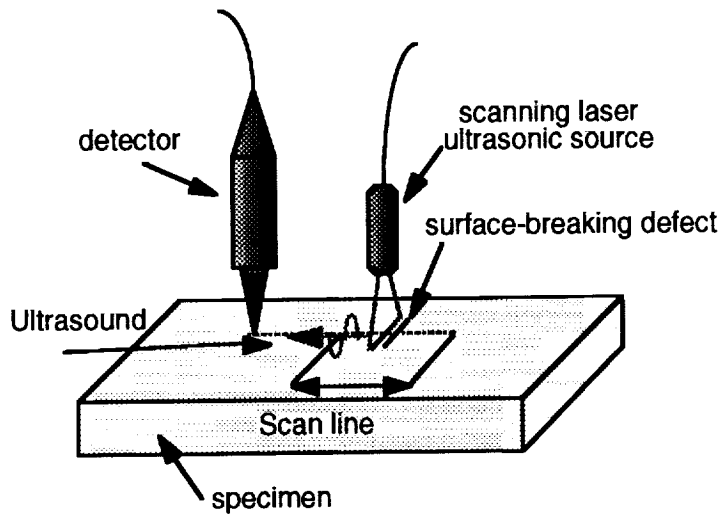


Figure 1. Principle of the Scanning Laser Source method with laser detection.

when the laser source approaches and passes over the defect. Proof of concept experiments have been carried out for flat specimens with EDM notches of various sizes, and an actual engine disk, all of which were provided by Allied Signal Engines.

Flaw Signature - Variation of Ultrasonic Amplitude

A typical characteristic signature for a surface-breaking notch of 0.2 mm depth on a flat specimen is shown in Figure 2. The following aspects of this signature should be noted:

(1) When the source is far ahead of the defect, the generated ultrasonic *direct* signal is of sufficient amplitude above the noise floor to be unambiguously picked up by the laser detector (Figure 3a). Also, a weak reflection from the flaw is barely visible amidst the noise.

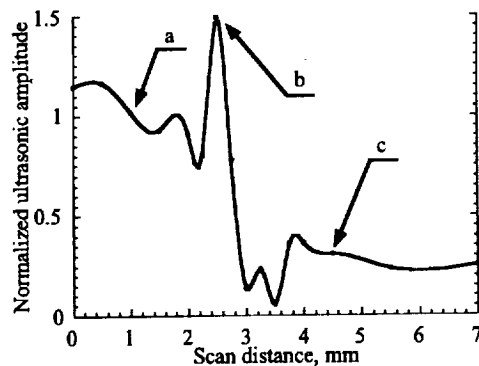


Figure 2. Typical characteristic signature of ultrasonic amplitude vs. SLS location as the source is scanned over a defect: (a) far ahead, (b) close to, and (c) behind the defect.

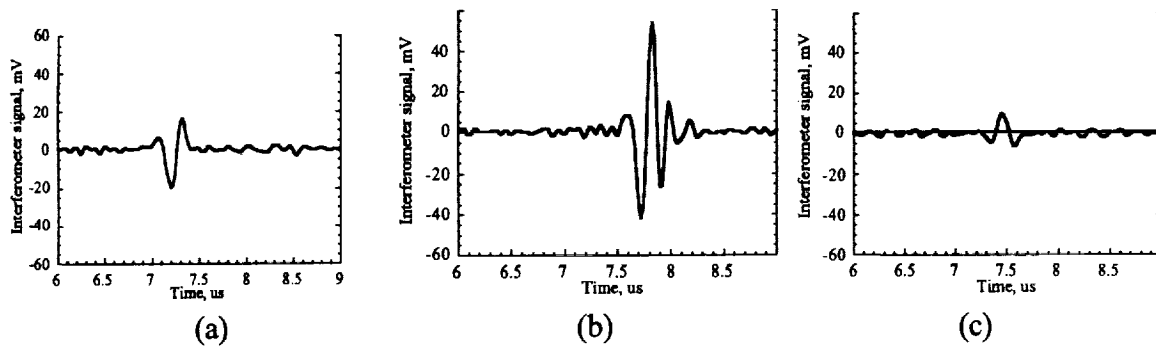


Figure 3. Representative ultrasonic signals detected by the Sagnac interferometer at a fixed location when the laser source is: (a) far ahead, (b) close to, and (c) behind the defect.

(2) As the source approaches the defect, the amplitude of the direct signal significantly increases (Figure 3b). This increase (from a level that was already sufficiently above the noise floor) is more readily detectable with a laser interferometer than any weak echoes from the flaw. We attribute this increase in signal amplitude not only to possible interference of the incident wave with the wave reflected by the defect (as the source is very close to the defect), but possibly more importantly to the changes in the conditions of generation when the laser source is in the vicinity of the defect.

(3) As the source passes over the defect, the ultrasonic signal amplitude drops noticeably again presumably due to changes in the conditions of generation when the source is right above the defect. Subsequently, as the source moves behind the defect, the amplitude increases again to some level that is compatible with the transitivity of the flaw (Figure 3c). Note that when the flaw depth is smaller than the wavelength of the generated ultrasound, a significant portion of the sound can pass by the flaw when the source is behind it.

These data were obtained for an aluminum specimen with an EDM notch (length 4 mm, width 0.3 mm, and depth 0.2 mm). The Scanning Laser Source used in this experiment had the following parameters: line length 4 mm, width 0.3 mm, thermoelastic generation at 4 mJ per pulse. A narrow-band Sagnac interferometer was used as the ultrasonic detector.

Flaw Signature - Variation of Ultrasonic Spectrum

Next, the spectral content of the generated ultrasonic signal was monitored as the SLS was scanned over a defect. The presence of the defect introduces a detectable frequency shift in SLS generated ultrasonic signals. This effect was observed using a broad-band heterodyne interferometer [6] for ultrasonic detection. The spectra of the SLS signals obtained during a scan over a 0.2 mm surface-breaking notch on a titanium specimen are shown in Figure 4. In the absence of a defect the SLS signal consists of relatively low frequency components with center frequency about 2 MHz (Figure 4a). As the SLS approaches the flaw (to within 0.3 mm) new spectral components in a 3-8 MHz frequency range appear in the detected signal (Figure 4b). This was the region where we observed maximum amplitude of the broadband signal, as described above. The high frequency components of the detected signal are still present when the SLS is almost above the defect (Figure 4c). The high-frequency components disappear from the spectrum of the detected signal when the SLS is behind the defect, and this is attributable to the fact that high frequency waves are mostly reflected away by the small flaw.

We attribute the changes in frequency content of the ultrasonic signal to the changes in the conditions of generation when the laser source is in the vicinity of the defect. To verify this, we reversed the positions of the laser ultrasonic source and the detector. The laser source was fixed at a distance of 20 mm from the defect, while a heterodyne interferometer probe was scanned across the

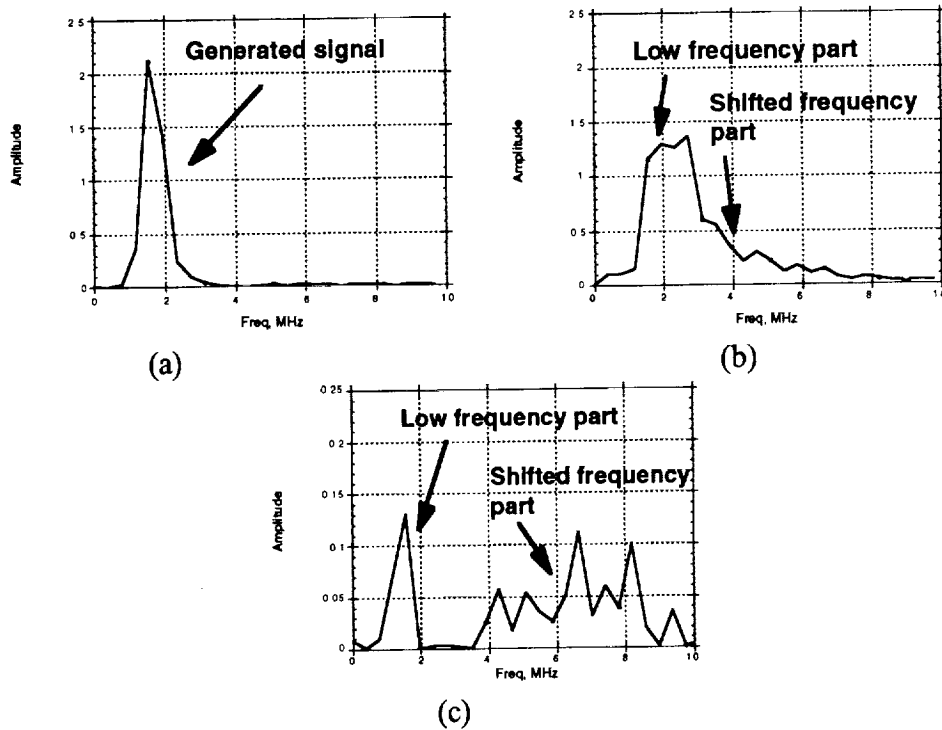


Figure 4. Spectrum of SLS signals: (a) far away from the defect, (b) as SLS approaches the defect, and (c) when SLS is virtually over the defect.

flaw area. In this case, as the laser detector approached the flaw an increase in the ultrasonic signal amplitude was observed due to interference between the incident and reflected signals. However, the spectrum of the signal was unchanged as expected. As before, any generated high frequency components were filtered out by the flaw and were not observed when the detector was behind the flaw.

Main Advantages of SLS Approach

All the advantages of laser based ultrasonics including non-contact and curved surface inspection apply to the SLS approach as well. Of particular importance are:

- (a) **Ease of Scanning:** The proposed method for detecting small surface-breaking flaws requires the scanning of a very narrow ultrasonic source over a surface and over any existing flaws. Conventional ultrasonic sources such as pzt-transducers, EMATs and capacitive transducers are not small enough or do not lend themselves to easy scanning. Only laser ultrasound generation sources are small enough for this method, and being non-contact, they can be easily scanned across a test surface of complex geometry.
- (b) **Coupling Independence:** The detection of the generated ultrasound is done at a fixed location and can be monitored using either a laser interferometer or a conventional pzt-transducer. The laser interferometer provides non-contact absolute measurements, and a pzt-detector provides higher sensitivity, and therefore this choice must be determined by the application. In either case, since the detection is at a fixed location, variabilities associated with pzt-coupling or laser speckles (for interferometric detection) are eliminated.
- (c) **Signal-to-noise improvement:** The SLS approach provides enhanced signal-to-noise performance compared to conventional pitch-catch mode of operation. This is because the presence of a flaw

is indicated by an *increase* in the amplitude of the detected ultrasonic signal rather than by the presence of a weak echo.

Application of SLS to Turbine Disk Inspection

The SLS approach was applied to the detection of fatigue cracks in the fan disk blade attachment slots of titanium engine disks. Cracking usually occurs very close to the slot to face transition, with some cracks actually breaking the transition region (see Figure 5a). The current inspection technique is a manual eddy current method. Our experiments show that laser ultrasonic inspection, performed using the conventional pitch-catch mode,

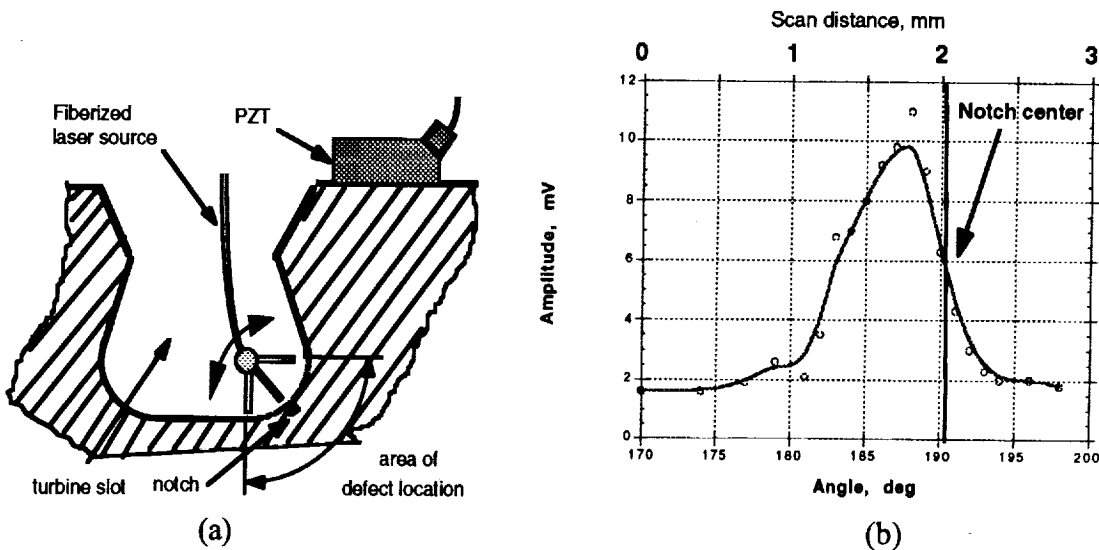


Figure 5. SLS approach applied to attachment slots in engine disks: (a) arrangement of testing, (b) flaw signature in the ultrasonic amplitude.

can only detect notches with a depth greater than 0.5 mm. In this case, the SLS approach can improve the sensitivity of inspection.

The geometry of the turbine disks is rather complicated, and a special rotary fixture was used to house the generating fiber and scan the laser source within the turbine slot. The detection of the ultrasonic signal was done using a pzt-transducer located on the easily accessible outside surface of the engine disk (see Figure 5a). SLS generation parameters were as follows: thermoelastic point source with diameter 0.2 mm, and 0.5 mJ energy per pulse. The inspected slot had an EDM notch with width 0.05 mm, length 0.75 mm, and depth 0.38 mm. The results obtained using the SLS technique are shown in Figure 5b. These results indicate that the characteristic flaw signature here is similar to that shown in Figure 2. This experiment shows that the SLS technique enables detection of smaller defects than can be detected in a pitch-catch mode using the same equipment.

CONCLUSIONS

A scanning laser source technique for detection of small defects has been developed. This technique provides distinct flaw signatures for small defects on flat and curved surfaces. It was shown that the amplitude and the spectrum of the generated ultrasonic wave changes as the SLS passes over a defect. A fiberized laser ultrasonic source has been used to detect small notches of 0.05 mm width on the surface of a turbine disk specimen.

ACKNOWLEDGMENTS

This material is based upon work performed at Northwestern University for the FAA Center for Aviation Systems Reliability operated by Iowa State University and supported by the Federal Aviation Administration under Grant No. 93-G-018 and for the Air Force Office of Scientific Research under Grant No. F49620-98-1-0285.

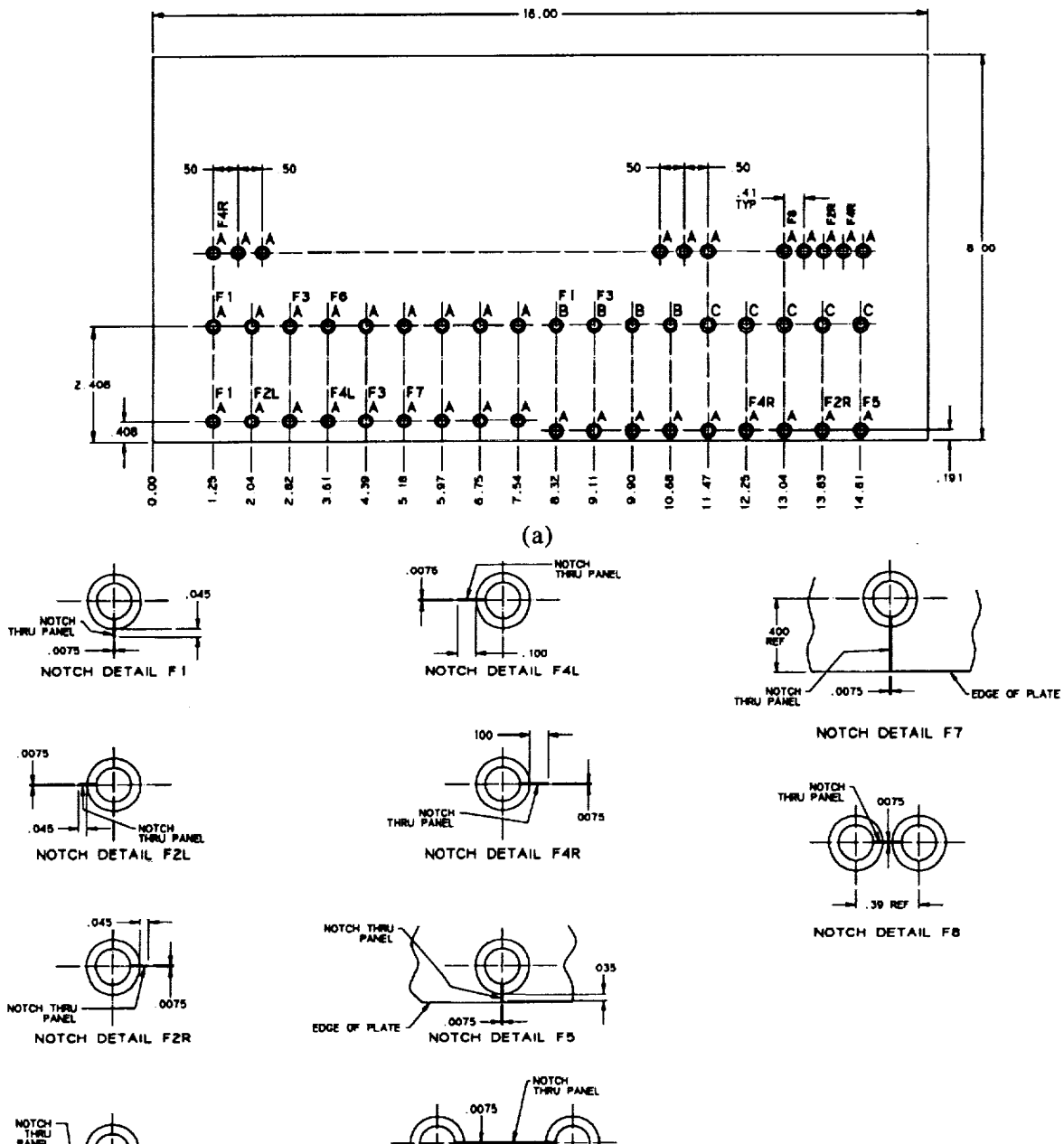
REFERENCES

1. C. B. Scruby and L. E. Drain, *Laser Ultrasonics*, Adam Hilger, New York (1990).
2. L.S. Wang, J. S. Steckenrider and Jan D. Achenbach in *Review of Progress in QNDE*, vol. 16A, eds. D.O. Thompson and D.E. Chimenti, (Plenum Press, New York, 1996), p. 507.
3. P. Fomitchov, A. Kromine, S. Krishnaswamy and J.D. Achenbach, in *Review of Progress in QNDE*, vol. 17A, eds. D.O. Thompson and D.E. Chimenti, (Plenum Press, New York, 1998), p. 675.
4. J. Huang and J. D. Achenbach, *J. Acoust. Soc. Am.*, 90(3), p. 1269, (1991).
5. P. Fomitchov, S. Krishnaswamy and J.D. Achenbach, *Optics and Laser Technology*, vol. 29, No 6, p.333 (1997).
6. B. Pouet, R. Ing, S. Krishnaswamy and D. Royer, *Appl. Phys. Lett.*, vol. 69, p. 3782 (1996).

RELIABILITY STUDY OF MAGNETO-OPTIC (MOI) IMAGING INSPECTION OF C-5 AIRCRAFT FUSELAGE

Jay L. Fisher, Gary L. Burkhardt, Jeffrey S. Stolte,
Janet P. Buckingham, Peter C. McKeighan, Jack Fitzgerald
Southwest Research Institute
P.O. Drawer 28510

Screening test specimens were constructed to represent typical structure and variations as determined from the above information. The primary test specimen is shown in Figure 1. This specimen was used to evaluate the effects of fastener-to-edge spacing, protruding fasteners, recessed fasteners, fastener material, flaw orientation (with respect to edges), liftoff, etc. Notches were used to simulate cracks. In some cases, this specimen was supplemented with others having additional variables, e.g., fastener size. Screening test specimen design is discussed below.



Photographic analysis showed that the actual distance between the fastener head and the edge was often much smaller than allowed by specification—in some cases, as small as 0.041 inch. Based on the photographic analysis, fasteners were put in the screening specimen with distances to the edge representing the manufacturer's minimum specified spacing, the minimum spacing found in the aircraft photographs, and an additional spacing with the fastener a large distance from the edge, which would represent a fastener row not adjacent to an edge. These conditions will be referred to as nominal, near, and far spacings, respectively. For each of these conditions, 0.045- and 0.10-inch flaws were placed in the specimen. The flaw orientation with respect to an edge can influence the MOI response; thus, flaws were included with orientations both parallel and perpendicular to the edge.

The aircraft manufacturer's specification for minimum fastener-to-fastener spacing is four times the fastener shank diameter plus 0.03 inch (measured from the fastener centers). In the photographs of C-5 structure supplied by SA-ALC, there were cases where the actual distances between the edges of the fastener heads were much smaller than allowed by the specification—in some cases, as small as 0.12 inch. Screening tests determined that this close fastener spacing was not significant for the aluminum and titanium fasteners, but was significant for the steel fasteners, as can be seen in Figure 2.

Further tests showed that the fastener head-to-head spacing below which the MOI response would be affected for steel fasteners was approximately 0.22 inch. An analysis of the aircraft photographs showed that only 4.8 percent of fasteners were spaced closely enough to meet this criterion. Because of this low percentage and because this situation would occur only for steel fasteners, flaws were not placed in closely spaced holes in the POD test specimens for nonconnecting flaws.

Although the MOI response to flaws generally becomes greater as flaw length increases, flaws which totally connect fastener holes or which totally to an edge (connecting flaws) produce an entirely different response than nonconnecting flaws. Whereas the nonconnecting flaw produces a protrusion of the fastener response directly over the flaw, a connecting flaw's observable response was a distortion in the "center hole" of the fastener response, as shown in Figure 3. This observation led to the conclusion that separate PODs should be developed for connecting and nonconnecting cracks.

A list of the variables considered and of their importance as determined from the screening tests is shown in Table 1.

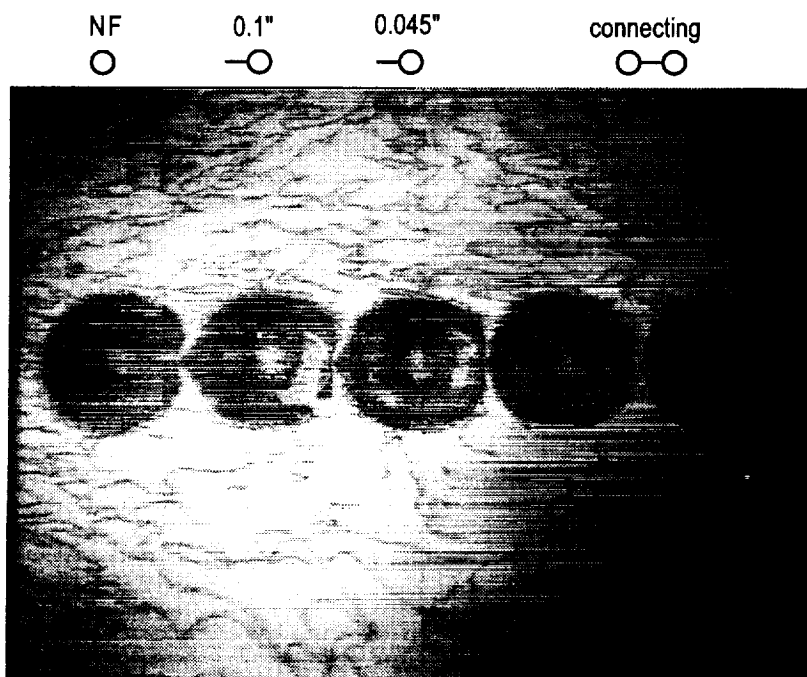


Figure 2. MOI images from closely spaced fastener holes with steel fasteners

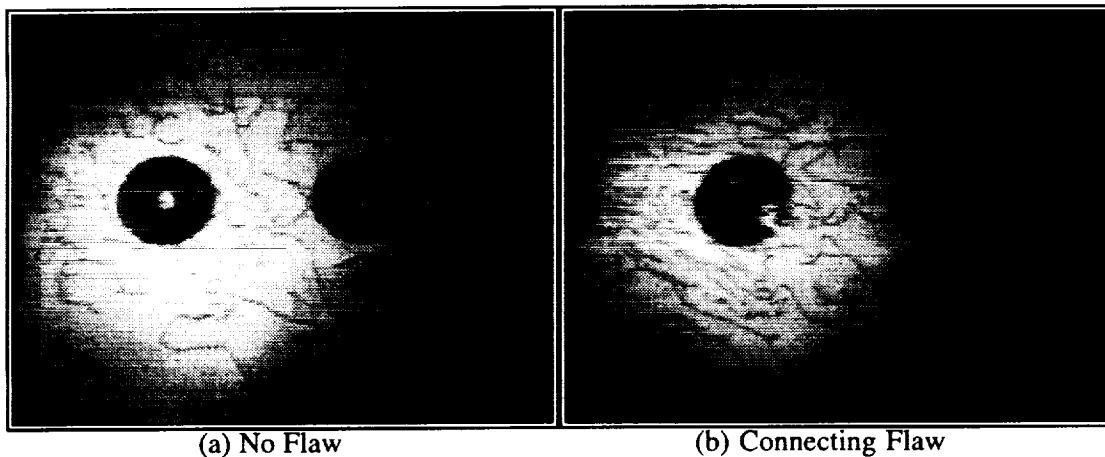


Figure 3. MOI images from fastener holes with titanium fasteners and a connecting flaw

TABLE 1. SUMMARY OF SCREENING TEST RESULTS

Factor Examined	Significance
Flaw Size	Important, especially connecting vs. nonconnecting
Flaw Orientation	Important if fastener-edge or fastener-fastener spacing is less than a certain value
Fastener Material	Important, especially steel compared to Al or Ti
Fastener Diameter	Not important
Fastener-to-Edge Spacing	Important if less than a certain value
Fastener-to-Fastener Spacing	Important if less than a certain value
Fastener Head Height	Important if fastener protrudes; not included in POD because of limited occurrence
Liftoff	Important—Value representative of maximum paint thickness (0.006 in) used in POD tests
Layer Thickness	Not important for first-layer flaws
Second-Layer Geometry	Not important for first-layer flaws
Skin Curvature	Important, but not included in POD tests because of limited occurrence
MOI Excitation Frequency and Power Level	Important

Based on the screening tests, design parameters were obtained for the test specimens to be used in the POD tests. These parameters are summarized in Table 2. The table includes important variables as identified by the screening tests and constants which were used in the specimen design but which were either not important as variables or which were chosen to represent typical aircraft conditions. Note that since 5/32-inch-diameter fasteners were used, the nominal fastener-to-edge and fastener-to-fastener distances were based on the manufacturer's minimum specification for this fastener size, as discussed in previous sections.

TABLE 2. POD TEST SPECIMENS DESIGN PARAMETERS

Variables	Characteristics
Flaw Size	Nonconnecting (0.011 to 0.245 inch) Connecting (fastener-to-fastener and fastener-to-edge)
Flaw Orientation	Parallel with edge Perpendicular to edge
Fastener-to-Edge Spacing	Near (0.161 inch from center or 0.04 inch from head)* Nominal (0.35 inch) Far (>0.35 inch)
Fastener-to-Fastener Spacing	Nominal (0.70 inch) Near (0.4 inch)—only used for connecting flaws
Fastener Material	Aluminum (NAS1097AD-5) Titanium (HL911-5) Steel (LS35270S05)**
Constants	
Fastener Size	5/32-inch-diameter shank
Skin Material	7075 T6 Aluminum
Skin Thickness	0.070 inch first layer 0.050 inch second layer
Liftoff (simulated paint thickness)	0.006 inch
*Near spacing not used for aluminum fasteners since aluminum is only used on stringer joints with no first-layer edges	
**Fastener has slight crown to head which protrudes approximately 0.005 inch above skin surface; this is within specifications for C-5	

4. TEST DESCRIPTION

NDI inspectors assigned to work on the C-5 were used for the POD testing. These inspectors were selected by SA-ALC from among the population of inspectors then currently used at Kelly Air Force Base (AFB) and were representative of the population eligible to conduct the inspections. The inspectors chosen were all experienced in eddy current testing (ET) and were certified Level II in ET based on MIL-STD-410D. None of the inspectors had prior experience with the MOI inspection technique.

MOI training was held at Kelly AFB and was conducted by PRI Instrumentation and an ET Level III from SwRI (who had been previously trained by PRI in the use of the MOI instrument and had significant experience with the screening tests). At the conclusion of this training session, the MOI instrument and several training specimens were left at Kelly AFB to allow the inspectors to practice using the instrument and become more familiar with the POD procedure. Finally, because some minor changes and additions were made to the POD procedure after the last training session, a review of the procedure was held before the POD testing began.

The POD test procedure, "MOI Procedure for Detection of Cracks Around Fasteners in C-5 POD Panels," was developed by SwRI specifically for this program and was based on several sources, including existing MOI procedures⁵⁻⁷, the MOI Operator's Manual⁸, PRI Instrumentation's MOI Training Course Book⁹, and SwRI's experience with screening specimens in the laboratory. The procedure was reviewed by the SA-ALC project monitor. The procedure is intended only for inspection of the POD panels and is not intended for inspection of an actual aircraft. It is intended, however, that the procedure could be used as a model for an aircraft inspection procedure.

The calibration and inspection method for nonsteel fasteners is relatively straightforward. Nonsteel fasteners are inspected with the rotating eddy current excitation mode. This mode allows fasteners to be inspected for flaws in any orientation with a single pass of the MOI imager. The calibration and inspection method for steel fasteners is more complicated and time consuming. First of all, steel fasteners must be degaussed properly before they can be inspected with the MOI technique. This step involves passing a degaussing unit over the steel fasteners and then viewing the MOI image of the fasteners to ensure that the fasteners were properly degaussed. The linear eddy current excitation mode was used for inspecting steel fasteners. This mode was necessary because flaws connecting two adjacent steel fasteners could not be reliably detected using the rotating excitation mode. Using the linear excitation mode means that each steel fastener must be inspected twice, once with the front-to-back linear excitation mode and once with the side-to-side linear excitation mode.

Four of the five trained inspectors were used for the POD testing. The POD testing, illustrated in Figure 4, was conducted at Kelly AFB for seven consecutive work days. The POD testing was monitored by the SwRI Level III and an NDI Engineer from Kelly AFB. Two MOI instruments were used so that two inspectors could work simultaneously. Each inspector used the same respective unit throughout the tests, with the exception that it was necessary for one inspector to change units for inspection of 12 standards.

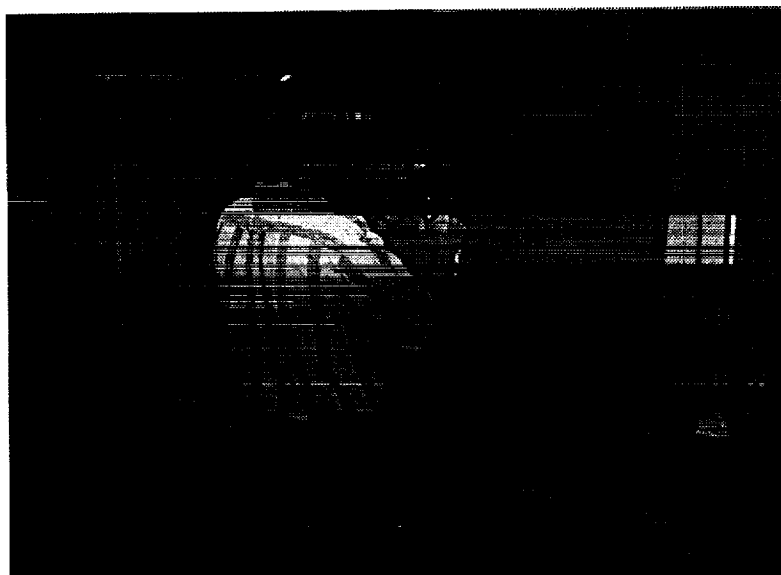


Figure 3. Photograph of MOI POD testing setup

RESULTS

POD curves for nonconnecting cracks with aluminum and steel fasteners are shown in Figures 4 and 5 (the curve for titanium is similar to that for steel). The results for first-layer nonconnecting cracks, using combined data from all inspectors, are summarized in Table 3. The table shows crack lengths detectable with a 90-percent POD (a_{90}) and crack lengths detectable at a 90-percent POD with a 95 percent lower confidence bound ($a_{90/95}$). It also shows the false-call rate. In the table, all lengths are reported as the distance from the edge of the fastener head to the crack tip. The target performance was an $a_{90/95}$ of 0.17 inch or less. Important results for nonconnecting cracks are:

- The target performance was met for the aluminum fasteners.
- If near-edge fasteners are eliminated from the inspection, then the target performance is met for titanium fasteners also. It should be noted that the near-edge condition was less than the minimum specified by the manufacturer, but was found to be present for 7 percent of the aircraft fasteners studied.

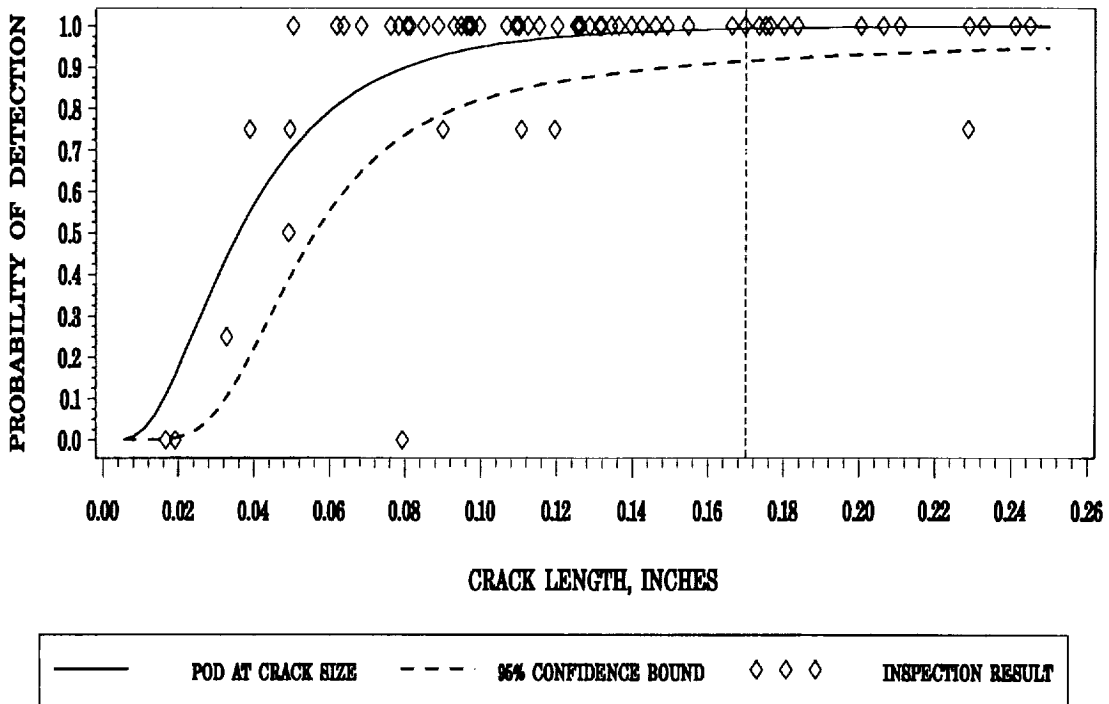


Figure 4. POD(a) for aluminum fastener material—all four inspectors

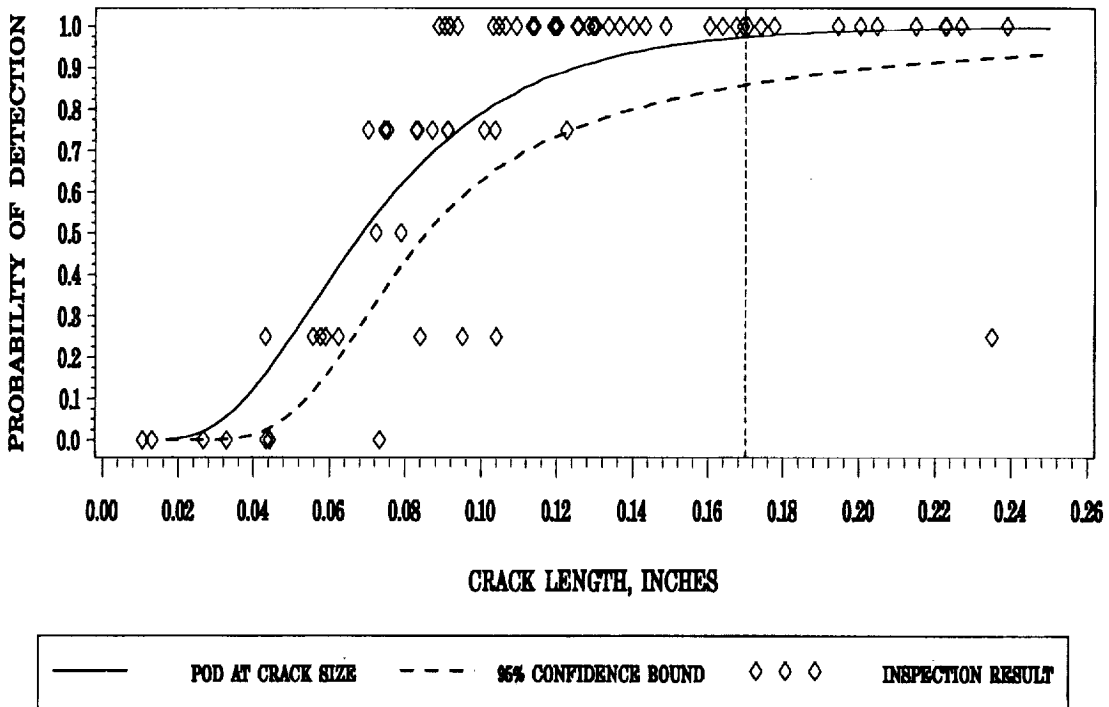


Figure 5. POD(a) for steel fastener material—all four inspectors

TABLE 3. DETECTION PROBABILITIES AND FALSE-CALL RATES FOR NONCONNECTING CRACKS

Fastener Material	a_{90} (in.)	$a_{90/95}$ (in.)	False-Call Rate (%)
Aluminum	0.080	0.151	0.19
Steel	0.124	0.205	0.25
Titanium	0.091	0.285	0.06
Titanium (without near-edge cracks)	0.067	0.151	---

- The target performance was not met for steel fasteners using the data from all inspectors.
- The results on titanium and aluminum fasteners were actually very similar, since there were no near-edge cracks used in the aluminum fastener data. (Aluminum fasteners are only used on stringer joints with no first-layer edges.)
- The false-call rate was less than one per 400 fasteners with steel fasteners, and even less with aluminum and titanium fasteners.

The results for first-layer connecting cracks (e.g., fastener-fastener and fastener-edge) are summarized in Table 4, using combined data from all inspectors. This table shows the percentage of cracks detected, the POD at a 95-percent confidence level, and the false-call rate.

TABLE 4. DETECTION PROBABILITIES AND FALSE-CALL RATES FOR CONNECTING CRACKS

Fastener Material	% Cracks Found	POD at 95% Confidence	False-Call Rate (%)
Aluminum	94	0.893	0.63
Steel	73	0.659	0.15
Titanium	93	0.873	0.30

Important results for connecting cracks are:

- For aluminum and titanium fasteners, the target performance was almost met. Two of the inspectors individually exceeded the target performance in aluminum by finding all 30 cracks connecting aluminum fasteners, and one inspector found 29 of 30 cracks connecting titanium fasteners. Therefore, it is likely that additional training and a rigorous qualification process could be used to meet the target performance for these fasteners.
- For both aluminum and titanium fasteners, performance was reduced by the presence of closely spaced fasteners. In aluminum, 2 out of 7 (29 percent) missed cracks were in the closely spaced fastener condition; in titanium, 3 out of 9 (33 percent), even though only 20 percent of the connecting cracks were linking closely spaced fasteners.
- For steel fasteners, the performance target was not met by any inspector.
- For steel fasteners, performance was severely reduced in the closely spaced fastener geometry; almost half of the missed cracks were in this geometry. Even so, the percent of cracks found—not including closely spaced fastener geometry—was only 83 percent, so limiting the inspection of steel fasteners in this manner would not provide acceptable results.

CONCLUSIONS

The Air Force criterion for acceptable performance on the C-5 was met for aluminum and titanium fasteners for nonconnecting cracks. For connecting cracks, the criterion was almost met for aluminum and titanium fasteners. For steel fasteners, the criterion was not met in either case.

As a result of this work, PRI has made improvements to the MOI system to address the difficulties that were found. It is planned to repeat the POD tests with the new instrumentation in the fall of 1998.

ACKNOWLEDGMENTS

This work was supported by the San Antonio Air Logistics Center/TIESM, Kelly Air Force Base. The efforts of Messrs. I. Rodriguez, H. Saldaña, and J. Riggs are acknowledged for the assistance they provided before, during, and after the fatigue cracking of the cracked standards. Messrs. H. King and G. Rodriguez also helped tremendously during the manufacture and design of the templates and test coupons. Finally, the cooperation of Kelly AFB NDI personnel is greatly appreciated.

REFERENCES

1. "Magneto-Optic Eddy Current Inspections of B-52 G/H Pressure Cabin Side Skin Determination of Detection Reliability," Boeing, Wichita, Enclosure A to Y-7W16-129-164 1130, reference Boeing letter Y-7W16-129-045-1130.
2. V. J. Brechling and F. W. Spencer, "Validation of the Magneto-Optic/Eddy Current Imager," U.S. Department of Transportation Report No. DOT/FAA/AR-95/100, November 1995.
3. F. W. Spencer and D. Schurman, "Reliability Assessment at Airline Inspection Facilities— Vol. III: Results of an Eddy Current Inspection Reliability Experiment," U.S. Department of Transportation Report No. DOT/FAA/CT-92/12, May 1995.
4. W. C. L. Shih, G. L. Fitzpatrick, D. K. Thome, R. L. Skaugset, and E. Y. C. Shih (PRI Instrumentation), "Aircraft Inspection with the Magneto-Optic/Eddy Current Imager (MOI)," presented at the International Conference on Surface Treatments in the Aeronautical and Aerospace Industries, Cannes, France, June 3–5, 1992.
5. Boeing MOI Inspection Procedure, "General Surface Inspection of Aluminum with the Magneto-Optic Imager (MOI)," March 15, 1992.
6. McDonnell-Douglas Inspection Procedure, "Magneto-Optic Imager (MOI) Inspection," December 15, 1991.
7. Lockheed MOI Inspection Procedure for L-1011.
8. "Magneto/Optic Eddy Current Imager Operator's Manual, Model 302 with Model 303 Supplement," PRI Instrumentation, 1990 and 1996.
9. "Aircraft Inspection with the Magneto-Optic/Eddy Current Imager (MOI) Training Course Book," PRI Instrumentation.

525

384874

1999037218

QUANTITATIVE INVESTIGATION OF SURFACE AND SUBSURFACE CRACKS NEAR RIVETS IN RIVETED JOINTS USING ACOUSTIC, ELECTRON AND OPTICAL MICROSCOPY

Z.M. Connor, M.E. Fine, and J.D. Achenbach
Northwestern University
2225 N. Campus Drive
Evanston, Illinois 60208 USA

ABSTRACT

The scanning acoustic microscope was previously shown to be useful for quantitatively investigating subsurface fatigue cracks at and near countersunk rivets in riveted lap joint specimens. Such cracks initially form on inner surfaces and are not visible on the outside surface. When combined with optical and electron microscopic examination of the surface and with fractography of fractured specimens, the formation and growth of subsurface cracks near rivets may be characterized in detail. A detailed study of crack formation and microcrack growth near rivets is presented. Observations were made on specimens fabricated from two pieces of Alclad 2024-T3 sheets riveted with 2017-T4 aluminum alloy flathead chamfered rivets. Specimens were fatigued in tension with an R ratio of 0.1. The interior crack lengths and crack growth rates as shown by the acoustic microscope are compared to the crack lengths and crack growth rates after the cracks broke the surface as shown by the light microscope. Plots of subsurface crack length vs. cycle number show slow almost linear growth vs. time. However, when the crack breaks through the outer surface, i.e. becoming a through the thickness crack, the crack growth rate increases rapidly. The length of the crack on the back surface of the countersunk panel remains longer than the length of the crack on the front surface of the specimen even with cracks several mm long; the growth rate along the crack front is constant. Fractographic examination of a specimen which was fatigued until a crack was just barely visible in the acoustic microscope but not seen on the surface reveals multiple cracks on each side of the rivet hole. The cracks in these specimens appears to be qualitatively identical to some cracks very close to single rivet cracks in full scale fuselage testing. FASTRAN II analysis, developed by Dr. James C. Newman, Jr.¹ was performed, and the predictions of crack length vs. cycles from this analysis are compared to the results obtained in these experiments.

1. INTRODUCTION

Since fatigue cracks have been found in aircraft, many studies have been performed involving prediction of the life of lap joints in the fuselage of an aircraft and the ability to detect fatigue cracks before they grew to an unsafe length. The nondestructive evaluation of these cracks while they are still small has been difficult as the cracks form on a subsurface of the joint and are a number of mm long by the time they reach a surface which is visible with either the optical microscope or the scanning electron microscope.

The load transfer conditions for riveted lap joint specimens are very different from unriveted specimens with a rivet hole. The load is concentrated at the rivets with load by-pass occurring in the panels so that the outer rows of rivets carry the largest load. Moreover, even if the load axis is along the center line of the riveted panels, there is a bending moment exerted on the outer rivets, and these are the rivets where failure is expected.^{2,3}

The process by which cracks nucleate and grow in riveted joints subjected to fatigue loading is a very complex one. Many variables come into play, including but not limited to, fretting, corrosion,

amount of clearance or interference fit between the rivets and the plate, amount of force applied during the riveting process, and amount of stress to which the joint is subjected.^{2,4}

Additionally, residual stresses are present in riveted joints. Fitzgerald and Cohen⁵ found these stresses to be compressive in the rivet and tensile in the sheet at low riveting forces, but at higher riveting forces, the stress in the sheet became compressive. Such compressive stresses are expected to increase the fatigue crack initiation time and reduce the crack propagation rate.

A study of riveted lap joints was undertaken by Mayville and Sigelmann⁶. Statistical experimental design was used to reduce the number of tests required. The different parameters studied were stress level, rivet spacing, rivet type, rivet orientation, number of rivet rows and skin thickness. The only ones which were shown to have a significant effect on fatigue life were stress level, rivet type and skin thickness. MSD almost always occurs in the top row (critical row) of rivets with cracks sometimes occurring in the second row of rivets. In Mayville and Sigelmann's investigation, the crack growth rate was found to be fairly constant for cracks up to 0.25 inches. This was determined by analysis of striation spacings on an actual aircraft. It was found that by increasing the bucktail diameter, the average number of cycles until crack initiation (defined as a 0.1 inch long crack) was increased by a factor of 2.

Piasek et al.⁷ characterized widespread fatigue damage in a full size fuselage test article. By visual in-situ nondestructive examination, cracks were found to initiate first in the upper row of rivets in a specimen containing four rows of rivets. After cracks had linked up at all upper row rivet locations, the pressure testing was stopped. The rivets used in this research were "button" head rivets.

By nondestructive examination (visual at 10x and eddy current), through cracks were found primarily in the upper row of rivets in the outer skin. These cracks all initiated either at the horizontal centerline of the rivet hole or in the upper half of the hole. No evidence of cracking was found on the inner surfaces. By in-situ visual examination, multiple cracks were not detected until approximately 83% of the life.⁷

By destructive examinations using the optical and scanning electron microscopes, outer skin cracks were found in the second row, and inner skin cracks were found in the third row. Cracks initiated at rivet hole corners, rivet hole surfaces and outer/inner skin surfaces. Evidence of fretting was found at the point of crack initiation for some cracks. Discontinuities at the surface cladding, at the rivet hole surface and at the inner skin corner were found to be crack initiation sites. The initiation sites for the fatal crack which linked up were along the lap splice joint interface in the area of fretting.⁷

Waterhouse⁸ found that the initial part of a fretting fatigue crack is open and fills with fretting debris which plays a role in the amount that the crack is held open. Also, the crack grows at an angle to the surface until it gets beyond the influence of the fretting action, and then it grows perpendicular to the applied stress.

Fretting has been found to definitely be the cause of cracks in some instances. When cracks nucleate away from rivet holes in aircraft joints, this is an indication that they were caused by fretting.⁹ Muller⁴ has shown that the amount of clamp up force used during the riveting process can also change the crack location. The crack will move away from the rivet hole when the riveting force becomes large enough. In the research presented hereinafter, it has been found that a nominal maximum fatigue stress of 103 MPa will cause the crack to nucleate away from the rivet hole and the crack will be off center, while a nominal stress of 154 MPa will cause the crack to nucleate at the rivet hole and the crack will be at the center line of the rivet and perpendicular to the loading direction. An intermediate stress between 103 MPa and 154 MPa will result in the crack moving up towards the centerline of the rivet.

A quantitative investigation of fatigue cracks at and near rivet holes in lapjoint specimens is reported herein. The effects of varying the maximum applied stress were included. For this study, the scanning acoustic microscope (SAM) was used to characterize subsurface cracks and the subsurface portion of the cracks after they broke the surface. The optical and scanning electron microscopes (SEM) were also used to characterize surface breaking cracks and to compliment the results of the

SAM. Finally, FASTRAN II crack length vs. cycle prediction, developed by Dr. James C. Newman, Jr.¹ was performed, and the predictions of crack length vs. cycles from this analysis was compared to the results obtained in these experiments at a nominal stress of 103 MPa.

1.1 EXPERIMENTAL METHODS

Riveted lap joint specimens were prepared by riveting together two Alclad 2024-T3 aluminum alloy panels, one with three countersunk rivet holes and one with three straight holes. The rivet holes were drilled and countersunk using a computer controlled machining center. The rivets were made of 2017-T4 aluminum alloy. The panels were riveted together on a manually operated hydraulic press where the rivets were compressed between two flat plates at a constant load of 44.6 kN to give a bucktail diameter of $6.12 \text{ mm} \pm 0.05 \text{ mm}$. A sketch of the riveted joint is shown in Figure 1.

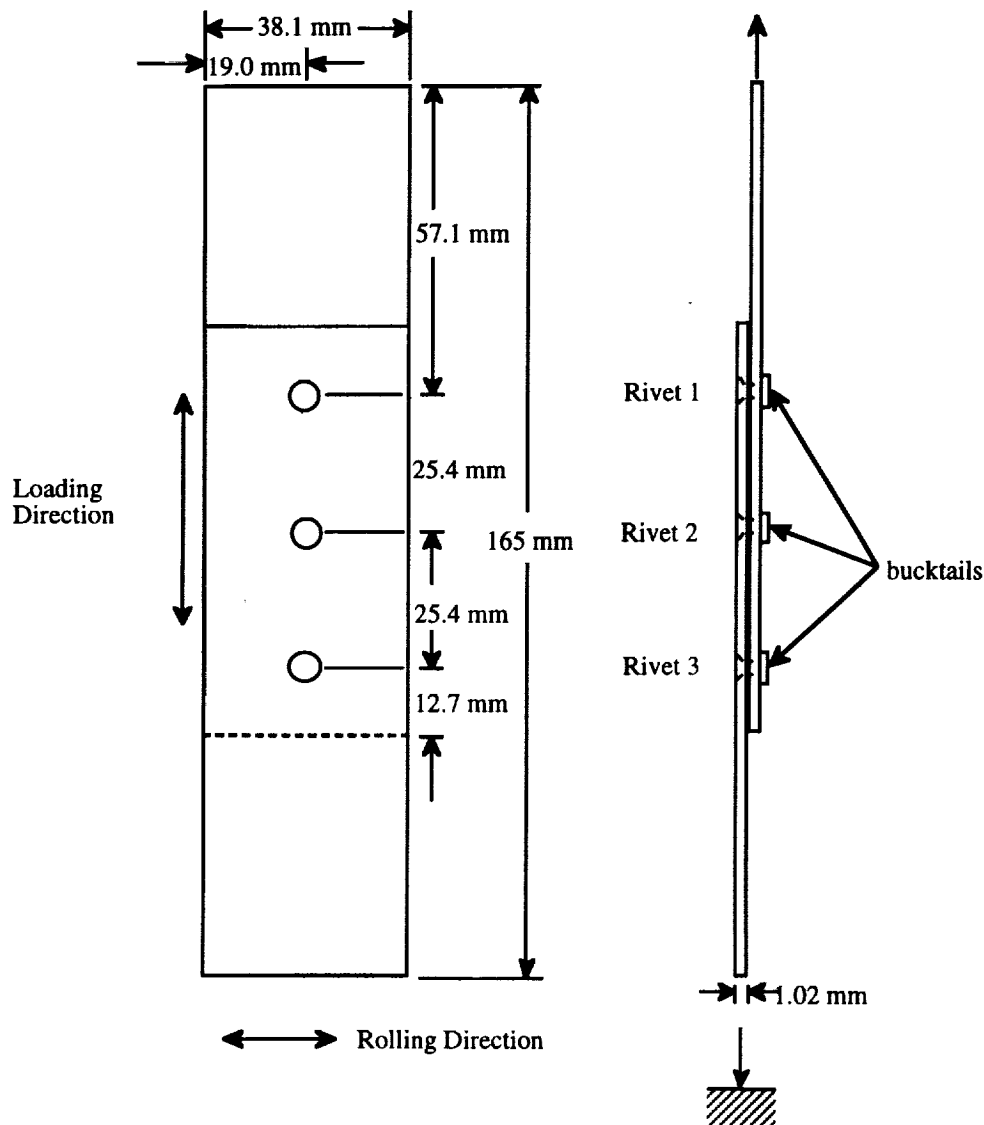


Figure 1. Sketch of Riveted Joint

An MTS servohydraulic uniaxial fatigue testing machine with a rating of 100 kN was used to perform the experiments. The three-rivet lap joint specimens were loaded in uniaxial tension with an R ratio of 0.1. The effect of different levels of maximum stress were investigated with the highest nominal stress employed being 206 MPa and the lowest stress being 103 MPa. Shims were used in the grips so that the load axis was along the initial center line of the specimen. A saw-tooth wave with a frequency of 5 Hz was applied with a function generator and fine tuned with the use of a digital recording oscilloscope. A positive R ratio was selected to prevent damage to the crack surface from crack closure.

The subsurface fatigue cracks were examined with the SAM after selected numbers of cycles and then returned to the fatigue apparatus for further cycling. Testing was discontinued and specimens were disassembled after various stages of subsurface fatigue cracking as revealed with the scanning acoustic microscope. After disassembly, the panels containing the fatigue cracks were pulled in tension until fracture to reveal the fatigue fracture surfaces which were examined microscopically using the SEM. Some tests were continued until long surface breaking cracks were obtained. Comparisons were then made between the crack lengths as shown with the SAM and with the optical microscope.

FASTRAN II analysis was performed on the specimens which were fatigued at a maximum stress of 103 MPa. FASTRAN II is a computer program developed by Dr. James C. Newman, Jr.¹ and predicts the crack length as a function of the number of cycles with selected variables input into the program. In this case, values were specified for the initial size of c , the half crack length, and a , the crack height. The crack configuration option used was for a surface crack. The input parameters were S_m , half the range of the stress amplitude; S_m , mean stress; width and thickness of the specimen; rivet spacing; bypass load; bending stress and interference fit.

1.2 RESULTS

In previous research and using the optical microscope, it has been shown that the first indication on the outer surface of the presence of a subsurface crack is surface rumpling consisting of plastic deformation markings and microcracks. This surface rumpling appeared near the rivet head of Rivet 3 identified in Figure 1. A scanning acoustic microscope C-scan image of a specimen with surface rumpling on one side of the rivet revealed subsurface radial cracks on both sides of the rivet. Roughly 87% of the cycles to an 8 mm (end-to-end) long crack are spent generating a surface breaking radial crack on one side of the rivet.^{10,11} The number of cycles between the first observance of a crack on the acoustic scans and the observance of surface rumpling as detected when viewing the replica of the surface of a specimen with an SEM was 55,000. When this specimen was pulled to fracture after 205,000 cycles, it was found to contain a true eyebrow crack, i.e. it did not go through the rivet hole. The SAM C-scan and the SEM micrograph of the crack both showed the crack to be 8.1 mm in length, and the crack was still not a surface breaking crack.^{12,13}

When specimens were fatigued at a maximum stress of 103 MPa and an R ratio of 0.1, it was found that "eyebrow" type cracks formed. When the maximum stress was increased to 206 MPa on a different specimen, a centerline type crack formed (A similar behavior was noted on stress increase with seven rivet specimens). At this high stress, the rivet is beginning to pull out, and there is competition between the specimen fracturing due to the crack or the specimen failing due to the rivet pulling out. The length of the crack as seen with the optical microscope was shorter than the length of the crack as seen with the SAM. The maximum bending stress due to the bending moment is on the back surface of the panel with the rivet head at Rivet 3.^{12,13}

Specimens were then tested at maximum stresses of 180 MPa, 154 MPa, and 129 MPa and 103 MPa. At 180 MPa and at 154 MPa, the fatigue cracks which formed were located radially at 3 and 9 o'clock around the rivet with respect to the stress direction as shown in Figure 2, but at 129 MPa and at 103 MPa, the fatigue crack was again an eyebrow type crack as seen in Figure 3. The initiation sites for specimens fatigued at 103 MPa were some distance from the rivet hole and on the inner surface of the countersunk panel as shown in Figure 4, while the fatigue cracks for the specimens fatigued at 154 MPa started at the corner where the knife edge intersects the hidden surface as shown in Figure

5. The crack begins in shear and then quickly turns to propagate normal to the direction of the applied stress. Figure 6 shows the crack on the left in Figure 5 at a higher magnification, and the transition from a shear crack to a crack normal to the direction of the applied stress is marked by a dotted line. Both kinds of cracks are seen in aircraft skins.

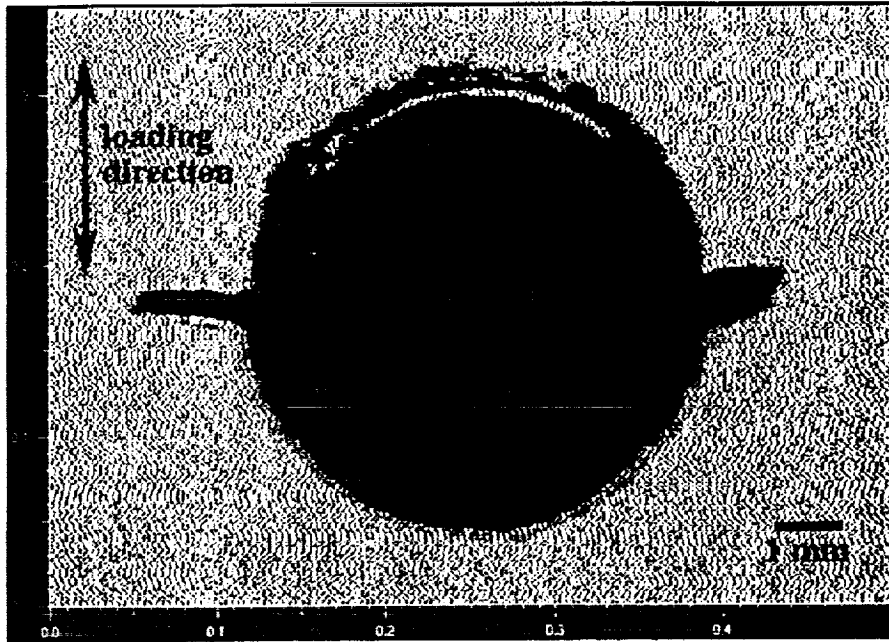


Figure 2. C-scan of type of crack which develops at a maximum stress of 154 MPa and 180 MPa.

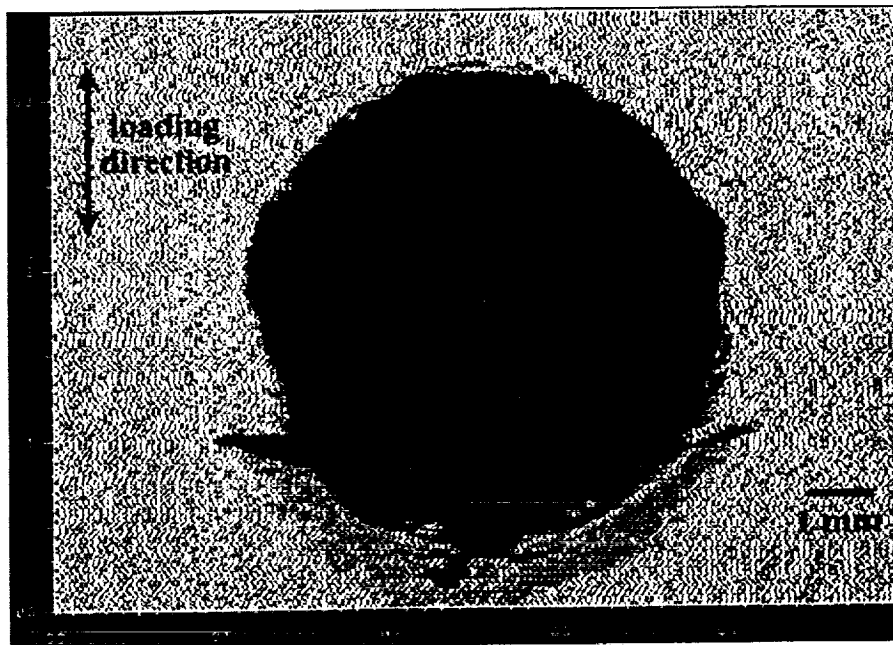


Figure 3. C-scan of type of crack which develops at a maximum stress of 103 MPa and 129 MPa.

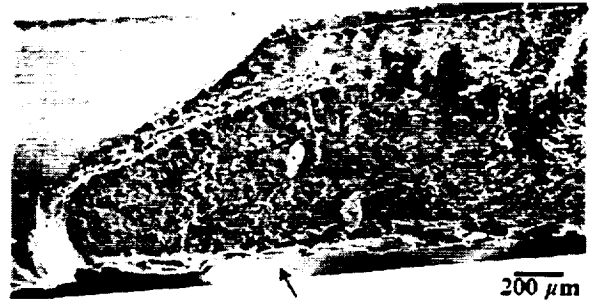
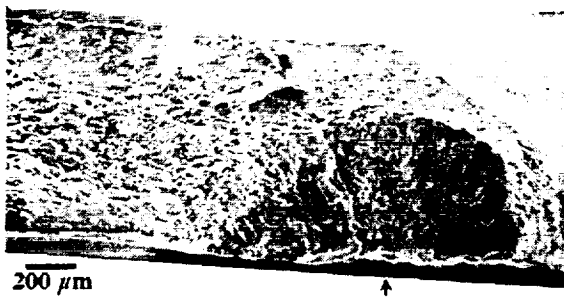


Figure 4. SEM micrograph of the fracture surface of a specimen which was fatigued at a maximum stress of 103 MPa. The crack initiation sites are some distance away from the rivet hole and on the inner surface.

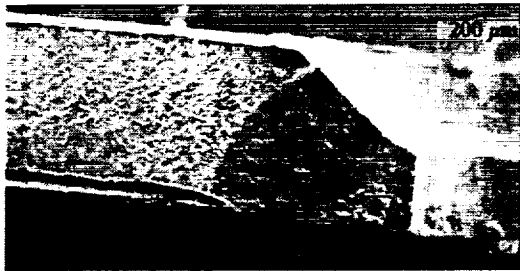


Figure 5. SEM micrograph of the fracture surface of a specimen which was fatigued at a maximum stress of 154 MPa. The crack initiation sites are at the corner where the knife edge intersects the hidden surface.

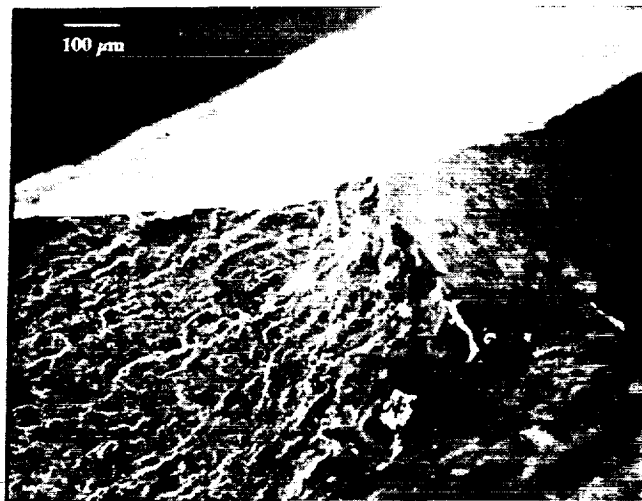


Figure 6. SEM micrograph of the crack on the left side in Figure 5. The transition from a shear crack to a crack which is propagating normal to the direction of the applied stress is given by the dotted line.

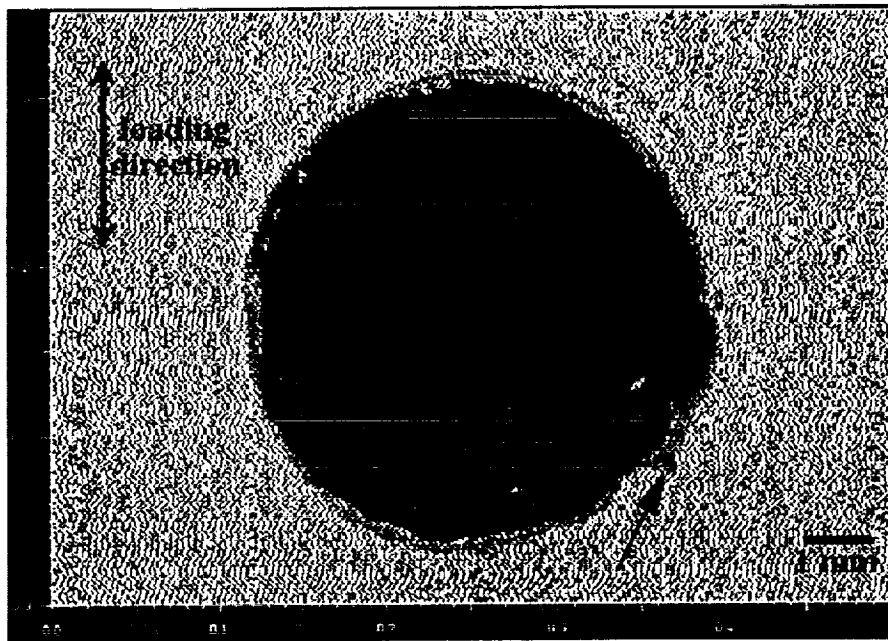


Figure 7. C-scan showing an early indication of a fatigue crack formed in a specimen at a maximum stress of 103 MPa. The indication is shown by the arrow.

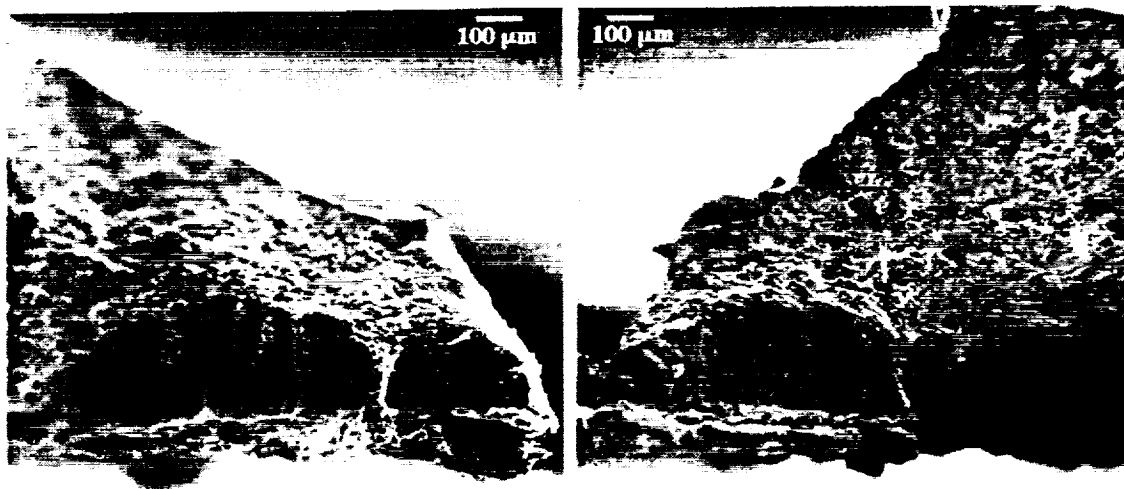


Figure 8. SEM micrograph of the fracture surface of the specimen shown in Figure 7. Multiple initiation sites are seen on each side of the rivet.

The subsurface cracks formed when a maximum stress of 103 MPa is applied propagate as asymmetrical semi-elliptical cracks until they reach the countersunk surface. When they appear on the outside surface, they are a short distance from the rivet head. As mentioned previously, prior to emergence of the macrocrack on the observable surface, an array of radial and circumferential microcracks are observed using optical and SE microscopy. These microcracks are a sign of fatigue damage and are the product of the propagating subsurface crack.

Figures 7 and 8 show an early indication of a fatigue crack formed at a maximum stress of 103 MPa as viewed with the SAM and the fracture surface as viewed with the SEM. There are several initiation sites as seen by the three microcracks on each side of the rivet hole. If the test had not been interrupted, these microcracks would have continued to grow until they linked up to form a single microcrack such as the one shown in Figure 4. Figure 9 shows an early indication of a fatigue crack formed at a maximum stress of 154 MPa as viewed with the SAM. The fracture surface as viewed with the SEM for this specimen is shown in Figure 5.

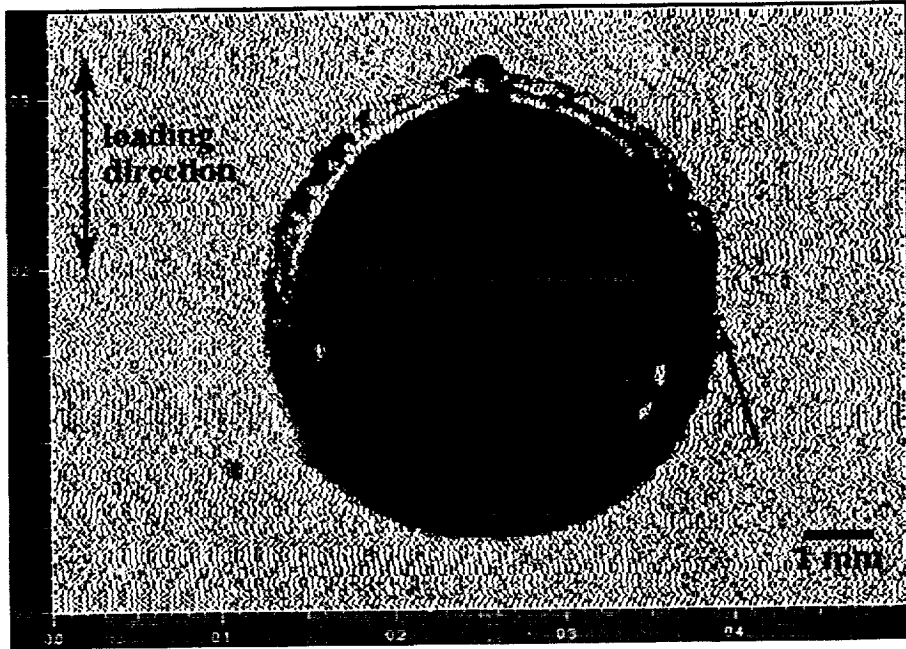


Figure 9. C-scan showing an early indication of a fatigue crack formed in a specimen at a maximum stress of 154 MPa. The indication is shown by the arrow.

Figure 10 is a plot of crack growth for a maximum stress of 103 MPa as obtained with the SAM. Crack growth was plotted as half the length of the crack from end-to-end, c , against the total number of cycles minus the number of cycles until a crack of length $, 2c$, was first observed. In this plot, we see that the subsurface crack growth is much slower than the crack growth for the longer surface breaking cracks.

Figure 11 is a plot of the crack growth of specimens fatigued at a maximum stress of 103 MPa and measured with the optical microscope and with the SAM. This plot shows slow, almost linear subsurface crack growth vs. time, but when the crack breaks through the outer surface, i.e. becoming a through crack, the crack growth rate increases rapidly. The length of the crack on the back surface of the countersunk panel remains longer than the length of the crack on the front surface of the specimen. However, the growth rate along the crack front is constant. Figure 12 is a plot of the crack growth of specimens fatigued at a maximum stress of 154 MPa as measured with the optical microscope and with the SAM. Both types of cracks are seen in aircraft.

The computer code, FASTRAN-II, developed by Dr. J. C. Newman, Jr.¹, is being used to compare our experimental results to the predictions of the code. FASTRAN-II uses the crack closure concept which says that the plastic deformation in the wake of the crack causes crack closure. The model calculates the crack opening stresses based on fatigue crack closure. The plot in Figure 13 gives the results of the FASTRAN-II analysis which was run and then compared with the acoustic microscope

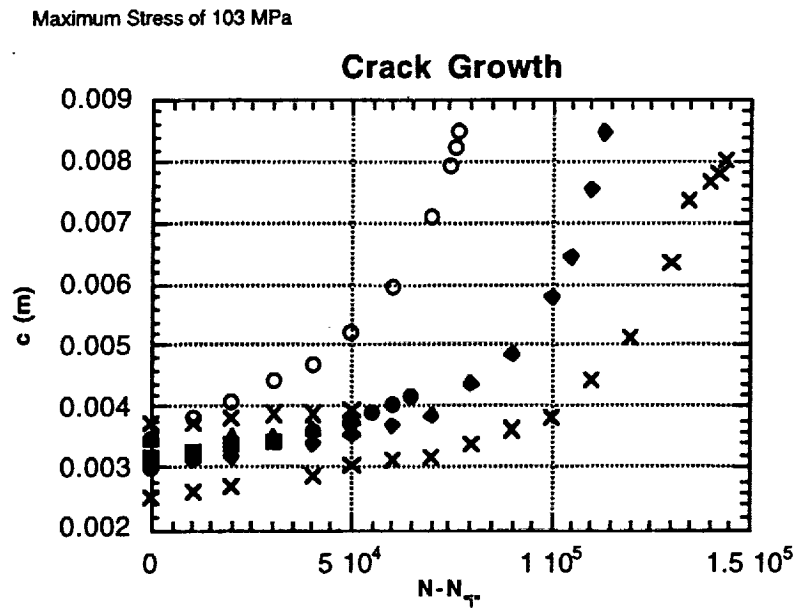


Figure 10. Plot of crack growth for a maximum stress of 103 MPa as obtained with the SAM.

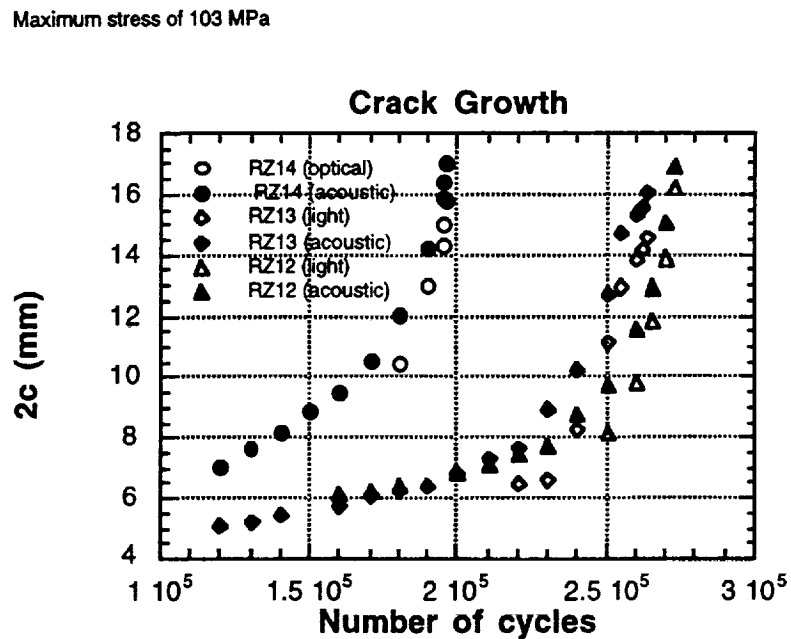


Figure 11. Plot of the crack growth of specimens fatigued at a maximum stress of 103 MPa as measured with the optical microscope and with the SAM.

Maximum Stress of 154 MPa

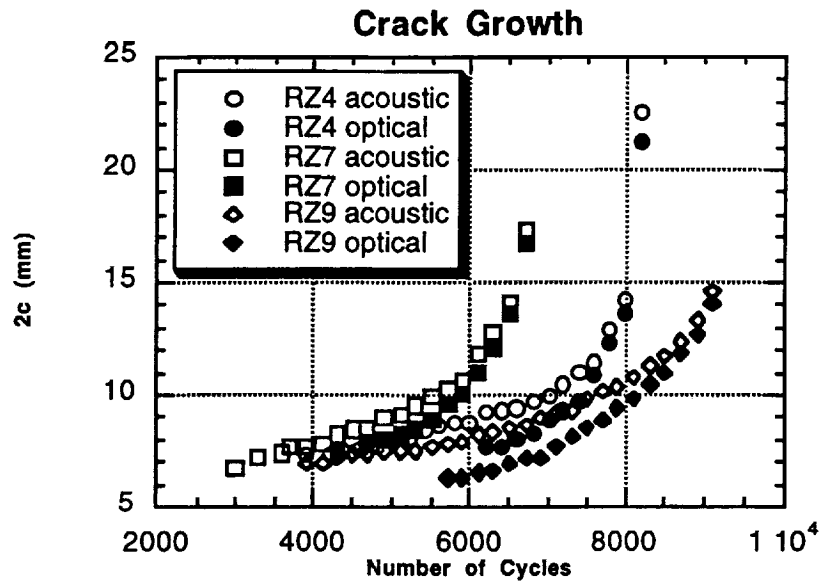


Figure 12. Plot of the crack growth of specimens fatigued at a maximum stress of 154 MPa as measured with the optical microscope and with the SAM.

Surface Crack and Acoustic Measurements

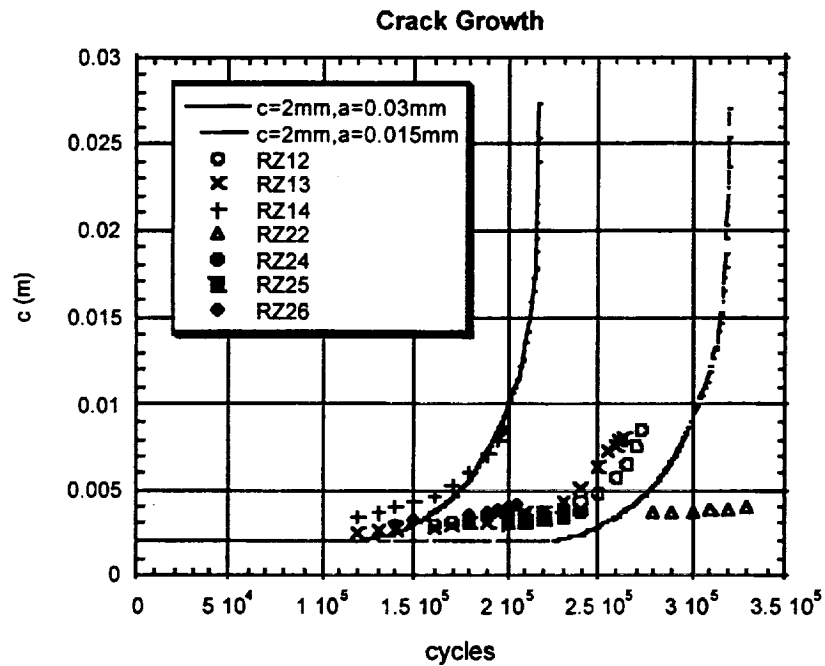


Figure 13. Plot comparing crack length vs. number of cycles as obtained with the SAM and as acquired using FASTRAN-II analysis.

measurements. There are 17 defined crack configurations from which to choose. The surface crack configuration was used as the crack initiates a slight distance from the rivet on the fretted surface at a maximum stress of 103 MPa. Different types of cyclic loads may be applied. We used constant amplitude. For the surface crack configuration, we specified an initial c , half-crack length and an initial flaw size, a . When a lapjoint configuration was used that assumes a corner crack at the knife edge, the curve was much sharper than the observed behavior. We used an initial crack size of 2 mm and initial flaw sizes of 15 μm and 30 μm .

CONCLUSIONS

The scanning acoustic microscope is useful for quantitatively investigating subsurface fatigue cracks that can't be observed optically or with the SEM. When combined with optical and electron microscopic examination of the surface and with fractography of fractured specimens, the formation and growth of subsurface cracks may be quantitatively characterized in detail revealing the fatigue crack initiation sites and determining the crack profile and growth kinetics. A riveted laboratory specimen was developed and the crack growth in these specimens appears to be qualitatively identical to the crack growth very close to single rivet cracks in full scale fuselage testing.

The sequence of events in the development of the eyebrow-type fatigue cracks are as follows: Fretting takes place between the mating surfaces, resulting in wear particles which may induce microcracks. (The location of the occurrence of fretting has been discussed previously.¹²) These microcracks that form grow out radially from the initiation sites and eventually link up to form a single microcrack. These cracks continue to grow radially until they eventually become surface breaking cracks. The growth rate along the crack front is constant so that the interior crack length remains longer with respect to the surface breaking crack length.

The crack configuration changes when the maximum stress changes. Fatigue cracks formed at a maximum stress of 103 MPa initiate and grow from the hidden side of the countersunk panel as semi-elliptical cracks, while fatigue cracks formed at a maximum stress of 154 MPa initiate and grow from the corner where the knife edge intersects the hidden surface. Analysis of the fracture surface of a specimen fatigued at a maximum stress of 103 MPa and with a crack barely visible under the acoustic microscope revealed several crack initiation sites on each side of the rivet hole. At 180 MPa, there is a competition between the specimen fracturing due to the crack or the specimen failing due to the rivet pulling out.

Reasonable agreement has been obtained between crack length vs. number of cycles curves acquired with the use of the SAM and with FASTRAN-II analysis when using an initial flaw size of between 15 and 30 μm .

ACKNOWLEDGMENTS

The research was funded by the Federal Aviation Administration, by a fellowship from the National Science Foundation and an Amelia Earhart fellowship from Zonta International.

REFERENCES

1. Newman, Jr., J. C., "FASTRAN II - A Fatigue Crack Growth Structural Analysis Program", NASA Technical Memorandum 104159, February, 1992.
2. Schijve, J.: "Multi-Site-Damage Fatigue of Riveted Joints", *Durability of Metal Aircraft Structures, Proceedings of the International Workshop on Structural Integrity of Aging Airplanes*, edited by S. N. Atluri, C. E. Harris, A. Hoggard, N. Miller, and S. G. Sampath, Atlanta Technology Publications, Georgia, 1992, pp. 2-27.

3. Jones, R., Rees, D. and Kaye, R.: "Stress Analysis of Fuselage Lap Joints", *Durability of Metal Aircraft Structures, Proceedings of the International Workshop on Structural Integrity of Aging Airplanes*, edited by S. N. Atluri, C. E. Harris, A. Hoggard, N. Miller, and S. G. Sampath, Atlanta Technology Publications, Georgia, 1992, pp. 118-131.
4. Muller, R. P. G., "An Experimental and Analytical Investigation on the Fatigue Behaviour of Fuselage Riveted Lap Joints", Ph.D. Thesis, Delft University of Technology, The Netherlands, 1995.
5. Fitzgerald, T. J. and Cohen, J. B.: "Residual Stresses in and Around Rivets in Clad Aluminum Alloy Plates", *Materials Science and Engineering*, A188, 1994, pp. 51-58.
6. Mayville, R. and Sigelmann, M., "Laboratory Study of Multiple Site Damage in Fuselage Lap Splices", Final Report, DOT/FAA/CT-93/74, December, 1993.
7. Piascik, R. S., Willard, S. A. and Miller, M., "The Characterization of Widespread Fatigue Damage in Fuselage Structure", FAA/NASA Symposium, edited by C. E. Harris, NASA CP 3274, May, 1994, pp. 563-580.
8. Waterhouse, R. B., "Theories of Fretting Processes," *Fretting Fatigue*, Applied Science Publishers Limited, edited by R. B. Waterhouse, London, England, 1981, pp. 203-219.
9. Hoepfner, D. Adibnazari, S. and Moesser, M. W., "Literature Review and Preliminary Studies of Fretting and Fretting Fatigue Including Special Applications to Aircraft Joints", Final Report, DOT/FAA/CT-93/2, April, 1994.
10. Connor, Z. M., Fine, M. E., and Moran, B., "A Study of Fatigue Crack Generation and Growth in Riveted 2024T3 Specimens", *Proceedings of FAA-NASA Symposium on Continued Airworthiness of Aircraft Structures*, 1996, Atlanta, GA, pp. 631-642.
11. Connor, Z. M., Li, W., Fine, M. E. and Achenbach, J. D., "Fatigue Crack Initiation and Growth in Riveted Specimens", *International Journal of Fatigue*, Vol. 19, Supp. No. 1, 1997, pp. S331-S338.
12. Connor, Z. M., Fine, M. E. and Achenbach, J. D., "Fatigue Crack Initiation and Propagation on Hidden Surfaces: Riveted Joints of Alclad 2024", presented at The First Joint DoD/FAA/NASA Conference on Aging Aircraft, July 8-10, 1997, Ogden, Utah, in press.
13. Connor, Z. M., M. E. and Achenbach, J. D., "Acoustic, Electron and Optical Microscopy Visualization of Surface and Sub-surface Cracks", *Review in Progress in Quantitative Nondestructive Evaluation*, Vol. 17B, eds. (Plenum, NY, 1997), pp. 1581-1588.

N
2
SINCE 2010

NON-CONTACT ULTRASONIC NDE SYSTEMS FOR AGING AIRCRAFT

Robert E. Green, Jr. and B. Boro Djordjevic
Center for Nondestructive Evaluation
The Johns Hopkins University
Baltimore, MD 21218-2689, USA
Telephone: 410/516-6115
Telefax: 410/516-7249
e-mail: robert.green@jhu.edu

526-38

1999037200

371697

81

ABSTRACT

This paper will describe the advantages of non-contact ultrasonic systems under development for the early detection of fatigue and corrosion damage in aging aircraft.

INTRODUCTION

Since aircraft of current design are complex, expensive structures and since the present funding situation severely limits the construction of new aircraft, there is an ever increasing need to assure their longer safe service life. Unnecessary time spent on the ground is uneconomical from a financial viewpoint and can be disastrous from a military viewpoint. Therefore, it is imperative that advanced reliable nondestructive evaluation techniques be developed to detect both fatigue and corrosion damage in aircraft currently in service. In order to survey a large structure accurately, economically, rapidly, and truly nondestructively, it is important to develop and optimize non-contact methods. Among the limited number of non-contact nondestructive evaluation techniques ultrasonics plays a prominent role. This has recently been emphasized in a National Research Council report entitled "Aging of U.S. Air Force Aircraft." Ultrasonics is listed under every critical NDE inspection need for aging aircraft.

ORIGIN OF FATIGUE DAMAGE

Fatigue damage resulting in microcrack and subsequent macrocrack formation constitutes one of the primary mechanisms for loss of structural integrity leading to failure of aircraft components. It has been well documented for all types of fracture that nucleation of cracks in metals occurs as a result of inhomogeneous plastic deformation in microscopic regions. This inhomogeneous plastic deformation can be in the form of slip bands, deformation bands, mechanical twinning, or localized strain concentration at grain boundaries, precipitates, dispersed particles, and inclusions. Moreover, the mechanisms responsible for these regions of inhomogeneous plastic deformation are all based on dislocation interactions. In particular, dislocation interactions with point defects, with other dislocations, with stacking faults, with grain boundaries, and with volume defects are known to create regions of severe localized plastic deformation, which develop into microcracks, which either coalesce or grow into macrocracks leading to ultimate fracture.

DETECTION OF FATIGUE DAMAGE

The ideal nondestructive evaluation technique would permit very early detection of fatigue damage so that proper assessment of the severity and rate of severity increase of the structural damage leading to failure can be made. Thus the most sensitive NDE techniques would be capable of detecting motion and pile-up of dislocations; the next most sensitive techniques would be capable of detecting

microcracks; the least sensitive systems would only be capable of detecting macrocracks. It is practically expedient to have NDE techniques which can successfully detect fatigue damage in each of these regimes since some components can tolerate larger regions of fatigue damage than others without serious concern for the structural integrity of the component. W.D. Rummel et al. (1) conducted a comprehensive statistical analysis of the detectability of artificially induced fatigue cracks in aluminum alloy test specimens. Based on the results of their measurements, it was concluded that the ultrasonic method was the most reliable for crack detection as well as to be the most accurate in measuring crack dimensions.

ULTRASONIC DETECTION OF FATIGUE DAMAGE

Basically, there are three different ultrasonic techniques which lend themselves to detection of the onset of fatigue damage namely body waves, surface waves, and ultrasonic attenuation. Surface wave techniques have been used for fatigue crack detection since 1962 and body wave techniques since 1964. However, both of these techniques are not sensitive to material changes which give warning of fatigue damage prior to macrocrack formation. The surface condition of the structure and proper coupling of transducers to the surface are special problems associated with the use of both body and surface waves.

ULTRASONIC ATTENUATION

In addition to velocity measurements for defect location and sizing, ultrasonic attenuation measurements based on nonlinear effects serve as a very sensitive indicator of internal loss mechanisms caused by microstructural alterations in the material prior to crack formation. These energy absorbing mechanisms are precursors to fatigue crack formation or corrosion damage and may be detected by properly implemented ultrasonic attenuation measurements. The first ultrasonic technique used to study the development of fatigue damage during fatigue cycling was the ultrasonic attenuation technique. As early as 1956, R. Truell and A. Hikata (2) observed changes in ultrasonic attenuation in the early stages of fatigue cycling on polycrystalline aluminum specimens. Similar measurements have continued up to the present time (3-10). Although, for over 40 years, this technique is known to be the optimum one to detect early fatigue damage, it has not proven useful for field use because of the problem of acoustically coupling the transducer to the structure in a reproducible fashion that does not influence the measured attenuation values. Experiments conducted in the early seventies to monitor the development of fatigue damage during cycling of an aircraft aluminum alloy show that ultrasonic attenuation can detect fatigue damage much earlier than conventional ultrasound reflection from a crack (Figure 1).

ULTRASONIC DETECTION OF CORROSION DAMAGE

Although the need to nondestructively detect corrosion damage in military aircraft has been recognized for many years, the fact that many aircraft currently in service are scheduled to fly well past their original design life, greatly increases the requirement for a reliable nondestructive method to detect corrosion. Recently a number of efforts have been initiated to nondestructively detect corrosion in aluminum alloy aircraft components, however, none of these techniques involve ultrasonic attenuation measurements. Since any corrosion product will result in an increase in ultrasonic attenuation, this technique has a very high probability of detecting even small amounts of hidden corrosion.

CONTACT OR WATER COUPLED ULTRASOUND

A major problem associated with the use of piezoelectric ceramic transducers is the requirement that they be acoustically bonded to the test material with an acoustical impedance matching coupling medium such as water, oil, or grease. Often more harmful, is the necessity of coupling the transducers to the test structure by immersing them in tanks of water or using water squirter systems.

Although the couplant allows acoustical energy to propagate into the test material, it causes several problems in addition to potential harm to the material. For velocity measurements, which are necessary for material thickness measurements and to locate the depth of defects, the coupling medium can cause transit time errors on the order of one percent. Partial transmission and partial reflection of the ultrasonic energy in the couplant layer, can lead to serious errors in absolute attenuation measurements. This latter fact is the reason that so few reliable absolute measurements of attenuation are reported in the scientific literature. The character of the piezoelectric transducer itself exerts a major influence on the components of the ultrasonic signal, since conventional transducers are limited in their frequency response and, since they are in contact with the surface of the material to be tested, they can load this surface and thereby modify the ultrasonic wave itself.

NON-CONTACT ULTRASOUND

A method of non-contact generation and detection of ultrasound is therefore of great practical importance. A non-contact technique affords the opportunity to make truly non-contact ultrasonic measurements at elevated temperatures, in corrosive and other hostile environments, in geometrically difficult to reach locations, in outer space, and to do this at relatively large distances from the test structure surface. These techniques greatly increase the capability of testing large structures without the present necessity of a coupling medium or either immersing the test material in a water tank or using water squirter coupling. Several non-contact ultrasonic techniques are presently available in various stages of development, namely capacitive pick-ups, electromagnetic acoustic transducers (EMATs), laser beam optical generators and detectors, and more recently air(gas)-coupled ultrasonic systems (Figure 2).

However, as the name implies, capacitive pick-ups cannot be used as ultrasonic generators and, even when used as detectors, the air gap required between the test structure surface is extremely small, which in essence causes the device to be very nearly a contact one. EMATs, on the other hand, have been successfully used for material defect characterization particularly in metal parts. One major problem with EMATs is that the efficiency of ultrasound generation and detection rapidly decreases with lift-off distance from the surface of the test object. They can obviously only be used for examination of electrically conducting materials. Because of the physical processes involved they are much better detectors than generators of ultrasound.

Laser ultrasonics affords the opportunity to make truly non-contact ultrasonic measurements in both electrically conducting and non-conducting materials, in materials at elevated temperatures, in corrosive and other hostile environments, in geometrically difficult to reach locations, and do all of this at relatively large distances, i.e. meters, from the test object surface. However, although laser ultrasonics has been under development for over 20 years (11) it has not yet been optimized. This is because expensive high power lasers are required for ultrasound generation and often to obtain an ultrasonic wave of sufficient amplitude to be practically useful, the surface of the test specimen must be ablated. Although much lower power lasers can be used for interferometric detection, unless the surface of the specimen is a good optical reflector, such detection systems will not work. This necessitates either painting the surface with an autoreflective paint or applying a similar stripple coating.

Through early research efforts, adequate knowledge of the physical interactions of laser light with materials has been gained such that commercial providers of laser ultrasonic technology have been established and have been successful in providing laser ultrasonic systems for specific applications. The United States Air Force has been actively supporting both research and development of advanced and applied laser based ultrasonic systems including efforts at Johns Hopkins. Most of this development work has concentrated on replacing conventional ultrasonic inspection systems with laser-based systems, therefore, the laser source and its unique ultrasonic characteristics have not been investigated in ways that could enhance the functionality of laser-based methods compared to their conventional counterparts.

LASER ULTRASOUND SYSTEMS

Laser generation of ultrasound in a material results from a rapid, localized heating of the material brought on by absorption of the laser pulse's optical energy. The rapid heating launches longitudinal waves into the material that partially mode convert to shear waves at the material surface. Unlike conventional piezoelectric transducers, both longitudinal and shear waves propagate through the material and may be detected in a single measurement at points removed from the source region. From this single measurement, both time-of-flight and attenuation may be determined simultaneously for the two ultrasonic modes as they travel through the same material from the source to the receiver. Thus, laser ultrasonic measurements could prove effective in identifying regions of incipient and actual fatigue and corrosion damage in metals.

A primary concern regarding laser ultrasonic systems is the poor signal-to-noise ratio exhibited by signals gathered with systems using laser transmitters and laser-based receivers. Attempts to improve the signal-to-noise of these signals using narrowbanding techniques (producing a toneburst from the laser source) or chirping methods (frequency modulating the source) have produced some success. Even with sophisticated equipment and ideal conditions, demonstrations of signal-to-noise improvements by factors of 3 to 10 are usual for these source modulation techniques. Further improvements to signal-to-noise must necessarily include the effects of the material on the laser ultrasonic signal. The laser ultrasonic process has been modeled successfully for many classes of materials (12). Since models allow predictions of the received laser ultrasonic signal, these models may be used to construct signal processing algorithms by which the signal-to-noise of actual signals may be improved. Indeed, preliminary application of simple methods has produced signal-to-noise improvements of 20-40 dB in ideal systems. Model-based signal processing methods need to be developed and assessed to determine if they can be used to extract the pertinent signal information concerning fatigue and corrosion damage.

LASER/EMAT ULTRASONIC SYSTEMS

For many materials systems, complete laser ultrasonic systems cannot be applied easily owing to the characteristics of optical ultrasonic detectors. For surfaces that are smooth and mirror-like, the receiver must be aligned with the specularly reflected light from the material surface. Such alignment would require contour following. For rough surfaces, light is scattered from the surface such that only a small fraction of the incident light enters the receiver. Large detection lasers must be used to get as much light to the detector as possible. Currently, these lasers are not only large but expensive. In other applications, the remote nature of laser-based reception is not required, but couplant-free transduction is required. EMATs do not require couplants and have been shown to be excellent receivers for laser ultrasound in nonmagnetic metal alloys. In such cases laser generation/EMAT detection systems may be ideal for detection of fatigue and corrosion in metals. EMATs can be constructed that are sensitive to both longitudinal and shear waves such that these can be received and analyzed together. Currently, work at Johns Hopkins is directed towards constructing a broadband EMAT for detection of laser-generated ultrasound (Figure 3). Owing to liftoff consideration, it is difficult to receive ultrasonic signals above 10 MHz using EMAT receivers. However, methods are being investigated to improve their high frequency response.

AIR(GAS)-COUPLED ULTRASOUND SYSTEMS

Air(gas)-coupled ultrasonic systems have been under development for some time and research is underway to optimize them for practical non-contact ultrasonic applications (13). These systems are relatively similar to conventional contact ones and, therefore, when optimized will play an important role in modern nondestructive evaluation. If coupling efficiencies through the air could approach those observed through water or gel couplants, one would expect air(gas)-coupled ultrasonic systems to be extremely inexpensive to implement since they would use, for the most part, the same electronics as conventional contact methods. Furthermore, scanning speeds could be increased,

couplant contamination problems could be eliminated, and complex geometries could be more easily scanned. An air-coupled ultrasonic system was developed in the Johns Hopkins University Center for NDE for C-scan imaging of cracks in wooden panel paintings for the Smithsonian Institution. Even though this unit permits generation of frequencies from below 100 kHz to 20 MHz, the C-scan system is usually operated around 500 kHz due to the currently available air-probe transducers. In addition to transmission C-scan imaging of cracks in wooden panel paintings, the system has been used successfully to scan graphite/epoxy prepregs and graphite/epoxy panels. Current effort is directed at measurement of adhesive bond quality between aluminum plates.

LASER/GAS-COUPLED ULTRASOUND SYSTEMS

Recently a hybrid method has been developed using lasers to generate sound and air(gas)-coupled transducers to detect the laser generated sound (Figure 4). Such a system offers the advantages of remaining remote from the sample and utilizing the most robust subset of both laser and air coupled ultrasonics. Since the laser light conversion to ultrasound takes place immediately beneath the surface of the target material, two of the four interface losses suffered in a fully air(gas)-coupled system would be eliminated. This system has proven successful in the laboratory to inspect graphite/epoxy tape placed cylinders and shows promise for process control of the tape placement process itself. Investigations are planned to investigate the advantages of this system for aging aircraft applications.

CONCLUSIONS

In the near future, new developments in laser ultrasonics, electromagnetic acoustic transducers (EMATs), and air(gas)-coupled ultrasound will permit design and construction of extremely efficient non-contact ultrasonic systems to detect fatigue and corrosion damage in aircraft structures based on both reflection of ultrasonic waves from cracks, but more importantly because of their non-contact nature permit ultrasonic attenuation detection of dislocation pileups, microcrack formation, incipient corrosion and other material changes prior to macrocrack and extended corrosion formation. Progress in these efforts will be highly relevant to the NASA, FAA, and Air Force mission of ensuring the safe, reliable in-service life of aircraft and aerospace vehicles especially those flown well past their original design lives.

REFERENCES

1. W.D. Rummell, P.H. Todd, Jr., R.A. Rathke, and W.L. Castner, "The Detection of Fatigue Cracks by Nondestructive Test Methods," *Materials Evaluation* 32, 205-212 (1974).
2. R. Truell and A. Hikata, "Fatigue in 2S Aluminum as Observed by Ultrasonic Attenuation Methods," Watertown Arsenal Technical Report No. WAL 143/14-47 (1956).
3. Robert E. Green, Jr. and John C. Duke, Jr., "Ultrasonic and Acoustic Emission Detection of Fatigue Damage," *International Advances in Nondestructive Testing*, 6, 125-177, Gordon & Breach, NY (1979).
4. Richard B. Mignogna, John C. Duke, Jr. and Robert E. Green, Jr., "Early Detection of Fatigue Cracks in Aircraft Aluminum Alloy Sheets," *Materials Evaluation* 38, pp. 37-42 (1980).

5. Robert E. Green, Jr., "Effect of Metallic Microstructure on Ultrasonic Attenuation," *Nondestructive Evaluation: Microstructural Characterization and Reliability Strategies*, Otto Buck and Stanley M. Wolf (eds.), Metallurgical Society of AIME, Warrendale, Pa, pp. 115-132 (1981).
6. Robert E. Green, Jr., "Nondestructive Acoustic Testing for Fatigue Damage," *McGraw-Hill Yearbook, of Science & Technology 1985* McGraw-Hill Book Co., New York, pp. 291-294 (1984).
7. Robert E. Green, Jr., "Nondestructive Materials Characterization," *Proceedings of 31st Army Sagamore Materials Research Conference, Materials Characterization for Systems Performance and Reliability*, J.W. McCauley and V. Weiss (Editors), Plenum Press, N.Y., pp. 31-58 (1986).
8. R.E. Green, Jr., *Nondestructive Evaluation of Materials, Annual Review of Materials Science* 20, 197-217 (1990).
9. Robert E. Green, Jr., "Non-Contact NDE Techniques," *Proceedings of The Air Force 3rd Aging Aircraft Conference, Wright-Patterson Air Force Base, Dayton, OH*, pp. 549-578 (1995).
10. R.E. Green, Jr., "Emerging Technologies for NDE of Aging Aircraft Structures," to be published in *Nondestructive Characterization of Materials in Aging Systems*, R.L. Crane et al. (Eds.), Materials Research Society, Vol. 503 (1998).
11. C.B. Scruby and L.E. Drain, *Laser Ultrasonics: Techniques and Applications*, Adam Hilger, Bristol, UK (1990).
12. J.B. Spicer and J.W. Wagner, "Comprehensive Modelling of Laser Ultrasonic Waveforms for Materials Characterization," *ASME AMD Acousto-Optics and Acoustic Microscopy*, 140, 163-179 (1992).
13. Allison Murray, Marion F. Mecklenburg, C.M. Fortunko, and Robert E. Green, Jr., "Air-Coupled Ultrasonic System: A New Technology for Detecting Flaws in Paintings on Wooden Panels," *Journal of the American Institute for Conservation* 35, 145-162 (1996).

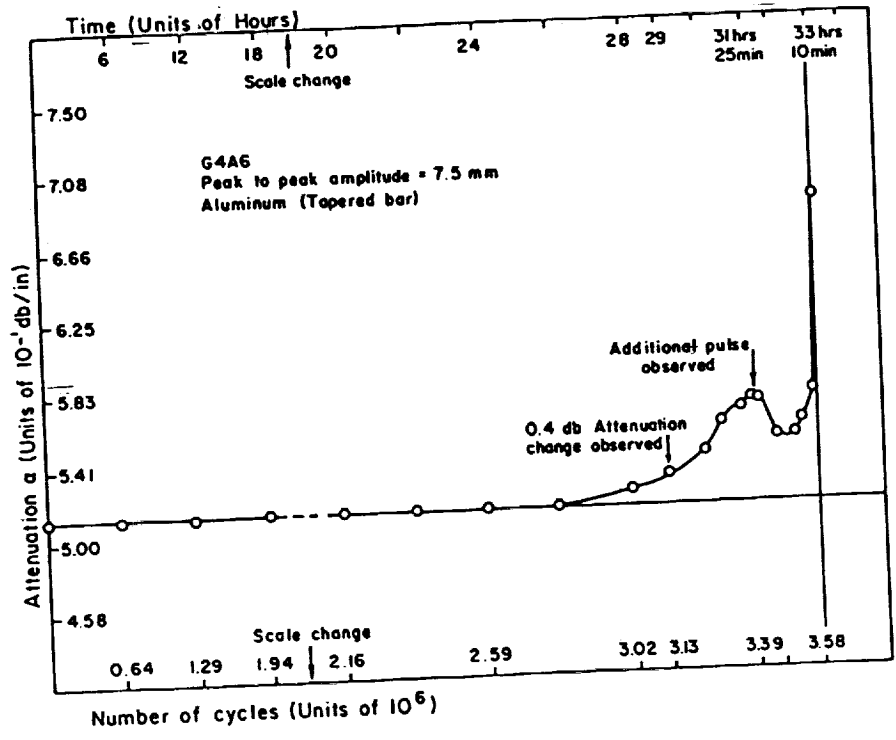


Figure 1. Ultrasonic Attenuation Gives Early Warning of Fatigue Failure in Aircraft Aluminum Alloys

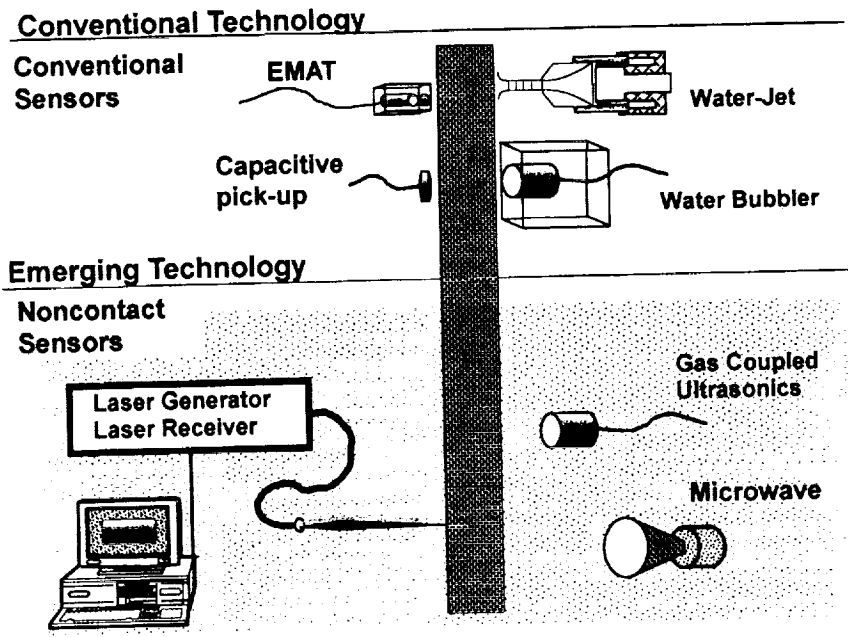


Figure 2. Conventional and Emerging Non-Contact Ultrasonic Techniques

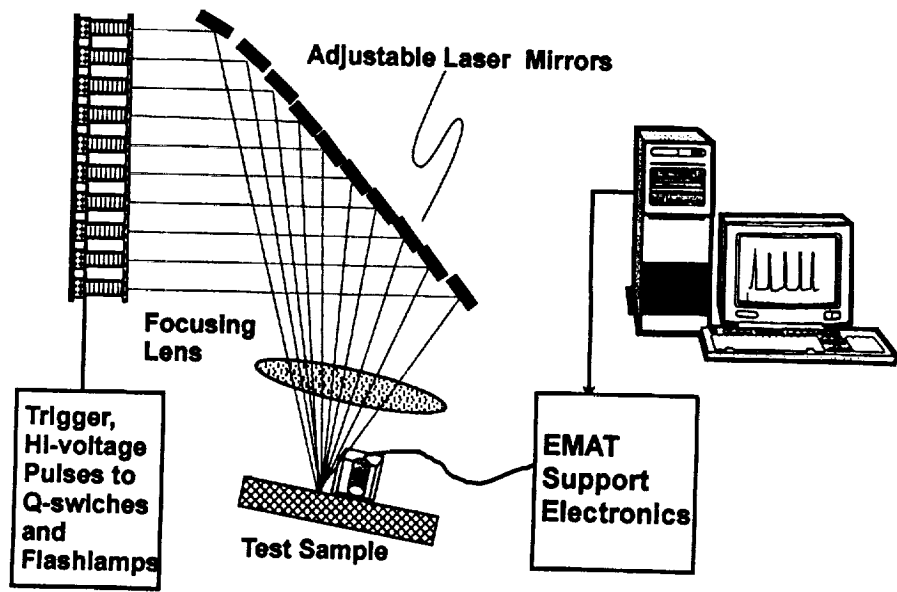


Figure 3. Ten Cavity Nd:YAG Laser System to Generate Narrow-Band Ultrasound with EMAT Detector

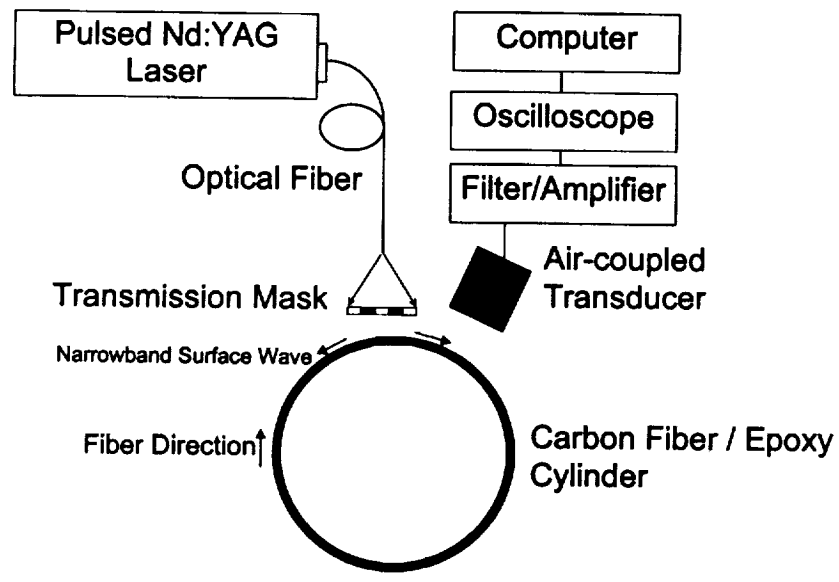


Figure 4. Laser Generation/Air Coupled Detection System for Graphite/Epoxy Cylinder Inspection

Evaluation of the Self-Nulling Rotating Eddy Current Probe System

**By: Don Hagemmaier and Kent Rengel
Boeing, Long Beach, CA**

**Buzz Wincheski and Min Namkung
NASA Langley Research Center, Hampton, VA**

**Presented at:
The Second Joint NASA/FAA/DoD Conference on Aging Aircraft
Aug. 31 - Sept. 3, 1998
Williamsburg, VA**

Abstract

In order to detect multi-site fatigue cracks located under flush-head rivets, automated eddy current equipment is required. To assure a reliable system, the eddy current probe must be centered easily over the installed rivets. To meet these requirements, the NDE Group at NASA LaRC developed the Self-Nulling Rotating Eddy Current Probe System (SNRECPS) which will be referred to as RPS in this document. The system was evaluated at the FAA, NDI Validation Center, in Albuquerque, New Mexico. The system was capable of detecting a 0.032 inch long crack with a 90/95% PoD.

Further evaluations were conducted at Boeing in Long Beach, California. These evaluations included fatigue cracks and notches in a range from 0.025 to 0.100 inch long under flush-head aluminum rivets and titanium or steel flush-head fasteners. The results of these tests are reported herein.

Subsequently, the system was loaned to the USAF Structures Laboratory for the purpose of detecting and measuring short cracks under flush-head rivets in a variety of fatigue test specimens. The inspection task was to detect and plot crack growth from numbered fasteners in lettered rows.

In January, 1998, the system was taken to Northwest Airlines Maintenance Base, in Atlanta, to inspect a DC-9, for multi-site cracks in three circumferential splices. The aircraft had 83,000 cycles. The inspection was conducted at 30 kHz from longeron 5 left to longeron 5 right. The system was calibrated using a 0.030 EDM first layer notch. The instrument gain was set to 19 mV from the notch. The reject level was set at 10 mV and the unflawed fasteners yielded a signal amplitude of 2 to 3 mV. Only one fastener location, out of about 2,500 tested, yielded a signal of 58 mV. The rivet was removed and visually evaluated. It appeared to be a slight gouge in the counter-sink zone. No fatigue cracks were detected. The same fastener locations were also inspected using the Boeing MAUS system at 60 kHz. No cracks were detected.

Thus far, the rotating probe eddy current system has been found to be very user friendly and capable of detecting first layer cracks on the order of 0.030 inch long or longer.

Introduction

During the course of this research, the Boeing NDE engineers validated the Self-Nulling Rotating Probe System (RPS) for the purpose of determining applications and limitations of the system for transfer of the technology to the aircraft operator's NDI personnel.

The Rotating Probe System, for the detection of fatigue cracks under airframe fasteners was developed and tested by NASA LaRC engineers prior to the end of 1993, which was less than one year after the original discovery of the Self-Nulling Probe effect.

. The Rotating Probe Method has been refined and built into a portable prototype instrument. Probability of Detection (PoD) testing of the system was performed at AANC hanger at Sandia National Laboratory in Albuquerque NM during the Spring of 1995. The results from this exercise were promising, but highlighted the need for further refinement. A second generation probe, based on the Sandia results, was developed and the results with a 90/95 % PoD was for a 0.032 inch long first layer crack in a 0.040 in. thick skin.

Several improvements have been incorporated into the latest version of the Rotating Probe System (see Figure 1). Hardware improvements have led to reduced weight, increased probe rotation speed, and simplification of the system assembly while increasing the overall robustness of the system. The main software enhancement has been the addition of the automated centering routine. Logic has been added to the software to calculate the position of the probe relative to the rivet center. This information is then displayed on the computer screen (along with the raw data) with an update rate of about 10 frames/second. The operator uses this feedback in order to position the probe over the fastener center. Once the probe is aligned, the data is processed and displayed in a second plot. In the default operating mode data acquisition will halt once the probe alignment criteria are met. This allows for the operator to interpret the data without having to maintain alignment of the probe over the rivet. Once data interpretation is completed, the button on the rotating probe head can be clicked to reactivate data acquisition.

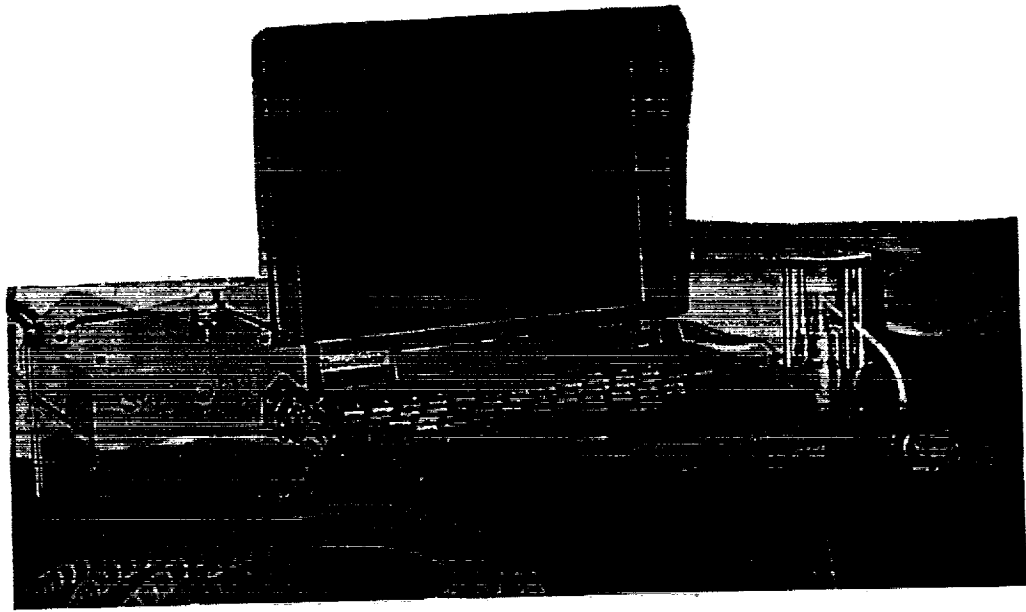


Figure 1. NASA LaRC Self-Nulling Rotating Probe Eddy Current System

Figure 2 shows the data display for a 0.035 inch long fatigue crack under an airframe rivet. The plot on the left side of the screen is a polar plot of the raw data acquired by the Self-Nulling Probe during one revolution about the rivet. The bulge in the otherwise circular plot is caused by the presence of the fatigue crack under the rivet head. Also contained within this plot is a dashed circle with (default) radius of 0.15 volts and an alignment vector from the origin to a location slightly below and to the right of the plot center. Alignment of the probe about the rivet is determined by this vector. The probe head is moved so as to bring the endpoint of the vector toward the origin. Once the length of the vector is below the radius of the dashed circle, the probe is determined to be aligned over the fastener. At this point, the data will be processed and the second plot will illuminate.

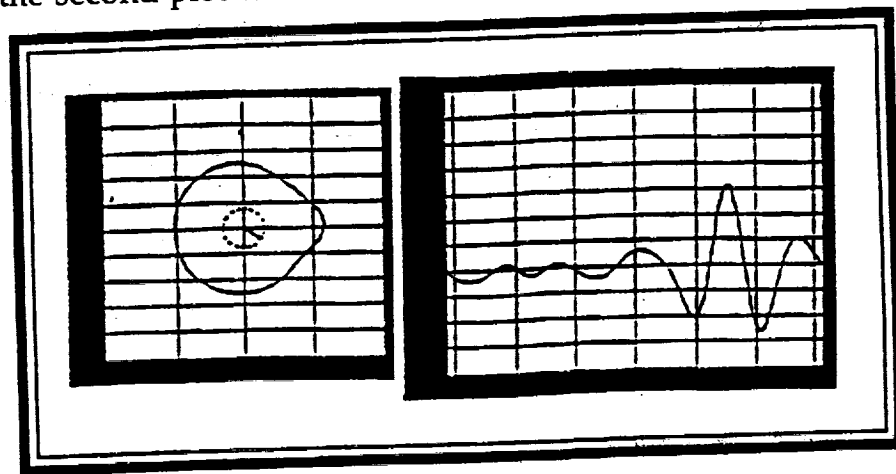


Figure 2. Real-time data display of Rotating Probe System. Displayed data is for 0.0935 inch fatigue crack under airframe rivet

The plot on the right side of the display shows the results of the spatial fourier bandpass filtering applied to the raw data. This is a Cartesian plot of the processed probe output amplitude versus angular position ($-\pi$ to π radians). This plot clearly shows the effects of the fatigue crack located - 1.5 radians (90 degrees.) from the top of the rivet. Above the plot, the peak amplitude of the processed data is presented (31.7 mV). This value is compared with a threshold (8 mV default) to determine if the rivet contains a flaw and the light adjacent to the peak value is illuminated accordingly.

One of the tasks of the Boeing contract was the detection of short cracks under installed flush-head fasteners (aluminum, titanium, and steel). This study consisted of designing and fabricating flawed (i.e., cracks plus notches) standards for the evaluation by the Rotating Probe System (RPS). The goal of the study was to determine the detectable crack/notch size in first and second layers in 0.063 and 0.082 inch thick skins.

System Evaluations

Instrument Evaluation Using Reference Standards

Initial tests were run using the crack/notch reference standards which were fabricated for a prior task. The design of the standards, having flush-head aluminum and steel fasteners is shown in Fig. 3. The standards contained both first layer cracks and notches ranging in size from 0.025 to 0.100 inch in length. The second layer contained only notches ranging in size from 0.025 to 0.100 inch in length.

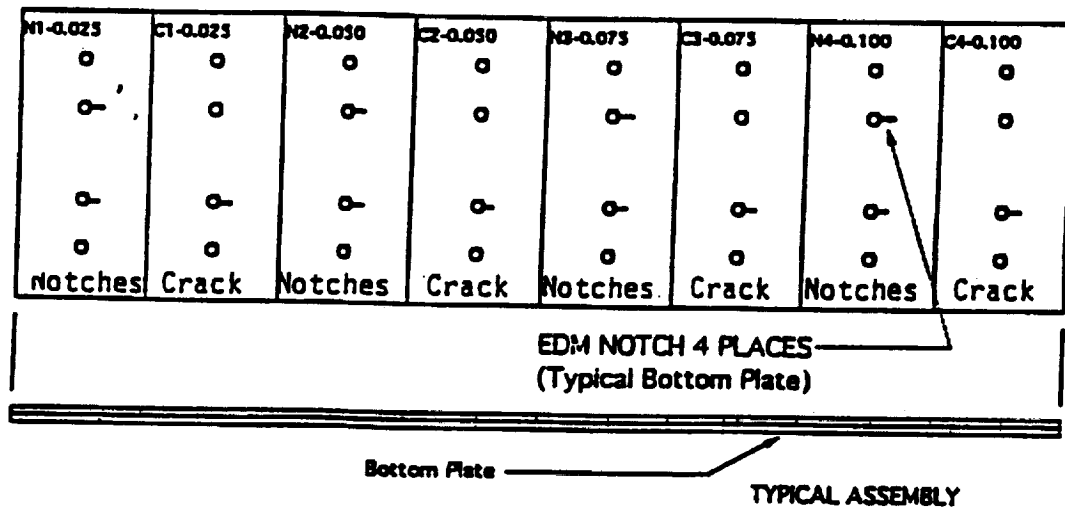


Figure 3. Cracked/Notched Reference Standards

The signal from an unflawed aluminum rivet yielded a response of 1.4 mV and for the 0.025 inch crack, 4.4 mV which yields a signal-to-noise ratio of 3.1 to 1. Generally,

a signal-to-noise ratio of 3 to 1 is usually sufficient for a reliable inspection. However, the Sandia tests required a 0.032 inch crack to achieve a 90/95% reliability.

The results obtained from the first layer cracks (C) and notches (N) under aluminum rivets is given in Table 1.

The signal obtained from an unflawed steel fastener was 7.2 mV which is considerably larger than obtained from the unflawed aluminum rivets of 1.4 mV. Clearly defined signals could not be obtained from the 0.025 and 0.050 inch long notches or cracks under the steel fasteners. The signal from the 0.075 inch notch was 31.2 mV and from the crack, 24.5 mV. The signal-to-noise ratio from the notch was 4.3-to-1 and for the crack, was 3.4-to-1. The signal from the 0.100 notch was 54 mV which yields a signal-to-noise ratio of 7.5 to 1 (see Table 1). The first layer detection was performed at 60 kHz

The scanning radius of the probe must be increased to keep the coil off the rivet due to the design of the probe. Contact of the ferrite ring of the probe with the steel fasteners causes very erratic signals and inaccurate data. Increasing the scanning radius by 1/4 segment (1/128 inch - 0.0078) increased detection reliability but the polar plot of the raw data was still not concentric and the Cartesian plot of the processed data had noise up to the 10% level. The plot images were printed and the set-up data recorded.

The operating frequency was reduced to 7 kHz to detect the second layer notches. The probe scanning radius was the same as used for first layer steel fasteners. The background noise at 7 kHz was 0.0. The 0.025 and 0.050 inch long notches could not be detected. The 0.075 inch notch yielded a signal of 11.2 mV and the 0.100 notch yielded a signal of 13.9 mV.

The 0.063 inch thick aluminum standards with notches and cracks (reported above) were re-scanned to verify repeatability of the instrument and set up data. All amplitude readouts were within +/-2% of previously saved data.

Stainless set screws were used to replace the steel ones used for lift-off and rotation adjustment. The steel screws were becoming stripped out from repeated adjustments.

EAA Equivalent Initial Flaw Size Specimen Tests

Description - Some 16 flat panel specimens, simulating 4 joint designs, were fabricated and delivered to the Structures Laboratory at WPAFB in Dayton for fatigue testing. The test plan required periodic inspection using eddy current (for cracks under fastener head) and microscopic (after the crack extended past the head of the rivet) to measure crack size. The test are to be terminated when the lead crack grows into a hole or links up with other multiple site damage (MSD). A tear-down

Table 1

Test Results for Flush-Head Al Rivets and Steel Fasteners
(Ref. Figure 3)

Notch location	Crack location	Length	Position	Response	Radius setting	Centering radius	File name
N1	/	.025"	90	3.7 mV	#6	.100 V	N1-025
N2	/	.050"	90	13.8 mV	#6	.100 V	N2-050
N3	/	.075"	90	36.0 mV	#6	.100 V	N3-075
N4	/	.100"	90	46.9 mV	#6	.100 V	N4-100
No Flaw	/	0	N/A	1.4 mV	#6	.100 V	N3-000
/	C1	.025"	90	4.4 mV	#6	.100 V	C1-025
/	C2	.050"	90	14.0 mV	#6	.100 V	C2-050
/	C3	.075"	90	25.3 mV	#6	.100 V	C3-075
/	C4	.100"	90	38.9 mV	#6	.100 V	C4-100
/	No Flaw	0	N/A	2.0 mV	#6	.100 V	C2-000
/	C3	.075"	90	24.5 mV	#6	.100 V	Fe C3-075
/	C4	.100"	90	22.9 mV	#6 1/4	.100 V	Fe C4-100
/	No Flaw	0	N/A	7.2 mV	#6 1/4	.100 V	Fe NF-000
N3	N3	.075"	90	31.2 mV	#6 1/4	.100 V	Fe N3-075
N4	N4	.100"	90	54.0 mV	#6 1/4	.100 V	Fe N4-100

inspection will be conducted and a Electron Microscope (SEM) will be used to determine crack sizes vs. number of cycles and to reveal undetected cracks.

The test panels are 22' wide by 56" long. Eight of the panels are fuselage longitudinal splice configurations, four being lap joint splices with .063" thick skins and four being butt splices with 0.086" skins.

Four (Type 2 Undoubler Lap Splice) panels with 0.063" thick 2024-T3 skins were inspected before shipping to WPAFB. The splice joints used 3/16" aluminum fasteners in three rows of 19. The top (A) and bottom (C) rows were the inspected critical rows. The "no flaw" amplitude responses ranged between 1.0 and 2.5 millivolts (mV) based on a set up of 3.1 mV on the 0.025" first layer notch, and 13.7 mV on a 0.050" notch.

Some of the panels had indications that required the fasteners to be removed and new fasteners installed. It was determined that these indications were caused by ferrous inclusions (possibly from the counter sinking tool) between the fastener head and the countersink. The indications ranged from 12.2 mV to 33.4 mV amplitude (about 0.030" and 0.063" notch equivalent). The fasteners that were removed in the C-row, of the Type 2 lap splice panels, were under the head of the longeron which made automatic installation of the rivets impossible. Reinstallation of the rivets caused dimpling of the panel and misalignment of the fastener head, at panel #2-C15 location causing the probe not to center align.

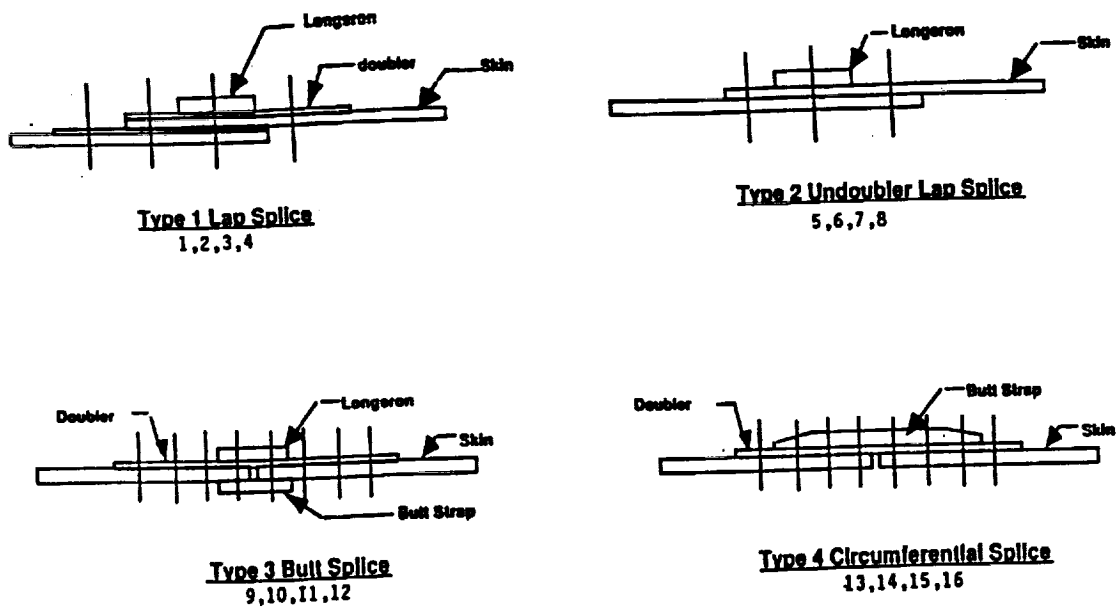


Figure 4. EIFS Splice Configurations

It was a good thing that that the newly assembled panels were scanned and the flaws found or the inspectors at WPAFB would have made false calls causing the eddy current inspection to be suspect.

The reference standards were fabricated and one set was sent to WPAFB to calibrate the instrument prior to inspection. They contain EDM notches with sizes ranging from 0.030" through 0.075" in length.

Dr. William Winfree, NASA LaRC, arranged for a Self-Nulling Rotating Probe (SNRP) system to be loaned to WPAFB for the EIFS program. Boeing engineers prepared a written operating instructions for the SNRP system to be used by the USAF inspectors.

The EIFS objective is to determine the equivalent initial flaw size distribution inherited in fuselage splice joints by experiment and crack growth analysis. The Self-Nulling Rotating Probe activity is associated with a study of the development of small flaw NDE for aerospace structures (Task 27) and an attempt to publish Self-Nulling probe procedures in the Boeing, Douglas Products Division, Non-Destructive Testing Standard Practice Manual (NDTSPM) as part of a technology transfer under Task 27, Phase II.

In October, NASA LaRC sent Long Beach the software upgrade on a 3.5" floppy. The upgrade included a simplified data storage and retrieval system, a revised second layer inspection program, and a new third layer inspection program (for Boeing lap joints). The results obtained with the new upgrade compared favorably with the previous version. Results were typical in that the upset fasteners that are bucked into the countersinks generally have about a 10% to 20% less amplitude than fasteners inserted into the countersink side.

WPAFB Visit -

In August 1997, the eddy current procedure, calibration standards, and the SNRP system was delivered to the USAF Structures Laboratory. The system was similar to the one at Boeing, Long Beach, except some adjustments were made to the software for second layer crack detection. The system did very well detecting the notches and stress cracks in the Figure 3 standards.

The standards that were manufactured by a vendor arrived at Long Beach only a few days before the trip was scheduled. The system had difficulty detecting the 0.030" and 0.040" notches in these standards. In most instances, the probe would not find the center of the fasteners and lock on to take an amplitude reading. It was concluded that the fasteners, which were bucked into the countersinks, were installed incorrectly. These standards were taken back to Long Beach and were disassembled which revealed poor filling of the countersink by the bucked fastener shanks. The standards were re-assembled, re-tested, and returned to WPAFB.

The NDT personnel, performing the inspections at WPAFB, are contracted inspectors. They arrived on August 14 and the NASA/Boeing team demonstrated the rotating probe system and went over the set up and calibration procedures for the EIFS panel inspection.

SNRP Inspection at WPAFB

All the fasteners were clearly identified for reporting purposes and an inspection sheet was provided for each assembly which identified the fastener rows to be inspected.

The WPAFB personnel sent us a plot of crack length versus cycles which showed a jogging (up/down) in the crack growth curves (Fig. 5). A phone conversation with the WPAFB personnel revealed that this jogging was caused by changing the probe rotation radius for first and second layer crack detection and not properly adjusting it between inspections. A phone call was made to NASA LaRC to ask if they could provide a second scanning head so that the inspectors could leave the scanning radius fixed between inspections, i.e., one scanner for first layer detection and a second for second layer detection. The second scanner solved the problem (see Figure 6).

The SNRP system will be returned to NASA LaRC upon completion of the EIFS testing at the USAF Structures Laboratory.

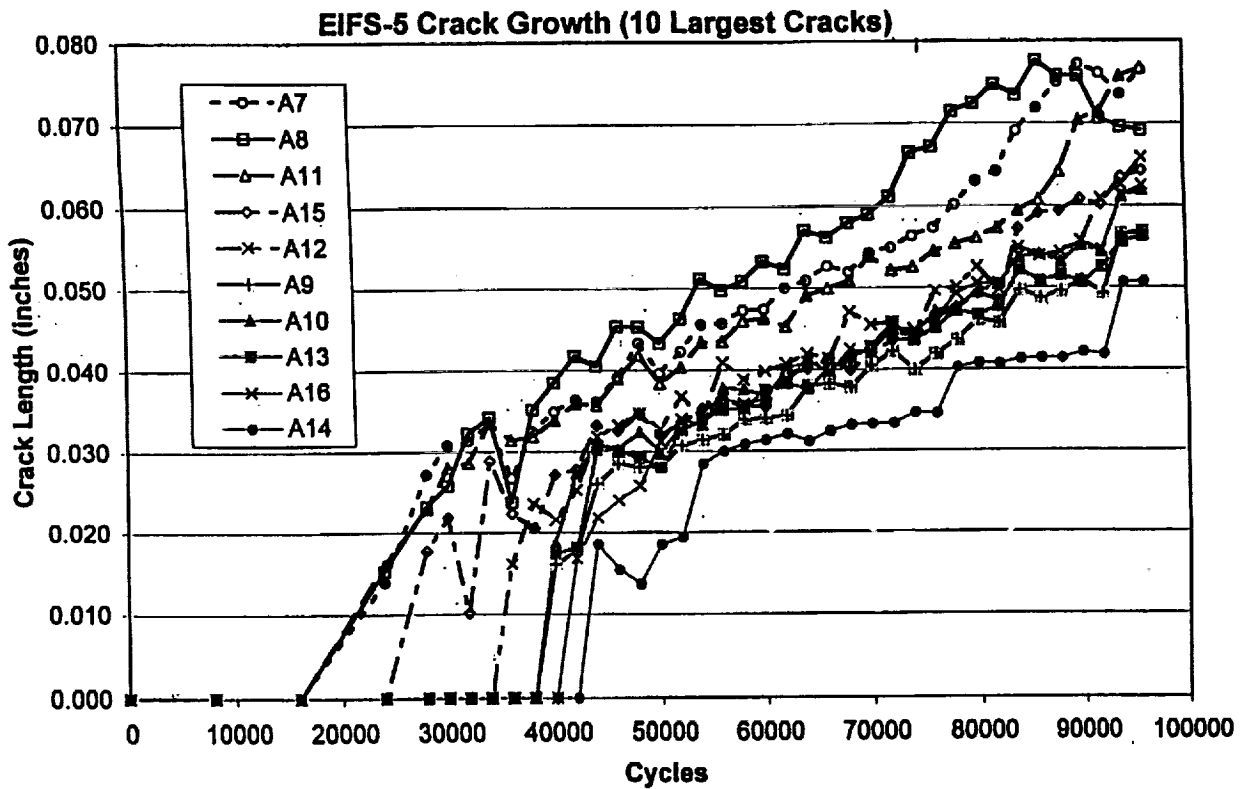


Figure 5 EIFS Erratic Crack Growth Plot

FAA/Boeing EIFS Testing

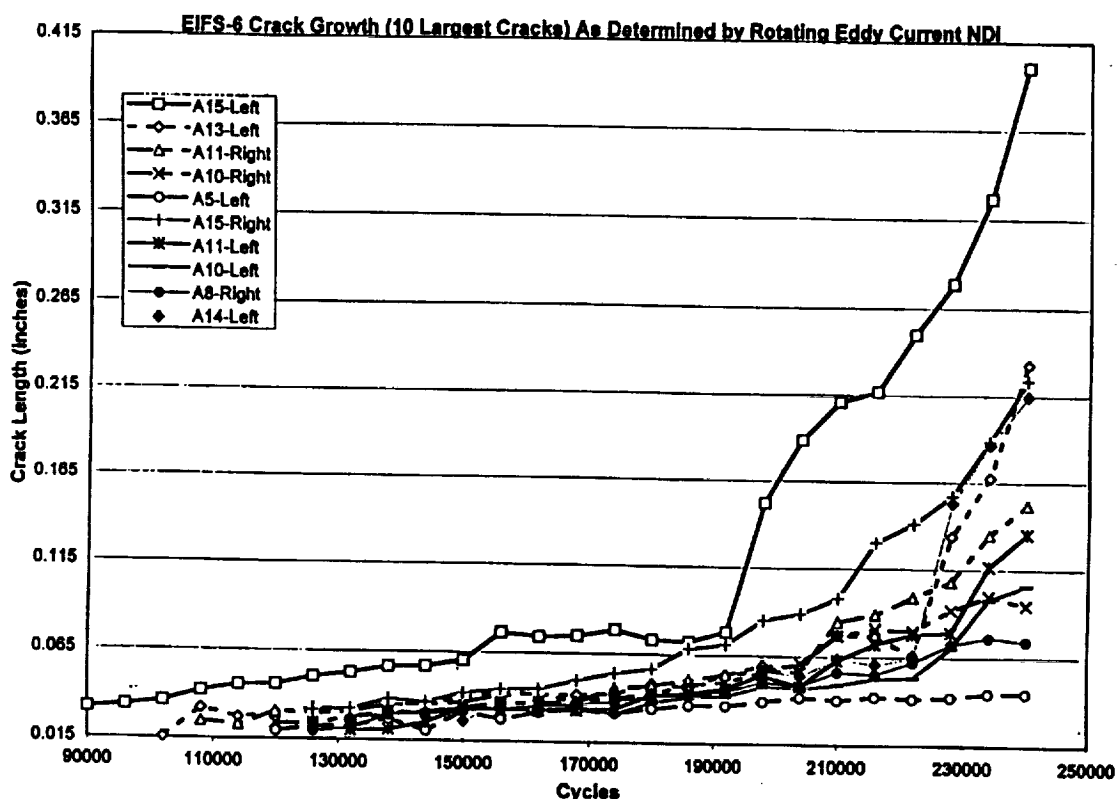


Figure 6. EIFS Uniform Crack Growth vs. Cycles Plot

SNRP System Validation

In order to validate the system, it needed to be evaluated on a high time (possibly cracked) aircraft. The authors contacted the Boeing, Douglas Products Division (DPD), Customer Service to arrange for a high time aircraft for inspection. A few selections were made but, for one reason or another, were canceled. Finally, DC-9 Fuselage 205, which had about 83,000 cycles became available for inspection at Northwest Airlines Maintenance Base in Atlanta.

The area selected for inspection was the three circumferential splices shown in Figure 7. The splices require eddy current inspection, for skin cracks, per DC-9 Series 20/30 SID NDI Manual. The inspection zone is from longeron 5 left to longeron 5 right.

On January 28 and 29th, a NASA/Boeing team went to Northwest to inspect the three splices with the SNRP System. Also in attendance were two engineers from Foerster Instruments who plan to market the SNRP System.

The system was operated at 60 kHz and calibrated to first layer EDM notches 0.030" and 0.075" long. The instrument gain was set at 19 mV from the 0.030" notch and 85 mV from the 0.075" notch. The rejection threshold was set at 10 mV. The background noise from the fasteners was 2 to 3 mV which yielded a good signal-to-noise ratio. Sta. Y=229 had 4 fastener rows and Sta. Y=588 and Y=803 had 6 fastener rows.

The inspection went very well and only one fastener, out of about 2,500, yielded a signal of 58 mV. The fastener was removed and visually and eddy current inspected. The open hole was re-evaluated with the SNRP system and found to be acceptable. Visual inspection confirmed a slight gouge in the countersink. The gouge was removed and a fastener installed.

The same three joints were eddy current inspected at 60 kHz, using the Boeing, St. Louis MAUS (Mobile Automated System). No flaw indications were obtained. The validation trip was considered very successful.

Boeing Seattle Evaluation

The scanner was received at Boeing, Seattle, in April 1997 for about a one month evaluation. A piece of fuselage skin from an in-service aircraft that has known size fatigue cracks was used for evaluation. The evaluation was done by Dave Doneux. The fifteen fastener locations had the following size cracks and millivolt (mV) readings:

<u>Fastener</u>	<u>Crack Size"</u>	<u>Millivolts</u>
1	.060	62.0
2	.040/.050	23.7
3	none	5.9
4	.030/.035	*2.5
5	.050	30.5
6	none	10.1
7	.070	47.6
8	.030/.030	*18.8
9	.030/.050	18.0/29.8
10	.050/.060	27.0/47.4
11	.070	26.0
12	.040	20.9
13	none	12.4
14	none	19.7
15	.035	*5.8

* Not Detected- Gate level set at 20 mV

All cracks that were 0.040" (1mm) or greater in length were detected. This equates to a 20+ millivolt signal (fastener #12). However the background noise (for uncracked fastener locations) ranged from 5.9 to 19.7 mV.

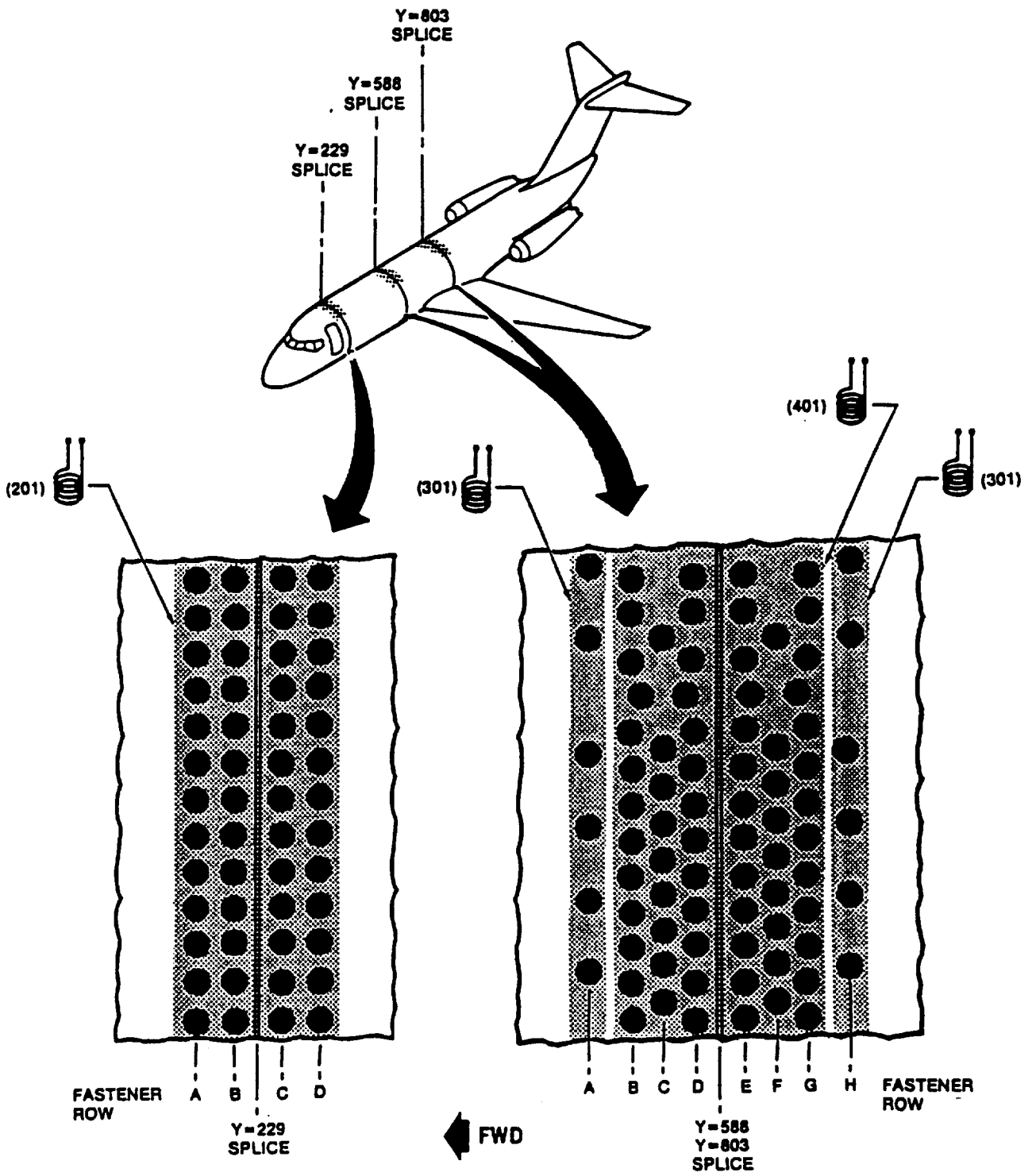


Figure 7. Circumferential Skin Splices

All cracks that were 0.040" (1mm) or greater in length were detected. This equates to a 20+ millivolt signal (fastener #12). However the background noise (for uncracked fastener locations) ranged from 5.9 to 19.7 mV.

Summary

Advantages:

1. One advantage of these SNRP system is that the software will not collect data until the probe is centered over the fastener.
2. The method used to change the probe's radius is good.
3. The detectable crack sizes (in inches) are:
 - 1st layer 0.040 thick at 60 kHz was 0.032 (Sandia PoD).
 - 1st layer 0.040 thick at 50 kHz was 0.040 (see 3.7).
 - 2nd layer 0.063/0.063 thick at 6 & 3.5 kHz was 0.100 (see 3.8).
 - 3rd layer 0.040/0.040/0.040 thick at 3.5 kHz was 0.15 (see 3.7).
 - 3rd layer 0.040/0.040/0.040 thick at 3.5 kHz was 0.100 regression fit and 0.120 binary fit (Sandia PoD).
4. Flaw detection repeatability is very uniform in response (mV).
5. The system is very user friendly.

Disadvantages:

1. The system cannot detect first layer cracks less than 0.075 inch long under flush-head steel fasteners.
2. The base of the probe housing that contacts the aircraft should have feet that contact in three locations rather than the flat plate presently used. This would improve fastener visibility and allow more stability on curved surfaces.
3. Frequency change should be made easier with an external adjustment.
4. If the instrument could also be made to run on dc current it would be more portable/useable.

THERMAL WAVE NDI OF DISBONDS AND CORROSION IN AIRCRAFT

Xiaoyan Han, L.D. Favro and R.L. Thomas
Wayne State University
Institute for Manufacturing Research and Department of Physics
Detroit, MI 48202, U.S.A.
Tel: (313)577-2970, 2727, 2792
Fax: (313)577-7743
han@thermal.physics.wayne.edu
skip@thermal.physics.wayne.edu
Bob@thermal.physics.wayne.edu

ABSTRACT

We describe advances in the application of thermal wave imaging to NDI of disbonds and corrosion in aging aircraft. This technique uses an infrared (IR) video camera to image the surface of the aircraft after the application of a short pulse of heat. The heat is applied by high-power xenon flash lamps. The camera and flashlamps are connected to the control computer by a 50-ft cable. This design makes it highly portable, as well as suitable for robotic manipulation. The computer is used to process the digital video data stream from the IR camera, as well as to display the resulting images. The imaging requires only a few seconds per square foot of aircraft surface. The system is capable of detecting and measuring as little as 1% metal material loss. Disbonded metal-to-metal doublers are readily detected, and disbonds and delaminations in graphite and boron fiber composite structures can be imaged and their depths measured. Examples of disbonds as deep as 36 plies under a boron patch are presented, along with an example of discrimination of impact damage on a ply-by-ply basis in a carbon fiber composite.

1. INTRODUCTION

Thermal wave imaging is carried out by using a flashlamp source to apply a spatially uniform pulse of heat to the part. An infrared video camera, under the control of a lunchbox computer, is then used to nondestructively image and characterize subsurface defects in aircraft, as shown schematically in Fig. 1. The system is portable, and can be operated by a single inspector, who can readily move around the aircraft. Figure 2 shows a photograph of the pulse echo thermal wave imaging system in operation to inspect a B747 aircraft for the presence of disbonded internal doubler structures. Two of the authors are shown operating the system from an extendable lift platform, from which they are using the hand-held imager. The imager consists of the infrared video camera, the flashlamp heat source, and a shroud which is used to direct the energy from the flashlamps onto the surface of the aircraft. This inspection was made with the computer also located on the lift platform. However, the imaging head is connected to the computer controller and power supplies for the flashlamps through an umbilical cable which is 50 feet in length, which permits operation with all the other equipment being located remotely.

In operation, the inspection of a square foot (or so) of the aircraft requires only a few seconds, and results in a sequence of thermal wave images, taken at a selectable set of time delays following the heat pulse, and corresponding to different depths beneath the surface. The electronic hardware and software for the system also allows the operator to set up several small areas of interest in the field of view, for which the temperature can be plotted as a function of time for the purpose of obtaining quantitative information about the depth of the defects beneath those regions. In this paper, we present examples in which these capabilities are utilized for inspection of composite and metal aircraft structures.

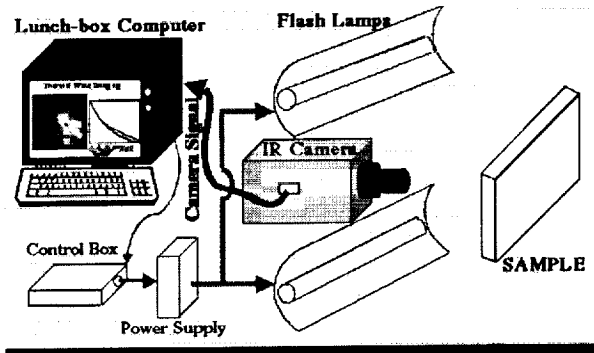


Fig. 1 Schematic diagram of the thermal wave imaging system.



Fig. 2 Photograph of the pulse echo thermal wave imaging system in operation to inspect a B747 aircraft for the presence disbonded internal doubler structures. Two of the authors are shown operating the system from an extendable lift platform, from which they are using the hand-held imager.

2. THERMAL WAVE IMAGING OF DISBONDS AND DELAMINATIONS IN COMPOSITES

In another paper from this Conference,¹ Dr. Michael T. Valley presents an extensive review of the results of a structured experiment evaluating thermal wave imaging systems for field-level inspection of composite structures on C-130, C-141, and F-15 aircraft by U.S. Air Force (USAF) personnel. Therefore, in this paper, we will only show a few examples of such images. In Fig. 3, we show the capability of the technique to image aluminum honeycomb structure beneath the five plies of boron-fiber-reinforced composite skin in a region of an F-15 test specimen. The image shown in Fig. 3 contains one type of representative defect: a machined core (simulated skin-to-core disbond), which is evident from the missing walls of the aluminum honeycomb (dark) in that region of the image.

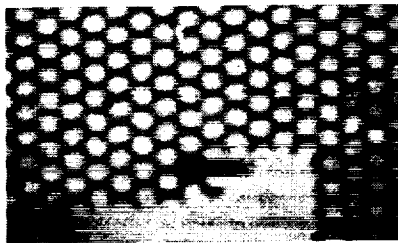


Fig. 3 Representative thermal wave image of an F-15 test specimen, showing a region of machined core.

Another example of simulated delamination/disbonds is shown in Fig. 4. This image was taken on a C-141 wing plank doubler calibration sample, from which pull tabs were removed after the adhesive curing process to produce air gap defects. In this example, the boron skin thicknesses ranged up to 15 plies, with the pull tabs placed between adjacent plies, a few plies up from the wing plank.

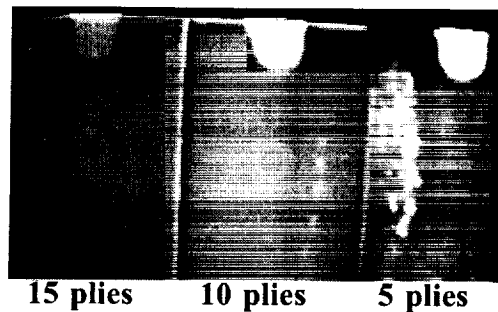


Fig. 4 Thermal wave image of simulated delamination/disbonds in boron composite doublers.

Although the previous two examples were for imaging through less than fifteen plies of boron composite skin, it is possible to image much deeper defects. Figure 5 shows a fabricated disbond underneath 36 plies of boron composite doubler on an L-1011 door structure. The disbond extends out from the 36-ply region, through the ply-drop-off region, to the edge of the doubler.



Fig. 5 Fabricated disbond underneath 36 plies of boron composite doubler on an L-1011 door structure. The disbond extends out from the 36-ply region, through the ply-drop-off region, to the edge of the doubler.

Delaminations can originate from impact damage in composite skins. An example thermal wave image of such damage is shown in Fig. 6, one of a sequence of thermal wave images which was taken following a heat pulse on a graphite epoxy test panel. Several delaminations are revealed, rotated from one another at 45° angles. The rotation is the result of the fiber tow rotation from ply to ply, together with the fact that the elliptically shaped delaminations follow the fiber directions.

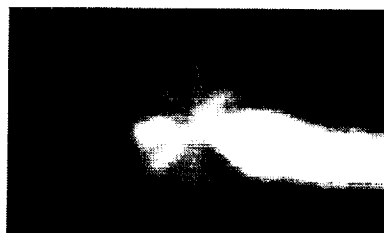


Fig. 6 Impact damage on a graphite composite panel, showing a set of elliptically shaped delaminations, together with a large delamination extending to one edge of the panel. The elliptical delaminations are rotated from one another at 45° angles, the result of the fiber tow rotation from ply to ply, together with the fact that delaminations follow the fiber directions.

An important class of composite structures used in commercial aviation are sound-deadening structures used in engine cowlings. An example of such a structure with a large number of programmed defects² is shown in Fig. 7 and Fig. 8, together with a hand-drawn sketch of the intended shapes and placements of the defects. The core material of this panel is aluminum honeycomb. Its skin consists of two layers. The one closest to the core is perforated fiberglass composite, with the perforation sizes and spacing being small compared to the size of the cells of the honeycomb. This is topped with a second skin of very fine metal mesh. These various layers are intended to deaden different parts of the audio spectrum from the engine. In this particular specimen, defects have been placed both between the mesh skin and the fiberglass layer, and between the fiberglass and the core. In many of these cases, the skin-to-core defects underlie the defects

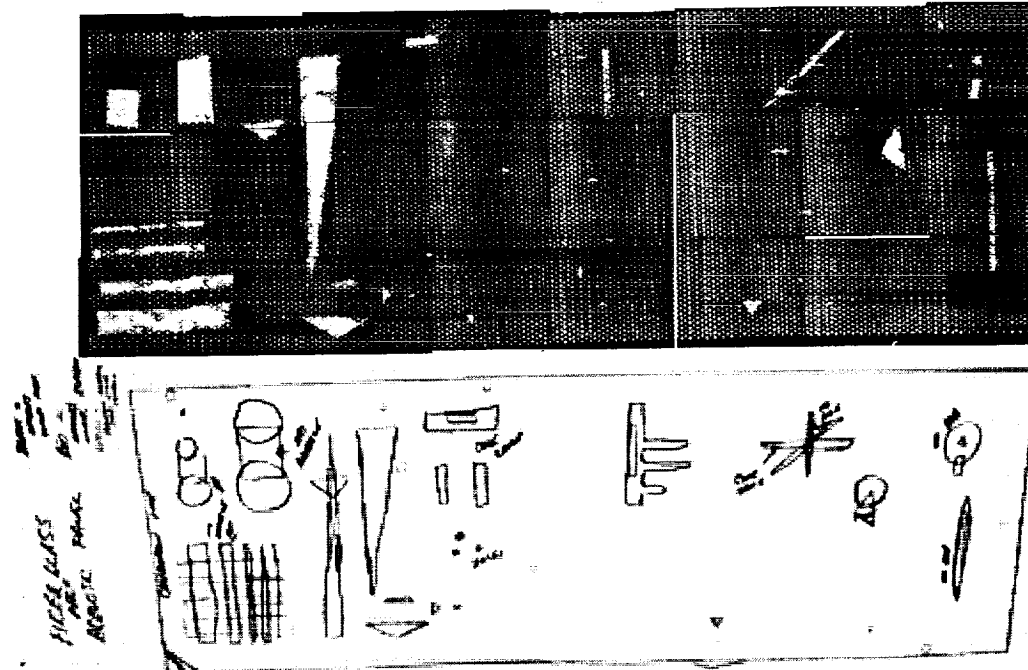


Fig. 7 Early-time thermal wave image of simulated defects between the wire mesh and the composite skin of a sound-deadening composite structure, whose core is aluminum honeycomb. The intended placement of defects is shown in the hand drawn sketch. The deeper defects appear in the following (later time) thermal wave image of Fig. 8. The background pattern arises from the perforations in the fiberglass layer between the mesh and the core.

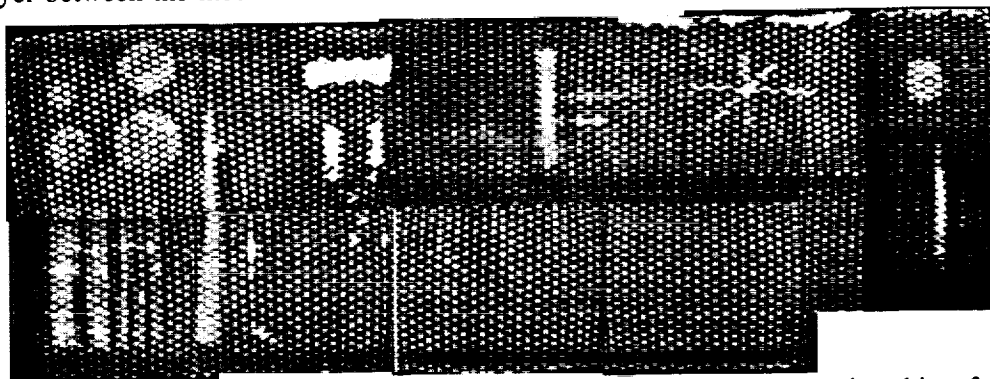


Fig. 8 Later-time thermal wave image of simulated defects between the composite skin of a sound-deadening composite structure and the aluminum honeycomb core. The intended placement of defects is shown in the hand drawn sketch. The shallower defects were shown in the preceding (earlier time) thermal wave image of Fig. 7. The background pattern (coarser grained than that in Fig. 7) reveals the walls of the honeycomb core.

between the wire mesh and the fiberglass, thus resulting in overlapping defects in the images. Figure 7 is an early-time thermal wave image showing the set of defects between the wire mesh and the fiberglass, as well as the small perforations in the fiberglass itself. Fig. 8 is a later thermal wave image revealing the deeper defects, as well as the structure of the cells in the honeycomb core. A comparison of Figs. 7 and 8, with reference to the sketch (shown in Fig. 7) shows that both sets of defects can be detected, including situations where defects overlap one another. In addition, in the left center of Fig. 8, one sees a number of defects such as that shown in Fig. 3, in which the core is damaged or cut away.

3. THERMAL WAVE IMAGING OF FLUID INTRUSION IN COMPOSITES

Thermal wave imaging can readily detect the presence of corrosion in the honeycomb region of composites. As an example of this capability, in Fig. 9 we show two thermal wave images of a composite spoiler structure, whose nomex honeycomb core had extensive fluid intrusion. The left image in Fig. 9 was taken from above the spoiler, and the right image was taken with the same surface of the spoiler held above the camera, allowing gravity to move the fluid toward the skin/honeycomb boundary. The fluid shows as dark regions, because of its heat-sinking influence at the skin.



Fig. 9 Thermal wave images of a composite spoiler structure, whose nomex honeycomb core had extensive fluid intrusion. The image taken from above shows wicking of the fluid up to the skin. When the spoiler is turned over and imaged from below, the fluid collects at the skin.

Fluid ingress can also be detected when it occurs in aluminum honeycomb composite structure, such as is used in the construction of the F-15 rudder (see Fig. 10).

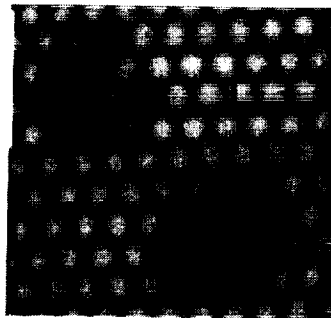


Fig. 10 Thermal wave images of fluid intrusion in the aluminum honeycomb core beneath a boron composite skin. The upper left region (dark gray) contains hydraulic fluid in the cells, whereas the lower right (black) contains water. The three squares have been placed on the image by the thermal wave imaging software, and indicate regions for which temperature-time curves will be plotted (described later in this paper).

4. THERMAL WAVE IMAGING OF SUBSURFACE CORROSION

Under the auspices of the U.S. Air Force, Dr. Michael O. Howard of ARINC has carried out a structured experiment to determine suitable NDE techniques for the inspection of C/KC-135 and B-52 fasteners in wing skins for the presence of corrosion. On the basis of the results of that ARINC experiment, two techniques were selected. One of these was an ultrasonic imaging technique, utilizing a so-called "dripless bubbler", developed by Dr. David Hsu and his colleagues at Iowa State University. The second was thermal wave imaging, in the form being discussed in this paper. There were 80 wing fasteners which were inspected in that structured experiment, and the WSU participation is exemplified in Fig. 11, which shows a comparison between one of our thermal wave images and the destructive optical images of the same fasteners.

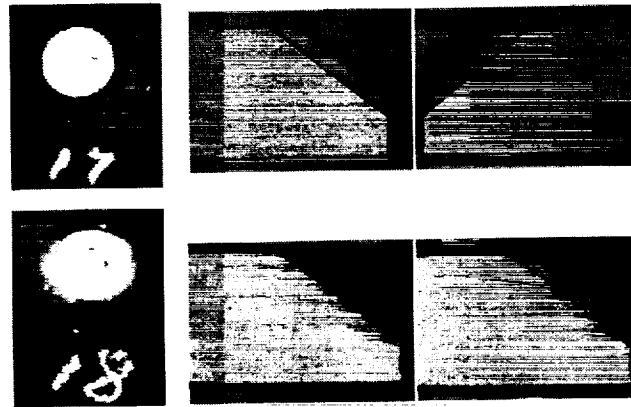


Fig. 11 Thermal wave images of intergranular corrosion in the vicinity of a C/KC-135 wing fastener (#18, lower left), together with optical images of sections of the countersink area. Corresponding images of an uncorroded fastener (#17, top row of images) is included for comparison.

5. QUANTITATIVE DEPTH DETERMINATIONS BY THERMAL WAVE ANALYSIS

Quantitative estimates of the depths of various defects can be made by means of thermal wave analysis. In previous work by this research group,³ we have shown that automated numerical analysis of the relative signals over corroded and uncorroded regions of an aircraft skin can be used to measure their relative skin thicknesses (and hence, the percentage of material loss in the corroded region) with a sensitivity and accuracy of about 1% material loss. To illustrate, we plot the comparison between thermal wave measurement and direct micrometer measurement of material loss in an aluminum corrosion calibration panel in Fig. 12.

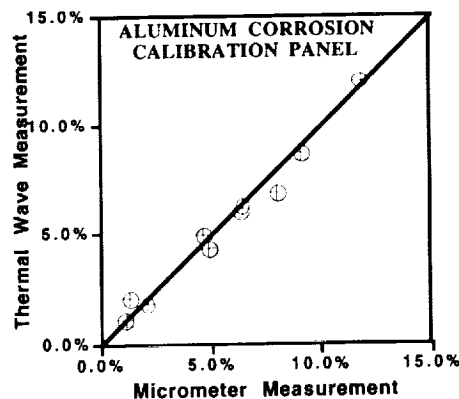


Fig. 12 Comparison between the thermal wave measurement and direct micrometer measurement of percentage material loss over an aluminum corrosion panel. The results show excellent agreement down to 1% material loss.

The time-dependence of the thermal wave signal on a region of the surface over a flaw, when compared to that over an undamaged region, can be used to measure the depth of the flaw. The time-dependence over a thick, undamaged region is inversely proportional to the square root of the time. Therefore, we plot the temperature-time behavior on a log-log scale. On such a plot, the undamaged region should show as linear, with a slope of minus one half. When a subsurface flaw, such as a delamination/disbond, is underneath the region of surface being plotted, thermal wave reflections from the boundary of the flaw return to the surface and cause a deviation from the inverse square root of the time, and do so beginning at a time which is proportional to the square of the depth to the flaw. This approach may be illustrated by revisiting the thermal wave image shown in Fig. 4, which is shown again in Fig. 13, together with four square regions of interest for which temperature-time plots are shown in Fig. 14. The square law behavior between the defect depths and the break times for these regions is shown in Fig. 15.

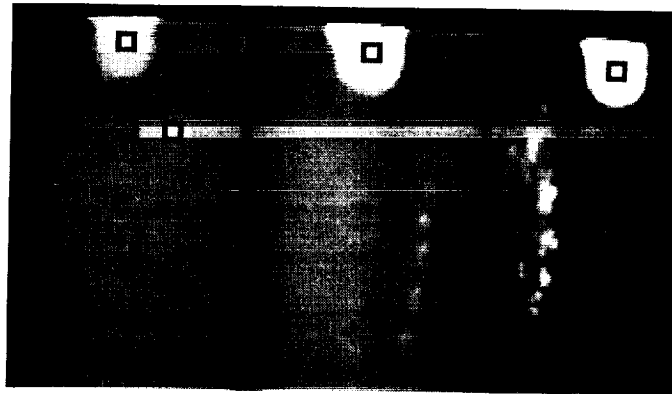


Fig. 13 Thermal wave image of three boron doublers over an aluminum plate, previously shown in Fig. 4, with four square regions of interest used to obtain the temperature-time curves in Fig. 14.

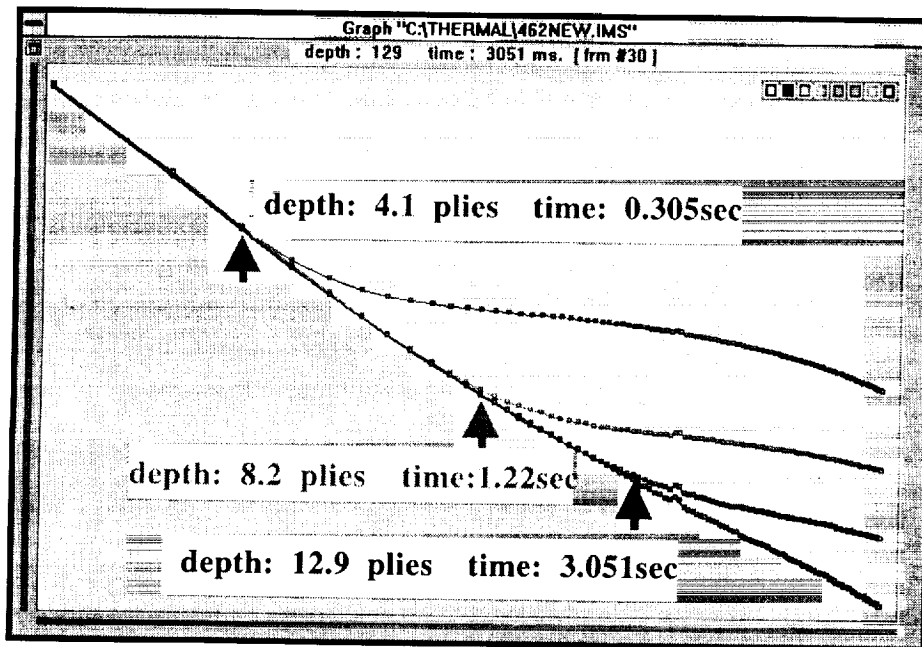


Fig. 14 Temperature-time curves (log-log scale) over the four regions indicated in the thermal wave image in Fig. 13. The curves over the top right, top middle, and top left delamination/disbonds break away from the reference curve at times which scale as the square of the depths, with assumed depths of 4 plies, 8 plies, and 13 plies, respectively. The square law relationship between the break time and the defect depth is shown in Fig. 15.

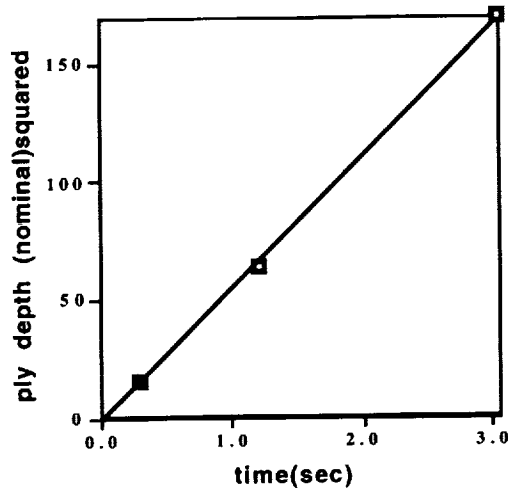


Fig. 15 Square law relationship between the break time and the defect depth, using the data from Fig. 14.

It may be noted in Fig. 14 that the reference region produces a log-log plot which is not quite a straight line. At early times, the behavior is influenced by the finite heat pulse width, and, at later times, by the fact that the skin is relatively thin. Consequently, the inverse square root behavior with time is not followed exactly. Nonetheless, Fig. 15 shows that the break times still are proportional to the squares of the depths, thus providing a quantitative tool for finding defect depths from thermal wave images. In practice, the operator need only calibrate on one known depth on a calibration sample, and the software will subsequently provide values of the depths for all other depths when the operator clicks the mouse to indicate the break points on corresponding temperature-time curves.

Another example of the application of this quantitative depth measurement is provided by the delamination sequence from impact damage on the graphite composite panel whose thermal wave image was shown earlier in Fig. 6. This image, together with a set of regions of interest, is shown again in Fig. 16. Using temperature-time plots similar to those shown above, we obtained the square behavior between delamination depths and break times shown in Fig. 17.

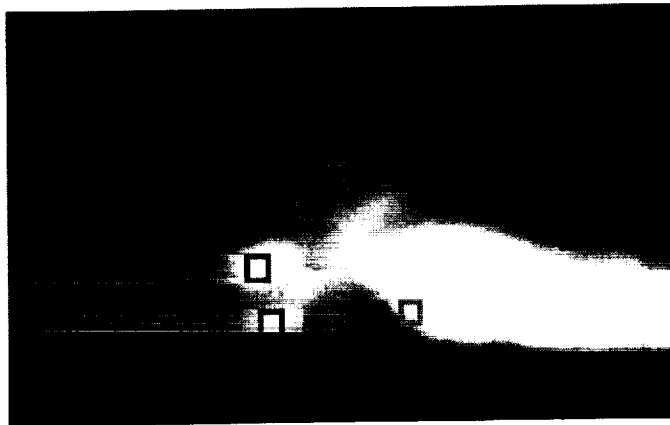


Fig. 16 Thermal wave image of impact-damage-induced delaminations in a graphite composite plate, previously shown in Fig. 6, with six square regions of interest used to obtain the plot shown in Fig. 17.

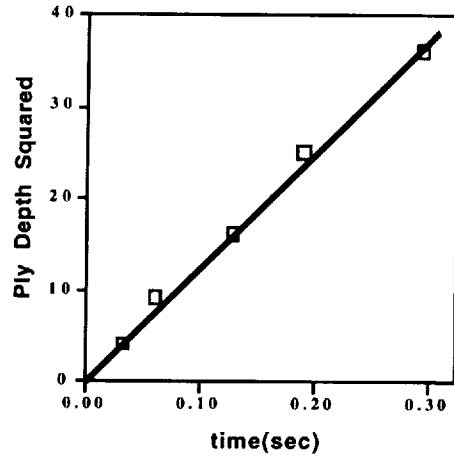


Fig. 17 Plot of the square of the deduced delamination depths, in units of a ply thickness, against break times measured from temperature-time plots in the regions of interest indicated by the squares in Fig. 16. This plot shows that the delaminations are in consecutively deeper plies, 2, 3, 4, 5, and 6 plies beneath the surface, with each delamination region rotated by 45° from the previous delamination.

6. CHARACTERIZATION OF FLUID INGRESS IN HONEYCOMB COMPOSITE CORE

We showed earlier, in Fig. 10, that thermal wave imaging can readily detect fluid ingress in aluminum honeycomb beneath boron composite skin, such as may occur in F-15 rudder structures. If we plot the temperature-time curves for the three regions indicated in Fig. 10 (see Fig. 18), it is

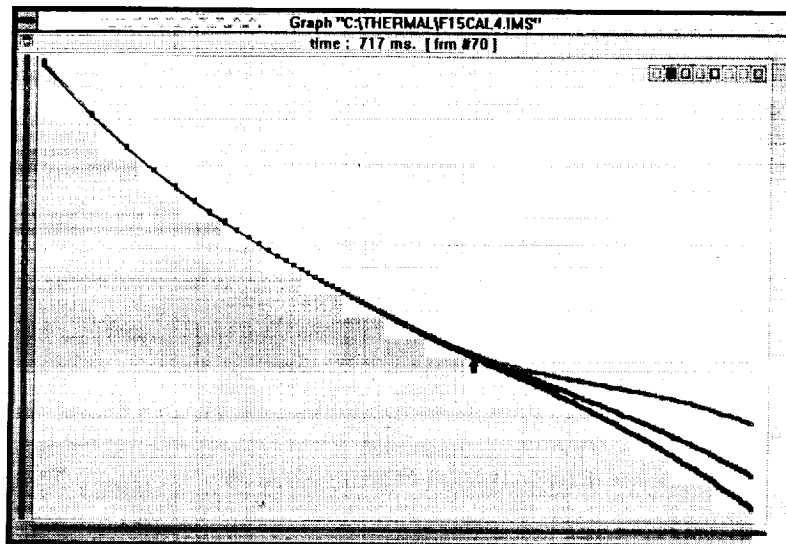


Fig. 18 Temperature-time plots for the three regions of interest indicated in the thermal wave image of fluid ingress, shown in Fig. 10. The top curve is the reference, the middle curve is for the hydraulic fluid ingress region, and the lower curve is for the water ingress region.

apparent that both the hydraulic fluid ingress and the water ingress regions are located at the same depths, namely beneath the five-ply composite skin, as indicated by the fact that the curves break from the background curve at the same time. It is also interesting to note that the curves at times later than the break time deviate from one another, as well as from the reference curve. The curve for water ingress decreases more rapidly, as one might expect because of its greater heat capacity. Thus,

it is possible from such plots, not only to locate the depth of these particular defects, but also to characterize them in terms of their different thermal properties.

CONCLUSIONS

Thermal wave imaging is a technique with numerous useful applications for NDE of aircraft structures. In this paper we have presented only representative examples of our own work in this area. In addition to the planned field use by the U.S. Air Force for composite inspection and for wing fastener corrosion inspection, which we have referred to and illustrated in this paper, there has been extensive use of the method for quality control in the F-22 Advanced Tactical Fighter Program.⁴ BF Goodrich Aerospace has carried out a probability of detection analysis, comparing thermal wave inspection with several other NDE techniques for application to metal skin/metal honeycomb structures for the NASA X-33/Venturestar space vehicle.⁵ The Navy is also using the technique for inspection of composite propellers on E2/C2 aircraft at the Cherry Point NADEP.⁶ It may therefore be concluded that thermal wave imaging is rapidly coming of age as an NDE method for aerospace applications, and it can be expected to find numerous other applications in the future.

ACKNOWLEDGMENTS

The authors would like to thank D. M. Ashbaugh and M.T. Valley of the FAA/AANC; S.R. Baughman of Lockheed Martin; R.J. Ducar of Nordam; M.A. Howard of ARINC; J.O. Taylor of BF Goodrich Aerospace; and S.M. Shepard of Thermal Wave Imaging, Inc., for useful discussions. The research was sponsored by the DOT/FAA William J. Hughes Technical Center's Airworthiness Assurance Center of Excellence (AAACE), under Contract Number DTFA-03-98-D-00008, and by the Institute for Manufacturing Research, Wayne State University.

REFERENCES

- ¹ M.T. Valley, D.P. Roach, L.R. Dorrell, D. M. Ashbaugh, and R. T. Mullis, "Evaluation of Commercial Thermography Systems for Quantitative Composite Inspection Applications," paper presented at this Conference.
- ² Test panels of this composite construction were kindly prepared by Mr. Robert Ducar of The Nordam Group, Tulsa, Oklahoma.
- ³ "Quantitative Thermal Wave Imaging of Corrosion on Aircraft," X. Han, L.D. Favro, T. Ahmed, Z. Ouyang, L. Wang, X. Wang, F. Zhang, P.K. Kuo, and R.L. Thomas, *Rev. Prog. in Quant. Nondestr. Eval.*, Vol. 16, Ed. D.O. Thompson and D.E. Chimenti, Plenum Press, New York, pp. 353-356 (1997).
- ⁴ "Applications for Thermal NDT on Advanced Composites in Aerospace Structures," Steve R. Baughman, *SPIE Vol. 3361*, pp. 311-319, 1998.
- ⁵ "Inspection of Metallic Thermal Protection Systems for the X-33 Launch Vehicle Using Pulsed Infrared Thermography", John O. Taylor and Henry M. Dupont, *SPIE Vol. 3361*, pp. 301-310; "Thermographic Inspection of Metallic Honeycomb Sandwich Structures," John Taylor and Henry Dupont, 25th Annual Review of Progress in Quantitative Nondestructive Evaluation, Snowbird, UT, 23 July, 1998, Plenum, to be published.
- ⁶ Private communication by Dr. Steven Shepard, Thermal Wave Imaging, Inc., Lathrup Village, MI.

AGING OF AIRFRAME MATERIALS: PROBABILITY OF OCCURRENCE VERSUS PROBABILITY OF DETECTION

D. Gary Harlow and Robert P. Wei
Department of Mechanical Engineering and Mechanics
Lehigh University
19 Memorial Drive West
Bethlehem, PA 18015-3085, USA
610-758-4127 (phone)
610-758-6224 (fax)
dgh0@lehigh.edu

ABSTRACT

The reliability of airworthiness assessment and the management of aging fleets of aircraft depend critically on the quality of tools for predicting damage nucleation and accumulation and its detection, i.e., on the interrelationship between the probabilities of occurrence and detection. To illustrate these interrelationships, a mechanistically based probability approach for one plausible scenario involving localized pitting corrosion and subsequent fatigue crack nucleation and growth is presented. A probability of detection based on typical non-destructive evaluation data is used for comparison and probabilistic assessment. The results suggest that the probability of detection using the state-of-the-art techniques is inadequate, and damage size should be quantitatively characterized as a part of an effective airworthiness assurance methodology. An appropriate nondestructive inspection target for damage sizes of about 0.10 mm with a probability of detection and a confidence level of sizing of at least 90% is suggested, versus the current capability of detection of 1.27 mm with a probability of detection of only 50%.

1. INTRODUCTION

Airworthiness, in a structural context, requires the assurance of continued structural integrity and safety of an aircraft throughout its planned period of operation from its current state to the next scheduled inspection and maintenance. Its accurate assessment depends critically on the development of a quantitative methodology that integrates information from state-of-the-art nondestructive evaluation (NDE) with validated methods for prediction of damage accumulation and structural integrity assessments. The mechanistic aspect of damage accumulation and the probabilistic aspects of its evolution and distribution are not adequately addressed in current methodologies. The criticality, or structural significance, of damage in relation to its probability of detection (PoD) by NDE techniques is not well established. In this paper, the issue of probability of damage occurrence (PoO) versus PoD is considered in terms of a mechanistically based probability model for plausible mechanisms of damage accumulation, or aging, in airframe materials. Specifically, a simplified mechanistic model for pitting corrosion and corrosion fatigue cracking in a typical airframe aluminum alloy (*e.g.*, 2024-T3) is used to illustrate the critical functions of modeling and detecting structural damage. The dichotomy between the PoO of structurally significant damage and the probability of its detection and the impact of PoD on the reliability of airworthiness assessments are highlighted.

2. POO, POD AND AIRWORTHINESS IN PERSPECTIVE

The overall problem in aging aircraft life extension and management (*i.e.*, in ensuring airworthiness) may be understood with the aid of Fig. 1. Airworthiness is typically assessed in relation to the "current or

initial state” of the structure (*i.e.*, at the time of schedule inspection and maintenance). To manage the maintenance and life extension of aircraft structures, a broad range of quantitative tools and supporting data are needed to assess their “*current state*” (*i.e.*, their integrity or safety) and to make probabilistic predictions regarding their “*future state*” (*i.e.*, their continued operational safety). These tools and databases are used to assess the airworthiness of the as-inspected structure and how it might be altered by damage accrued during subsequent service. For these assessments, a set of structural analysis and life prediction tools based on the “*pristine*” initial state and validated by experimentation and service experience, is typically used, in conjunction with NDE information on the current state of the aircraft. They, then, serve as a basis for certification, maintenance planning and overall fleet management.

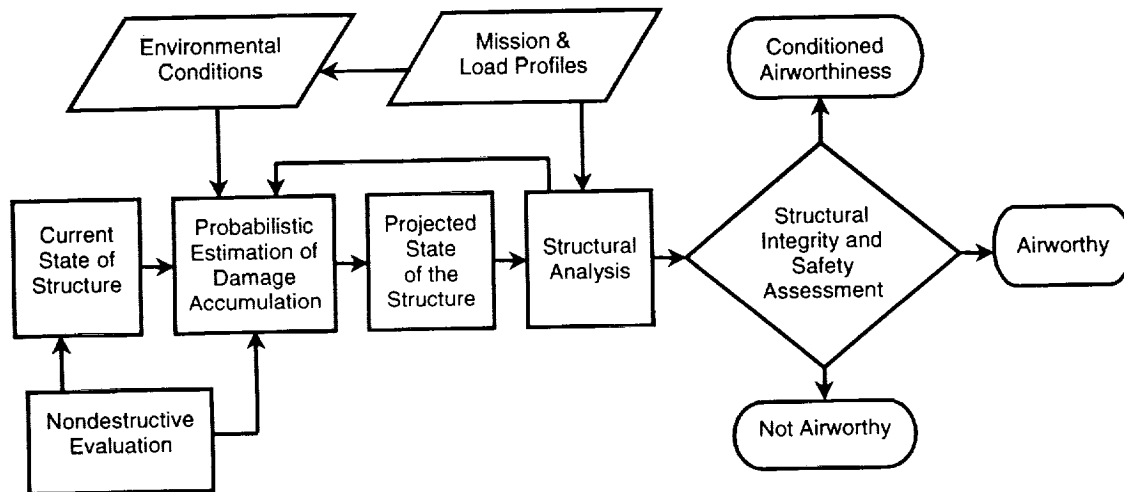


Figure 1. Airworthiness, structural integrity and durability assessments.

These tools require a quantitative understanding, characterization and modeling of the elemental processes of damage, the assessment of damage by NDE, and the incorporation of the various models and NDE information into a suitable probabilistic framework for service life prediction and reliability assessment. Their successful development and utilization depend on the integration of the supporting technologies of materials science, structural mechanics and NDE. A common practice used as part of the damage tolerance approach to the design and life management of aircraft components and structures is to consider the effect of a single dominant crack of length 1.27 mm in the assessment of fatigue crack growth life. Considerable efforts have been expended in the analysis of a single crack emanating from a rivet hole. NDE methods have evolved to conform to this design approach and its predictions. Specifically, being able to detect accurately damage of size 1.27 mm has become the standard to target. In aging aircraft systems, however, multi-site damage (MSD) and widespread fatigue damage (WFD), which can degrade aircraft components and structures and decrease their residual strength and life, are of increasing concern.

Structural integrity and durability are strongly affected by material degradation through localized corrosion and corrosion fatigue crack nucleation and growth. It is now widely recognized that MSD and WFD are frequently initiated from localized corrosion damage. Recent studies have shown that pitting corrosion is a principal form of localized corrosion damage in aluminum alloys. An estimate of the influence of initial pit size (with radii from 10 to 200 μm) on fatigue lives at different stress levels, based simply on crack growth analysis, has been made¹ and is shown in Fig. 2. There is a severe reduction in life as the initial damage size increases. Specifically, for large stresses the reduction exceeds an order of magnitude, but for smaller stresses the reduction can be as large as 5 orders of magnitude. These small

damage sizes, which are considerably smaller than the 1.27 mm target, can have a drastic impact on fatigue life. The estimated results show that the NDE problem is more challenging than previously envisioned, in that much smaller damage needs to be detected. Thus, the accuracy and reliability of NDE must be reexamined and improved, if it is to be an effective part of fleet management programs. Because PoD *per se* reflects an inability to determine a given size of damage with certainty, the probabilistic implication of PoD on the reliability of airworthiness assessment, therefore, must be addressed as well, and is considered below in relation to the state-of-the-art of NDE.

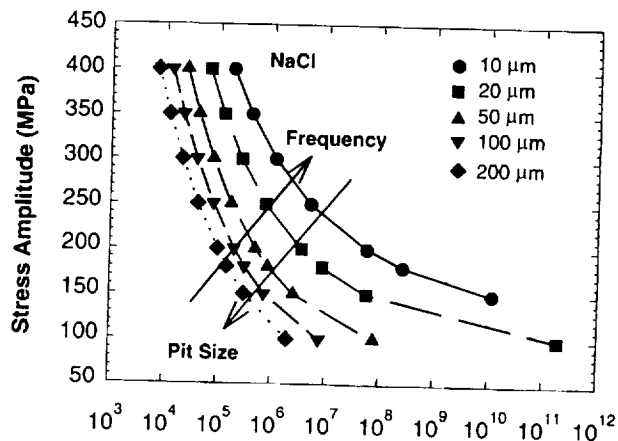


Figure 2. The influence of stress and initial pit (crack) size on fatigue life.

3. STATE-OF-THE-ART OF NDE

The PoD of damage by NDE practice is typically derived from detect/non-detect calls for damage along with signal responses that are believed to reflect the damage (crack) size, without determining the actual size^{2,4}. Performance capability depends upon the nature and distribution of the signals generated under the conditions of operation. The signal and decision thresholds and saturation limit criteria are important factors in the analysis. The possible detect/non-detect calls are as follows: (i) damage exists and is detected; (ii) no damage exists but one is identified; (iii) damage exists but is not detected; and (iv) no damage exists and none is detected. The PoD can be defined in a variety of ways^{2,3}, but it is established typically through a controlled set of experiments in which specimen geometry and damage sizes are independently established. Information on damage sizes is provided only to the analyst, and sizing information is not requested of the NDE inspectors⁴. False calls (items (ii) and (iii)) greatly influence the upper and lower tails of the PoD curve, but have little effect on its central value⁵. One way to account for false calls is to construct a better physical model for the NDE procedure. Another is to use relative operating characteristic curves, or by appropriately weighting the data⁵. None of these approaches are accepted universally. Thus, accurate estimates for the PoD are not easy to obtain and suitable procedures have not been fully established. Due to the key role of NDE in structural integrity analysis and service life management, however, these issues must be addressed.

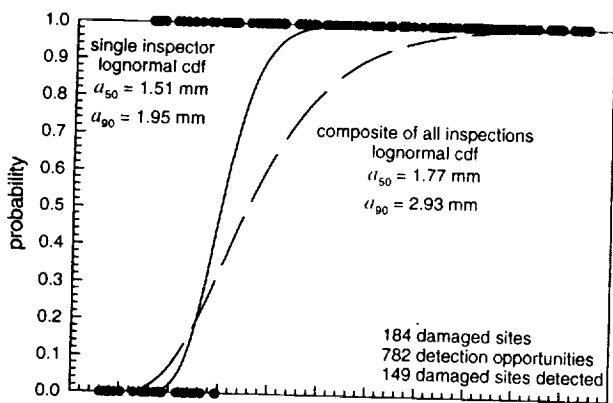


Figure 3. PoD curves for one "good" and all 45 inspectors, and simulated data for the one inspector⁴.

Based on the foregoing protocol, estimations of the PoD have been made recently using data from state-of-the-art eddy-current methods involving 45 inspectors⁴. The data were obtained from blind NDE measurements on a set of specimens with known damage. There were 184 damaged sites for first layer cracks in rivet joints joined with countersunk rivets, with a total of 782 detection opportunities (*i.e.*, cracks). The NDE was considered successful, if a damaged site were detected. PoD curves were estimated based on the crack size and NDE (detect/non-detect) data, and are shown in Fig. 3. The solid and dashed curves represent the maximum likelihood estimates for a

lognormal distribution for one "good" inspector and for all inspectors, respectively. The median and 90 percentile crack sizes for the good-inspector PoD are seen to be 1.51 and 1.95 mm, respectively; both of which are greater than the target of 1.27 mm. The scatter for all 45 investigators (dashed line) is much greater, and the median and 90 percentile are 17 and 50% greater, respectively. This information illustrates the concern that current NDE methods are inadequate in relation to the requirements for PoD.

The fact that damage sizes typically are not reported as a part of the current NDE practice is an issue for the reliable prediction of future states and may be considered in relation to Fig. 3. Because the actual data were not available, a simulated set of crack sizes was developed, based on the solid PoD curve, for the detect/non-detect (1/0) observations and is also shown in Fig. 3. The simulated data suggest that cracks as small as 0.5 mm might be detected, but those as large as 1.5 mm might be missed. The absence of sizing information and the uncertainty in damage detection (even for cracks larger than 1.27 mm) render the ability to ensure continued airworthiness and to schedule subsequent inspection and maintenance problematic. A simplified mechanistic model for pitting corrosion and corrosion fatigue crack growth is used to highlight the dichotomy between the PoO of structurally significant damage and the probability of its detection, and the impact of PoD on the reliability of airworthiness assessments.

4. A SIMPLIFIED MECHANISTIC MODEL

To develop tools for ensuring airworthiness and managing the fleet of aging aircraft, it is essential to integrate life prediction modeling for damage growth and accumulation with NDE. Their effectiveness would be greatly enhanced through the use of a multidisciplinary approach. This approach would embody the development, utilization, and integration of the supporting technologies of corrosion and materials science, structural mechanics and NDE. To show the benefits of this integration and to illustrate the use of mechanistically based probability modeling, a simplified model for pitting corrosion and corrosion fatigue crack nucleation and growth is presented. The specific example is a simplification of aircraft fuselage pressurization-depressurization cycling, and considers a hemispherical pit/semi-circular crack in a large plate. The model is used for estimating the PoO and in considering the impact of the PoD of damage on airworthiness. The PoO also provides a rational basis for estimating the distribution of damage for use in WFD analyses.

Figure 4 shows a schematic diagram of the development of corrosion and corrosion fatigue crack growth. The micrograph is a typical localized severe pit in which constituent particles are visible. Clusters of particles determine the rate and extent of pit growth, and naturally, the larger clusters

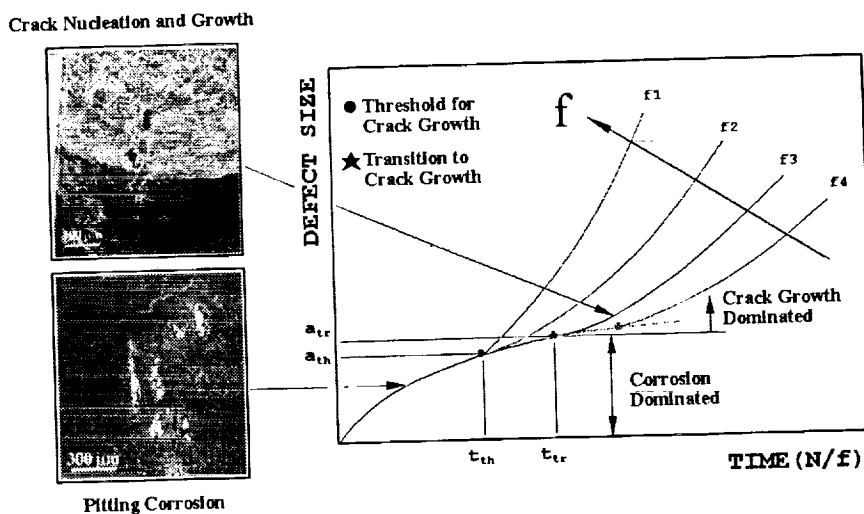


Figure 4. Schematic diagram of the development of corrosion and corrosion fatigue crack growth.

lead to more severe damage^{6,7}. Severe pits that occur in high stress regions of components or structures are sites from which corrosion fatigue cracks nucleate and grow. The micrograph for crack nucleation and growth shows the extent of a pit from which a crack emanated. Most of the principal features of this damage process are included in the simplified model considered herein. In addition, randomness associated with material properties and their sensitivity to the environment are represented explicitly in the model.

The random variable (rv) of interest is the size of the damage as a function of time. For this illustration, localized damage is described by a single variable; *i.e.*, during pitting the variable is the pit depth and for cracking it is the crack depth. A complete description of the proposed model can be found in refs 8 and 9; however, the key aspects are repeated here for completeness.

To model pitting corrosion, the pits are assumed to be hemispherical throughout and grow at a constant volumetric rate that is determined by Faraday's law augmented by a temperature dependent Arrhenius relation. The pit depth a , up to the transition size a_{tr} at which a crack initiates, is given by

$$a = [(3MI_{p_0}/2\pi nF\rho) \exp(-\Delta H/RT)t + a_0^3]^{1/3}; \quad a \leq a_{tr}, \quad (1)$$

where $M = 27$ is the molecular weight of the material; $n = 3$ is the valence; $F = 96514$ C/mol is Faraday's constant; $\rho = 2.7 \times 10^3$ kg/m³ is the density; $\Delta H = 40$ kJ/mol is the activation enthalpy; $R = 8.314$ J/mol-K is the universal gas constant; the absolute temperature $T = 293$ K is an average of typical values when the aircraft is on the ground; I_{p_0} is the pre-exponential term in the Arrhenius representation for corrosion current; a_0 is the initial pit radius; and t is the time required for a pit to develop to a depth of a .

The mechanistically based model for the corrosion fatigue crack growth rate $(da/dN)_c$ is assumed to be the standard power law form, and the driving force ΔK is for a semi-circular crack in an infinite plate. If $t \geq t_{tr}$, the transition time from pitting to cracking, and $N = ft$, where the frequency $f = 10$ cyc/day depicts an aircraft used for short haul service, then

$$a = [a_{tr}^b + bC_c f (2.2\Delta\sigma/\sqrt{\pi})^{n_c} (t - t_{tr})]^{1/b}; \quad b = (2 - n_c)/2; \quad n_c = 3.55. \quad (2)$$

The coefficient C_c characterizes the material properties, including microstructural and environmental parameters, and a far field stress range $\Delta\sigma = 300$ MPa is used to reflect typical stresses for critical locations in a fuselage panel.

Since pitting controls the damage growth until corrosion fatigue crack growth dominates, transition can be characterized by⁶

$$\Delta K \geq \Delta K_{th} \quad \text{and} \quad (da/dt)_{crack} \geq (da/dt)_{pit} \quad (3)$$

where ΔK_{th} is the threshold driving force and the derivatives are the appropriate time-based pit and corrosion fatigue crack growth rates.

Variability is modeled through I_{p_0} , a_0 , C_c , and ΔK_{th} , which are chosen to be mechanistically and statistically independent of time. Scatter in material properties, environmental sensitivity, and resistance to fatigue crack growth is reflected in C_c . Material and manufacturing quality is represented by a_0 and ΔK_{th} . Finally, I_{p_0} reflects the scatter associated with the electrochemical reaction for pit growth. The

three-parameter Weibull distribution has been found to characterize adequately ΔK_{th} , a_o , C_c and I_{Po} , and is shown in refs 1, 7, 10 and 11.

5. IMPACT OF POO AND POD ON AIRWORTHINESS

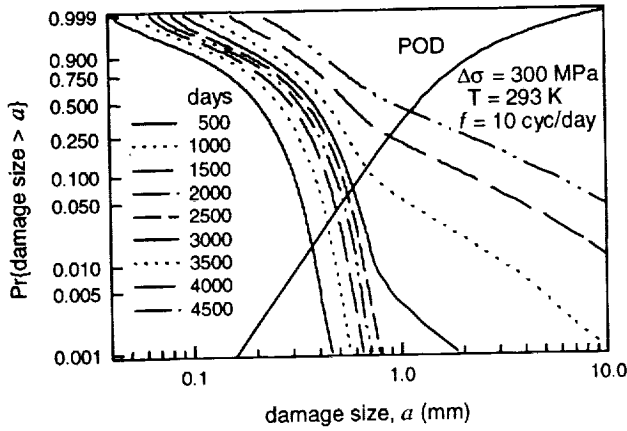


Figure 5. PoO of damage size versus time.

and 0.9 mm. Clearly, the probability of finding a large damage for longer times, and greater damage, is quite high.

The final curve on Fig. 5 is a log-logistics form for the PoD for eddy-current methods¹². The parameters for this PoD are assumed to be a median $m = 1.27$ mm, which is based on the current damage tolerance approach, a 90% detection of 2.54 mm and a minimum detection level $a_{min} = 0$. This PoD is used commonly as a reference. The portion of the figure of concern is that above the PoD. In that region the PoO is greater than the PoD. If the damage size were small, there would be no need for concern. If the damage size is larger, however, the consequence is magnified. For example, after 4500 days the PoO of a damage of size greater than 1.27 mm is about 50%, but the PoD for that damage size is only 50%. In other words, about half of the damage of that size would not be detected. For larger damage sizes, the PoD appears to be adequate. Nevertheless, a caution must be given. As indicated on the graph, the PoO of very large damage is small, which means that to certify that such a damage does not exist would require a thorough search over an extensive area. Obviously, if the applied stress is reduced, then the time to expect large damage increases; however, the inspection dilemma is only delayed.

A graph of the average damage size versus time is given in Fig. 6 to accentuate the tension between the PoO and the PoD and to portray the effect that corrosion has on the life of a structure. The rvs are assumed to be equal to their means. Two models for the time-dependent average damage size, in which the initial size ($a_o = 5 \mu\text{m}$) is identical for both, are presented. The model represented by the solid curve includes pitting corrosion, which is dominant up to t_{tr} , and corrosion fatigue crack

Based on the foregoing model, the PoO and evolution of damage are calculated and used in assessing the capability of current NDE methods, the impact of PoD on airworthiness assessments and the influence of corrosion on service life. Figure 5 is a graph of the probability that the damage size exceeds a specified level a at a given time t . The times, ranging from 500 to 4500 days, encompass typical behavior. For the shorter times, 500 to 2500 days, pitting predominates; however, for the longer times cracking is critical. This is depicted by the rather abrupt change in the shape of the probability curves. There is variability in the transition size a_{tr} from pitting to cracking due to the underlying rvs, but it ranges between 0.6

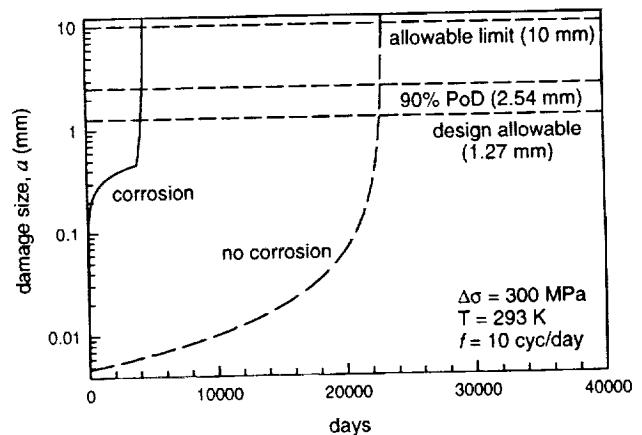


Figure 6. Average damage size modeled by pitting corrosion with corrosion fatigue crack growth and corrosion fatigue crack growth only.

growth, and the dashed curve represent a model for corrosion fatigue crack growth alone. The three dashed horizontal lines represent the USAF allowable size for a single crack (1.27 mm), the PoD of 90% (2.54 mm) shown in Fig. 5, and a reasonable allowable limit for a fuselage panel (10.0 mm).

The predicted life with corrosion is significantly shorter than that based purely on corrosion fatigue crack growth. At a damage size of 1.27 mm, the predicted life with corrosion is only 19% of that without corrosion. It is to be noted that the onset of fatigue crack growth would occur at a threshold damage size $a_{th} = 39 \mu\text{m}$, when $\Delta K = \Delta K_{th}$. Because of the competition between corrosion and fatigue (eqn. (3)), the actual transition would take place at the transition point $a_{tr} = 460 \mu\text{m}$. The time for pitting damage to reach a_{th} is only on the order of a few days, and to reach a_{tr} is about 4,000 days. The remaining life beyond a_{tr} is identical for the two models. Thus, the impact on the life and integrity of a structure from pitting corrosion is extreme, and is consistent with the findings in Fig. 2. It is reflected by a reduction of potential life to about 4,200 days from about 22,700 days; all of which is associated with the truncation of early fatigue crack growth of about 18,500 days by pitting corrosion. The more striking observation from Fig. 6 is that the remaining life after the damage exceeds the allowable size of 1.27 mm is extremely small regardless of the assumed model. The residual life after the 90% PoD is even less. When the applied stress is reduced the situation is not quite as severe, e.g., for $\Delta\sigma = 100 \text{ MPa}$ the remaining average life, with pitting corrosion, is approximately 30%, but the fraction diminishes to just 15% beyond the 90% PoD value. In this example, the possible elevation of local stresses by corrosion was not included, for example, through pillowing¹³. The use of damage driving forces based on “pristine” conditions would have to be modified.

Clearly, substantial improvements in the ability of NDE techniques to reliably detect much smaller damage are warranted. Equally important is the ability to detect precisely the size of damage. An acute dilemma for NDE may be illustrated using Fig. 6. Typically damage inspection intervals are established as a fraction of the predicted life. For this example, however, a safe inspection criterion based on an assumption of pitting and corrosion fatigue crack growth together would be only about 10% of the life predicted by considering corrosion fatigue crack growth alone. In other words, inspection would be necessary relatively soon after the unprotected alloy has been exposed to the environment. In reality, aircraft structures are protected quite well; however, when they have been compromised by corrosion, corrective action becomes urgent. The consequence of this observation is that the resolution for NDE must improve drastically. The PoD needs to be high, at least 90%, for damage sizes between 10 and 50 times smaller than that indicated by the PoDs shown above; i.e., down to the order of 0.1 mm.

To highlight the concern with the current NDE practice of providing detect/non-detect calls, typically without information on damage size, an illustrative example for purely corrosion fatigue crack growth is considered. A model given by eqn. (2) is used to characterize fatigue crack growth. Mean values for the rvs are used so that the computation is deterministic. It is assumed that the minimum damage size is 0.3 mm which is slightly below a typical detection limit⁴. The results are shown in Fig. 7. The solid line is assumed to be the material’s actual crack growth response, with a “design” life of about 800 days. Based on this response, the first inspection, for example, might be scheduled at 400 days and the second at 600 days.

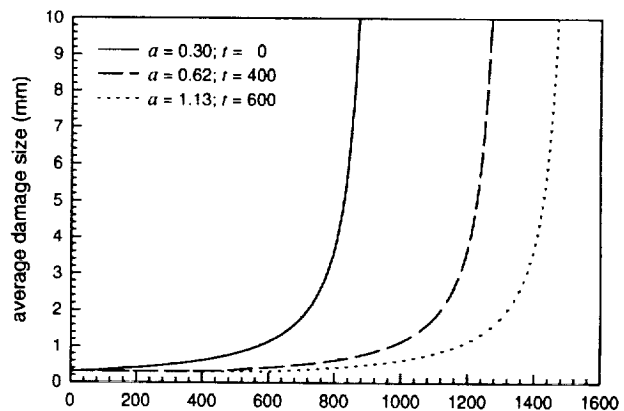


Figure 7. Underestimation of damage in life prediction assuming a corrosion fatigue crack growth model.

The damage (crack) sizes at these times would be 0.62 and 1.13 mm, respectively. Based on the PoD for all NDE inspectors (Fig. 3), crack growth would not be detected at the first scheduled inspection and with a probability of less than 10% at the second. The aggressive maintenance option would be to reapply the first inspection interval and reschedule the second inspection at 800 days. This choice anticipates a life of about 1,200 days (dashed curve), but there would be a significant risk for reaching the "design" life during this period. The more conservative approach would be to adhere to the originally planned second inspection. At this point, the PoD would still be too low and the potential risk for failure during subsequent service would be extremely high (see dotted curve). Without information on the damage size, it is difficult to make reliable assessments of continued airworthiness. Clearly, underestimating the current state-of-damage can lead to overly optimistic estimates on life and continued airworthiness. This example was based on NDE data for first layer damage in a riveted joint. The problem becomes more acute for second or third layer damage because of the severe degradation in NDE reliability¹⁴. The key conclusion to be drawn is that current state-of-the-art NDE methods are not adequate for detecting damage at the sizes that can significantly affect life prediction.

Current NDE methods do not provide suitable accuracy. Even with the best NDE equipment available, the levels of reliable detection are still a factor of 2 to 4 times too large, and the ability to provide sizing information is uncertain. The consequence of this observation and the previous illustration is that the capability for NDE needs to be improved. The PoD should be high, at least 90%, for damage sizes at least one order of magnitude smaller than that indicated in Figs 3 and 5, along with capability for accurate determination of the size of damage at these levels. Coupled with these requirements is the mandate to inspect extremely large structures, some of which have nearly inaccessible locations. Furthermore, the reported PoD analyses are only for simple configurations, but the accuracy and confidence may be significantly reduced for more complex ones, such as multi-layer joints. Also, all of the NDE studies heretofore did not include the complications of corrosion, which is known to adversely affect some NDE techniques². Obviously, the relationship between allowable limits, actual damage sizes, and detection accuracy is critical for proper aircraft maintenance and management.

6. SUMMARY

Airworthiness assessment and management of aging fleets of aircraft depend critically on the quality of tools for predicting damage nucleation and accumulation, and on the reliability and accuracy of its timely detection. In this paper, an approach and methodology for predicting the PoO of damage is outlined, and is used to assess the state-of-the-art and requirements for NDE. A simplified mechanistically based probability model is used for estimating the PoO of damage in aircraft materials subjected to localized (pitting) corrosion and corrosion fatigue crack growth. The results show that the service lives are significantly reduced by early corrosion damage. They served to highlight the dichotomy between the probability for damage accumulation and its detection, in that the PoD is too low for structurally significant corrosion and early fatigue damage. In its current usage, the PoD simply represents the probability for detecting the existence of damage above a given size. PoD in the fullest sense, however, is much more complex, and must include information on size, geometry and location of damage, and it must account for the dependence on inspectors and techniques. The PoD needs to exceed 90% for damage sizes that are 10 to 50 times smaller than the current level of 1 to 2 mm. The ability for providing accurate NDE measurements of damage sizes is essential for making reliable airworthiness assessments. It is recognized that both modeling and detection of damage need to be substantially improved in the development of effective tools for airworthiness assessment and fleet management. Because of the importance of corrosion in aging aircraft and because corrosion damage is not clean, accurate NDE measurements are a challenge, especially in detecting corrosion damage underneath a rivet head or in the 2nd and 3rd layers of a typical joint.

A method for predicting the PoO of damage was demonstrated through the use of a simplified mechanistic model for pitting corrosion and corrosion fatigue crack growth. The method facilitates the prediction of the evolution and distribution, and the PoO of damage in terms of their size, geometry and location. It can serve as a basis for quantitative estimations of the distribution of damage for use in WFD analyses to replace the more *ad hoc* approach used heretofore.

ACKNOWLEDGEMENT

This research was supported in part by the Air Force Office of Scientific Research under Grants F49620-96-1-0245 and F49620-98-1-0198 and by the Federal Aviation Administration under Grant 92-G-0006.

REFERENCES

1. R.P. Wei, C. Li, D.G. Harlow and T.H. Flournoy, "Probability Modeling of Corrosion Fatigue Crack Growth and Pitting Corrosion," *ICAF97: Fatigue in New and Aging Aircraft*, vol. 1, R. Cook and P. Poole, eds (London: Engineering Material Advisory Services Ltd., 1998), 197-214.
2. W.D. Rummel, G.L. Hardy, and T.D. Cooper, "Applications of NDE Reliability to Systems," *Nondestructive Evaluation and Quality Control, Metals Handbook 9th Ed.*, Vol. 17, ASM International, Metals Park, OH, 1989, pp. 674-688.
3. A.P. Berens, "NDE Reliability Data Analysis," *Nondestructive Evaluation and Quality Control, Metals Handbook 9th Ed.*, Vol. 17, ASM International, Metals Park, OH, 1989, pp. 689-701.
4. F.W. Spencer and D. Schurman, "Reliability Assessment at Airline Inspection Facilities Volume III: Results of an Eddy Current Inspection Reliability Experiment," DOT/FAA/CT-92/12, III (1995).
5. R.W. Hyatt, G.E. Kechter, and R.G. Menton, "Probability of Detection Estimation for Data Sets with Rogue Points", *Materials Evaluation*, Vol. 49, 1991, pp. 1402-1408.
6. C.-M. Liao, G.S. Chen and R.P. Wei "A Technique for Studying the 3-Dimensional Shape of Corrosion Pits," *Scripta Materialia*, 35 (11) (1996), 1341-1346.
7. C.-M. Liao, "Particle Induced Pitting Corrosion of Aluminum Alloys" (Ph.D. Dissertation, Lehigh University, 1997).
8. R.P. Wei and D.G. Harlow, "A Mechanistically Based Probability Approach for Predicting Corrosion and Corrosion Fatigue Life," *ICAF: Durability and Structural Integrity of Airframes*, vol. 1, A.F. Blom, ed. (London: Engineering Material Advisory Services Ltd., 1993), 347-366.
9. D.G. Harlow and R.P. Wei, "Probabilistic Aspects of Aging of Airframe Materials: Damage Versus Detection," *The 3rd Pacific Rim International Conference on Advanced Materials and Processing*, M.A. Imam, R. DeNale, S. Hanada, Z. Zhong and D.N. Lee, eds. (The Minerals, Metals & Materials Society, 1998), 2657-2666.
10. G.S. Chen, K.-C. Wan, M. Gao, R.P. Wei and T.H. Flournoy "Transition from Pitting to Fatigue Crack Growth - Modeling of Corrosion Fatigue Crack Nucleation in a 2024-T3 Aluminum Alloy," *Materials Science & Engineering*, A 219 (1996), 126-132.
11. D.G. Harlow and R.P. Wei, "A Probability Model for the Growth of Corrosion Pits in Aluminum Alloys Induced by Constituent Particles," *Engineering Fracture Materials*, 59(3) (1998), 305-325.
12. A.P. Berens, P.W. Hovey and D.A. Skinn, "Risk Analysis for Aging Aircraft Fleets: Volume 1 - Analysis," USAF WL-TR-91-3066 (1991).
13. J.P. Komorowski, N.C. Bellinger, and R.W. Gould, "The Role of Corrosion Pillowing in NDI and in the Structural Integrity of Fuselage Joints," *ICAF97: Fatigue in New and Aging Aircraft*, vol. 1, R. Cook and P. Poole, eds (London: Engineering Material Advisory Services Ltd., 1998), 251-266.
14. D. Hagemmaier and G. Kark, "Eddy Current Detection of Short Cracks Under Installed Fasteners," *Materials Evaluation*, Vol. 55, 1997, pp. 25-30.

CRACK DETECTION AND MONITORING OF AGING AIRFRAMES

Neal Phelps
Ogden ALC

Scott May
United States Air Force

Eric Hauge, Tamara Leeks and Pat Johnson
Boeing Phantom Works

Steve Ziola and John Dorigi
Digital Wave Corporation

Abstract

Reducing structural operation and support (O&S) costs is a primary objective for those responsible for system operation and sustainment. Flying aircraft longer and harder than originally expected, as we do today, makes this objective difficult to achieve. One way to reverse this trend and lower O&S costs of aging aircraft, is to perform automated inspections of the airframe. Present day computer technologies make it possible to install a small, autonomous computer and sensor system on an aircraft to monitor difficult and costly to inspect structural locations. The health of the monitored location could be determined by the end user through normal operations (Standard Flight Data Recorder download) providing a significant reduction in scheduled maintenance. This paper will provide an overview of an approach that will autonomously detect and monitor crack growth in aircraft structures. The overview will discuss the final results developed under the AFRL F-16 Crack Monitoring System Proof of Concept Program, provide background on system requirements and summarize the preliminary design of the electronics and software necessary for on-aircraft crack monitoring.

Introduction

A proof-of-concept Crack Monitoring System (CMS) was developed under USAF Contract F33615-95-D-3203, Delivery Order No. 0006. The scope of the contract consisted of four tasks: 1) Requirements Definition, 2) CMS Preliminary Design, 3) F-16 Concept Testing, 4) Technology Transfer. Details of this work can be found in the reference 6 report or one of its references. This paper will summarize the approach for an acoustic emission crack monitoring system and the results of the proof of concept study in section 1. The preliminary design for a flight CMS will be summarized in section 2.

Requirements for design and implementation of a Crack Monitoring System for use on an F-16 aircraft were developed. Many of the requirements were obtained directly from other documents, typically military standards or F-16 specific documents. Since the demonstration aircraft is an F-16, the requirements developed for the CMS could, in most instances, be considered the worst case conditions, and therefore could be applied, with engineering judgment, to other weapon systems.

The CMS preliminary design contains information that describes the results of trade studies used to arrive at the overall system architecture. Numerous design options have been considered. A single design that demonstrates feasibility is summarized in this paper. The design goals which have been given heavy consideration in the preliminary design effort include, but are not limited to, minimum weight, minimum

power consumption, system cooling, and minimum cost. Some of these goals may not seem important for a single application, but we must keep in mind that the final production system may be used in multiple locations on a single aircraft. Additionally it must be useful on more than one model or type of aircraft.

1.0 Technique Description and Test Results

This section will summarize an automated approach used detect crack events and predict crack tip source locations. Results of an automated analysis of the data from an F-16 bulkhead fatigue test will also be presented.

1.1 Automated Source Location using Broad Band Acoustic Emission

The Broadband Acoustic Emission technique can be viewed as a direct technique since it is based on the use of measurements that directly model a physical phenomenon. It is well suited for detecting small defects and monitoring their growth (high frequency ~ 50 kHz to 2MHz). It uses acoustic wave-front time of arrival (TOA) monitoring to accurately predict source location. Other fields that use Broadband Acoustic Emission or Passive Ultrasonics include: SONAR (Underwater Acoustics), Seismology (Low Frequency), RADAR (Electromagnetic Waves) and Ultrasonics (High Frequency). The fundamental steps to perform the technique are:

1. Collect Acoustic Emission (AE) time history data.
2. Down-select, de-noise and compress collected AE waveform data.
3. Find first significant waveform peak.
4. Compute time of arrival (TOA) using first peak detection.
5. Compute 3-D source location from time of arrival data and sensor location information.
6. Estimate TOA from predicted source locations to each sensor location and difference with measured TOA from waveform peaks. This is the residual (an assessment of uncertainty).

A completely automated algorithm to determine the location, in three dimensions, of each crack event analyzes the monitored acoustic emission events. A plot of the source locations then provides a picture of the crack location and geometry. For each event, a signal waveform is obtained for each sensor that is monitoring the structure. To determine the source location in three dimensions, at least four sensors are needed. More than four sensors provide redundancy and the chance to locate an event even if one or more sensors are not functioning properly. The raw acoustic emission waveforms are first processed by noise reduction routines. Wavelet transform methods [2] are used to filter and reduce the noise in the signals. The waveform peaks are located and the first significant peak is taken as the arrival of the event at that sensor. The time of arrival (TOA) to this peak, which is the time of arrival of the event at that sensor, is then calculated. Waveform data from eight sensors with the time of arrival marked at the first peak for each is shown in Figure 1.1.

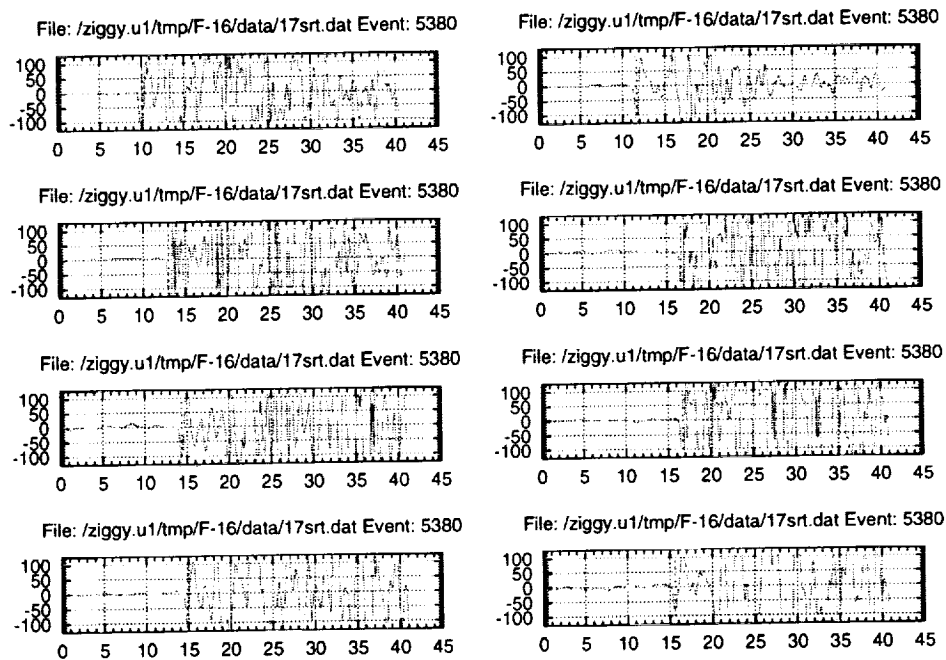


Figure 1.1, Waveforms from one event with TOA marked on each signal.

The TOA values are computed for all sensors. These times are used to calculate the 3-D source location. Knowing the position of the sensors, the time of flight (wave propagation time) between them and the wave propagation speed in the material that is being monitored, a set of equations can be written with the source location as the unknown. A nonlinear least square analysis is used to compute the best source location to fit the system of equations. A measure of the accuracy of the calculated source location is made by a residual computation. Taking the calculated source location, an estimate of the TOA to each sensor can be made. This estimate is compared to the TOA calculated from the first peak of the waveform. If the normalized difference in these two values is small, then it is assumed that the source location is good. This residual number is a measure of the uncertainty in the source location that was calculated.

1.2 Results from Concept Testing

During the fatigue test of the F-16 FS 479 bulkhead at Lockheed-Martin Tactical Aircraft Systems (LMTAS), a Digital Wave Corporation Fracture Wave Detector (FWD) system was used for detection and monitoring of the crack growth. Eight sensors were used to ensure that accurate source location could be performed. For 3-D source location, a minimum of four sensors must be used. Since the method for determining the source location utilizes a nonlinear least squares approach, the more sensors the better (within reason). Eight sensors were chosen as a conservative number for this test, although six sensors would most likely be used in an operational environment.

The acoustic emission data gathered during the test was analyzed using the automated source location algorithm. The reference documenting the results from this test is included in the reference 6 report. Figure 1.2 shows the bulkhead, the fretting at the crack location and the AE predicted crack source locations. Further analysis of the data was performed by breaking the results into the time blocks in which they occurred. The source locations detected during each block of loading were plotted along with the crack lengths determined from a Lockheed-Martin fractographic analysis. The final comparison is

shown in Figure 1.3. Source locations from each block plotted in a different shade. The final length of each crack front is represented by the solid black lines. The dots on the end of the crack lines are there only to be able to pick out the crack ends among the source locations. Overall, the crack location and geometry appear to agree very well with the fractography analysis of the crack surface.

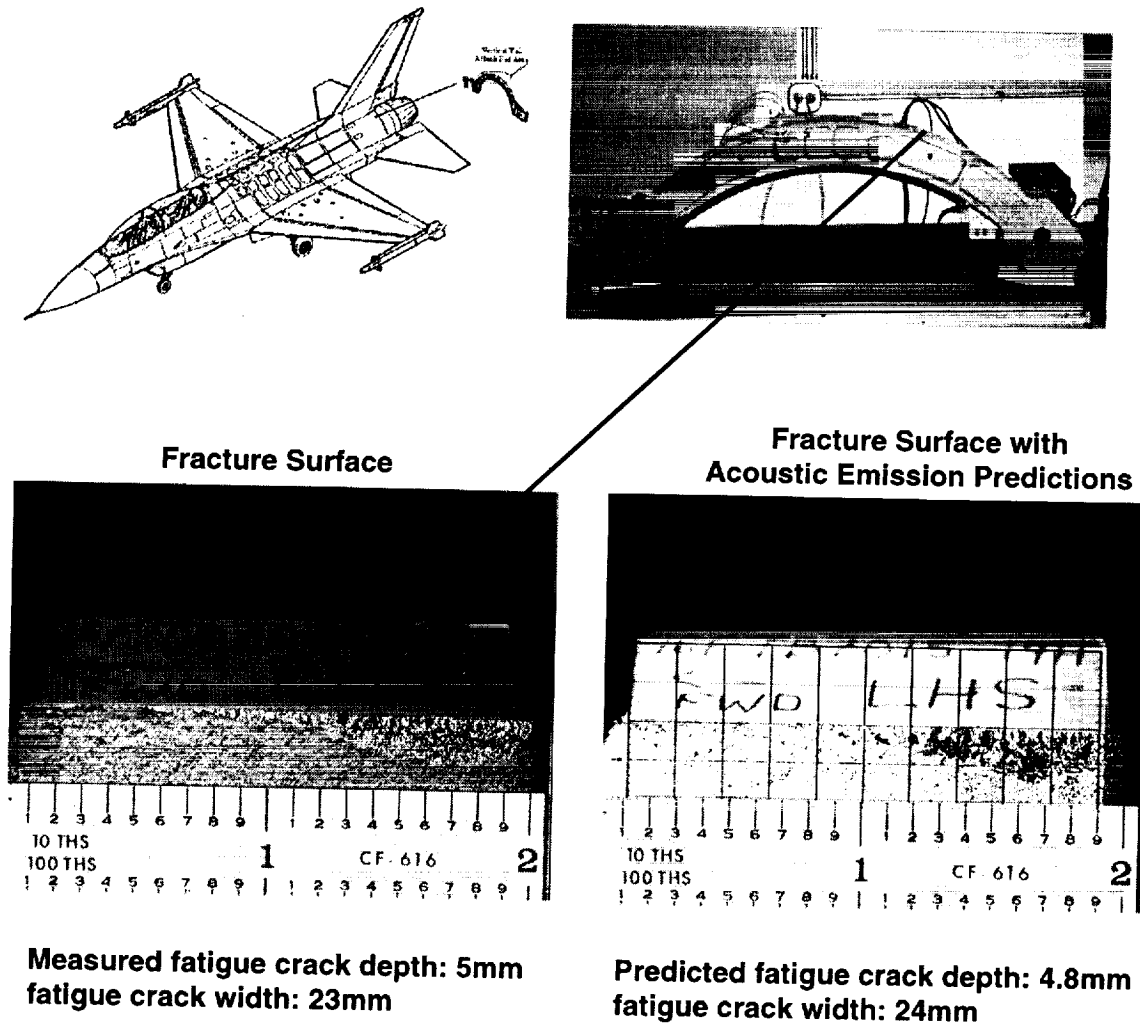


Figure 1.2, Illustration of F-16 bulkhead test results

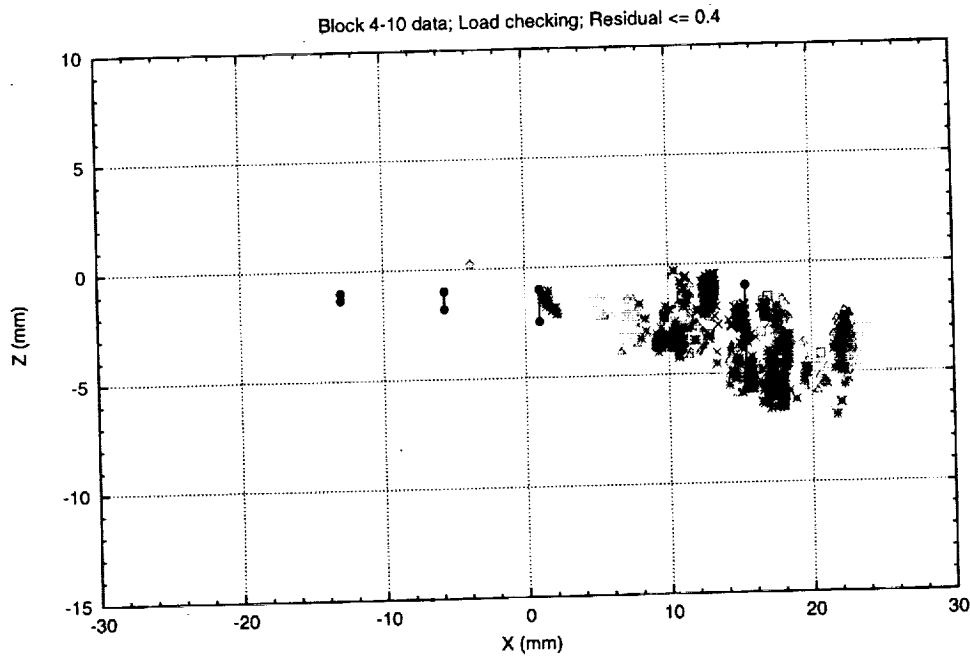


Figure 1.3, Source locations by block compared to crack front depths from LMTAS fractography.

When examined block by block, there are some discrepancies between the crack predictions by the source location algorithm and the conclusions from the LMTAS fractography analysis. The fractography report showed small crack initiations on the left side of figures 1.2 and 1.3. The CMS prediction did not. The results of an analysis performed at Boeing (Seattle) concluded that the crack had first initiated on the right side of the fracture surface. This agrees more closely with the source location predictions. Because of this discrepancy between the fractographic analyses, there is a question of how small a crack the acoustic emission system can detect. Further testing should be performed to determine the size of a flaw that can be detected with the acoustic emission monitoring system. However, overall this crack monitoring system proved that it could detect crack growth in a part by monitoring and analyzing the acoustic emission events.

1.3 Background Noise Level Evaluation for F-16 at Buckley Air National Guard

A test was performed at Buckley Air National Guard Base in Denver, Colorado to characterize the background noise level of an F-16. A total of 16 acoustic emissions sensors were attached to the F-16 at a variety of locations (figure 1.4). The first objective of this test was to determine the frequency spectrum of the structural noise created by the F-16 engine running at levels from idle to full afterburner while on the ground. The second objective was to determine if the acoustic emission system could detect signals on the level of crack growth energies while the engine was running. The third objective was to evaluate the EMI environment of the F-16 due to electronic systems. Reference 6 includes a more detailed description of this test.

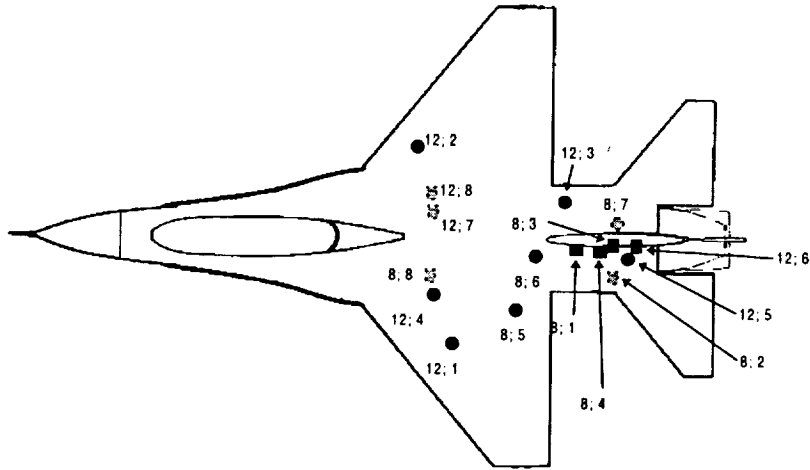


Figure 1.4, Sensor locations during the F-16 noise tests (top view). The first number is the system A/D bit resolution, the second is the sensor number. Gray represents sensors under the aircraft.

1.3.1 Discussion of Test Results

The test results indicated that structural noise consisted mainly of continuous signals dominated by frequencies less than 200 kHz and that there were no continuous EMI signals that would interfere with the performance of a crack monitoring system. To start the aircraft, a small jet engine (secondary engine) is started using compressed air. This engine is then used to start the main engine. The secondary engine is located on the FS341 bulkhead, near sensor 8. The signals from this portion of the testing are shown in Figure 1.5. The frequency content of the signals is in the 100 kHz range, well below any of the frequencies of interest in crack growth detection.

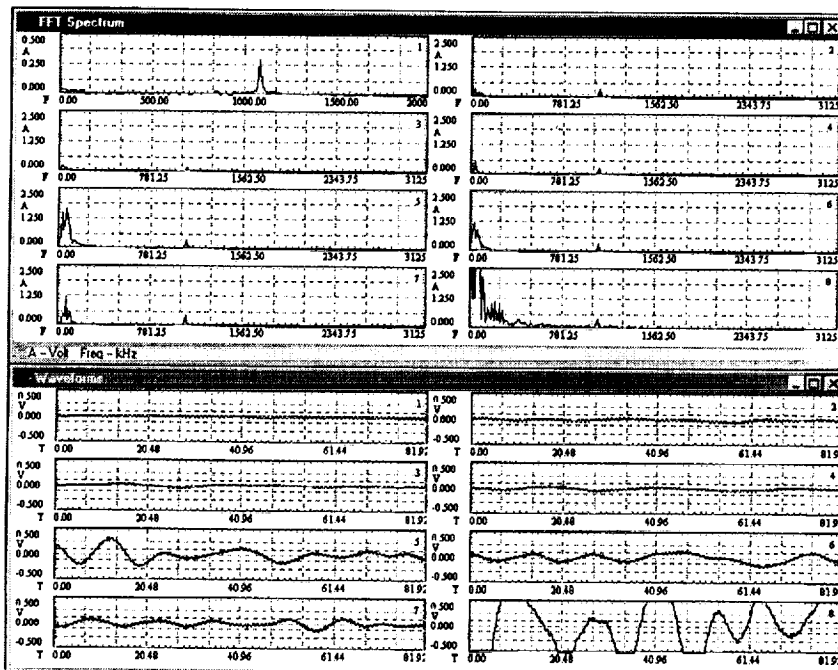


Figure 1.5, Frequency response (top) and time traces (bottom) for signals detected during engine startup.

A single EMI event was observed during the testing, shown in Figure 1.6. This occurred during the aircraft radar operation tests. No events were detected during either the electronic or flight-control tests. The frequency content of the EMI signal overlaps that contained in crack growth events, however, there are no wave propagation characteristics in the signals. Therefore, signals such as these could be easily eliminated from the data set.

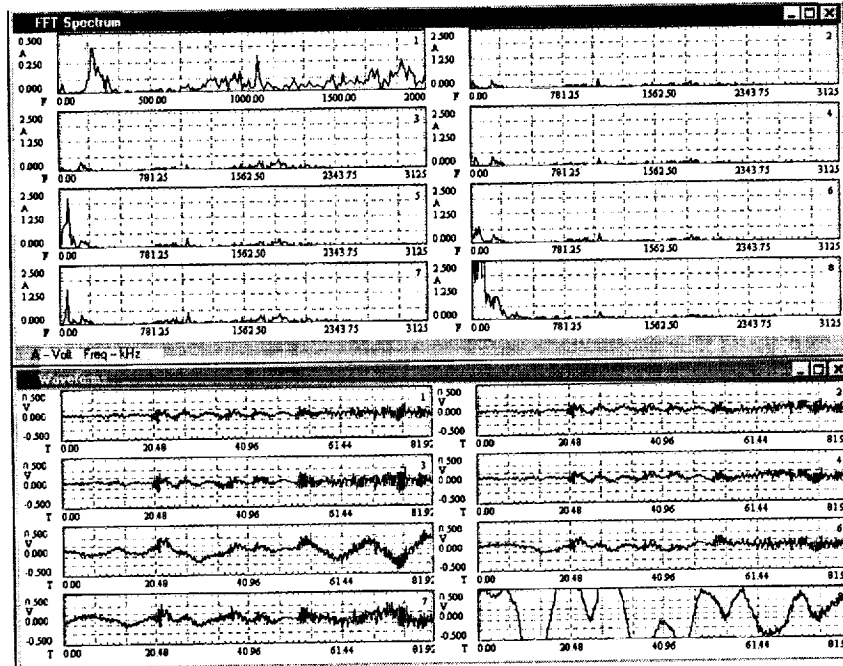


Figure 1.6, EMI event detected during radar tests.

1.3.2 Noise Test Conclusions

Based on the F-16 noise tests, the noise from electronics, flight actuators and engines should not interfere with the monitoring of crack growth using acoustic emission. All mechanical noise was 200 kHz or less, which is much less than the frequencies of interest in crack growth. The EMI noise was minimal, and is easily distinguishable from the crack growth signals.

2.0 Design Package

A design for a flight CMS that meets the requirements set out for a military aircraft application has been proposed. The flight portion of the CMS consists of the CMS Processing Unit (CMSPU) and the Broadband Acoustic Emission (BAE) sensors along with their preamplifiers and associated cabling. The only component that is located off the aircraft is the CMS Data Processing System (CMSDPS) which is used for data downloading and processing. Trade studies were performed to examine individual components of the CMSPU: 1) computer bus, 2) enclosures, 3) application specific integrated circuit (ASIC) vs. discrete ICs, 4) off-the-shelf (OTS) single board computer (SBC) vs. custom SBC, 5) OTS system boards vs. custom system boards, 6) storage media, and 7) enclosure cooling techniques. Each

trade study outlined a number of design options that exist for the CMS and an optimal solution based on the current design goals was chosen.

2.1 Requirements

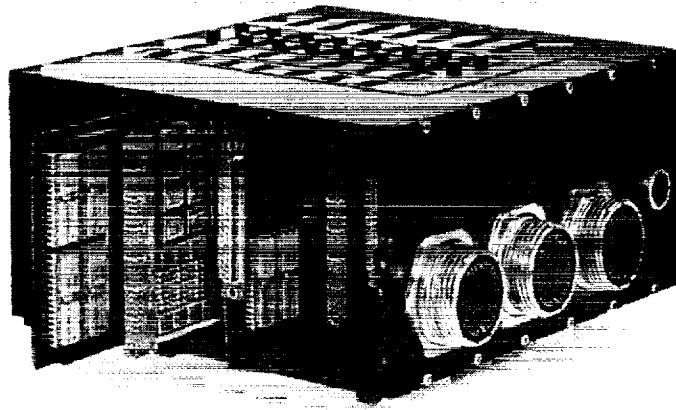
The requirements necessary for design and implementation of an aircraft structural CMS for use on the F-16 have been specified [6]. The material was obtained from a number of sources that define environmental and other general requirements pertaining to equipment installed on F-16 aircraft. Also included are functional and operational requirements that describe required levels of performance and methods of operation for the CMS. The requirements were compiled with input from software developers, hardware developers and USAF personnel representing the end user of the CMS. The requirements were divided into five main categories: environmental requirements, size/ weight/location requirements, interface requirements, functional requirements, and operational requirements. Details are available in the Requirements Document listed in reference 6.

2.2 Preliminary Design

This section contains a summary of the preliminary design information and results for a CMS. The scope of the design effort included defining the CMS architecture, performing trade studies on significant components, and defining a preliminary system in enough detail to assess feasibility and determine approximate system performance and cost. Trade studies on system architecture, system design strategies and system components have been performed in order to produce a preliminary design that meets all of the performance and end user requirements. The preliminary CMS system consists of a single rugged enclosure containing a number of system boards. The CMS boards include a single board computer, a memory board, an analog I/O board, a 1553B interface, and a number of Acoustic Emission (AE) signal conditioning / analog-to-digital (ADC) boards. A ground unit, the Crack Monitoring System Data Processing System (CMSDPS), will be used to download data off the aircraft and for subsequent data processing. This design satisfies all of the requirements specified in the CMS requirements document. An overview of the down selected design is provided in Table 2.1. The goal in the CMS design is to maximize the number of AE channels per board, keeping in mind all of the functions each AE channel must incorporate. Two approaches can be taken to implement the required design. The first is to use discrete surface mounted integrated circuits (ICs). There is no one IC that can accomplish all of the functions required of the AE signal conditioning board. The second approach is to develop an application specific IC (ASIC), to accomplish the required functions. The ASIC approach was chosen because of improved system performance and increased channel density. The storage device for the CMS presents a unique design challenge because of the shock and vibration environment in which it is required to operate. The optional devices considered were ruggedized hard drives, OTS flash memory devices, and custom flash memory devices. The solid state technology coupled with the nonvolatile feature of flash memory offer numerous advantages in the rugged CMS environment. The OTS flash memory option was chosen primarily because of low risk and Non-recurring engineering (NRE).

Table 2.1, Summary of CMS Design Results

<u>Trade Study</u>	<u>Result</u>
Computer Bus	3U Compact PCI
Enclosure	3U 8-slot 0.8" pitch
ASIC vs. Discrete IC	ASIC
Single Board Computer	Off the Shelf
System Boards	Off the Shelf (if possible)
Storage Device	Off the Shelf Flash (if possible)
Cooling	Forced Air Convection
System Dimensions	8.6 in - 9.3 in - 9.8 in
System Weight	17.2 lb
Power Consumption	110 Watts



3.0 Conclusions

The requirements and a preliminary design for the CMS have been discussed in this paper. Numerous design options have been considered to implement the CMS architecture and a nominal design has been selected. The selected design demonstrates feasibility for the CMS system. The requirements outlined in the requirements document can be met by the nominal system. Concept testing of an F-16 FS479 bulkhead showed that the system was capable of detecting a fatigue crack. Analyzing the acoustic emission data and plotting the crack source locations showed that the crack location and geometry was accurately predicted by the source location routines. All tasks relating to the USAF Contract (F33615-95-D-3203), Delivery Order No. 0006, for a Crack Monitoring System, have been successfully completed. The feasibility of a CMS system for use on an F-16 military aircraft has been demonstrated. The foundation has been laid for follow-on efforts to be pursued.

Acknowledgements

The authors would like to acknowledge the following individuals for their support, insight and contributing work on this project and the area of acoustic emission technology:

Nick Strapko and Richard Luke, Lockheed Martin Tactical Aircraft Systems
Mark Defazio, ASC/YP
Dr. W. Prosser, NASA Langley
Dr. Roy Ikegami, Boeing Phantom Works
Dr. Michael Gorman, Digital Wave Corporation

References

1. S. May, N. Phelps, I. Searle, S. Ziola "F-16 Structural Crack Monitoring by means of Broadband Acoustic Emission", The First Joint NASA/FAA/DoD Conference on Aging Aircraft.
2. A. Grapps, "An Introduction to Wavelets", *IEEE Computational Science and Engineering*, Summer 1995, Vol. 2, Num. 2.
3. I. Searle, S. Ziola, and B. Seidel, "Crack Detection on a Full Scale Aircraft Fatigue Test", Proceedings of SPIE Smart Structures and Materials 1997 Conference, Vol. 3042, pp. 267-277.
4. M. R. Gorman, "Determining Fatigue Crack Growth in Aircraft by Monitoring Acoustic Emission", *Naval Research News*, v.XLIV, n. 1, 1992, pp. 24-27.
5. Searle, I., Ziola, S., Seidel, B. "Crack Detection of a Full Scale Aircraft Fatigue Test", SPIE Smart Structures and Materials Conference Proceedings, 3042-34, San Diego, California, March 1997.
6. AFRL F33615-95-D-3203 Final Report, "F-16 Crack Monitoring System Proof of Concept"

Abbreviations

AE	Acoustic Emission
ASIC	Application Specific Integrated Circuit
BAE	Broadband Acoustic Emission
CMS	Crack Monitoring System
IC	Integrated Circuit
NRE	Non Recurring Engineering Costs
OTS	Off The Shelf
ROM	Rough Order of Magnitude
SBC	Single Board Computer

MULTI-ELEMENT ULTRASONIC LINEAR ARRAYS FOR RAPID LAP-JOINT INSPECTION

Robert A Smith and Stephen J Willsher
Defence Evaluation and Research Agency
Griffith Building - A7
DERA, Farnborough, GU14 0LX, UK
Telephone: +44 1252 395655
Telefax: +44 1252 397223
E-mail: rasmith@dera.gov.uk

ABSTRACT

Rapid detection and characterization of disbonding and corrosion in lap joints is a high priority for both military and civil transport aircraft operators. Approaches to this requirement have followed two clearly different routes: the development of novel large-area inspection systems, and the enhancement of current ultrasonic or eddy-current methods to reduce inspection times. This paper deals with the use of multi-element transducers to increase the scanning speed for ultrasonic lap-joint inspection. Array technology has been very widely used in the medical ultrasound field although rarely above 10 MHz, whereas lap-joint inspection requires a pulse center-frequency of 12 to 20 MHz in order to resolve the separate interfaces in the lap joint. A specification for a 128 mm-long multi-element linear array of 4 mm x 2 mm ultrasonic elements for use with the ANDSCAN[®] scanning software was sent to selected NDT manufacturers with experience in the medical imaging field. This paper analyses the performance of the transducer that was produced and evaluates its use in scanning systems of different configurations. Preliminary trials have produced scanning speeds along the lap-joint in excess of 0.18 m/min (or 7" per minute) - limited by the data acquisition card in the computer. After upgrading this card, a speed of up to 3.6 m/min (11'8" per minute) should be possible with a flaw detector capable of a pulse-repetition-frequency (PRF) of 8 kHz, although this may then be limited by the time taken to update the C-scan information in the computer.

1. INTRODUCTION

The requirement for rapidly detecting corrosion and disbonds in lap joints of transport aircraft has prompted the development of various new NDT methods and large-area imaging systems. However, there is still great potential for speeding up conventional methods, such as eddy-currents and ultrasonics, using automated or semi-automated scanners. Currently there are several systems available that scan either a single transducer in a raster scan, or several single-element transducers simultaneously (1-3). Another method for increasing scanning speed even further is to electronically scan through a linear array of transducer elements and manually move this array along the lap joint. Thus DERA is developing both ultrasonic and eddy-current arrays and evaluating their inspection performance and the potential speed of inspection.

A considerable amount of research and development on linear-array transducers has been completed in the past for the medical-ultrasound industry where such devices have been commonplace for at least 20 years. However, they have been noticeably absent from the in-service NDT world during that period. Recent years have seen the development of piezo-composite transducers which, by their very nature, are highly suitable for use as arrays and there have been several moves to introduce these arrays into NDT (4-5). In addition, piezo-composite arrays can be flexible (6-8) and this could prove essential because the

most obvious problem with using array technology on in-service structures is that of maintaining coupling (for ultrasonics) or stand-off (for eddy-currents) on uneven surfaces. Thus a substantial part of DERA's development program will be looking at this problem. This paper concentrates on the development of an ultrasonic array with a sufficiently high frequency range for lap-joint inspection, and a rapid scanning system to plot the C-scan results.

2. LINEAR-ARRAY TRANSDUCER

The prototype array transducer which was designed and manufactured to a DERA specification by Diagnostic Sonar Ltd (DSL) from Livingston, Scotland, can be seen in Figure 1 mounted in a simple trolley. The array had to interface to a conventional flaw detector and operate at a center frequency of over 12 MHz in order to resolve the front and back of the various aluminum lap-joint skins, and preferably even the front and back of the bond. Each scan-line was required to have an entry beamwidth of between 2 mm and 4 mm.

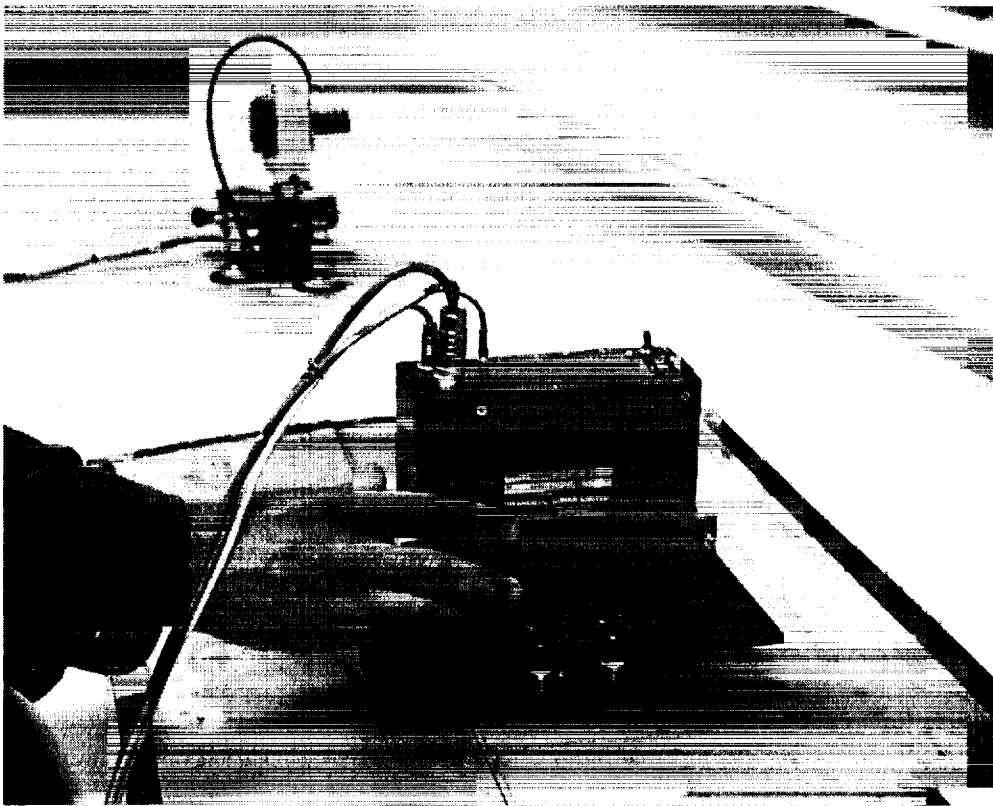


Figure 1. Lap-joint array developed by Diagnostic Sonar Ltd to DERA's specification (9). The prototype carriage is designed to keep the ultrasound beams normal to the surface.

The array has been described previously (9), and uses a poly-vinylidene fluoride (PVDF) piezoelectric sheet sandwiched between a backing block and the stand-off material. For this lap-joint application an aluminum stand-off was chosen by DSL although other materials will also be investigated at DERA. A water stand-off is likely to give the cleanest ultrasonic signals but this will require a recirculating system with quite a high flow rate. The array comprises 64 electroded elements of size 4 mm x 2 mm (or 0.16" x 0.08"), spaced at 2 mm (0.08") centers, fired in pairs (see Figure 2). After each firing either the

transmitting pair or the receiving pair are alternately incremented along by 2 mm (0.08"). Thus the result is 128 scan-lines spaced at 1 mm (0.04") centers.

The ultrasonic performance of the linear array has been initially assessed and the center frequency of approximately 12 MHz is sufficiently high to enable bond inspection and depth scans of corrosion sites. However, at present the bandwidth is not as wide as is desirable for these inspections and this aspect is being addressed.

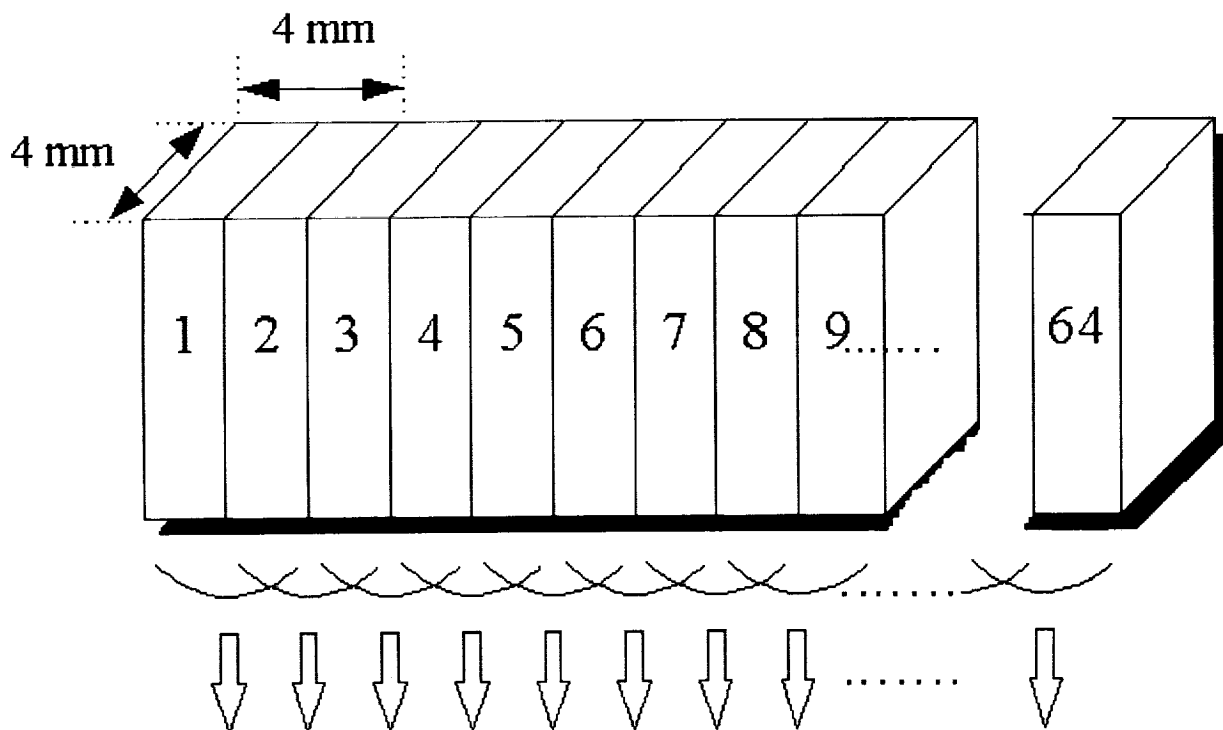


Figure 2. Schematic diagram of scan-line firing sequence for linear-array probe with 64 elements.

The multiplexer electronics, contained in the array itself, allows three modes of operation:

- single element with operator selection of the element,
- continuous cycling triggered by the flaw detector's firing pulse, or
- computer control of the firing element.

The ANDSCAN software allows use of all of these modes and the last two are being assessed to decide which gives the optimum performance. Both have their advantages: cycling triggered from the flaw detector gives the fastest scanning speed but computer control avoids any loss of data points due to the asynchronous acquisition rates.

In the normal scanning configuration the array probe is connected to the flaw detector which is set to dual-transducer mode. There are additional connections to the computer for transmitting digital scan-line information, and to a power supply (see Figure 3).

In addition, the array can be used as a high-resolution paintbrush-type probe with just a flaw detector and no scanning system or computer. The sensitivity to small defects is greatly increased over a single-element paintbrush probe and the scan rate would be equivalent to that of a 4 mm x 128 mm paintbrush probe.

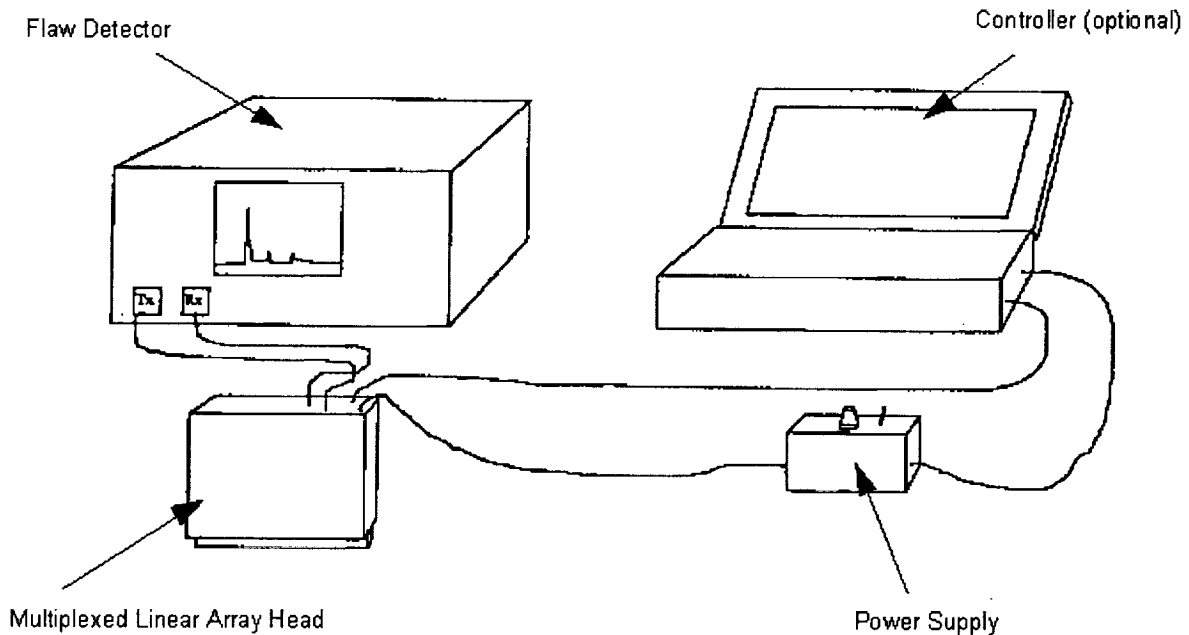


Figure 3. Schematic diagram of the operating configuration which includes a controlling computer, if required, which can also be used for the C-scanning software.

3. THE SCANNING SYSTEM

There are two different situations for rapid lap-joint inspection: long lengths of narrow lap splices and wider areas of doubler reinforcement. Hence it is important to provide suitable scanning systems for both of these instances. However, by far the most common application for rapid inspection on aging aircraft is the great lengths of narrow lap joints on large transport aircraft.

A method was required to track the linear position of the array as it moves along a lap joint which could be over 10 m long. This tracking system needed to be interfaced to C-scanning software and the DERA-developed ANDSCAN[®] system was the obvious choice (10,11). A modification to the standard R-theta scanning arm used a sprung extension potentiometer to measure the radial distance (see Figure 4). This enabled the standard software package to be used after a previous modification for use with multi-element arrays (12).

A trolley is used to hold the array perpendicular to the surface whilst allowing it to move up and down with spring pressure downwards. The array can also swivel about an axis parallel to the extension string. The use of a wheeled trolley also helps to maintain movement in a straight line although deviations will be correctly mapped because the scanning arm is still sensitive to angle as well as radial distance.

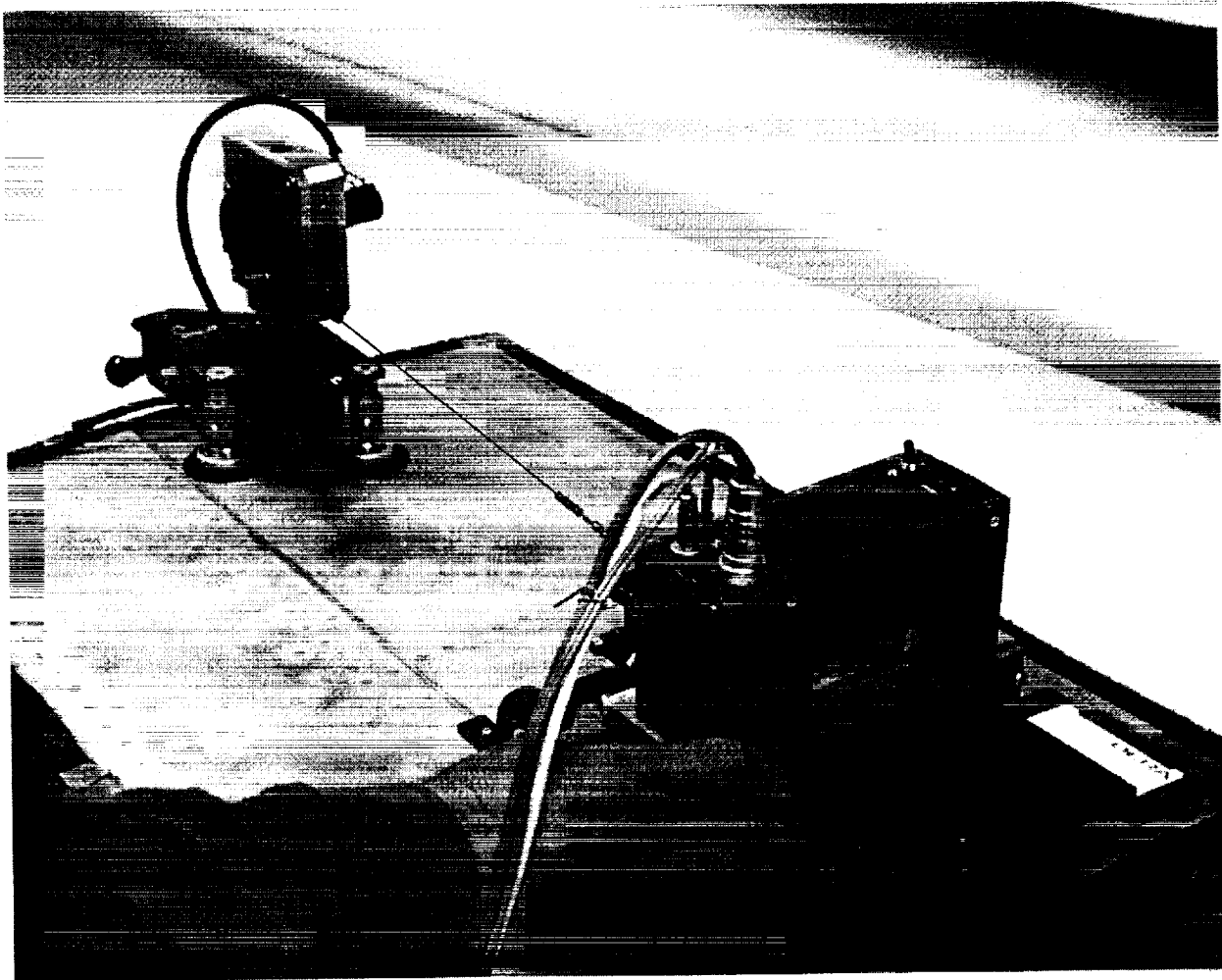


Figure 4. An ANDSCAN[®] positioning system fitted with a sprung extension potentiometer measures the distance along the lap joint.

Provided angular movement does not become rapid or oscillatory the measurement of angular position allows re-scanning of an area without the need to accurately re-position the trolley. However, it is important that the direction of movement is always towards or away from the ANDSCAN base unit because the software assumes that the array lies perpendicular to the extension string.

Another scanning method that is appropriate for a large area - wider than 128 mm - is a manual X-Y scanner. This is another option for interfacing with the ANDSCAN software (see Figure 5). In this case the scanner has been developed at DERA as a combination of two radial arms from the well-known R-Theta scanner originally produced for ANDSCAN. This configuration has advantages for wider areas because the array is always orientated the same way for each swathe. In contrast, the R-Theta scanner requires the array to be perpendicular to the radial direction and is less appropriate for multiple swathes across a large area.

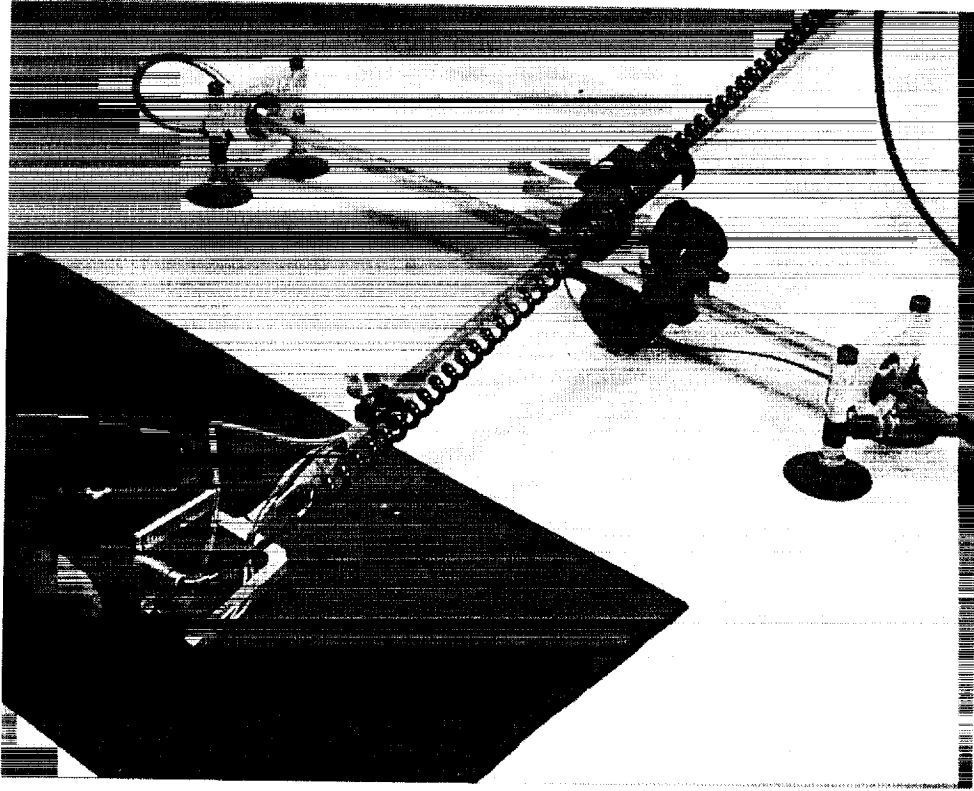


Figure 5. An X-Y scanner for ANDSCAN with a smaller linear array attached, showing that orientation of the array is maintained.

4. RESULTS

A rapid inspection method is primarily concerned with defect detection rather than characterization, although if the same equipment can achieve both then this is very advantageous. Thus the important performance criteria for such a method are: in-plane spatial resolution to ensure critical defect sizes are detected, out-of-plane spatial resolution (equivalent to temporal resolution) to give adequate distinction between closely-spaced interfaces, and other frequency characteristics such as the center-frequency and bandwidth which would be important for spectroscopic measurements such as roughness measurement.

Defect detection capabilities are partly dependent on in-plane spatial resolution so a test block containing different sized flat-bottomed holes and slots was used (see Figure 6). The aim of the specification for the linear array was to achieve a 2 mm (0.08") resolution and the amplitude C-scan of the above test block in Figure 7 demonstrates the ability to detect 1.5 mm-wide (0.06") slots and resolve 1.5 mm-diameter (0.06") holes spaced at 2.5 mm (0.10") centers. However, the time-of-flight scan (or depth scan) in Figure 7 does not show the 1.5 mm (0.06") diameter holes. This was because the amplitude of the reflections from these smallest holes was insufficient to cross the gate threshold set on the flaw detector.

Preliminary trials have produced scanning speeds along the lap-joint in excess of 0.18 m/min (or 7" per minute) - limited by the data acquisition card in the computer. This was measured with a spot size (and therefore resolution) of 1 mm (0.04") and a 128 mm-wide (5") swathe. However, acquisition cards are now available with much improved acquisition features which are ideal for this particular application. After upgrading the data acquisition card, maximum scanning speeds should dramatically increase. Linear speeds up to 3.6 m/min (11'8" per minute) should be possible with a flaw detector capable of a

pulse-repetition-frequency (PRF) of 8 kHz, although this may then be limited by the time taken to update the C-scan information in the computer.

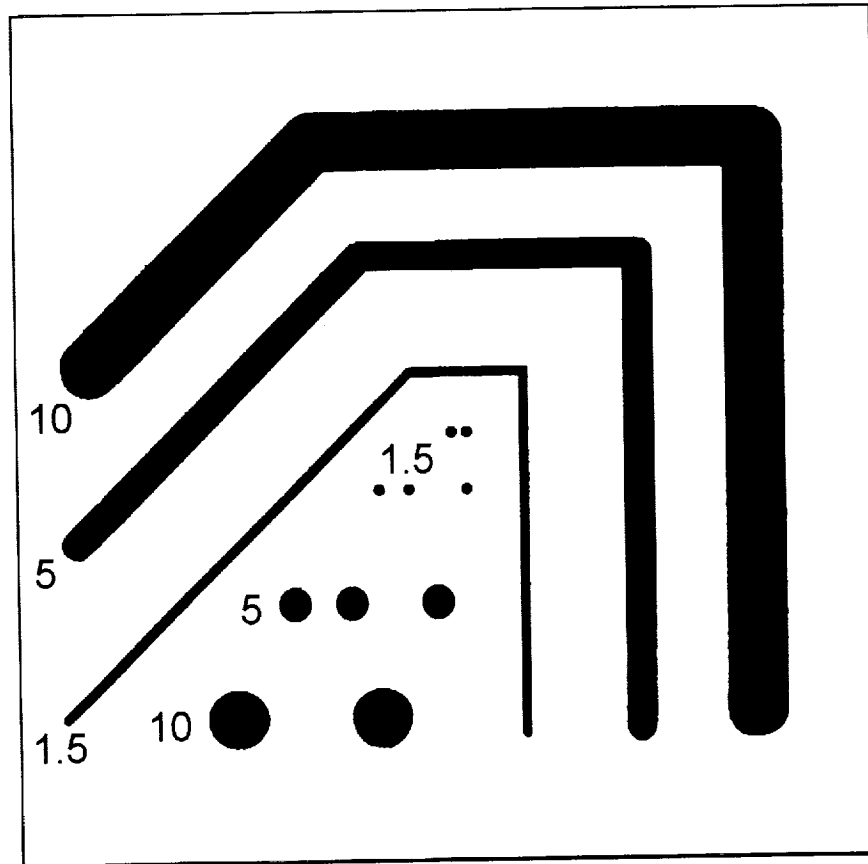


Figure 6. Diagram of resolution test specimen with flat-bottom holes and slots in 9 mm (0.36") thick aluminum. The labels give the slot width, or hole diameter, in mm. The closest 1.5 mm (0.06") diameter holes are spaced at 2.5 mm (0.10") centers.

CONCLUSIONS

A new rapid lap-joint inspection has been developed using simple additions to conventional equipment. Ultrasonic resolution of 1.5 mm (0.06") and scanning resolution of 1 mm (0.04") at a speed in excess of 0.18 m/min (or 7" per minute) has been demonstrated - limited by the data acquisition card in the computer. This was measured with a spot size (and therefore scan step-size) of 1 mm (0.04") and a 128 mm-wide (5") swathe. After upgrading the data acquisition card, a speed of up to 3.6 m/min (11'8" per minute) should be possible with a flaw detector capable of a pulse-repetition-frequency (PRF) of 8 kHz. Further work is required to optimize the ultrasonic performance the coupling onto curved or undulating surfaces, and the scanning speed.

ACKNOWLEDGMENTS

The authors are grateful to Mr Lyn Jones and Dr David Bruce of the NDE Group at DERA for assistance in the development of the linear array transducer and the scanning system, and to Mr David Lines of Diagnostic Sonar Ltd for the multiplexer design and transducer development.

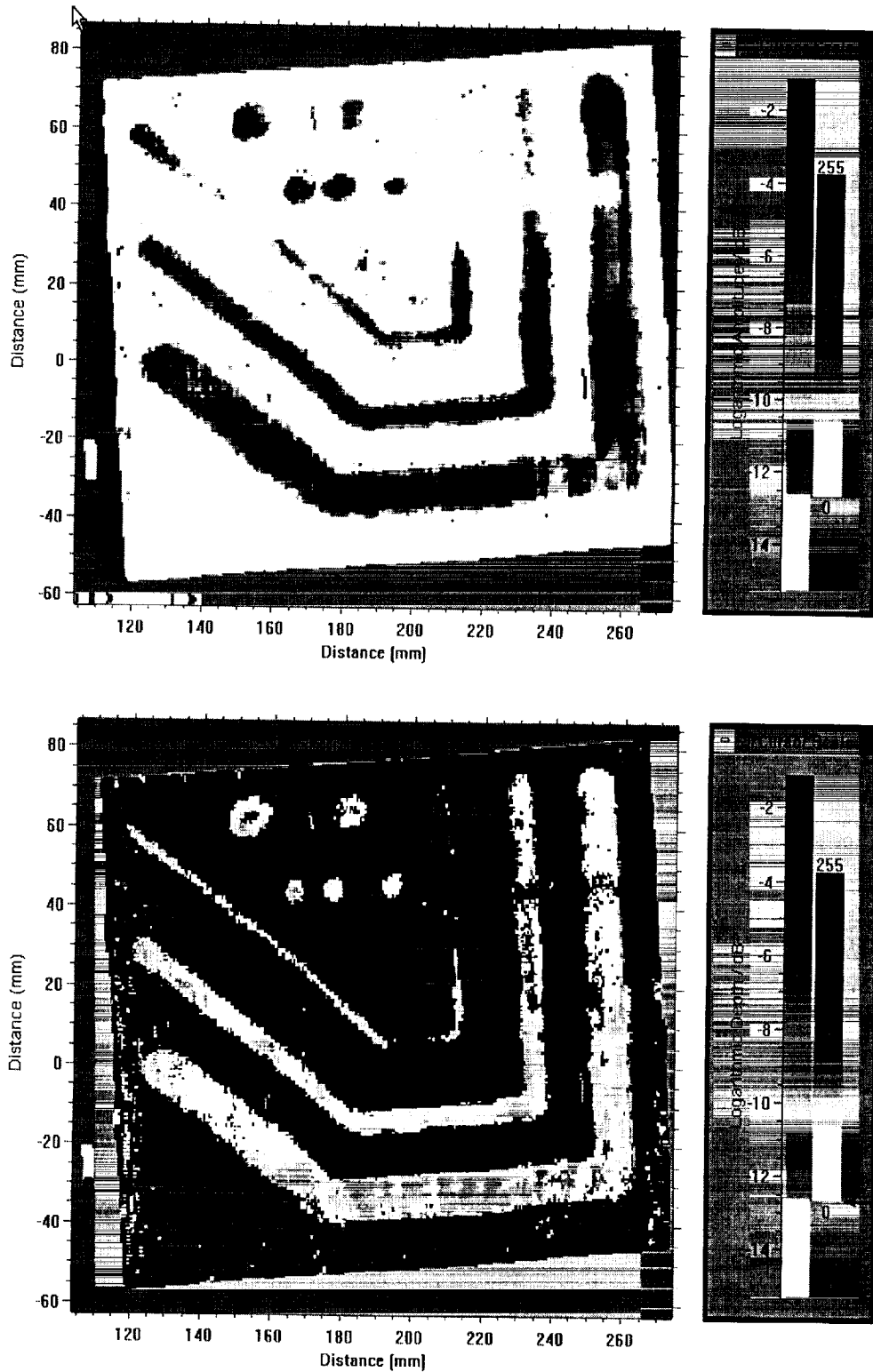


Figure 7. Defect-gated amplitude C-scan (top) and depth scan (bottom) of an aluminum resolution test specimen. On the amplitude scan the 1.5 mm (0.06") diameter holes spaced at 2.5 mm (0.10") can just be resolved. These were the first scans obtained with the array and can probably be improved upon.

REFERENCES

1. Reighard M K, Van Oordt T W and Wood N L, "Rapid ultrasonic scanning of aircraft structures." *Materials Evaluation*, Vol 49, No 12, pp 1506-1514, 1991.
2. Khalid A, Chen S, Fan A, Satter T and Bridge B, "Development of a climbing robot for the deployment of NDT sensors in hazardous environments." *Insight - Journal of the British Institute of NDT*, Vol 36, No 12, pp 943-948, 1998.
3. Backes P G, Bar-Cohen Y and Joffe B, "The Multifunction Automated Crawling System (MACS)." *Proc IEEE Int Conf on Robotics and Automation*, Albuquerque NM, pp 335-340, April 1977.
4. Savakus H P, Klicker K A and Newham R E, "PZT-Epoxy piezoelectric transducers: a simplified fabrication process." *Mater Res Bull*, Vol 16, pp 677-680, 1980.
5. Hayward G and Hossack J, "Unidimensional modelling of 1-3 composite transducers." *J Acoust Soc Am*, Vol 88, pp 599-608, 1990.
6. Powell D J and Hayward G, "Flexible ultrasonic transducer arrays for nondestructive evaluation applications - Part I: The theoretical modelling approach." *IEEE Transactions on Ultrasonics, Ferroelectrics, and Frequency Control*, Vol UFFC-43, No 3, pp 385-392, 1996.
7. Powell D J and Hayward G, "Flexible ultrasonic transducer arrays for nondestructive evaluation applications - Part II: Performance assessment of different array configurations." *IEEE Transactions on Ultrasonics, Ferroelectrics, and Frequency Control*, Vol UFFC-43, No 3, pp 393-402, 1996.
8. Reynolds P and Hayward G, "Design and construction of a new generation of flexible ultrasonic transducer arrays." *Insight - Journal of the British Institute of NDT*, Vol 40, No 2, pp 101-106, 1998.
9. Lines D A, "Rapid inspection using integrated ultrasonic arrays", *Insight - Journal of the British Institute of NDT*, Vol 40, No 8, pp 573-577, 1998.
10. Smith R A, "Evaluation and accuracy assessment of ANDSCAN - a non-destructive portable scanner, Part 1. ANDSCAN hardware and software," *Insight - Journal of the British Institute of NDT*, Vol 37, No 4, pp 284-289, 1995.
11. Smith R A, "Evaluation and accuracy assessment of ANDSCAN - a non-destructive portable scanner, Part 2. NDT applications and specialised features; accuracy and repeatability," *Insight - Journal of the British Institute of NDT*, Vol 37, No 5, pp 352-357, 1995.
12. Willsher S J and Smith R A, "Multi-element ultrasonic scanning of in-service air-frames", *Insight - Journal of the British Institute of NDT*, Vol 40, No 3, pp 154-159, 1998.

USE OF ACOUSTIC EMISSION MONITORING TO DETECT, LOCATE AND MEASURE MULTIPLE SITE DAMAGE (MSD) FATIGUE CRACK GROWTH UNDERNEATH RIVET HEADS

Stuart L. McBride
AEMS Acoustic Emission Monitoring Services Inc.
Kingston, Ontario, K7L 1X4, Canada
Tel/Fax: (613) 544-6792
aems@kos.net

Jason P. Scott
Department of Mechanical and Aerospace Engineering, Carleton University
Ottawa, Ontario, K1S 5B6, Canada

Graeme F. Eastaugh
National Research Council Canada, Institute for Aerospace Research
Ottawa, Ontario, K1A 0R6, Canada

ABSTRACT

This presentation describes an investigation into the feasibility of using acoustic emission monitoring (AEM) for the detection and measurement of multiple site damage (MSD) fatigue cracks underneath the rivet heads of a fuselage skin splice during laboratory fatigue testing. There are currently no other known laboratory or in-service methods for the measurement of cracks under rivet heads. Furthermore, the only technique available for constructing crack growth curves for such situations is that of counting microscopic fatigue striations.

A special MSD test specimen was used to simulate a fuselage splice. The specimen was manufactured from aluminum alloy 2024-T3 and was roughly representative of the skin splices in some pressurized transport aircraft fuselages. Constant amplitude fatigue loading was used to simulate fuselage pressurization cycles, and cracks were allowed to nucleate naturally, i.e., without the use of artificial notches. The four central rivet holes in the critical rivet row of the specimen were monitored using two pairs of piezo-electric sensors placed in a line 3.8 cm from the critical rivet row. The fatigue test was terminated shortly after "visual initiation" - the appearance of the first crack beyond a rivet head. Post-test analysis was performed using standard AEMS Inc. interactive software, except for some new algorithms that were developed to remove fretting and rubbing noise at each rivet location. Crack growth curves showing crack face area vs. cycles were constructed for the period of crack growth underneath the rivet heads. For these curves, the relationship between acoustic events and crack growth increments was obtained by a separate calibration test on a coupon specimen containing a single countersunk open hole. The AEM results were compared with fractographic measurements.

The investigation indicated that the AEM techniques used could detect small hidden cracks under rivet heads and that it might be possible to obtain useful crack growth curves showing crack face area vs. cycles from AEM data alone. Individual crack growth curves could be obtained when there was only one crack on one side of a rivet hole. Otherwise, there was ambiguity in the time-of-flight data and only curves showing aggregate crack area could be constructed. Acoustic events translated into clearly defined crack growth curves at all the monitored holes. Such curves initiated at all holes at between 60% and 70% of the visual initiation period of the specimen, indicating that hidden MSD had developed long before the first crack was detected visually. The crack face areas associated with these AEM detection points were estimated to be about 0.1 sq. mm - i.e., about 10% of the area of a visibly detectable crack. Additional tests are planned to confirm the results, determine the consistency and accuracy with which crack growth curves can be constructed, and develop routine test and analysis procedures for application by trained (NDE) technicians.

1. INTRODUCTION

This paper describes an investigation into the feasibility of using acoustic emission monitoring (AEM) for the detection, location and monitoring of multiple fatigue cracks under the rivet heads in a fuselage skin splice during laboratory fatigue testing and the construction of crack growth curves.

The investigation was a collaborative research project involving AEMS Acoustic Emission Monitoring Services Inc. (AEMS Inc.), Carleton University and the National Research Council Institute for Aerospace Research (NRC/IAR). It used a special multiple site fatigue damage (MSD) test specimen developed by the NRC and Carleton University and AEM technology developed by AEMS Inc. for laboratory testing⁽¹⁻³⁾ and full-scale structural testing⁽⁴⁻⁷⁾. The MSD test specimen⁽⁸⁾ was manufactured from aluminum alloy 2024-T3 and is generally representative of the skin splices in some pressurized transport aircraft fuselages. The acoustic emission tests were conducted as part of a wider investigation of the MSD fatigue and corrosion/fatigue characteristics of fuselage splices being conducted by the NRC and Carleton University. Cracks were allowed to develop naturally in the specimen during the test without artificial notches. Fatigue loading was terminated shortly after the first crack appeared beyond a rivet head.

The objectives of the AEM tests were:

- a) To determine if fatigue cracks can be detected, located and monitored under several rivet heads simultaneously.
- b) To determine if fatigue crack growth curves (plots of crack face area vs. fatigue cycles) can be determined for growth under the rivet heads and for a short distance beyond the rivet heads.
- c) To determine the size of the smallest fatigue crack underneath the rivet heads which can be detected by AEM.
- d) To determine effective procedures for the routine AEM of MSD test specimens.

The tests show that, under laboratory conditions, cracks under rivet heads can be detected, located and monitored by AEM. Evidence of damage in the rivet holes is detectable by AEM at 10-20% of the number of load cycles required to produce one fatigue crack which is large enough to be detected visually outside a rivet head. The source mechanism for these data has not been determined at this time but it is believed to be due to damage in the countersink material or to precrack deformation processes. Later in the fatigue test, at 50-60% of the number of load cycles required to produce one fatigue crack which is large enough to be detected visually outside a rivet head, acoustic emission commences which increases rapidly for subsequent load cycles. This activity is attributed to growing fatigue cracks. The results show that it is feasible to obtain crack growth curves from this data for cracks hidden beneath rivet heads. These fatigue crack growth curves could be used for damage tolerance analysis of aircraft fuselage splices.

2. EXPERIMENTAL

This section describes the MSD test specimen, acoustic emission calibration and analysis procedures and the general experimental procedure. The acoustic emission analysis method used here was applied to the data when mechanical testing was completed. The method could be implemented, however, during data acquisition. This would provide crack growth curves which could be automatically updated and displayed as the test progresses.

2.1 DESCRIPTION OF MSD TEST SPECIMEN

The MSD test specimen consists of two sheets of 0.040 inch thick 2024-T3 clad aluminum alloy joined by a three-row riveted lap splice⁽⁸⁾ as shown in Figure 1. Straps and doublers are bonded to each side of the sheets to control the stress distribution before and during crack development so as to simulate the conditions experienced by the longitudinal fuselage splice of a pressurized transport aircraft. The configuration of the specimen and the stress level used in the tests here are roughly representative of narrow-body transport aircraft. The rivet holes are countersunk to a knife-edge and so represent a worst-case condition. Cracks are allowed to nucleate naturally, i.e., without the use of artificial notches. The AEM sensor arrays used to monitor the MSD test specimen (Figure 1) were selected to optimize the line-of-sight between the potential crack sites and the sensors. Mechanical testing consisted of uniaxial constant amplitude load cycling at a frequency of 2 Hz. The loading conditions used consisted of a maximum load of 7,219 lbs with an R value of 0.02. Under these conditions, the maximum stress 1 inch from the critical rivet row is 14 ksi.

2.2 ACOUSTIC EMISSION PROCEDURES

Acoustic emission data was continuously recorded during load cycling for each sensor pair using the AEMS-1002M acoustic emission data acquisition system. The data was transferred via modem to AEMS, Kingston for interpretation. AEMS Inc. equipment and software embody automatic and semi-automatic techniques for distinguishing acoustic signals related to crack growth at the rivet holes from those related to fretting and rubbing at the same rivet holes and from extraneous noise. Analysis of the acoustic emission data involved mainly the development of procedures to remove fretting noise from the data set. The algorithms used to remove signals not related to crack growth are the standard multi-purpose algorithms available in AEMS Inc. analysis software. These algorithms were applied in the same manner to all acoustic emission data. For the MSD specimen tests, some preliminary work was required to characterize the ambient acoustic and electrical noise, optimize equipment settings and dampen extraneous acoustic noise produced by the mechanical testing equipment. In addition, some new algorithms were added to the software to improve the extraction of fretting and rubbing noise at the rivet holes from the acoustic data. These algorithms were applied to the recorded data after mechanical testing was completed. Two types of calibration are required for the successful application of AEM to the location of growing fatigue cracks and the quantitative determination of the amount of crack growth.

2.2.1 Difference-in-Arrival-Time (Δt) Calibration

Difference-in-arrival-time (Δt) calibration is accomplished by the application of acoustic emission simulation signals at various locations in the structure. The locations selected here for the application of acoustic emission simulation signals are close to each sensor, just outside each linear sensor array along the line connecting the sensors (see Figure 1). The resulting recorded Δt values are then used to construct constant Δt contours which can be superimposed on the structure as shown in Figure 1 and subsequently used to relate acoustic emission data to structural locations. The validity of this calibration is separately checked by applying acoustic emission simulation signals at each of the rivet locations.

2.2.2 Material Calibration

Material calibration was carried out independently of the MSD test by AEM of fatigue crack growth in a simple coupon specimen of the same thickness and material as the MSD specimen and which contained a countersunk hole similar to the rivet holes in the MSD specimen. This coupon was fatigued under stress conditions similar to those which occur in the MSD test specimen. Since the coupon specimens do not have rivets installed in the countersink holes, calibration data obtained in this manner is not complicated by interfacial rubbing and fretting noise. Table 1 lists the experimental parameters used for these acoustic emission calibration tests.

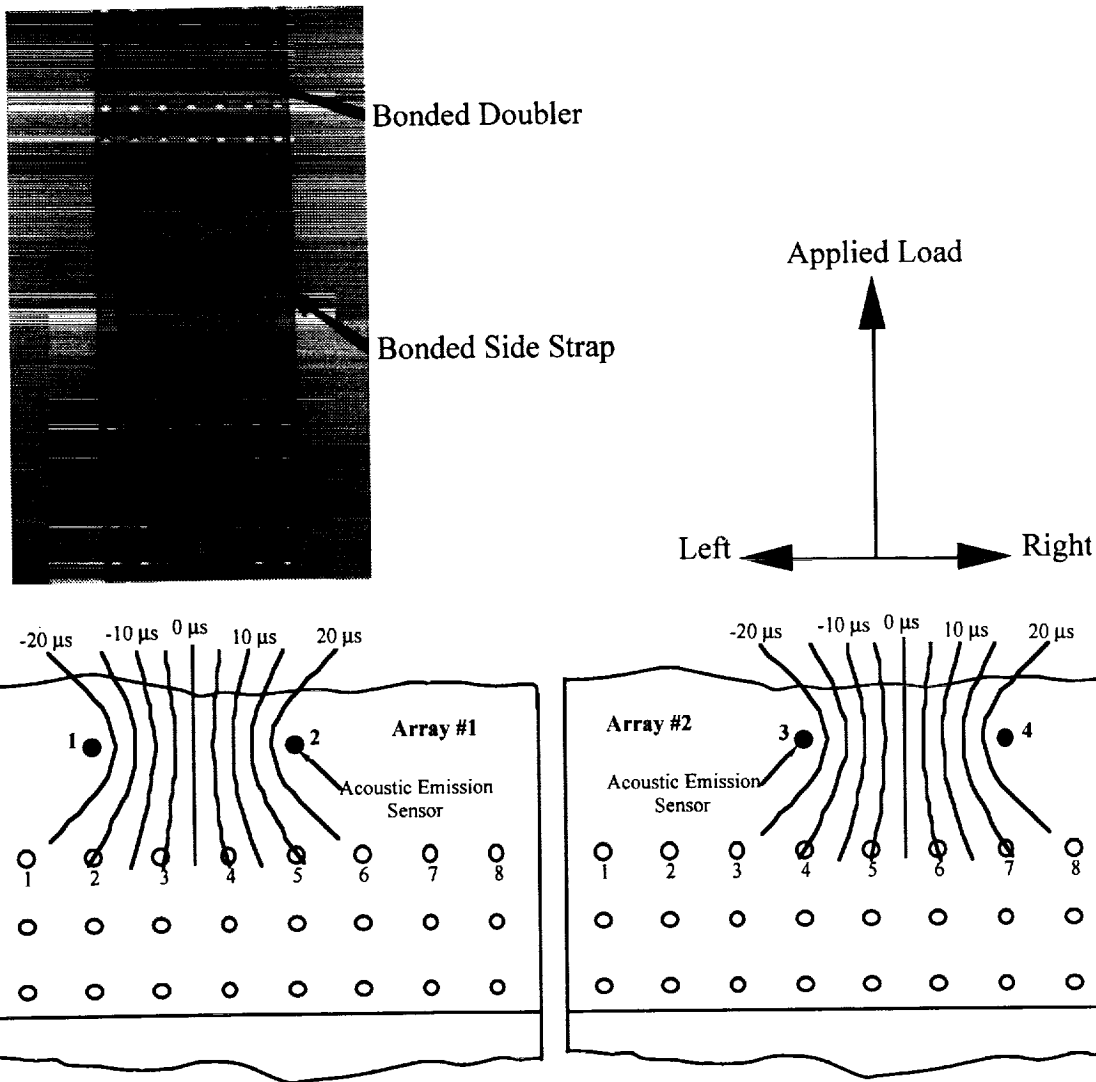


Figure 1 Photograph of the MSD test specimen and illustration of the rivet rows showing the location of the acoustic emission sensors. The horizontal distance between rivet holes is 1 inch. The loci shown are the lines of constant difference-in-arrival-time (Δt) used to locate acoustic emission sources.

TABLE 1. ACOUSTIC EMISSION CALIBRATION TEST PARAMETERS

Test Parameter	Value or Range
Parameters used in separate acoustic calibration tests on single sheet coupons containing a single countersunk hole.	
SEN and 100° Countersink Specimens	12" x 1" x 0.04"
Maximum Stress (S_{max})	5-15 ksi
Stress Intensity Factor Range (ΔK)	10-15 MPa \sqrt{m}
Load Ratio (R)	0.05
Acoustic Emission Amplitude Threshold	≥ 45 dB relative to 1 μV
AEM Detection Range	$\geq 94\%$ of Maximum Load

An alternative method of calibration could be based on the acoustic emission data obtained from one crack which is large enough to be observed visually outside the rivet head. This internal calibration method (which was not used here) would assure that the calibration was valid for stress conditions characteristic of rivet holes in the riveted splice.

2.3 GENERAL TESTING PROCEDURE

For the MSD test specimen reported here, the cycling frequency was 2 Hz and the test was continued with acoustic emission data being recorded until a crack emerged from beneath one of the rivet heads. The MSD test specimen (Figure 1) was continuously acoustic emission monitored during constant amplitude cyclic loading until visible cracks were detected at rivets 4 and 5 at 136,000 load cycles. Following this, the critical rivet row was cut out of the specimen so as to provide one-inch square specimens each containing a rivet. The rivets were then carefully removed and the countersink of each rivet hole examined for cracks. A small loading fixture was used to apply a tensile load to each specimen to increase the visibility of cracks. Visible cracks were detected only in the countersunk sheet. Crack face areas were estimated from crack lengths measured on the surface of the countersink by assuming a through-crack with a circular crack front centered at the initiation site located at the countersink knife edge. Cracks were not clearly visible on the faying surface of the sheet because they were obscured by fretting damage. The acoustic emission results are presented in the form of plots of derived crack face area versus fatigue cycles. These plots can be used in their present form for damage tolerance analysis or they can be converted to plots of crack length versus fatigue cycles by invoking the rivet hole geometry. The total crack face area determined by fractographic examination is shown in each figure for comparison. The acoustic emission data and the associated source location (Δt) were analyzed to estimate the crack growth at each rivet location. An optical microscope was used periodically during the tests to measure any visible cracks.

3. RESULTS AND DISCUSSION

The material calibration tests on open-hole coupons (Table 1) indicated that acoustic emission events due to fatigue crack growth occurred only above 94% of maximum cyclic load. This phenomenon is a known one in AEM and was confirmed in the analysis of MSD test specimen data. It will simplify the analysis of future tests by allowing it to be focussed on that portion of the load cycle when the load is increasing from 94% to 100%.

Figure 2 illustrates the location and sizes of the fatigue cracks in the MSD test specimen observed at the end of the test for rivets number 3, 4, 5 and 6 in the MSD test specimen. Figure 2 shows that:

- a) the cracks on the right side of rivet 4 and rivet 5 extend outside the rivet head. These cracks were observed visually on the specimen before disassembly.
- b) all other cracks were entirely hidden by rivet heads prior to disassembly.
- c) crack growth is primarily in a direction perpendicular to the applied load.
- d) crack initiation normally occurs in the upper half of the rivet hole.
- e) several cracks are present in each rivet hole.

Table 2 summarizes the locations and sizes of these cracks. The acoustic emission data is used here to determine the fatigue crack face area as a function of the number of constant amplitude load cycles. This determination is carried out for the aggregate fatigue crack growth associated with each individual rivet hole. When it is possible to associate acoustic emission data with a single crack, the crack growth curve was separately determined.

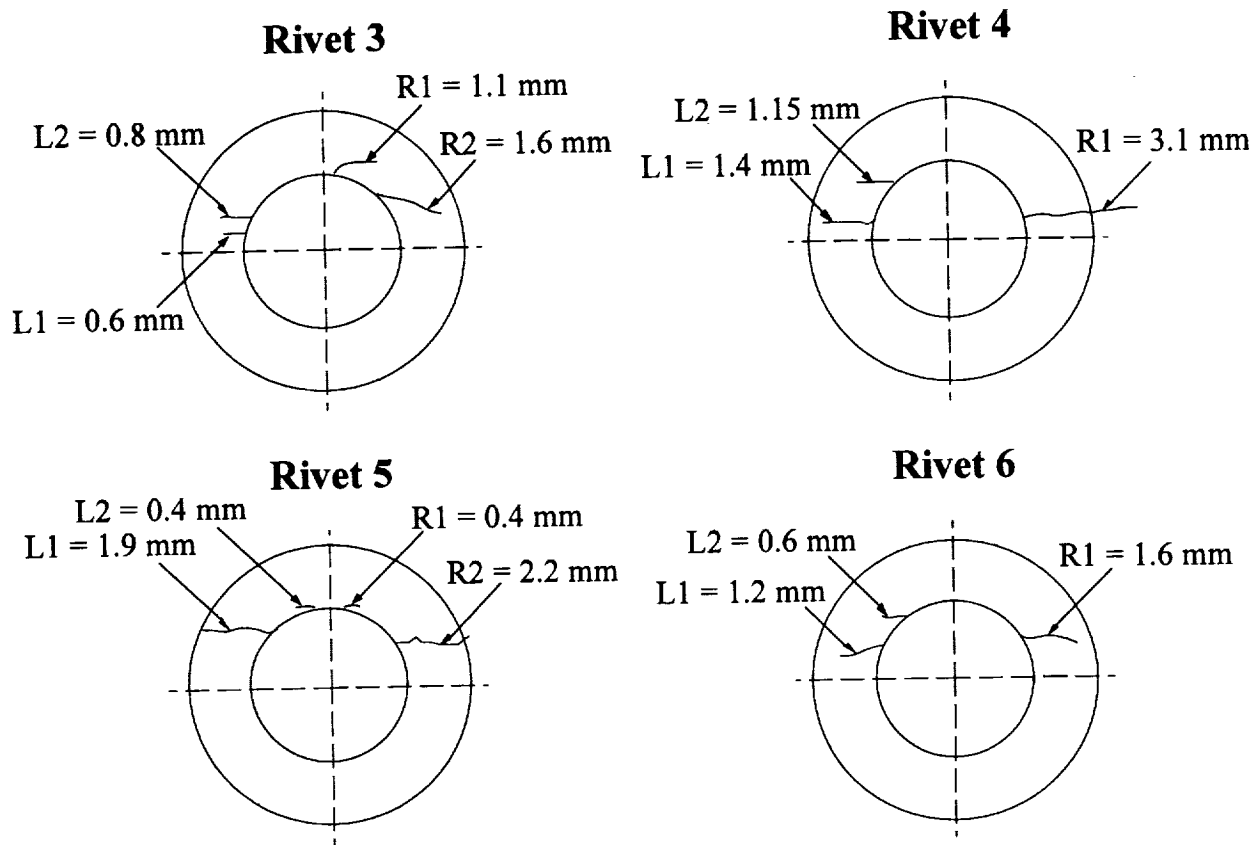


Figure 2. Location and size of fatigue cracks in each of the rivet hole countersinks.

TABLE 2. OPTICAL MICROSCOPE MEASUREMENTS OF CRACK SIZE (FIGURE 2)

Rivet Number	Crack Location	Measured Crack Length (mm)	Crack Face Area (mm ²)
Summary of crack locations, crack lengths and crack face area. These data are derived from the optical microscope measurements (Figure 2).			
3	left 1	0.6	0.12
	left 2	0.8	0.20
	right 1	1.1	0.22
	right 2	1.6	0.56
4	left 1	1.4	0.56
	left 2	1.2	0.29
	right 1	3.1	2.20
5	left 1	1.9	0.95
	left 2	0.4	0.02
	right 1	0.4	0.02
	right 2	2.3	1.30
6	left 1	1.2	0.36
	left 2	0.7	0.09
	right 1	1.6	0.56

Crack growth plots showing aggregate crack face area against cycles for each of the four rivets monitored are shown in Figure 3. Since the acoustic data for the single cracks on the right side of rivets 4 and 5 could be unambiguously separated from the other data, crack growth curves for these individual cracks were determined and are shown in Figure 4. The crack face areas were computed from the acoustic emission data for each rivet after removal of rivet rubbing and fretting noise. The removal of rubbing and fretting noise from the data set was accomplished for each rivet by applying the same algorithm to all data from each rivet. For the plots of individual cracks all acoustic data for one side of the rivet, including rubbing and fretting noise, were separated from the data for the whole rivet location prior to the application of the algorithm. When each side of a rivet is treated individually in this manner, there is theoretically less likelihood of crack events being treated as fretting noise by the algorithm, and so the net estimate of crack growth might be slightly greater. The crack face areas obtained from the fractographic examination are listed in Table 2 and are marked on each graph in Figures 3 and 4 for comparison with the crack face areas estimated using acoustic data. The agreement between acoustic and fractographic measurements is good, particularly for the individual cracks in Figure 4.

Most of the crack growth plots show a few apparent crack growth events early in the fatigue test followed by a quiescent period and then a succession of closely spaced crack events. The early events are believed to be due to damage in the rivet hole but cannot be unambiguously identified as fatigue crack propagation. They are included here as crack growth events pending further investigation of the source of these early events and the meaning of the quiescent period.

Based on the earlier calibration tests on single hole coupons, the acoustic emission equipment is estimated to have been capable of detecting crack increments in the MSD specimen of 0.02 mm^2 or more. The acoustic emission amplitude threshold used was 45 dB relative to $1 \mu\text{V}$ at the preamplifier.

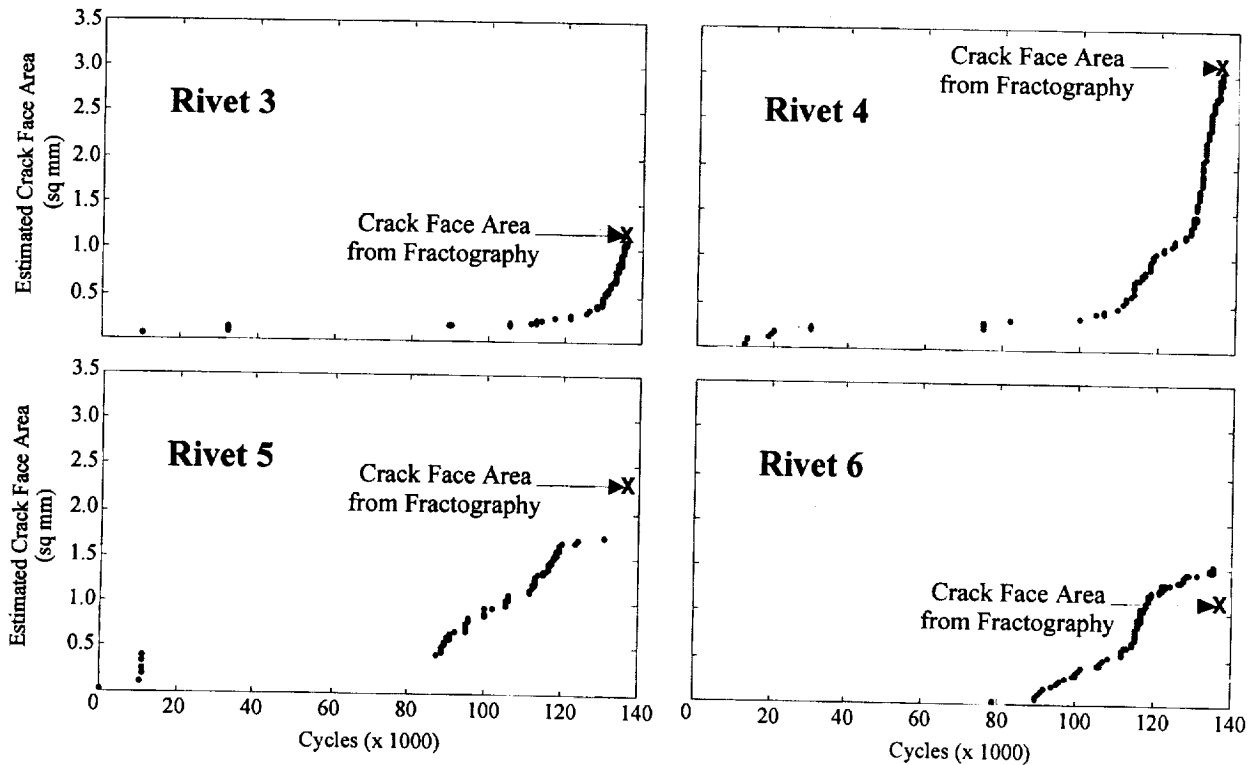


Figure 3. Estimated crack face area for rivets 3, 4, 5 and 6 derived from the data which remains after removal of fastener rubbing and fretting noise. The crack face area from fractography is the sum of the crack face areas listed in Table 2.

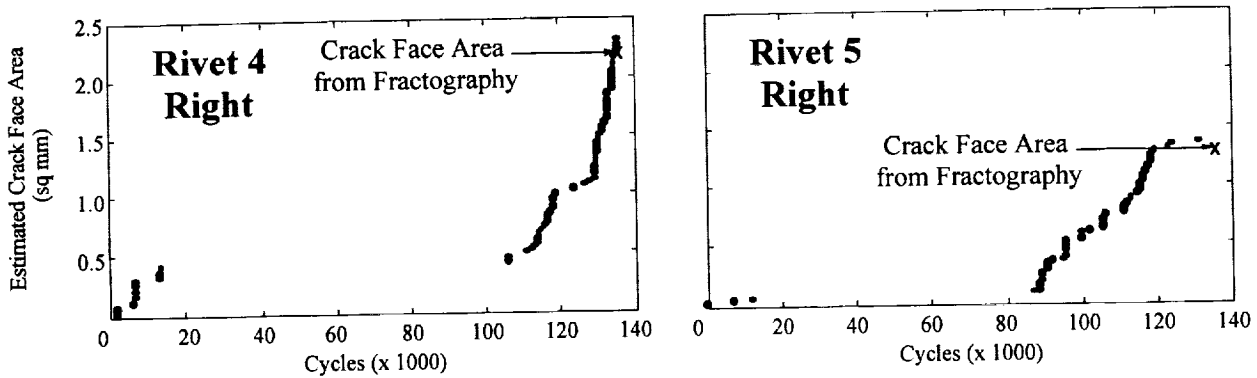


Figure 4. Estimated crack face area for the right side of rivets 4 and 5 derived from the data which remains after removal of fastener rubbing and fretting noise. The crack face areas from fractography are those listed in Table 2.

Experience has indicated that, due to the presence of rubbing and fretting noise at the rivet holes, an accumulation of crack events corresponding to a total crack increment of at least 0.1 mm^2 would be required to give a reliable indication of the presence of a crack under constant amplitude loading. This area increment corresponds to a crack length of about 0.5 mm for a crack which initiated at the bottom of a rivet hole countersink. Acoustic emission that was clearly attributable to crack growth started at rivet 4 at 75,000 load cycles (55% of the number of load cycles required to produce one fatigue crack that is large enough to be detected outside a rivet head). Well defined crack growth curves started at the other three rivets a short while later, indicating that hidden MSD existed under all four rivets well before visual initiation. The individual crack growth plot for rivet 5 right in Figure 4 indicates that this well defined crack growth may be detectable starting at crack face areas as low as 0.1 mm^2 , a crack length of about 0.5 mm, but further tests are needed for statistical confirmation.

An interesting feature of the crack growth plot for rivet 4 is the temporary flattening out of the growth curve in the region of 120,000 cycles. A similar phenomenon appears to have occurred at rivets 5 and 6, except that the final acceleration of the crack area growth rate is not evident - possibly because the test was terminated too soon for it to occur. These features may be related to the geometric discontinuity at the edge of the countersink, crack interaction, or local effects of stresses introduced by riveting.

The results presented above indicates that acoustic emission can be used to measure fatigue crack growth beneath rivet heads in a MSD test specimen subjected to constant amplitude cyclic loading. Further work is planned to confirm this capability. Similar results might be achievable in full-scale laboratory tests on transport aircraft fuselages or fuselage panels, where constant amplitude loading is representative of service use. The use of AEM during variable (programmed) loading has not been addressed here but previous work by one of the authors has demonstrated the potential for using acoustic emission to monitor and measure fatigue crack growth under fastener heads in full-scale structural tests in which programmed loading was used⁽⁴⁻⁷⁾. To obtain crack growth results in such a case, a calibration of the relation of acoustic emission to crack growth under the full-scale test loading conditions is required. Such a calibration could be determined by applying the full-scale test spectrum to a representative coupon specimen in the laboratory.

While the acoustically measured crack growth data presented in this paper was in part obtained by creating and applying new analysis procedures after the MSD specimen test was completed, these procedures are such that they can be applied uniformly in an automated or semi-automated manner to future tests. Consequently, an on-line analysis during data acquisition could be developed to provide crack growth curves which are automatically updated and displayed as the test progresses.

4. SUMMARY AND CONCLUSIONS

Acoustic emission was used successfully to detect, locate and monitor crack growth under rivet heads in a MSD specimens designed to simulate a riveted fuselage splice. Analysis of the acoustic emission data based on an independent coupon test calibration produced crack growth curves (fatigue crack face area versus number of load cycles) which are in good quantitative agreement with the crack sizes determined fractographically after completion of mechanical testing. AEM was shown to be equally effective at estimating the aggregate crack growth of multiple cracks present within the same rivet hole (Figure 3) or at determining the growth of those single fatigue cracks which could be individually distinguished by AEM (Figure 4).

The results presented here indicate that acoustic emission can be used to measure fatigue crack growth beneath rivet heads in a MSD test specimen subjected to constant amplitude cyclic loading. Similar results might be achievable in full-scale laboratory tests on transport aircraft fuselages or fuselage panels, where constant amplitude loading is representative of service use. The use of AEM during variable (programmed) loading has not been addressed here, but previous work by one of the authors has demonstrated the potential for using acoustic emission to monitor and measure fatigue crack growth under fastener heads in full-scale structural tests in which programmed loading was used^(4,7). To obtain crack growth results in such a case, a calibration of the relation of acoustic emission to crack growth under the full-scale test loading conditions is required.

In summary, we conclude the following:

- a) Acoustic emission can be used in a MSD environment to detect, locate and monitor fatigue cracks which are hidden by rivet heads in a fuselage skin splice.
- b) Fatigue crack growth is first clearly detectable at about 50% to 60% of the number of constant amplitude load cycles at which a crack, emerging from under a rivet head, is first detected visually. Further tests are needed to provide statistical confirmation of the reliability of AEM estimates of the associated crack lengths.
- c) Apparent crack indications occur at 10% to 20% of the number of constant amplitude load cycles at which a crack, emerging from under a rivet head, is first detected visually. The source mechanism for these data has not been established but they are believed to be due to damage within the rivet hole and may be associated with fatigue crack initiation.
- d) Crack growth curves (plots of crack face area versus number of constant amplitude fatigue cycles) can be determined for crack growth under the rivet heads. These crack growth curves are based on an independent AEM calibration determined from fatigue testing of a coupon manufactured from the MSD specimen material. Independent calibration is not necessary, however, if the crack face area can be determined for one crack which is detectable visually outside the rivet head or if fractographic measurements of the crack face areas have been made in a previous test on a similar specimen.
- e) On-line analysis during data acquisition could be used to provide crack growth curves which are automatically updated and displayed as the test progresses.

5. ACKNOWLEDGEMENTS

The authors gratefully acknowledge the access to this test which was kindly provided by Carleton University (Professor P. V. Straznicky) and the National Research Council of Canada (Mr. D. L. Simpson). Partial funding of this work was provided by the National Research Council of Canada and the Department of National Defence (3GB12W7711-7-7370).

6. REFERENCES

1. S. L. McBride and K. Gong, Acoustic Emission Monitoring of Plastic Deformation and Fatigue Crack Propagation in an Aluminum Alloy which Exhibits Localized Yielding, to be published.
2. S. L. McBride, K. Gong and Y. Hong, The Relation Between Acoustic Emission and Crack Growth Parameters During Fatigue in Aluminum Alloys and Steels, to be published.
3. AEMS Inc., Acoustic Emission Monitoring of Multiple Site Damage (MSD) Fatigue Cracks Under Rivet Heads in a Laboratory Specimen Which is Representative of a Fuselage Skin Splice, Report submitted to the National Research Council, Institute for Aerospace Research (1998).
4. S. L. McBride and J. W. Maclachlan, Identification of Acoustic Emission Signals Due to Crack Growth, Crack Face Rubbing and Structural Noise in the CC-130 Hercules Aircraft, Review of Progress in Quantitative Nondestructive Evaluation, 2A, pp. 517-531 (1983).
5. S. L. McBride, M. R. Viner and M. D. Pollard, Acoustic Emission Monitoring of Aging Aircraft Structures, Review of Progress in Quantitative NDE, 11B, pp. 2275-2282 (1992).
6. S. L. McBride, M. D. Pollard and Y. Hong, Enhanced Fatigue Crack Detection in Aging Aircraft Using Continuous Acoustic Emission Monitoring, Review of Progress in Quantitative NDE, 12, pp. 2191-2197 (1993).
7. S. L. McBride, G. Deziel and S. Le Guellec, Acoustic Emission Monitoring of Full-Scale Fatigue Tests on Canadian Forces Aerospace Structures, 1994 USAF Structural Integrity Program Conference, pp. 239-254 (1995).
8. G. F. Eastaugh, D. L. Simpson, P. V. Straznicky and R. B. Wakeman, A Special Uniaxial Coupon Test Specimen for the Simulation of Multiple Site Fatigue Crack Growth and Link-up in Fuselage Splices, AGARD-CP-568 (1995).

BONDED REPAIR TECHNIQUES USING SOL-GEL SURFACE PREPARATIONS

Kay Y. Blohowiak, Kenneth A. Krienke, Joseph H. Osborne
Boeing, Phantom Works,
Seattle, WA 98124-2499
Tel: (253) 773-2055
Fax: (253) 773-5941
E-mail: kay.y.blohowiak@boeing.com

James J. Mazza
AFRL/MLSA, WPAFB, OH

Georgette B. Gaskin, Jonahira R. Arnold
Naval Aviation Systems Team, Patuxent River, MD

William S. DePiero, Joseph Brescia
US Army TACOM-ARDEC, Picatinny Arsenal, NJ

ABSTRACT

This joint development program is a concerted SERDP-funded Tri-Service effort to develop sol-gel surface treatments for adhesive bonding on aluminum, titanium, and steel surfaces. Sol-gel formulations and processes applicable to epoxy adhesive systems were developed. These nonchromated, water-based sol-gel coating systems are comprised of environmentally-acceptable materials and can be applied on the substrate by spraying, brushing, or swabbing for various repair applications. The joint R&D project focuses on development, optimization, and implementation of these sol-gel processes for repair and remanufacture of aircraft structures. The goals of this program are to design a process that 1) increases durability, 2) improves process robustness, 3) decreases repair time, 4) uses simple equipment and processes, 4) uses environmentally-friendly materials, and through all of these 5) increases affordability. Depot sites, including NADEP-North Island, NADEP-Cherry Point, Warner Robins ALC, and Corpus Christi Army Depot are involved in the requirements generation and testing cycle to ensure end-user needs are being met and technology transition issues are assessed. Current and potential applications of this technology on aerospace hardware and manufacturing and repair criteria are discussed.

1.0 INTRODUCTION

Corrosion and fatigue of aircraft structure are two of the biggest problems limiting the lives of military aircraft. Adhesively bonded repair/reinforcement is a key approach for maintaining the Air Force's aging fleet, especially as a remedy for fatigue cracks. Bonding is also important for maintaining other DoD weapons systems. Bonded repairs provide substantial cost savings and reduced aircraft downtime when compared to component replacement. Bonded repairs have several advantages over traditional repair approaches using mechanical fasteners: improved structural efficiency, improved fatigue life due to elimination of fastener holes, and weight savings.

Metal treatment prior to bonding is a key factor for both the initial adhesion of a bonded joint and its long-term environmental durability. Current metal prebond surface preparations, especially for on-aircraft repair, are either inconvenient to use, contain hazardous materials, and/or do not provide the performance necessary for successful long-term durable bonds. Past bond failures, primarily due to

inadequate surface preparation, have been a limiting factor in the current use of bonded repairs, especially for primary structure.

Conventional approaches of preparing metal surfaces for bonding (anodizing and etching) promote adhesion by producing a high surface area structure which has both mechanical and physical (Lewis acid-base, dispersion, hydrogen bonding, etc.) interactions with the adhesive primer. Hazardous materials (strong acids, hexavalent chromium, volatile organic compounds) and complexity associated with the state-of-the-art processes tend to limit the use of adhesive bonding technology, particularly for on-aircraft repair.

Previous work by Boeing and others has demonstrated the potential for sol-gel technology to revolutionize metal adhesive bonding by providing an environmentally-compliant, high-performance, simple and inexpensive approach for surface preparation. The term "sol-gel" is a contraction for "solution-gelation." It involves the growth of metal-oxo polymers and is based on hydrolysis and condensation reactions to form inorganic polymer networks. Sol-gel chemistry is a versatile process that is capable of producing adherent thin films on metals and composites. Using appropriate precursors, films promoting adhesion of organic resins, such as adhesives, paints, and coatings can be produced. Adhesion is a result of the chemical interaction at the interfaces between the metal and the sol-gel and the sol-gel and the primer. Our approach is to use waterbased sol-gel chemistry to develop thin film coatings that effectively produce a gradient from the metallic surface, through a hybrid inorganic/organic layer, to the organic resin.

Incorporation of primer constituents in the sol-gel solutions to create a one-step process is also being investigated. Formulation of a hybrid primer, which would be part inorganic and part organic, is being derived to function as a one-step process. This primer takes advantage of the best reactivity and mechanical advantages of each component and provides durable bonding. Additionally, we are evaluating the use of the one-step sol-gel primers as an adhesive primer applied over phosphoric acid anodize (PAA) surface preparation on aluminum alloys. This will provide an environmentally-compliant surface preparation system for parts processing associated with depot-level component fabrication.

The team structure for this development and evaluation effort is shown in Figure 1.

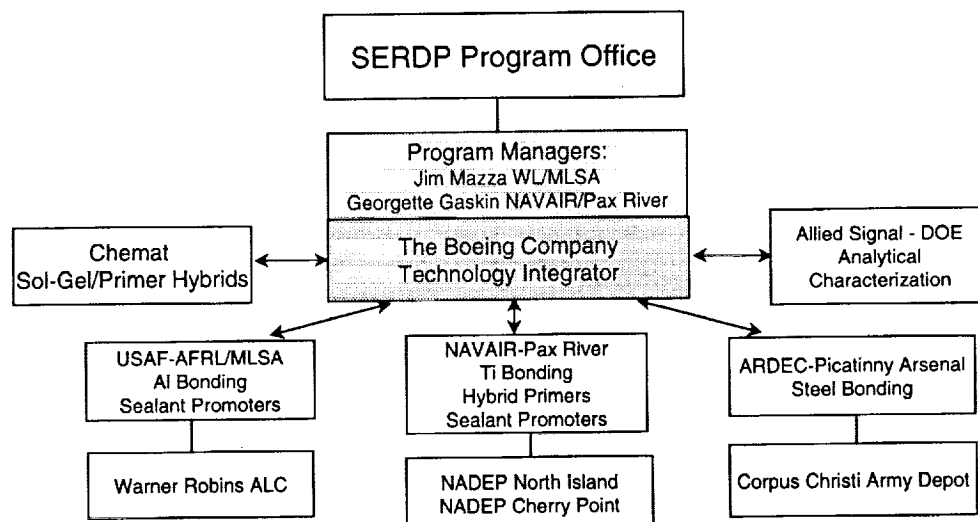


Figure 1. Program Structure for the Tri-Service Sol-Gel Technology for Low-VOC Nonchromated Adhesive and Sealant Applications Program

1.1 PREVIOUS STUDIES

In previous studies at Boeing, a sol-gel process using the Boegel-EP formulation, was developed for aluminum and titanium alloys. Mechanical testing and environmental exposure testing demonstrated the feasibility of obtaining strong, durable bonds using these sol-gel processes in the laboratory. However, laboratory processes are not always applicable in a field repair environment. Additionally, it was desirable to eliminate any grit blasting steps due to the time, cost, and potential for contamination that they present. In the last contract effort, SAIC Subcontract #45000083283, it was also demonstrated that manual abrasion techniques, such as abrasion with Scotchbrite, sanding, or use of a wirewheel, show potential as deoxidation methods for use with the Boegel-EP system. The parameters for appropriate surface activation of the aluminum alloy substrate prior to sol-gel processing will be fully defined and characterized in this proposed effort to maximize reproducibility in the bonding process.

The bonding of titanium using standard surface preparation techniques has not been an easy or reproducible process for aerospace hardware. The very passive nature of titanium and the difficulty in chemical processing of the titanium alloys have made manufacturers shy away from designing in bonded titanium parts for primary or secondary structure. There are several programs that have used titanium bonding successfully; however, the surface preparation techniques that are used are often arduous and involve hazardous chemicals and processes. Additionally, there is not a universally acceptable technique available for the repair of titanium bonded structure in the field. In previous efforts, we have demonstrated that sol-gel processes can be used to obtain strong and durable bonds on alumina grit blasted titanium alloys.

Steel bonding applications, particularly in use for helicopter rotor blade erosion caps, have been a particular surface treatment durability problem. In previous efforts, Chemat has addressed some of the issues regarding the peculiarities of stainless steels as bonding substrates. In our current program, we are examining stainless steel bonding, particularly for the AM355 and 301 alloys, and are delineating what is required for surface activation and preparation to obtain durable, consistent bonds.

2.0 RESULTS AND DISCUSSION

2.1 TEST METHODS

Screening studies were conducted on test panels of bare Al 2024-T3 and 7075-T6, Ti-6Al-4V, stainless 301 and AM355. The sol-gel system tested consisted of dilute aqueous mixtures of γ -glycidoxypropyltrimethoxysilane (GTMS) and tetra-n-propoxyzirconium (TPOZ) with an acetic acid catalyst. The pH of the solution is approximately 5-6. The panels were typically sprayed with the sol-gel solution using an airless or high volume, low pressure (HVLP) sprayer using a spray-drench technique. The spray-drench technique involves spraying the substrate surface until it is fully covered and excess solution just begins to run off. Alternatively, the sol-gel was applied by swabbing with a brush or cheesecloth.

The panels were dried under ambient conditions for a minimum of 30 minutes. The dried panels were primed with an adhesive bond primer, either the waterborne, chromated Cytec BR 6747-1M, or the waterborne nonchromated Cytec BR 6757. Control specimens were prepared for all the metals: phosphoric acid anodize or Pasa Jell 105 for aluminum; chromic acid anodize, Pasa Jell 107, or phosphate fluoride for titanium; and ferric chloride etch for stainless. Test panels were bonded in an autoclave using BMS 5-101, Type II, Grade 10 250°F-cure adhesives, 3M AF 163-2M or Cytec FM 73M.

Screening level testing was conducted using the ASTM D 3762, Wedge Test. Progress of the crack along the bondline was measured periodically after the initial driving of the wedge and after exposure to 140°F and/or 160°F and >95% relative humidity. Lap shear testing was conducted per BSS 7202 using either finger panels or wide-area lap panels bonded with the same adhesive. Peel testing was conducted per ASTM D 3167.

2.2 BOND PERFORMANCE TESTING ON ALUMINUM

Adhesive-bonded repairs on aluminum aircraft range from adhering composite patches on damaged portions of aluminum skin, bonding of doublers, and reinforcement of corrosion degraded areas, to moisture-induced delamination of aluminum skins from aluminum honeycomb core. Often these repairs are carried out on the aircraft and therefore need to use equipment and procedures appropriate for this environment.

Currently, surface preparation techniques such as phosphoric acid anodize or Pasa Jell 105 are used to provide an appropriate surface for bonding. These methods use hazardous materials and generate waste materials that must be disposed of in an appropriate fashion. More recently, the grit blast/silane process has been used as an environmentally friendly process alternative technique. Drawbacks of this process include the need to contain and collect grit blast residue, and excessive process times.

Our standard Boegel-EP epoxy bonding sol-gel formulation was tested on 2024-T3 aluminum alloy substrates using several different surface preparation techniques. The wedge test data (conditioned at 140°F and >98% relative humidity) comparing the sol-gel treated specimens to those treated with other standard bonding techniques are shown in Figure 2. Sol-gel specimens were bonded with the waterborne Cytec BR 6747-1, while the phosphoric acid anodize containment system (PACS) processed and grit blast/silane controls were primed with Cytec BR 127. This initial data showed us that the sol-gel technique was viable as a surface preparation method for repair operations.

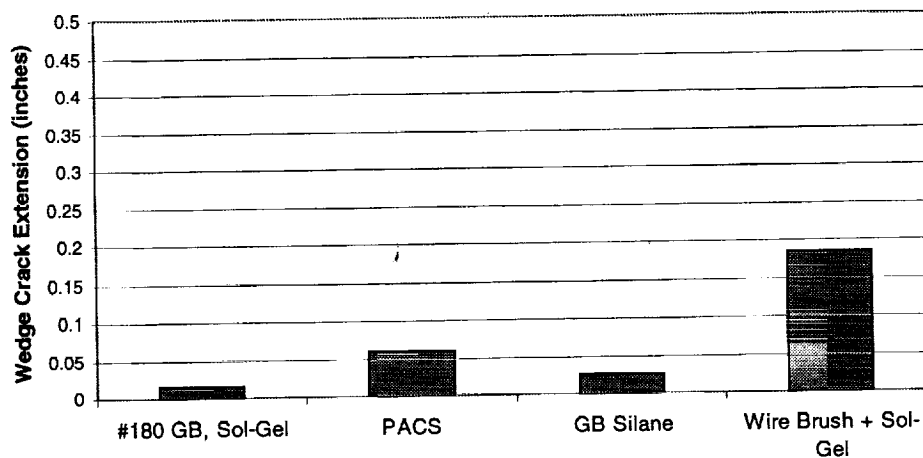


Figure 2. Comparison wedge test data after one week exposure at 140°F and >98% RH for 2024-T3 specimens given different surface treatments bonded with 3M AF 163-2M 250°F-cure adhesive.

Since our initial efforts, several improvements have been made to optimize the formulation and process. First, the amount of acetic acid used in the mixture, which is added to control the hydrolysis and condensation of the sol-gel components and stabilize the mixture, has been reduced. This brings the pH of these sol-gel mixtures to approximately 5-6. This will minimize any concern of corrosion in

faying surfaces or at fasteners and potentially eliminate the need for masking cracks during repair sequences. Secondly, testing has indicated that a separate heat cure of the sol-gel coating is not necessary to achieve good hot/wet durability. Simple ambient drying of the waterbased coating at room temperature gave excellent wedge test results. Figure 3 shows the results of these comparisons.

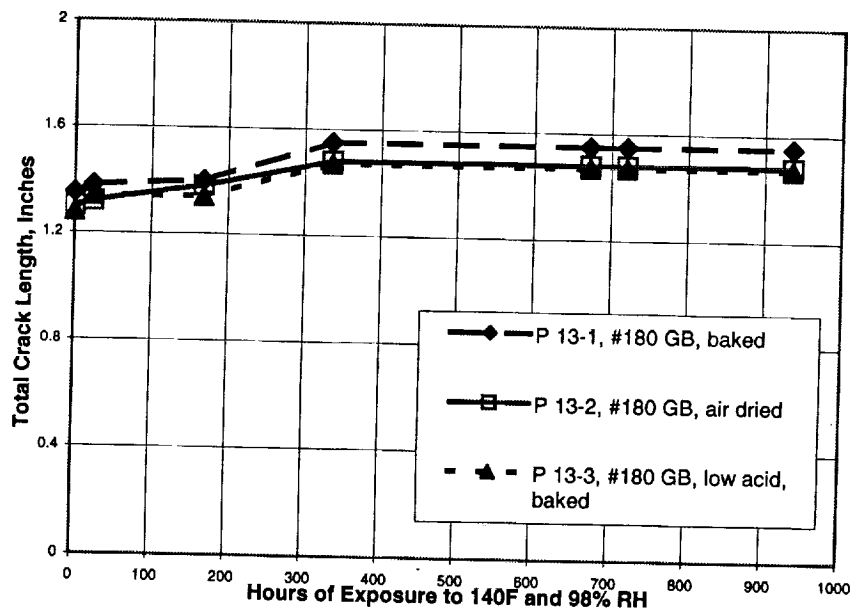


Figure 3. Comparison of formulation improvements in the wedge test performance of the Boegel-EP system on 2024-T3 aluminum using Cytec BR 6747-1 primer and 3M AF 163-2M 250°F-cure adhesive.

The most critical factor in obtaining good performance with the sol-gel systems is the surface activation of the metal alloy. Our previous work indicated a large difference in hot/wet performance when using different deoxidation and cleaning techniques prior to sol-gel coating. For example, the data indicate that good durability can be achieved when using a method as simple as mechanical deoxidation with alumina-grit sandpaper. However, it has been apparent that a certain degree of uniformity and completeness is required of the sanding process to get good durability in the bonded system. Mechanical deoxidation and cleaning methods such as sanding, wire brush, and abrasion with Scotchbrite all show potential use as pretreatment methods for field repair. Wedge test data using these mechanical deoxidation methods is shown in Figure 4.

Our current activities focus on identifying what surface chemistries are optimum and how to achieve the appropriate surface activation using both environmentally friendly and simple equipment and material. A designed experiment is currently being conducted at the Air Force Research Laboratory examining different surface activation methods on aluminum alloys and the factors leading to consistent bond performance at the metal to sol-gel interface.

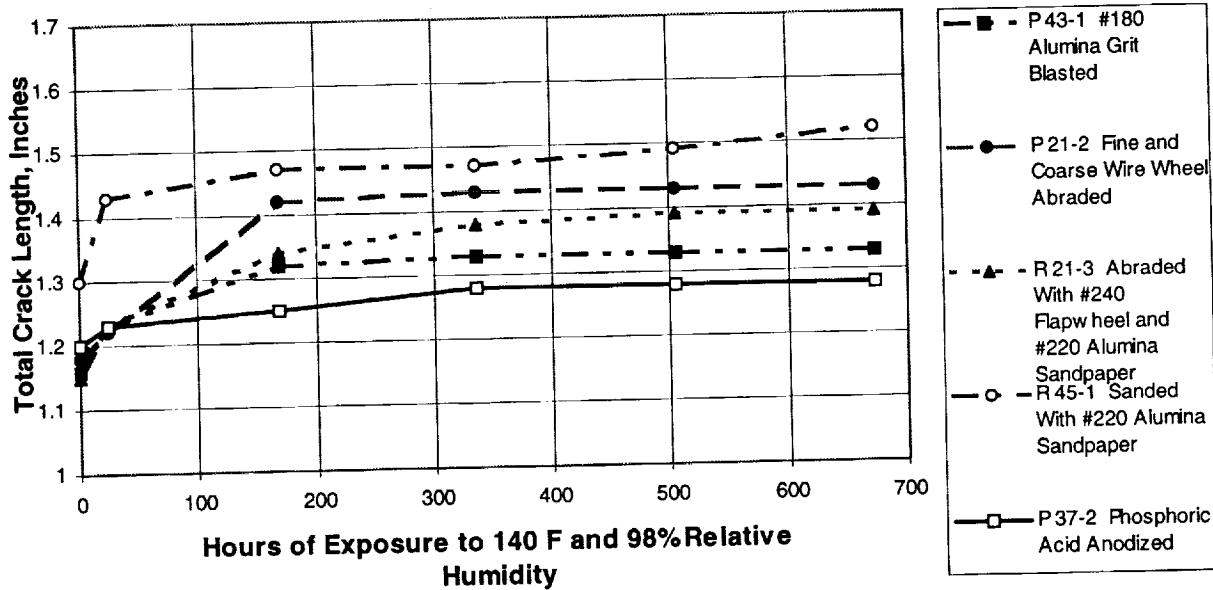


Figure 4. Comparison of mechanical deoxidation and cleaning methods in the wedge test performance of the Boegel-EP system on 2024-T3 aluminum using Cytec BR 6747-1 primer and 3M AF 163-2M 250°F-cure adhesive.

2.3 BOND PERFORMANCE TESTING ON TITANIUM

Titanium bonding applications range from primary structural bonding applications of titanium to titanium, composite, or honeycomb on vehicles such as the F-18 or Joint Strike Fighter (JSF). Additionally, applications exist such as the bonding of titanium lightning strips or erosion caps on the rotor blades of helicopters such as the CH-47s. With all of the parts comprised of titanium alloys, repair methods for use on titanium hardware are especially critical. Unfortunately, there are currently no easy, safe, environmentally friendly methods available for durable adhesive bonding repair of titanium structures. Pasa Jell 107 is currently used in many applications, as well as tank processes such as chromic acid anodize or phosphate fluoride etching, but all involve the use of toxic or environmentally hazardous materials and generate hazardous waste.

Figure 5 shows the results of our first round robin testing involving the Boegel-EP process on titanium substrates, with a comparison being made between specimens made by Boeing personnel and specimens made by NAVAIR personnel. This initial data shows that very consistent, durable bonded interfaces can be achieved when using grit blasting (GB) as the pre-treatment step on titanium substrates. Other methods though, such as sanding or using a flapwheel fitted with #240 alumina grit sandpaper, can be used to clean and deoxidize titanium surfaces. Albeit, further testing needs to be conducted to optimize the results of these sanding methods on the harder titanium substrates.

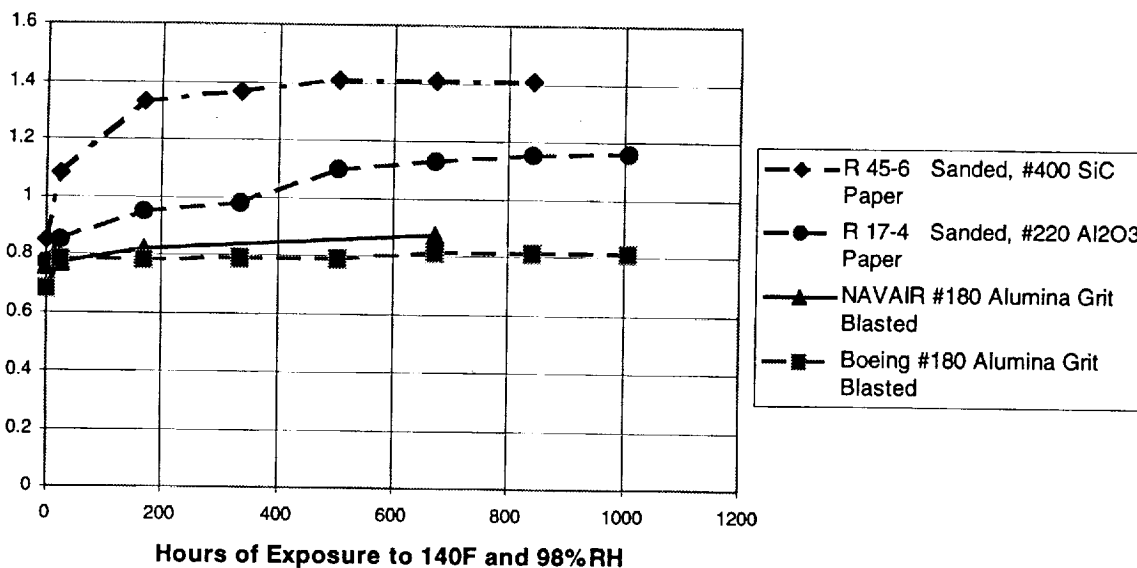


Figure 5. Comparison of wedge test performance of the Boegel-EP process on Ti-6Al-4V substrates with various surface pretreatments that had been prepared by Boeing and Navy personnel using Cytec BR 6757 primer and 3M AF 163-2M 250°F-cure adhesive.

When it is not possible to grit-blast the surface, an alkaline pretreatment is also acceptable. Alkaline pretreatments give durable performance with the sol-gel coating by providing a titanium surface chemistry conducive to durable sol-gel interfaces in hot/wet conditions.

2.4 BOND PERFORMANCE TESTING ON STEEL

Various spacecraft hardware and military hardware, such as the erosion caps on the Apache AH-64 rotor blades, require adhesive bonding of stainless steel hardware. Currently, the surface preparation process for bonding of stainless AM355 or 301 hardware is the ferric chloride/hydrochloric acid etch (FCHAE) process. Improvements to the FCHAE process added a grit blasting step that has dramatically increased the durability of the bonded system. However, the process is still based on an immersion technique and uses hazardous materials generating rinse water that needs to be treated and disposed of properly.

The Army has adopted a pollution prevention strategy that has source reduction and/or material substitution as the most desirable approach for minimizing hazardous waste reduction. The goal of this part of the research effort is to investigate the potential replacement of an immersion tank process with one that will produce structural adhesive bonds with equivalent strength and durability without generating significant amounts of hazardous waste or using other environmentally-undesirable materials.

Figure 6 shows the wedge crack extension results when the Boegel-EP coating system was applied to a grit blasted, 0.040"-thick, stainless 301 surface. This data is compared with the original ferric chloride (FCHAE) baseline method and improved FCHAE process controls run at the Army Picatinny Arsenal. With the new improved FCHAE system, the sol-gel data shows comparable durability. However, the process is expected to show substantial benefits in repair time and hazardous materials usage.

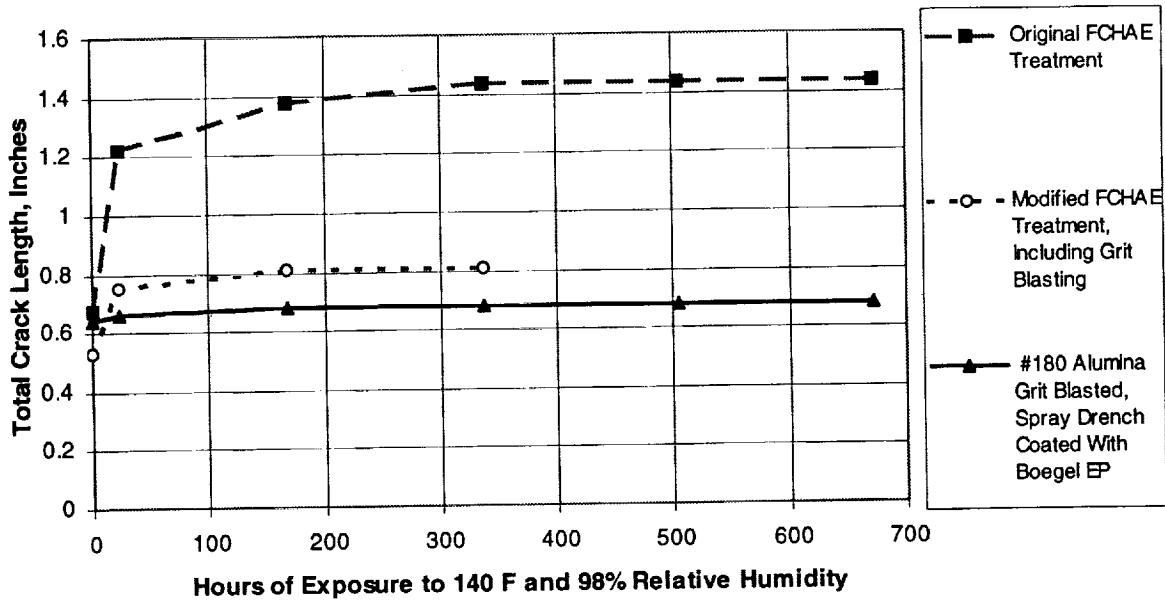


Figure 6. Wedge test comparison of the Boegel-EP process on stainless 301 with the FCHAE baseline and improved FCAHE processes using Cytec BR 6747-1 primer and 3M AF 163-2M 250°F-cure adhesive.

CONCLUSIONS:

Sol-gel surface preparations using the Boegel-EP coating formulation result in durable adhesive bonds on aluminum, titanium, and steel substrates. Optimization of surface cleaning and preparation techniques will make these robust, dependable systems for remanufacture and repair bonding in the field or at a depot site. Sol-gel processing reduces repair process flow-time, uses environmentally-acceptable materials, minimizes waste, improves worker safety, and gives durable, consistent bonding performance. We are continuing to conduct studies to better understand and control the interfacial surface chemistry to obtain reproducible systems for bonding, painting, and corrosion control. However, some applications are currently available or will soon be available for implementation in a shop or field repair environment.

ACKNOWLEDGMENTS

This effort was partially funded by the Strategic Environmental Research and Development Program (SERDP). The program development is being partially conducted under SERDP Project #PP-1113.

A NEW NON-CONTACTING NDT SYSTEM FOR DETECTION OF DISBONDS IN COMPOSITE AND METAL STRUCTURES

J. M. Webster^a, T. Thevar^a J. Mew^b.

^aHolographics Inc.

44-01 11th Street, L.I.C., New York, USA.

^bUniversity of Portsmouth,

School of Computing Studies and Mathematics, Milton Campus, UK.

ABSTRACT

The non-contacting Acoustic/Doppler system discussed in this paper is unique and employs a proprietary design acoustic transducer which produces an air coupled shock or pressure wave. This is achieved by discharging a high voltage capacitor within a period of $<5 \mu\text{sec}$. The transducer design configuration produces a single brief, but extremely high velocity shock wave of broadly unidirectional characteristics launched into the air and used to impact and excite the object undergoing testing. The objective of the impact is to excite natural relaxation frequencies in the object. Surface relaxation frequencies for any given material are dependent upon the underlying substructure of the object. In many respects this technique is analogous to tapping a surface with the edge of a coin.

The technique depends upon the hypothesis that any change in substructure will locally affect the surface frequency response spectrum. Our results show both deep subsurface defects as well as supporting structures. Present standoff distance between the NDT transducer and the object undergoing test is up to four meters.

Remote interrogation of the relaxation frequencies on the surface of the object undergoing NDT is accomplished with a highly customized scanning laser Doppler velocimeter. An analog velocity time domain signal received from each data point is passed into the processing compute, then it is immediately processed to a Fast Fourier Transform (FFT). This data is then stored in the computer as individual frequency bands over the pre-selected frequency range. A velocity based image is computed and presented on a monitor overlaid on an image of the object which was simultaneously grabbed by a CCD camera. Techniques for computerized automatic analysis of the images are being developed and will be discussed in a separate paper.

1. INTRODUCTION

The non-contacting acoustic Doppler system discussed in this paper is unique and employs a proprietary design acoustic transducer which produces an air coupled shock or pressure wave, similar to that produced from a small explosion. This is achieved by discharging a high voltage electrical capacitor within a period of $<5 \mu\text{sec}$. The discharge is contained within a small ceramic chamber with an annular design anode providing an exit for the hot gasses which are a result of the discharge, figure 1. The result of this proprietary configuration is that a single brief, but extremely high velocity shock wave of broadly unidirectional characteristics is launched into the air and used to excite the object undergoing testing. It has been successfully employed in NDT operations at stand off distances of up to 3.5 m, however, this does not represent its limitations, but rather the limitation of our present facility.

1.1 Excitation:

The objective of the brief impact of white noise is to excite natural relaxation frequencies in the object and avoid any "blanketing" effect that would be present if continuous wave white noise was applied. Surface relaxation frequencies for any given material are dependent upon the underlying substructure of the object. In many respects this technique is analogous to tapping a surface with the edge of a coin: if there is a subsurface defect such as a debond then the resulting relaxation frequencies make a hollow sound. This is a very subjective and non-quantifiable method of NDT, because the human ear is very limited in its response in terms of volume and frequency. Beside the physiological audible response being very difficult to quantify, background noise is normally present in any workplace and would add difficulties to the evaluation. Furthermore, physical contact is not always an option. However, properly applied, the study of these relaxation frequencies is a very good non-destructive testing technique. In the case of this technology we are recording and analyzing the resulting relaxation frequencies excited by our acoustic pressure wave up to 50 kHz.

The technique depends upon the hypothesis that any change in substructure will effect the surface resonance frequencies, which are uniquely peculiar to any given area and given uniformity of the underlying structure. Our results show both subsurface defects as well as local changes in the supporting structures.

Figure 1 is an illustration of our prototype acoustic transducer. The electrical discharge is formed in the small chamber between the cathode and anode. The high voltage discharge is varied between ten to fifty joules, dependent upon such variables as stand off distance and type of composite. The annular design of the anode permits the extremely high pressure hot gasses formed within the discharge chamber to be exhausted and launched at an extremely short duration acoustic wave into the air. The velocity of the wave is estimated to be between Mach fifteen to twenty at the exit of the transducer. Measured at ten centimeters distance into its travel, it has a velocity of approximately Mach four depending upon the configuration of the transducer employed and the input power, then drops to Mach one at approximately 30 cm.

1.2 Scanning Laser Vibrometer:

Remote interrogation of the relaxation frequencies which occur upon the surface of the object undergoing non-destructive testing are accomplished with a customized scanning laser Doppler interferometer. This device normally employs a 3 mW He-Ne laser to scan the surface of the object undergoing NDT with an array of up to 512 x 512 data acquisition points which may be deployed and shaped at the operators choice. Time domain data is received from each data point into the processing computer and immediately processed to FFT representation.

Data, after processing to an FFT, is stored in the computer as individual frequency bands over the pre-selected frequency range. Optionally a number of FFT frequency lines can be selected: for example 512, 1024 or 2048. There is a roll off in sensitivity above 80%, thus the useable bands are 400, 800 and 1600 respectively. Information is stored at each frequency band, together with fault and noise data. The information pertaining to the objects surface response is recorded for each frequency condition at a specific band in the recorded frequency spectrum.

The data is analyzed in individual frequency bands in order to isolate data pertaining to any recorded fault condition. Figure 2 illustrates diagrammatically a typical section of the information recorded. In any record we have a number of potential sources of noise. The main cause we have termed gross bending modes which appear at low frequencies and other sinusoidal bending appears at somewhat higher frequencies. Noise is also present in a random form usually isolated to individual frequency or

over very narrow band widths. The analysis procedure has is the subject of an ongoing research project and is the subject of a separate paper in this conference proceedings where results of other application are shown. The objective of the analysis program is to select those information carrying frequencies and thus minimizing noise whilst accentuating the signal information. The understanding of this noise elimination procedure is central to the successful operation of this technology and has permitted an automatic analysis software feature to be designed that will accurately detail and characterize faults with the minimum of operator input.

Experiments so far conducted do indicate that surface finish or color is not an important factor in the samples to which it can be applied. We have used it successfully on both black, white and colored surfaces, and those which are either polished and matte finish.

3. RESULTS

Unfortunately, due to the limitation of the publication they are in grayscale. The original image is actually in six colors corresponding to auto ranged velocity values. The first, in figure 3, is a record obtained from a "Textron Doubler". This was provided by the Federal Aviation Administration. It is a boron composite patch which is proposed for use on aluminum constructed aircraft as a doubler repair. It is currently in use on military aircraft. There are five preprogrammed debonds in the test sample, all of which are clearly shown in terms of velocity, particularly in 3D representation.

The second result is illustrated in figures 4, 5 and 6. This is a composite repair test panel with the fault map shown in figure 4. This test specimen was designed to represent possible faults which might be present in a typical repair to a carbon composite area, which had been damaged. Preprogrammed into this test panel are eight faults, varying in size and depth, some of which are on the rear of the specimen and others on the scarf. Figure 5 shows the presence of seven of the faults. The eighth fault not only proved illusive for us, but also for other NDT systems, which were tested on this panel. Most of the alternative techniques require surface contact with the object undergoing test. This result is presented as isolines. One of the advantages of this system of NDT is that its output is in the form of an image, which is easily assimilated by an operator. Figure 6 is a different representation of the same source data and shows the deposition of the resin which damped the relaxation frequencies and therefore clearly show the ability of the system to detect not only faults, which may be contained within the repair, but also the presence of a repair or joint.

The result of the scarf repair test, among many others in our records does show that this technology can "see through" both the surface layers of composite and the central honeycomb core to defects located against the rear side of the material undergoing NDT. Furthermore, an analysis of the frequency bands will show the fault size. It is expected in the future that we will be able to characterize the depth of the fault from the frequencies recorded, which are accessible in the final data and available to the inspector.

With respect to depth of penetration, we have demonstrated in this paper we can detect fault through honeycomb cores to the rear of the object. The maximum number of carbon composite layers which we have tested and detected faults is 14 layers above a honeycomb core. We have had no specimens above this thickness to test.

4. DISCUSSION AND CONCLUSIONS

This technology is new and potentially offers a different and radically alternative approach to the NDT of composite materials. Additionally to the results shown in this paper, we have successfully applied the technology to glass composite AWAC Raydome's in a blind (POD) test and to the detection of

corrosion in lap joints where initial work indicated that 5% metal can be deduced from the resulting frequency spectra; it is fully expected that this will be improved with further work..

It is a large area coverage system which operates remotely from the object with a stand off distance of at least 3.5 meters and does not require any surface contact or interface. Furthermore it is not particularly sensitive to surface color or finish. Results have been obtained from both solid and honeycomb core materials where defects can be located even at the rear of the specimen with respect to the point of measurement.

Patents granted or pending:

Webster J. M. Acoustic wave generating apparatus US patent Number 5616865. April 1997.

Webster J. M. Method and apparatus for the non-destructive inspection of composite materials and semi-monocoque structures. US Patent 5505090. April 1996.

Webster J. M. and Mew J. Automatic analysis of defects in composite materials. US patent filed.

Contact: Dr John M. Webster. E-mail: john_webster@compuserve.com

Acknowledgments: This work was sponsored by DARPA Phase II # DAAH01-95-C-R182 Contract "Development of an Optical/Acoustic Method for the Remote Non-Destructive Inspection of Large Area Composite Materials for Structural Defects". Approved for Public Release Distribution Unlimited.

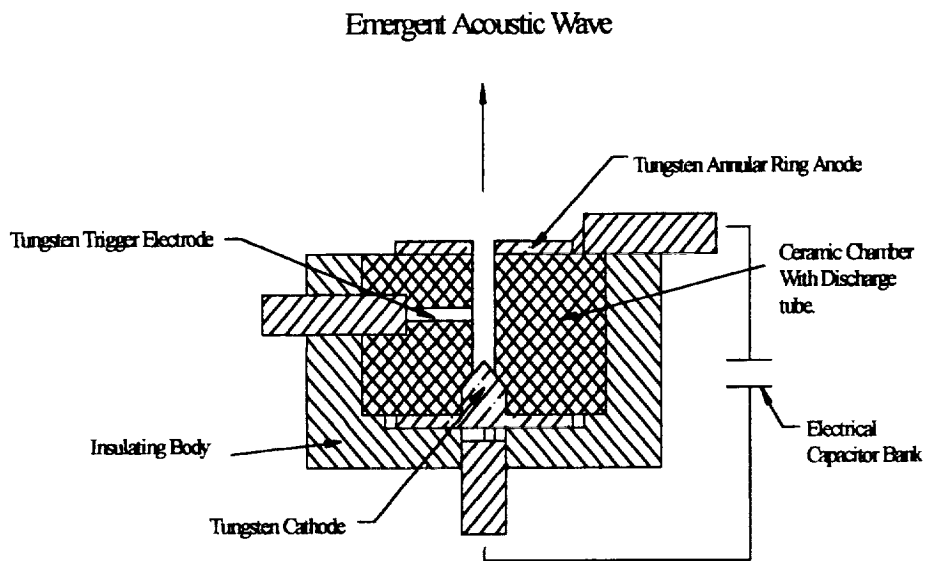


Figure 1. Impulse transducer

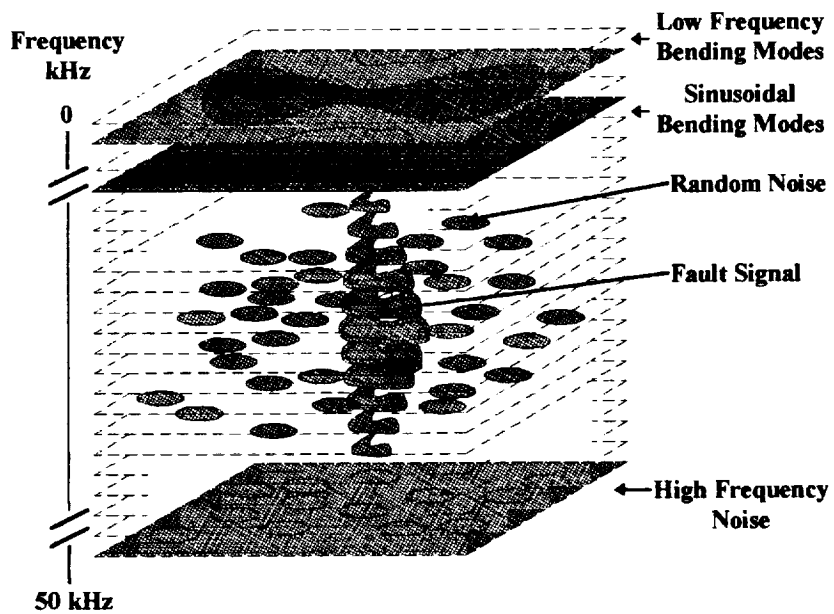


Figure 2. Diagrammatic visualization of FFT spectrum

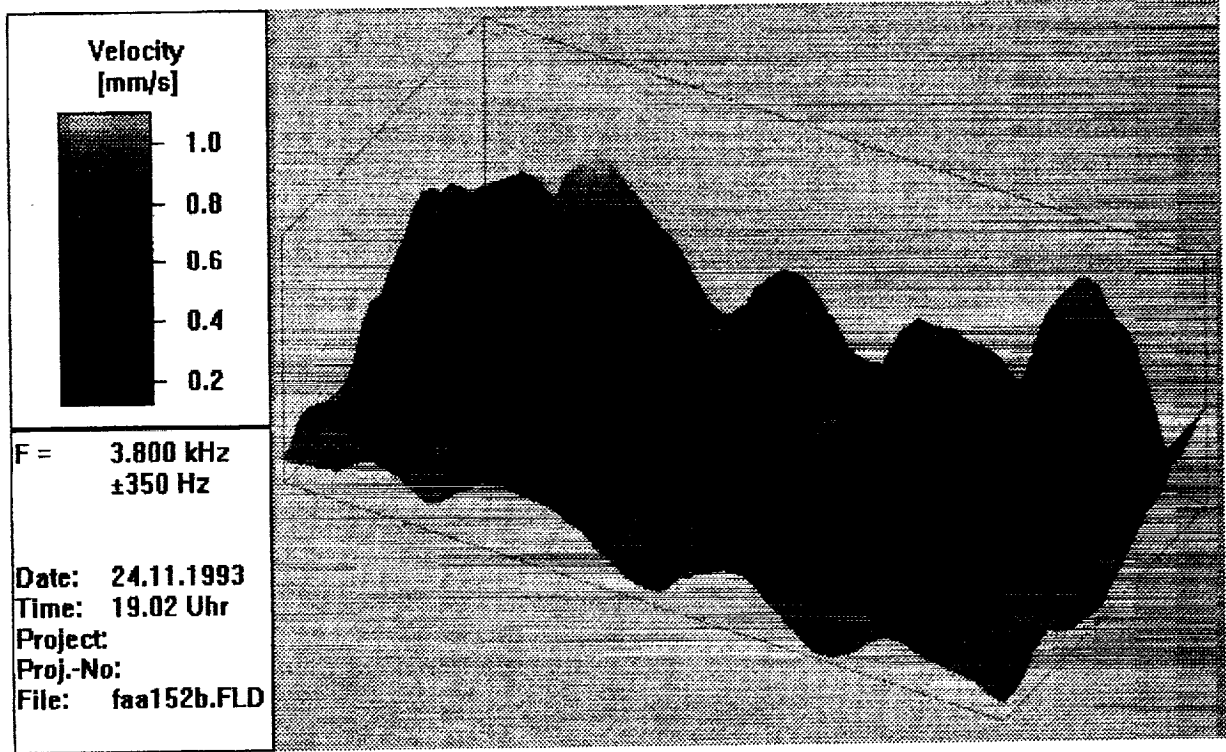


Figure 3. Textron doubler

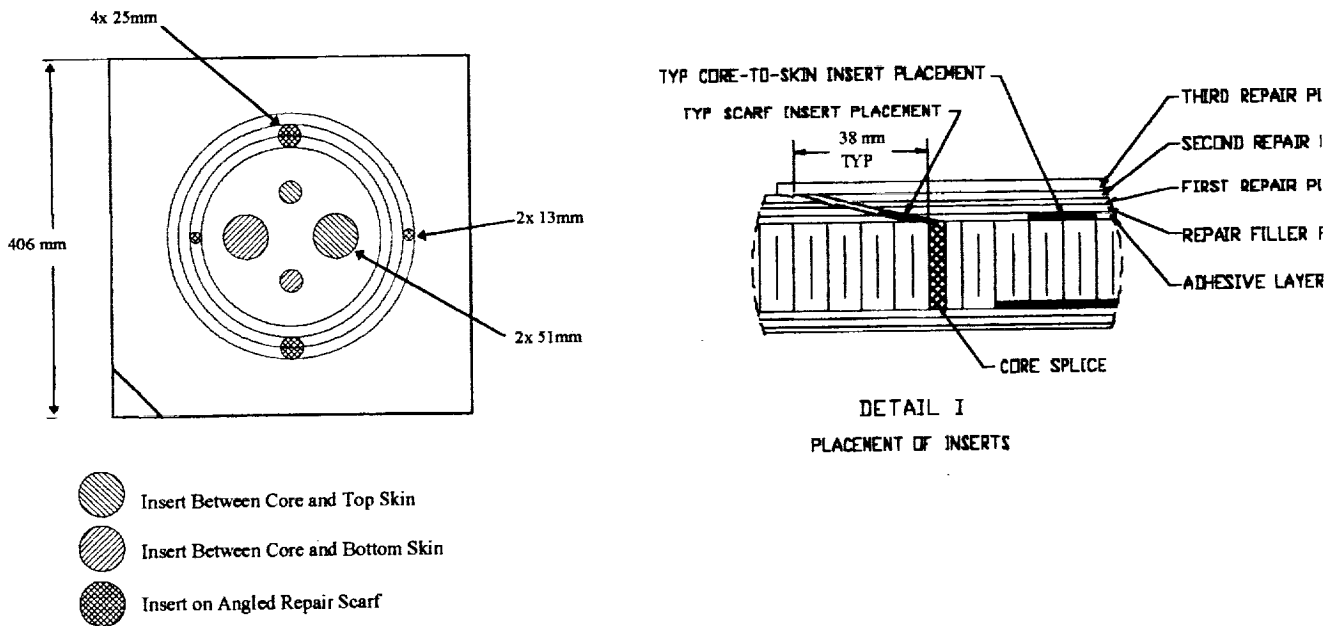


Figure 4. Carbon scarf repair simulation panel manufactured by Boeing. Note defects below and on top of the honeycomb

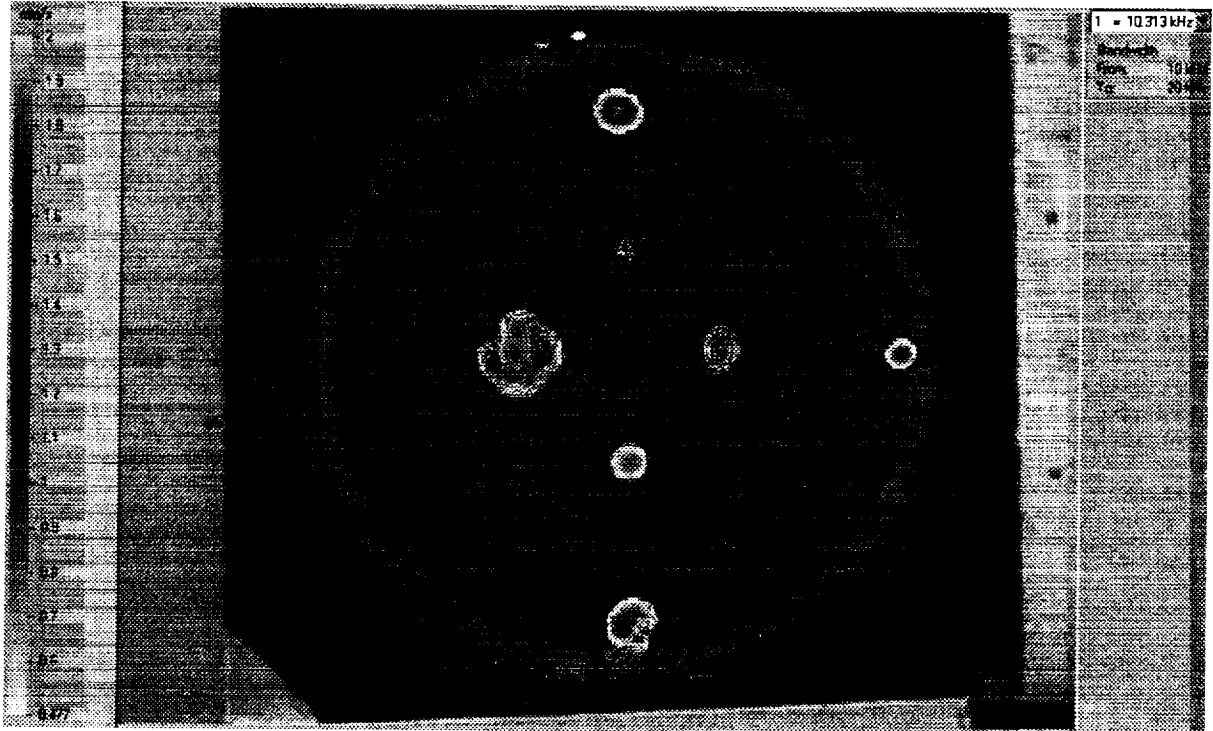


Figure 5 Result showing seven faults

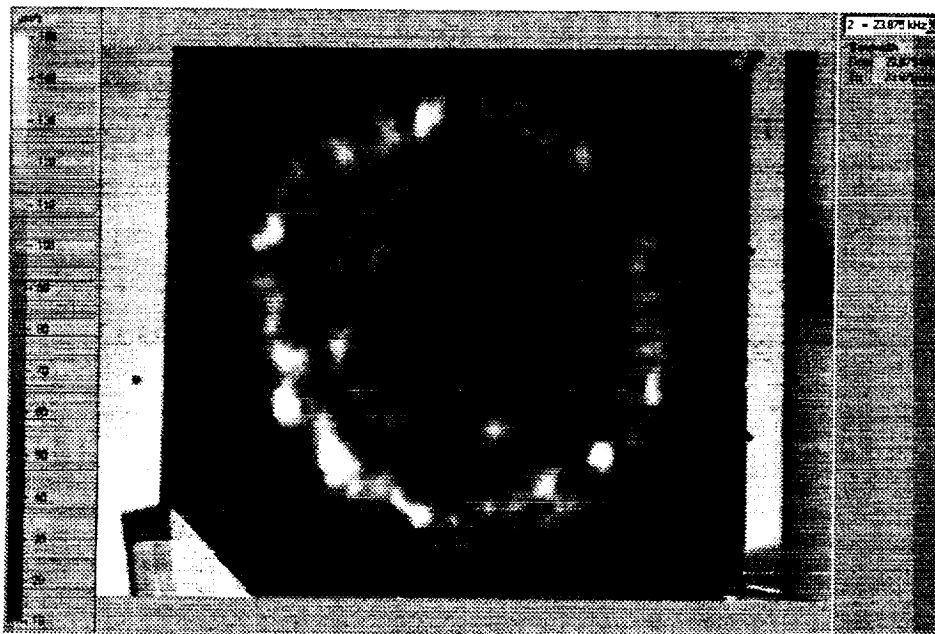


Figure 5 Different calculation from the same data set scan but now showing the resin used to effect the repair

A SMART PATCH APPROACH FOR BONDED COMPOSITE REPAIR/REINFORCEMENT OF PRIMARY AIRFRAME STRUCTURES

Alan A. Baker, Stephen C. Galea and Ian G. Powlesland

Airframes and Engines Division, Defence Science & Technology Organisation - Aeronautical & Maritime Research Laboratory, 506 Lorimer Street, Fishermens Bend, Victoria 3207, Australia.

Ph: +61 3 9626 7495;

Fax: +61 3 9626 7089;

alan.baker@dsto.defence.gov.au

ABSTRACT

The application of bonded composite patches to repair or reinforce defective metallic structures is becoming recognised as a very effective versatile remedial procedure for many types of problems. Immediate applications of bonded patches are in the fields of repair of cracking, localised reinforcement after removal of corrosion damage and for reduction of fatigue strain. The application of bonded composite patches or reinforcements to repair or restore properties of defective secondary structures has become routine in the Royal Australian Air Force (RAAF). However, bonded repairs to critical damage in primary components are generally limited due to certification concerns and are generally acceptable only on the basis that a margin on design limit-load (DLL) capability is retained in the loss (total absence) of the repair. To certify such repairs substantial analysis and testing programs are required, as well as a stringent inspection program during service to ensure structural integrity is not compromised.

For certification and management of critical repairs for very high cost components, the "Smart Patch" approach may be an acceptable solution from the airworthiness perspective and be cost effective for the operator and may even allow some relaxation of the certification requirements. Assuming patch disbonding due to bond environmental degradation is not a concern and that the static requirements are satisfied, then full credit for the patch in slowing crack growth could be justified by a continuous safety-by-inspection approach based on self-assessment of the patch system integrity using a "smart patch" approach.

In the most basic form of the "Smart Patch", in-situ sensors can be used as the nerve system to monitor in-service the structural condition (health or well-being) of the patch system and the status of the remaining damage in the parent structure. This application would also allow the operator to move away from current costly time-based maintenance procedures toward real-time health condition monitoring of the bonded repair and the repaired structure. These systems would allow timely decisions on preventative and scheduled maintenance before failure of the repair or repaired structure. To this end a 'stand-alone' patch health monitoring device which is in close proximity to sensors on a repair is being developed. More specifically this paper describes a laboratory demonstration on bonded doublers of an F-111 skin doubler specimen. The instrumentation will measure, process and store sensor measurements during flight and then allow this data to be down loaded, after the flight, onto a PC, via remote (wireless) data access.

1 INTRODUCTION

For economic reasons there is a current trend to operate military aircraft well past their original design life. However, this results in a rapidly increasing number of airframe corrosion and cracking problems

and gives rise to the urgent need for cost-effective, efficient repair procedures. This situation is extremely relevant to the Royal Australian Air Force (RAAF) where many aircraft types, such as the F-111, P3C and F/A-18, will have exceeded their design life well before they can be replaced.

The application of bonded composite patches or doublers to repair or reinforce defective metallic structures is becoming recognised as a very effective versatile repair procedure for many types of problems¹. Immediate applications of bonded patches are in the fields of repair of cracking, localised reinforcement after removal of corrosion damage and for reduction of fatigue strain. The bonded repair to the cracked structure - crack patching - allows the restoration of strength and stiffness of the structure, as well as slowing crack growth by reducing stress intensity. The application of bonded composite patches to fix defective secondary structures has become routine.

However the application of bonded composite repairs to cracked primary structure is generally acceptable only on the basis that a margin on design limit-load (DLL) capability is retained in the loss (total absence) of the repair².

This is essentially the application of a fail-safe approach, viz.:

- When a cracked single-load-path component maintains sufficient residual strength to withstand DLL times a safety factor (often 1.2). In this case regular inspection is required, to ensure that the critical crack length for failure at this stress is not exceeded, based on the predicted growth rate for the unpatched crack.
- When a redundant (multiple) load path component can withstand DLL times the safety factor if the cracked path has failed. This is a standard procedure now for such structures so should not pose any particular problems. In this case inspection is required to ensure that the alternate load path is not cracked to the extent that it would not withstand the elevated stress.

The conservative approach in the single load path case eliminates the possibility of repairing a crack already above critical size or a small crack with high growth rate. However, a repair to a crack greater than critical size was undertaken in Australia to the lower wing skin of an F111 aircraft, following an extensive certification program^{2,3}. To certify the repair a substantial analysis and testing program, to ascertain 1) residual strengths, 2) damage tolerance and 3) durability, was required.

In the single load-path cases the inspection requirement based on growth of the unpatched crack may be acceptable where the initial crack size is small (or non-existent, for example in the case of a preventative doubler rather than a patch). However, there will be many repairs, for example those with cracks approaching critical size, where this inspection requirement will not be cost-effective. The repair can then be undertaken only by giving full credit for the reinforcement in restoring residual strength and reducing the rate of crack growth. That is when the cracked/patched structure can be managed as on a slow crack growth or damage tolerant basis. Essentially, as discussed in reference 2, there is a need to prove that the cracked/patched structure meets damage tolerance requirements – this includes slow crack growth, even if the original structure was designed on a safe-life basis.

Assuming patch disbonding due to bond environmental degradation is not a concern and that the static requirements are satisfied, then full credit for the patch in slowing crack growth could thus be justified by:

- i. Safe Life Approach in Safe-Life Zone: Based on demonstrating that strains are below threshold in the safe life zone PLUS
- ii. Damage Tolerance Approach in Damage Tolerance Zone: Based on predictable slow disbond growth. OR
- iii. Continuous Safety by Inspection Approach: Based on self-assessment of the patch system integrity using “smart patch” approach³.

Figure 1 illustrates the safe-life and damage tolerant zones at the ends and in the middle, respectively, of a generic patch.

The aim of the 'smart patch' approach is for continuous monitoring of patch performance to ensure that load transfer is maintained. The need to follow the correct patch design and process procedures is unchanged. The smart approach simply allows a relaxation of the probability of failure requirements, particularly in relation to environmental degradation. However, it must be stated from the outset that the viability of any smart approach now depends on establishing its reliability or probability of detection - which is similar to the problem of probability of detection in NDI. Certainly self-checking and significant redundancy would have to be included in the system to provide the required level of confidence.

Smart patch approaches are technically feasible but will be economically viable only for repairs to very significant and costly primary structure. For certification and management of critical repairs for very high cost components, the "Smart Patch" approach may be an acceptable solution from the airworthiness perspective and be cost effective for the operator and should allow some relaxation of the certification requirements.

In the most basic form of the "Smart Patch", in-situ sensors can be used as the nerve system to monitor in-service the structural condition (health or well-being) of the patch system and the status of the remaining damage in the parent structure. This application would also allow the operator to move away from current costly time-based maintenance procedures toward real-time health condition monitoring of the bonded repair and the repaired structure. These systems would allow timely decisions on preventative and scheduled maintenance before failure of the repair or repaired structure. The sensors, which may for example be resistance-foil⁴ or piezoelectric strain gauges^{5,6,7} or optical fibres^{8,9,10}, are ideally (for robustness) embedded in the composite patch or more simply bonded to its surface. Current studies at Airframes and Engines Division (Aeronautical and Maritime Research Laboratory, AMRL) and the DSTO Centre of Expertise for Structural Mechanics, are focused on the assessment of new techniques in order to achieve in-situ real-time measurement of patch integrity and effectiveness^{7,10}

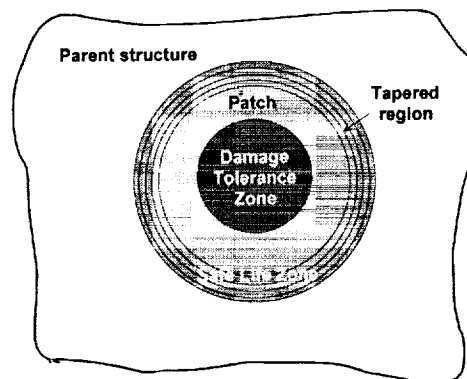


FIGURE 1 - Schematic of a generic external bonded repair showing safe-life zone (no disbonding allowed in this zone) and damage tolerant zone (stable disbonding growth allowed in this zone) 2.

This paper reports on a program of work at AMRL aimed at developing a fully self-contained miniaturised sensor signal conditioning and data acquisition system, attached in close proximity to sensors on a repair, for storing recent in-flight high-load readings of patch health. That is, this paper describes a laboratory conceptual demonstration of a 'stand-alone' patch health monitoring device that monitors the health of bonded doublers on an F-111 skin doubler specimen. The wireless feature will assist in allowing this smart patch concept to gain acceptance in practice, since wiring associated with

the sensors, actuators and instrumentation will be difficult, if not impossible, to implement on real aircraft structures without OEM approval.

2 SMART PATCH APPROACH

A generic patch system is shown in Figure 1 which shows (1) a safe life region where disbonds in the adhesive grow rapidly, leading to repair failure, and (2) a damage tolerant region of the patch system over the damaged parent region where limited disbond growth is acceptable since growth is generally stable². Therefore the specific objectives are to detect disbond growth in the safe life zone of the patch (which is unacceptable) and monitor damage growth in the parent material (below the damage tolerance zone) - delaminations for composites or cracks for metals.

One approach to introduce redundancy, improve reliability and increase the probability of detection, in order for the smart patch concept to be more readily accepted, is to develop and implement a variety of sensors and sensing techniques into the system. The issue of power supply is closely interrelated with the choice of sensor (and actuator) and damage detection technique used. Figure 2 illustrates some of the more promising combinations of sensors/actuators, damage detection techniques and power sources. For our conceptual demonstrator a primary cell (Lithium/Manganese cell of dimensions 25 mm diameter 3.2 mm thick) was used, in conjunction with the strain ratio technique (explained below) using resistance-foil and piezoelectric film strain sensors.

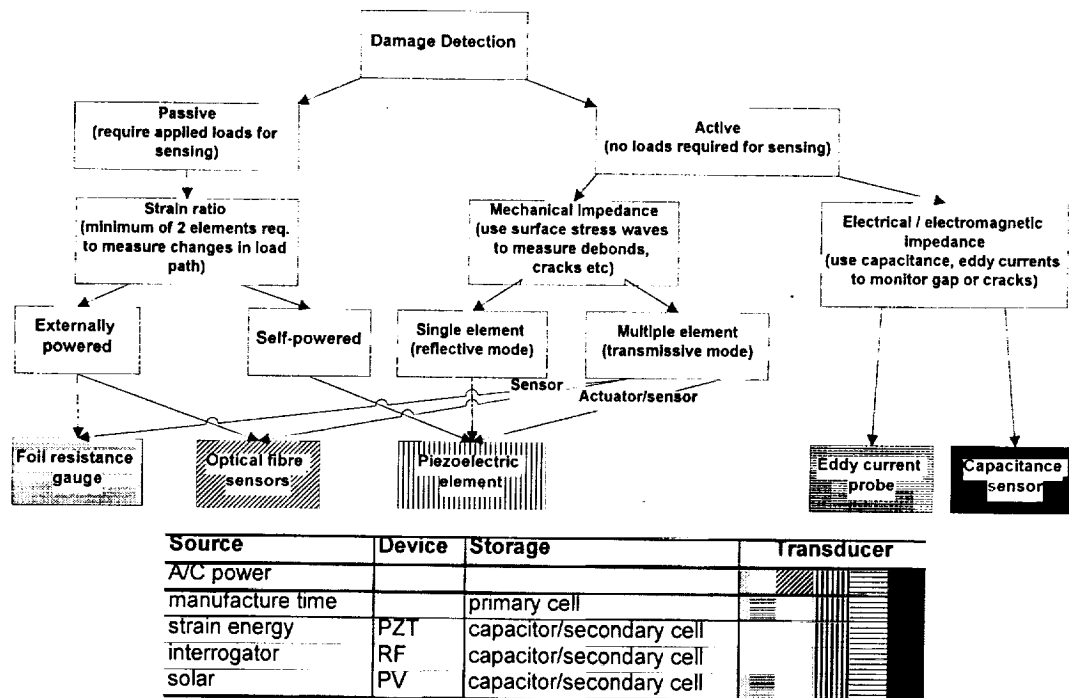


FIGURE 2: Flow diagram showing some more promising damage detection techniques, with possible corresponding transducers and power sources.

The "smart" approach being studied in DSTO is based on strain sensors, such as resistance-foil strain gauges bonded to the ends of the taper region and on the surface of the component away from the patch, as shown in Figure 3, and the monitoring of the ratio (patch strains) / (strain in the component) during service life. Any decrease in this ratio is an indication of disbonding of the patch in this critical region. In this approach there is no requirement for measurement of the actual loading: disbonding is indicated by the reduction in relative strain. Ideally, the gauges are automatically monitored by an on-board miniaturised computer which would provide a warning (e.g. via a wireless link) should the

indication of disbonding become significant. The system could also monitor the growth of the crack in the parent structure. This could be combined with the damage-tolerance approach in the crack region or alternatively the “smart” capability could also include monitoring of crack and disbond growth.

The smart patch approach for detecting disbond growth in a repair system during service operation was planned for in-service management of a large (120+ ply) boron/epoxy (B/E) doubler reinforcement for the wing pivot fitting (WPF) of Australian F-111 aircraft. Fatigue cracks can initiate in the upper-skin of the F-111 Wing Pivot Fitting (WPF) stiffener runout region shown in Figure 4a. A strain reduction of over 30 % is required to avoid plastic yielding, during Cold Proof Load Testing (CPLT), in this region ¹¹ and also to increase the in-service inspection interval. The required strain reduction is particularly challenging because of the thick steel structure and high loading. To achieve the required strain reduction without causing damage to the structure, B/E doublers, as depicted in Figure 4a and b, were designed and developed ^{4,12}.

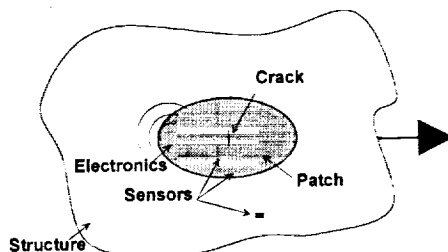


FIGURE 3 - Schematic of the smart patch concept.

The approach taken is to apply resistance-foil strain gauges (see Figure 4b) on the ends of the taper on the B/E doubler and on the surface of the steel WPF away from the doubler and monitor the ratio (doubler strains) / (strain in the steel fitting) during service life. Any decrease in this ratio is an indication of disbonding of the doubler. It is important to note there is no requirement in this approach for measurement of the loading. A similar approach is being used to monitor the structural integrity of a large (5 m x 1 m) 6 mm thick doubler used to reduce cracking around welds in the aluminium deck of an Royal Australian Navy Frigate ¹³. Figure 5 shows results obtained from tests on F-111 representative bonded joint specimens (representing a section through the doubler) subjected to CPLT loads and the F-111 loading spectrum.

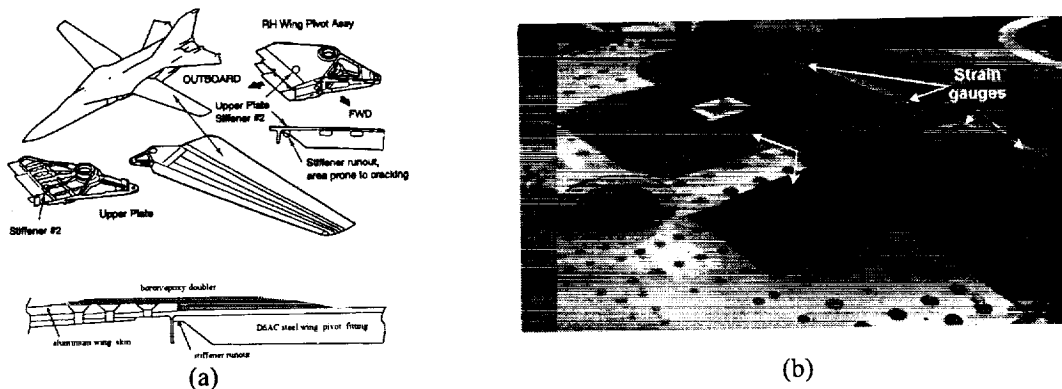


FIGURE 4 - (a) Schematic showing (top) location of critical area in the F-111 wing pivot fitting and (bottom) detail of the critical area and the 120 ply thick B/E doubler ^{2,4}. (b) Photograph of B/E doublers on F-111 with the location of resistance-foil strain gauges for doubler health monitoring.

Disbonding is indicated by the reduction in relative strain, as shown in Figure 5a. The disbands initiated and grew mainly from the corners of the doubler and growth was very much less in the centre.

In the aircraft doubler system the sides are tapered normal to the doubler axis, so stress concentrations in these corners will be much less severe; however, the results show the effectiveness of the monitoring approach proposed. This early attempt at in-service monitoring of the doubler gauges (using strain gauge wiring passing through and over the wing fairing which covers the doubler), although highly effective for aircraft undergoing the CPLT, proved too cumbersome to be practical for service use.

In this program of work, resistance-foil strain gauges and piezoelectric film (PVDF) sensors are being used to detect and monitor damage in the safe life zone of an F-111 skin doubler specimen (region E in the specimen in Figure 5a). The specimen is subject to cyclic loading and a stand-alone wireless access data logging device, developed at AMRL, is used to monitor and store patch state-of-health values, which are then downloaded by a wireless infrared (IR) link to a PC. The device is basically a small two-channel battery-powered signal-conditioning and data-acquisition system, with integrated real time processing of its readings, storage for the processed results and a wireless communication link.

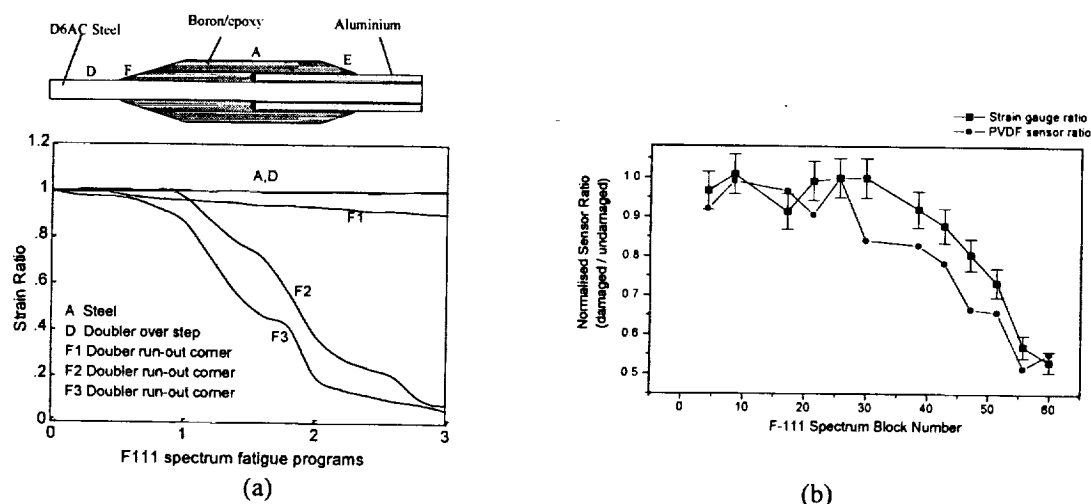


FIGURE 5 - (a) Plot of strain ratio reduction due to disbond growth as a result of fatigue cycling (bottom) and representative bonded joint specimen showing strain gauge positions (top). The F gauge results plotted are on the corners of the doubler⁴. (b) Plot of strain ratio for representative skin doubler specimens which effectively simulates strains in region E⁷.

Another 'smart' approach being developed in DSTO is based on the use of MEMS Micro-Electro-Mechanical-Systems which are incorporated into the adhesive bond line. These systems detect incipient patch environmental-degradation by detecting the presence of chemical species that are indicators of undesirable reactions taking place at the metal adhesive interface¹⁵.

2.1 SENSORS AND FAILURE CRITERIA

For the demonstrator there appeared to be three reasonably well developed families of sensor; resistive (foil, wire or semiconductor strain gauges), piezoelectric film (PVDF, PVF₂) and piezoelectric ceramic (PZT). Of these resistance-foil strain gauges are probably the most commercially mature technology and piezoelectric film is probably the one that shows the most promise in high cyclic strain applications. This is an important consideration as our initial testing fatigued the resistance-foil gauge grids prior to the patch bond failing.

Normally it is desirable to detect damage over a reasonable area. This could potentially be achieved by having one large sensor or several elements connected to act effectively as a large sensor. However, the down side is that this averaging effect will reduce the sensitivity of such a system. One alternative is to have individual channels for each of a number of individual (or small groups) sensors. This

appears attractive but if the centralised electronics failed the whole device may be inoperative. Another alternative is to have individual autonomous pairs of far field and area of interest sensors. This alternative has the potential to provide a degree of robustness against single sensor or electronics failure, and provides a system which is easily scalable for different geometry patches. It also provides information on the extent of damage – that is the system can track the damage (even in the event of an element failing).

The smart patch prototype is based on the technique of monitoring strains at two locations for each unit, i.e. one on the far-field (e.g. parent structure) and the other in the safe-life zone of the patch. Two prototypes were constructed, one using resistance-foil strain gauges and the other used piezoelectric film (PVDF) sensors as the sensing elements. Although a single figure for a given pair was all that was technically required, additional parameters were recorded to increase confidence in the system. The main one being a timestamp of the last time the far field gauge saw significant strain.

2.2 DATA ACQUISITION, PROCESSING AND STORING DATA

Two triggering approaches were initially considered. The first was to have a device which is normally dormant and activated by some external trigger. The external trigger could be supplied by a transducer such as a piezoelectric element: however, the device would need to perform a self check in order to assess if the external triggering system is functioning. This option was not used in the conceptual prototype because of the added complexity and the possible associated reduction in overall reliability. The second approach is to have the device periodically sampling. In order to meet the limited power requirements variable sampling rates would be employed. That is the sample rate is a function of the (activity) strain level of the parent strain gauge, where the maximum sample rate is about 3 samples/sec during times of high (activity) strain and the minimum sample rate is about 10 samples/hour during periods of low (activity) strain. It is envisaged that this technique would still achieve about 3 - 5 years of life for the device, based on using resistance-foil strain gauges.

2.3 DATA TRANSFER

The patch state-of-health values would ideally be transferred by the operator to a small portable hand held battery powered unit via ultrasonic, infrared (IR), RF or other means. The hand held interrogating device would provide the remote link and would indicate the state-of-health of the patch, which could then be loaded into a centralised data base. An alternate option is to interrogate the device using a (portable) PC. The second option was adopted in this laboratory conceptual demonstration because of ease of setting up the equipment. Also, for this demonstration an IR link is used since this is the simplest and most convenient option. However, this technique requires the availability of a line of sight between the device and the interrogator, and thus provides a severe restriction since this device will in practice be covered for protection or possibly be embedded in the patch - thus for many applications line-of-sight technique may not be applicable. Therefore, future work will include incorporating an RF link, since this will allow interrogation through non-metallic layers, such as epoxy, fibre glass layers, B/E layers, etc. An additional advantage with the RF link is that some implementations (eg. those based on identification tag technology) require no power from the device for communication, ie. it is powered from the interrogator, whereas the IR link requires power from the device. However, using the IR link on the conceptual prototype was sufficient to demonstrate the basic philosophy.

It is possible in certain applications that neither RF or IR will be appropriate. In such cases a direct mechanical link may be able to propagate a wave carrying the stored information to the interrogator. This could possibly be implemented by a piezoelectric transducer on the inside of the structure feeding a wave to an interrogator placed against the outside of the structure. A variation on this, would be to

use ultrasonic signals to carry the information. As the information was in digital form it could be much less dependant on operator technique than conventional NDI processes.

3 EXPERIMENTAL SET-UP AND PROCEDURE

The F-111 skin doubler specimen consisted of a 3.13 mm thick aluminium inner adherend with tapered 29 ply unidirectional boron/epoxy doublers bonded to each side to retain symmetry as shown in Figure 6. The doublers are bonded to the aluminium substrate using FM73 epoxy structural adhesive. The boron doublers are tapered at the ends at a taper, or step-up, rate of 1 ply every 4 mm. These specimens are based on the representative dog-bone specimens described by Baker et al.⁴ and the uniaxial loading is applied at a frequency of about 4 Hz.

Resistance-foil strain gauges are located on the far-field and the 4th step of the boron doubler on each side of the specimen, as shown in Figure 6. Two 28 μm thick piezoelectric film (PVDF) sensors, one located in the far-field on the aluminium adherend (parent structure) and the other covering the first two steps of the doubler, were applied to each side of the specimen as shown in Figure 6. The PVDF film, as supplied, was coated on both sides with a thin layer of conductive silver ink¹⁴ and electrical wires were bonded to the top and bottom surfaces by using conductive silver-loaded epoxy. These far-field sensors are approximately 20 mm long (loading direction) by 30 mm wide and sensors over the taper are approximately 6 mm long by 30 mm wide. Note that the direction of maximum sensitivity of the PVDF film corresponded to the applied load direction.

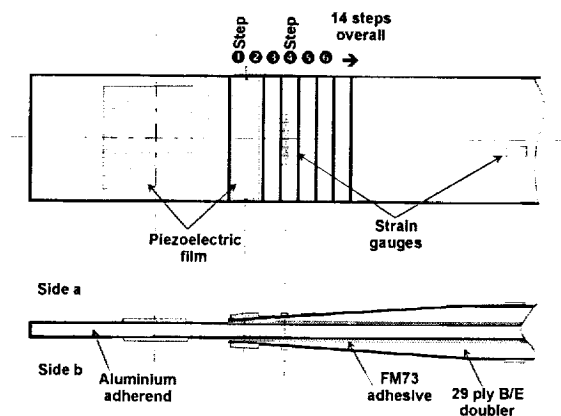


FIGURE 6 - Schematic of specimen showing sensor locations.

Two patch health monitoring devices are used in the conceptual demonstration. One device, designated as PHMa, was connected to resistance-foil gauges on side a of the specimen. The second device, PHMb, was connected to piezoelectric film (PVDF) sensors on side b. Therefore the former device effectively monitors $\epsilon_{\text{step4}}/\epsilon_{\text{far-field}}$ on side a and the latter device monitors $\epsilon_{\text{step1-2}}/\epsilon_{\text{far-field}}$ on side b. In order to verify the results from devices PHMa and PHMb additional sensors were monitored independently, i.e. on side a the piezoelectric film (PVDF) sensors, the central foil gauge on step 4 and the far-field foil gauge, and on side b, the central foil gauge on step 4 and the far-field foil gauge were monitored.

Constant amplitude sinusoidal loading with maximum/minimum loads of 8/-20 kN (case 1) and 20/2 kN (case 2) were applied. Note that, a 20 kN load achieves strains of the order of 3,100, 2,050 and 700 $\mu\epsilon$ in the aluminium, 1st and 4th steps of the doubler, respectively. Initially resistance-foil strain gauges were attached to the aluminium adherend and over the 1st step; however, because of the high strain levels required to initiate damage in the doubler these gauges fatigued after approximately 50,600 and 37,000 cycles of loading conditions 1 and 2, respectively. No damage had been detected in the boron doubler at this stage even though the loading was quite severe. Therefore the failed resistance-foil

strain gauges were replaced by the piezoelectric film sensors and testing was continued, using case 2 loading condition, until the specimen failed in the aluminium adherend near the grips.

4 DISCUSSION

The patch health monitoring device shown in Figure 7 was not optimised for size and weight; however, it easily fits in the palm of an average hand and has a mass of about 25 grams. The electronics could be easily compressed and lightened by greater use of surface mount components, and it is estimated that by using off-the-shelf components the device could be reduced to a size of approximately 50 mm by 50 mm by 4 - 7 mm. The thickness is dependent on the battery, which in turn will be dependent on the service requirements. Figure 7 also shows photographs and a schematic of the demonstrator set-up.

The specimen was subjected to 37,000 cycles at +20/+2 kN cyclic load before the piezoelectric film sensors were applied. Figure 8 shows data from the patch health monitoring device (i.e. ratio of step 1+2/far-field strains), as well as the ratio of the step 4/far-field strains (reference gauges), against the number of loading cycles. This figure shows that after applying the piezoelectric film sensors a further 20,000 cycles (total of 57,000 cycles) were applied before the patch health monitoring device on side b, PHMb, showed a 50% drop in patch state-of-health value – thus indicating that the damage had progressed past the 1st step since this device measured the ratio of the averaged strain over the first two steps/far-field strain. This figure demonstrates quite clearly that the device has detected and is monitoring the damage growth in the tapered end of the doubler (even though the sensor averaged the strain over the first two steps). The device then indicated that after a further 2,000 cycles the damage had propagated past the 2nd step. The resistance-foil gauges, on side b, indicated that the damage had then progressed to and past the 4th step after another 14,000 cycles and 27,000 cycles respectively. The test was continued in the hope that damage would initiate on side a, however the specimen failed in the aluminium near the grips before damage was observed on side a. The specimen was subjected to a total of 151,000 cycles. The test also showed that the piezoelectric film sensors are robust and extremely fatigue resistant. These sensors withstood a total 114,000 cycles at a peak strain of 3,100 $\mu\epsilon$.

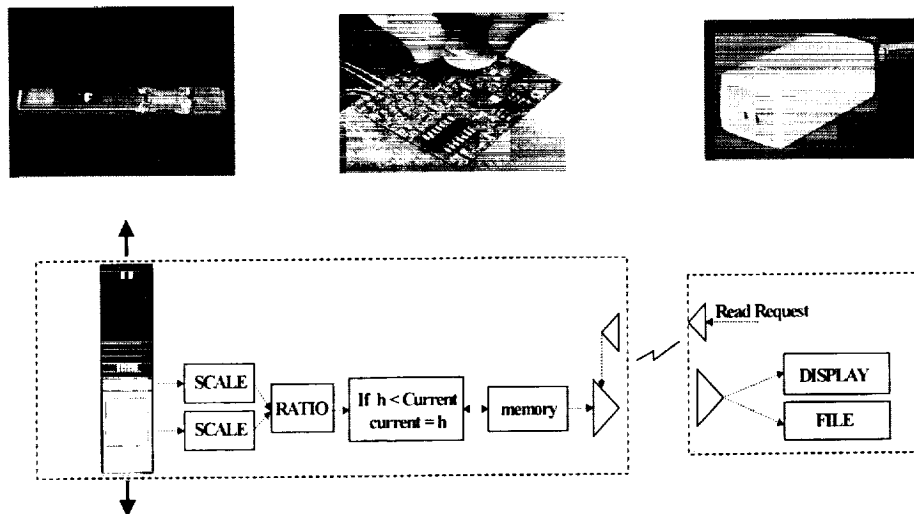


FIGURE 7 – Photographs and flow chart of the demonstrator experimental set-up.

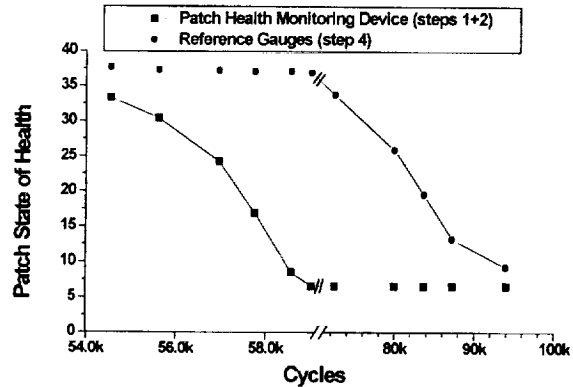


FIGURE 8: Plot of variation of patch state of health (ratio of critical region strain/far-field strain) with increasing number of applied loading cycles.

5 CONCLUSION AND RECOMMENDATIONS

The “smart patch” approach which is based on self-monitoring would considerably alleviate the certification requirements for implementing bonded composite repairs to primary aircraft structures. This approach relies on the ability to detect automatically disbonding in the patch, ie. the ‘smart patch’ approach is basically a continuous safety-by-inspection approach for the bonded repair. However, this approach brings its own problem of reliability assurance. Smart patch approaches are technically feasible but will be economically viable only for repairs to very significant and costly primary structure.

Previous experimental work at the AMRL has shown that the concept of a patch health monitoring systems by using ratios of (patch strain)/(strain in the component) appears to be quite promising. Therefore, the “smart” approach being studied in the DSTO is based on strain sensors bonded to the ends of the taper region and on the surface of the component away from the patch and the monitoring of the strain ratio during service life. Any decrease in this ratio is an indication of disbonding of the patch in this critical region. In this approach there is no requirement for measurement of the actual loading: disbonding is indicated by the reduction in relative strain. Ideally, the gauges are automatically monitored by an on-board miniaturised computer which would provide a warning (e.g. via a wireless link) should the indication of disbonding become significant. The system could also monitor the growth of the crack in the parent structure. This could be combined with the damage-tolerance approach based on slow disbond growth for the crack region or alternatively the “smart” capability could also include monitoring of crack and disbond growth.

Main aspects of the (remotely interrogated) patch health monitoring device were outlined in this paper. Two devices were built and experimentally demonstrated on a laboratory specimen containing a boron/epoxy doubler using both resistance-foil and piezoelectric film sensors as the strain sensors. The results show that the patch health monitoring device was able to successfully detect and monitor damage in the safe-life region of the patch (i.e. the tapered region of the doubler). The latter sensors appeared to be extremely fatigue resistant and robust.

However, this device has several areas needing further investigation and refinement. One area is the very difficult problem of interrogating the ‘smart patch’ through the aircraft fuselage/skin when the patch is situated in inaccessible internal locations. The second major area is to ensure all components (particularly the battery) perform properly over an extended operational temperature and altitude range. Although only one patch state-of-health value and two times are recorded on the prototype, further development of the electronics would allow a greater number of other parameters to be

recorded as well. For example, other parameters recorded could be the number of times the strain exceeds a given strain level or variables affecting corrosion rate etc.

ACKNOWLEDGMENTS

The authors would like to thank Roger Vodicka and Tom Radtke for useful discussions related to the experimental program, and Leigh Conder and Steve Van Der Velden for work on the electronics, debugging, programming and testing.

REFERENCES

- 1 A. A Baker, "Bonded Composite Repair of Metallic Aircraft Components", AGARD-CP-550 Composite Repair of Military Aircraft Structures, Paper 1, 1994.
- 2 A. A. Baker, "On the Certification of Bonded Composite Repairs to Primary Aircraft Structures", Proceedings of Eleventh International Conference on Composite Materials (ICCM-11), Gold Coast Australia, 1997.
- 3 A.A. Baker, L.R.F Rose, K.F Walker. and E.S.Wilson, "Repair Substantiation for a Bonded Composite Repair to a F-111 Lower Wing Skin," Proceedings of the Air Force 4th Aging Aircraft Conference, Colorado July 1996.
- 4 A. A. Baker, R. J. Chester, M. J. Davis, J. A. Retchford and J. D. Roberts, "The development of a Boron/Epoxy doubler system for the F111 Wing Pivot Fitting - Materials Engineering Aspects" *Composites* **24**, pp. 511 - 521, 1993.
- 5 S. C. P. Galea "Monitoring Damage in Bonded Composite Repairs of Cracked Metallic Components Using Surface Strain Measurements," *Proceedings of Eleventh International Conference on Composite Materials (ICCM-11), Gold Coast Australia, 1997.*
- 6 D. Rees, W. K. Chiu and R. Jones, "A Numerical Study of Crack Monitoring in Patched Structures Using a Piezoelectric Sensor" *Smart Materials and Structures* **1**, pp 202 - 205, 1992.
- 7 R. Vodicka and S. C. P. Galea, "Use of PVDF Strain Sensors for Health Monitoring of Bonded Composite Repairs", *DSTO Technical Report 0684*, June 1998.
- 8 C.-C. Chang and J. Sirkis, "Multiplexed Optical Fibre Sensors for Air Frame Repair Patch Monitoring", *Experimental Mechanics* **36**, pp. 353-359, 1996.
- 9 E. Tapanes and S. C. P. Galea, "Use of Optical Fibre Sensors to Detect and Monitor Damage in Bonded Composite Repairs of Cracked Metallic Components" *Proceedings of Eleventh International Conference on Composite Materials (ICCM-11), Gold Coast Australia, 1997.*
- 10 I. McKenzie, R. Jones, W. K. Chiu, D. Booth, S. Galea, "The Monitoring of Crack Growth Beneath Bonded Repairs using a Bragg Grating Array", *Proceedings of the Far East and Pacific Rim Symposium on Smart Materials, Structures, and MEMS, 10 - 13 December, 1997.*
- 11 A. F. Cox, "Fatigue Cracking in the Upper Plate of Wing Pivot Fittings in F111 Aircraft", *Defence Science and Technology Organisation, Aeronautical Research Laboratory, Report ARL-MAT-R-121*, 1988.
- 12 L Molent, R. J.Callinan, and R. Jones, "Design of an all Boron/Epoxy Doubler Reinforcement for the F-111C Wing Pivot Fitting:Structural Aspects", *Composite Structures* **11**, pp. 57-83, 1989.
- 13 I. Grabovac, R. A. Bartholomeusz and A. A. Baker, "Composite Reinforcement of a Ship Superstructure - Project Overview", *Composites* **24**, pp. 501-509, 1993.
- 14 Atochem N.A., 1987. *Kynar Piezo Film Technical Manual*, Atochem N.A. - Piezo Film Sensor Division, Valley Forge, PA.
- 15 A.A. Baker and L Meadows, "Air Force Research Area Critical Issues Paper: Smart Materials and Structures for Military Airframes", *Defence Science and Technology Report DSTO-GD-0176*, May 1998.

EVALUATION OF COMMERCIAL THERMOGRAPHY SYSTEMS FOR QUANTITATIVE COMPOSITE INSPECTION APPLICATIONS

Michael T. Valley, Dennis P. Roach, Larry R. Dorrell
Sandia National Laboratories
Airworthiness Assurance NDI Validation Center
3260 University Blvd. SE, Access Road B
Albuquerque, NM 87106
505-843-8722 (x8760 fax)
mtvalle@sandia.gov

Dennis M. Ashbaugh
SAIC
Airworthiness Assurance NDI Validation Center
3260 University Blvd. SE, Access Road B
Albuquerque, NM 87106

Roy T. Mullis
WR-ALC/TIEDM
420 2nd Street, Suite 100
Robins AFB GA 31098-1640

ABSTRACT

The expanded use of composite structures and the development of new composite repair techniques on U.S. Air Force (USAF) aircraft has created the need for improved portable, quantitative NDI methods and systems that can be used by field-level USAF NDI personnel. Recent advancements in thermal imaging technologies offer new inspection capabilities that can reliably meet this need. As part of a multi-phase program to field this technology, commercially available thermography systems are being assessed in structured experiments and on-aircraft field evaluations. The recently completed structured experiments evaluated quantitative inspection capabilities for bonded composite repair doublers and composite honeycomb structures and repairs. Specifically, test specimens included real and simulated C-130 underwing doubler repairs, C-141 underwing and plank riser doublers, C-141 engine cowlings, and F-15 rudders. Specimen flaws included disbonds, delaminations, and water and hydraulic fluid ingress in both repaired and unrepaired structures. This paper discusses test specimen design, experiment results, and the suitability of thermography for each composite inspection task under consideration.

1. INTRODUCTION AND BACKGROUND

The test results reported in this paper come from a project that will produce new composite inspection capabilities ready for use on operational USAF aircraft. This capability is being fielded with a multi-phase program that evaluates commercially available systems in structured experiments and field evaluations (conducted by USAF NDI staff), produces reference standard manufacturing data, delivers a prototype inspection system, and generates an NDI procedure manual and training program. The project phases, objectives, and status are:

- **Phase 1 - System Identification/Evaluation**

Objective: Survey commercial thermography systems to assess the state of the art in inspection capabilities and produce a list of candidate thermography systems for formal testing and evaluation. **Status:** More than 50 thermography systems vendors were identified. Only 6 systems were considered viable candidates for quantitative composite inspection applications

- **Phase 2 - Structured Experiments**

Objective: Evaluate selected thermography systems to determine which system best meets the USAF inspection needs. Use the vendor survey results from phase I to design an evaluation experiment that determines the inspection capabilities and limits. **Status:** Two companies, Bales Scientific, Inc. and Thermal Wave Imaging, Inc. (TWI) in partnership with Wayne State University (WSU), participated in the experiments completed in April 1998. Based on the test results, the TWI/WSU team inspection system was selected for on-aircraft field testing.

- **Phase 3 - Reference Standard Development**

Objective: Design and manufacture sample reference standards and develop manufacturing technical data. **Status:** Preliminary standards were used by each inspection team during the structured experiments. Lessons learned from these tests were implemented in the final designs. The final specimens are being manufactured for delivery to the Air Force in October 1998.

- **Phase 4 - Field Evaluation**

Objective: Perform field evaluation of the selected thermography system on USAF aircraft. Develop an NDI procedure manual and training program. Train USAF staff. **Status:** Field testing and the first training course are scheduled to begin in October 1998.

- **Phase 5 - Documentation and System Procurement**

Objective: Use lessons learned from field testing to prepare a final NDI procedures manual and training program. Deliver an inspection system to the Air Force. **Status:** Final system and documentation delivery is scheduled for April 1999.

2.0 EXPERIMENT DESIGN

2.1 Test Specimen Design

Assorted flaw generation techniques were evaluated experimentally to determine which flaw engineering approaches produce realistic thermography inspection results. The following describes the induced test specimens flaws and manufacturing process. A sample F-15 rudder specimen design is shown in figure 1. Though not shown in figure 1, many specimens' flaws were collocated spatially, but at differing depths, to assess the impact of near surface flaws on the detection/identification of deeper flaws.

1. **Pull Tab** - A 0.003" to 0.004" thick stainless steel shim stock is placed between adjacent composite plies. The shims are treated with RAM Silicone mold release to prevent permanent bonding of the insert to the adhesive. These inserts are removed after the adhesive curing process to produce an air gap disbond. These flaws were used in the C-130 wing doubler, F-15 rudder, and C-141 wing (external underwing doubler and plank riser doubler) specimens.

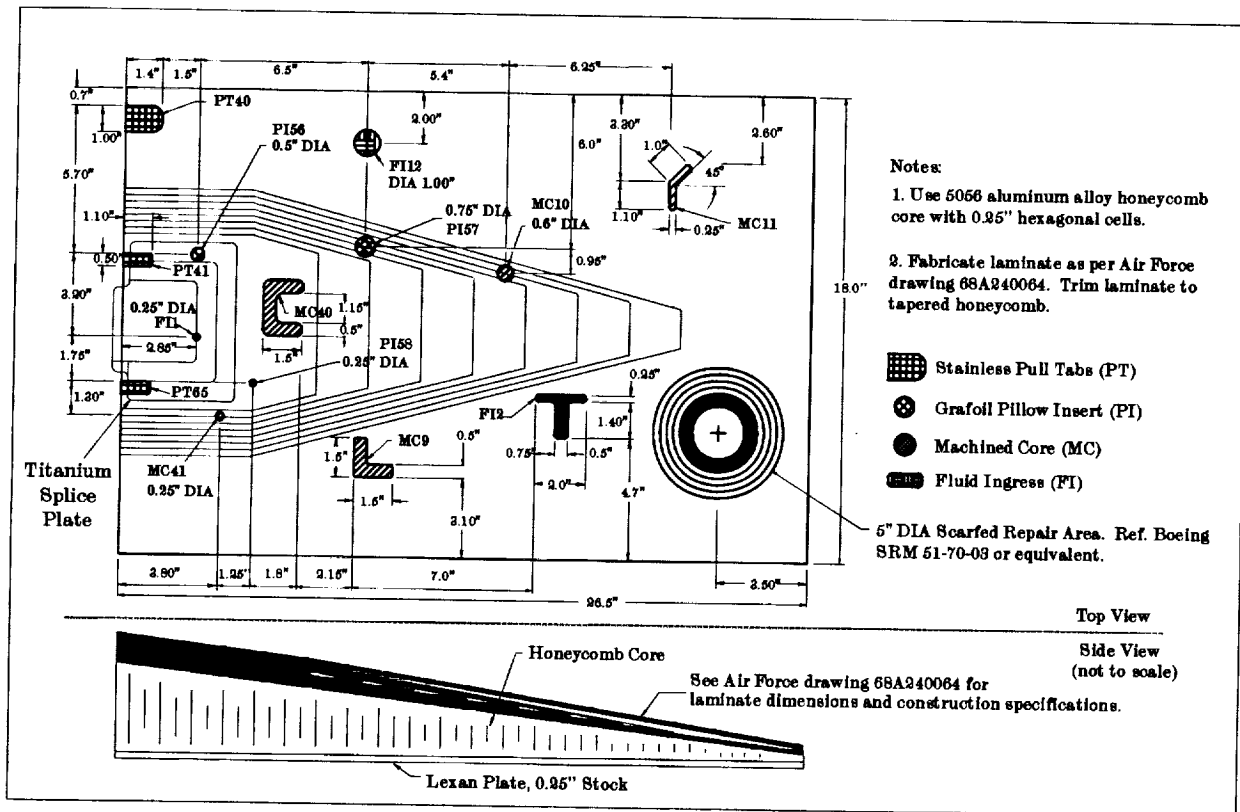


Figure 1. Sample design drawing for an F-15 rudder test specimen.

2. **Pillow Insert** - Experimental results suggested that interply delaminations could be created using either Kapton tape around 3 layers of tissue paper or grafoil inserts. Grafoil inserts were used in the structured experiments reported in this paper. These flaws were used in the C-130 wing doubler, F-15 rudder, and C-141 wing (external doubler and plank riser) specimens.
3. **Machined Core** - Air gap disbonds between the aluminum honeycomb and the composite laminates (or aluminum skin) were generated by machining thin recesses in the honeycomb cells. To maintain the air gap during manufacturing, the laminate portion of the honeycomb assembly is cured separately and then joined to honeycomb using a secondary bonding process. These flaws were placed in the engine cowling and F-15 rudder specimens.
4. **Pin Hole** - Small (about 0.125" diameter) holes were drilled in the parent material to create a vacuum leak during curing. This produced irregular shaped disbonds with random tentacles between the boron-epoxy doublers and parent aluminum. These flaws were used in the C-130 wing doubler and C-141 wing (underwing and plank riser) specimens.
5. **Fluid Ingress** - Both water and MIL-H-83282C hydraulic fluid were injected into individual cells in the honeycomb panels. The honeycomb was sealed with a Lexan sheet glued to the specimen back. Some cells were full and some were half full. The fluid ingress regions ranged from a single 0.25" cell to multiple cells spanning a region with a characteristic lateral dimension of 2.0". In some instances adjacent cells had differing fluids. Mixed fluid cells were not used. Fluid ingress was only induced in the F-15 rudder specimens.

6. Surface Grind - In some locations the aluminum surface had 10-20% of the material removed by grinding to simulate a region where corrosion had been removed. This process created a region of uneven adhesive thickness but did not create a disbond. These "flawed" areas were used to assess the ability of thermography systems to distinguish between a flawed region requiring a repair and a previously repaired region not requiring additional repair work. These flaws were used in the C-130 doubler and C-141 wing (underwing doubler and plank riser) specimens.
7. Scarfed Repair - Scarfed repairs were made in the F-15 rudder specimens in accordance with the F-15 rudder structural repair manual and pertinent Air Force specifications. In some cases, the repaired region was also populated with machined core disbonds, grafoil pillow inserts, and fluid ingress regions to determine if thermography could detect flaws in a previously repaired region.

2.2 Test Stands and Inspection Impediments

Four test stands were manufactured to fixture the specimens in configurations that create inspection conditions similar to those found in an operational environment. These inspection conditions presented inspection/access impediments that provided the opportunity to assess the NDI system fieldability and usability. The test stands, and a description of each simulated impediment, are provided in figures 2-5.

The TWI/WSU inspection team used a relatively small, lightweight, hand held inspection system that was able to easily adjust to the test stand induced impediments. However, each stand highlighted fieldability problems for the Bales' inspection system. The Bales' inspection system used in the experiments was mounted on a movable cart. The size of the cart and its limited range of motion created the following problems for the Bales thermography system:

1. The table with the engine cowling stand had to be moved to the inspection system.
2. The cart was too large to fit on the F-15 rudder stand. Adjustments were made to accommodate the inspection system. In the field, a custom stand or lift may be needed.
3. The height of the C-130 stand was at the limit of the inspection system adjustment. If the specimen had been placed any higher, special accommodations would have been required.
4. The inspection system could not be used inside the C-141 wing plank riser stand. The test specimens were removed from the stand and inspected on the floor. The current system as configured for the experiments is not capable of performing in-wing inspections.

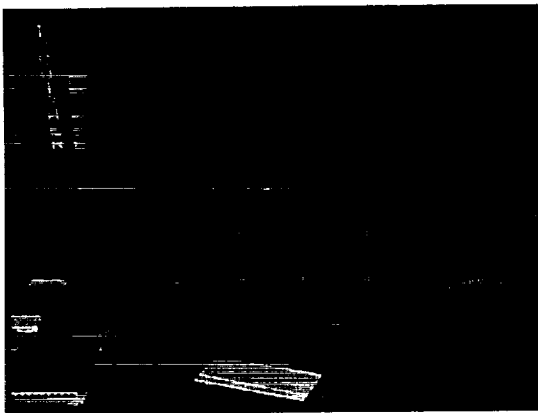


Figure 2. C-141 engine cowling test stand. All inspections were performed with the test specimen vertical and the test stand location fixed (i.e., the equipment had to be moved into the proper inspection position). The test frame with the mounted specimen was placed on a table during the inspections.

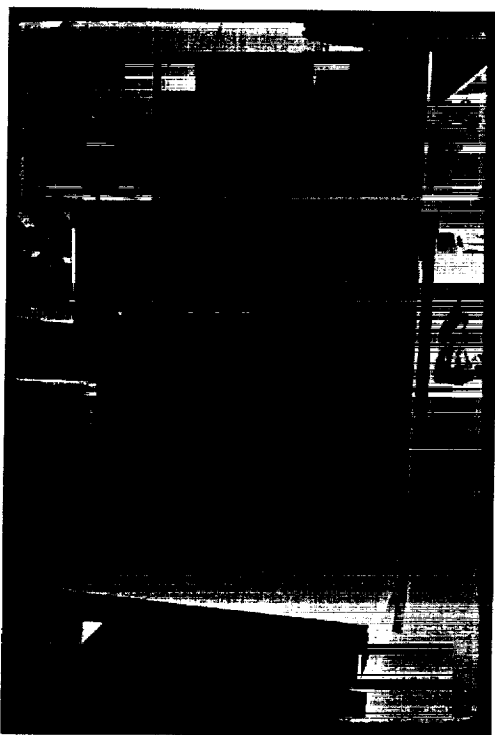


Figure 3. F-15 rudder test stand. All inspections were performed with the specimen vertical and the inspector/equipment restricted to the stand base. Support equipment could be remote if a sufficiently long umbilical was used.

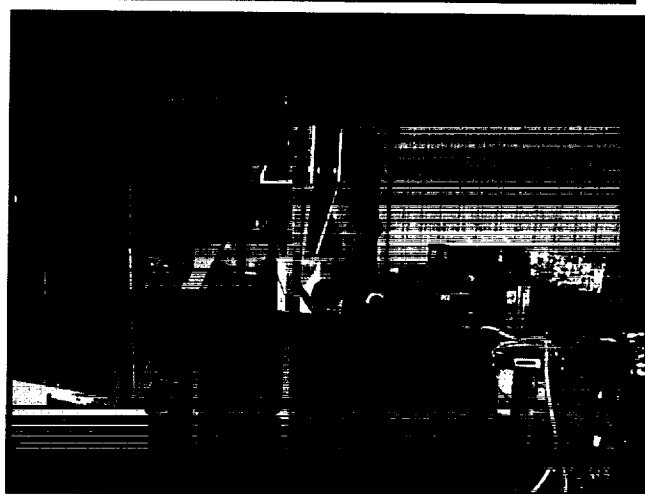
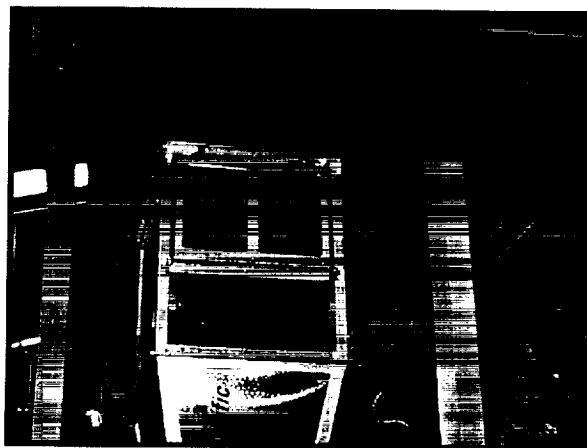


Figure 4. C-130 wing composite repair test stand. The test specimen is mounted overhead and inspected Bales Scientific setting up to inspect the specimen.

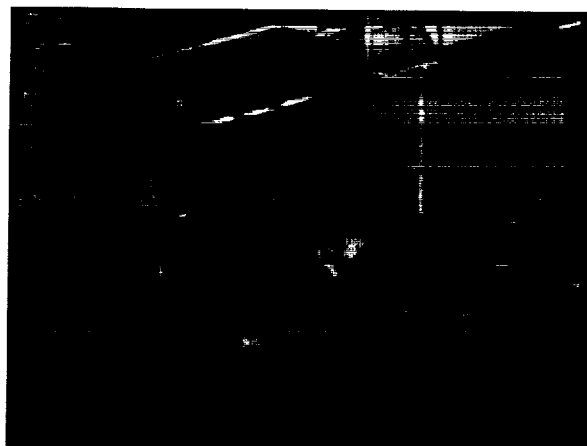
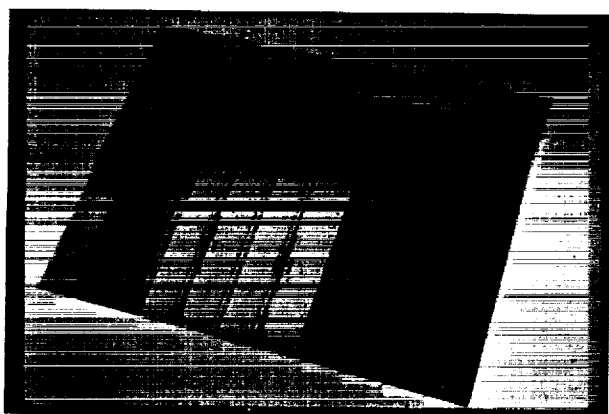


Figure 5. C-141 riser test stand. The inspections required that the inspector and equipment enter the stand through a 21" x 28" access port. The right image shows the inspector and TWI system being lowered into the stand to inspect the wing plank risers.

3. ANSWER DETERMINATION AND DATA LOGGING

The engineered test specimens were manufactured in accordance with design drawings and specifications. Mylar template overlays were used to position the flaws. After the specimens were constructed, each was inspected in an ultrasound immersion tank. The ultrasound images were overlaid and registered with the design drawings to compare the actual flaw locations/sizes with the design. The software used to perform the registration and overlay operation allowed the transparency of the top image to be varied to visualize differences. This same overlay and registration operation was used to analyze the experiment results where the thermal image results were inconclusive.

To the extent practical, the data was collected in a manner that allowed for semi-automated data analysis using computer software. Specifically, each experimenter recorded their results in electronic forms on a computer database module developed to support this experiment. The data entry required that the experimenter enter the flaw type (including identifying the fluid type for ingress situations), flaw size (characteristic dimension), flaw ply depth (if a delamination), a raw inspection image, and a color annotated image highlighting the detected flaw. This approach minimized the opportunity for human error and helped ensure consistency in the grading.

4. TEST RESULTS

To fully assess the competing inspection system capabilities, some flaws were programmed with a size, location, and/or characteristic that was intended to be undetectable with state of the art thermography capabilities and beyond the current Air Force inspection needs. The test design intentionally tried to preclude 100% success. Scores less than 100% do not mean USAF requirements can't be met.

<i>Grading Metric</i>	<i>TWI</i>
% Implanted Flaws Detected	94
Minimum Flaw Sizing Error (%)	0
Maximum Flaw Sizing Error (%)	50
Average Flaw Sizing Error (%)	6 (33)
Minimum Ply Depth Error (# Plies)	0
Maximum Ply Depth Error (# Plies)	4***
Average Ply Depth Error (# Plies)	0.9

Table 1. C-130 underwing composite doubler test results. * The 33 % average sizing error for Bales is misleading. This is principally due to a single sizing error on a 0.125" diameter flaw. Ignoring this one error resulted in an average sizing error of 6%. ** The Bales inspection system did not have the ability to identify the depth of interply delaminations. *** The TWI maximum ply depth measurement error occurred in a flaw located beneath a tapered ply region where the "answer" varied spatially. The single reported value was correct for part of the flaw region but was off by 4 plies at the deepest point. This reported error may be misleading/incorrect and may be due to the manner in which it was reported.

4.1 C-130 Wing Plank Test Results

A single C-130 wing plank composite doubler test specimen was used. The 3'x3' specimen consisted of 0.187" thick 7075-T6 aluminum plate with a 2'x2' octagonal 7 ply composite boron-epoxy doubler (with a 181 fiberglass outer protective layer). Two 1" wide x 0.125" thick 7075-T6 straps with fasteners (one strap with steel and the another with aluminum fasteners) were assembled on the back of the specimen to simulate a wing skin assembly. The doubler contained 16 programmed flaws (8 grafoil inserts, 4 pull tabs, 2 surface grinds, and two pinhole induced "natural flaws") and multiple unprogrammed disbonds and delaminations. The flaws ranged in size from a minimum of 0.125" in diameter to the largest flaw with a maximum dimension of 4.0". The C-130 specimen test results for are presented in table 1.

<i>Grading Metric</i>	<i>Bales</i>	<i>TWI</i>
% Implanted Riser Flaws Detected	75	100
% Implanted Flaws Correctly Identified	92	85
Minimum Sizing Error (%)	0	0
Maximum Sizing Error (%)	67	63
Average Sizing Error (%)	19	20
Minimum Ply Depth Error (# Plies)	N/A	0
Maximum Ply Depth Error (# Plies)	N/A	6
Average Ply Depth Error (# Plies)	38%	1.8

Table 2. C-141 wing plank riser specimen test results.*The Bales' inspection system cannot identify flaw ply depth. However, using the relative timing of the flaw's appearance in the acquired images, Bales reported the relative flaw depth (e.g., top half, middle, bottom half). The results provided indicate the percentage of the time the relative depth measurement was correct.

4.2 C-141 Wing Plank/Underwing Doubler Results

Sixteen C-141 wing plank weep hole riser specimens and 8 C-141 underwing doubler specimen were inspected. The inspected riser repairs consisted of a 15 ply boron-epoxy doubler with a 181 fiberglass prepreg outer protective layer. Each underwing doubler had 8 boron-epoxy plies and a fiberglass layer. Both the weep hole repairs and underwing doublers were placed on actual C-141 wing plank sections provided by the Air Force. Eight underwing doubler test specimen were used with 26 programmed flaws and multiple natural flaws ranging in size from 0.25" in diameter to a maximum flaw dimension of 2.7". Sixteen riser doublers specimens were used with 16 programmed flaws and multiple natural flaws ranging in size from 0.25" in diameter to a maximum flaw dimension of 1.9". Some of the underwing doublers and riser doublers were unflawed. The test results for these specimens are presented in tables 2 and 3. It should be noted that TWI did not use their automated flaw depth measurement software for these specimens. As a result, the ply depth errors increased significantly over the results they attained on the C-130 and F-15 test specimens.

<i>Grading Metric</i>	<i>Bales</i>	<i>TWI</i>
% Implanted Plank Flaws Detected	69	88
% Implanted Flaws Identified	94	76
Minimum Sizing Error (%)	0	0
Maximum Sizing Error (%)	88	200
Average Sizing Error (%)	20	30
Minimum Ply Depth Error (# Plies)	N/A	1
Maximum Ply Depth Error (# Plies)	N/A	14
Average Ply Depth Error (# Plies)	4.7	4.7

<i>Grading Metric</i>	<i>Bales</i>	<i>TWI</i>
% Implanted F-15 Flaws Detected	88	88
% Implanted Flaws Correctly Identified	77	100/93
% Fluid Flaws Correctly Identified	20	60
Minimum Sizing Error (%)	0	0
Maximum Sizing Error (%)	50	100/400
Average Sizing Error (%)	9.6	10.5/20.9
Minimum Ply Depth Error (# Plies)	N/A	0
Maximum Ply Depth Error (# Plies)	N/A	2/8
Average Ply Depth Error (# Plies)	48%	0.5/1.4

Table 4. F-15 rudder specimen test results. * See table 2 comments. The two TWI values (# / #) represent total results and results excluding tapered specimen regions where the answers varied spatially.

4.3 F-15 Rudder Test Specimen Results

Six F-15 tests specimen were used. Five specimens had a uniform 6 ply laminate skin bonded to tapered 5056 aluminum honeycomb and one had a tapered 8 to 24 ply laminate skin on tapered honeycomb with a titanium bracket inserted between the middle plies. There were 52 flaws and 4 scarfed repairs, with flaws both in the repairs and beneath the bracket. The flaw sizes ranged from 0.25" in diameter to 3.3" along the maximum flaw dimension. The test results for these specimens are presented in table 4.

Quantitative Lateral Flaw Size Measurements					
	Skin Thickness (inches)	% Flaws Detected	Minimum Error (%)	Maximum Error (%)	Average Error (%)
Boles	0.040	33	55 h, 36 v	55 h, 36 v	55 h, 36 v
TW	0.040	100	0		0.70
Boles	0.050		0 h, 20 v	36 h, 46 v	22 h, 33 v
TW	0.050	66	0	20	10
Boles	0.060	66	60 h, 14 v	94 h, 33 v	77 h, 24 v
TW	0.060	100	22	25	24
Boles	0.070	33	17 h, 28 v	17 h, 28 v	17 h, 28 v
TW	0.070	33	0		0
Boles	0.080	25	N/A	N/A	N/A
TW	0.080	25	23	23	23
Boles	0.100	0	N/A	N/A	N/A
TW	0.100		N/A	N/A	N/A
All		33	0 h, 14 v	94 h, 46 v	31 h, 30 v
All		50	0	25	12

Table 5. Engine cowling test specimen inspection results. Where more than one flaw dimension was measured, “h” and “v” refer to the measurement errors in the horizontal and vertical directions.

4.4 C-141 Engine Cowling Test Specimen Results

One engine cowling specimen with six regions of differing 2024-T3 aluminum skin thickness was used. The specimen was 24.0” wide x 12.0” high and was bonded to 1.0” thick 5052 aluminum honeycomb. There were 20 core to skin disbond flaws with characteristic flaw dimensions ranging from 0.25” to 2.2”. Some of the flaws were located in the 1.0” wide x 24.0” long honeycomb butt joint splice that spanned the middle section of the specimen. The test results are presented in table 5.

4.5 Subjective Evaluation Results

In addition to the objective results provided in tables 1-5, a subjective evaluation was performed to rate the system viability. Evaluation results are provided in tables 6-7 using the following scoring metrics. Two scores in a single category means the score varied between inspection applications/specimen types.

Score Definition

- 1 Ready for use or needs minor modifications. Minimal financial/schedule impacts. No technical risks.
- 2 Well defined modifications are needed. Some financial/schedule impacts. Low technical risk.
- 3 Technology shows promise but requires some applied research or development. Financial and schedule impacts are beyond project scope. Moderate to high technical risks.
- 4 Significant problems exist. Extreme financial and/or schedule impacts. Very high technical risks. Involves extended research beyond the existing project scope.
- 5 Problem requiring significant technological advancement or major change in vendor’s corporate philosophy. Not resolvable in foreseeable future.

<i>Rank</i>	<i>Evaluation Criteria</i>	<i>BALES Score</i>	<i>TWI Score</i>
High	Accuracy	Table 2	Table 2
High	Sensitivity	Table 2	Table 2
High	Data Analysis Capabilities	2, 3	
High	Versatility	2, 3	1, 2
	Portability		
Medium	Complexity	2	2
	Human Factors		
Low	Inspection Time	1	1
	Availability		
Low	Cost	1	1
	Field Support Capabilities		

Table 6. Evaluation criteria results summary.

<i>SPECIMEN CATEGORY</i>	<i>BALES SCORE</i>	<i>TWI SCORE</i>
Engine Cowling	2	1
C-130	1	1
F-15	1	1
C-141 Underwing Doubler	2	1
C-141 Plank Riser	2	1

Table 7. Inspection accuracy & sensitivity evaluation criteria results by specimen category.

CONCLUSIONS

Both evaluated inspection systems demonstrated reliable, high sensitivity flaw detection capabilities with a zero false call rate. The Bales' inspection system provided the best imagery, but was the least flexible from a portability and fieldability standpoint. The TWI system, which was the only system that demonstrated the ability to measure flaw depth and identify all flaw types (including correct fluid type identification when the fluid was not beneath another flaw type), was selected for on-aircraft field testing to be conducted by the Air Force in the fall of 1998.

ACKNOWLEDGEMENTS

This project was performed under contract to Warner Robins Air Logistics Center (WR-ALC/TIEDM) with funding provided by the Air Force Air Mobility Command. Project oversight is provided by the Aging Aircraft and Systems Office, ASC/SMA, Wright Patterson AFB, Ohio. The structured experiments were performed at the FAA Airworthiness Assurance NDI Validation Center, operated by Sandia National Laboratories for the William J. Hughes FAA Technical Center.

HIDDEN CORROSION DETECTION TECHNOLOGY ASSESSMENT

Wally C. Hoppe
University of Dayton Research Institute
300 College Park Avenue
Dayton, Ohio, 45469-0120, USA
(937) 229-3711 - telephone
(937) 229-3712 - fax
hoppe@udri.udayton.edu

ABSTRACT

The US Air Force issued a delivery order to the University of Dayton Research Institute to optimize existing corrosion detection technologies and couple these with an automated system to provide significant maintainability improvements to the C/KC-135 and similar type aircraft. Major tasks on the program and overall program status are reviewed. Special emphasis is placed on the NDE evaluation and validation methodologies developed and applied on this program. This methodology is briefly described and trial test results are presented. These results demonstrate the feasibility of applying this methodology to assess hidden corrosion detection technologies.

1. INTRODUCTION

The aging of US Air Force aircraft is well documented. The problems associated with maintaining these aircraft are also well documented. Damage includes cracking, corrosion, multi-site damage, widespread fatigue damage, stress-corrosion cracking, and crack-corrosion interactions. Inspection, disposition decisions, repairs, rework and upgrades are becoming increasingly important. Aircraft availability decreases as maintenance costs and depot flow days increase. In order to keep these aircraft in service, reduce costs, reduce flow days and increase availability, with the result of optimizing fleet readiness, it is important to improve nondestructive inspection methods. New methods must be developed. The application of others must be expanded. Capabilities must be improved by providing for better discrimination between damaged and undamaged material/structure. And, false calls must be reduced. New methods must be transitioned for depot and field level use. Automation will also play a role in reducing costs and improving capability.

An important element to the acceptance and implementation of improved NDE methods will be validation. Validation consists of an independent, quantitative assessment through the use of controlled tests, procedures and protocols, to evaluate the capability of the inspection method to detect and quantify damage on test specimens that will be independently characterized.

In the spring of 1997, the US Air Force issued a delivery order to the University of Dayton Research Institute (UDRI) titled Automated Corrosion Detection Process/System for Cost-Effective Maintainability Improvement. Under this program, UDRI is tasked with optimizing, evaluating, and selecting several nondestructive inspection (NDI) technologies for integration into an automated inspection system directed at detection of hidden corrosion in the KC-135. Of central importance to the process is the development of appropriate validation methodologies. There are several tasks on this program. This paper will give a brief overview of the program objectives and some early results.

2. DISCUSSION

A brief overview of the KC-135 inspection challenges will be presented first, followed by a review of the program tasks. The topic of specimens will be addressed. A description of our detection assessment methodology will be given, followed by a presentation of a feasibility test that has been performed.

2.1 BACKGROUND ON C/KC-135

The KC-135 is an interesting case of an aging aircraft. The average age of this aircraft is over 35 years with almost 600 aircraft still in service¹. It is the intent of the Air Force to continue to fly these aircraft perhaps 40 more years. According to a U.S. General Accounting Office report², the Air Force has not yet identified a replacement aircraft, and recently, they modified their plans for a replacement, delaying its insertion into service until the year 2013. This same report states that depot flow days have increased from 158 days in 1991 to 245 days in 1995, forcing a gradual extension of the depot cycle from four years to five years. The KC-135 is not flown aggressively, making corrosion the most important life-limiting form of damage. At this point, corrosion is considered an economic issue, but even so, increases in flow days and maintenance costs are having a direct impact on the fleet readiness. Furthermore, what is an economic issue today may develop into a safety problem in the future.

Corrosion occurs in many forms on the KC-135. Crevice corrosion in the lap joints and doublers is of primary interest on this program. Crevice corrosion has associated with it metal thinning, surface roughness, and pilling. The KC-135 has intergranular and exfoliation corrosion around steel fasteners on the upper wing skins. Corrosion can occur between wing skins and spars, between the lower wing skin and the main landing gear trunnion, and between fuselage wing skins and steel doublers around pilot windows. Stress corrosion cracking of components made from large 7075-T6 aluminum forgings has also been found. Reference [1] provides information on other types of corrosion reported on the KC-135.

The materials and manufacturing practices in use at the time these aircraft were built have led to favorable conditions for the initiation and growth of crevice corrosion in lap joints and doublers. Large portions of the skin are made of 2024 and 7075 aluminum alloys. Joints were assembled typically without any sealant or zinc chromate. With time and exposure to the environment, corrosion has resulted.

There are several types of construction features in the structure that complicate the inspection: material composition (alloy type), skin thickness, fastener type, and the presence of substructures.

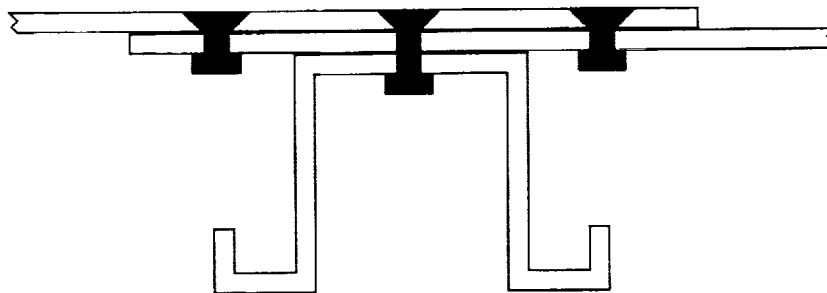


Figure 1. Sketch of lap joint cross section. Shown here are the layers of skin, the stringer, and the rivets.

The skin structures that are of interest to us are the lap joints (see figure 1), splice joints, stringers and sonic straps. These structures are fastened with spot welds or rivets (aluminum or steel, button head or countersunk). Combinations of these "simple" structures result in very complex skin structures. Furthermore, the C/KC-135 has many different mission configurations, as well as repairs and modifications. There are approximately 900 linear feet of lap joints and 1000 square feet of doublers (including triplers and quadruplers) on each aircraft. Considering the alloys, skin configurations, aircraft configurations, repairs, patches, modifications, and assembly tolerances, the inspection of the KC-135 presents a significant inspection challenge.

2.2 THE AUTOMATED CORROSION DETECTION PROGRAM

As mentioned earlier, the goal of this program is the optimization, evaluation and selection of one or more inspection technologies to integrate into an automated inspection system to detect hidden corrosion on the KC-135. The goal is to be able to accurately and reliably detect and characterize corrosion to less than 10 percent thickness loss. In this section each of the major tasks of the program will be described.

While not attempting to include every known inspection technology, UDRI competitively selected several technologies to participate in the program. These include both contact and noncontact methods and four different physical principles. Participating organizations are listed in Table 1. Other technologies may be evaluated for participation as appropriate.

TABLE 1. PARTICIPATING NDE RESEARCH ORGANIZATIONS

Organization	Technology
Wayne State University	Thermography
Physical Research, Incorporated	Magneto-Optical Imaging - Eddy Current
Analytical Services and Materials	Ultrasonics
Advanced Research Applications Corporation	Radiography
NASA-LaRC	Thermography
NASA-LaRC	Radiography

Each of the first four organizations listed in Table 1 has completed optimization of their respective technologies as applied to the detection of crevice corrosion in lap joints and doublers. In the fall of 1998, the capability of each of these six technologies listed above will be determined in a controlled assessment test. This evaluation/validation will be described below. Following the evaluation, we will select one or more inspection technologies with an acceptable level of detection capability for continuation in the program. The selected technologies must lend themselves to automation, and be sufficiently mature to begin this phase of development. Throughput and other implementation/logistic issues will also play a role in the continuation decision.

As part of this program, UDRI has made an assessment of several automation concepts, investigating their claimed capabilities, advantages, disadvantages, costs and risks. At this point in the program, we are intending to pursue a crawler robot as the delivery mechanism for the different inspection modes. While the goal of the program is automation, the program is not intended as a robotic development effort. The significant NDI issues are more important.

Undoubtedly, more than one technology will be required to produce a complete inspection of the lap joints and doublers. With this in mind, we will be considering different data fusion schemes. Other tasks

on the program include investigating NDI reproducibility and a Nondestructive Evaluation (NDE) requirements survey. The goal of our investigation into NDI reproducibility is to establish a framework for defining those technology specific parameters critical for assuring reproducible inspection results. The NDE requirements survey has compiled responses from over 60 knowledgeable individuals in the aerospace industry with primary emphasis on the Air Force. The survey has investigated different types of damage, damage location, inspection needs, equipment availability, and other issues. Data has been compiled in a database that can be queried in many different ways. A summary of the survey is being prepared.

The efforts on this program are many-faceted, and are all important to the program; however, the main thrust of the program is the evaluation of the NDI technologies, and the integration and demonstration of an automated system. In order to evaluate the different technologies, UDRI has developed a validation methodology. UDRI has also obtained an assortment of specimens. Specimens and validation methodology will be briefly described below.

2.3 SPECIMENS

Any validation methodology requires appropriate specimens. The development and search for specimens is an ongoing effort in the aging aircraft community. Generally, there are two different types of specimens. First, there are real inspection articles, with real damage. In this case, these would be pieces of real aircraft fuselage skin panels with actual corrosion. These specimens allow for double-blind tests. They are single use, and require destructive break-open and independent characterization. Selection and availability of such specimens are severe constraints. Specimens with too much, or too easy-to-find corrosion provide little information in a test. Similarly, specimens with too little or too difficult-to-find corrosion have limited usefulness, but are necessary in the evaluation of the likelihood of false calls.

The second type of specimen is a manufactured one. It contains either real or artificial corrosion, and possibly some corrosion by-product (simulated or real). Since it is engineered, it should have well defined corrosion levels. It provides for single-blind tests, and can be used many times. While there are advantages to this type of specimen, there is always the question whether it accurately simulates reality. On the other hand, it offers considerable control of test variables. There are many ideas with regard to engineered test panels. Essentially, any validation methodology will require both types of specimens.

As part of this program, UDRI has acquired a number of candidate specimens from two aircraft. In particular, a KC-135 aircraft was recently cut up at Tinker Air Force Base. This aircraft had been previously stationed in Hawaii, and contained extensive corrosion damage. The decision was subsequently made to scrap the aircraft. Mr. Don Nieser (OC-ALC/LACRA) and other individuals at Tinker Air Force Base worked aggressively to have this aircraft cut up and the pieces used to study corrosion, fatigue, and nondestructive testing. UDRI received several pieces of the fuselage, two pieces of a wing, and an intact portion of the tail. The fuselage pieces are of various sizes, but typically are many feet wide by many feet long. Each contains some combination of lap joint, doubler, stringer and/or other structure. UDRI is screening these panels to look for adequate levels of corrosion to make appropriate specimens for evaluation tests. We are considering complexity of the structures as well as areas without corrosion for false call assessment. Figure 2 shows two typical KC-135 panels. UDRI has also acquired several pieces of a 707 fuselage, the commercial version of the KC-135. This fuselage had been used in extensive fatigue tests for the Navy. The pieces we received are also being screened for appropriateness as test specimens.

We have also engineered several other panels, each having material removed from one side and assembled into skin structures with simulated corrosion by-products in the void. Each panel has been designed with a different purpose in mind. Figure 3 shows the machined surface of one specimen. The



Figure 2. Two KC-135 panels. These panels were cut from a KC-135 at Tinker Air Force Base in March 1998. The longer of the two panels is about 8 feet long.

squares are 2 X 2 inches, each with a different amount of material removed. This specimen is designed to test for a correlation between NDE output and the thickness loss. Without such a correlation it would be senseless to perform further testing. This test will also look at noise and saturation levels in the output image. This specimen, with its sharp corners and uniform thickness profile within the squares will not be used for probability of detection (POD) assessment.

Another specimen contains 8 sets of lines, each set consisting of three lines. All sets of equal-width, equal-separation line pairs have the same depth of material removed. Line widths and separation distances vary from 1 inch to 0.008 inches. This line pair specimen is designed to ascertain an estimated spatial resolution for each NDE technique. Again, this specimen will not be used for POD assessments.

Obviously, sharp corners and uniform areas of thickness loss are not representative of real corrosion.

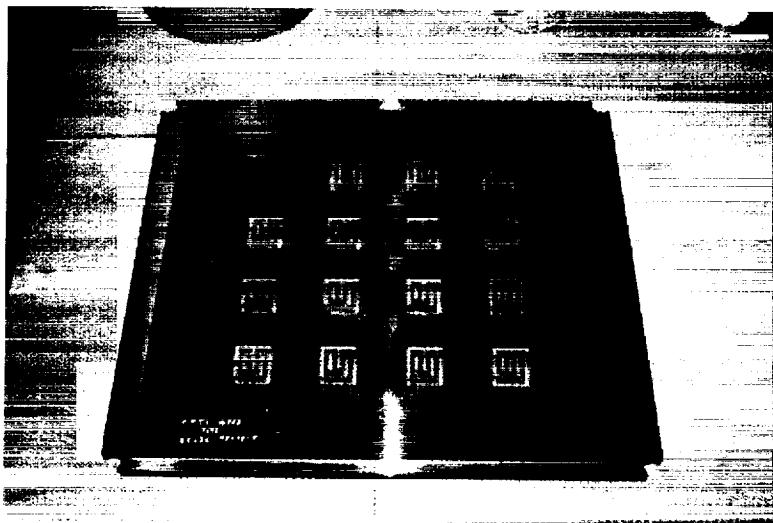


Figure 3. Correlation panel. The machined squares are each two inches by two inches.

With this in mind, we created another specimen that was designed to provide a random profile of thickness loss. The profile was computer-generated using a simple algorithm to "grow" the thickness loss in depth and spatial extent about several seed points. The machined area covers a region of about 4 X 4 inches, and the material removed ranges from zero to 0.018 inches (0 to 45% loss). Currently, this is considered a trial specimen designed to measure output as a function of thickness loss and from this to estimate POD. Depending on its success, additional specimens can be easily created. We are also investigating other methods of manufacture. In addition, we are continuing to investigate different specimen designs, including engineered specimens with a combination of machined and real corrosion generated thickness loss.

2.4 CORROSION DETECTION TECHNOLOGY ASSESSMENT METHODOLOGY

A short discussion of a methodology for corrosion detection assessment is given below, followed by a description of a feasibility test that was conducted using this method. Finally, the results of the test are given.

2.4.1 Discussion of Assessment Methodology

Early in this program, we received input from several individuals representing several organizations concerning the development of a methodology for assessing the capability of different inspection systems to detect and characterize corrosion. These individuals and their organizations are listed in Table 2. The input that we received from these individuals dealt with the topics of specimens, corrosion metrics, analysis methods, and procedures and protocols, among other things. The general philosophy of the test was provided and in some cases, details were included as well. The responses varied.

TABLE 2. INDIVIDUALS PROVIDING INPUT ON DETECTION ASSESSMENT.

Contributor	Organization
D. Nieser	OC-ALC/LACRA
D. Kinsie	AFRL/MLS-OL
J. Gallagher	AFRL/CCL
W. Rummel	D&W Enterprises, LTD
M. Golis	Advanced Quality Concepts
G. Hardy	Retired
F. Spencer	Sandia National Laboratories
C. Smith	FAA Technical Center
A. Berens	University of Dayton Research Institute

In addition to UDRI's efforts, there has been and continues to be considerable work directed at corrosion detection assessment. For instance, ARINC³ has done work in this area, as has Sandia National Laboratories⁴ with the Airworthiness Assurance NDI Validation Center. While much progress on this topic has been made, there is still much to learn, and consensus on a method of corrosion detection validation has yet to be reached. Our approach has been to learn what we can from the various sources, and to provide a proposed method that will contribute to the advancement of this field. This proposed method is not specifically built upon the input of any one of the resources given above. It is, however, designed to be an integrated, self-consistent whole that will lend itself to analysis similar to well established crack detection technology assessment methods⁵.

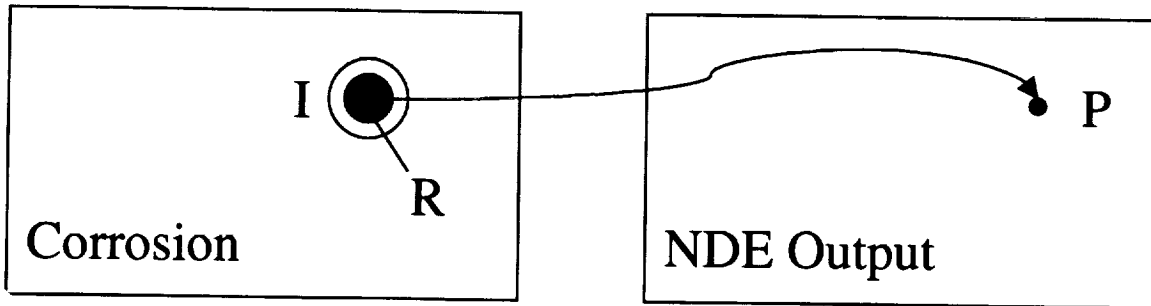


Figure 4. Diagram of concept underlying corrosion detection assessment methodology

Conceptually, our method is based upon the premise that for each NDE technology being evaluated, the output at a given point, P, is a function of the thickness loss in a small region, R, of the test panel. This is shown conceptually in Figure 4. An output image is the collection of output pixels. In order to determine the probability of detecting a given level of thickness loss, we define independent inspection cells, I, such that the output at the point P is independent of the corrosion everywhere outside the cell. The size of the independent cells is determined from the tests conducted on the resolution test panels (line pair specimen). A collection of non-overlapping independent cells then represents independent inspection opportunities for that test panel. Data pairs are established consisting of the output at the center of the cells and a thickness loss parameter from within the cells. This parameter may be the actual average thickness loss or alternatively the actual maximum thickness loss within the region, R, inside the cell, I. The output is then plotted as a function of this thickness loss parameter. Since two cells with nominally the same thickness loss parameter may have different corrosion profiles, the plot of output versus thickness loss will include scatter in the data. This scatter of the data about some trend curve reflects the variation in corrosion profile from cell to cell, as well as noise and other variables. By appropriately modeling the trend curve and residuals, it is possible to calculate the probability of detection (POD) as a function of thickness loss for a given threshold, technique, and spatial resolution.

From this perspective, it is obvious that certain engineered specimen concepts are inadequate. If a specimen thickness loss profile is uniform, it presents an unrealistic profile of corrosion. The scatter in the data as determined from such specimens would not reflect what will be observed on real aircraft panels. Similarly, engineered corrosion clusters that contain sharp edges are unrealistic. To make the methodology described herein work, each specimen must have its corrosion profile fully characterized with some independent method and must truly represent the kinds of damage that is expected on real aircraft. Real corrosion test panels must also be fully and independently characterized. Test panels with different corrosion profile characterizations may give different POD results. Therefore, a complete independent characterization of the test panel serves to distinguish the corrosion found on one panel from the corrosion found on another panel. For instance, a panel with many pits will look different than one with few pits and extensive general attack, and may then result in different POD capabilities.

By modeling the output in regions of no thickness loss, the probability of a false call can be established. False calls are threshold excursions in regions of no thickness loss. Systems with better discrimination have fewer false calls and overcalls for the same POD for a given critical thickness loss. In this scheme, different technologies can be compared by examining their respective discrimination capabilities for a given detection level.

2.4.2 Description of Feasibility Test

To demonstrate the feasibility of this assessment methodology, we tested it using the random profile panel discussed above. In this trial test, the single Al 2024 panel (0.040 inches thick – 12 inch square) was inspected from the side opposite the machined surface using ultrasonics and eddy current. The ultrasonic data was used as a reference characterization of the panel. It was done in immersion using a 25 MHz, 0.25-inch diameter, 0.5-inch spherically focussed transducer. Time-of-flight data was collected relative to the front surface reflection with a 100 MHz sampling rate. This gives a thickness resolution of approximately 1.25 mils in aluminum. The 6-dB spot size was calculated to be about 0.005 inches in water. Sample points were separated by 0.010 inches, and the step size between lines was 0.010 inches. Each time-of-flight measurement was converted to an estimated thickness.

The eddy current inspection was considered to be the method under test. It was performed at 35 KHz, with a 0.26-inch diameter shielded absolute coil. This produced a skin depth of 0.025 inches and an eddy current level at the back of the sheet that was about 20% of front surface current level. The liftoff signal was placed in the horizontal channel, and the vertical channel was used for the inspection. Sample points were separated by 0.040 inches in both the scan and index directions.

2.4.3 Results of Feasibility Test

Figure 5 shows grey scale images of the ultrasonic and eddy current inspections. Each image has been preprocessed for presentation (cropped, rotated, flipped, scaled, centered...). Figure 6 shows 128 non-overlapping, randomly selected independent inspection cells (0.32 inches diameter).

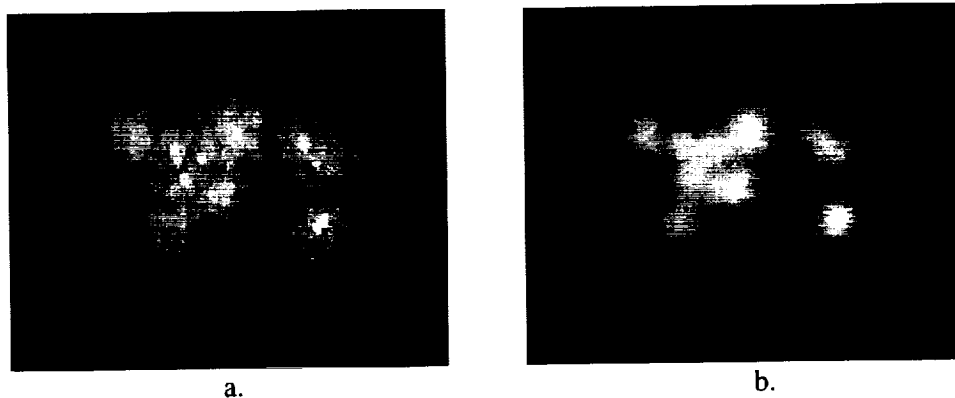


Figure 5. Inspection results for random profile specimen. The first image, (a), is the grey scale output for the UT inspection. The second image, (b), is the output for the eddy current inspection.

There are 59 cells with no material removed, which were excluded from the analysis. Figure 7 is a plot of output versus average material removed for the remaining 69 cells. These averages were calculated over 0.26-inch diameter regions centered on the conservatively sized cells. Also shown in this figure is a straight-line best-fit to the data. In order to calculate a POD curve, we assume that the data can be modeled as a straight line given by the best-fit, and that the scatter about the fit can be modeled by a normal distribution with standard deviation given by that of the residuals. The figure also displays a threshold that was used to calculate a POD for this particular inspection. This POD is shown in Figure 8. This simple test and analysis demonstrates the feasibility of our proposed methodology for determining

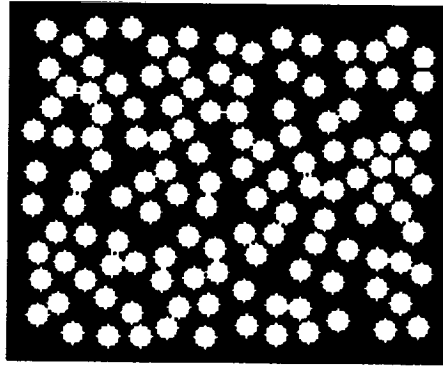


Figure 6. A collection of 128 non-overlapping independent inspection cells. Each cell is 0.32 inches in diameter and was randomly selected. The selection routine excluded a border region to avoid edges of the image.

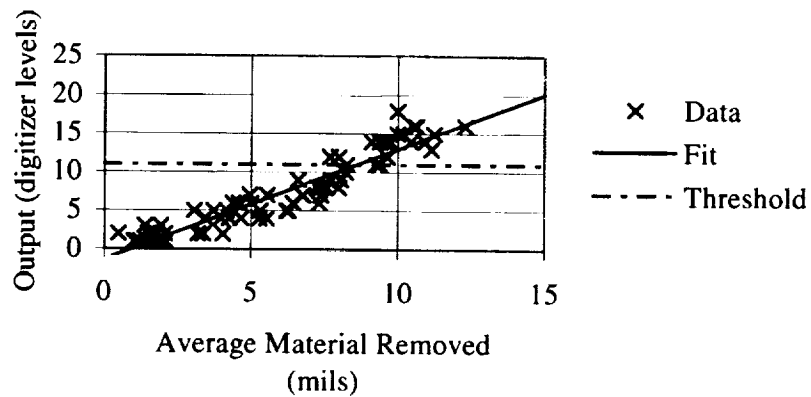


Figure 7. Analysis results. Output versus average material removed for independent cells excluding those with no material removed.

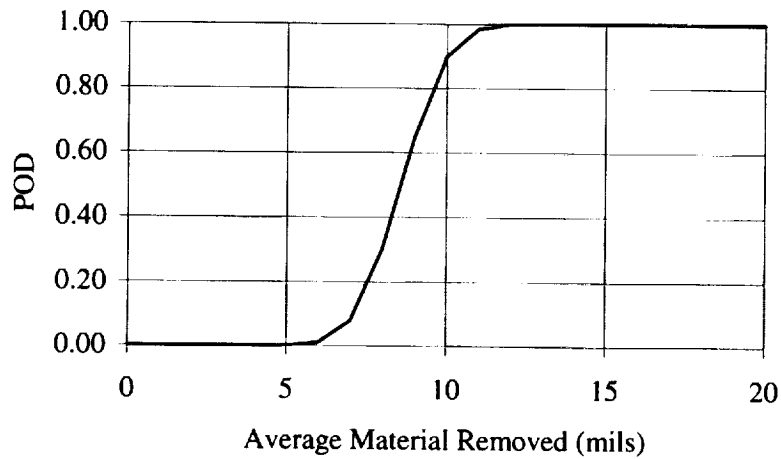


Figure 8. Estimated probability of detection based on the threshold in Figure 7.

the POD for a detection technology. Full-scale implementation will include a more rigorous analysis of the fit and residuals, with tests for normality and equal variance at different material loss levels. Confidence limits will also be determined.

There are many items that have not been addressed in this presentation of our validation methodology. These include the experimental plan with procedures, protocols, specimen definitions, test matrix, record keeping and reporting requirements. The test matrix includes repeatability and sensitivity tests and defines such things as test sequence and the specimens to use for each test. Furthermore, in each evaluation there are a host of issues that must not be ignored, such as image preprocessing, data formats, pixel resolution differences, file handling and archiving. NDI system calibration is also essential. Another important element of this evaluation is the independent characterization of the test specimens. In the above feasibility study, we used a high-frequency focused ultrasonic inspection for this purpose, but ultimately this will be inadequate. Better alternatives exist, such as topographic radioscopy. Each of these items is discussed in detail in our experimental plan.

CONCLUSION

A corrosion detection validation methodology has been demonstrated to be feasible. Using this methodology and an associated experimental plan, we are evaluating several NDE technologies and are selecting those that will continue on the Automated Corrosion Detection Program. We will then enter the integration phase of the program in which a prototype automated inspection system will be assembled. In parallel, we will continue development of our validation methodology including the investigation of different specimen concepts. Later in the program, we will demonstrate this automated system on the intact tail section that is currently residing in a facility in Oklahoma City. At some later point, a full implementation of an automated system such as the one to be demonstrated on this program should play a significant role in reducing costs and flow days, and ultimately improving the readiness of the fleet. This system and the validation methodologies should also be applicable to other aircraft inspection problems.

ACKNOWLEDGMENTS

This work was funded through USAF Contract F09603-95-D-0175, Delivery Order RZ05. Mr. Charles Buynak (AFRL/MLLP) is the contract monitor. Mr. Norm Schehl (UDRI) performed the eddy current inspection of the random profile test panel.

REFERENCES AND FOOTNOTES

1. "Aging of U.S. Air Force Aircraft – Final Report", National Material Advisory Board, 1997.
2. "U.S. Combat Air Power: Aging Refueling Aircraft Are Costly to Maintain and Operate", General Accounting Office, Chapter Report, 08/08/96, GAO/NSIAD-96-160.
3. Alcott, J., "An Investigation of Nondestructive Inspection Equipment: Detecting Hidden Corrosion on USAF Aircraft", Materials Evaluation, Vol. 52, No. 1, January 1994, pp. 64-73.
4. Roach, D., Harmon, K., Jones, C., Walkington, P., "Aircraft Inspection Validation Experiments and the Use of NDI Validation Samples", Materials Evaluation, Vol. 53, No. 7, July 1995, pp. 803-807.
5. MIL-STD 1823, Nondestructive Evaluation System Reliability Assessment (1994).

Pre-Corroded Fastener Hole Multiple Site Damage Testing
Second Joint NASA/FAA/DoD Conference on Aging Aircraft

Joe Luzar *
Associate Technical Fellow
Boeing Information, Space & Missile Systems
Wichita, Kansas
316-523-5408
joe.luzar@wichita.boeing.com

Patrick S. Johnson
Senior Specialist Engineer
Boeing Phantom Works
Seattle, Washington
253-773-9564
patrick.s.johnson@boeing.com

ABSTRACT

Multiple Site Damage testing was performed on uncorroded and pre-corroded open hole panels fabricated from new 2024-T3 clad aluminum (0.062"t) to assess corrosion damage effects on crack growth rates, crack growth lives, linkup loads, and residual strength. The pre-corroded test panels were artificially corroded with a modified ASTM B368 Accelerated Salt Fog process prior to testing. Testing was at laboratory ambient conditions. The panels were tested in two phases. First, constant amplitude cyclic loading was applied and fatigue crack growth data was recorded. Next, a saw cut central lead crack was introduced and the panel was loaded to failure. Metallurgical examination of a representative sampling of crack faces provided statistical corroded material loss measurements ranging from 24% to 37% corresponding to local stress increases of approximately 30% to 60%. Franc2d/l analysis was used extensively to calculate the required normalized stress intensity factors. Test results are compared to analysis and indicate that corrosion effects on crack growth, crack growth rates, crack linkup loads, and residual strength can be accounted for by simple net section stress increases proportional to material loss.

Six 2024-T3 clad MSD test panels fabricated from new sheet stock (Figure 1) were tested in this program. Two (2) panels were tested in the baseline uncorroded condition. The remaining four (4) test panels were fabricated oversize, artificially corroded, final machined, and then tested. The finished hole detail with double through thickness EDM notches is shown in Figure 2. The holes and EDM notches were fabricated after the artificial corrosion process. The panel thickness (0.062"), fastener hole diameter ($1/4$ "") and fastener pitch (1") were selected as being representative of typical aircraft lap joint geometry. The panel width (W), the number of open holes (n), and the lead crack size (2a) were selected to maximize the load differences between the Swift Linkup load and the minimum load calculated by either Net Section Yield or Linear Elastic Fracture Mechanics, assuming double through thickness 0.050" MSD cracks in the adjacent two holes to the lead crack. Initial sizing was done in collaboration with similar testing at Wichita State University performed by Joe Camenzind and Dr. Bert Smith. Sizing results are shown in Figure 4 and compared to other MSD crack size scenarios. The final adjacent hole MSD crack sizes (a_{msd}) was selected as 0.150" so that multi cracked hole crack growth data could be recorded prior to cutting the discrete lead crack and loading to failure.

Testing was accomplished in 2 phases at ambient laboratory temperature and humidity conditions with anti-buckling guides in place on both sides of the test panels above and below the fastener hole row. The

first phase was cyclic loading with no lead crack. The test panels were constant amplitude loaded at 1-3 Hz and at a load ratio of 0.1 with maximum stresses ranging from 7.4 to 11.2 ksi (Figure 9).. Crack growth data was recorded for 10 cracks per panel (Figure 3) until the average MSD crack size propagated to 0.150". At this point, the test was temporarily stopped (the specimen remained gripped but unloaded) and the center most 7 holes were saw cut to form a central lead crack. This resulted in a lead crack of approximately 6.55" with two adjacent holes on either side of the lead crack having double MSD cracks. The second test phase then loaded the test panels to static failure under load control at a load rate of 20 kips per minute. Intermediate lead/MSD crack linkup loads and failure loads were recorded (Figure 10).

Two of the four artificially corroded panels representing the extremes of visible corrosion damage were examined after testing to determine the actual corroded material loss. Each monitored crack face was examined with a Quantex Image Analysis system to measure the remaining areas from which thickness losses were calculated. Crack face regions were used to eliminate errors due to static overload necking during final failure loading. Representative crack face photographs are shown in Figure 5. Average material loss on one panel was 26.6% with the second panel at 32.5%. Individual crack face material losses ranged from 24% to 37%.

Crack growth rate and crack growth life analysis results are presented in Figures 8 and 9 and are based on normalized stress intensity factors (Figure 7) derived from a symmetric Franc2d/l half panel model (Figure 6a). The model was constrained in the vertical direction along the lower panel edge and uniformly loaded in the vertical direction along the upper panel edge. Double through thickness cracks were modeled at each of the holes and propagated with the Franc2d/l automatic sequence to derive the analysis stress intensity factor history. Unique hole SIF data was used with specific crack face material loss data to determine hole specific crack growth rate data (Figure 8). Average SIF data used with average crack face material loss data was used for crack growth life analysis (Figure 9). Both analyses accounted for corrosion damage effects by simple stress increases proportional to material losses. The current data confirms earlier test results and substantially expands the range of corrosion damage that can be categorized by simple stress increases proportional to material losses.

Analytical lead crack and adjacent MSD crack linkup loads were calculated as the minimum of; 1) simple net section yield load, 2) critical lead crack Linear Elastic Fracture Mechanic load, 3) critical adjacent MSD crack Linear Elastic Fracture Mechanic load, or 4) the Swift linkup load. Franc2d/l modeling was used for calculating stress intensity solutions for this studies specific crack configuration. A brief description of each failure criterion follows.

1) Simple Net Section Yield Load:

This analysis assumes panel failure when the net section stress reaches material yield. Net section area is calculated by subtracting the lead crack, any holes, and any MSD cracks from the original width and then multiplying this net width by the material thickness. The applicable formula is;

$$P_{crit(NSY)} = F_{ty}t[W - 2a_{lead} - (\text{Number of holes})(\text{Hole diameter}) - (\text{Number of MSD cracks})(\text{Average MSD surface crack length})]$$

2) Critical Lead Crack Linear Elastic Fracture Mechanics Load:

This analysis assumes panel failure when the lead crack fractures. Failure load is based on the material Plane Stress Fracture Toughness, panel width, panel thickness, lead crack

size and the Stress Intensity Beta solution. Normalized stress intensity factors were calculated using Franc2d/l. The applicable formula is;

$$P_{\text{crit(LEFM, lead crack)}} = \frac{K_a W t}{\beta_{\text{(Franc2D/L, lead crack)}} \sqrt{\pi a_{\text{(lead crack)}}}}$$

3) Critical MSD Crack Linear Elastic Fracture Mechanics Load:

This analysis assumes panel failure when the adjacent MSD cracks fracture. Failure load is based on the material Plane Stress Fracture Toughness, panel width, panel thickness, MSD crack size and Franc2d/l normalized stress intensity solutions. The applicable formula is;

$$P_{\text{crit(LEFM, MSD crack)}} = \frac{K_a W t}{\beta_{\text{(Franc2D/L, MSD crack)}} \sqrt{\pi a_{\text{(MSD crack)}}}}$$

4) Swift Linkup Load:

The Swift linkup load is that load that results in the plastic zones of the lead crack and the adjacent MSD crack intersecting. This criteria was first hypothesized by Tom Swift and appears to work reasonably well for materials having relatively large specific toughness (=Ka/Fty) such as 2xxx aluminum alloys. This analysis is based on remaining ligament length between the lead crack tip and the adjacent MSD crack tip, the flow stress (average of the yield and ultimate strengths), the lead crack size, the MSD crack size, and the associated Stress Intensity Beta values. The applicable formula is;

$$P_{\text{crit(Swift linkup)}} = \sqrt{\frac{\pi(\text{ligament})(S_{\text{flow}})^2}{\beta_{\text{(Franc2D/L, lead crack)}} \sqrt{\pi a_{\text{(lead crack)}}} + \beta_{\text{(Franc2D/L, MSD crack)}} \sqrt{\pi a_{\text{(MSD crack)}}}}$$

where the plastic zone radius is given by the contemporary definition;

$$R_{\text{py}} = \frac{(K / S_{\text{flow}})^2}{2\pi}$$

and is predicated on solution of the following ligament plastic zone relation;

$$\text{Ligament} = 2R_{\text{py(lead crack)}} + 2R_{\text{py(MSD crack)}}$$

Linkup loads for each of these criteria are tabulated in Figure 10 with corroded panel linkup loads being calculated as proportional to the remaining material thickness. The Swift Linkup criteria proved the best correlation with test data for all of the test panels with analysis loads within 5% of test values.

Calculated residual strength loads based on Net Section Yield, Critical Lead Crack Linear Elastic Fracture Mechanics, or non-linear Franc2d/l analysis are compared to actual test loads (Figure 10). The

best match (2% to 6%) resulted from the non-linear Franc2d/l analysis which accounted for slow stable tearing prior to final fracture. Without slow stable tearing affects, the error ranged from 12% to 17%.

The Franc2d/l slow tearing residual strength model (Figure 6b) used the following inputs:

Elements:

- Outside plane strain core region ----- eight-noded, quadratic, plane stress
- Within plane strain core region ----- eight-noded, quadratic, plane strain
- Elements along the crack path were 0.04 inches wide (horizontal dimension).
- The plane strain core region encompassed exactly two rows of elements (~0.095" total height).

Material Properties:

- Material type: 2024 clad aluminum plate, T-L orientation
- Young's Modulus, E = 10.6 Msi
- Poisson Ratio, n = 0.33
- Thickness outside the corroded region = 0.062 inch
- Thickness within the corroded region = 0.062 inch
- Uniaxial Yield Stress = 40 ksi
- Critical CTOA = 4.5 degrees
- Material non-linear plastic hardening curve data [Newman]:

Strain (in/in)	Stress (ksi)	Strain (in/in)	Stress (ksi)
0.00000	0.0	0.03800	55.1
0.00319	33.4	0.06200	59.5
0.00600	42.1	0.10000	62.4
0.01000	47.9	0.14000	63.1
0.01600	50.6	0.20000	63.8

Boundary Conditions:

- Left hand edge used symmetry boundary condition.
- Bottom edge used symmetry boundary condition.
- Top edge used applied displacement boundary condition of $U_y = 0.005$ in.

Initial Crack and Crack Path Definition:

Initial crack extended 0.03 inches beyond the edge of the outermost hole. The crack path was defined to lie along the horizontal line of symmetry. The crack was defined to open the nodes along 38 elements (each of length 0.04 in) giving it a total growth of 1.52 inches.

Crack Tip Opening Angle Evaluation:

The CTOA was defined to be evaluated two nodes behind the crack tip. The mid-side node was included in this count so that this distance was a constant 0.04 inches behind the crack tip throughout the entire analysis.

Analysis Control Parameters:

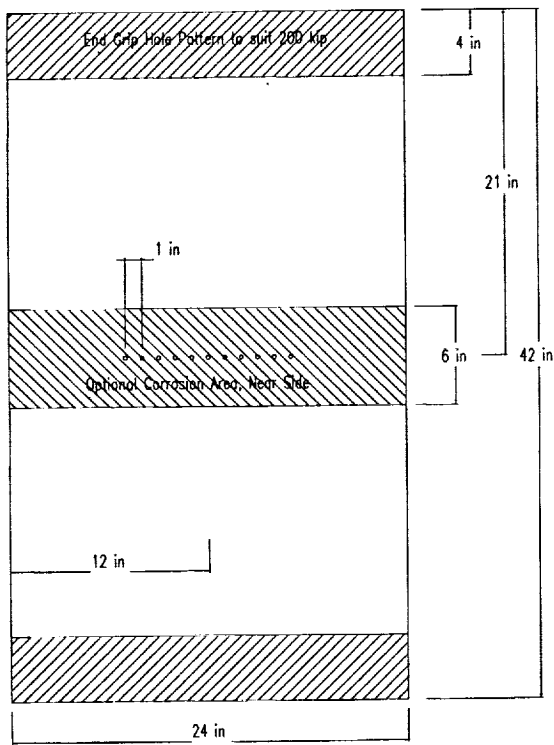
- Load Sub-Steps: 100
- Max Iterations: 200
- Appl Disp Factor: 50
- Final Step: 38
- Analysis Mode: Incremental/Unzipping
- Global Tolerance: 0.001
- Load Factors: 0
- Accelerate Iter: None
- Increment Method: Fixed

References

- 1) Swift, T., "Widespread Fatigue Damage Monitoring Issues and Concerns", presented at The 5th International Conference on Structural Airworthiness of New and Aging Aircraft, Hamburg, Germany, June 16-18, 1993.
- 2) Gruber, M. L., Wilkens, K. E., and Worden, R. E., "Investigation of Fuselage Structure Subject to Widespread Fatigue Damage", Boeing Commercial Airplane Group, presented at the FAA-NASA Symposium, Continued Airworthiness of Aircraft Structures, Atlanta, Georgia, August 1996.
- 3) Moukawsher, E. J., Grandt Jr., A. F., and Neussl, M. A., "Fatigue Life of Panels with Multiple Site Damage", Journal of Aircraft, V33, N5, pgs. 1003 - 1013.
- 4) Moukawsher, E. J., Heinemann, M. B., and Grandt Jr., A. F., "Residual Strength of Panels with Multiple Site Damage", Journal of Aircraft, V33, N5, pgs. 1014 - 1021.
- 5) Camenzind, J. W., "Effect of Multiple Site Damage (MSD) on Residual Strength, The Linkup Failure Mode", Aerospace Engineering Department, Wichita State University, 5 May 97.
- 6) Camenzind, J. W., "Effect of Multiple Site Damage (MSD) on Residual Strength, An Investigation of the Linkup Criterion of Flat Aluminum Panels", Aerospace Engineering Department, Wichita State University, 13 May 97.
- 7) Luzar Jr., J. J., "Corroded Material Crack Growth Rate Test Results", Boeing Defense and Space Group, presented at The First Joint DOD/FAA/NASA Conference on Aging Aircraft, Ogden, Utah, July 1997.
- 8) Swenson, D. and James, M., "FRANC2D/L: A Crack Propagation Simulator for Plane Layered Structures", User's Guide, Kansas State University.
- 9) Newman, J.C., Jr., Dawicke, D.S., Sutton, M.A., and Bigelow, C.A., "A Fracture Criterion for Widespread Cracking in thin-sheet Aluminum Alloys," International Committee on Aeronautical Fatigue, 17th Symposium, Stockholm Sweden, June 9-11, 1993, pp 13.

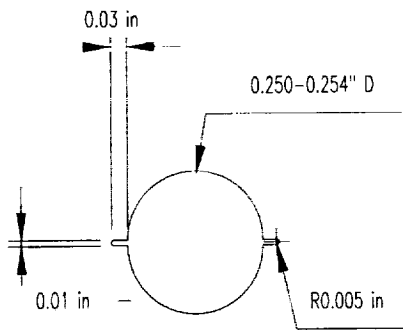
Nomenclature

2a	Surface lead crack length, inch
amsd	MSD surface crack length, inch
B2a	Lead Crack Nondimensional Stress Intensity Factor
Bmsd	MSD Crack Nondimensional Stress Intensity Factor
cavg	Average surface MSD crack length
CTOA	Crack Tip Opening Angle
d	Specimen hole diameter, inch
LEFM	Linear Elastic Fracture Mechanics
MSD	Multiple Site Damage
N	Cycle count
NSY	Net Section Yield
Pcrit (lefm, lead crack)	Critical Lead Crack Fracture Mechanics Load, kips
Pcrit (lefm, MSD crack)	Critical MSD Crack Fracture Mechanics Load, kips
Pcrit (net section yield)	Critical Net Section Yield Load, kips
Pcrit (Swift Linkup)	Critical Swift Linkup Load, kips
Scrit (lefm, lead crack)	Critical Lead Crack Fracture Mechanics Stress, ksi
Scrit (lefm, MSD crack)	Critical MSD Crack Fracture Mechanics Stress, ksi
Scrit (net section yield)	Critical Net Section Yield Stress, ksi
Scrit (Swift Linkup)	Critical Swift Linkup Stress, ksi
t	Specimen thickness, inch
W	Specimen width, inch



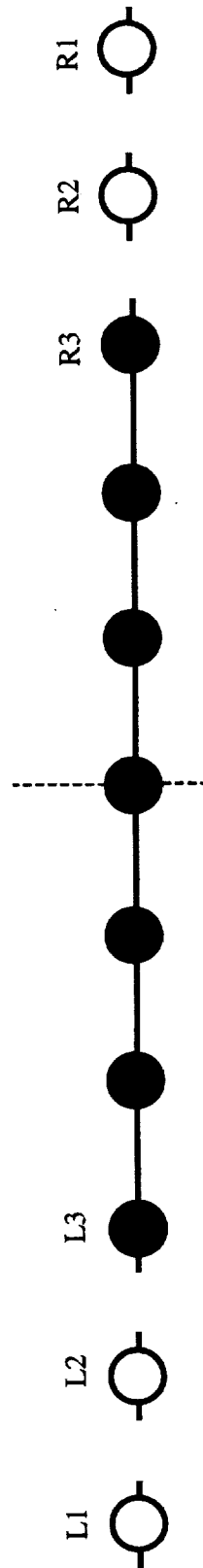
Final MSD Panel Configuration
(Longitudinal rolling direction is normal to applied load)

Figure 1



Finished EDM Hole Detail

Figure 2



(Note: The indicated Lead Crack was saw cut after crack growth testing was completed.)

Hole Numbering Scheme

Figure 3

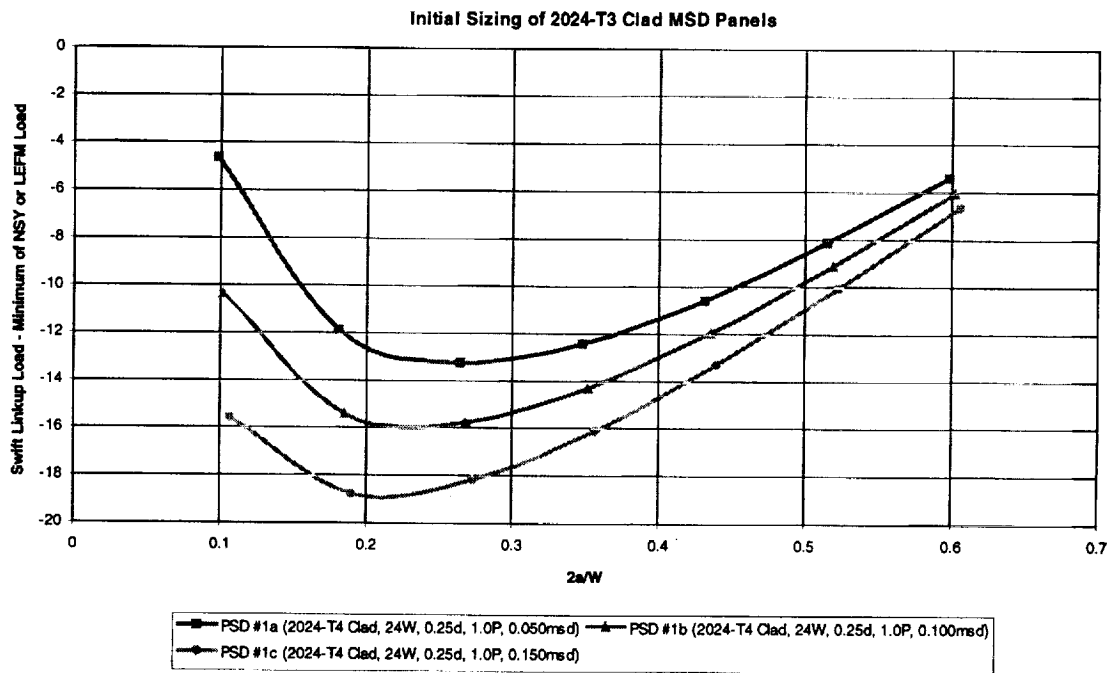
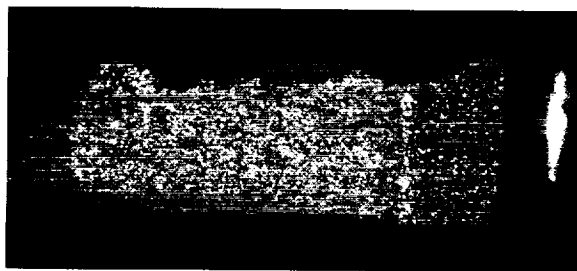
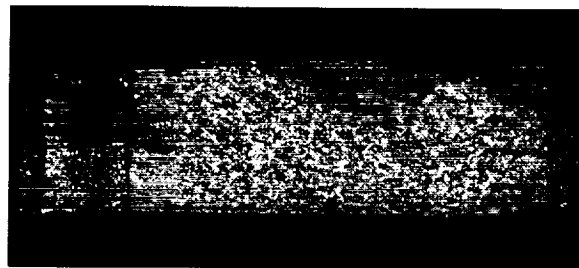


Figure 4: Test Panel Sizing Data

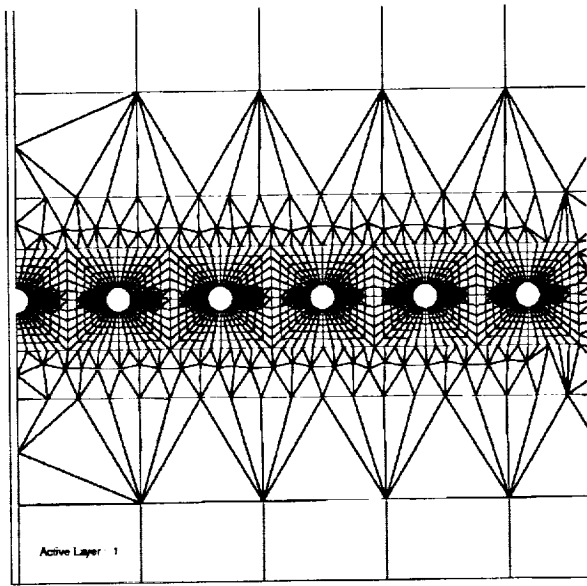


Hole L1 - Left Crack Face



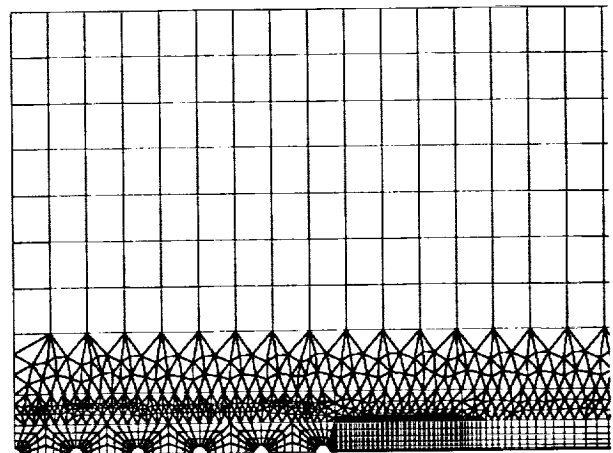
Hole L1 - Right Crack Face

Figure 5: Typical Corrosion Damage



Franc2d/L Fine Mesh Half Panel Model for Crack Growth Stress Intensity Solutions

Figure 6a



Franc2d/L Fine Mesh Quarter Panel Model for Residual Strength Slow Stable Tearing

Figure 6b

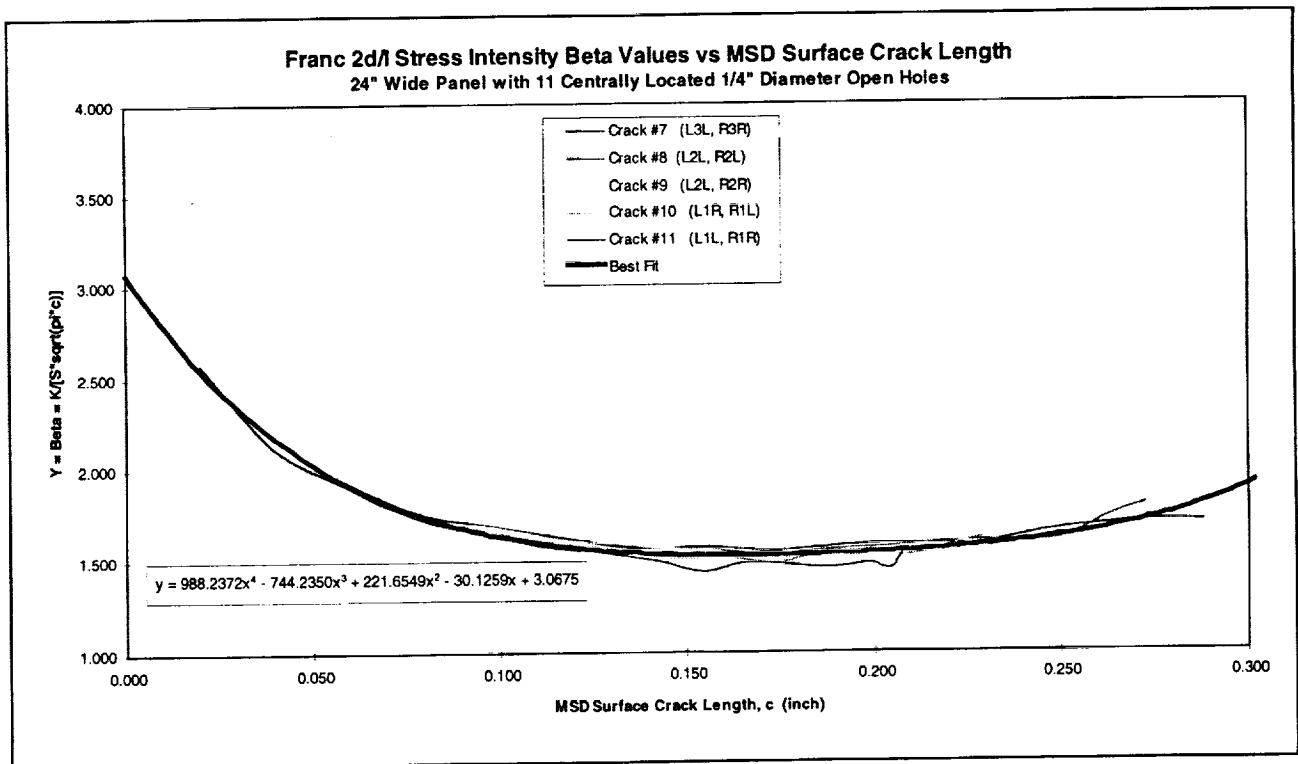


Figure 7: Normalized Stress Intensity Factors – Crack Growth Analysis

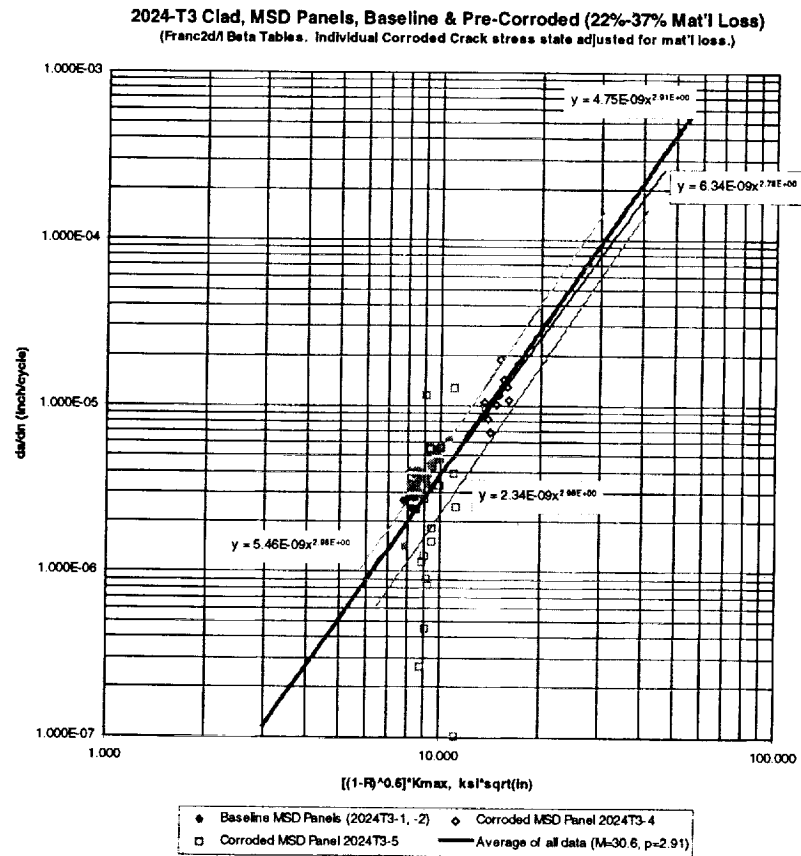


Figure 8: Baseline and Pre-Corroded Crack Growth Rates (from Test Data)

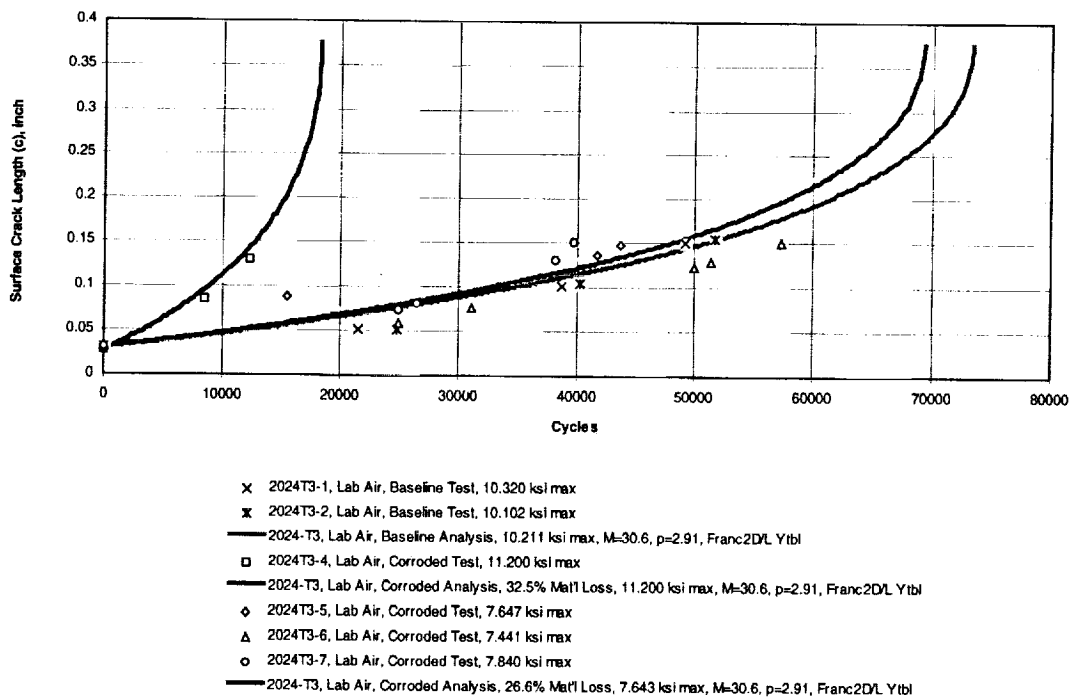


Figure 9: Crack Growth Test vs Analysis Comparison

	2024-T3 (Uncorroded Baseline)		2024-T3 (Corroded, 32.5% Mat'l Loss)		2024-T3 (Corroded, 26.6% Mat'l Loss)	
	Link Onset	Fracture	Link Onset	Fracture	Link Onset	Fracture
	Basic Geometry and Material Data					
Ka =	138	138	138	138	138	138
Ftu(B) =	60	60	60	60	60	60
Fty(B) =	40	40	40	40	40	40
W =	24	24	24	24	24	24
d =	0.25	0.25	0.25	0.25	0.25	0.25
t =	0.062	0.062	0.042	0.042	0.046	0.046
Adjacent Hole MSD Data						
Total # of adjacent holes =	4		4		4	
MSD Crack Length, amsd =	0.15		0.15		0.15	
LEFM Beta Value, Bmsd =	2.861		2.861		2.861	
Lead Crack Data						
Total Lead Crack Length, 2a =	6.548	10.548	6.548	10.548	6.548	10.548
LEFM Beta Value, B2a =	5.265	6.814	5.265	6.814	5.265	6.814
Calculated Critical Loads (kips)						
Pcrit (net section yield) =	37.825	33.361	25.623	22.599	28.064	24.752
Pcrit (lfm, lead crack) =	57.005	44.047	38.617	29.838	42.294	32.680
Pcrit (lfm, MSD crack) =	104.555	N/A	70.827	N/A	77.573	N/A
Pcrit (Swift linkup) =	21.585	N/A	14.622	N/A	16.015	N/A
Pcrit (Franc2d/l Residual Strength, 2a=12.870) =	N/A	30.330	N/A	20.546	N/A	22.503
Pcrit (net section yield, 2a=12.870) =	N/A	27.602	N/A	18.698	N/A	20.479
Calculated Critical Stresses (ksi)						
Scrit (net section yield) =	25.420	22.420	25.420	22.420	25.420	22.420
Scrit (lfm, lead crack) =	38.310	29.601	38.310	29.601	38.310	29.601
Scrit (lfm, MSD crack) =	70.265	N/A	70.265	N/A	70.265	N/A
Scrit (Swift linkup) =	14.506	N/A	14.506	N/A	14.506	N/A
Scrit (Franc2d/l Residual Strength, 2a=12.870) =	N/A	20.383	N/A	20.383	N/A	20.383
Scrit (net section yield, 2a=12.870) =	N/A	18.550	N/A	18.550	N/A	18.550
Recorded Test Loads (kips)						
2024T3-1	20.5	29.9				
2024T3-2	20.6	29.5				
2024T3-4				19.7		
2024T3-5					16.3	20.1
2024T3-6					16.3	22.2
2024T3-7					15.3	21.2
Analysis vs Test Results	5.0%	2.1%	-----	4.3%	0.3%	6.3%

**Linkup and Residual Strength Analysis vs Test Results
2024-T3 Clad MSD Panels with and w/o Corrosion**

Figure 10

ADVANCED CORROSION RESISTANT COATINGS FOR OUTER MOLD LINE APPLICATIONS

Joseph H. Osborne, Kay Y. Blohowiak
Boeing Phantom Works
Seattle, WA 98124
253/773-2569
253/773-5941
joseph.h.osborne@boeing.com

S. Ray Taylor, Chad Hunter
University of Virginia
Charlottesville, VA 22903

Gordon Bierwagon, Brendon Carlson
North Dakota State University
Fargo, ND 58105

Joshua Du, Mathew Damron
Chemat Technology, Inc.
Northridge, CA 91324

Dan Bernard
Deft Inc.
Irvine, CA 92714

Michael S. Donley
Air Force Research Laboratory
WPAFB, OH 45433-7750

ABSTRACT

A coating system comprised of a sol-gel-based conversion coating and chromated primer shows corrosion protection equivalent to the same primer over alodine. Nonchromated primers do not perform well when applied over nonchromated conversion coatings, including sealed anodize. Electrochemical testing (EIS, ENM) of the coating systems shows that waterborne coating systems to be more porous than high solids coatings. The EIS results rank the performance of coating systems in the same order as does salt spray. Response of the coating systems to a damage event is shown by EIS to depend on the presence of active inhibitors. Hybrid inorganic/organic hybrid polymers show promise as coating materials and offer opportunities for including nonchrome inhibitors in different ways to control their release. Traditional topcoat coatings offer little or no additional transport barrier. Advanced fluoropolymer topcoat formulations increase the barrier properties of the coating system and can help protect the substrates from corrosion.

1. INTRODUCTION

The Air Force has funded numerous programs to advance technology in the coating systems used on their weapon systems. The goal of the research efforts has been to increase performance and lower costs. In the past decade, environmental concerns have added an additional goal to reduce the use of volatile organic compounds and hazardous materials, such as hexavalent chromium, from the coating systems. The combination of these goals makes for a very challenging technical effort.

In general, these programs have been primarily focused on the traditional elements of coating systems looking for materials and processes that can be used as drop-in replacements. The Advanced Corrosion Resistant Aircraft Coating program (ACRAC) is designed to develop coatings using a systems approach. The goals of the program are to meet the Air Forces top priority requirements of corrosion protection, environmental compliance (OSHA and EPA), and durability of appearance. To achieve these goals, innovative nontraditional materials and processes are being investigated. The approach is to leverage existing sol-gel and nonchrome inhibitor technologies to provide adhesion and corrosion protection. The sol-gel approach is also being pursued to develop hybrid organic-inorganic polymer materials for coatings. These hybrids are tailorable to optimize both mechanical properties and incorporation and delivery schemes of corrosion inhibitors. Advanced formulation technologies for topcoats including polymer systems and fillers as well as powder and plasma application techniques are being investigated.

A key feature of the program is to integrate all elements together and evaluate the system for corrosion resistance and performance. Cyclic corrosion exposure and electrochemical techniques are being used to monitor the response of the coating systems to accelerated corrosion testing. The electrochemical methods also give information about the mechanisms of behavior of the coating systems in use.

The target vehicle for the ACRAC coating is the KC-135. There are over 500 vehicles in the Air Force inventory and they expect to be deployed for at least the next 20 years. A coating system that performs well and meets the corrosion and performance requirements of the KC-135 should be adaptable to the AMC fleet in general. Fielding a nonhazardous high performance coating system will significantly decrease the maintenance and operating costs of the transport fleet.

To accomplish the ACRAC program objectives, a team of experts in coatings formulation and application, sol-gel technology, and coating system evaluation has been assembled. The team members are shown in Figure 1 with their primary contributions to the program.

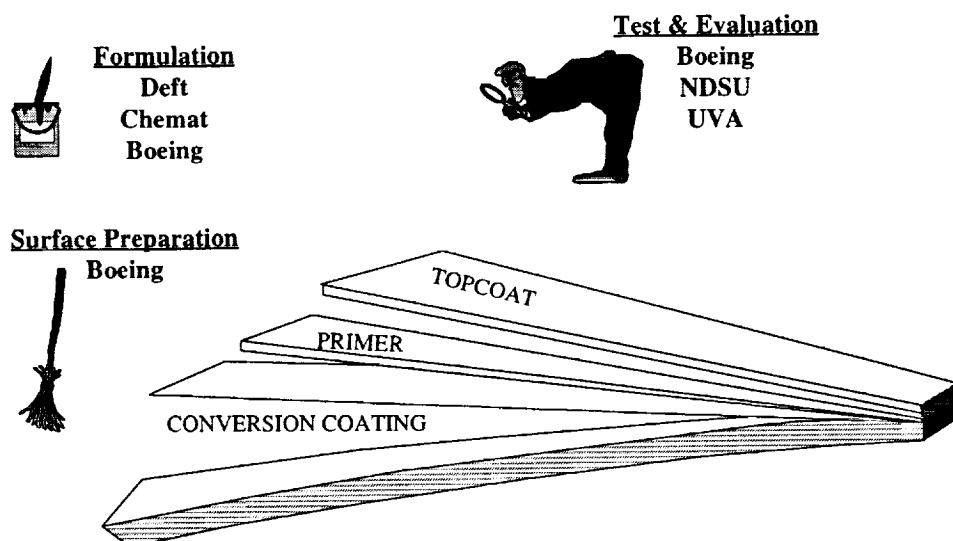


Figure 1 – ACRAC Team Members

2. PROGRESS IN SOL-GEL COATINGS

Two approaches to developing sol-gel materials for coating systems that we are focusing on are 1) sol-gel thin films and 2) sol-gel thick film hybrid coating systems. The requirements for both coatings are to promote adhesion between the metal substrate and the overlying organic primer or topcoat and to provide corrosion protection.

2.1. THIN FILM

The thin film approach uses metal oxide films with organic coupling agents. In concept this coating will replace the function of the traditional chromate conversion coating. The sol-gel system developed at Boeing consists of a dilute aqueous zirconium and functionalized silicon alkoxide solution that is spray applied to the cleaned metal surface. The film is dried in place with no thermal curing required.

The silicon component carries an organic group that is chosen so as to be chemically compatible with the organic polymer system in the primer or topcoat. A glycidoxyl group is typically used for epoxy primers. The coating system is thin (typically 50-200 nm) and forms a gradient coating as shown in Figure 2. A key feature is that chemical bonding is possible between the substrate and the primer and topcoat. This gives superior adhesion relative to chromate conversion coatings that rely on mechanical interlocking, hydrogen bonding, and dispersion forces for adhesion.

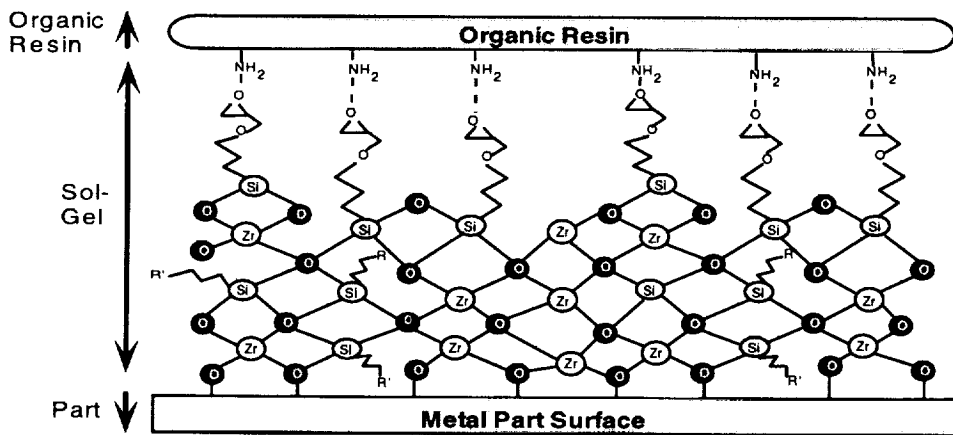


Figure 2 – Sol-Gel coating structure

Testing with mil-spec epoxy primers shows that the thin sol-gel coating, referred to as Boegel-EP, provides excellent adhesion of primer to aluminum substrates. Similar sol-gel chemistries are being tested in other programs for adhesion to steel and titanium with equally good adhesion results. Use on aluminum structure fastened with stainless steel or titanium fasteners should not pose adhesion difficulties. This will be tested as part of the transition phase of the program.

The Boegel sol-gel coating by itself does not have significant corrosion resistance. The primed system using Boegel and chromated primers shows equivalent performance to chromated primers applied to alodined surfaces. Nonchrome primers applied to Boegel do not perform well. This is a common result for nonchrome primers applied over nonchrome surface preparations.

Table 1 shows the primers and conversion coatings used in a test of nonchrome primers and conversion coatings. All of the candidate primers are being tested to the requirements of MIL-P-85582 Class N, the specification for water reducible solvent resistant epoxy primers. The Spraylat and Dexter products are being flight tested on Navy airplanes. The conversion coatings include chromated Alodine 1200S (MIL-C-5541 Type 1A) and dilute chromate sealed Boric Sulfuric Anodize (BSAA, MIL-A-8625 Class 1C) as control conversion coatings. Boegel-EPII, unsealed BSAA, and bare

deoxidized panels are the nonchromate candidates. All of the primers pass wet and dry adhesion tests on all of the conversion coatings.

Table 1 – Primers and conversion coatings tested

Nonchromate Primers	Conversion coatings
Deft 44-W-16	Alodine 1200S
Deft 44-W-18	Boegel-EP
Courtaulds	Sealed Boric Sulfuric Acid Anodize
Dexter/Crown Metro 10PW22-2	Unsealed Boric Sulfuric Acid Anodize
Spraylat EWDY048A/B	Deoxidized only
Courtaulds MIL-P-85582 chromated	

The results of corrosion testing of the Table 1 primers and conversion coatings are summarized in Table 2. Figure 3 shows panels that were exposed to salt spray. The electrochemical data for these panels will be discussed later.

Table 2 – Primer and conversion coating results matrix

Conversion Coating	NSS Results – 2500 hour exposure
Alodine 1200S	All pass
Boegel-EP	All nonchrome primers fail MIL-P-85582 control passes
Boric Sulfuric Acid Anodize Dilute chromate sealed and unsealed	One candidate marginal pass, all others fail MIL-P-85582 control passes
Deoxidized (Boeclene acid deox)	All nonchrome primers fail MIL-P-85582 control passes

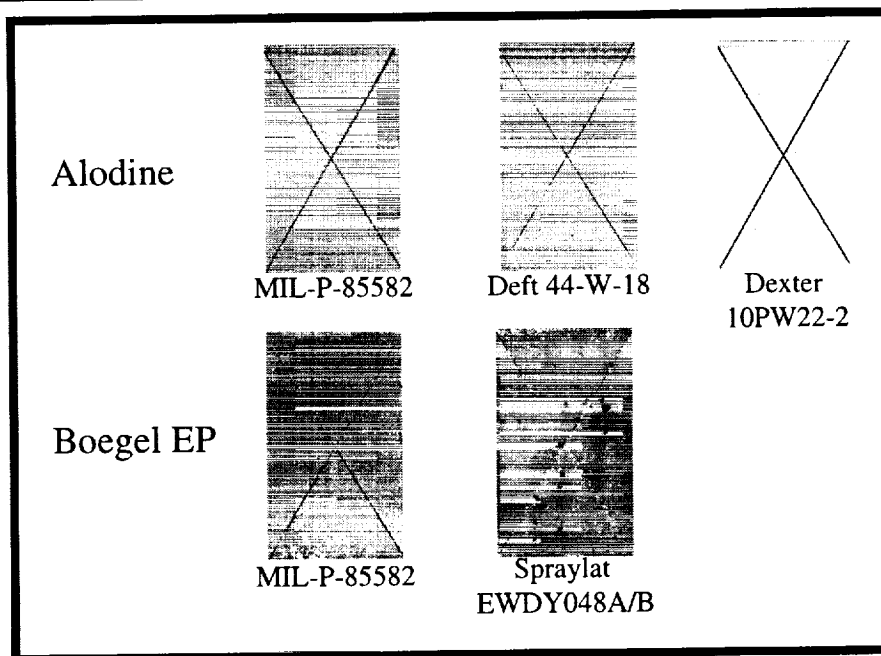


Figure 3 – Salt spray exposure panels for primers applied to alodine and Boegel-EP. Al2024 substrates.

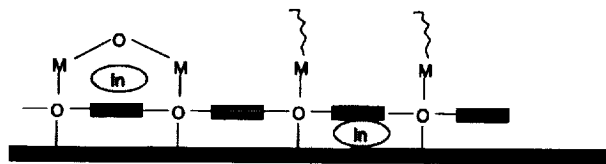
The nonchrome primers tested were “first generation” primers aimed at meeting MIL-P-85582 Class N requirements. Second generation primers are being developed and are showing better performing.

The significant conclusion from this data is that some chromate in the system is essential. The failures of the primers applied to sealed MIL-A-8625 Type 1C coatings (Boric sulfuric anodize) shows that nonchromate inhibitor technologies are still not sufficiently developed for acceptable performance.

Incorporation of state-of-the-art nonchrome inhibitors into the thin sol-gel matrix has had limited success to date. Various cerates, vanadates, and borates have been mixed into the Boegel coating solution. Limited solubility of some inhibitors and blistering of primers applied to sol-gel coatings using more soluble materials are the typical problems. Stand-alone salt spray performance is improved by a day or two, but not more than three days. Initial analysis indicates that these inhibitors interact with the sol-gel chemistry to create "weak" spots in the coating.

Inhibitors can be added to the Boegel chemistry, however. Adding chromates into the coating solution produced a sol-gel coating that passed 7 days salt fog exposure with no corrosion pits. Paint adhesion is still excellent. Primed panels are in long term testing. This implies that the sol-gel chemistry must be adapted to best deliver the nonchrome inhibitors to active sites on the aluminum surface. Figure 4 shows several schemes for incorporating inhibitors into the sol-gel matrix. Chromates and the inhibitors studied to date rely primarily on the entanglement/trapping mechanism. Chemically incorporating inhibitors into the sol-gel matrix will take advantage of the hybrid capabilities of the sol-gel coatings.

I. Entanglement / Trapping



II. Chemical Incorporation into Polymer

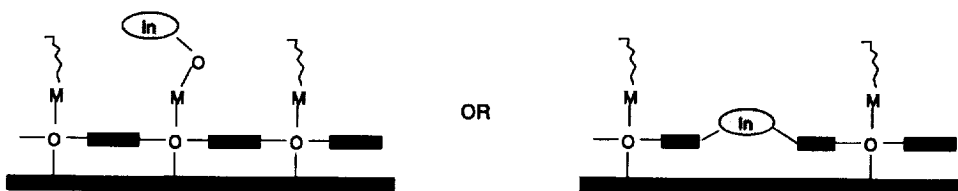


Figure 5 – Incorporation of inhibitors into sol-gel matrix.

2.2. THICK FILM HYBRID COATING SYSTEMS

The goals for the hybrid coating systems are to replace the functionality of both the conversion coating and the primer. As a consequence the hybrid coating must provide excellent adhesion to both substrate and topcoat, provide long term corrosion protection, and be resistant to the fluids used in aircraft. This coating approach is a possible technological basis for a "permanent" coating system.

Several approaches have been investigated for developing hybrid coating systems. The most promising is one composed of an epoxy silane based alumina/silica sol solution containing Shell EPI-REZ® 5522-WY-55 or similar epoxy resins. This chemistry produces room temperature curable systems that can be pigmented with titanium dioxide or corrosion inhibitors. This coating shows good adhesion properties.

Incorporation of inhibitors into the hybrid coating systems has shown the same performance problems as seen with the thin film sol-gel coatings. Limited corrosion protection and blistering have been issues. Inhibitor materials encapsulated into organic shells or ceramic particles are being developed to control the solubility and mode of incorporation into the sol-gel matrix.

3. PROGRESS IN TOPCOATS

Concepts for advanced topcoats are in the initial stages of study. Previous work has shown that formulation changes can have a dramatic effect on the cleanability of flat coatings. These are being pursued as well as the use of nontraditional flattening agents, advanced fluorinated polymers, powder systems, and plasma deposited coatings.

One aspect of flat coatings is the balance between the critical pigment volume concentration (CPVC) and permeability of the coating. For corrosion resistance and cleanability a lower PVC is desired. Achieving low gloss requires a high PVC. Technologies to lower gloss without exceeding the CPVC are being investigated.

Figure 6 shows the EIS data for primer and primer plus traditional MIL-C-85285 flat topcoat coatings. The topcoat is electronically "transparent" meaning that it contributes little to the overall barrier properties of the coating system. Fluoropolymer coating systems have approximately the same PVC but should be better electrochemical barriers due to their hydrophobic nature. Increased barrier properties should provide superior corrosion protection.

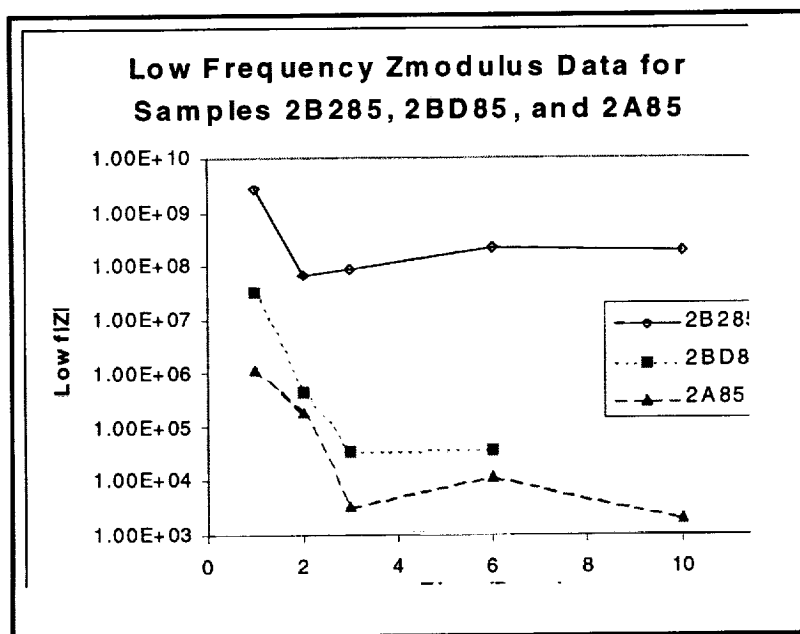


Figure 6 – EIS data for primer and primer with topcoat coating systems.

4. PROGRESS IN EVALUATION TECHNIQUES

Understanding the transport and barrier properties of a coating is key information to guide development of coating systems. Electrochemical techniques can give a relative ranking of coating performance in a relatively short time (days to weeks) as opposed to months for traditional salt fog exposure testing. These techniques also give information regarding the performance of the coatings in terms of their transport properties and corrosion resistance.

4.1. ELECTROCHEMICAL EVALUATION OF DAMAGE TOLERANCE

A test method unique to the ACRC program is the determination of electrochemical response of a coating system to a damage event. In this test, electrochemical impedance spectroscopy (EIS) is used to characterize the coating for several days. A defect is then created in the coating and the response of the system is monitored for another several days. Figure 5 shows schematically the method used to make the defect.

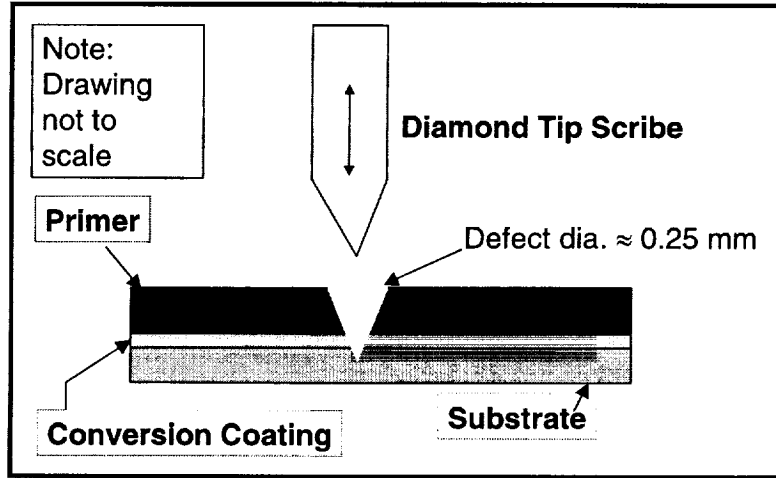
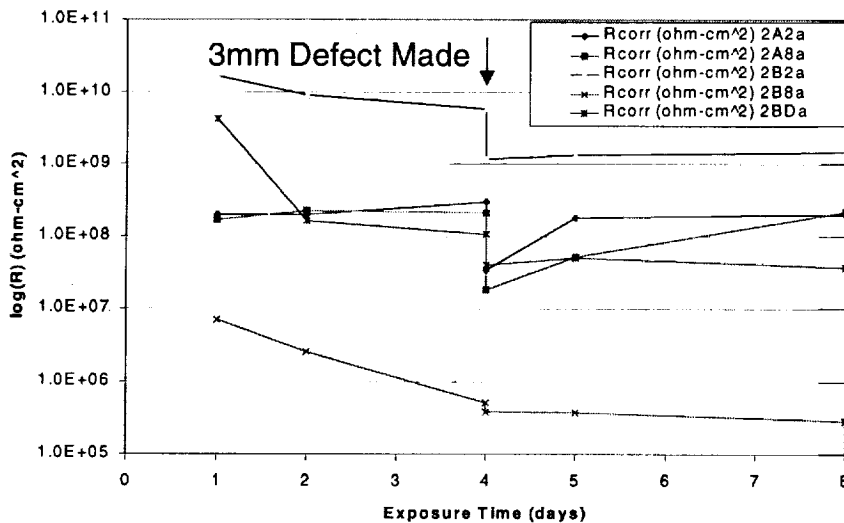


Figure 5 – Schematic for defect production

Figure 6 shows test results for several coating systems. The high solids MIL-P-23377 primer consistently has the highest R_{corr} value. Water based primer systems are more porous as indicated by the lower R_{corr} . All systems show response to defect production and some recovery after, indicating a “healing” of the defect area. It is this response of the coating system to damage that is desired to protect the underlying metal structure from corrosion until such time as the damage is repaired. This 8-day test provides information equivalent to that gained in the traditional salt spray testing that takes up to three months to complete.



Boegel/23377
 Alodine/44-W-18
 Alodine/Dexter
 Boegel/Dexter
 Boegel/44-W-18

Figure 6 – R_{corr} vs. exposure time with defect. Primers and conversion coatings are as described in Table 1.

4.2. ELECTROCHEMICAL NOISE METHOD (ENM)

Electrochemical Noise measures small fluctuations of current in a circuit caused by “instantaneous” corrosion events occurring on a surface. The noise data is used to calculate an average resistance value for the system that is proportional to rate of corrosion events occurring at the surface. Figure 7 shows ENM data for nonchrome primers applied to alodine and Boegel on Al2024 and Al7075 substrates. The results are consistent with those obtained from salt spray testing shown above in Table 1 and Figure 3. ENM differentiates between the coating systems in as little as 7 days. Salt spray testing takes at least 4 weeks.

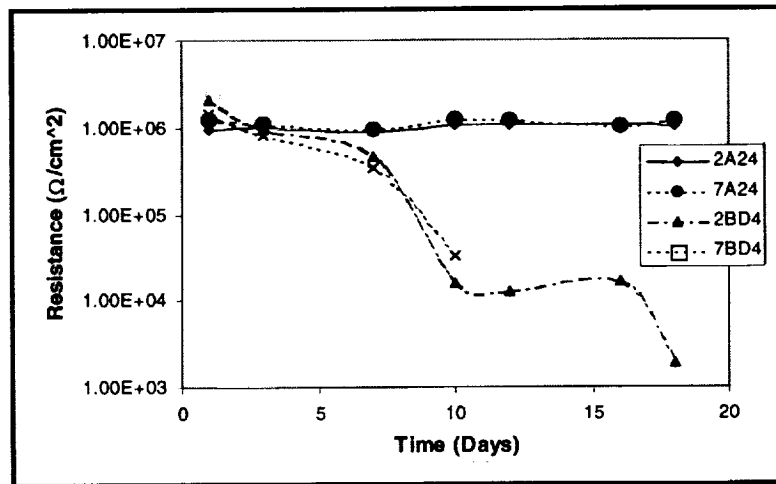


Figure 7 – ENM data for nonchrome Dexter primer over Alodine and Boegel. The “2” and “7” indicate Al2024 or Al7075 substrates. The “A” and “B” indicate Alodine or Boegel.

5. TRANSITION PLAN

Technologies developed in the ACRAC program will be transitioned to fleet vehicles through the CTIO at WPAFB. The primary target vehicle for coating systems developed in the ACRAC program is the KC-135. There are a large number of these vehicles in the Air Force inventory and they are expected to be deployed for at least the next 20 years. The cost to paint one KC-135 at the depot after PDM is estimated to be \$250K. Figure 8 shows the current processing steps and those proposed using advanced coating processes. The Phase I leverages as much existing technology as possible for drop-in replacement of the current process steps. Phase II implements advanced technologies. Demonstrations of technical feasibility conducted with the Coatings Technology Integration Office (CTIO) are planned for the first quarter of 2000. Actual application of the coating system to a KC-135 will occur if the process has been realistically demonstrated in a production (i.e. no laboratory) environment.

Process step	Current	Phase I	Phase II
alkaline clean			
Clean "brighten"	MIL-C-38335	solid state cleaning	solid state cleaning
Conversion coating	Alodine 1200S	sol-gel conversion coat	Hybrid coating
Primer	MIL-P-23377	MIL-P-85582 Class N	
Topcoat	TT-P-2756	MIL-C-85285	Advanced topcoat

Figure 8 – Finishing sequence for the KC-135

6. CONCLUSION

The ACRAC program is taking a systems approach to developing corrosion resistant durable coatings for military aircraft. Significant progress has been made in developing nonchromated conversion coatings that provide superior adhesion of organic coatings to metal structure. Effective materials for corrosion protection and methods of delivering them to active sites remains a need area. Hybrid inorganic and organic polymer systems are being developed that show promise for use as durable coating materials for military aircraft.

ACKNOWLEDGMENTS

This effort was funded by the Defense Advanced Research Projects Agency administer through the Air Force Research Laboratory, Wright Patterson Air Force Base.

EFFECT OF AIRCRAFT WASHING ON THE LIFE OF CORROSION PREVENTION COMPOUNDS

Krishnakumar Shankar
School of Aerospace and Mechanical Engineering
University College, Australian Defence Force Academy
The University of New South Wales, Canberra, ACT 2600 Australia
Ph: 61-2-6268 8584, Fax: 61-2-6268 8276
E-Mail: k-shankar@adfa.edu.au

Natasha Tindall
HS 816 Squadron, Royal Australian Navy
Naval Air Station, Nowra, NSW 2600 Australia

Bruce Hinton and Maria Salagaras
Defence Science and Technology Organisation
Aeronautical and Maritime Research Laboratory
POBox 4331, Melbourne, Victoria 3001 Australia

ABSTRACT

Corrosion Prevention Compounds (CPCs) are now commonly employed to combat corrosion in aircraft structures, particularly for controlling crevice corrosion in airframe skin splice joints. On the other hand, for fixed and rotary wing aircraft operating in severe corrosive conditions as in the marine environment, frequent washing with fresh water is also employed to remove salt deposits and inhibit the onset of corrosion. Unfortunately, while both these remedies are independently effective, it has been found that aircraft washing tends to reduce the effectiveness of the corrosion prevention compounds. This paper describes the results of an experimental program aimed at determining the effect of frequent washing on the effective life of CPCs in crevice joints. The tests were conducted on crevice washer specimens treated with three different kinds of commercially available Water Displacing Corrosion Preventive (WDCP) compounds and exposed to continuous salt spray testing as per ASTM Standard B-117. After thirty days of exposure, specimens treated with CPCs but not subjected to washing had developed less than twenty percent of corrosion compared to unwashed specimens without any CPCs, whereas corrosion in untreated specimens subjected to frequent washing was about half of that in untreated unwashed specimens. After thirty days of exposure to salt fog and frequent washing, the specimens treated with CPCs had developed the same amount of corrosion as the untreated specimens. A comparison of the performance of the different CPCs studied showed while some of them may remain effective up to a period of about two weeks, in most cases frequent washing causes corrosion to develop over a significant part of the crevice in a matter of six to seven days, highlighting the necessity of reapplication of the CPCs every time the aircraft is washed.

1. INTRODUCTION

In today's world of increasing economic pressures, the prevention and control of corrosion in airframe structures is a matter of high priority to both military and civilian aircraft operators, who have been investing large amounts of money and effort to stretch the effective operational life of equipment in service to the maximum extent possible. While corrosion may be regarded as a natural aging process that may be considered acceptable in aircraft that have exceeded their expected operational life, the fact is that even airframes in the prime of their life succumb to attacks of corrosion, with either debilitating or expensive consequences, especially when they operate in highly aggressive, corrosion inducing, environments. Most aircraft operators have embarked upon active Corrosion Prevention and Control programs, with a view to delaying the onset of corrosion as far as possible, monitoring airframe structures closely for detecting corrosion as soon as it sets in, and taking active measures either for elimination or for maximum

amelioration, where eradication is not possible. The traditional method of preventing corrosion is the exclusion of aqueous environment from the metal surface using paint coatings. While this is still the primary method employed, two other control mechanisms that have come into use in the last two decades for reinforcing or supplementing the protection offered by paint coatings, are application of Water Displacing Corrosion Preventive compounds and fresh water washing.

1.1 WATER DISPLACING CORROSION PREVENTIVE COMPOUNDS

A common method adopted for combating corrosion in both civilian and military aircraft is the application of Water Displacing Corrosion Preventive Compounds (WDCPs) which have been found to be highly effective in preventing the onset of corrosion, as well as inhibiting its further growth once an attack sets in. Typical commercial WDCP products are Boeshield T9™, WD40™, CRC 3-36™, LPS 1™, LPS 3™, and ARDROX 3961™. In addition to possessing good corrosion inhibiting properties, they also have excellent penetrating and water displacing properties. In general most WDCPs contain an oil, grease or wax based film former, a volatile, low -surface tension carrier solvent, a non-volatile hydrophobic additive, and various corrosion inhibiting compounds¹. The WDCPs are particularly suited for use in crevice joints, such as airframe skin lap and butt splices. Upon application the carrier solvent penetrates deep into the crevices, and evaporates leaving a residual film containing the hydrophobic additives and the corrosion inhibitors. Most WDCPs are formulated to meet the requirements set by various specifications such as the US Military Specification MIL-C-81309, UK Joint Services Designation such as PX-24 or Boeing Materials Specifications such as BMS 3-23. WDCPs are relatively inexpensive and easily applied, either from aerosol cans or by brushing the liquid on to the surface. They are therefore widely used throughout the industry, without perhaps adequate laboratory or field research concerning their effectiveness, life expectancies or possible side effects such as influence on fatigue life of the components^{2,3}.

1.2 AIRCRAFT WASHING

A practice commonly adopted under Corrosion Prevention and Control schemes for aircraft operating in aggressive conditions such as marine environment or concentrations of industrial pollutants, is to subject them to frequent washing to remove the deposits of salt and corrosive chemicals from the metallic surfaces. This has been found to be very effective in delaying the attack of corrosion. The Royal Australian Navy has a number of Defence Instructions such as AP 119A-0202-1, NAP 7210.024-2-000 and NAP 7210.024-6-2-2 for aircraft washing procedures^{4,6}. Instructions detail the frequency of washing and the use of cleaning agents. Cleaning procedures vary according to the base location of the aircraft - ship or shore, the operating conditions, and the level of grime which has built up on the aircraft since the previous wash. Aircraft involved in maritime operations are required to undergo a fresh water wash after any period of low flying or exposure to foul weather. For ship borne aircraft an external aircraft foam cleaning is carried out every seven days, with daily fresh water rinsing. For land-based aircraft foam cleaning is carried out every 14 days, and fresh water rinsing is carried out as required⁴. The detergent to be employed as well as the ratio of the detergent to fresh water mixture according to whether it is a normal wash, light duty or heavy duty wash, are also specified^{5,6}. It is to be noted the Naval husbandry procedures require that Corrosion Prevention Compounds be reapplied on the relevant structural components every time the aircraft is subjected to a wash. While this procedure may be viewed as overly conservative, it is a safe approach, since there has been no previous studies on the removal of WDCPs or on the reduction in their effectiveness due to fresh water or detergent cleaning of aircraft.

1.3 OBJECTIVE OF EXPERIMENTAL INVESTIGATION

The present experimental work was undertaken with the objective of investigating the effect of frequent washing on the effectiveness of Water Displacing Corrosion Preventive compounds in protecting airframe structures from crevice corrosion. The aim was to determine the effective life of the WDCPs within the crevices between the joints, when they are being frequently subjected to fresh water cleaning, in comparison to their effective life when no washing is undertaken. It is hoped that the study will facilitate a more scientific approach to determining the frequency of

aircraft washing and/or reapplication of the corrosion prevention compounds after washing, with the result of either saving in husbandry costs and effective utilisation of material and man-hours in corrosion maintenance of the Navy's aircraft.

2. EXPERIMENT

The experimental program consisted of accelerated corrosion testing of crevice washer specimens treated with three different types of commercial WDCPs commonly employed in the aircraft industry, as well as a set of untreated specimens, in a salt spray environment. The control group of specimens were kept unwashed, while the test specimens were subjected to frequent washing using a detergent mix in accordance with specifications of the Australian Navy's aircraft husbandry program.

2.1 CREVICE WASHER SPECIMENS

The crevice specimens employed in the experiment were constructed using aluminium coupons attached to crevice washers as per ASTM G78 Standard⁷. The coupons were made of square 4mm thick square pieces of aluminium alloy 2024-T3 sheet, 25mmx25mm in size, with a 6mm hole drilled through the centre. Both surfaces of the aluminium sheets were given a surface finish of 120 grind, and were unpainted. The teflon washers had an inner diameter of 6mm, outer diameter 15mm and contained 12 crevices (see Figure 1). The crevice washers were attached to either side of the aluminium piece, secured by a nylon fastener (see Figure 2). Thus each specimen provided 24 crevices and 24 exposed areas (between the crevices) which could be monitored during the trial. The nylon fasteners were tightened using a torque slightly more than finger tight, care being taken to reproduce the same torque for all the 128 specimens prepared. After the application of CPCs, the specimens were assembled in specially prepared plastic racks in the salt spray corrosion chamber.

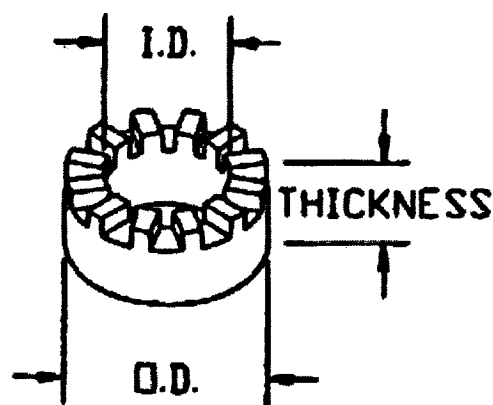


Figure 1. Schematic of Crevice Washer

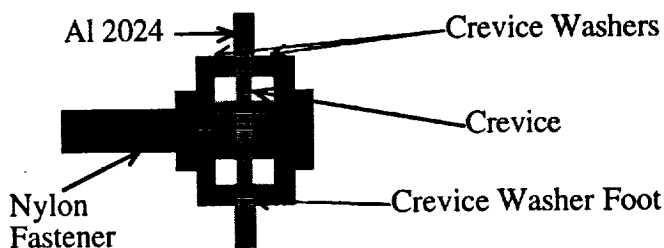


Figure 2. Assembly of Crevice Washer Specimen

2.2 TREATMENT WITH WDCPS

The 128 specimens prepared were divided into two groups of 64, the test group A, which were subjected to frequent washing, and the control group B, which were not washed at all. Both groups were further divided into 8 subgroups, each of which was exposed to the salt fog for a predetermined interval of time (see Table 1). Each subgroup contained 4 pairs of specimens, one pair of which was left untreated, while the other three pairs were treated with a different type of WDCP, selected from commercial products commonly employed in the aircraft industry. For proprietary reasons, the trade names of the WDCPs are being withheld and they are designated as

CPC1, CPC2 and CPC3 for the purposes of reporting. CPC1 is an oily type of Water Displacing Corrosion Preventive, which produce a thin film of about 3 to 4 microns after drying. CPC2 is a greaseless WDCP, whose film thickness is about 25 microns upon drying. CPC3 is of the soft waxy type, with a dry film thickness of approximately 50 microns. The specimens were treated with WDCPs in accordance with the instructions of the manufacturers and allowed to dry for 24 hours before being placed in the corrosion chamber. The test matrix presented in Table 1 below shows details of the different test conditions that were employed in the experiment.

TABLE 1. TEST MATRIX

Group No.	Washed/Unwashed	No CPC	CPC1	CPC2	CPC3	Exposure time (hrs)
1A	Washed	2	2	2	2	94
1B	Unwashed	2	2	2	2	92
2A	Washed	2	2	2	2	162
2B	Unwashed	2	2	2	2	162
3A	Washed	2	2	2	2	254
3B	Unwashed	2	2	2	2	253
4A	Washed	2	2	2	2	325
4B	Unwashed	2	2	2	2	322
5A	Washed	2	2	2	2	418
5B	Unwashed	2	2	2	2	418
6A	Washed	2	2	2	2	485
6B	Unwashed	2	2	2	2	485
7A	Washed	2	2	2	2	579
7B	Unwashed	2	2	2	2	581
8A	Washed	2	2	2	2	650
8B	Unwashed	2	2	2	2	652

2.3 WASHING PROCEDURE

Half the total number of specimens were treated as the control group and were not subjected to any washing, while the other 64 specimens were subjected to frequent washing. The specimens in the latter group were washed 4 times a week. To accommodate practical constraints the washing was performed at irregular intervals, ie. on Mondays, Tuesdays, Thursdays and Fridays. The specimens were washed employing a sponge in accordance with the Navy guidelines, using a mixture of one part of detergent solution to 2 parts of fresh water. The foam was rinsed using running tap water. The full details of the washing procedure and the experimental investigation is provided elsewhere⁹.

2.4 ACCELERATED CORROSION TESTING

The accelerated corrosion testing was performed using a Singleton Salt Fog Corrosion Chamber in accordance with the ASTM Standard Practice B117 for Operating Salt Spray Testing Apparatus⁸. The specimens were subjected to continuous salt fog exposure, except for interruptions of about an hour for removal of specimens for washing and examination every other day. The accelerated testing was conducted for a total of about four weeks. At intervals of about 3 to 4 days, sixteen specimens - a pair of unwashed and a pair of washed specimens from each of the four sets treated

with a different WDCP condition - were removed from the salt spray chamber, cleaned, disassembled and inspected for corrosion. The actual number of hours of exposure to salt spray environment for each group of specimens is listed in Table 1.

2.5 CORROSION MONITORING

When the specimens were removed from the salt spray chamber at the end of their designated exposure times, they were disassembled, washed under running tap water and photographed, before being cleaned with a 70% nitric acid solution. They were then examined under an optical microscope to gauge the extent of pitting corrosion developed. The main measure employed to quantify the extent of corrosion was to visually identify its spread over the surface of the crevices, as well as the exposed surface between the crevices on either side of the Aluminum test pieces. This is expressed as a percentage of the total crevice area or of the exposed surface area available for corrosion. The extent of surface area covered by corrosion, both within the crevices and in the exposed areas, was considered to be the most acceptable form of quantifying corrosion in this trial, although it is to be admitted that one drawback of this measure of corrosion is that it does not allow for the consideration of the severity of corrosion.

Two other methods of quantifying the extent of corrosion were also attempted: measurement of weight loss and the measurement of pit depth. In the former case, it was found that a large fraction of both washed and unwashed specimens actually gained weight by the end of the accelerated corrosion testing period, most likely due to CPC and corrosion product build-up remaining in the corrosion pits even after cleaning. As for the measurement of pit depth, the large number of pits on the specimens made it impossible to measure the depth of every pit in order to obtain the average pit depth as required by ASTM Standard 46-94. Therefore, an attempt was made to record what appeared to be the largest pit on the specimen, but a tabulation of the results did not show any correlation between the recorded maximum pit depth and the time of exposure to salt spray. This could be attributed to the incomplete removal of the accumulated corrosion products from within the pits, as well as misapprehension as to the deepest pit on the specimen. In any case the measurement of pit depth alone would not account for the cross-sectional shape or number of the pits. Hence the study has been restricted to measurement of the extent of corrosion in terms of the area of surface coverage both in the crevices as well as the exposed surfaces between the crevices.

3. EXPERIMENTAL RESULTS

The experimental results are presented in Figures 3 to 8. In each case the abscissa is the exposure period in days while the ordinate indicates the percentage of surface area over which corrosion has developed. The extent of corrosion measured in the 24 crevices of each specimen (12 on either side of the aluminium sheet) is labelled as crevice corrosion, whereas the corrosion measured in the exposed areas in between the crevices under the two washers is labelled as surface corrosion.

3.1 EFFECT OF FRESH WATER WASHING ON SPECIMENS WITHOUT CPC

For specimens subjected to salt spray testing without any treatment with CPCs, the percentage area of surface corrosion between crevices and the percentage area of crevice corrosion are plotted against the period of exposure in Figures 3(a) and 3(b) respectively. The broken lines in the figures indicate the corrosion monitored on unwashed specimens, while the solid lines indicate corrosion measured on specimens that were subjected to regular fresh water washing. The beneficial effect of frequent washing, with no other protection against corrosion employed, is evident from the figures. The untreated unwashed specimens developed almost hundred percent corrosion on the exposed surfaces within twenty days while even after exposure for about thirty days the surface corrosion in untreated specimens washed regularly is less than 50%. The plots in Figure 3(b) show that the washed specimens develop corrosion over 70% of the areas within the crevices within 10 to 20 days, indicating that washing is not as effective in preventing crevice corrosion in untreated specimens as it is in controlling surface corrosion. This could be attributed to the fact that the washing procedure removes salt build-up from the exposed surface but leaves the aluminium's natural corrosion inhibiting oxide coating intact. Removing the salt coating

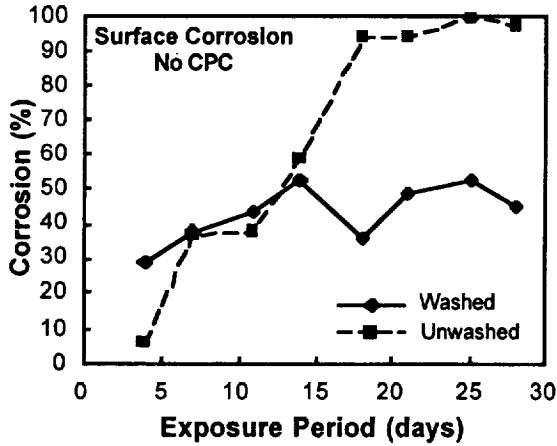


Figure 3(a). Surface Corrosion in Specimens with No CPC

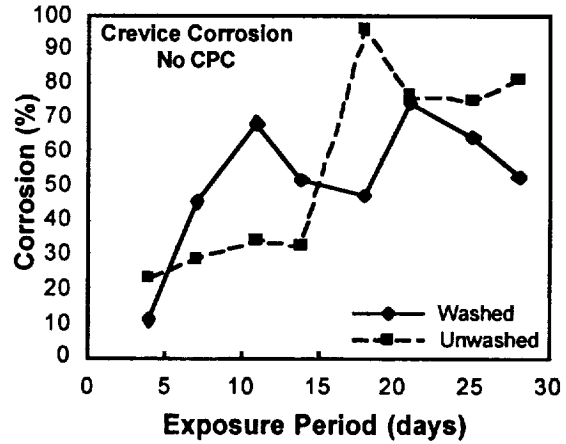


Figure 3(b). Crevice Corrosion in Specimens with No CPC

means that the aluminium is not attacked by concentrated salt deposits. Since washing would not be as effective in removing salt and corrosion products from within the crevices the effects of washing in suppressing the formation of corrosion is less pronounced within the crevices. Still, frequent washing with fresh water and detergent appears to be a good deterrent for both surface and crevice corrosion.

3.2 EFFECTIVENESS OF CPCs WITHOUT FREQUENT WASHING

The efficacy of Water Displacing Corrosion Compounds in keeping corrosion at bay is displayed in Figures 4(a) and 4(b). In these figures show the percentage areas of surface corrosion are plotted against the period of exposure to salt spray, for the control specimens which

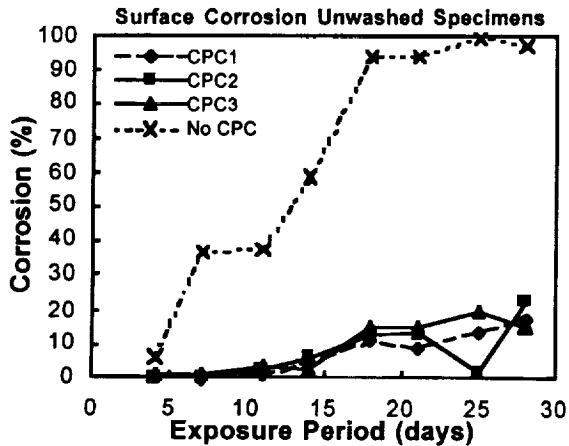


Figure 4(a). Surface Corrosion in Unwashed Specimens

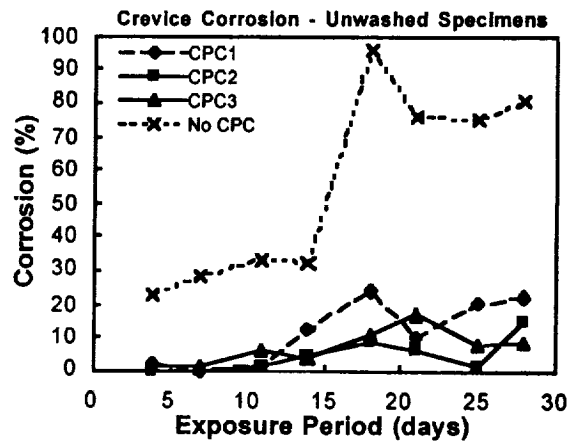


Figure 4(b). Crevice Corrosion in Unwashed Specimens

were not subjected to frequent washing. It can be seen that in both cases, specimens without any treatment developed 100 percent corrosion within about 2 weeks of exposure. If an arbitrary value of twenty percent corrosion is taken to indicate the breakdown of the CPC, then for the three CPCs studied virtually no breakdown has occurred until the end of the four week trial period. Considering crevice corrosion, only CPC1, which has the least dry film thickness, shows signs of breaking down towards the end of the four week trial, while CPC2 and CPC3 remain just as effective in crevices as on exposed surfaces. In comparison, the unprotected or bare specimens

reach twenty percent corrosion within the first week, with an average corrosion coverage of approximately ninety percent after fifteen days.

3.3 COMBINED EFFECTIVENESS OF CPCs AND FREQUENT WASHING

Figures 5(a) and 5(b) respectively, indicate the effectiveness of CPCs on the specimens which are subject to frequent fresh water washing. The breakdown of CPCs is significant and almost immediate for both types of corrosion, surface as well as crevice, as evidenced by the plots. For surface corrosion CPC1 reaches twenty percent within the first five days, ie. just two washes, while all three CPCs have broken down by the fourteenth day. Again, using our arbitrary criterion of 20% corrosion as the indication of failure, it is seen that in the crevice areas under the washers, all three CPCs breakdown before the tenth day. On average CPC3 with the thickest dry film coating appears to provide the best crevice protection while CPC1 provides the best surface protection. By the end of a three to four week period it is evident that specimens that were initially coated with CPCs are as much affected by corrosion as those originally unprotected.

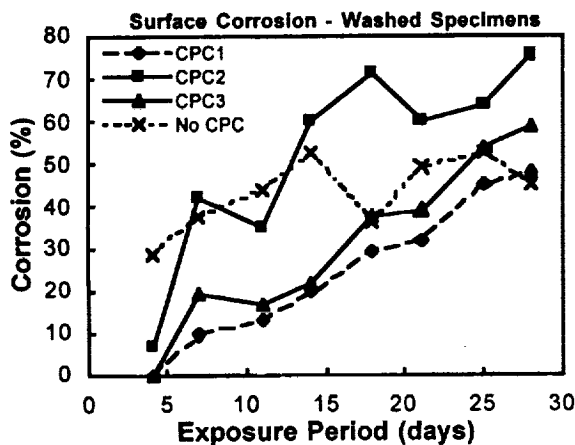


Figure 5(a). Surface Corrosion in Specimens Subjected to Washing

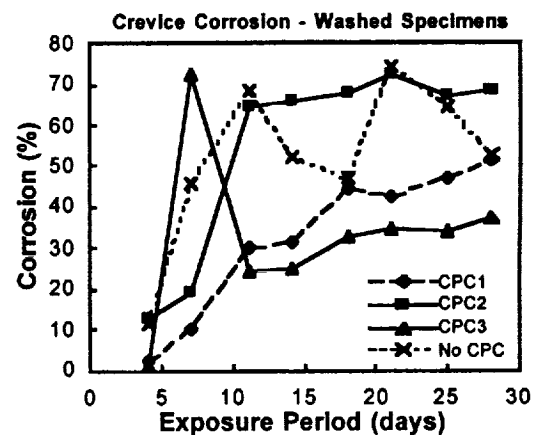


Figure 5(b). Crevice Corrosion in Specimens Subjected to Washing

3.4 EFFECTIVENESS OF CPCs WHEN SUBJECTED TO FREQUENT WASHING

The data from the plots in Figures 4 and 5 are presented separately for each individual CPC in Figures 6 to 8. Figures 6(a), 7(a) and 8(a) respectively depict the comparison of the growth of corrosion damage on the exposed surfaces between the crevices in the washed and unwashed conditions for each of the three compounds CPC1, CPC2 and CPC3. The comparison of crevice corrosion growth with increasing periods of salt spray exposure between the washed and unwashed groups of specimens is displayed in Figures 6(b), 7(b) and 8(b) respectively for the three compounds investigated. It is evident from these graphs that all three CPCs were successful in containing corrosion to within 20% of the total available crevice and exposed surface areas, when the specimens were not subjected to frequent washing, whereas in the specimens subjected to frequent washing all three CPCs broke down fairly quickly, resulting in corrosion coverage well above the twenty percent mark. This confirms that CPC coatings are adversely affected by washing and need to be reapplied.

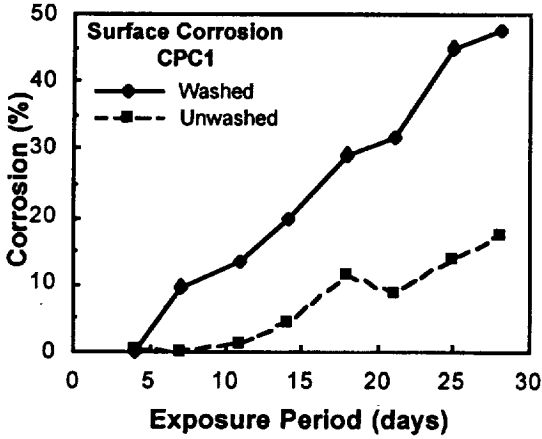


Figure 6(a). Comparison of Surface Corrosion in Specimens with CPC1

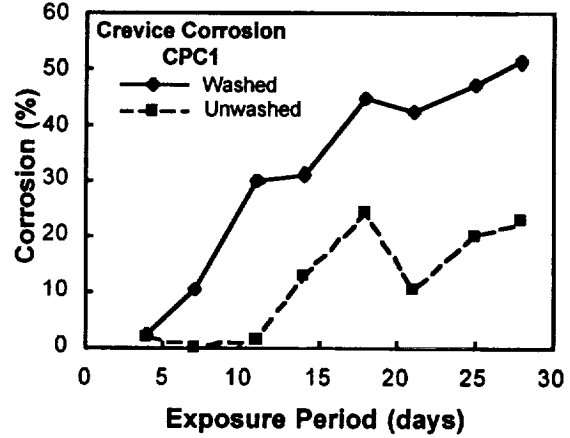


Figure 6(b). Comparison of Crevice Corrosion in Specimens with CPC1

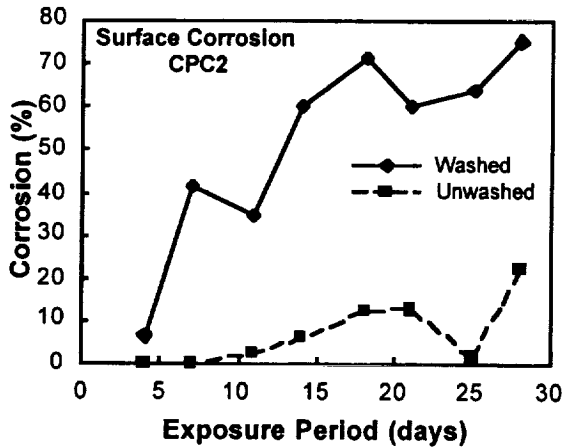


Figure 7(a). Comparison of Surface Corrosion in Specimens with CPC2

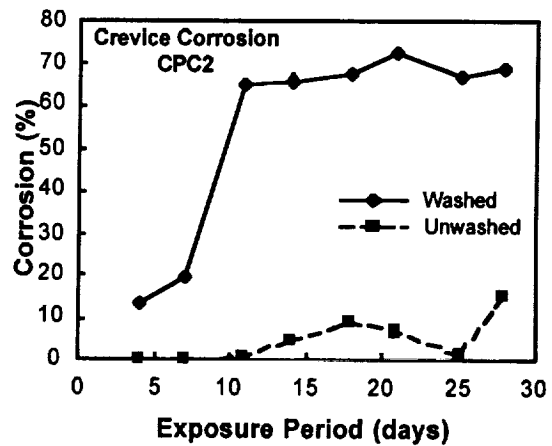


Figure 7(b). Comparison of Crevice Corrosion in Specimens with CPC2

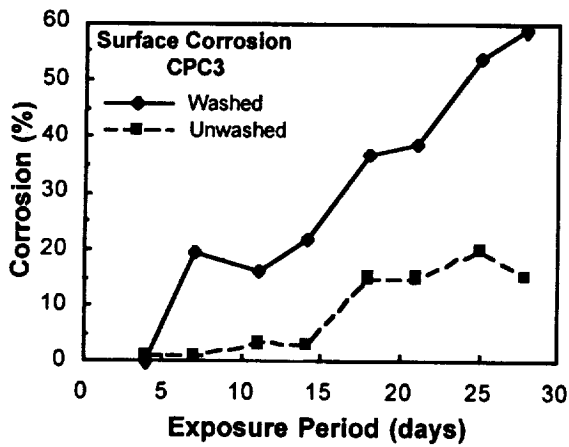


Figure 8(a). Comparison of Surface Corrosion in Specimens with CPC3

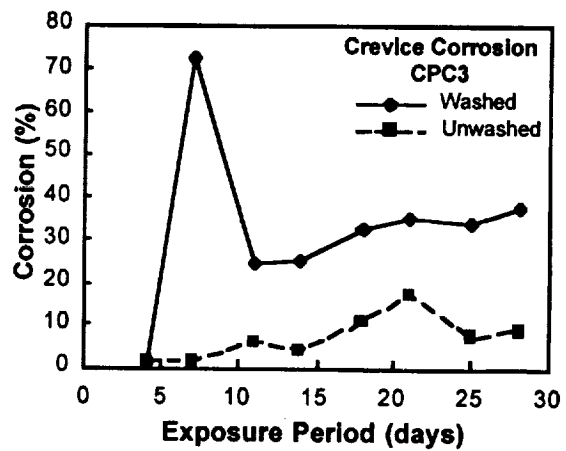


Figure 8(b). Comparison of Crevice Corrosion in Specimens with CPC3

CONCLUSION

The results of an experimental investigation on the effectiveness of Water Displacing Corrosion Prevention compounds have been presented. The results from the tests indicate that:

- The use of frequent washing with fresh water has a beneficial effect in controlling the growth of corrosion damage. Compared to unwashed specimens which get fully corroded in the salt fog environment within about 20 days, specimens that are washed every alternate day develop only 50 to 70% corrosion even after four weeks. Fresh water washing, however, is more effective in inhibiting surface corrosion than crevice corrosion.
- Water Displacing Corrosion Preventive Compounds on their own are very effective and reliable in inhibiting both surface and crevice corrosion in aluminium alloys. Less than twenty percent corrosion is developed in both cases even after continuous exposure to salt fog for four weeks, provided the specimens are not subjected to washing.
- The combination of CPCs and frequent washing, without reapplication of the CPCs, however, is only as effective as fresh water washing by itself. Frequent washing significantly reduces the effectiveness of the CPCs. After two or three washes, the CPCs are virtually ineffective, if no recoat is applied. Comparing between different CPCs, it appears that the thin film CPC studied was more durable on exposed surfaces, whereas the thick film CPC appeared to retain its protective capacity for the longest period within the crevices.

REFERENCES

1. B.Hinton, K.Shankar, P.Trathen, M.Salagaras, L.Wilson and G.Devereux, *Control of Corrosion on Aluminium Alloys with Corrosion Prevention Compounds*, Paper No. 335, 13th International Corrosion Congress, Melbourne, Australia, 25-29 November 1996.
2. Machin, A.S. and Mann, J.Y., *The Influence of Water-Displacing Organic Corrosion Inhibitors on the Fatigue Behaviour of 2024-T3 Alclad Aluminum Alloy Bolted Joints*, ARL-STRUC-R-390, 1979.
3. Hoepfner, D. W., Adibnazari, S. and Moesser, M. W., *Literature Review and Preliminary Studies of Fretting and Fretting Fatigue Including Special Applications to Aircraft Joints*, DOT/FAA/CT-93/2, United States Federal Aviation Administration, Atlantic City, 1994.
4. Royal Australian Navy, *Corrosion in Naval Aircraft*, Defence Instruction (Navy) AP 119A-0202-1, 1992.
5. Royal Australian Navy, *Organisational Maintenance, General Aircraft Maintenance Manual, Wash Helicopter*, Defence Instruction (Navy) NAP 7210.024-2-000, 1995.
6. Royal Australian Navy, *Technical Manual of Husbandry Inspection Operations Model S-70B-2 Helicopter*, Defence Instruction (Navy) NAP 7210.024-6-2-2, 1995.
7. American Society for testing and Materials, *Standard Guide for Crevice Corrosion Testing of Iron-Base and Nickel-Base Stainless Alloys in Seawater and Other Chloride-Containing Aqueous Environments*, ASTM G78-95, Annual Book of ASTM Standards, Vol.3, 1996.
8. American Society for testing and Materials, *Standard Practice for Operating Salt Spray (FOG) Testing Apparatus*, ASTM B117-94, Annual Book of ASTM Standards, Vol.3, Section 03.02 - Wear and Erosion, Metal Corrosion, 1996.
9. Tindall, N., *The Effect of Washing on the Life of Corrosion Preventative Compounds (CPCs) in Crevices*, B.Engg. Thesis, School of Aerospace and Mechanical Engineering, University College, Australian Defence Force Academy, University of New South Wales, Australia, 1997.





REPORT DOCUMENTATION			Form Approved OMB No. 0704-0188	
Public reporting burden for this collection of information is estimated to average 1 hour per response, including the time for reviewing instructions, searching existing data sources, gathering and maintaining the data needed, and completing and reviewing the collection of information. Send comments regarding this burden estimate or any other aspect of this collection of information, including suggestions for reducing this burden, to Washington Headquarters Services, Directorate for Information Operations and Reports, 1215 Jefferson Davis Highway, Suite 1204, Arlington, VA 22202-4302, and to the Office of Management and Budget, Paperwork Reduction Project (0704-0188), Washington, DC 20503.				
1. AGENCY USE ONLY (Leave blank)		2. REPORT DATE January 1999	3. REPORT TYPE AND DATES COVERED Conference Publication	
4. TITLE AND SUBTITLE The Second Joint NASA/FAA/DoD Conference on Aging Aircraft			5. FUNDING NUMBERS WU-538-10	
6. AUTHOR(S) Charles E. Harris, Editor				
7. PERFORMING ORGANIZATION NAME(S) AND ADDRESS(ES) NASA Langley Research Center Hampton, VA 23681-2199			8. PERFORMING ORGANIZATION REPORT NUMBER L-17819A	
9. SPONSORING / MONITORING AGENCY NAME(S) AND ADDRESS(ES) National Aeronautics and Space Administration Washington, DC 20546-0001			10. SPONSORING / MONITORING AGENCY REPORT NUMBER NASA CP-1999/208982/PART1	
11. SUPPLEMENTARY NOTES				
12a. DISTRIBUTION / AVAILABILITY STATEMENT Unclassified-Unlimited Subject Category: 39 Distribution: Standard Availability: NASA CASI (301) 621-0390			12b. DISTRIBUTION CODE	
13. ABSTRACT (Maximum 200 words) The purpose of the Conference was to bring together world leaders in aviation safety research, aircraft design and manufacturing, fleet operation and aviation maintenance to disseminate information on current practices and advanced technologies that will assure the continued airworthiness of the aging aircraft in the military and commercial fleets. The Conference included reviews of current industry practices, assessments of future technology requirements, and status of aviation safety research. The Conference provided an opportunity for interactions among the key personnel in the research and technology development community, the original equipment manufacturers, commercial airline operators, military fleet operators, aviation maintenance, and aircraft certification and regulatory authorities. Conference participation was unrestricted and open to the international aviation community. Appendix B contains the name and addresses of the 623 participants in the Conference.				
14. SUBJECT TERMS fatigue, fracture, corrosion, structural integrity, aircraft, NDE, NDI nondestructive evaluation, inspection, aging aircraft, fleet management			15. NUMBER OF PAGES 403	
			16. PRICE CODE A18	
17. SECURITY CLASSIFICATION OF REPORT Unclassified	18. SECURITY CLASSIFICATION OF THIS PAGE Unclassified	19. SECURITY CLASSIFICATION OF ABSTRACT Unclassified	20. LIMITATION OF ABSTRACT UL	

